NASA/CR–2011-215960

Modeling High-Speed Civil Tiltrotor Transports in the Next Generation Airspace

William W. Chung, Dennis Linse, Al Paris, and Dan Salvano
Science Applications International Corporation (SAIC)
McLean, Virginia

Ted Trept and Tom Wood
Bell Helicopter Textron, Inc.
Hurst, Texas

Huina Gao, Dave Miller, Ken Wright, and Ray Young
Sensis Corporation
Reston, Virginia

Victor Cheng
Optimal Synthesis, Inc.
Los Altos, California

Prepared for Ames Research Center under
Contract No. NAS1-NNA06BC41C

October 2011

The NASA STI Program Office . . . in Profile

Since its founding, NASA has been dedicated to the advancement of aeronautics and space science. The NASA Scientific and Technical Information (STI) Program Office plays a key part in helping NASA maintain this important role.

The NASA STI Program Office is operated by Langley Research Center, the Lead Center for NASA's scientific and technical information. The NASA STI Program Office provides access to the NASA STI Database, the largest collection of aeronautical and space science STI in the world. The Program Office is also NASA's institutional mechanism for disseminating the results of its research and development activities. These results are published by NASA in the NASA STI Report Series, which includes the following report types:

- TECHNICAL PUBLICATION. Reports of completed research or a major significant phase of research that present the results of NASA programs and include extensive data or theoretical analysis. Includes compilations of significant scientific and technical data and information deemed to be of continuing reference value. NASA's counterpart of peer-reviewed formal professional papers but has less stringent limitations on manuscript length and extent of graphic presentations.

- TECHNICAL MEMORANDUM. Scientific and technical findings that are preliminary or of specialized interest, e.g., quick release reports, working papers, and bibliographies that contain minimal annotation. Does not contain extensive analysis.

- CONTRACTOR REPORT. Scientific and technical findings by NASA-sponsored contractors and grantees.

- CONFERENCE PUBLICATION. Collected papers from scientific and technical conferences, symposia, seminars, or other meetings sponsored or cosponsored by NASA.

- SPECIAL PUBLICATION. Scientific, technical, or historical information from NASA programs, projects, and missions, often concerned with subjects having substantial public interest.

- TECHNICAL TRANSLATION. English-language translations of foreign scientific and technical material pertinent to NASA's mission.

Specialized services that complement the STI Program Office's diverse offerings include creating custom thesauri, building customized databases, organizing and publishing research results . . . even providing videos.

For more information about the NASA STI Program Office, see the following:

- Access the NASA STI Program Home Page at *http://www.sti.nasa.gov*

- E-mail your question via the Internet to help@sti.nasa.gov

- Fax your question to the NASA Access Help Desk at (301) 621-0134

- Telephone the NASA Access Help Desk at (301) 621-0390

- Write to:
  NASA Access Help Desk
  NASA Center for AeroSpace Information
  7115 Standard Drive
  Hanover, MD 21076-1320

NASA/CR–2011-215960

Modeling High-Speed Civil Tiltrotor Transports in the Next Generation Airspace

William W. Chung, Dennis Linse, Al Paris, and Dan Salvano
Science Applications International Corporation (SAIC)
McLean, Virginia

Ted Trept and Tom Wood
Bell Helicopter Textron, Inc.
Hurst, Texas

Huina Gao, Dave Miller, Ken Wright, and Ray Young
Sensis Corporation
Reston, Virginia

Victor Cheng
Optimal Synthesis, Inc.
Los Altos, California

National Aeronautics and
Space Administration

Ames Research Center
Moffett Field, California 94035-1000

October 2011

Available from:

NASA Center for AeroSpace Information
7115 Standard Drive
Hanover, MD 21076-1320
(301) 621-0390

National Technical Information Service
5285 Port Royal Road
Springfield, VA 22161
(703) 487-4650

TABLE OF CONTENTS

List of Figures vii
List of Tables xiii
Nomenclature xvii
Summary 1
1 Introduction 3
2 CTR Design Approach and Results 5
2.1 Mission Requirements Under NextGen 6
2.2 General Design Approach 9
2.3 Comparative Design Summary 22
2.4 10-Passenger CTR (CTR10) 26
2.5 30-Passenger CTR (CTR30) 35
2.6 120-Passenger CTR (CTR120) 45
2.7 Design Recommendations 69
2.8 Generating Input Data for BADA 70
2.9 Noise Footprint 70
3 CTR Modeling for NAS Performance Analysis 81
3.1 Introduction 81
3.2 BADA Performance Model Entries 81
3.3 Performance Data Collection 92
3.4 BADA Model Determination 94
3.5 BADA Model Verification 112
3.6 BADA Modeling for the Nacelle Conversion Operations 120
3.7 Verification of CTR Flight Performance Integrated Into the NAS Simulation Tools 130
4 CTR Concept of Operations 139
4.1 STOL and VTOL 139
4.2 Runway-Independent Operations 141
4.3 Noninterference Operations 142
4.4 Developing CTR Flight Profiles Via Pilot-in-the-Loop Simulation 143
4.5 Developing Desired Flight Parameters for the CTR Fleet for the NextGen Performance Analysis 156
4.6 Potential Certification and Safety Issues 157

TABLE OF CONTENTS (cont.)

5 CTR Operations in NextGen 163
5.1 NextGen Concept of Operations 165
5.2 NextGen Capabilities Applied to CTR Operations 167
5.3 NextGen ConOps Applied to CTR Operations 168
6 CTR Fleet Performance Analysis under NextGen 173
6.1 NextGen Performance Metrics for CTR 176
6.2 NextGen Performance Analysis Tools 184
6.3 Assumptions for NextGen Performance Analysis 185
6.4 Descriptions of the NAS Analysis Test Matrix 190
6.5 Results From the Baseline (Test Points 0.0, 0.1) 195
6.6 Results From the CTR120 Fleet (Test Points 1.1–1.4) 198
6.7 Results From CTR90 and CTR120 Mixed CTR Fleet (Test Points 2.1–2.4) 204
6.8 CTR30, CTR90, and CTR120 Mixed Fleet Results (Test Points 3.1–3.4) 208
6.9 Results From the CTR10 Fleet Scenarios (Test Point 5.0) 212
6.10 Results of VTOL/STOL CTR Operations (Test Point 6.0) 212
6.11 Sensitivity Analysis of CTR Load Factor (Test Point 7.0) 212
6.12 Results of Sensitivity Study of Taxi-Out/Taxi-In Time (Test Point 8.0) 215
6.13 CTR NAS Performance Under NextGen Analysis Summary 215
7 Environmental Impact of the CTR Fleet 219
7.1 Noise Impact at EWR 219
7.2 Overview of the Emission Impact of a CTR Fleet 238
7.3 Summary 240
8 Summary and Recommendations 243
8.1 CTR Technology 243
8.2 BADA and NAS Simulation 244
8.3 NextGen ConOps 244
8.4 CTR ConOps 245
9 References 247

Appendix A. BADA Overview 251
Appendix B. Airplane Mode Performance Trim Matrix 257
Appendix C. Conversion Mode Performance Matrix 261
Appendix D. CTR30 and CTR120 BADA Model Determination 265

TABLE OF CONTENTS (concluded)

Appendix E. CTR90 BADA Model Linear Sizing 287
Appendix F. CTR90 BADA Performance Model Comparison 315
Appendix G. CTR30, CTR90, and CTR120 BADA Model Verification 321
Appendix H. Pilot-in-the-Loop Flight Simulation Results 341
Appendix I. CTR Performance Deck 355
Appendix J. Tradeoff Analysis of CTR Flight Profiles 365
Appendix K. ACES Test Scenarios Setup 389
Appendix L. Possible VTOL/STOL Landing Locations at Newark Liberty International Airport for Civil Tiltrotor Aircraft 391
Appendix M. AvTerminal Analysis 399
Appendix N. Conventional Itineraries Analysis 405
Appendix O. CTR Itineraries Analysis 411

LIST OF FIGURES

Figure 2-1. The tiltrotor aircraft history of Bell Helicopter. 5
Figure 2-2. Turboprop and turbojet range characteristics up to 160 passengers. 8
Figure 2-3. Generic NextGen mission profile. 9
Figure 2-4. NextGen hypothetical development schedule. 12
Figure 2-5. Design methodology applied to the NextGen tiltrotor configurations. 13
Figure 2-6. CTR10 and CTR30 acoustic requirements related to rotor tip speed vs. gross weight 15
Figure 2-7. CTR90 and CTR120 acoustic requirements related to rotor tip speed vs. gross weight 16
Figure 2-8. An example of the impact of exhaust nozzle discharge coefficient on net power. 18
Figure 2-9. Buffet-free design chart for wing loading. 20
Figure 2-10. Impact of compressibility on propulsive efficiency. 21
Figure 2-11. Front view comparison of the NextGen designs. 23
Figure 2-12. Profile view comparison of the NextGen designs. 23
Figure 2-13. NextGen CTR range compared to fixed-wing aircraft. 24
Figure 2-14. NextGen CTR width compared to fixed-wing aircraft. 25
Figure 2-15. NextGen CTR fuselage length compared to fixed-wing aircraft. 25
Figure 2-16. Cabin layout of the CTR10 configuration. 27
Figure 2-17. CTR10 normalized engine power available. 28
Figure 2-18. Effect of true airspeed on power available. 28
Figure 2-19. CTR10 normalized net nacelle thrust. 29
Figure 2-20. Three-view drawing of the CTR10 configuration in helicopter mode. 32
Figure 2-21. CTR10 OEI STO hover ceiling, ISA and ISA+20°C. 33
Figure 2-22. CTR10 partial speed-altitude envelope, ISA. 34
Figure 2-23. CTR10 payload-range curve, ISA cruise. 34
Figure 2-24. Cabin layout of the CTR30 configuration. 36
Figure 2-25. CTR30 normalized engine power available. 39
Figure 2-26. Effect of true airspeed on power available. 39
Figure 2-27. CTR30 normalized net nacelle thrust. 40
Figure 2-28. Three-view drawing of the CTR30 configuration in airplane mode. 42
Figure 2-29. Three-view drawing of the CTR30 configuration in helicopter mode. 43
Figure 2-30. CTR30 OEI STO hover ceiling, ISA and ISA+20°C. 44
Figure 2-31. CTR30 partial speed-altitude envelope, ISA. 44
Figure 2-32. CTR30 payload-range curve, ISA. 45
Figure 2-33. The cabin layout of the CTR120 configuration. 47

LIST OF FIGURES (cont.)

Figure 2-34. Bell tiltrotor handbook drag methodology correlation. 49
Figure 2-35. LSAF correlation with 25-foot JVX rotor data from the NASA Ames OARF.....51
Figure 2-36. Impact of rotor rpm on cruise propulsive efficiency.....52
Figure 2-37. Sensitivity of design gross weight and hover/cruise balance point. 54
Figure 2-38. Relationship between disk loading and blade aspect ratio.....54
Figure 2-39. Productivity index for CTR120 with a design range of 1,500 nmi. 55
Figure 2-40. Impact of range on design gross weight.....57
Figure 2-41. Impact of range on productivity index. 57
Figure 2-42. Impact of disk loading and design speed on design gross weight (25,000 feet). 58
Figure 2-43. Impact of disk loading and design speed on engine size (25,000 feet). 59
Figure 2-44. Impact of disk loading and design speed on productivity index (25,000 feet). 59
Figure 2-45. Impact of disk loading and design speed on design gross weight (27,500 feet). 60
Figure 2-46. Impact of disk loading and design speed on engine size (27,500 feet). 60
Figure 2-47. Impact of disk loading and design speed on productivity index (27,500 feet). 61
Figure 2-48. Impact of disk loading and design speed on design gross weight (30,000 feet). 61
Figure 2-49. Impact of disk loading and design speed on engine size (30,000 feet). 62
Figure 2-50. Impact of disk loading and design speed on productivity (30,000 feet). 62
Figure 2-51. Productivity index for CTR120 with a design range of 1,200 nmi. 63
Figure 2-52. Three-view drawing of CTR120 configuration in airplane mode. 66
Figure 2-53. Three-view drawing of CTR120 configuration in helicopter mode. 66
Figure 2-54. Installed rotor Figure of Merit for CTR120 design (5k/ISA+20°C). 67
Figure 2-55. CTR120 OEI STO hover ceiling (ISA and ISA+20°C). 68
Figure 2-56. CTR120 partial speed-altitude envelope (ISA). 68
Figure 2-57. CTR120 payload-range curve (ISA). 69
Figure 2-58. 10-passenger SEL noise contours for approach, 3-degree. 73
Figure 2-59. 10-passenger SEL noise contours for approach, 6-degree. 73
Figure 2-60. 10-passenger SEL noise contours for approach, 9-degree. 74
Figure 2-61. 10-passenger SEL noise contours for takeoff, VTO. 74
Figure 2-62. 10-passenger SEL noise contours for takeoff, STO. 75
Figure 2-63. 30-passenger SEL noise contours for approach, 3-degree 75
Figure 2-64. 30-passenger SEL noise contours for approach, 6-degree. 76
Figure 2-65. 30-passenger SEL noise contours for approach, 9-degree. 76
Figure 2-66. 30-passenger SEL noise contours for takeoff, VTO. 77

LIST OF FIGURES (cont.)

Figure 2-67. 30-passenger SEL noise contours for takeoff, STO. 77
Figure 2-68. 120-passenger SEL noise contours for approach, 3-degree. 78
Figure 2-69. 120-passenger SEL noise contours for approach, 6-degree. 78
Figure 2-70. 120-passenger SEL noise contours for approach, 9-degree. 79
Figure 2-71. 120-passenger SEL noise contours for takeoff, VTO. 79
Figure 2-72. 120-passenger SEL noise contours for takeoff, STO. 80
Figure 3-1. CTR VTOL/STOL mission phases mapped to BADA-supported configurations. 92
Figure 3-2. CTR10 airframe drag in airplane mode based on provided trim performance data. 95
Figure 3-3. CTR10 thrust performance under various operating conditions. 97
Figure 3-4. CTR10 descent thrust ratio across altitude envelope. 98
Figure 3-5. CTR10 descent thrust specific fuel consumption over various mission phases. 99
Figure 3-6. CTR10 low-power-descent fuel flow variant. 100
Figure 3-7. CTR10 effect of MTOW variation on maximum attainable altitude at 300-fpm residual ROC. 101
Figure 3-8. Climb schedule over the altitude envelope for the CTR10 at MTOW and airplane mode. 102
Figure 3-9. CTR10 LRC schedule over the altitude envelope in airplane mode at MTOW. 103
Figure 3-10. Descent schedule for the CTR10 at MREF and airplane mode. 104
Figure 3-11. CTR10 approach and landing descent thrust scale factor 106
Figure 3-12. Takeoff thrust scale factor for the 10-passenger CTR. 107
Figure 3-13. Aerodynamics for IC mode of the CTR10. 108
Figure 3-14. Aerodynamics for AP mode of the CTR10. 108
Figure 3-15. Aerodynamics for STOL LD mode of the CTR10. 109
Figure 3-16. CTR10 aerodynamics for VTOL LD mode. 109
Figure 3-17. CTR10 aerodynamics for STOL TO mode. 110
Figure 3-18. CTR10 Aerodynamics for VTOL TO mode. 110
Figure 3-19. CTR10 STOL TO C_{DO} coefficients. 111
Figure 3-20. CTR10 VTOL TO C_{D0} coefficients. 111
Figure 3-21. Overall CTR flight profile. 120
Figure 3-22. CTR10 fuel burn, Flight Profile Points 2 to 4 for STOL and VTOL operations. 125
Figure 3-23. CTR10 fuel burn, Flight Profile Points 8.1 to 12, STOL operations at various GS angles. 126
Figure 3-24. CTR10 fuel burn, Flight Profile Points 8.1 to 12, VTOL operations at various GS angles. 126
Figure 3-25. CTR30 fuel burn, Flight Profile Points 2 to 4, STOL and VTOL operations 127
Figure 3-26. CTR30 fuel burn, Flight Profile Points 8.1 to 12, STOL operations at various GS angles 127
Figure 3-27. CTR30 fuel burn, Flight Profile Points 8.1 to 12, VTOL operations at various GS angles. 128

LIST OF FIGURES (cont.)

Figure 3-28. CTR10 conversion-mode static trim comparison data. 129
Figure 3-29. CTR30 conversion-mode static trim comparison data. 129
Figure 3-30. CTR120 conversion-mode static trim comparison data. 130
Figure 3-31. CTR10 VTOL TO C_{D0} coefficients. 131
Figure 3-32. CTR10 altitude and TAS responses comparison. 133
Figure 3-33. CTR30 altitude and TAS responses comparison. 134
Figure 3-34. CTR90 altitude and TAS responses comparison. 135
Figure 3-35. CTR120 altitude and TAS responses comparison. 136
Figure 4-1. VTOL landing pad dimensions with a 100-foot-effective RS. 141
Figure 4-2. VTOL and STOL landing areas at MIA. 146
Figure 4-3. Initial CTR approach profile. 147
Figure 4-4. The Bell Helicopter Partial Task Simulator (PTS) 149
Figure 4-5. BA609 cockpit with the third-person view 149
Figure 4-6. CTR takeoff profile from PITL experiment. 152
Figure 4-7. CTR approach profile from the PITL experiment. 152
Figure 4-8. Productivity Index for the CTR fleet in selected origin-destination city-pairs 157
Figure 4-9. Regulations over BA-609 certification. 158
Figure 6-1. NVI NRA major U.S. airport delay projections for 2025. 173
Figure 6-2. Current baseline major U.S. airport delay projections for 2025. 174
Figure 6-3. CTR regional networks. 175
Figure 6-4. Operational and service performance metrics. 176
Figure 6-5. Composition of scheduled trip times. 179
Figure 6-6. Arrival time distribution and 15-minute standard. 180
Figure 6-7. Flow corridors. 182
Figure 6-8. Optimized profile descent. 182
Figure 6-9. Trip circuity. 183
Figure 6-10. Circuity in practice. 183
Figure 6-11. ACES vertiport relationship between average delay and daily operations. 187
Figure 6-12. CTR120 fleet regional networks. 198
Figure 6-13. CTR90 and CTR120 mixed fleet regional networks 204
Figure 6-14. CTR30, CTR90, and CTR120 mixed fleet regional networks 208
Figure 6-15. Cumulative total delay reduction from CTR substitution. 216
Figure 6-16. Cumulative average delay reduction from CTR substitution. 216

LIST OF FIGURES (concluded)

Figure 7-1. CTR30 vertical takeoff (VTO) departure comparison, Run 13, SEL (A-weighted) contours....220

Figure 7-2. CTR30 3-degree-approach comparison, Run 05, SEL (A-weighted) contours. 221

Figure 7-3. CTR30 3-degree-approach, RNM 3 vs. RNM 7 with restricted hemisphere set. 221

Figure 7-4. CTR30 3-degree-approach profile for INM input....225

Figure 7-5. SEL noise footprint of a CTR30 3-degree final approach: RNM vs. INM. 226

Figure 7-6. SEL noise footprint of a CTR30 3-degree extended approach. 227

Figure 7-7. SEL noise footprint of a CTR120 3-degree approach....227

Figure 7-8. SEL noise footprint of a CTR90 3-degree approach....228

Figure 7-9. SEL noise footprint of a CTR30 VTO departure from EWR. 228

Figure 7-10. Possible vertiport sites for the CTR fleet at EWR. 230

Figure 7-11. SEL noise footprint for outbound NEC EWR flights. 231

Figure 7-12. SEL noise footprint for outbound NEC EWR flights 231

Figure 7-13. SEL noise footprint for inbound NEC EWR flights. 232

Figure 7-14. SEL noise footprint for inbound NEC EWR flights. 232

Figure 7-15. SEL noise footprint for all NEC EWR flights. 234

Figure 7-16. SEL noise footprint for all NEC EWR operations. 234

Figure 7-17. DNL noise footprint for assumed all CTR NEC EWR operations. 235

Figure 7-18. DNL noise footprint for assumed all CTR NEC EWR flights over population distributions. 235

Figure 7-19. DNL noise footprint comparison for a 3-degree (left) and a 9-degree (right) approach at EWR....236

Figure 7-20. DNL noise footprint comparison for 3-degree (top), 9-degree (middle), and rerouted 9-degree (bottom) approach at EWR. 237

Figure 7-21. CTR and conventional block fuel per seat vs. distance. 241

LIST OF TABLES

Table 2-1. Proposed CTR fleet operational modes in NextGen....6
Table 2-2. Design goals for the NextGen aircraft....7
Table 2-3. NextGen mission profile segment details....9
Table 2-4. Comparison of NextGen design characteristics....22
Table 2-5. Summary of the CTR10 configuration characteristics....30
Table 2-6. Summary of the CTR30 configuration characteristics....38
Table 2-7. CTR120 design requirements....46
Table 2-8. Summary of CTR120 configuration characteristics....64
Table 2-9. Summary of CTR120 weights....65
Table 2-10. CTR120 drag breakdown....65
Table 2-11. Noise level adjustments....72
Table 3-1. Airframe type characteristics....82
Table 3-2. Airframe geometry characteristics....82
Table 3-3. Airframe mass characteristics....83
Table 3-4. Flight envelope parameters....83
Table 3-5. Flight operations schedule parameters....84
Table 3-6. Airframe aerodynamic characteristics....85
Table 3-7. Propulsion system thrust characteristics....88
Table 3-8. Propulsion system fuel flow characteristics....90
Table 3-9. Airframe ground movement characteristics....91
Table 3-10. CTR10 calculated stall speed in CR configuration (NAC 0 degrees)....96
Table 3-11. CTR10 MCP climb at 1.23 VSTALL static trim verification results....114
Table 3-12. CTR10 Long-range cruise static trim verification results....115
Table 3-13. CTR10 MCP cruise static trim verification based on known maximum KTAS schedule....115
Table 3-14. CTR10 MCP cruise static trim verification based on BADA-predicted MCP available....116
Table 3-15. CTR10 long-range cruise mission profile verification....117
Table 3-16. CTR10 maximum continuous power cruise mission profile....117
Table 3-17. CTR10 conversion-mode level-flight static trim verification....118
Table 3-18. CTR10 conversion-mode static trim verification....119
Table 3-19. Airplane mode time to transit and fuel burn per nmi at 1,500 feet level flight, 200 KTAS....122
Table 3-20. CTR10 time, distance, and fuel burn per flight profile phase with STOL conversion....122
Table 3-21. CTR10 time, distance, and fuel burn per flight profile phase with VTOL conversion....123
Table 3-22. CTR30 time, distance, and fuel burn per flight profile phase with STOL conversion....123

LIST OF TABLES (cont.)

Table 3-23. CTR30 time, distance, and fuel burn per flight profile phase with VTOL conversion 123
Table 3-24. CTR90 time, distance, and fuel burn per flight profile phase with STOL conversion 124
Table 3-25. CTR90 time, distance, and fuel burn per flight profile phase with VTOL conversion 124
Table 3-26. CTR120 time, distance, and fuel burn per flight profile phase with STOL conversion 124
Table 3-27. CTR120 time, distance, and fuel burn per flight profile phase with VTOL conversion 125
Table 3-28. Static trim verification check case configurations defined 128
Table 3-29. Flight time performance comparison between ACES and CTRPD 132
Table 3-30. Summary of CTR10 flight time and fuel burn comparison by flight segments 133
Table 3-31. Summary of CTR30 flight time and fuel burn comparison by flight segments 134
Table 3-32. Summary of CTR90 flight time and fuel burn comparison by flight segment 135
Table 3-33. Summary of CTR120 flight time and fuel burn comparison by flight segment 136
Table 3-34. Estimated CTR taxi fuel flow 137
Table 4-1. Proposed CTR fleet operational models in NextGen 142
Table 4-2. Planned PITL test matrix 151
Table 4-3. Takeoff and landing runway length requirements under STOL configuration 153
Table 4-4. CTR10 nacelle and airspeed settings 154
Table 4-5. CTR30 nacelle and airspeed settings 154
Table 4-6. Origin-destination city-pair cruise speed and cruise altitude developed based on Productivity Index 157
Table 4-7. CTR in NextGen design, dimension, and mass properties 160
Table 6-1. Summary of departures and seats by region 175
Table 6-2. Operational performance metrics 178
Table 6-3. Service performance metrics 179
Table 6-4. Capabilities of simulation platforms investigated 184
Table 6-5. CTR markets 185
Table 6-6. CTR departures 185
Table 6-7. CTR unimpeded block hours 186
Table 6-8. CTR airframes at 8.6 block hours per day 186
Table 6-9. CTR operations and average delay per airport/vertiport 188
Table 6-10. Conventional aircraft performance assumptions 189
Table 6-11. Delay metric selection 192
Table 6-12. Delay metric for OPSNET 45 airports 192
Table 6-13. Test matrix 194

LIST OF TABLES (concluded)

Table 6-14. Test Point 0.0, conventional fleet with mixed equipage 196
Table 6-15. Test Point 0.1, conventional fleet with fix-based routes 197
Table 6-16. CTR 120-passenger fleet operations 199
Table 6-17. Conventional fleet flights with mixed equipage replaced by CTR120 fleet 200
Table 6-18. Savings of CTR120 fleet (table 6-16) over conventional mixed-equipage fleet (table 6-17) 201
Table 6-19. Conventional fix-based flights replaced by CTR 120-passenger fleet operations 202
Table 6-20. Savings of CTR120 fleet (table 6-16) over conventional fix-based fleet (table 6-19) 203
Table 6-21. CTR90 and CTR120 mixed fleet operations 205
Table 6-22. Conventional mixed-equipage flights replaced by CTR90 and CTR120 operations 206
Table 6-23. Savings of CTR90/120 mixed fleet (table 6-21) over conventional mixed-equipage flight (table 6-22) 207
Table 6-24. CTR30, CTR90, and CTR120 fleet operations 209
Table 6-25. Conventional mixed-equipage flights replaced by CTR30, CTR90, and CTR120 operations 210
Table 6-26. Savings of CTR30/90/120 mixed-fleet (table 6-24) over conventional mixed-equipage flights (table 6-25) 211
Table 6-27. Fuel burn comparison between CTR VTOL and STOL operations 213
Table 6-28. High load factor option: use of CTR90 to replace CTR120 in Test Point 2.4 (mixed CTR90 and CTR120 fleet) 214
Table 6-29. Effect of one additional minute of taxi time per flight on daily fuel consumption 215
Table 6-30. Cumulative delay reduction from CTR replacement 215
Table 7-1. Over-flight conditions used to generate NPD data 223
Table 7-2. Outbound flights scheduled for the CTR fleet at EWR 229
Table 7-3. Inbound flights scheduled for the CTR fleet at EWR 229
Table 7-4. Assumed mixed CTR flights at EWR for DNL comparison 233
Table 7-5. CTR emissions summary 239

NOMENCLATURE

4DT	Four-Dimensional Trajectory
AATE	Advanced Affordable Turbine Engine
AC	Advisory Circular
AC	Airworthiness Certificate
ACES	Airspace Concept Evaluation System
ACP	Auto-Configure Properties
ADS-B	Automatic Dependent Surveillance-Broadcast
ADS-R	Automatic Dependent Surveillance-Rebroadcast
ADVENT	Adaptive Versatile Engine Technology
AEDT	Aviation Environmental Design Tool
AGL	Above Ground Level
ANSP	Air Navigation Service Provider
AOE	All Engines Operating
AP	Approach
APMT	Aviation Environmental Portfolio Management Tool
APU	Auxiliary Power Systems
ASPM	Aviation System Performance Metrics
ASQP	Airline Service Quality Performance
ATC	Air Traffic Control
ATM	Air Traffic Management
BADA	Base of Aircraft Data
BADA.APF	BADA Airline Procedure File
BADA.GPF	BADA General Parameters File
BOS	Boston Logan International Airport
BWI	Baltimore Washington International Airport
CAS	Calibrated Airspeed
CDA	Continuous Descent Arrival or Continuous Descent Approach
CDA	Concept Design and Analysis
CDTI	Cockpit Display of Traffic Information
CESTOL	Cruise-Efficient Short Takeoff and Landing
CFD	Computational Fluid Dynamics
CFR	Code of Federal Regulations
ConOps	Concept of Operations
COPTER	Comprehensive Program for Theoretical Evaluation of Rotorcraft

CR	Cruise
CSPR	Closely-Spaced Parallel Runway
CTA	Controlled Time of Arrival
CTR	Civil Tiltrotor
CTRDAC	Civil Tiltrotor Development Advisory Committee
CTRPD	Civil Tiltrotor Performance Deck
DA	Decision Altitude
DCA	Ronald Reagan Washington National Airport
DCP	Differential Collective Pitch
DGW	Design Gross Weight
DNL	Day-Night Average Sound Level
DOF	Degree of Freedom
DOT	Department of Transportation
DPs	Departure Procedures
EA	Enterprise Architecture
EASA	European Aviation Safety Agency
ECS	Environmental Control System
EFB	Electronic Flight Bag
EPNdB	Effective Perceived Noise in Decibels
ESF	Energy Share Factor
ESTOL	Extreme Short Takeoff and Landing
ETOPS	Extended Twin-Engine Operations
EWR	Newark Liberty International Airport
FAA	Federal Aviation Administration
FAF	Final Approach Fix
FAR	Federal Aviation Regulation
FATO	Final Approach and Takeoff Area
FBPP	Fuel Burn Post Processor
FBW	Fly-by-Wire
FCS	Flight Control System
FIS-B	Flight Information Services-Broadcast
FMS	Flight Management Systems
GC	Great Circle
HEETE	Highly Efficient Embedded Turbine Engine
HP-TBO	High-Performance Trajectory-Based Operations

HQRs	Handling Qualities Ratings
IAD	Dulles International Airport
IAP	Instrument Approach Procedure
IC	Initial Climb
ICAO	International Civil Aviation Organization
IF	Initial Fix
IFR	Instrument Flight Rules
IMC	Instrument Meterological Conditions
INM	Integrated Noise Model
IPSA	Interagency Portfolio and System Analysis
ISA	International Standard Atmosphere
ITAR	International Traffic in Arms Regulations
IWP	Integrated Work Plan
JFK	John F. Kennedy International Airport
JHL	Joint Heavy Lift
JPDO	Joint Planning and Development Office
KCAS	Knots Calibrated Airspeed
KTAS	Knots True Airspeed
LAS	Las Vegas-McCarran International Airport
LAT	Latitude
LAX	Los Angeles International Airport
LCTR	Large Civil Tiltrotor Aircraft
LD	Landing
LDL	Landing Length
LGA	New York LaGuardia International Airport
LON	Longitude
LPV	Lateral Navigation With Precision Vertical Guidance
LRC	Long-Range Cruise
LSAF	Lifting Surface Aerodynamics and Performance Analysis of Rotors in Axial Flight
LTO	Landing and Takeoff
LZ	Landing Zone
MAP	Missed Approach Point
MCP	Maximum Continuous Power
Mdd	Drag Divergence Mach
MGW	Maximum Gross Weight

MIA	Miami International Airport
MREF	Reference Mass
MRP	Maximum Rated Power
MSL	Mean Sea Level
MTOW	Maximum Takeoff Weight
NAC	Nacelle
NAS	National Airspace System
NAVAID	Navigational Aid
NCO	Net-Centric Operations
NEC	Northeast Corridor
NEC9	Northeast Corridor Nine
NextGen	Next Generation Air Transportation System
NGIP	NextGen Implementation Plan
NIO	Noninterference Operations
nmi	Nautical Miles
NPD	Noise Power-Distance
NRA	NASA Research Announcement
NVI	New Vehicle Integration
NYC	New York City
OARF	Outdoor Aerodynamic Research Facility
O-D	Origin-Destination
OEI	One-Engine-Inoperative
OEM	Original Equipment Manufacturer
OEP	Operational Evolution Partnership airports
OPD	Optimized Profile Descent
OPSNET	Operations Network
OWE	Operational Weight Empty
PANYNJ	Port Authority of New York and New Jersey
PC	Production Certificate
PD	Performance Deck
PFA	Power for Ascent
PFD	Power for Descent
PHL	Philadelphia International Airport
PI	Productivity Index
PIT	Pittsburg International Airport

PITL	Pilot-in-the-Loop
PLA	Powered Lift Aircraft
PLF	Power for Level Flight
PM	Particulate Matter
PNT	Positioning, Navigation, and Timing
PRESTO	Preliminary Evaluation and Sizing Tool
PRM-A	Precision Runway Monitor-Alternative
PTS	Partial Task Simulator
PWN	Piece-Wise-NPD
RIO	Runway-Independent Operations
RNAV	Area Navigation
RNM	Rotorcraft Noise Model
RNP	Required Navigation Performance
ROC	Rate of Climb
ROCD	Rate of Climb/Descent
RS	Rotor Span
RTA	Required Time of Arrival
SAE	Society of Automotive Engineers
SAIC	Science Applications International Corporation
SEL	Sound Exposure Level
SFC	Specific Fuel Consumption
SID	Standard Instrument Departure
SNI	Simultaneous Noninterference
SSA	Shared Situational Awareness
SST	Supersonic Transports
STARS	Standard Terminal Arrival Routes
STO	Short Takeoff
STOL	Short Takeoff and Landing
SVS/EVS	Synthetic Vision Systems/Enhanced Vision Systems
TAF	Terminal Area Forecast
TAS	True Airspeed
TBO	Trajectory-Based Operations
TC	Type Certificate
TCAS	Traffic Collision Avoidance System
TEM	Total Energy Model

TFM	Traffic Flow Management
TIS-B	Traffic Information Services-Broadcast
TLOF	Touchdown and Lift-Off Area
TO	Takeoff
TOC	Top of Climb
TOD	Top of Descent
TOL	Takeoff Length
TR	Tiltrotor Requirement
TSFC	Thrust Specific Fuel Consumption
UAS	Unmanned Aircraft Systems
VAATE	Versatile Affordable Advanced Turbine Engine
VASC	Vertical Ascent in Ground Effect
VFR	Visual Flight Rules
VLJ	Very Light Jet
VLRC	Long-Range Cruise Velocity
VMC	Visual Meterological Conditions
VTO	Vertical Takeoff
VTOL	Vertical Takeoff and Landing
WAAS	Wide Area Augmentation System
WRT	With Respect to

MODELING HIGH-SPEED CIVIL TILTROTOR TRANSPORTS IN THE NEXT GENERATION AIRSPACE

William W. Chung,[1] Dennis Linse,[1] Al Paris,[1] Dan Salvano,[1] Ted Trept,[2] Tom Wood,[2] Huina Gao,[3] Dave Miller,[3] Ken Wright,[3] Ray Young,[3] and Victor Cheng[4]

Ames Research Center

SUMMARY

This study focuses on the impact of Civil Tiltrotors (CTRs) on the National Airspace System (NAS) under the Next Generation Air Transportation System (NextGen). To develop a better understanding of this impact, the study took a high-fidelity approach to analyzing the flight performance of a CTR fleet in evaluating NAS performance. Three difference sizes of CTRs (with seat configurations of 10, 30, and 120 passengers) were developed using major Original Equipment Manufacturer (OEM) design practices to assess the case for CTR operations in the NAS based on performance, market demand, and NAS capacity. The flight performance of the three CTRs was evaluated based on mission requirements and tiltrotor manufacturing technology such as airframe, engine, rotor, and manufacturing materials, assuming an in-service date of 2025. The flight performance of a fourth CTR (with a seat configuration of 90 passengers) was scaled from the performance of the other three CTRs, and checked against published reports, to complete the fleet mix for a NAS performance analysis. Flight performance based on weight, speed, and altitude was then translated to conform to the Base of Aircraft Data (BADA) aircraft performance model taking into account the CTR's unique nacelle conversion and a range of cruise, takeoff, and approach and landing profiles.

The enhanced BADA data were then applied to a NAS performance analysis to evaluate the impact of the CTR fleet in the Next Generation Airspace System (NextGen). The CTR fleet concept of operations (ConOps) assumes noninterference operations (NIO) and runway-independent operations (RIO) capabilities, since these unique capabilities of the CTR can offer potential improvements to the performance of NAS (i.e., increased capacity and reduced delay, while meeting required safety standards).

NAS performance in terms of throughput, delays, and capacities was evaluated using Airspace Concept Evaluation System (ACES), a distributed, agent-based simulation of the NAS consisting of NAS models and simulation control and assessment tools. The effects of a fleet of 30-, 90-, and 120-passenger aircraft (CTR30, CTR90, and CTR120) were first evaluated in the Atlanta, Las Vegas, and North East Corridor regions in 2025, using current projections of passenger growth and capacity consitent with those of the Federal Aviation Administration (FAA) and the Joint Planning and Development Office (JPDO). The selection of these three regional scanarios resulted from the projection of significant 2025 delays in these regions, and the estimated effect on NAS delay reduction of substituting CTR service for conventional scheduled service on routes under 500 statute miles. A preliminary investigation of a CTR10 fleet was also considered in a notional business model. Environmental effects such as noise and emission of a CTR fleet were also considered.

---

[1] Science Applications International Corporation (SAIC), 1710 SAIC Drive, McLean, VA 22102.

[2] Bell Helicopter Textron, Inc., 600 E. Hurst Boulevard, Hurst, TX 76053.

[3] Sensis Corporation, 11111 Sunset Hills Road, Suite 130, Reston, VA 20190-5373.

[4] Optimal Synthesis, Inc., 95 First Street, Suite 240, Los Altos, CA 94022-2777.

1 INTRODUCTION

Civil Tiltrotor (CTR) aircraft have the unique operating ability to take off and land like rotorcraft and cruise like conventional fixed-wing aircraft. CTRs are capable of performing both vertical takeoff and landing (VTOL) and short takeoff and landing (STOL) operations. These unique capabilities give CTRs the flexibility to operate under a different concept of operations (ConOps) including runway-independent operations (RIO) using VTOL and STOL, or STOL at stub runways, to bring the traveling public to their destinations in a timely manner. The assumption is that CTR fleet operations under RIO or using underutilized runways can directly increase the capacity to the National Airspace System (NAS) if major issues such as cost of new investment to the infrastructure and safety, and environmental issues such as noise and emission are justified by the value of such operations. Past studies (refs. 1-3) have found there is potential for a CTR fleet to improve NAS capacity based on unique CTR unique attributes. Other studies (refs. 4,5) investigating STOL operations have reviewed runway requirements, availability, and cost factors for operations in the NAS and in the New York and Washington Terminal areas, finding that a fleet of 40-passenger CTRs could reduce delay times in the NAS by replacing turboprop traffic with CTRs, providing CTR-specific runways can be developed. From these studies, it is clear that for the CTR to realize its advantage over fixed-wing aircraft and rotorcraft, and to increase the NAS capacity and reduce delays, a noninterfering flight operation with CTR-specific stub runways, helipads, or vertiports is essential. As the major infrastructure of the NAS is evolving under the Next Generation Air Transportation System (NextGen) with a target date of 2025 (as well as the maturing CTR technology (refs. 6-8) addressing the performance, cost of operations, and noise), this effort focuses a systems study to address the issues associated with deploying a fleet of CTRs by exploring the trades among procedures, CTR capabilities, and overall NextGen performance.

To develop a NAS performance trade study in capacity and delay, performance characteristics of four CTR sizes (with seat configurations of 10, 30, 90 and 120 passengers) in climb, cruise, descent, and hover were developed in all flight phases to better estimate the impact of CTR operations in the NAS with a high degree of fidelity of CTR flight characteristics. CTR design technology is based on an in-service date by 2025 for all four sizes of CTR. Performance of the 10-passenger CTR (CTR10) is derived, in part, from design heritage from the Bell/Agusta BA609, and the 30-passenger CTR (CTR30) is derived, in part, from design heritage from the Bell/Boeing V-22. The 120-passenger CTR (CTR120) is a completely new design developed by means of design synthesis tools, based on the weight, range, and cruise performance requirements. Design trades in payload, cruise speed, and cruise altitude are evaluated. Detail description of the design methodology and results are presented in section 2.

These CTR10, CTR30, and CTR120 performance data, which include coefficients of lift, drag, and thrust, and fuel flow rate at various flight conditions in airplane and conversion modes, were converted to the Base of Aircraft Data (BADA) modeling framework (refs. 9,10) for the follow-on NAS performance analysis effort described in section 6. The 90-passenger CTR (CTR90) performance is derived by scaling (through regression analysis) CTR10, CTR30, and CTR120 performance after fitting their performance data into BADA modeling format. Development of the fitting and scaling in BADA modeling framework, and verification with the designed performance results, are presented in section 3. An overview of the BADA modeling is presented in appendix A; the CTR airplane mode trim matrix used in developing drag and thrust coefficients is presented in appendix B; the CTR conversion mode trim matrix is presented in appendix C; linear-fittings of drag and thrust coefficients based on the trim matrix for the CTR30 and CTR120 are presented in appendix D; regression analysis results for the CTR90 from CTR10, CTR30, and CTR120 performance data are presented in appendix E; comparison of the CTR90 performance with an OEM designed 90-passenger CTR is presented in appendix F; and verifications of CTR30, CTR90, and CTR120 performance are presented in appendix G.

Flight profiles for the four different passenger sizes of CTRs were developed using a fixed-based high-fidelity pilot-in-the-loop (PITL) flight simulation experiment to investigate the RIO issues at an Operations Network (OPSNET) 45 airport; man-machine interface issues at various flight phases, and operational issues associated with the conversion characteristics at the takeoff and approach, and landing phases were examined in the PITL simulations. Established flight profiles were later used to determine optimal cruise speed and altitude for the CTR fleet. Procedures in establishing a noninterfering CTR operation and RIO for a terminal area were developed based on a sample airport in the NAS, i.e., Miami International, and evaluated via the PITL simulation for the CTR10 and CTR30. Flight profiles for approach and landing, and takeoff were evaluated based on flight characteristics of CTRs in conversion mode, pilot workload, approach and landing cueing requirements, and one-engine-inoperative (OEI) requirements for VTOL and STOL operations. These results are presented in section 4.

The objective of this study is to investigate the impact that a CTR fleet may have under NextGen. For that purpose, NextGen technology and overall ConOps (ref. 11) were evaluated to identify relevant technology and ConOps applicable to CTR operations, such as performance-based services (e.g., Area Navigation/ Required Navigation Performance (RNAV/RNP)), and Four-Dimensional Trajectory (4DT)-Based Operations. These assessments are presented in section 5.

The CTR fleet's flight performance and ConOps developed in previous sections were applied directly to NextGen performance tradeoff analysis by providing higher fidelity CTR fleet operational performance attributes, specifically in takeoff, climb, cruise, descend, and approach and landing. The NAS performance impact due to the CTR fleet, specifically in delay and capacity, was investigated and reported in section 6. Conventional fixed-wing fleet's flight services, such as number of flights and flight schedules, were restructured as more slots were made available by shifting some of the passenger demand to the CTR fleet with RIO (ref. 12) and NIO capabilities. Delay and throughput performances at Northeast Corridors (NEC), Atlanta, and Las Vegas regions where CTR fleets were deployed were investigated based on targeted market, demand and capacity forecasts, and fleet-mix assumptions. A footprint of the CTR traffic at EWR was developed and studied to conduct environmental impact analysis in noise and emission.

Finally, section 7 summarizes CTR design technology, BADA modeling for CTR, NAS performance analysis, and the CTR fleet impact to the NextGen ConOps.

2 CTR DESIGN APPROACH AND RESULTS

The main design requirement for this study was to develop a civil tiltrotor (CTR) fleet of four aircraft with seat configurations accommodating 10, 30, 90, and 120 passengers. Bell Helicopter Textron Inc., under subcontract to Science Applications International Corporation (SAIC), designed the CTR10, CTR30, and CTR120 aircraft for this study. The CTR90 design was derived from a regression-analysis-based interpolation of CTR30 and CTR120 characteristics; this effort was performed by SAIC. The approach to developing the CTR90 design and its resultant characteristics are described in section 3.

The CTRs in this study were developed at a conceptual design level built on Bell's design experience that began in the 1950s and includes the design, manufacture, and flight testing of seven different tiltrotor aircraft. These include the XV-3, XV-15, V-22 (joint Bell-Boeing team), Pointer, UAV 911, UAV 916, and BA609. Five of these aircraft are illustrated in figure 2-1. Of these aircraft, the Bell-Agusta BA609 will be the first civil-certified tiltrotor. Relevant lessons learned from this first-of-a-kind experience are incorporated in this study.

Ground rules, consistent with the conceptual nature of this study, were established to guide the design process. They are as follows:

1) Each design must have a technical basis in an existing engineering design, analysis, or technology plan.
2) The design of each configuration is to be based on practical considerations reflecting how an OEM might proceed with the development of a fleet of aircraft.
3) Design solutions are driven by engineering analysis only (marketing analysis is beyond the scope of this study).
4) Use productivity index (in engineering terms) to evaluate trade study results instead of a cost analysis.
5) Use parametric weight methods only (no detailed analysis is to be conducted during this study).

Figure 2-1. The tiltrotor aircraft history of Bell Helicopter.

The CTR10 and CTR30 designs were derivatives of existing CTRs, and only the CTR120 design was the result of a new design synthesis. The decision to use a design modification approach to develop the CTR10 and CTR30 designs is discussed in section 2.2.2, Technology Insertion.

The remainder of this section addresses the design effort. It includes discussions of the primary mission requirements (section 2.1), the general design approach (section 2.2), a comparative summary of the designs (section 2.3), design details of the CTR10, CTR30, and CTR120 aircraft (sections 2.4, 2.5 and 2.6), design recommendations (section 2.7), generation of input data to construct BADA-equivalent CTR models (section 2.8), and noise footprints corresponding to takeoff and landing profiles developed in the Bell Helicopter Partial Task Simulator (section 2.9). Details of the Pilot-in-the-Loop (PITL) simulation results are provided in section 5.

2.1 Mission Requirements Under NextGen

Operational, mission, and design requirements were addressed before the design of the NextGen fleet began.

2.1.1 Operational Modes

Multiple potential operational scenarios were considered for the NextGen fleet. An evaluation of the relationship between these scenarios and each of the four classes of aircraft was made. The results are summarized in table 2-1. This assessment was made with usage in mind and not necessarily to define design requirements for this study. However, the scenarios noted in table 2-1 could impact future designs depending on which one was determined to be the critical requirement. For example, a city center elevated helipad would dictate different sizing requirements than a ground-based heliport with a 200-foot runway.

The operational mode reflected in the design and simulation work in this study is most closely related to flights in and out of airports with co-located vertiports. Additional discussion of the operational modes is presented in section 4.

2.1.2 Mission Goals

From a design perspective, the primary mission-related requirements that must be defined are: takeoff ambient meteorological conditions, takeoff profile, payload, design range, cruise altitude, and cruise speed. To this end, goals were set to address these requirements and are defined in table 2-2.

TABLE 2-1. PROPOSED CTR FLEET OPERATIONAL MODES IN NEXTGEN

Passenger Seat Capacity	Metroplex Usage				
	City Center Vertiport to City Center Vertiport	City Center Vertiport to Airport Vertiport	Airport Vertiport to Airport Vertiport	Airport Vertiport to Uncongested Runway	Runway to Runway
10	√	√	√	√	No
30	√	√	√	√	No
90	No	No	√	√	No
120	No	No	√	√	No

TABLE 2-2. DESIGN GOALS FOR THE NEXTGEN AIRCRAFT

Number of Passengers	10	30	90	120
Takeoff Condition	5k/Hot	-->	-->	-->
Takeoff Procedure(1)	VTOL(2)	VTOL(2)	VTOL	VTOL
Payload, lbs	2,200	6,600	19,800	26,400
Design Range, nmi	800(2)	1,000(2)	1,000	1,500
Cruise Altitude, 1000's ft	25	25	30[2]	30(2)
Cruise Speed, ktas	Fallout	Fallout	300(2,3)	350(2)

(1) VTOL is assumed to be a Transport Category procedure (same as Cat A).
(2) Target.
(3) At 90-percent MCP.

The takeoff ambient condition selected was the same as that used in the NASA 90- and 120-passenger designs (refs. 8,13). It is approximately equivalent to an International Standard Atmosphere (ISA)+20°C takeoff from Denver, Colorado. It is considered to be a good design point because it encompasses a large percentage of the U.S. population.

Although the takeoff procedure has been identified as a Vertical Takeoff (VTO), it does not necessarily require that the design must be able to hover with one engine inoperative (OEI). It does mean that the takeoff is not a Short Takeoff (STO) procedure utilizing a runway and that the aircraft can either fly away or safely land if an engine becomes inoperable.

Previous studies have suggested variations on these requirements; however, the dominant question in this study, relative to goals, was in regard to design range. Several sources (refs. 6,7) that were reviewed suggest a good design range is on the order of 600 nmi. Both studies point to the fact that one reason a civil tiltrotor can compete with jets at ranges below 600 nmi is because it has a better block time. Other studies (refs. 8,13) by NASA of large civil tiltrotors have targeted longer ranges as goals on the order of 1,000 to 1,200 nmi.

There are several scenarios and considerations that can result in a preferable design range that would be anywhere from 600 to 1,200 nmi, or more. These include, but are not limited to,

1) Commuter operations, 500–600 nmi.
2) Commuter operations with round-trip capability to remote airports without refueling, 1,000–1,200 nmi.
3) Commuter operations, 500–600 nmi with fuel capacity for long legs but reduced payload to be used in disaster relief.
4) Longer-range markets, 1,000–1,500 nmi.

Given the considerations above, range goals for this study varied with the number of passengers in a trend similar to fixed-wing aircraft as shown in figure 2-2 and were not the result of a detailed market analysis. The range data in figure 2-2 was taken from an annual aviation publication (ref. 14). The range of number of passengers does not include the larger aircraft; however, it provides a trend against which the NextGen CTRs can be compared. One difficulty is interpreting published performance data. Many fixed-wing aircraft cannot take off with a full load of both passengers and fuel. These limitations were not defined; therefore, the data shown in figure 2-2 is based on maximum still-air range versus maximum passenger capacity.

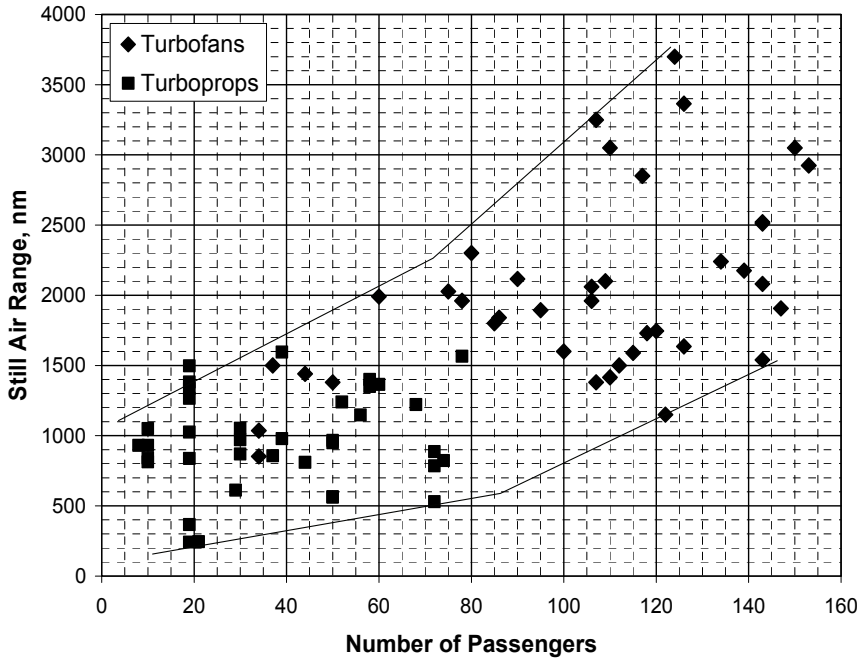

Figure 2-2. Turboprop and turbojet range characteristics up to 160 passengers.

The design range for the CTR10 and CTR30 aircraft was a target-only since these aircraft were based on modifications to existing tiltrotors resulting in inherent limitations. The range capability of these two aircraft became a fallout. The initial design range of 1,500 nmi for the CTR120 design was part of a preliminary set of design requirements/goals developed by the NASA/SAIC team.

Design cruise altitudes were selected based on a desire to integrate into controlled airspace. Definitive limitations were not available, and certain restrictions inherent in the case of the CTR10 and CTR30 designs were not or could not be changed. Design cruise speed was selected based on goals established in previous NASA studies (refs. 1,2). Cruise altitude and speed were traded during the design of the CTR120 design. Trends in cruise altitude and airspeed for turboprops and turbofans were not developed. This information was not available in a useable format, and no further research was conducted on the subject.

As discussed in subsequent design sections, not all the goals were met. In some cases the goals such as design speed for the CTR120 design could be met; however, they were changed for what was considered to be a preferred design point based on an assessment of productivity.

2.1.3 Mission Profile

All of the NextGen designs were evaluated using the same mission profile to provide a consistent comparison of their capabilities. It is a simple range mission consisting of warm-up, takeoff, conversion, climb, cruise, descent, reconversion, landing, and reserve segments. The takeoff condition corresponds to Denver on a hot day (ISA+20°C). The cruise segment varies depending on the fallout aircraft capability or the design goal and was flown at standard day conditions. The reserve segment is based on Instrument Flight Rules (IFR) reserve requirements in accordance with FAA Federal Aviation Regulation (FAR) Part 91.167 (Fuel requirements for flight in IFR conditions).

Figure 2-3 graphically presents the characteristics of the mission. Table 2-3 provides the details of each mission segment. This mission profile was used to size the CTR120 design.

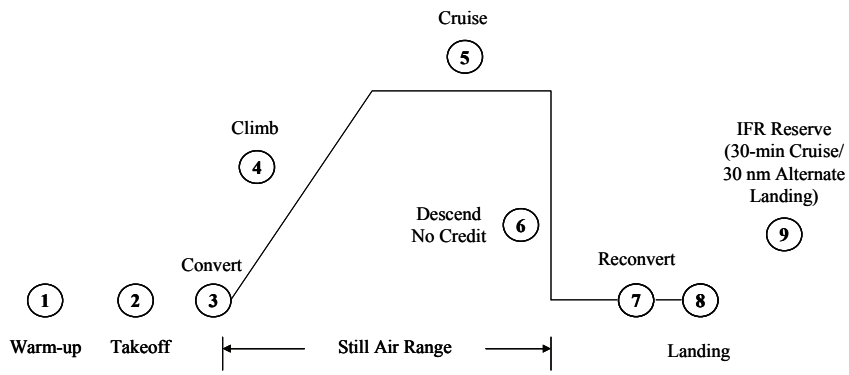

Figure 2-3. Generic NextGen mission profile.

TABLE 2-3. NEXTGEN MISSION PROFILE SEGMENT DETAILS

Mission Segment	Segment Type	Altitude (1000's ft)	Day	Time (min)	Distance (1) (nm)	Airspeed (ktas)	Payload (# of pax)	Power Available (%)	Engine Rating (-)
1	Warm-up	5	ISA+20	5	0	0	as req'd	100	IRP
2	Hover OGE	5	ISA+20	2	0	0	"	100	MRP
3	Convert	5	ISA	0.25	n/a	Varies	"	100	MCP
4	Climb	n/a	ISA	n/a	n/a	1.23 Vstall	"	100	MCP
5	Cruise	best alt	ISA	n/a	Fallout	Vlrc/Vmcp (2)	"	100	MCP
6	Descend	n/a	ISA	n/a	no credit	n/a	"	100	MCP
7	Reconvert	5	ISA	0.25	n/a	Varies	"	100	MCP
8	Hover OGE	5	ISA+20	1	0	0	"	100	MRP
9	IFR Reserve	10	ISA	30	no credit	Vlrc	"	100	MCP
	(2 parts)	5	ISA+20	n/a	30	Vlrc	"	100	MCP

(1) Total distance equals range (not including 30 nm of segment 9)
(2) Vlrc (long range cruise @ 0.99 specific range); Vmcp (100% MCP) required for 120-passenger sizing

The one variant in the assessment of range was the mode of takeoff. Although the initial goal was for a VTO takeoff, the CTR10 and CTR30 designs were also evaluated for STO takeoff performance in order to maximize range. This, however, has potential implications in terms of terminal operations.

Since the aircraft in this study were designed for commercial use, they fall under FAA Transport Category rules. This requires that all takeoff and landing weights are defined by OEI capability. This has a more significant impact on the smaller twin-engine aircraft than on the larger four-engine aircraft.

2.2 General Design Approach

This section addresses those subjects that are of a more general nature and may be equally applicable to each design in this study. They include the configuration description, technology insertion, design synthesis methodology used, noise requirements, engine technology, and general design constraints and/or limiting factors in the area of structure and aerodynamics.

A more detailed discussion of all other related subjects is provided for each of the designs in sections 2.4, 2.5, and 2.6. This includes design requirements, cabin layouts, engine performance, weights, aerodynamics, and the design process and results.

2.2.1 CTR Configuration

This study considered two types of tiltrotor configurations: 1) conventional corresponding to existing aircraft, and 2) an unconventional approach for a new design. Because of the modification approach used for the CTR10 and CTR30 designs, these configurations, by definition, are considered to be conventional tiltrotors.

The CTR90 and CTR120 designs are new designs and warrant configuration trade studies. Variations in configuration, including low wings, fixed engines, and wing tip extensions were considered and have been evaluated by Bell in the past with mixed results. There are good engineering reasons for considering these alternative configurations. However, issues such as control power, number of engines, engine residual thrust, wing lift efficiency, drag, nacelle cooling, exhaust deflection, drive system arrangement, and structural impact must all be traded at a more detailed level than is possible in this study in order to define the best configuration. Therefore, for this study all of the NextGen CTR designs are configured as conventional tiltrotors, which are well understood.

The airframe consists of a high wing configuration with engines in tilting nacelles like the BA609 and the V-22. Since there is no definition for a conventional tiltrotor empennage, a T-tail design geometrically similar to the BA609 was used for aircraft in the NextGen CTR fleet. A retractable tricycle landing gear arrangement was adopted without nose wheel steering. Wing tip extensions were not used. Because of the large size differences in the fleet, some configuration variations will inherently exist (for example, the change in number of engines as the aircraft size increases). All of the CTR fuselages are of composite construction and contain pressurized cabins that operate at a maximum cabin pressure altitude of 8,000 feet.

The lift-propulsion system consists of engine, drive system, rotors, and wing. The engine and main drive system components are integral to the tilting nacelle. The nacelle also includes blowers and radiators for transmission and hydraulic system cooling. The nacelle is split into zones for fire protection. A bypass duct augmented by a bypass blower ensures that particles do not enter the engine. This design also protects the engine from ice.

The engines are representative of advanced technology engines based on the Army's Advanced Affordable Turbine Engine (AATE) and Versatile Affordable Advanced Turbine Engine (VAATE) programs. Ground heating was not addressed in this study due to the lack of final engine and engine nacelle definition. Exhaust deflection might be required for both the CTR10 and CTR30 configurations. The expected nacelle engine height of the CTR90 and CTR120 configurations would most likely not produce any ground heating concerns. Inlet particle separators integral to the engine are not required.

The drive system arrangement depends on the number of engines; however, all of the CTR configurations include prop-rotor, tilt axis, and mid-wing gear boxes. The drive systems in this study are conventional in nature. A "variable" rpm transmission was not used. An interconnect shaft is included in all aircraft. Many of the accessories are driven off of the mid-wing gearbox. Although the CTR90 and CTR120 designs will use four engines they must still use an interconnect shaft to fully use the three remaining engines during an OEI event.

The rotor blades are of composite construction and do not include blade fold. Gimbaled rotors are used in the CTR10 and CTR30 designs. Stiff in-plane rotors are used in the CTR90 and CTR120 designs. The number of blades varies over the CTR fleet, primarily as a consequence of several considerations including weight, disk loading, tip speed, maneuver requirements, and design experience.

The wing is of composite construction consisting of a leading edge, torque box, fixed trailing edge, and control surfaces. The leading edge section includes deice capability. The torque box includes a front spar at 5-percent chord and an aft spar at 50-percent chord. Fuel is carried in multiple crashworthy bays within the

torque box. The fixed trailing edge contains the interconnect shaft and subsystem lines required for control surface actuation, as well as providing hydraulics and electrical power to the nacelles. The control surfaces, referred to as flaperons, act as both flaps and ailerons.

Details of the subsystems in the aircraft such as the Environmental Control System (ECS), fly-by-wire flight controls, hydraulics, electrical, and anti-ice/deice will not be described in detail. However, inherent in the parametric analysis of this study is a system redundancy to ensure that a critical failure has a chance of less than one in a billion of occurring. The NextGen CTRs are all-weather capable with the ability to fly into known icing. AC generators provide the electrical power for rotor anti-ice/deice capability. The CTR30, CTR90, and CTR120 designs all have Auxiliary Power Systems (APU) to support ECS and wing deice, and to provide ground power.

Avionics suites will not be described. They can vary significantly and estimates of requirements and capability in the NextGen time frame were not addressed during the design phase of this study. However, the avionics parametric weights have been found over time to remain at a relatively consistent level of weight, even though capability has improved.

2.2.2 Technology Insertion

One of the objectives of the design process was to incorporate advances in technology. To understand what level of technology would potentially be available, hypothetical design and development schedules were established that a manufacturer might follow under ideal circumstances. Ideal circumstances for this study have been defined to mean:

1) A market demand exists.
2) A business case can be made for each design.
3) Staffing is not an issue.
4) A manufacturer would be willing to commit the resources necessary to the development of the four classes of NextGen CTRs in order to be in service by 2025.

These schedules were based on a projected in-service NextGen start date of 2025 and are shown in figure 2-4.

A NextGen study team decision was made to assume that each aircraft would go from detail design to first production delivery in five years. This schedule is very aggressive and based on the assumption that all decisions necessary for a successful program would be made before detail design started, including teaming arrangements. The result of the schedule analysis was the identification of a general technology insertion date of 2017 that would be applicable to all designs at some stage in their development before the in-service date. This date applies equally to both engine and design technologies.

Projected technology improvements by 2017 are not based on trend lines but on technology projections developed under the DoD Joint Heavy Lift (JHL) Concept Design and Analysis (CDA) contract. This is important for two reasons: first, the effect of scale has been addressed by design and analysis, and second, there is an engineering design and research basis for all of the technology factors applied to the NextGen CTRs. For this study the assumption is that these technologies will be funded and demonstrated in time for application to the NextGen designs. Due to the restricted nature of the JHL contracted effort, only general information concerning technology benefits applied to NextGen may be reported herein.

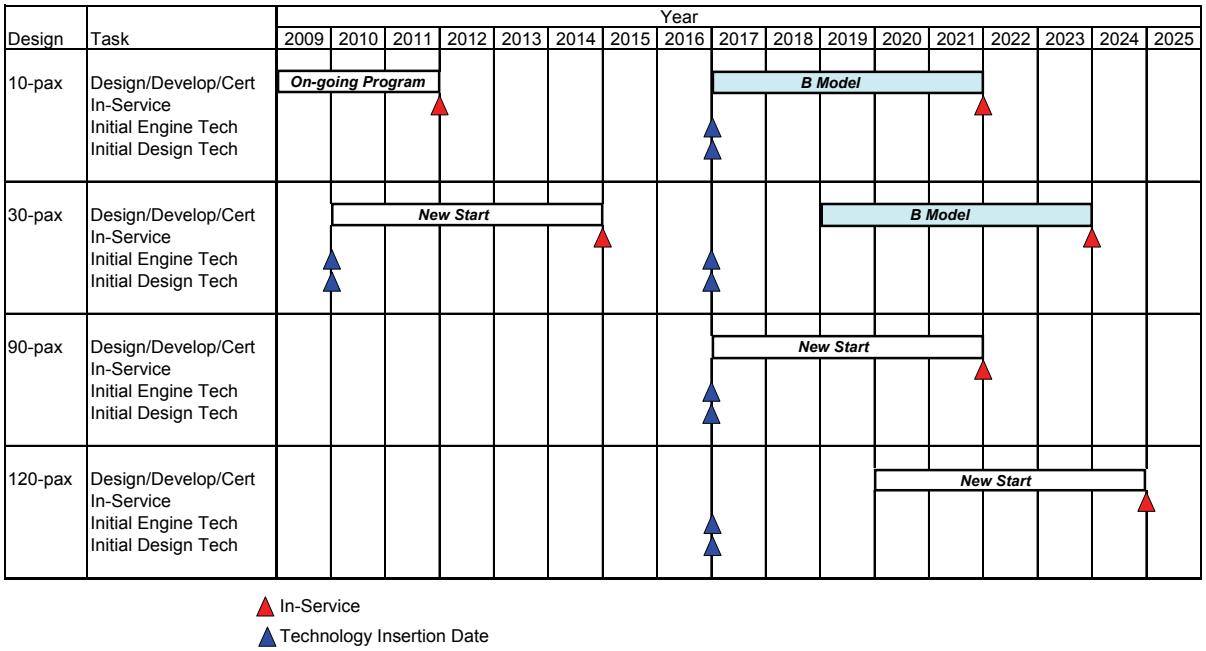

Figure 2-4. NextGen hypothetical development schedule.

2.2.2.1 10 Passenger (CTR10)

The NextGen CTR10 design has its heritage in the Bell-Agusta BA609. The BA609 will be the first civil-certified tiltrotor in the world. The BA609 has undergone an extensive flight test program to date. In terms of design and technology the BA609 represents a mature nine-passenger civil tiltrotor design using mid- to late-1990s technology.

Traditionally in the aviation industry a "new start" design evolves into follow-on versions. In all cases a significant improvement in capability is the goal but at significantly reduced nonrecurring development costs. Therefore, the CTR10 NextGen design is based on a hypothetical "B" model evolving from the BA609. Although the start date of the "B" model is shown to be in time for projected technology improvements, the assumption is that the primary objective would be an engine upgrade only. Additional technology upgrades would only be applied if they did not represent a large investment in additional certification-related testing.

2.2.2.2 30 Passenger (CTR30)

The NextGen CTR30 civil tiltrotor design is based on the assumption that it would be developed around the lift/propulsion system of the U.S. Navy/Marine Corps/Air Force V-22 tiltrotor. Evolving the military V-22 into a civil 30-seat design would not be a "B" model version as in the case of the BA609. However, it more than likely would not be a "new start" because of cost considerations. Figure 2-4 shows that the CTR30 design could have an early start date followed by a "B" model that would reflect a significant improvement in engine technology. Although the first design would not be a true "new start," it would benefit from state-of-the-art technology in those areas where new components are required.

2.2.2.3 90 Passenger (CTR90)

The CTR90 design is considered to be a new start. It would rely on the insertion of technology available at the start of its detail design phase, which is in the year 2017.

2.2.2.4 120 Passenger (CTR120)

The approach to the CTR120 design is the same as that for the CTR90 design. It would also rely on the insertion of 2017 technology. Even though the detailed design begins in the year 2020, attempting to assess the impact of an additional three years in technology is beyond the scope of this study.

2.2.3 Design Methodology

Two different methods were used to develop the NextGen designs. As noted earlier, the CTR10 and CTR30 aircraft were future-technology derivatives of, or used major systems from, existing aircraft. The CTR120 design was developed by synthesis of a completely new design. The core program used to develop these three aircraft is the Preliminary Evaluation and Sizing Tool (PRESTO) (ref. 15) developed by Bell Helicopter. However, the final designs only evolve after a systematic interaction between the requirements, detailed design tools, Bell's aircraft database, and PRESTO. An overview of this process is illustrated in figure 2-5.

PRESTO is a program developed to size both helicopters and tiltrotors. It is also capable of developing what is referred to as "point design" performance. This capability allows the user to predict aircraft and mission performance for a fixed design, and also provides the capability to conduct an evolutionary design. An evolutionary design is a process that automatically updates the weight empty as various subsystem or component characteristics are changed while all other are held fixed. This method lies somewhere between "point design" analysis and true synthesis. PRESTO is capable of design synthesis to multiple sizing requirements and mission profiles for a given design. It was developed to allow synthesis with certain characteristics held constant. For example, a tiltrotor can be sized to a fixed engine, fixed rotor diameter, fixed-wing area, or fixed weight empty.

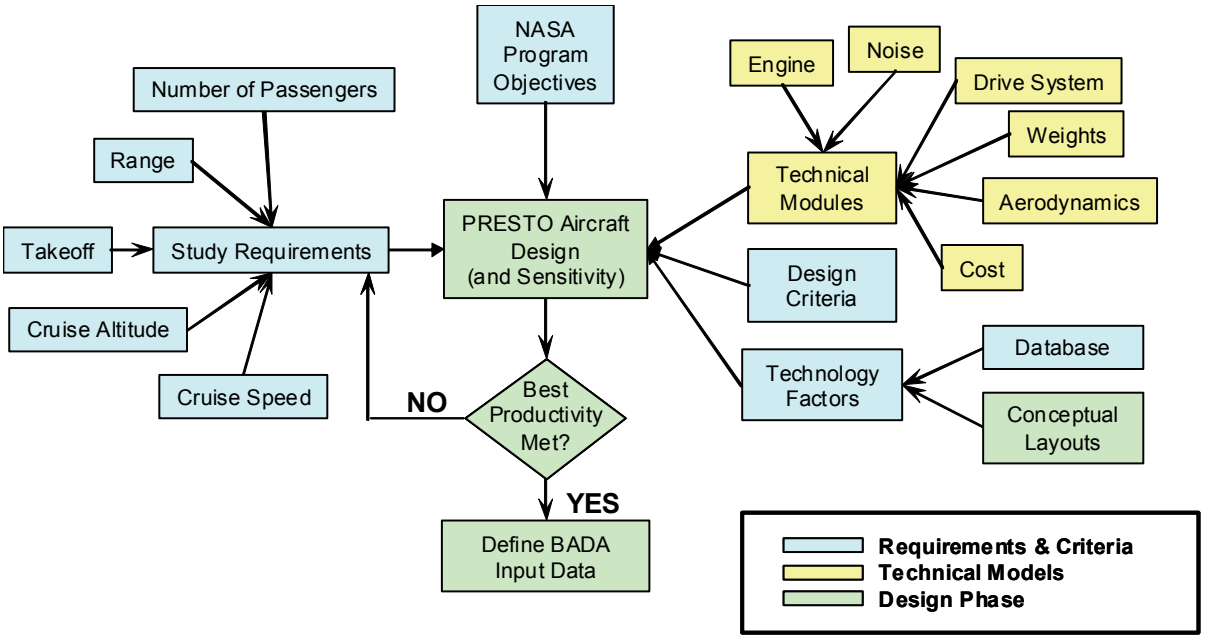

Figure 2-5. Design methodology applied to the NextGen tiltrotor configurations.

The PRESTO system was based on the philosophy of level of effort. As a result it is capable of being used with several levels of modeling complexity. The levels of complexity reflect typical stages that a synthesis may be in and the corresponding input data that is available. Regardless of the level of complexity, PRESTO predicts the aerodynamic, weight, and engine characteristics using physics-based models that can be calibrated off-line with higher fidelity programs such as Bell's Comprehensive Program for Theoretical Evaluation of Rotorcraft (COPTER). Models can also be adjusted by technology factors. Where analytical capability is not available and flight test data is, empirical trends have been developed. Once a design has been completed, PRESTO is capable of multiple airplane performance analyses. This includes hover performance, hover ceilings, speed-altitude envelopes, payload range, specific range, and mission performance.

2.2.4 Noise Requirements

Civil noise certification regulations for tiltrotors are currently patterned after noise regulations for helicopters. As for helicopters, the noise limits are often referred to as 'Stage' limits (refer to Title 14, Code of Federal Regulations (CFR), Part 36). The test conditions and limits are similar to helicopters, although different applicability dates apply. Separate limits are applied to the three noise certification flight conditions of flyover, takeoff, and approach operating in VTOL mode.

Since no tiltrotor aircraft have been certificated to date, the tiltrotor regulations are technically treated as guidelines within International Civil Aviation Organization (ICAO) (http://www.icao.int/) Annex 16. Regarding the certification of the BA609 tiltrotor, both FAA and European Aviation Safety Agency (EASA) have requested that Bell voluntarily use these guidelines as certification requirements. Bell has agreed to this request.

The stage limit definitions applicable to this study are as follows:

Stage 1: No Stage 1 tiltrotors are envisioned.

Stage 2: The current guideline has adopted the Stage 2 helicopter limits for tiltrotors. Stage 2 helicopters are those for which an application for a new type certificate was made after March 6, 1986. This limit will be applicable to all tiltrotors certified in the near future. Those tiltrotors, and acoustical changes to those tiltrotors, must meet Stage 2 noise limits.

Stage 3: Stage 3 noise limits for tiltrotors will be developed after one or more tiltrotor certifications have successfully been accomplished. It is anticipated that the limits will be the same as the current Stage 3 noise limits for helicopters. Adoption of the Stage 3 tiltrotor limits will likely parallel the adoption of Stage 4 helicopter limits in the 2016–2025 time frame.

Stage 3 helicopters are those for which application for a new type certificate was made after March 21, 2002. Those helicopters, and acoustical changes to those helicopters, must meet Stage 3 noise limits.

It is noted that although most countries have adopted Stage 3 noise limits into law, the FAA has not yet formally adopted Stage 3 into the Federal Aviation Regulations. However, the FAA has in principal agreed to adopt the standard and requires it for new helicopter certifications.

Compared to Stage 2, the Stage 3 limits are 4 EPNdB lower for the flyover condition, 3 EPNdB lower for the takeoff condition, and 1 EPNdB lower for the approach condition.

Stage 4: Adoption of Stage 4 tiltrotor noise limits will likely be in the 2035–2040 time frame unless community noise becomes an issue as the tiltrotor fleet grows and countries press for an earlier adoption.

The assumption under this study was that each configuration would meet civil noise certification limits. Therefore, a relationship between noise requirements, noise predictions, and rotor tip speed in helicopter mode was developed for application to the design and/or sizing of the NextGen aircraft. The limits are defined in figures 2-6 and 2-7.

The Bell Acoustics group developed the data for figures 2-6 and 2-7. The data in these figures is based on an empirical prediction methodology that evolved from flight-test-acquired noise characteristics of the XV-15 aircraft. To date only Stage 2 and 3 noise levels have been defined for tiltrotors. The Stage 4 requirements are based on an assessment by Bell Helicopter only and do not reflect any current published information or known requirements under consideration.

Based on the hypothetical development schedule in figure 2-4, the CTR30 tip speed was defined using Stage 3 requirements. The resultant operating tip speed at 100-percent rpm is 700 fps. The CTR120 design is a new start, and its corresponding tip speed at 100-percent rpm of 650 fps is based on the Stage 4 requirement. This was based on the assumption that its operational life would extend well into the projected Stage 4 time frame and that the time frame might move forward as noted above. The 90-passenger design would fall into the same category.

Although no credit was taken for specific tip shape treatments, it was estimated that the design tip speed could be increased by approximately 15 fps (to meet an equivalent noise level) if a low-noise tip shape design was used. The net result could be a reduction in design gross weight.

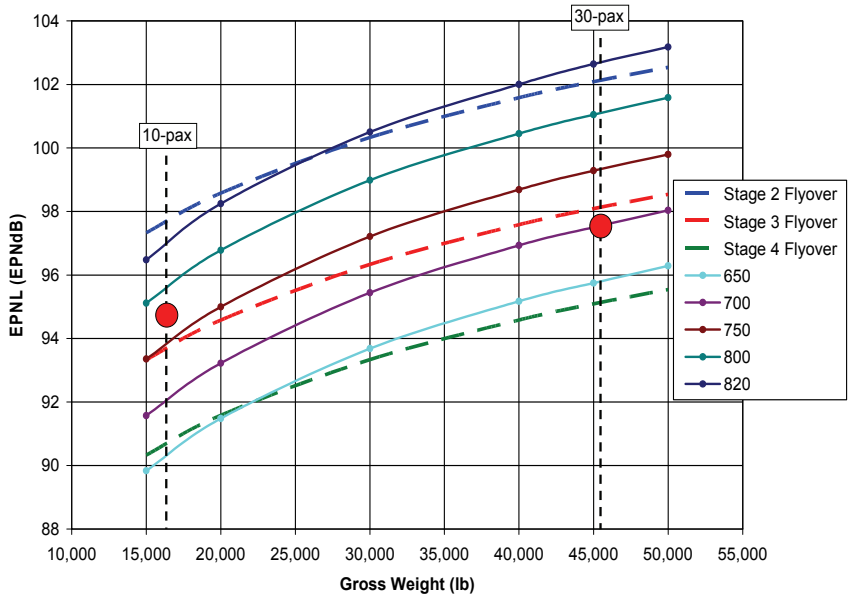

Figure 2-6. CTR10 and CTR30 acoustic requirements related to rotor tip speed vs. gross weight.

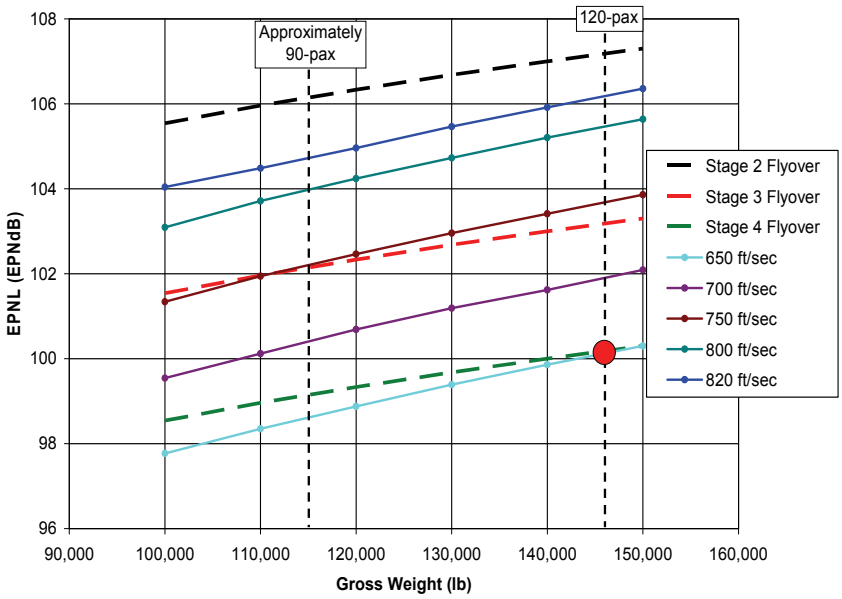

Figure 2-7. CTR90 and CTR120 acoustic requirements related to rotor tip speed vs. gross weight.

2.2.5 Engine Technology and Modeling

This section briefly describes the level of technology used to support this study. It also describes how the data is developed for input into the PRESTO design program.

2.2.5.1 Advanced Technology

Advanced technology engine programs are currently under way that will potentially provide significant improvements in operating cost, weight reduction, and fuel consumption in the not too distant future. Technologies were selected that would potentially be available to the NextGen CTR designs in accordance with the development schedules defined in section 2.2.2, Technology Insertion.

The result was the selection of Advanced Affordable Turbine Engine (AATE) technology for the CTR10 design and Versatile Affordable Advanced Turbine Engine (VAATE) technology for the CTR30 and CTR120 designs. Because the CTR90 is based on an interpolation of the CTR30 and CTR120 characteristics, its performance is inherently based on VAATE technology.

The AATE program has the goals of a 25-percent reduction in specific fuel consumption (SFC), a 65-percent improvement in shaft horsepower-to-weight ratio (shp/wt), a 20-percent improvement in design life, a 35-percent reduction in production and maintenance cost, and a 15-percent reduction in development cost.

The VAATE program has the goal of a 200-percent increase in engine thrust-to-weight ratio (with an equivalent power-to-weight ratio for turbo-shaft configurations), a 25-percent reduction in engine fuel consumption, and a 60-percent reduction in engine development, procurement, and life cycle maintenance cost. The Adaptive Versatile Engine Technology (ADVENT) and the Highly Efficient Embedded Turbine Engine (HEETE) are subprograms within the VAATE program. ADVENT is focusing on improvements in the turbine section while also integrating the engine with highly efficient inlets and exhaust systems. The

HEETE program mainly focuses on improving the compressor to achieve much higher compressor operating pressure ratios.

2.2.5.2 Modeling Engine Data for PRESTO

Multiple engine cycle decks based on AATE and VAATE technology were used to develop the generic characteristics of engine performance to be applied to the NextGen CTR designs. The engine cycle decks were used to create estimated installed engine performance based on experience gained from the V-22 and BA609 flight test programs. The installation losses include a secondary cooling flow estimate of 15 percent of the engine mass flow to perform nacelle and oil cooling.

A major component of installed engine performance is inlet recovery. For the installed engine performance for the NextGen CTRs a normalized V-22 inlet recovery table was created and used to predict the inlet recovery expected on the future tiltrotor aircraft in this study. The other major component to the predicted installed performance is the amount of engine back pressure to use when performing the engine cycle deck run. Most helicopters use a turboshaft engine which has low engine back pressure and exhaust exit velocity while airplanes use a turboprop engine that has high engine back pressure and exhaust exit velocity. Low engine back pressure increases the engine performance/efficiency but low engine mass flow exit velocity creates momentum drag at high flight speeds.

Before NextGen design work was started, a study was performed to investigate the effect of engine back pressure and engine exhaust flow parasitic drag on the net installed performance. Since conducting this study for each design as part of the iterative design process was beyond the scope of this effort, only one set of design conditions was evaluated. The takeoff and cruise goals of the CTR120 design were selected for this task. The study involved decreasing the exhaust nozzle effective exit area and plotting the net engine horsepower efficiency (see figure 2-8). As the exhaust area is decreased the engine horsepower is decreased while the engine exhaust net thrust increases. By converting the net thrust to an equivalent engine horsepower the net installed horsepower can be estimated. This was balanced against the impact on hover performance. As a result of this study an engine exhaust nozzle discharge coefficient of 0.45 percent was selected for the cycle decks of both engine technologies, and the results incorporated in the engine performance applied to all of the NextGen designs.

Using the data developed from the process described above, a normalized engine model was developed for the PRESTO program. The normalized or "rubber" engine model allows PRESTO to synthesize a design to a set of requirements with the engine rated power being a fallout. However, the basic characteristics of the engine remain unchanged. This process has proven to be accurate as long as the final engine rating is within a reasonable percentage of the reference rating on which the "rubber" engine model is built.

The PRESTO engine model requires input for power available, fuel flow, and engine residual thrust. For the AATE engine technology evaluated for this study, the engine SFC ranged from 0.34 to 0.36 lbm/hr/hp. For the VAATE engine technology evaluated for this study, the engine SFC ranged from 0.32 to 0.34 lbm/hr/hp.

Because tiltrotor nacelles require compartment and oil cooling there is a momentum drag that is closely associated with the operating conditions of the engine. For this study momentum drag was book kept with engine residual thrust resulting in net nacelle thrust. Examples of the PRESTO engine input data are provided in the aircraft design sections as appropriate.

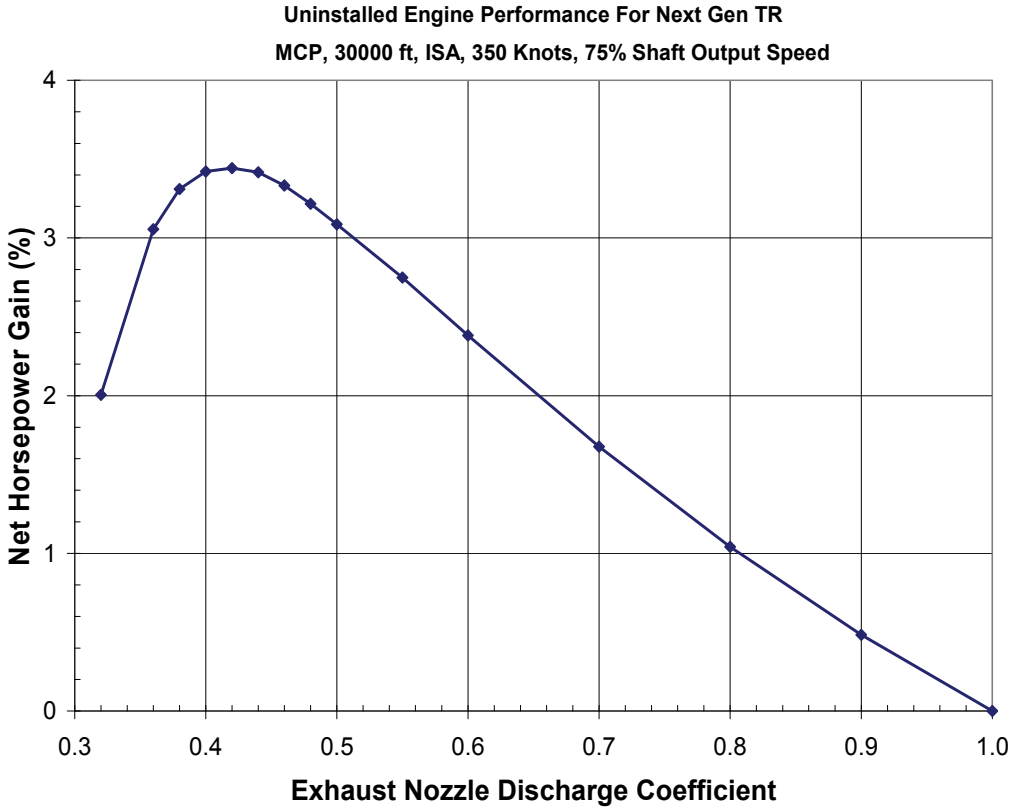

Figure 2-8. An example of the impact of exhaust nozzle discharge coefficient on net power.

2.2.6 Design Constraints

This section discusses the design constraints and limiting factors that were considered during the design of the NextGen CTRs. Not all constraints could be assessed by analysis in this study; consequently, some were addressed based on Bell's experience base with designs of similar size and configuration.

2.2.6.1 Structural and Aeromechanical Stability Constraints

The NextGen CTR fleet includes a significant range of sizes. The CTR120 design is on the order of nine times larger than the CTR10 design in terms of weight with a geometric scale factor of approximately 2.7:1. The manner in which scale impacts design constraints was not analyzed; however, physical and aeromechanical constraints were identified and applied based on Bell's experience.

Bell Helicopter has designed and analyzed rotors for aircraft significantly larger than that of the CTR120. Using these studies for guidance, several limitations have been assumed regarding structure and aeromechanical stability. These include wing aspect ratio, wing thickness-to-chord ratio (t/c) and prop-rotor rpm in airplane mode.

A wing aspect ratio of 6.5 has been identified as a good balance between structural weight and fuel efficiency. Wing t/c was held to a minimum of 18 percent to provide adequate clearance for the conversion spindle and interconnect shaft. Both aspect ratio and t/c are approximate limits. A more rigorous design study would be required for optimizing the configuration.

Because a conventional tiltrotor configuration was assumed for this study, it inherently results in a drive system whose rpm varies only with engine rpm. In order to reduce fuel flow in airplane mode, the lowest possible rotor rpm was selected to reduce the incompressible and compressible related profile power. Recent design studies have shown that a conventional tiltrotor rotor and drive system can be designed to operate over a range between 70 percent in cruise mode and 100 percent in helicopter mode at NextGen cruise speed and altitude goals.

If the NextGen CTRs are designed to accommodate operating in normal airport ground traffic patterns, a requirement to be able to taxi long distances would have to be accounted for. This is a requirement that has implications in the design of the landing gear and is already inherent in the Bell parametric weight equations. The Bell database for landing gear consists primarily of fixed-wing designs.

2.2.6.2 Aerodynamic and Performance Constraints/Limiting Factors

There were three constraints either applied to or evaluated for all designs. The primary aerodynamic constraint was buffet onset in airplane mode. In airplane mode two performance constraints were imposed: rate-of-climb at top of climb and minimum power speed for climb.

For this study it was assumed that transport category certification would apply to all NextGen designs. Consequently, in accordance with FAA FAR part 25.251, Vibration and Buffeting, a buffet-free operational envelope was developed for the NextGen aircraft. Under this FAR there are two major requirements that affect NextGen: 1) "there may be no perceptible buffeting condition in the cruise configuration in straight flight at any speed up to Vmo/Mmo, except that stall warning buffeting is allowed," and 2) "for an airplane with Md (design Mach number) greater than 0.6 or with a maximum operating altitude greater than 25,000 feet, the positive maneuvering load factors at which the onset of perceptible buffeting occurs must be determined with the airplane in cruise configuration….and for a sufficient range of speeds and load factors for normal operation."

For the CTR10 and CTR30 designs buffet onset was a true constraint since the configurations were the result of aircraft modifications. For the CTR120 design, however, buffet onset became a sizing requirement.

In accordance with AC25-7A, the FAA, at this time, allows the buffet onset boundary to be "established only by pilot event." Since this is a paper study only, the approach has been to: 1) consider the design parameters that affect buffet onset; 2) define a buffet onset boundary; and 3) evaluate its impact on aircraft design. Some of the major design parameters affecting buffet onset include wing design, cruise Mach number, cruise lift coefficient, maneuver requirements, and design margin. The buffet onset boundaries for the CTR10 and CTR30 designs have a basis in flight test data; however, they were modified to reflect the characteristics of the NextGen designs.

The CTR120 buffet onset boundary was developed by combining the characteristics of a set of known but proprietary boundaries. During this study, design cruise altitude and speed targets were specified; however, these design requirements were considered to be variables and open to trades. Since defining buffet onset boundaries are detailed in nature, and the exact characteristics of altitude and speed were not known, a generic approach was taken. The primary assumption was that the buffet onset boundary would reflect the low Mach number characteristics typical of a thick wing tiltrotor and the high Mach number characteristics typical of modern high-speed jets. This may be somewhat optimistic but not too far removed from the limits of possibility. The buffet onset boundary is defined as the lift coefficient corresponding to buffet onset as a function of Mach number.

The resultant buffet onset boundary, combined with margins, was used to define the buffet-free boundary. The buffet-free boundary was used to define limitations of the CTR10 and CTR30 flight envelopes and to define the buffet-free-design wing loadings for the CTR120 aircraft. The wing loadings required for buffet-free operations are presented in figure 2-9 as a function of altitude and speed. The curves in figure 2-9 are based on the assumption that a good design is capable of a 30-degree banked turn with an additional incremental "g" capability for transients. The "g" loading is based on a proprietary design process and will not be provided; however, it does include additional margin for weight risk associated with new designs. The wing loadings corresponding to the maximum takeoff gross weight for the CTR10, CTR30, and CTR120 designs are shown in figure 2-9. Both the CTR10 and CTR30 aircraft are operationally limited to cruise at 25,000 feet. The CTR30 design is marginal; however, it is capable of a 30-degree banked turn with some margin. It can only fly at higher gross weights if it reduces altitude.

Depending on power available, performance-based cruise altitudes may or may not be constrained by buffet. Therefore, there is an additional constraint that has been applied based on a rate-of-climb capability. For this study it has been assumed that, as a minimum, the rate-of-climb capability at the top of climb must be no less than 500 fpm. This has been used to ensure that the CTRs can climb to a new altitude should air traffic control require it unless it is already at its operational ceiling (which is not necessarily the performance-based service ceiling). At a lower rate-of-climb capability the CTR may have no option but to decrease altitude if there is a conflict with other aircraft at the same altitude.

The NextGen aircraft minimum power speed for climb was defined by en route climb-related certification requirements. For this study the BA609 certification basis part TR.69 (similar to FAA FAR part 23.69) was selected. TR.69 states, “All engines operating. The steady gradient and rate of climb must be determined….with (1) not more than maximum continuous power on each engine; (2) the landing gear retracted; (3) the wing flaps retracted or in the autoflap position; and (4) a climb speed not less than 1.23 VSR1 (1g stall).” Therefore, climb performance was based on climbing at 1.23 times the 1g stall speed.

Although not a clearly defined constraint, compressibility is a limiting factor in terms of achieving a good design. This is particularly important in terms of the CTR120 cruise altitude and speed requirements. Figure 2-10 is a generic chart created to illustrate the relationship between prop-rotor efficiency, rotor compressibility onset, design requirements, and rotor cruise rpm.

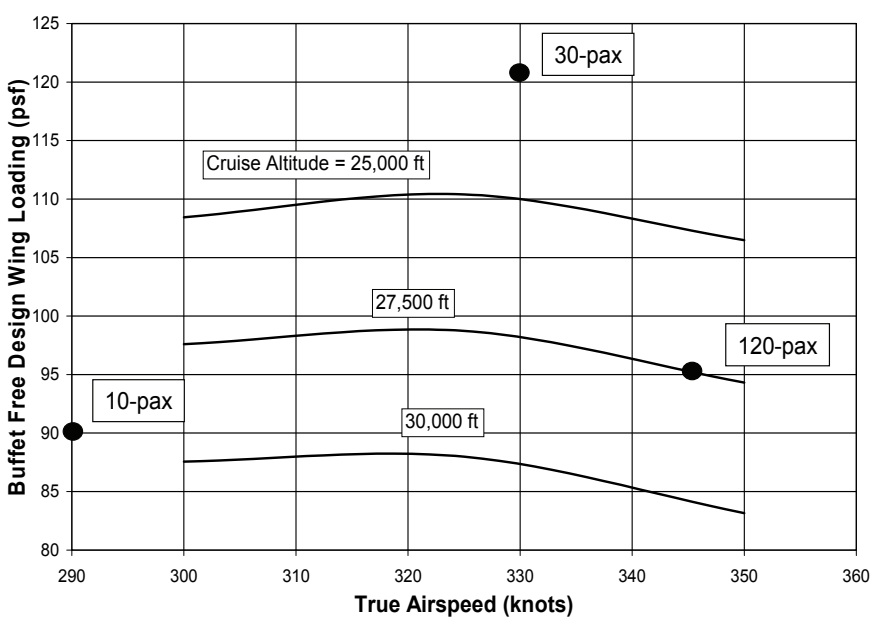

Figure 2-9. Buffet-free design chart for wing loading.

The onset of compressibility is affected by the drag divergence characteristics of the rotor airfoils; therefore, a major consideration is the rotor cruise rpm. Figure 2-10 also shows the impact of changing the design tip speed at 100-percent rpm. As design tip speeds are reduced to meet more demanding noise requirements, there is a benefit, as expected, in terms of alleviating compressibility effects for a given cruise-rpm-to-hover-rpm ratio.

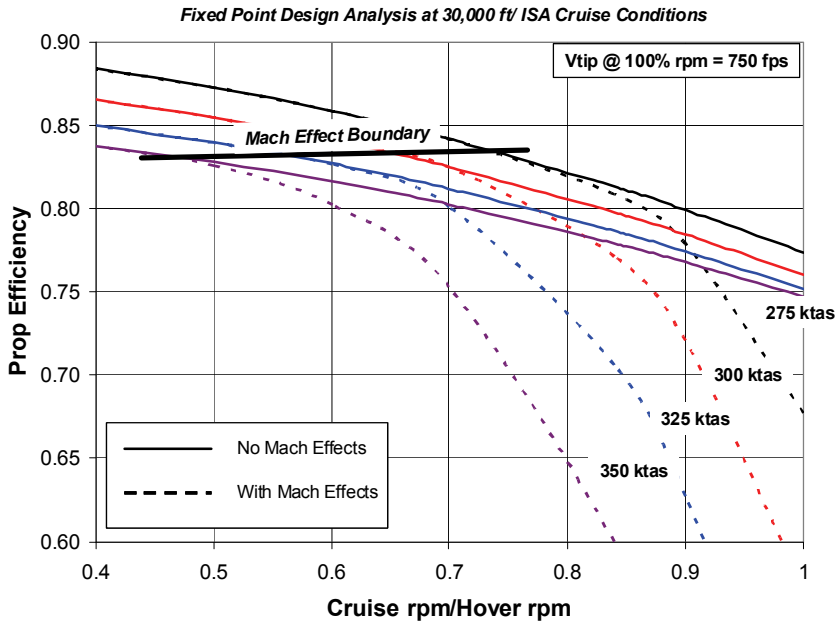

(2-10a)

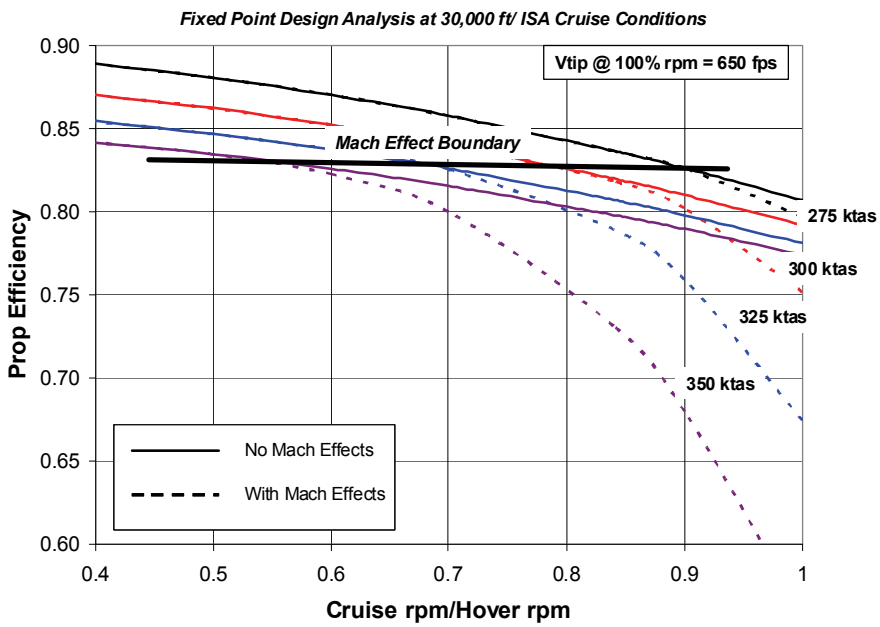

(2-10b)

Figure 2-10. Impact of compressibility on propulsive efficiency.

2.3 Comparative Design Summary

A summary of characteristics of the NextGen fleet is given at this point to provide a relative feel for the designs before proceeding through the design details. Table 2-4 provides a comparison of the top-level geometric, drive system, and aerodynamic characteristics for each design. As discussed in section 2.2.2, Technology Insertion, the CTR10 and CTR30 designs are derivatives of, or modifications to, the Bell-Agusta 609 and Bell-Boeing V-22 aircraft. To avoid proprietary rights and International Traffic in Arms Regulations (ITAR) issues, only those characteristics of the CTR10 and CTR30 designs that are either in the public domain or are unique characteristics resulting from the NextGen design effort are noted. All other information that is not available is denoted "n/a."

In order to obtain an appreciation of the relative sizes of the NextGen fleet, scaled front and side views of the CTR120 design are presented in figures 2-11 and 2-12. These views are not accurate representations of all characteristics, just approximations for effect. The CTR90 design is based on a linear interpolated design that is described in section 3.

TABLE 2-4. COMPARISON OF NEXTGEN DESIGN CHARACTERISTICS

Number of Passengers		10	30	90 (1)	120
Weights:					
Design Gross Weight, DGW	lb	16800	46460		147647
Maximum Gross Weight, MGW (Full Fuel & Payload)	lb	16192	46430		147647
Empty Weight + Trapped Fluids	lb	11022	32160		98737
Payload	lb	2200	6600	19800	26400
Operating Load	lb	470	670	870	1070
Number of Crew	ND	2	3	4	5
Fuel System Capacity	lb	2500	7000		21441
Geometry:					
MR Radius	ft	13.0	19.0		36.1
Number of Blades per Rotor	ND	3	4	6	6
Wing Span	ft	33.8	45.8		100.4
Length Fuselage	ft	n/a	61.6		111.9
Engine/Xmsn:					
Number of Engines	ND	2	2	4	4
Engine Takeoff Power Rating (SLS - uninstalled)	eshp	3000.0	9000.0		9372.0
MCP Xmsn rating @ mast (100%rpm)	hp	n/a	4412.0		13063.0
Aero/Performance Related:					
Main Rotor Tip Speed (100% rpm)	fps	775	700	665	650
Main Rotor Tip Speed, A/P mode (70%rpm)	fps	651	588	466	455
Flat Plate Drag (alpha=0) (3)	sq ft	11.0	23.4		56.3
Design Cruise Altitude	ft	25000	25000	27500	27500
Design Cruise Speed (2)	ktas	n/a	n/a	340	345
Range (5k/ISA+20 deg C takeoff)					
@ max payload, max fuel & Vlrc	nm	821	804		1331
@ max payload, max fuel & Vmcp	nm	750	671		1179 (4)

(1) Characteristics based on linear interpolation between 30 and 120-pax designs
(2) 90 and 120-pax design cruise speeds based on Vmcp
(3) Drag does not include nacelle cooling drag which is inherently built into engine residual thrust.
(4) Vmcp = 345 kts for sizing and mission cruise not exactly the same; Vmcp for mission legs > 345 ktas

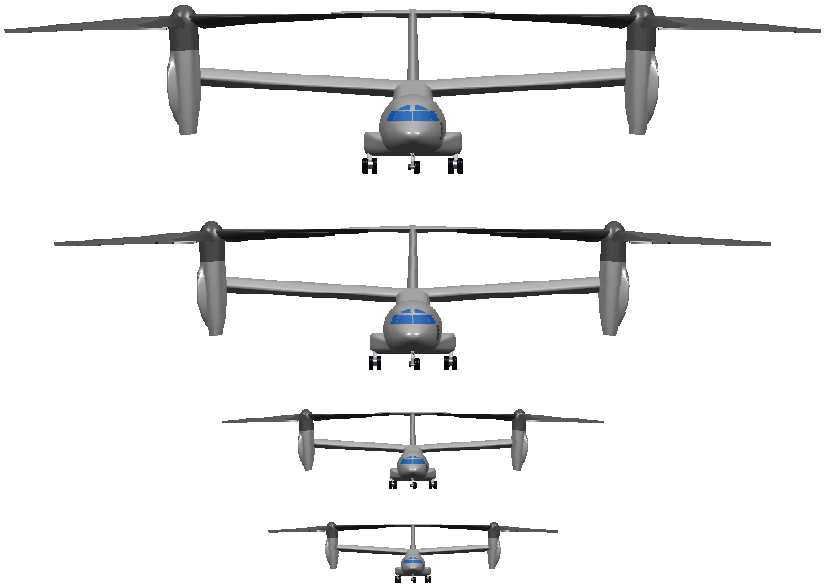

Figure 2-11. Front view comparison of the NextGen designs.

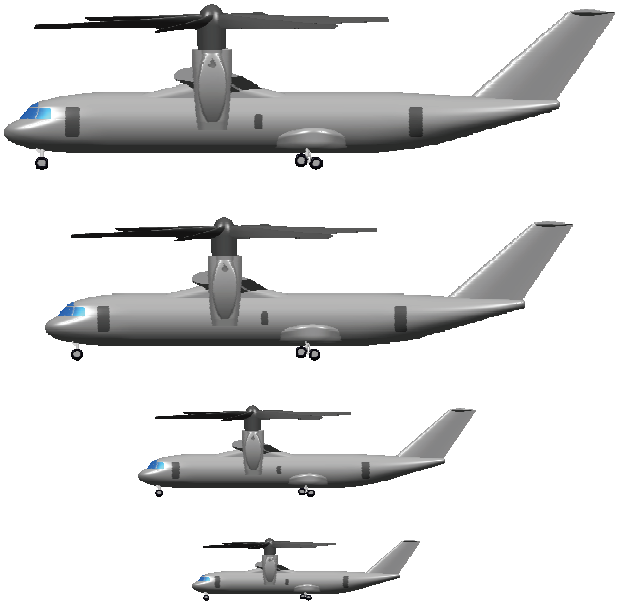

Figure 2-12. Profile view comparison of the NextGen designs.

Figures 2-13, 2-14, and 2-15 are presented, as a function of the number of passengers, to compare final NextGen CTR range, fuselage length, and aircraft width characteristics to original CTR goals and fixed-wing aircraft trends. The most noticeable difference is in overall width. The NextGen CTR wing span is in line with fixed-wing aircraft, however, the overall width is considerably different because of the inclusion of the CTR rotors. Therefore, if the NextGen CTR designs must be able to approach current airport terminal areas there is a question of clearance with the jet-way. However, the overall width of the CTR designs is not greater than that of a B-777 or a B-747-8. This design consideration was not addressed in this study.

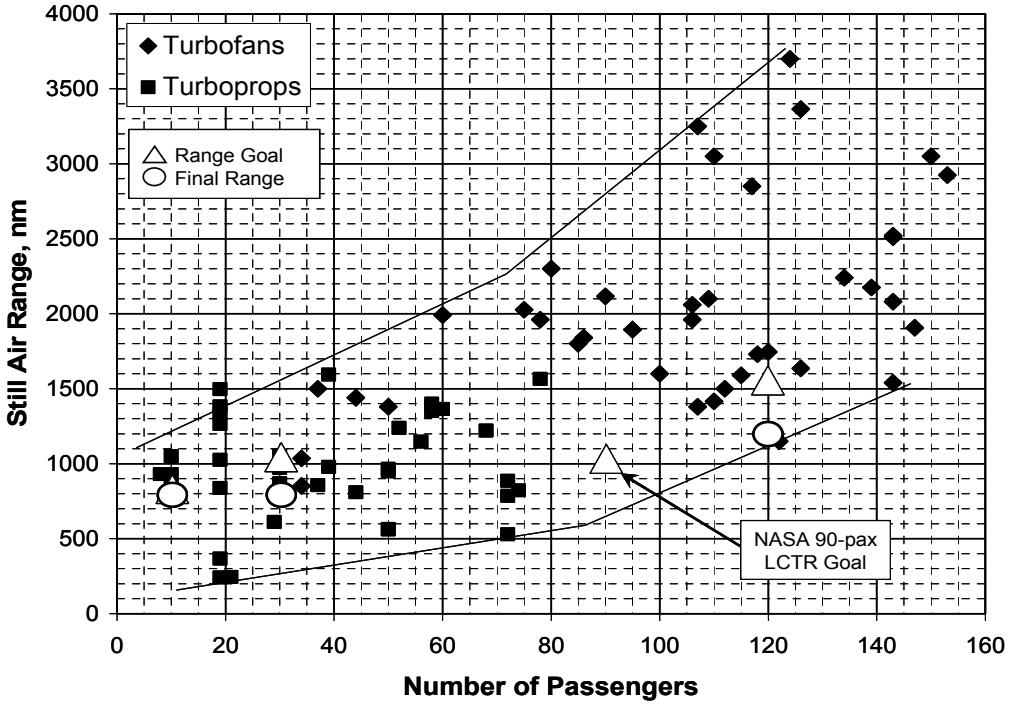

Figure 2-13. NextGen CTR range compared to fixed-wing aircraft.

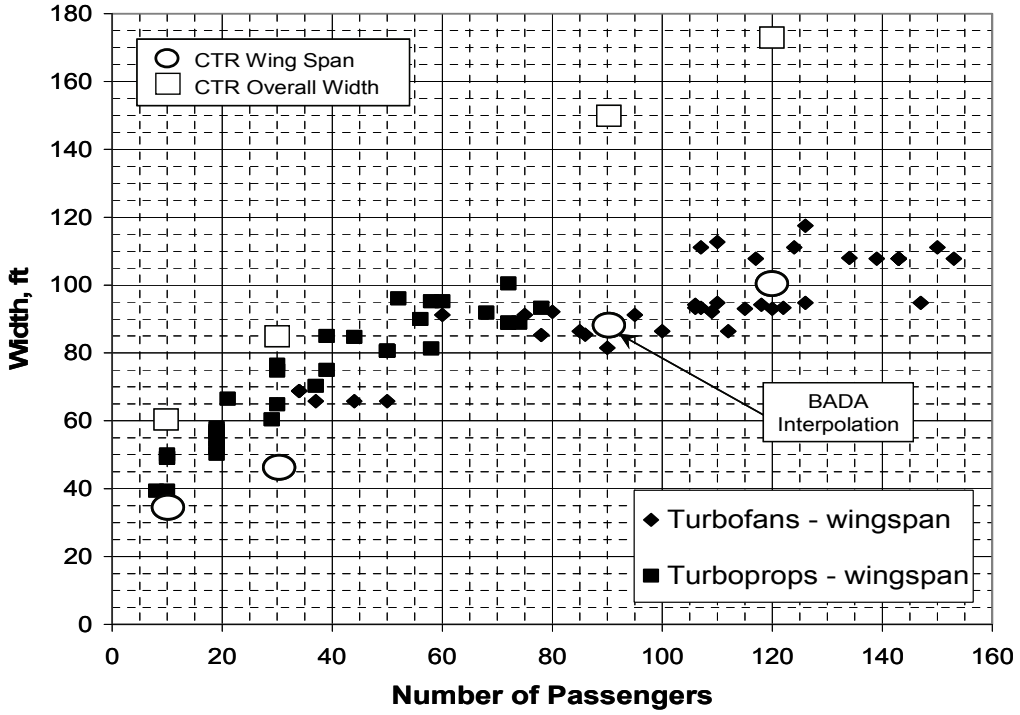

Figure 2-14. NextGen CTR width compared to fixed-wing aircraft.

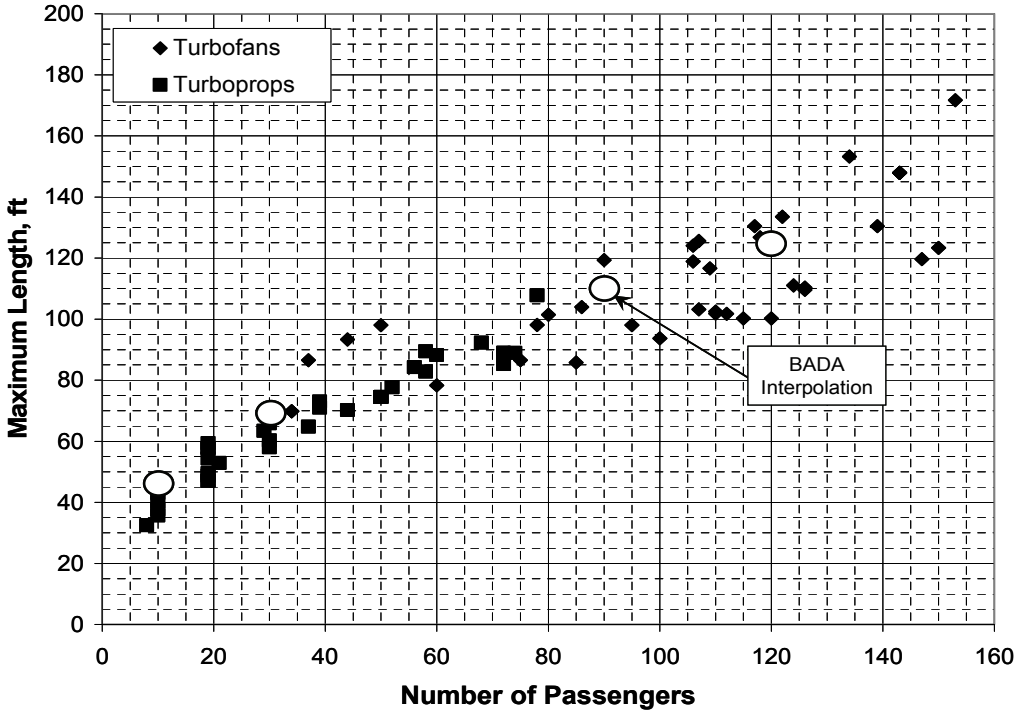

Figure 2-15. NextGen CTR fuselage length compared to fixed-wing aircraft.

2.4 10-Passenger CTR (CTR10)

The baseline for the CTR10 is a hypothetical "B Model" version of the BA609 as defined in section 2.2.2.1, 10 Passenger. It incorporates advanced technologies available in 2017 to the extent possible. The advantage of evolving the CTR10 design from the BA609 is the fact that the aircraft has been in flight test for several years, and the performance and weight of the configuration are well understood.

The CTR10 design uses the basic airframe of the BA609. The external lines are the same with only one exception, the impact of installing a new engine in the nacelle. The new engine is based on AATE technology, which is described in section 2.2.5, Engine Technology and Modeling.

2.4.1 Design Requirements

Because the CTR10 is a notional BA609 derivative, the structural and performance requirements were not changed. Therefore, the maximum gross weight is the same as that of the BA609, 16,800 lbs. Tip speed is the same as the BA609 and is currently close to the Stage 3 noise requirement. At this time it has been assumed that this will be acceptable in the future for the "B" model.

2.4.2 Cabin Layout

It should be noted that in developing the CTR10 configuration based on the BA609, several issues had to be considered. The first was related to seating. To increase the seating from nine to ten passengers without stretching the fuselage required a change in the seating arrangement. One of the forward facing seats had to be converted into a side facing bench seat for two passengers. This is the only internal modification that was made. There may be some special considerations and restrictions based on FAA rules that make this configuration untenable if used for paying passengers; however, side facing bench seats are used in corporate jets. No adjustments have been made to weights for potential structural considerations in mounting a bench seat.

There is a certification demarcation line between nine and ten passengers in terms of emergency egress requirements in the event of ditching. The potential impact is in regard to available exits and their size. The impact of this issue was not addressed.

This aircraft is not designed or required to have a flight attendant. There is no lavatory or galley. All baggage is stored in a compartment behind the aft pressure bulkhead with access from outside the aircraft only.

Figure 2-16 shows the current cabin arrangement and its proposed modification. The current seat width and seat pitch are 16 and 32 inches, respectively.

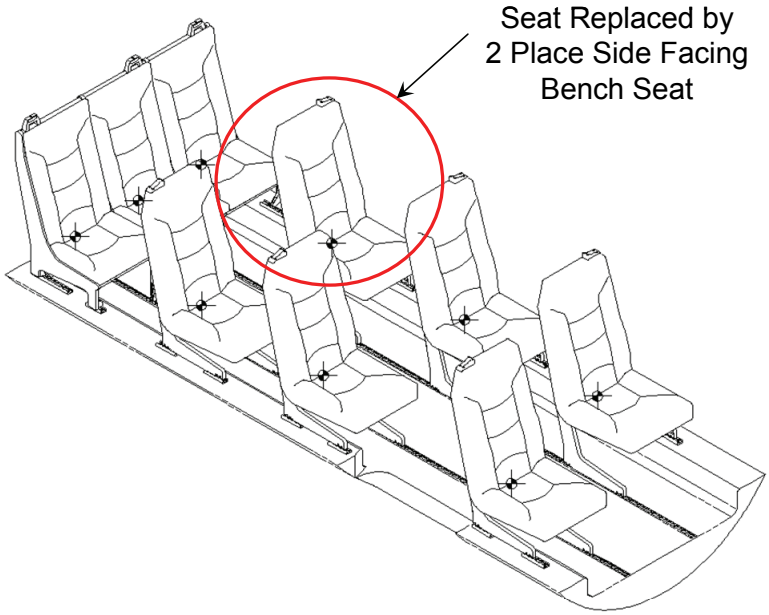

Figure 2-16. Cabin layout of the CTR10 configuration.

2.4.3 Engine Performance

Installed engine power available, fuel flow, and net nacelle thrust data were developed by Bell Helicopter's Propulsion group based on a 3,000 shp engine with AATE technology. Installed data was developed in the manner described in section 2.2.5, Engine Technology and Modeling, assuming a 0.45 exhaust nozzle discharge coefficient. Because of the high cruise speeds and Mach numbers typical of a tiltrotor, data was provided for a range of pressure altitudes up to 30,000 feet and Mach numbers up to 0.60. Engine performance was generated for both hover and cruise rpm.

The engine data used to build the PRESTO model was based on a military rating structure. Consequently for this study the maximum rated power (MRP), which is a 10-minute rating, was used for takeoff power. The implication with respect to a civil rating structure was not addressed. Normalized power available, ram recovery, and net nacelle thrust are shown respectively in figures 2-17, 2-18, and 2-19 for the AATE PRESTO engine model. In figure 2-19, the symbol "δ" represents atmospheric pressure ratio, and the symbol "Θ" represents atmospheric temperature ratio. The rated SFC of the engine is approximately 0.35.

One potential issue is exhaust deck heating. The drive system rating is the same as the BA609; therefore, engine power levels should not exceed those of the BA609. However, the engine exhaust is closer to the ground than for the BA609 which exhausts out of the side of the nacelle. Until more detailed studies can be performed with this engine technology no exhaust deflection solutions have been incorporated.

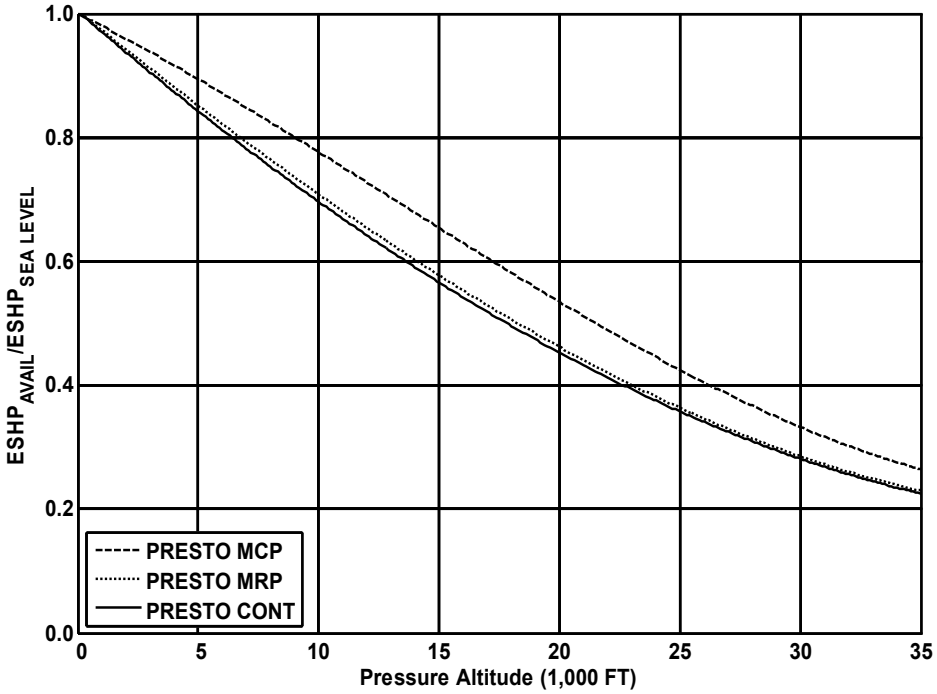

Figure 2-17. CTR10 normalized engine power available.

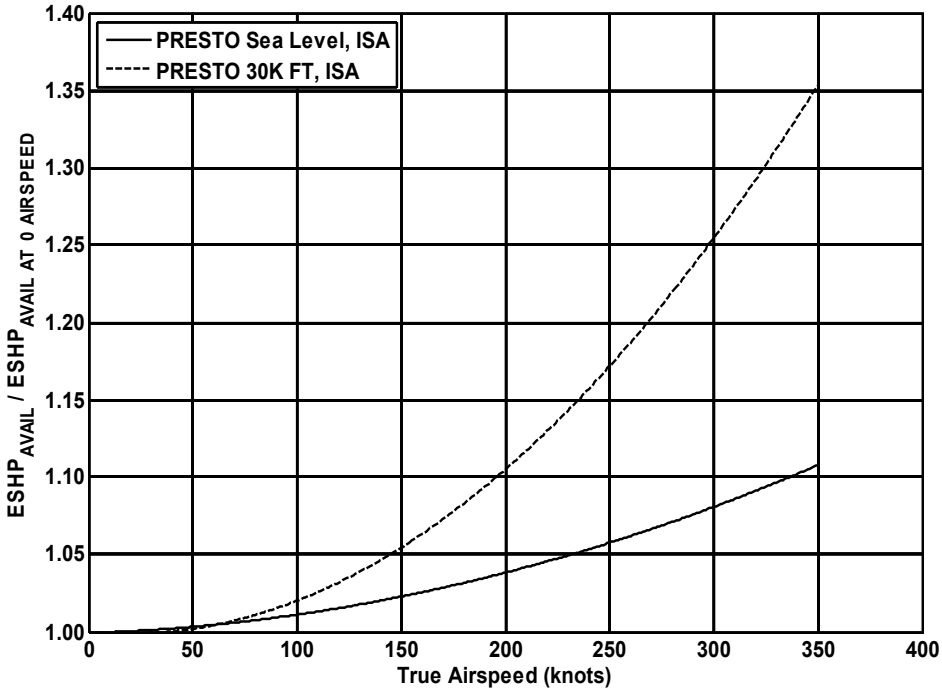

Figure 2-18. Effect of true airspeed on power available.

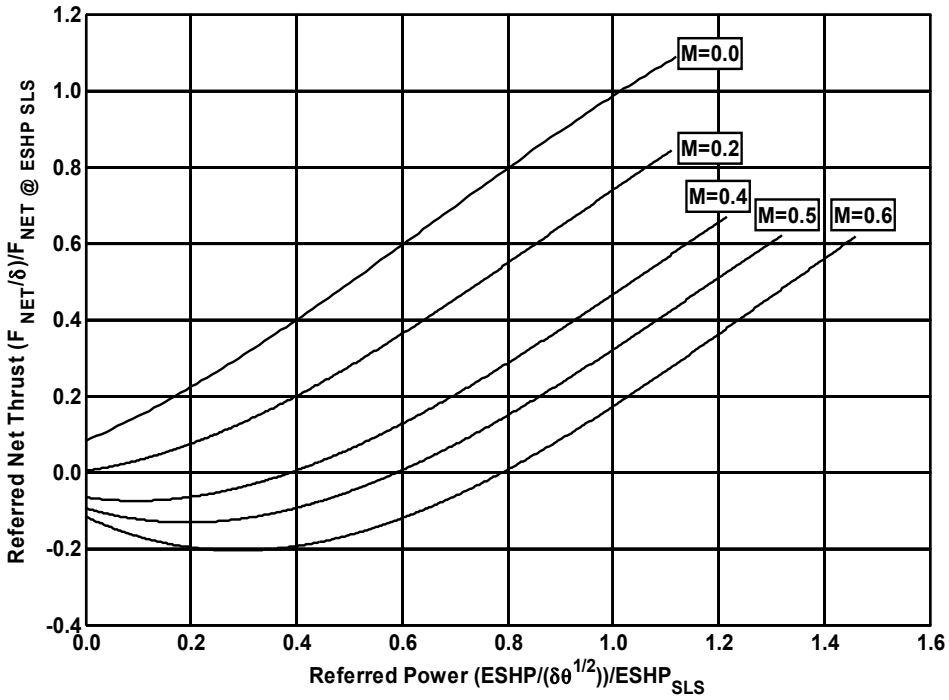

Figure 2-19. CTR10 normalized net nacelle thrust.

2.4.4 Weights

Although the "B" model development approach is assumed to start at a point in time where technology advances are projected to be available, this configuration, as noted earlier, relies on existing structure to the greatest extent possible. Therefore, weight reduction based on technology improvements was only achieved in those areas that might not require significant additional qualification or regression testing; for example, window treatment and furnishings technology.

The process for estimating the weight empty of the CTR10 design involved several steps. The Bell Helicopter Weights group calculated a set of parametric weights (Industry Standard Group Weight Statement format) for the BA609. These weights were then corrected to actual weights by correlation factors. The last step was to apply technology factors based on a technology insertion date of 2017.

The most significant weight reduction was associated with the AATE engine technology. Engine dry weight and related component weight savings accounted for approximately 50 percent of the total weight savings. The remaining 50 percent was primarily due to new materials. Because the "B" model is a modification to a proprietary civil product, specifics of the baseline weights and technology benefits cannot be presented. However, it can be stated that the "B" model was able to take advantage of approximately 25 percent of the potential benefits that could be realized from a "new start" design.

The crew weight assumed 200 lbs/person with a 70 lb allocation for additional operating load. Passenger weight was assumed to be 220 lbs/passenger allowing for baggage. A summary of weights for the CTR10 design is provided in table 2-5.

TABLE 2-5. SUMMARY OF THE CTR10 CONFIGURATION CHARACTERISTICS

Weights:		
Design Gross Weight, DGW	lb	16800
Maximum Gross Weight, MGW (Full Fuel & Payload)	lb	16192
Design Payload	lb	2200
Empty Weight + Trapped Fluids	lb	11022
Operating Load	lb	470
Number of Crew	ND	2
Fuel System Capacity	lb	2500
Geometry:		
MR Radius	ft	13.0
Number of Blades per Rotor	ND	3
Thrust Equivalent Chord	in	14.8
Solidity	ND	0.0908
Wing Span	ft	33.8
Wing Chord	ft	5.4
Wing Area	sq ft	183.0
Horizontal Span	ft	n/a
Horizontal Tail Area	sq ft	n/a
Tail Type	ND	T-tail
Vertical Span	ft	n/a
Vertical Tail Area	sq ft	n/a
Length Fuselage	ft	n/a
Fuselage Height	ft	n/a
Fuselage Width	ft	5.8
Nacelle Length (not including spinner)	ft	n/a
Nacelle Height	ft	n/a
Nacelle Width	ft	n/a
Engine/Xmsn:		
Number of Engines	ND	2
Engine Ratings, SLS, uninstalled		
2.5-min OEI Power	eshp	3055.0
Takeoff Power	eshp	3000.0
Max Continuous Power	eshp	2508.0
MCP Xmsn rating @ mast (100%rpm)	hp	n/a
Aero/Performance Related:		
Disk Loading at MGW	psf	15.2
Wing Loading at MGW	psf	88.5
Main Rotor Tip Speed (100% rpm)	fps	775
Main Rotor Tip Speed, A/P mode (70%rpm)	fps	651
Hover Download	%T	n/a
Flat Plate Drag (alpha=0)	sq ft (2)	11.0
Oswald A/C efficiency "e"	ND	n/a
Incompressible Clmax (zero flaps)	ND	n/a
Design Cruise Altitude	ft	25000
Design Cruise Speed	ktas	n/a
Vlrc @ MGW/Std Day/Design Cruise Altitude	ktas	260
(Vlrc is speed at 0.99 best range speed)		
Vmcp @ MGW/Std Day/Design Cruise Altitude	ktas	284
(Vmcp is speed at 100% MCP available)		
Range (5k/ISA+20 deg C takeoff)		
@ max payload, max fuel & Vlrc	nm	821
@ max payload, max fuel & Vmcp	nm	750

2.4.5 Aerodynamics

The aerodynamic characteristics of the CTR10 design were developed by applying corrections to BA609 aerodynamics. The aerodynamic characteristics of the BA609 are well understood and based on the results of wind tunnel testing substantiated by flight test. Since the rotor aerodynamics are the same as those for the BA609, only airframe aerodynamics were modified.

For PRESTO analysis the key aerodynamic characteristics required to calculate performance are airframe maximum lift coefficient, the airframe drag polar, rotor aerodynamics, and the effect of compressibility. Only the drag polar was modified to reflect configuration changes in the engine installation. The BA609 PT7-6A engine exhaust exits on the side of the nacelle. The advanced technology engine is installed to exhaust out the aft end of the nacelle. The resultant incompressible equivalent flat plate drag area of the CTR10 configuration was 11.0 square feet.

As noted in the engine discussion, nacelle cooling flows changed with the installation of the advanced technology engine; however, the resultant drag is more accurately book kept in the nacelle net thrust and not in airframe drag.

2.4.6 Design Process Discussion

Because the CTR10 aircraft is the result of an aircraft modification program, design synthesis was not used. The final design and performance capability was defined using the PRESTO "fixed point" analysis. The primary objective was to achieve the range goal of 800 nmi after an OEI-capable takeoff with a maximum payload and maximum fuel. The takeoff condition is representative of Denver on a hot day (5k/ISA+20°C).

A weight empty was estimated for the CTR10 configuration with a 3,000 shp engine (MRP). The takeoff gross weight for this configuration was 16,192 lbs, which included 2200 lbs of payload and 2500 lbs of fuel. PRESTO was run to assess OEI performance for VTO and STO takeoff conditions. The resultant STO takeoff gross weight capability was 16,181 lbs. This was considered to be close enough for a solution. A detailed assessment of the STO takeoff distance was not made; however, it is on the order of 1,000 and 1,500 feet to clear a 50-foot obstacle depending on the takeoff procedure. To refine the STO takeoff distance would require a more in-depth analysis.

The VTO takeoff capability was 15,424 lbs. This equates to only six passengers if taking off with full fuel. Further engine trades were not conducted to push the VTO capability to the maximum gross weight of 16,192 lbs. An approximate increase in the OEI-to-maximum-continuous-power (MCP) ratio from 1.21 to 1.31 would be required and is within the realm of today's engine characteristics. There are additional studies that could be conducted to optimize the performance including the use of water/alcohol injection. The uninstalled power available ratings are given in table 2-5.

2.4.7 Results

The following sections present the results of the CTR10 design process.

2.4.7.1 Design Description

A summary of the CTR10 design characteristics is provided in table 2-5. Because of the close relationship between the CTR10 design and the BA609, only that information which is in the public domain (ref. 16) or unique to the NextGen design is provided.

2.4.7.2 Three-View Drawing

Figure 2-20 presents a three-view drawing of the proposed CTR10 configuration in helicopter mode.

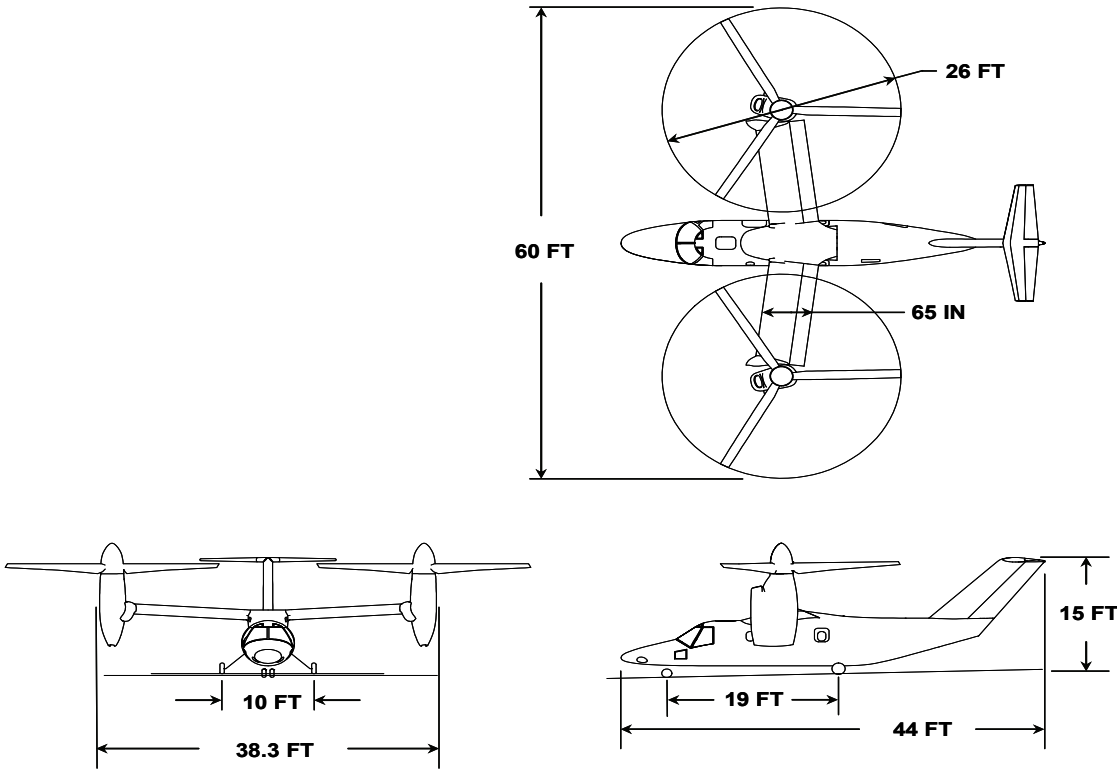

Figure 2-20. Three-view drawing of the CTR10 configuration in helicopter mode.

2.4.7.3 Performance Characteristics

This section provides aircraft and mission performance characteristics of the CTR10 design to the extent possible. Figures 2-21, 2-22, and 2-23 provide a takeoff ceiling for OEI VTO and STO ceilings, a partial speed-altitude envelope, and a payload-range curve, respectively.

The CTR10 has a full passenger VTO takeoff capability at 5k/ISA conditions, however, as noted earlier, that is reduced to six passengers at 5k/ISA+20°C. The alternative for a full passenger load at the hi/hot condition is a STO takeoff with the current design.

The speed-altitude envelope shown in figure 2-22 is at the maximum gross weight of 16,192 lbs. At the ISA operational ceiling of 25,000 feet, the long-range cruise speed is approximately 260 knots true airspeed (KTAS). During a range mission the long-range cruise speed will vary between 250 and 260 knots. Maximum true airspeed capability at 100-percent MCP is approximately 283 knots.

The payload-range data in figure 2-23 shows four scenarios for a 5k/ISA+20°C takeoff that address both a VTO and STO takeoff. The range for a maximum payload of 10 passengers using a VTO takeoff is 510 nmi. Although maximum fuel load is not available, this is still a competitive range for the commuter market. With a STO takeoff, maximum payload and fuel can be carried resulting in a range of 821 nmi, which exceeds the original goal. At the range goal of 800 nmi, the passenger load capability is respectively 10 and 7 for STO and VTO takeoffs.

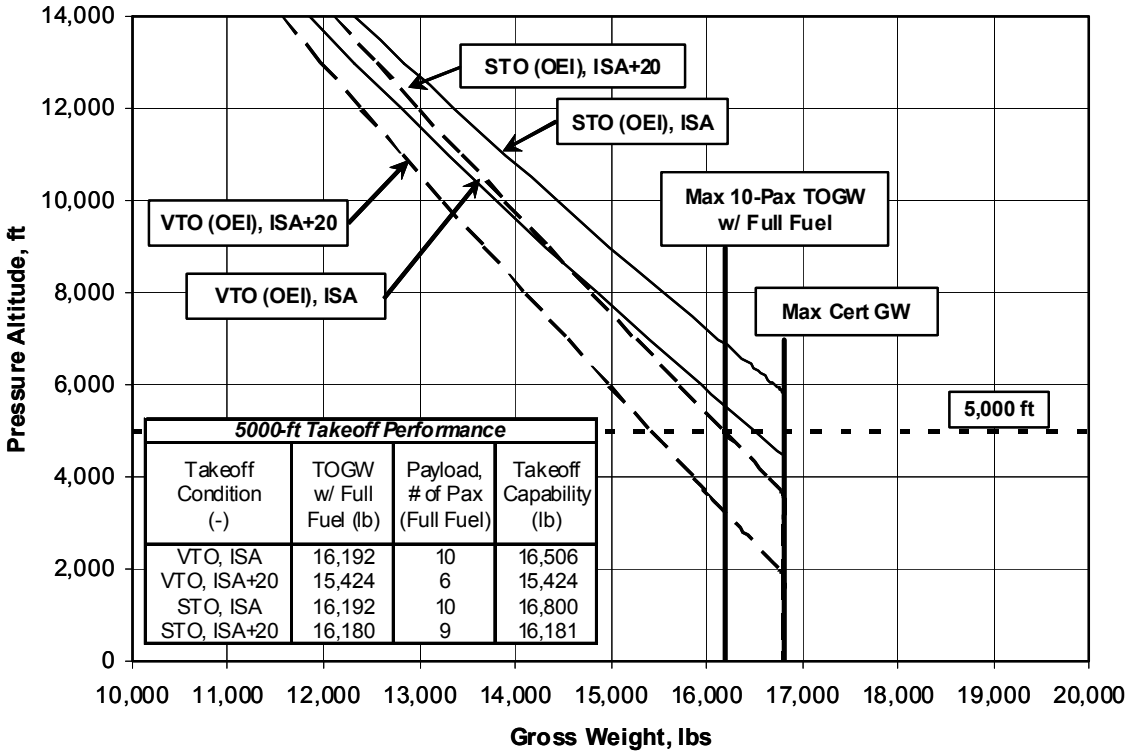

5000-ft Takeoff Performance

Takeoff Condition (-)	TOGW w/ Full Fuel (lb)	Payload, # of Pax (Full Fuel)	Takeoff Capability (lb)
VTO, ISA	16,192	10	16,506
VTO, ISA+20	15,424	6	15,424
STO, ISA	16,192	10	16,800
STO, ISA+20	16,180	9	16,181

Figure 2-21. CTR10 OEI STO hover ceiling, ISA and ISA+20°C.

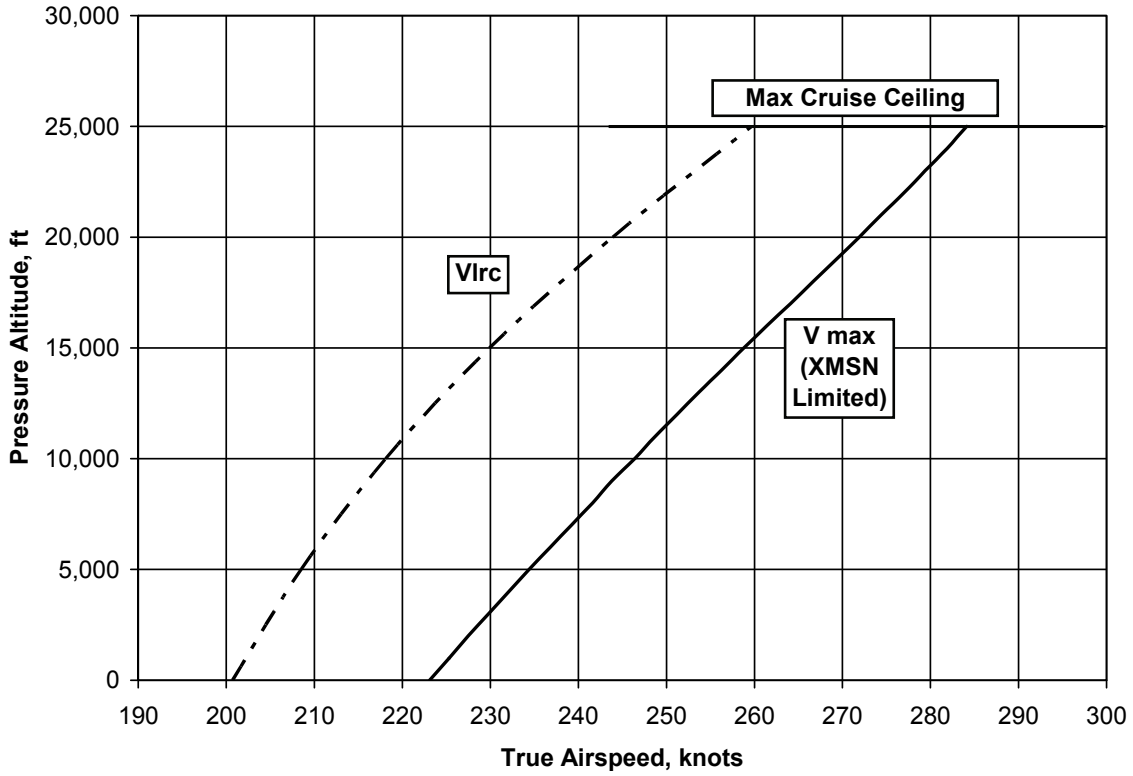

Figure 2-22. CTR10 partial speed-altitude envelope, ISA.

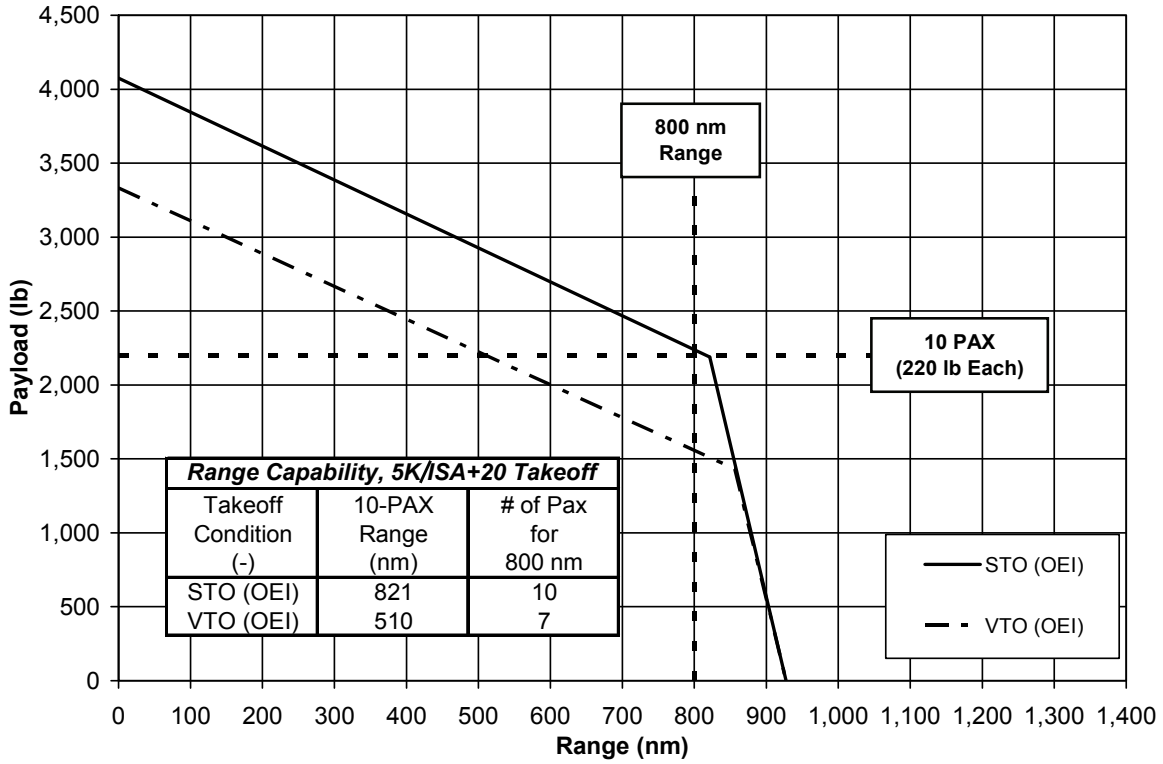

Range Capability, 5K/ISA+20 Takeoff		
Takeoff Condition (-)	10-PAX Range (nm)	# of Pax for 800 nm
STO (OEI)	821	10
VTO (OEI)	510	7

Figure 2-23. CTR10 payload-range curve, ISA cruise.

2.5 30-Passenger CTR (CTR30)

The baseline for the CTR30 configuration is the V-22. For the purposes of this study the development schedule shown in section 2.2.2, Technology Insertion, was followed. The CTR30 design was envisioned as a two-step development similar to the CTR10 design. The first aircraft would be designed with pre-2017 technology. This would be followed by a "B" model advanced technology engine program starting in 2019.

Because the V-22 is a military aircraft, more extensive modifications have been incorporated to define the CTR30. The V-22 is a production aircraft; consequently, the performance and empty weight characteristics are very well understood. The core of the CTR30 design is the V-22 lift propulsion system. This includes the wing, nacelles, rotor blades, and drive system. Nacelle modifications were held to the minimum required to accommodate a new technology engine.

2.5.1 Design Requirements

The CTR30 design is based on a hybrid set of requirements by definition only because major components of the V-22 lift-propulsion system were used. However, in terms of performance, the primary requirement was an OEI transport category takeoff capability at 5k/ISA+20°C conditions using a 2.5-minute OEI rating. Cruise speed and altitude were not requirements but a fall out of the design. These characteristics were limited by the decision to use existing V-22 drive system and wing components.

Empennage sizing was based on a static stability requirement only. The horizontal tail sizing requirement was based on a static stability margin of 5 percent. Vertical tail sizing was based on a requirement for neutral directional stability. Bell has been successful in using differential collective pitch (DCP) in the rotors to augment directional stability as in the BA609; however, inherent negative airframe static stability based on additional augmentation capability is considered beyond the scope of this study.

The fuselage is designed for civil passenger transport. As such, requirements in terms of emergency exits, galley, lavatories, and the number of attendants are set by FAA rules. The details are described in section 2.5.2, Cabin Layout. The cabin is pressurized to operate at a maximum aircraft operating altitude of 30,000 feet. Because the geometry of the lift-propulsion system of the V-22 did not change, rotor-to-fuselage clearance became a requirement for defining the cabin cross section.

The positive limit maneuvering load factor is a required input in the parametric weight equations. It was defined as 2.5 g based on the methodology specified in FAA FAR part 25.337.

The CTR30 rotor tip speed at 100-percent rpm was required to be 700 fps based on the noise requirements presented in section 2.2.4. This was believed to be consistent with Stage 3 acoustic requirements in terms of magnitude as well as timing of implementation.

2.5.2 Cabin Layout

The CTR30 cabin does not include separate first-class seating. The seating arrangement was a fallout of the maximum cross section consistent with the rotor-to-fuselage clearance requirement. There are ten rows of three seats across and one aisle. The seat pitch of 36 inches and seat width of 21 inches are considered to be in line with the desires of the customer community. The width of the aisle is 20 inches and is set by FAA FAR part 25.815.

The cabin provides an additional seat for one flight attendant per FAR part 121.391. The cabin has one lavatory and no galley. The lavatory is in line with industry practice. Overhead stowage is not provided in the cabin. Baggage is carried in a baggage compartment behind the aft pressure bulkhead with access from outside of the aircraft only. The cabins were designed to meet FAA requirements with respect to emergency egress. The cabin includes 34- x 72-inch forward and aft entry doors. Two full-size exits are required by FAR part 25.807 for aircraft with a seat configuration of 24–40 passengers.

Figure 2-24 shows the current cabin arrangement.

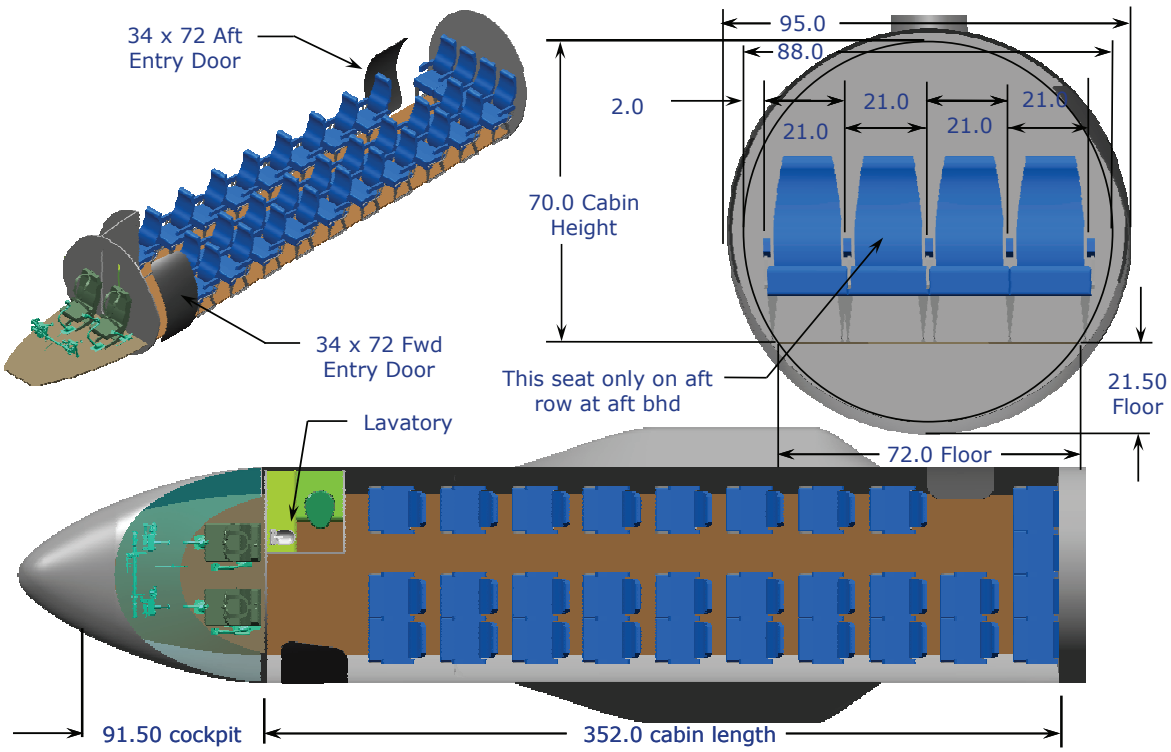

Figure 2-24. Cabin layout of the CTR30 configuration.

2.5.3 Engine Performance

Installed engine power available, fuel flow, and net nacelle thrust data were developed by Bell Helicopter's Propulsion group based on an 11,000-shp engine using VAATE technology. This data was used as reference data only to construct the normalized engine input required by PRESTO.

Installed data was developed in the manner described in section 2.2.5.2 assuming a 0.45 exhaust nozzle discharge coefficient. Because of the high cruise speeds and Mach numbers typical of a tiltrotor aircraft, data was provided for a range of pressure altitudes up to 35,000 feet and Mach numbers up to 0.60. Engine performance data was generated for both hover and cruise rpm.

The available engine data for this study used a military rating structure. There was no attempt to convert it into a commercial rating structure; consequently, the MRP (10-minute rating) was used for takeoff power.

The uninstalled power available is given in table 2-6. The 2.5-minute OEI power was assumed to be 120 percent of MRP. This assumption is higher than is currently available in large advanced technology engines, although it could be achieved with water/alcohol injection. However, this rating was used primarily as an equivalence to a combined 30-second OEI and 2-minute OEI rating structure to simplify the takeoff analysis. In a development program a more definitive rating structure would be requested of the engine manufacturer, at which time tradeoffs between ratings would be made. Normalized power available, ram recovery, and net nacelle thrust are shown respectively in figures 2-25, 2-26, and 2-27 for the VAATE PRESTO engine model. The rated SFC is approximately 0.33.

2.5.4 Weights

The process for developing the weight empty of the CTR30 configuration is the same as that described in section 2.4.4 for the CTR10 design with the exception that parametric weights analysis started with the V-22 configuration. As with the CTR10 design this configuration relies on existing structure to the greatest extent possible. Weight reduction was taken in areas that might not require significant additional flight test time; however, extensive airframe changes were required for the 30-passenger design. The main impact on weight empty occurred in the areas of the fuselage, fuselage-wing junction (removal of wing fold), empennage, and the engine installation. Blade fold was also removed from the weights, however, the impact on blade design was not assessed.

To the extent that the configuration constraints of commonality were applied, military requirements were changed to reflect civil requirements for a commercial aircraft where possible. Cabin pressurization was provided to reflect a maximum ceiling of 30,000 feet. This provided some altitude margin although the operational service ceiling was limited to 25,000 feet to maintain a buffet-free maneuver capability.

Passenger and crew weights were the same as defined for the CTR10 in section 2.4.4, Weights. An additional allocation of 70 lbs of operating load associated with the crew was included. A summary of weights for the CTR30 design is provided in table 2-6.

TABLE 2-6. SUMMARY OF THE CTR30 CONFIGURATION CHARACTERISTICS

Weights:		
Design Gross Weight, DGW	lb	46460
Maximum Gross Weight, MGW (Full Fuel & Payload)	lb	46430
Design Payload	lb	6600
Empty Weight + Trapped Fluids	lb	32160
Operating Load	lb	670
Number of Crew	ND	3
Fuel System Capacity	lb	7000
Geometry:		
MR Radius	ft	19.0
Number of Blades per Rotor	ND	4
Thrust Equivalent Chord	in	n/a
Solidity	ND	n/a
Wing Span	ft	45.8
Wing Chord	ft	8.33
Wing Area	sq ft	382.0
Horizontal Span	ft	11.4
Horizontal Tail Area	sq ft	55.0
Tail Type	ND	T-tail
Vertical Span	ft	12.6
Vertical Tail Area	sq ft	85.0
Length Fuselage	ft	61.6
Fuselage Height	ft	7.9
Fuselage Width	ft	7.9
Nacelle Length (not including spinner)	ft	n/a
Nacelle Height	ft	n/a
Nacelle Width	ft	n/a
Engine/Xmsn:		
Number of Engines	ND	2
Engine Ratings, SLS, uninstalled		
2.5-min OEI Power	eshp	10880.0
Max Rated Power (10-min)	eshp	9215.0
Max Continuous Power	eshp	7187.0
MCP Xmsn rating @ mast (100%rpm)	hp	4412.0
Aero/Performance Related:		
Disk Loading at MGW	psf	20.5
Wing Loading at MGW	psf	121.5
Main Rotor Tip Speed (100% rpm)	fps	700
Main Rotor Tip Speed, A/P mode (84%rpm)	fps	588
Hover Download	%T	n/a
Flat Plate Drag (alpha=0)	sq ft	23.4
Oswald A/C efficiency "e"	ND	n/a
Incompressible Clmax (zero flaps)	ND	n/a
Design Cruise Altitude	ft	25000
Design Cruise Speed	ktas	n/a
Vlrc @ MGW/Std Day/Design Cruise Altitude	ktas	340
(Vlrc is speed at 0.99 best range speed)		
Vmcp @ MGW/Std Day/Design Cruise Altitude	ktas	334
(Vmcp is speed at 100% MCP available)		
Range (5k/ISA+20 deg C takeoff)		
@ max payload, max fuel & Vlrc	nm	804
@ max payload, max fuel & Vmcp	nm	671

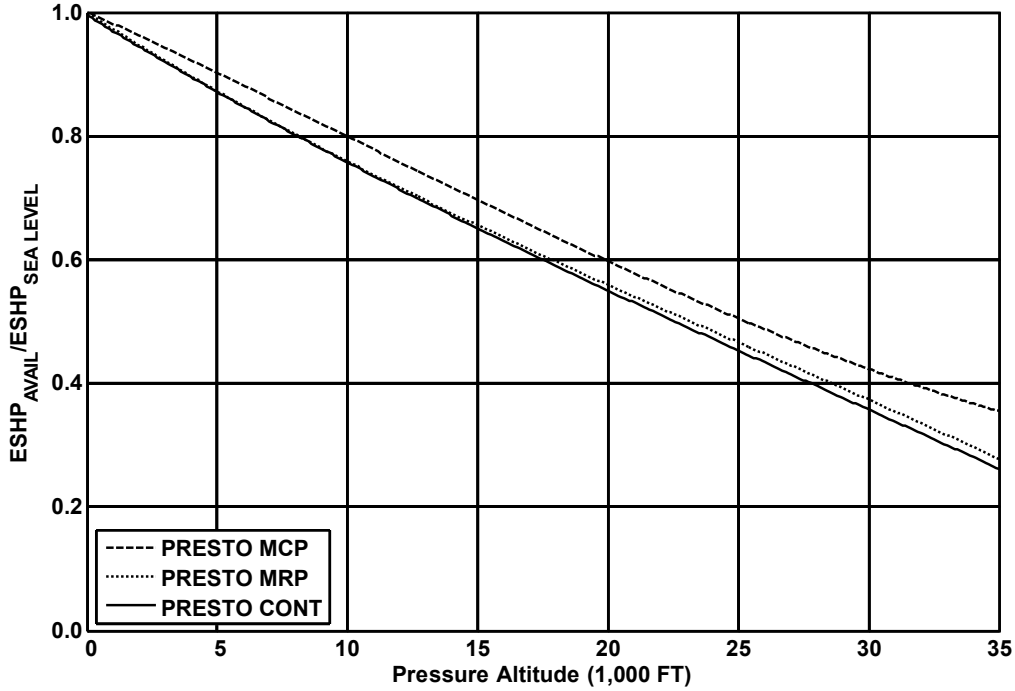

Figure 2-25. CTR30 normalized engine power available.

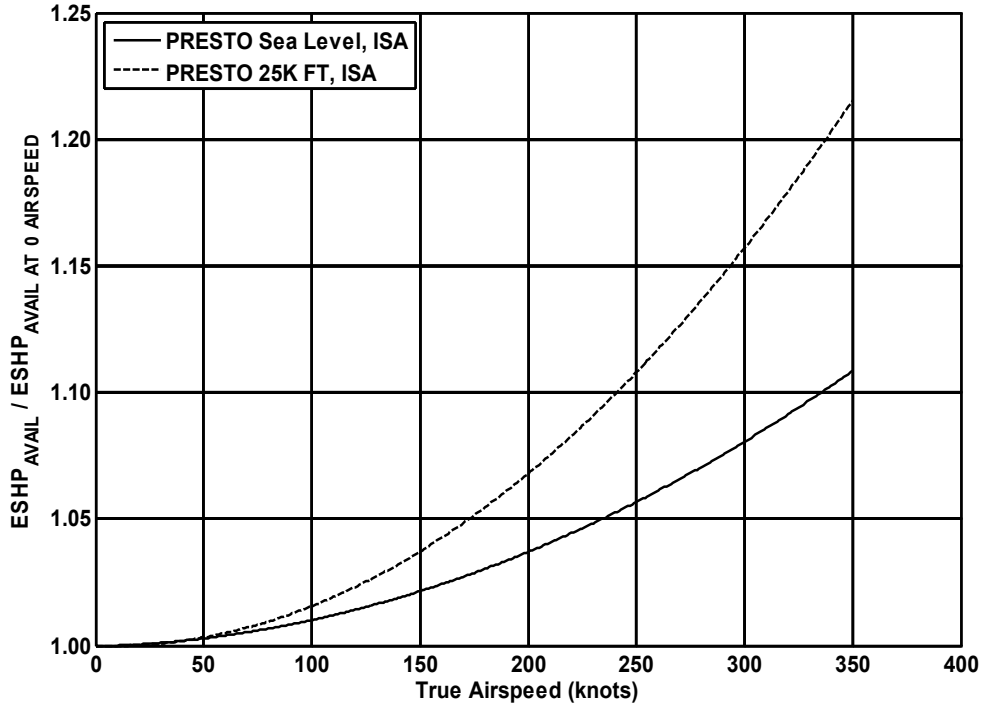

Figure 2-26. Effect of true airspeed on power available.

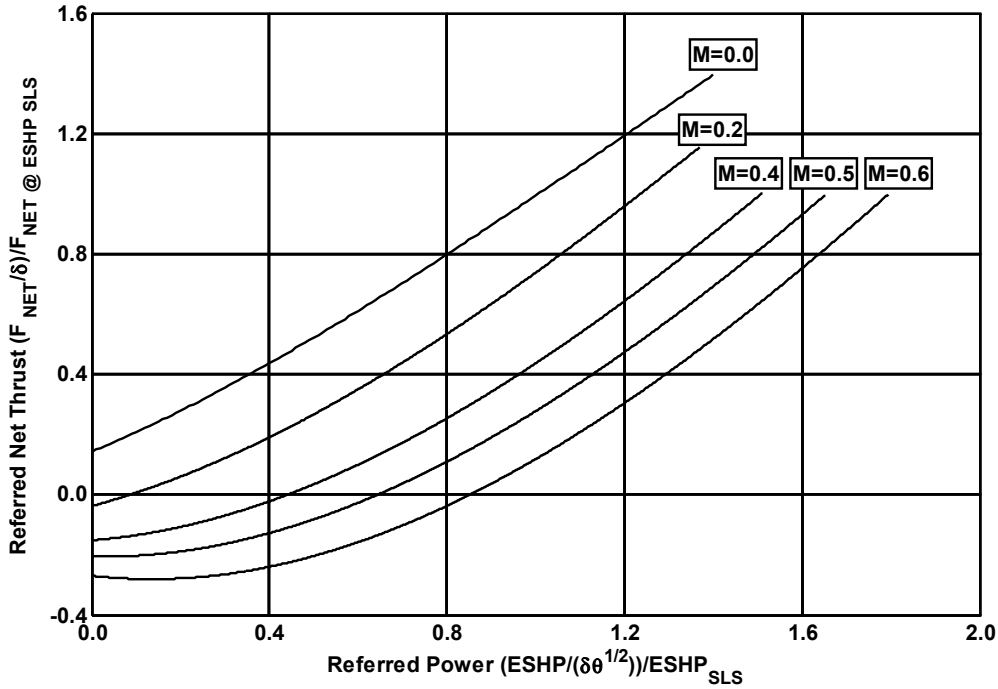

Figure 2-27. CTR30 normalized net nacelle thrust.

2.5.5 Aerodynamics

The aerodynamic characteristics of the CTR30 design were developed by applying corrections to V-22 aerodynamics. The aerodynamic characteristics of the V-22 are well understood and substantiated by flight test.

The aerodynamic characteristics of the rotor are similar to those of the V-22; however, corrections were made for the effect of changing the number of blades per rotor from three to four. The greatest impact in hover was the effect of an increase in solidity. The greatest impact in cruise was the higher hub drag, again due to solidity, which is essentially independent of rpm.

A significant change occurred in the airframe aerodynamics due to a reduction in drag. This was mostly the result of the lack of an aft ramp requirement, changes in the landing gear sponsons, the use of a T-tail empennage configuration, and the removal of military-related excrescences. The resultant incompressible equivalent flat plate drag area of the CTR30 configuration was 23.4 square feet.

For PRESTO analysis the key aerodynamic characteristics required to calculate performance are airframe maximum lift coefficient, the airframe drag polar, rotor aerodynamics, and the effect of compressibility. In constructing the drag polar, the induced drag was assumed to be unchanged by the configuration modifications. The maximum lift coefficient was also assumed to be the same. Only the minimum drag of the polar was corrected. Rotor and airframe compressibility effects as a function of Mach number were unchanged.

There was also a change in nacelle drag because of the installation of the new VAATE technology engine. This was primarily associated with changes in the cooling flows which were book kept in the nacelle net thrust and not in airframe drag.

2.5.6 Design Process Discussion

The CTR30 aircraft was treated as an aircraft modification program. This configuration uses as many V-22 components as possible, including the rotor blade, drive system, and wing. Consequently, they were not resized. The fuselage, empennage, and engines were completely new designs. The rotors resulted in a hybrid design as a consequence of the noise requirements in section 2.2.4. The nacelles were modified into a commercial configuration. The fuel system capacity and engine were the primary variables in terms of sizing.

The fuselage and empennage were completely replaced. As a consequence the wing folding mechanism was removed. The wing incidence was set at 3 degrees (leading edge up) to improve fuselage attitude at the high cruise altitudes of this configuration. The fuselage was sized by cabin requirements (see section 2.5.2) and did not vary once the layout was completed. A T-tail configuration was selected for the empennage sized to meet the static stability requirements in section 2.5.1, Design Requirements.

The hover rpm was reduced to meet the Stage 3 noise requirements shown in figure 2-6. Consequently, the rotor system was changed from a three-bladed gimbaled rotor to a four-bladed gimbaled rotor to compensate for the reduced tip speed. The geometric and aerodynamic characteristics of the blades are the same as the V-22 with the exception that blade fold has been removed. One goal in a modification program would be to keep as many of the blade tools as possible. The potential impact that was not evaluated was with respect to blade dynamics. A cursory assessment indicated that a redesign of the blade properties could actually reduce weight empty.

The fuel capacity of this configuration was set at 7,000 lbs. The initial goal was to have sufficient fuel on board for a 1,000-nmi range with a maximum payload of 30 passengers. However, to achieve the range goal would have required cruising at a higher wing loading. The higher wing loading would have resulted in a reduced buffet-free boundary and was not considered as an option. The fuel system used the full capacity of the wings outboard of the wing/body junction; however, this was not sufficient fuel capacity so additional fuel was required to be carried in the sponsons.

The design went through several iterations in an attempt to meet the initial range goal shown in figure 2-2. PRESTO was used to conduct this partial synthesis to address the changes noted above. The takeoff condition was 5k/ISA+20°C.

2.5.7 Results

The following sections present the results of the CTR30 design process.

2.5.7.1 Design Description

A summary of the CTR30 design characteristics is provided in table 2-6. New design features evolving from this study are reported, as well as any of the characteristics that are inherently V-22 but also in the public domain (ref. 17).

2.5.7.2 Three-View Drawings

Figures 2-28 and 2-29 respectively present three-view drawings of the CTR30 configuration in airplane mode and helicopter mode.

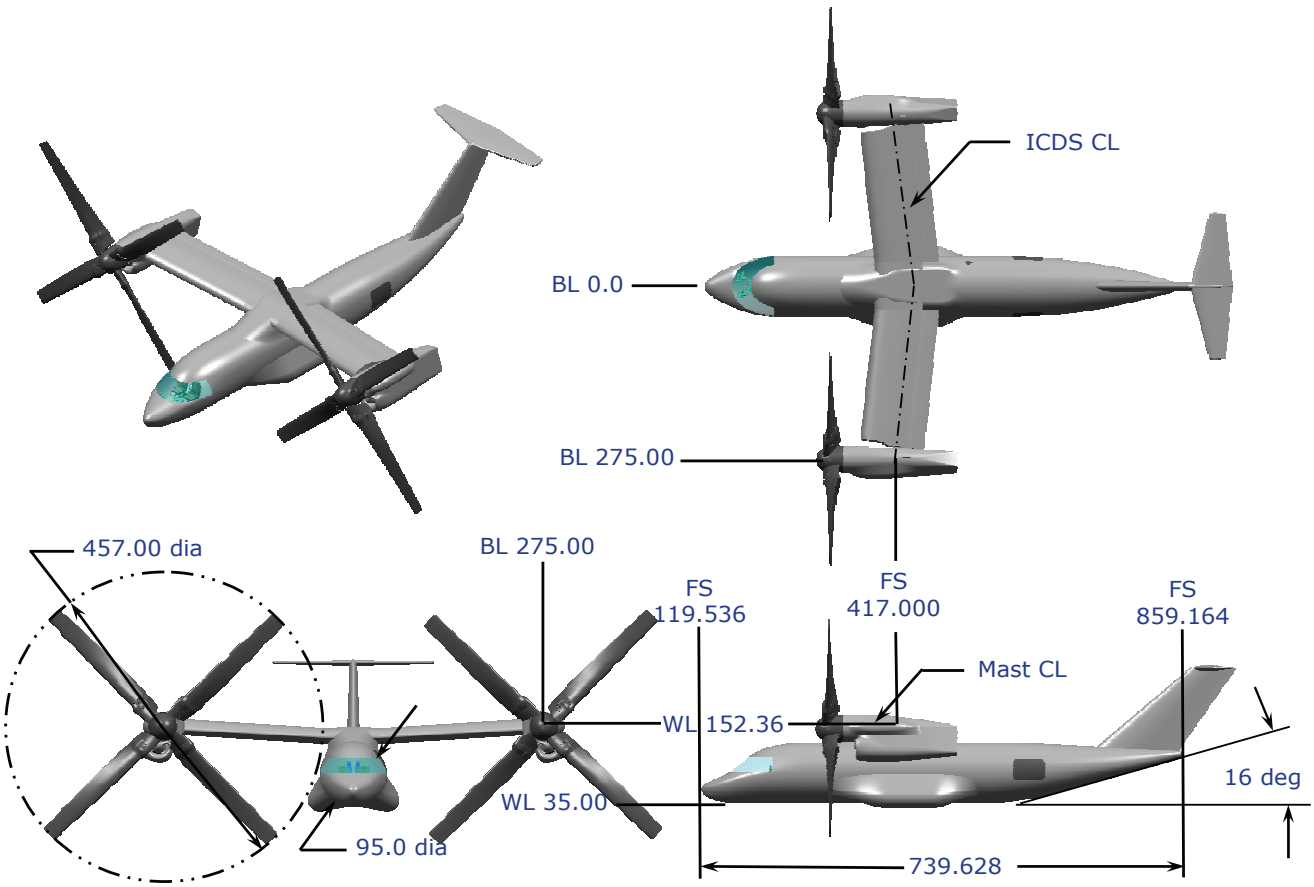

Figure 2-28. Three-view drawing of the CTR30 configuration in airplane mode.

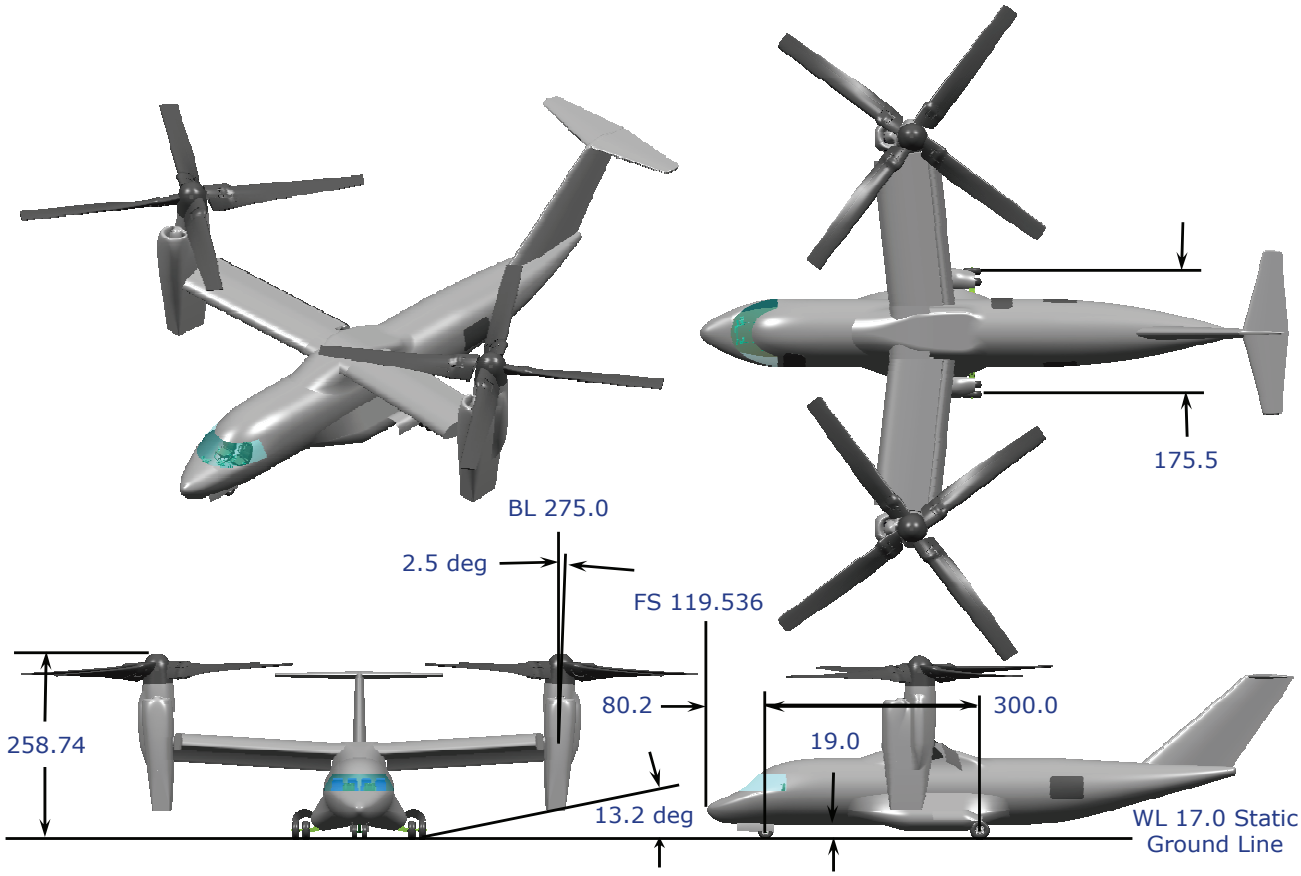

Figure 2-29. Three-view drawing of the CTR30 configuration in helicopter mode.

2.5.7.3 Performance Characteristics

This section provides aircraft and mission performance data that are pertinent to this study. Figures 2-30, 2-31, and 2-32 respectively provide a takeoff ceiling, speed-altitude envelope, and payload-range data for ISA and ISA+20°C ambient conditions.

The CTR30 has a full passenger STO takeoff capability at 5k/ISA+20°C. The speed-altitude envelope shown in figure 2-31 is at the maximum takeoff gross weight of 46,430 lbs. Maximum true airspeed capability at 100-percent MCP is 333 knots. At the operational ceiling of 25,000 feet, the long-range cruise speed is 287 KTAS. Based on the NextGen mission profile from section 2.1.3, the CTR30 long-range cruise speed varies between 275 and 285 knots.

Figure 2-32 shows that the CTR30 range capability using a 5k/ISA+20°C STO takeoff is 804 nmi. The original goal was not achieved; however, the fallout range capability coupled with the cruise speed appears to be competitive with performance in the literature.

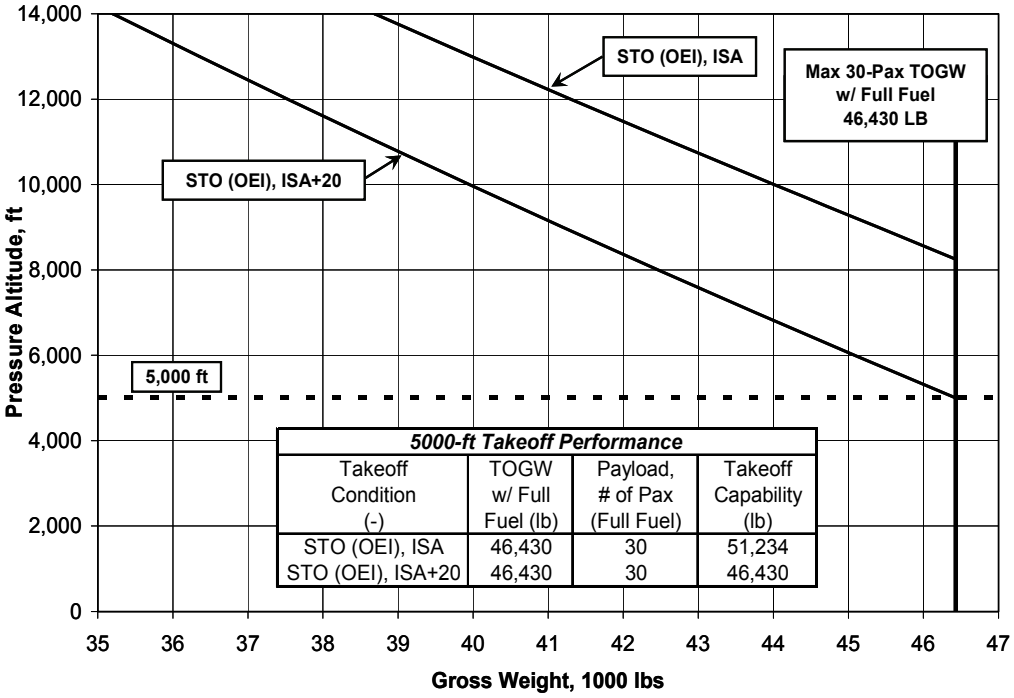

5000-ft Takeoff Performance			
Takeoff Condition (-)	TOGW w/ Full Fuel (lb)	Payload, # of Pax (Full Fuel)	Takeoff Capability (lb)
STO (OEI), ISA	46,430	30	51,234
STO (OEI), ISA+20	46,430	30	46,430

Figure 2-30. CTR30 OEI STO hover ceiling, ISA and ISA+20°C.

Figure 2-31. CTR30 partial speed-altitude envelope, ISA.

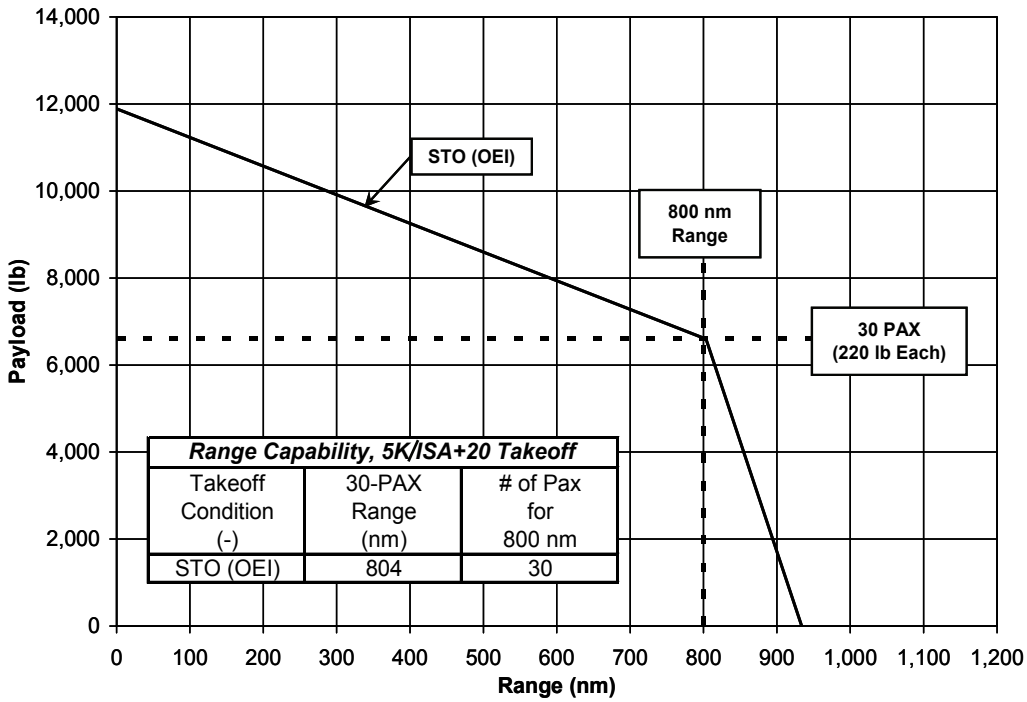

Figure 2-32. CTR30 payload-range curve, ISA.

2.6 120-Passenger CTR (CTR120)

The CTR120 is the result of a full synthesis. It was designed to meet the NextGen goals defined in section 2.1.2. Advanced technology projected to be available by the year 2017 was applied to the entire aircraft. The final design solution is the result of several trade studies conducted using the design synthesis branch of the PRESTO program.

2.6.1 Design Requirements

The initial set of design requirements listed in table 2-7 was selected by the SAIC/NASA NextGen study team. Table 2-7 includes the initial set of requirements and the final set that evolved during the study. Some requirements were a fallout and were noted as such; for example, tip speed, design disk loading, and wing loading. Others were specified as targets and changes to final values were noted; e.g., cruise altitude and cruise speed. Other requirements were changed to reduce design gross weight; e.g., maximum payload and fuel capacity.

Empennage sizing was based on a static stability requirement only. The horizontal tail sizing requirement was based on a static stability margin of 5 percent. Vertical tail sizing was based on a requirement for neutral directional stability. These requirements are the same as those for the CTR10 as discussed in section 2.5.1, Design Requirements.

TABLE 2-7. CTR120 DESIGN REQUIREMENTS

Requirements	Initial	Final
Sizing Details		
Service entry date	2025	unchanged
Design start date (technology date)	2017	unchanged
Payload	26400	unchanged
- Number of pax	120	unchanged
- Weight per pax, lb	220	unchanged
Crew		
- Number of crew	not specified	5
- Weight per crew member	not specified	200
Max Payload	32000	26400
Range, nm	1500	1200
Design speed, ktas	350	345
- Power setting, % MCP	< or = 100% MCP	100% MCP
- Altitude, ft	30000	27500
- Ambient, nd	ISA	unchanged
Rotor tip speed, fps		
- Hover	To be Defined	650
- Cruise	Sizing Fall-out	455
Fuel capacity	mission fuel + 5%	mission fuel
Design Mission Profile		
Takeoff (warm-up & taxi)	5-min; 5k/ISA+20; 100% Takeoff Power	unchanged
HOGE	2-min; 5k/ISA+20; 100% MRP; OEI capable	unchanged
Climb	@ 100% MCP	unchanged
Cruise	@ Vbr; 30000; ISA	@ Vmcp; 27500; ISA
Descend (no distance credit)	n/a	unchanged
HOGE	1-min; 5k/ISA+20 deg; OEI capable	unchanged
IFR Reserve		
- 30 nm	5k/ISA+20	unchanged
- 30 min @ Vbr	10k/ISA	unchanged
Design		
Wing Loading, psf	Sizing Fall-out	95.2
Disk Loading, psf	Sizing Fall-out	18.0
Engine		
- Technology level	2017	2017 (VAATE)
- Takeoff rating	5-min Takeoff rating	10-min (MRP)
MCP Transmission sizing	5k/ISA+20 deg C HOGE @ TOGW and 100%MCP	unchanged
Seat Pitch, in	32	see next two entries
Seat Pitch (first class), in	not specified	38
Seat Pitch (coach), in	not specified	32
Seating, nd	4x3 & 6x18	unchanged
Rotor radius constraint	Fall-out	unchanged
Blade loading, nd	Good banked turn and 10k/isa hover at DGW	unchanged
Blade fold constraint	No blade fold	unchanged
Weights		
Weight for sizing geometry (DGW)	Mission takeoff gw	unchanged
Structural design gross weight	= DGW	unchanged
Design load factor		
- airplane mode	2.5 g's minimum	unchanged
- helicopter mode	2.0 g's minimum	unchanged
- Definition	@ DGW	unchanged

The fuselage is designed for civil passenger transport. As such, requirements in terms of emergency exits, galley, lavatories, and number of attendants are set by FAA rules. The details are described in section 2.6.2, Cabin Layout. The cabin is pressurized to operate at a maximum altitude of 30,000 feet.

2.6.2 Cabin Layout

The CTR120 cabin is divided into first and coach classes. There is seating for 12 in first class and 108 in coach. There are three rows of four seats across in first class. The seat pitch is 38 inches and the width is 28 inches. Economy class consists of 18 rows of 6 seats across. The seat pitch is 32 inches and the seat width is 21 inches. Per FAR part 25.817, this is the maximum seating across with only one aisle. The width of the aisle is 20 inches per FAR part 25.815.

The cabin provides additional seats for three flight attendants, which is the number of attendants required per FAR part 121.391. The cabin has one lavatory in first class and two in coach. There is also a forward and aft galley. There are two stowage closets and overhead stowage in the cabin.

The cabin was designed to meet FAR part 25.807 emergency egress requirements. The cabin includes 34- x 72-inch forward and aft entry doors, two 34- x 72-inch service doors and two 20- x 38-inch emergency exits. Figure 2-33 shows the current cabin arrangement.

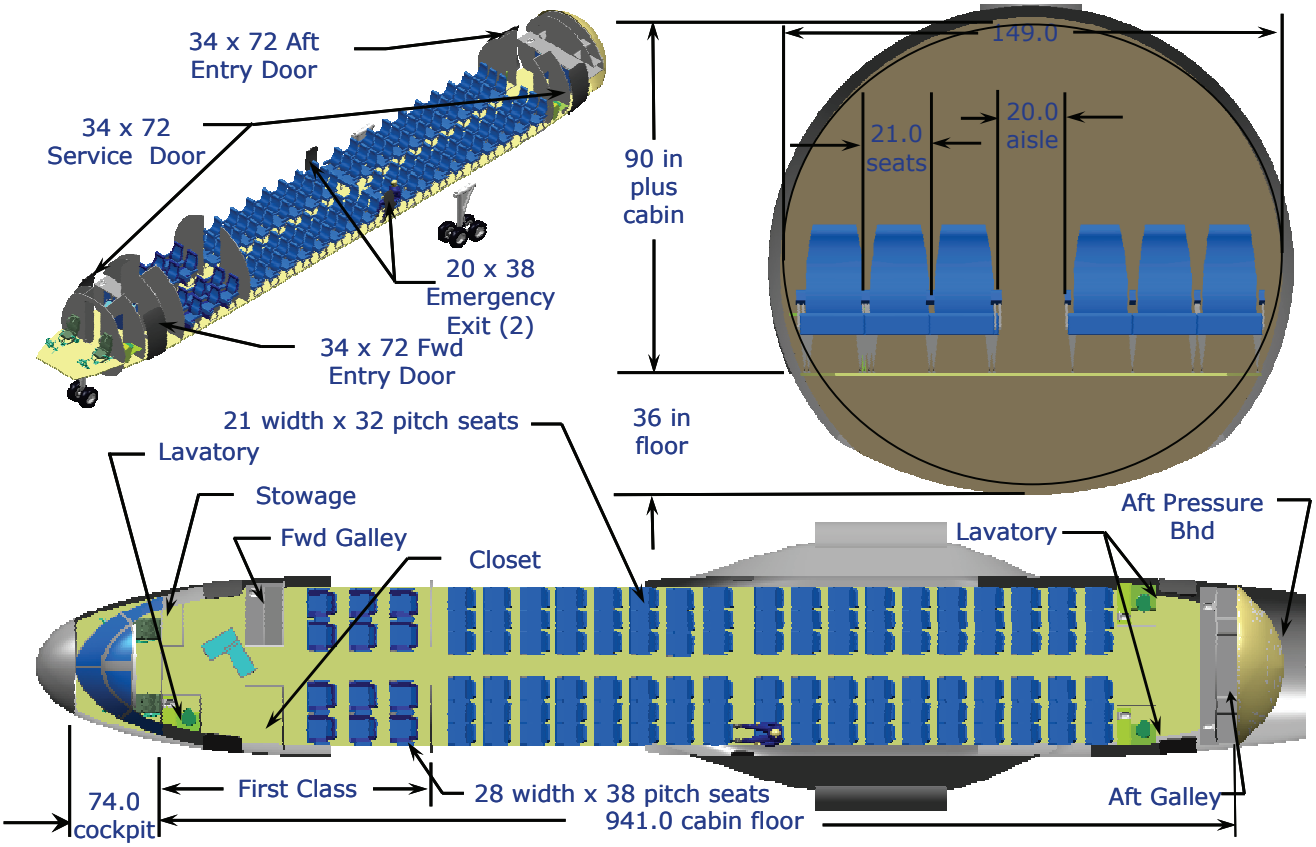

Figure 2-33. The cabin layout of the CTR120 configuration.

2.6.3 Engine Performance

The engine data provided by the Propulsion group is the same as that applied to the CTR30 configuration, which was based on VAATE technology. Normalized fuel flow, effect of airspeed (ram recovery), and net nacelle thrust data used as input into the PRESTO model are the same as those shown in figures 2-25 thru 2-27. As it turns out, the CTR30 and CTR120 engine ratings were within 2 percent of each other with the only difference being the number of engines.

A fixed-engine configuration was considered; however, the additional complexity of two engines per nacelle was beyond the scope of this study and consequently a conventional tiltrotor tilting engine was used. One of the main considerations for such a study would have to be recovery of lost residual thrust in hover, which can be on the order of 2 percent of the takeoff gross weight.

2.6.4 Weights

Bell Helicopter parametric weight equations are an integral part of the PRESTO design synthesis tool. As such, only those inputs that are required by PRESTO are provided by the Weights group. Technology factors are applied that reflect the 2017 technology developed under the JHL study contract (ref. 6). Because the CTR120 aircraft is on the order of 2–3 times heavier than the largest production tiltrotor, it was essential to account for scale effects. Previously evaluated (ref. 6) scale effects are inherently built into the PRESTO weights methodology. The weights are based on a maximum cruise altitude for pressurization of 31,800 feet.

Passenger and crew weights were the same as defined for the CTR10 in section 2.4.4, Weights. An additional allocation of 70 lbs of operating load associated with the crew was included. A weight statement for the final CTR120 design solution can be found in section 2.6.7.1, Design Description, table 2-9. The data is presented in the Industry Standard Group Weight Statement format.

2.6.5 Aerodynamics

Since the CTR120 design is a full synthesis, the aerodynamic analysis is based on the modeling capability of the PRESTO program. The aerodynamic models address hover and forward-flight isolated rotor power required, hover performance losses due to rotor/airframe interaction, rotor-induced download in hover, rotor compressibility, and the airframe drag polar.

PRESTO uses physics-based models that are calibrated by detailed design codes. The calibration was accomplished during the JHL study (ref. 6) and only repeated for this study as required. The primary programs used to calibrate rotorcraft performance are the Lifting Surface Aerodynamics and Performance Analysis of Rotors in Axial Flight (LSAF) and Comprehensive Program for Theoretical Evaluation of Rotorcraft (COPTER) programs. Computational Fluid Dynamics (CFD) programs were used primarily to evaluate aerodynamic characteristics of the airframe.

The rotor geometry is a hybrid of the V-22 blade and a previously designed large-scale rotor.[6] The planform taper of the V-22 blade was retained; however, to enhance cruise performance a thinner blade in terms of thickness-to-chord (t/c) ratio was selected. Because the previous large-scale rotor design is comparable in size to the CTR120 rotor, which was substantiated as feasible by analysis and used a thinner blade, its t/c distribution was selected. The change in t/c resulted in improved cruise performance and a new family of airfoils. The airfoils were scaled[6] from the V-22 defining sections corresponding to nondimensional radial stations at 0.25, 0.50, 0.75, and 1.00. These airfoil tables were used to define the CTR120 rotor performance.

PRESTO uses a simplified rotor performance model with equivalent compressibility corrections applied at the rotor performance level. The compressibility characteristics of the individual airfoils are not used by

PRESTO. Therefore, rotor compressibility must be calibrated off-line. This was done using the LSAF program. It was determined that the current PRESTO model was a good representation of the compressibility effects. To improve the rotor compressibility characteristics would require additional airfoil design work.

The vertical airframe drag in hover, or download, is based on an empirical model developed over the years under Bell Independent Research and Development programs. This methodology has been substantiated indirectly on two different flight test aircraft and directly for one configuration during a full-span powered wind tunnel test of the BA609 configuration.

The forward flight airframe aerodynamic characteristics of lift and drag were developed using CFD and handbook drag estimation methods. The maximum incompressible lift coefficient was defined as 1.85 based on CFD analysis of a similar configuration. The PRESTO model of the impact of Mach number on maximum lift coefficient was also confirmed with CFD.

The equivalent flat plate drag was calculated off-line using a Bell handbook method for conceptual designs. This method has been correlated against four flying tiltrotors. In the conceptual phase excrescence drag is based on historical values. As the design progresses more detailed drag estimates can be made. However, not until an aircraft is built can final hardware differences relative to the original paper design be identified. These differences are then evaluated to update the aircraft drag database.

A correlation curve has been developed to illustrate the accuracy range of the handbook method. Scales have been removed because of the proprietary and sensitive nature of the data. The results are shown in figure 2-34.

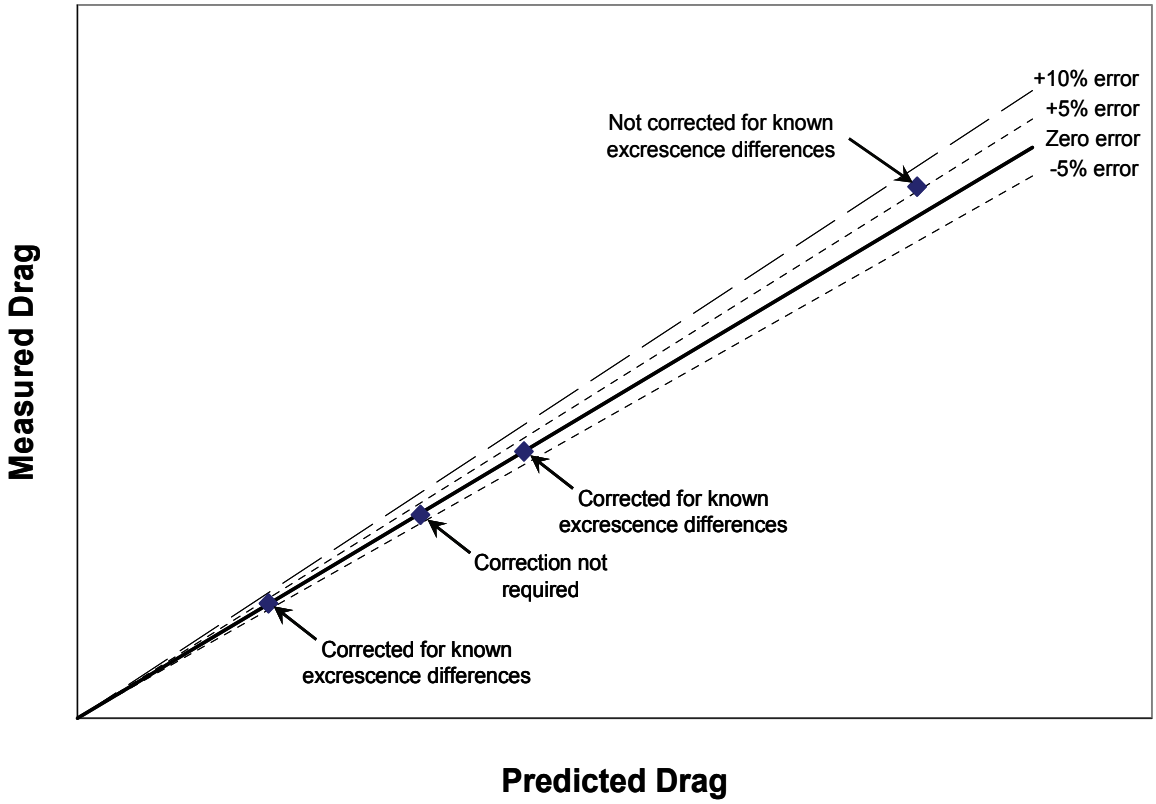

Figure 2-34. Bell tiltrotor handbook drag methodology correlation.

This design used a very clean fuselage and a wing-thickness-to-chord ratio (t/c) of 18 percent. Although the t/c is high, the drag divergence Mach (Mdd) number for the airframe was set to a goal of 0.6. In a detailed design certain constraints would have to be addressed such as sufficient volume for interconnect shafts and conversion spindles; however, it may be possible to achieve the Mdd goal of 0.6.

2.6.6 Design Process Discussion and Trade Studies

A generic summary of the design process used in this study was shown in figure 2-5 in section 2.2.3, Design Methodology. This involves the development of PRESTO inputs, conducting trades studies to define specific characteristics such as design speed, altitude, and disk loading, and conducting the final synthesis.

Before the CTR120 design synthesis was started a benchmark configuration was developed. This configuration was used to support drag and isolated rotor performance calibration. The NASA 120-passenger large civilian tiltrotor aircraft (LCTR) design (ref. 6) was used as the benchmark. It also served to ensure that no unusual PRESTO design convergence problems existed. The LCTR weight empty fraction, mission profile, rated engine SFC, and equivalent flat plate drag area were used to synthesize the benchmark case. The result was a configuration that overall matched the LCTR in takeoff gross weight and geometry within 2 percent of the NASA design.

The benchmark geometry from PRESTO was used as input for the analysis of drag and isolated rotor performance. A Bell handbook method for estimating drag for conceptual designs was used to predict clean component drag. The resultant drag values were then reduced to equivalent skin friction drag coefficients using the calculated wetted areas from PRESTO for the benchmark case. This is a simplified drag method for synthesis, which was recalibrated for the final solution. Excrescence drag for this design was developed by evaluating existing aircraft; correcting for those items not on the CTR120 configuration, and then converting the result into a percentage of the clean component drag. This resulted in an excrescence drag of 10 percent applied to the CTR120 design.

Isolated rotor data for the CTR120 design was based on predictions using the Bell Helicopter prescribed wake analysis, LSAF. For this study LSAF was calibrated to measured data from a 25-foot rotor test. The data was obtained during a test at the NASA Ames Outdoor Aerodynamic Research Facility (OARF). A conservative approach was used with respect to the higher blade loadings. This was accomplished by adjusting the LSAF prescribed wake parameters to match the OARF data as closely as possible without applying stall delay to the rotor airfoil data tables. The resultant correlation is shown in figure 2-35.

The rotor configuration used for the CTR120 was based on previous design work (ref. 6) that determined the best solution was a six-bladed stiff in-plane rotor. The PRESTO parametric analysis confirmed that six blades was the most effective solution for minimizing design gross weight and still maintaining a blade aspect ratio in Bell's range of experience. The trend of decreasing gross weight with increased number of blades, while maintaining blade aspect ratio, was very similar to that shown in previous NASA work (ref. 1).

Using the resultant wake parameters from the LSAF calibration and six blades, isolated rotor performance was predicted based on the new airfoil sections discussed in section 2.6.5. Although the correlation of LSAF was with test data for a three-bladed rotor, the trend for number of blades and solidity was confirmed through LSAF correlation with test data for three- and four-bladed rotors of different solidity obtained under a Bell Independent Research and Development Program. The resultant nondimensional isolated rotor performance was corrected by PRESTO for the effect of rotor-airframe aerodynamic interactions.

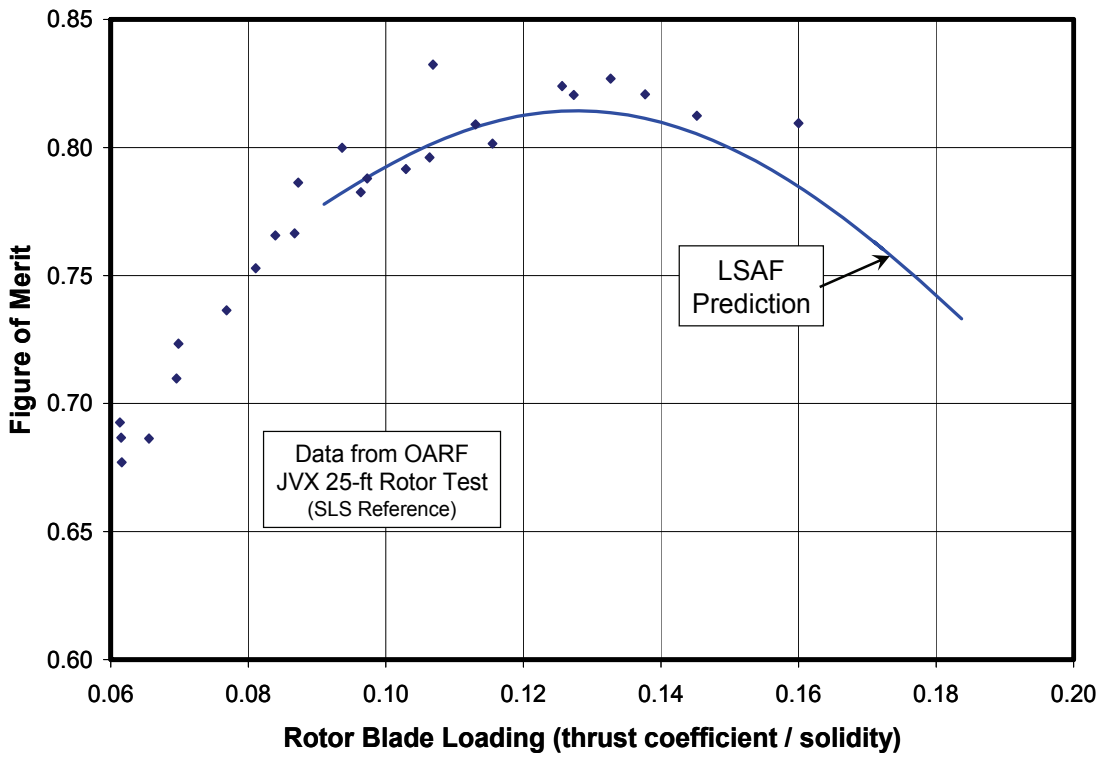

Figure 2-35. LSAF correlation with 25-foot JVX rotor data from the NASA Ames OARF.

A PRESTO run was made to check the weights methodology. The input weights file used the factors representative of 2017 technology. The results of the run were then checked by the Weights group using the off-line equations that PRESTO weights are based on.

Several trade studies were conducted to support the final design synthesis. They included the effect of disk loading, cruise altitude, cruise speed, and design range. For these trade studies several design and configuration characteristics were established. They included:

1) Wing aspect ratio = 6.5 (a balance between wing structural weight and design mission fuel).
2) No wing extensions (benefits when trading aerodynamic end-plating and aspect ratio have been shown to reduce fuel required; however, the development of a structural design solution to assess the impact on empty weight was beyond the scope of this study).
3) Wing t/c set to 18 percent (see section 2.2.6.1, Structural and Aeromechanical Stability Constraints).
4) Set the airplane mode rotor-to-fuselage clearance at 18 inches (this is a soft requirement, not the result of an analysis).
5) No variable speed transmission (using state-of-the art drive system design to support the hypothetical start date of 2017).
6) Define cruise rpm as 70 percent of takeoff rpm.
7) Number of blades, 6.

The selection of a wing aspect ratio of 6.5 was based on the results from a previous study (ref. 6). The only time that aspect ratio changed during the trade studies was when the minimum gap between the rotor in airplane mode and the side of the fuselage was less than 18 inches.

Lowering the cruise rpm to 70 percent of hover rpm is guided, in part, by results from other design studies; doing so imparts significant improvements in cruise performance relative to tiltrotors currently flying. This raises other issues that need to be addressed, however, including accessories that are directly operated off of the drive system. The PRESTO calculation provided in figure 2-36 shows the impact of the ratio of cruise rpm to hover rpm on prop efficiency and the impact of compressibility. A 5.7-percent gain in prop efficiency was achieved by reducing cruise rpm from 84 percent to 70 percent of hover rpm.

For this study the engine fuel flow was based on the cruise rpm of the cycle decks that were available. This may be conservative; however, it should not be assumed that operating at low rpm in cruise automatically means poor fuel efficiency without a variable-speed transmission. In a detailed design the engine manufacturer would be required to provide a balance between fuel efficiency and power available. Therefore, the highest fuel efficiency would not necessarily occur at 100-percent rpm but at something closer to the cruise rpm.

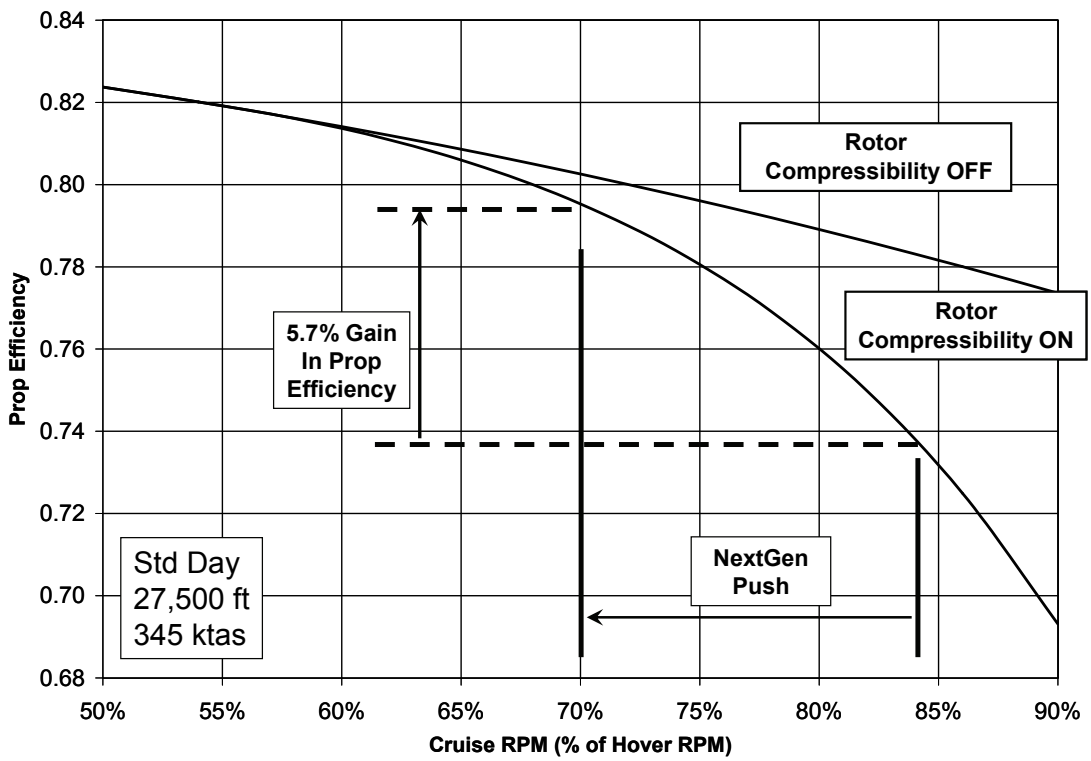

Figure 2-36. Impact of rotor rpm on cruise propulsive efficiency.

The final input required in PRESTO corresponds to the drive system and accessory losses. PRESTO uses loss equations when data is available in the proper format. Since it is preferable to use loss equations, rather than losses as a percent of power required, the approach was to scale losses from known aircraft.

The first major step in the design synthesis process is the sizing of the engine and transmission. For this study three sizing conditions were specified: 1) an All Engines Operating (AEO) hover at 100-percent MRP, 2) an OEI transport category takeoff at 100-percent OEI power, and 3) a maximum continuous cruise speed at 100-percent MCP. The ambient condition for the takeoff sizing point was 5k/ISA+20°C. The cruise condition was for a standard atmosphere and the selected cruise altitude and cruise speed. Each condition was evaluated at the design gross weight. For the CTR120 design the transmission was sized by the takeoff condition.

For the VTO transport category takeoff (previously known as a Cat A takeoff) the aircraft must have sufficient power to fly away or land after losing an engine at the critical "takeoff decision point." It was assumed that during the takeoff the OEI power available was equivalent to 85 percent of the power required to hover at the takeoff weight.

Before the engine and transmission could be sized, however, a trade was conducted to address the impact of OEI power available on aircraft size as a function of disk loading. Although a normalized engine model was developed in terms of lapse rates and the impact of speed, the OEI rating was left as a variable in the rating structure for the study.

The selection of a ratio of OEI power to MCP power combined with other characteristics defines the relationship between a design sized by hover versus one sized by cruise. The approach was to define a power ratio that would then be held constant for all subsequent trade studies. An assessment of several large engine studies, as well as existing engines, showed that power ratios for a 2.5-minute OEI rating relative to MCP can be as high as 1.42, and a 30-second OEI rating as high as 1.72. The power ratio can be increased even further by the use of water/alcohol injection, with power pushes as high as an additional 15 percent. Water/alcohol injection would introduce a weight penalty which could impact decisions regarding the selection of an OEI/MCP power ratio. There is also the issue of a combined 30-second and 2-minute OEI rating and what its effective equivalence is in terms of transport category takeoffs. The subject of engine rating requires much further study and is complex in terms of defining the relationship to takeoff performance.

The results are shown in figure 2-37 for a range of power ratios. This trade study was based on a synthesis using the initial goals of a 30,000-foot cruise altitude, 350-knots cruise speed, and 1,500-nmi range. This figure has been normalized since it was a preliminary study and did not reflect the final weights.

Figure 2-37 shows that the minimum design gross weight increases as the OEI/MCP ratio decreases. This is expected since the lower ratio means that a larger engine is required for the same takeoff capability. The trend is highly nonlinear with diminishing returns between ratios of 1.4 and 1.5. The minimum gross weight points in figure 2-37 correspond closely to the demarcation between a cruise design (lower disk loadings) and a hover design (higher disk loadings) in terms of power required.

There is also a relationship between design disk loading and blade aspect ratio to be considered for a given number of blades. The results are shown in figure 2-38 and are based on a rotor with six blades. Current design experience at Bell includes a range of blade aspect ratio between 9 and 14. This range corresponds to OEI/MCP ratios between 1.4 and 1.5.

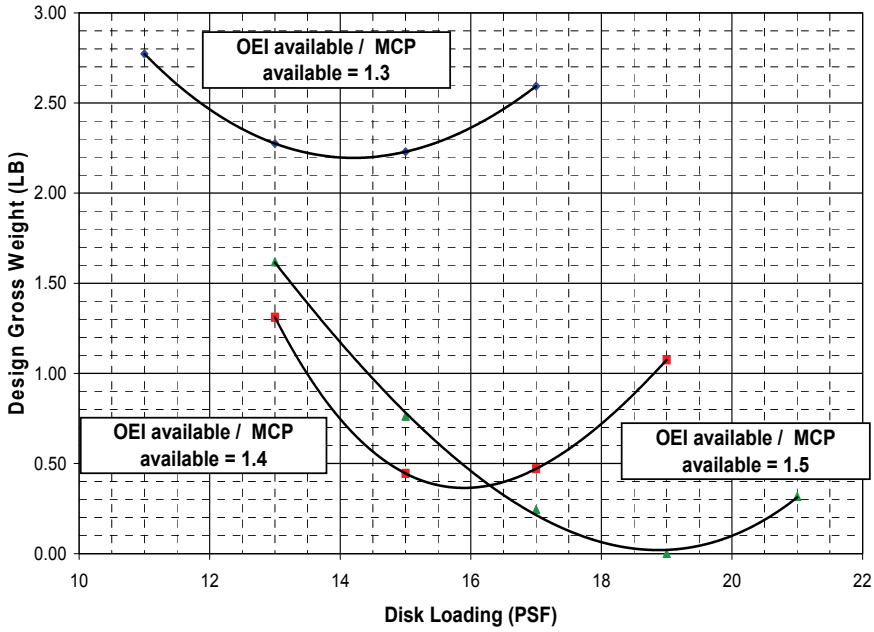

Figure 2-37. Sensitivity of design gross weight and hover/cruise balance point.

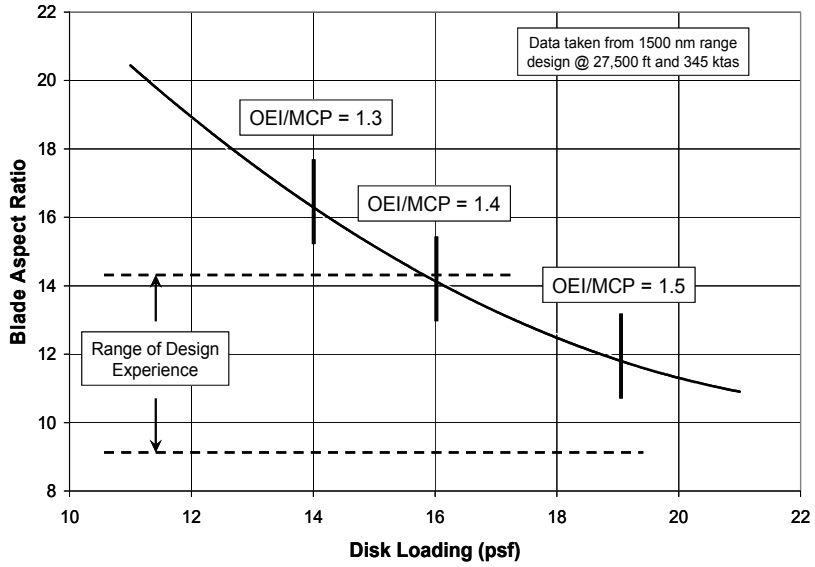

Figure 2-38. Relationship between disk loading and blade aspect ratio.

An OEI/MCP ratio of 1.5 was selected for the remaining trade studies. This is aggressive; however, it is difficult to determine the exact relationship between this power ratio and a final rating structure that could include combinations of 30-second and 2-minute OEI ratings. It does result in a blade aspect ratio that falls roughly in the middle of Bell's design experience. If, during more advanced design studies, it was found that the OEI/MCP ratio needed to be reduced to 1.4, the impact would be 0.3 percent in design gross weight, 5 percent greater overall aircraft width, and a blade aspect ratio within the current design range experience. A much more detailed analysis would be required to define the final engine rating structure suitable for the takeoff requirements for this study.

With a ratio of 1.5 for OEI to MCP power selected, the next trade study was an evaluation of the relationship between cruise speed, cruise altitude, and disk loading on the design gross weight and engine rating. This was initially conducted for a 1,500-nmi range. Disk loading sweeps were conducted at 25,000-, 27,500-, and 30,000-foot pressure altitude for speeds ranging from 300 to 350 KTAS.

A productivity index was used to evaluate the relative merit of each design point since a cost analysis was beyond the scope of this study. Although the definition is in engineering terms, its derivation (ref. 18) is based on the classical definition in terms of cost.

Productivity Index = (Payload * Range) / ((Weight Empty + Block Fuel) * Block Time)

Costs have changed since this design was originally done, which could result in a different relationship between some of the terms; however, this was not investigated and the relative trends should hold.

The results of this trade study were then combined into one set of data to depict productivity as a function of cruise altitude and speed. The results are shown in figure 2-39. Each point in figure 2-39 corresponds to the disk loading associated with the highest productivity and an aspect ratio of 6.5.

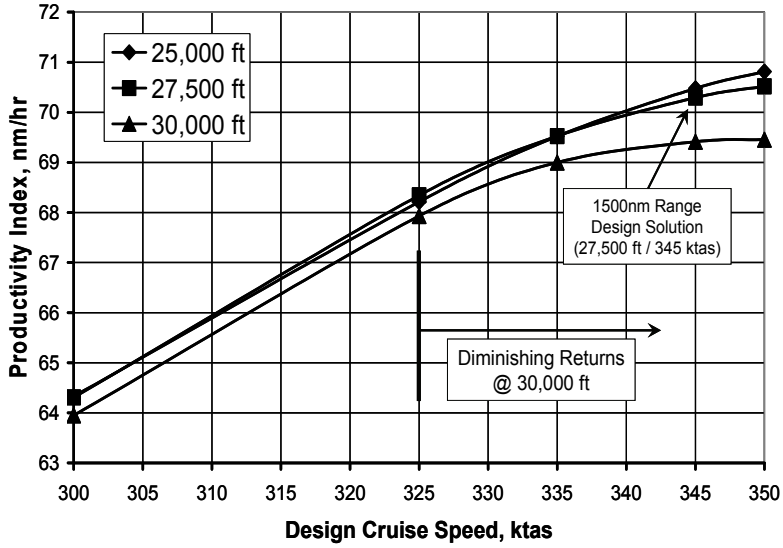

Figure 2-39. Productivity index for CTR120 with a design range of 1,500 nmi.

Figure 2-39 shows that the best productivity can be achieved at altitudes below the 30,000 foot design goal. If, however, other compelling reasons exist for remaining at 30,000 feet, there is the question of whether the design cruise speed should remain at 350 KTAS. There is a significant point of diminishing returns in terms of productivity that begins between 325 and 335 KTAS at 30,000 feet.

The selection of the design solution for a 1,500-nmi-range design was somewhat subjective; however, figure 2-39 does show that a cruise altitude of 27,500 feet tends to yield an overall better design in terms of productivity up to 335 KTAS. The design cruise speed was selected to be 345 knots since it appears to be the point of diminishing returns for productivity at 27,500 feet. The disk loading that corresponds to a 27,500-foot/345-KTAS solution is 18 psf.

There is still an unanswered question with respect to whether there is a minimum altitude below which the CTR120 design would not fit into the NextGen operations. This would require further study, the results of which could push the recommendation of cruising at 27,500 feet up or down.

The previous trade resulted in a conclusion that the original cruise altitude and cruise speed goals stated in table 2-2, section 2.1.2, Mission Goals, should be amended. However, the question of whether the range goal is appropriate is much more elusive. Figure 2-2 in section 2.1.2, Mission Goals, showed a range trend as a function of the number of passengers for turboprops and turbofans. The boundaries of that figure are subjective; however, they suggest that the shortest range required to stay in the fixed-wing class may be on the order of 1,200 nmi. This is the same as the range selected for the NASA 120-passenger LCTR design. However, there are other considerations in a range study including whether the NextGen CTRs are a unique class of aircraft to themselves in terms of market demand, e.g., daily commuter versus longer range overnight. As noted in section 2.1.2, Mission Goals, a range of 500–600 nmi is a competitive range when comparing CTRs to fixed-wing aircraft. There is one other consideration, however, for long legs which could take advantage of the VTOL capability of the CTR— disaster relief.

Therefore, a range trade study was conducted to be inclusive of the 500-nmi competitive range and the 1500-nmi study target to find a rationale for the final CTR120 design goals. This trade included ranges of 500, 800, 1,000, 1,200, and 1,500 nmi to enhance the definition of any possible nonlinearity. The analysis was done at a cruise altitude of 27,500 feet. A disk loading of 18 psf, corresponding to the 1,500-nmi design solution, was held constant for this trade. Although the best disk loading solution varies somewhat with speed, it was not considered to be a factor in evaluating the relative impact of range. The results are shown respectively in figures 2-40 and 2-41 for design gross weight and productivity index.

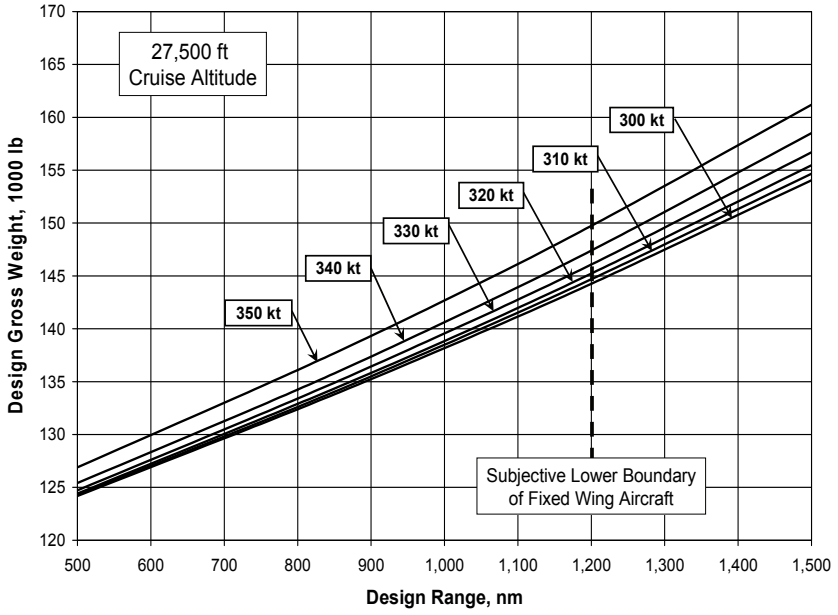

Figure 2-40. Impact of range on design gross weight.

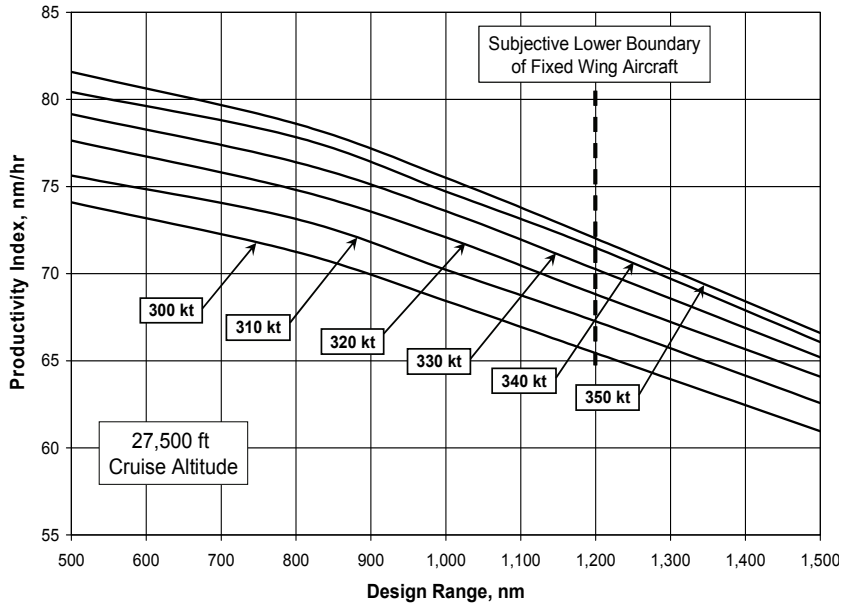

Figure 2-41. Impact of range on productivity index.

From this study it was concluded that reducing the design range increased productivity significantly. There was a tendency for productivity to start to break at approximately 900 nmi; however, at the same time there was no indication that 600 nmi was an optimum. That conclusion probably cannot be drawn from these results because there are other considerations at the lower ranges that have not been accounted for.

The final decision was to reduce the design range from 1,500 nmi to 1,200 nmi but with the following rationale. The change resulted in an 8-percent increase in productivity which would improve the design's competitive position (still remaining within the subjective envelope of fixed-wing aircraft) and maintain long legs for other missions such as disaster relief. One question would be, "Can the approximate 15-percent increase in design gross weight (synonymous with fly-away cost) be justified by increasing the design range from 600 to 1,200 nmi?" An alternative that was not evaluated, but presented in section 2.1.2, was to design to a range of 600 nmi and provide fuel capacity for a 1,200-nmi range at reduced payload.

With the range goal changing to 1,200 nmi, a final trade study, similar to that for 1500 nmi, was conducted to confirm the design altitude, cruise speed, and disk loading for the final design synthesis. The results are presented in figures 2-42 thru 2-44 for a 25,000-foot cruise altitude. Trades at altitudes of 27,500 and 30,000 feet respectively are shown in figures 2-45 thru 2-47 and figures 2-48 thru 2-50.

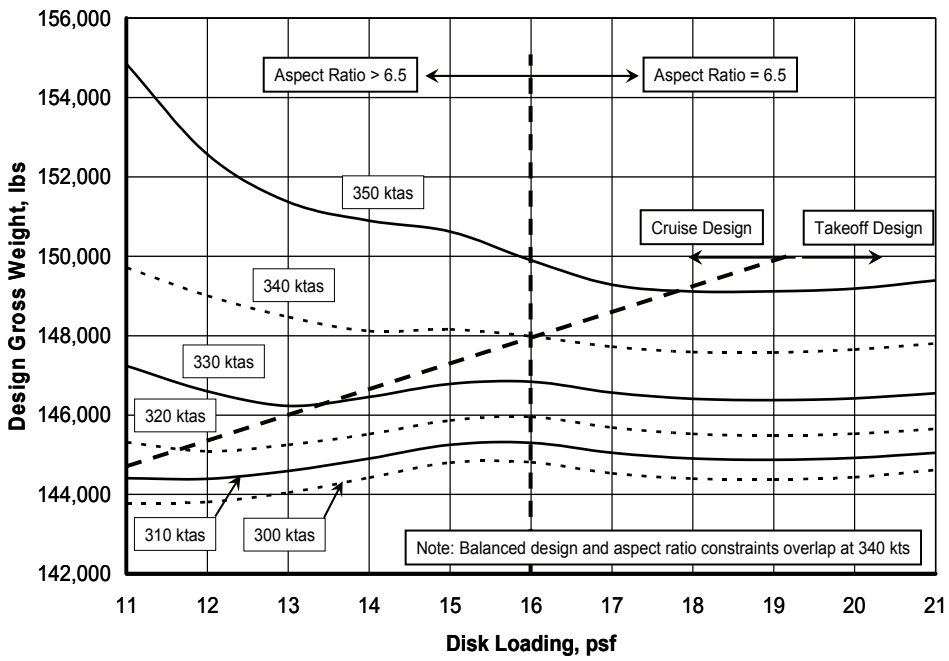

Figure 2-42. Impact of disk loading and design speed on design gross weight (25,000 feet).

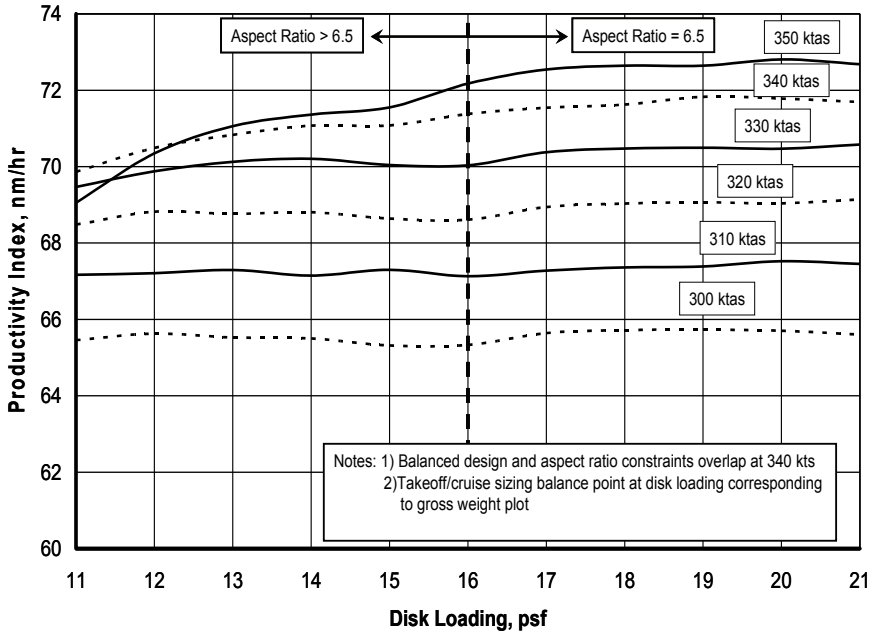

Figure 2-43. Impact of disk loading and design speed on engine size (25,000 feet).

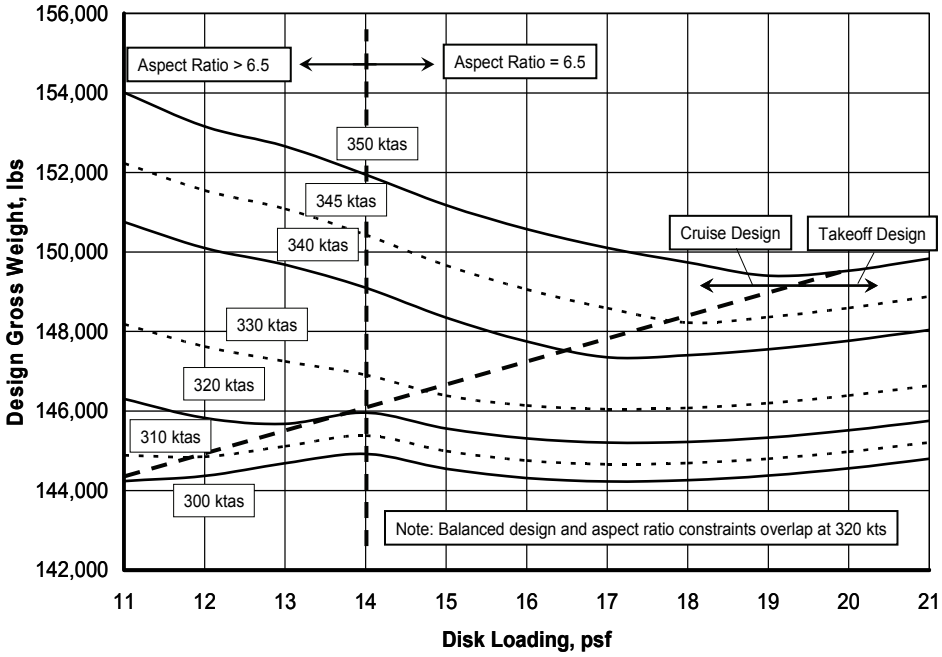

Figure 2-44. Impact of disk loading and design speed on productivity index (25,000 feet).

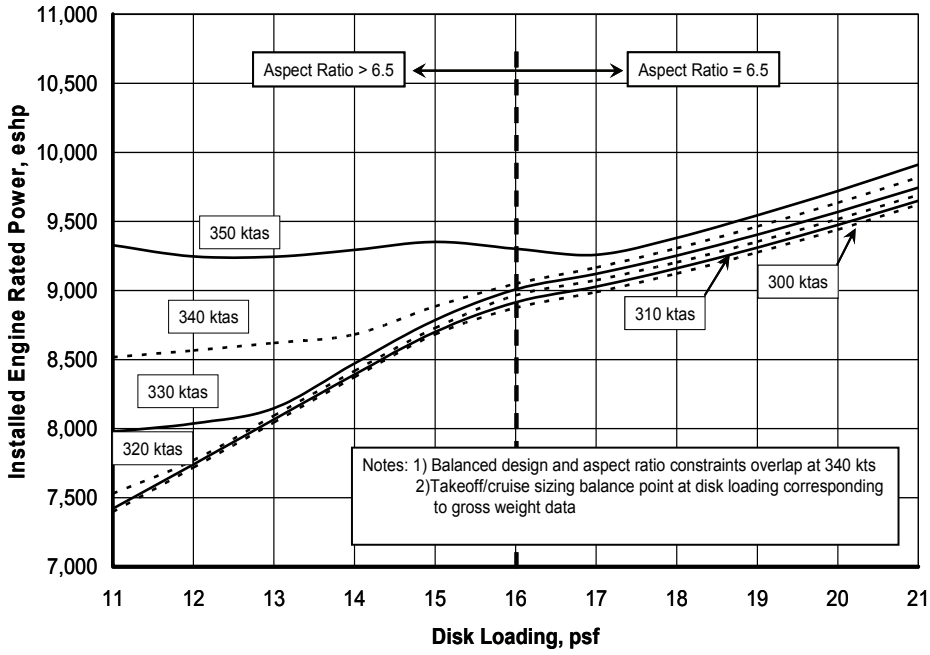

Figure 2-45. Impact of disk loading and design speed on design gross weight (27,500 feet).

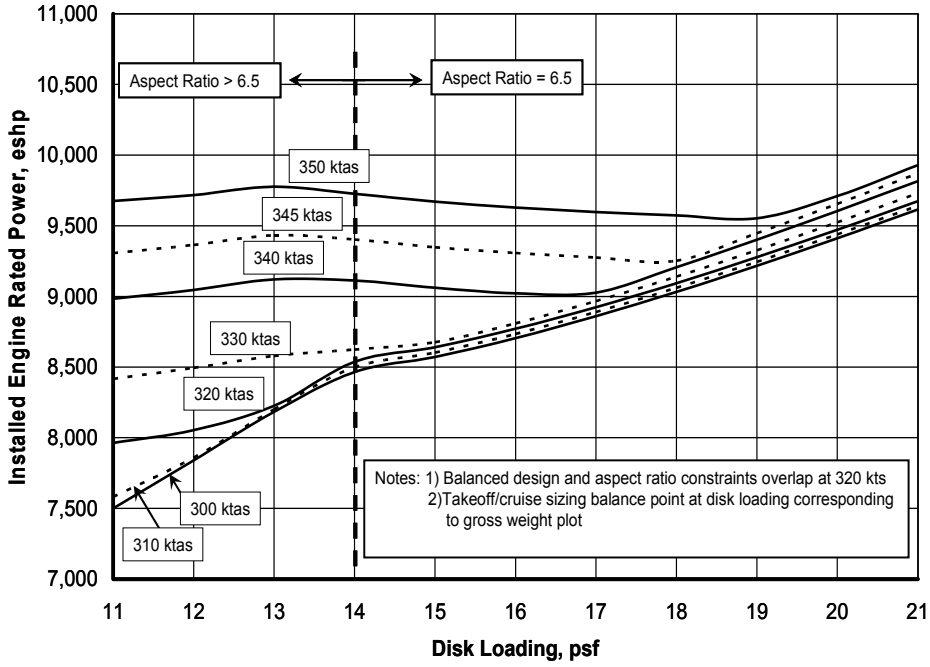

Figure 2-46. Impact of disk loading and design speed on engine size (27,500 feet).

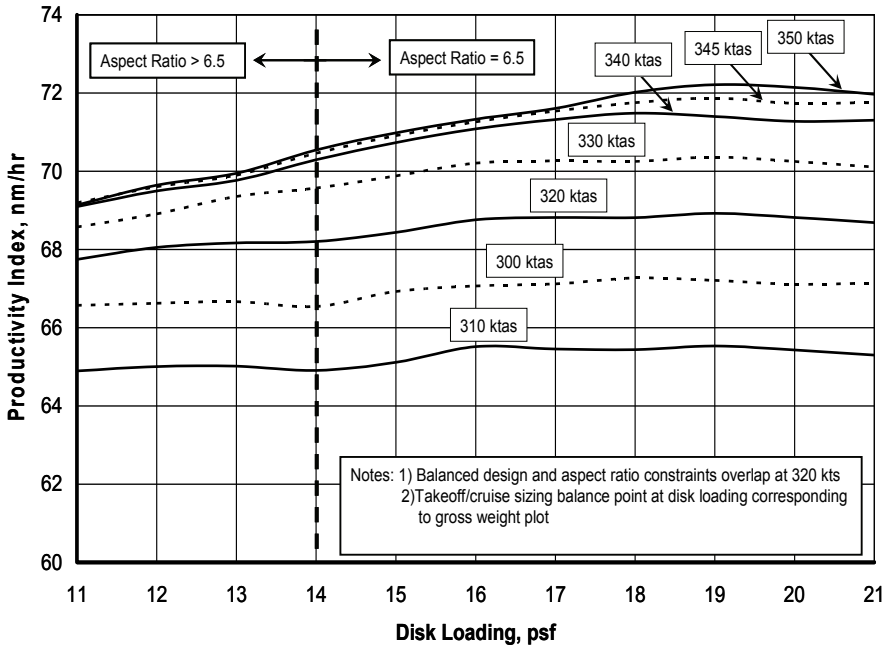

Figure 2-47. Impact of disk loading and design speed on productivity index (27,500 feet).

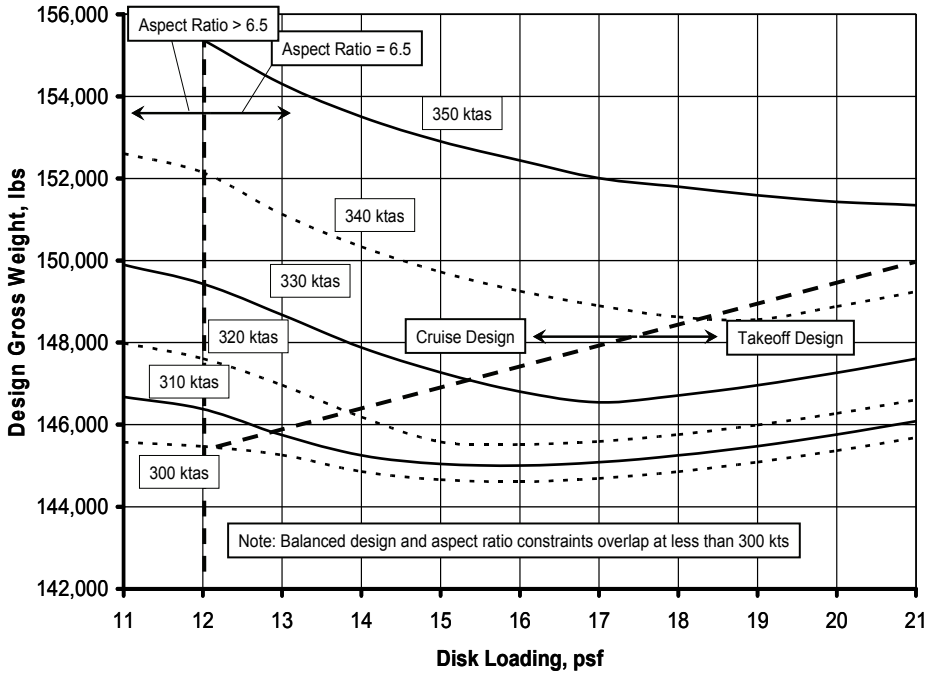

Figure 2-48. Impact of disk loading and design speed on design gross weight (30,000 feet).

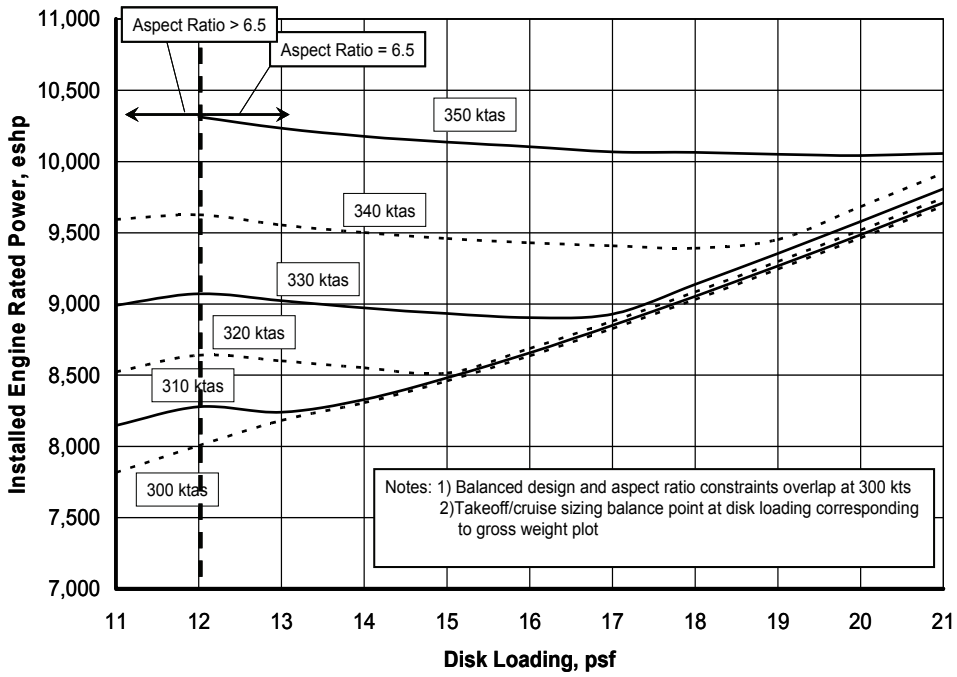

Figure 2-49. Impact of disk loading and design speed on engine size (30,000 feet).

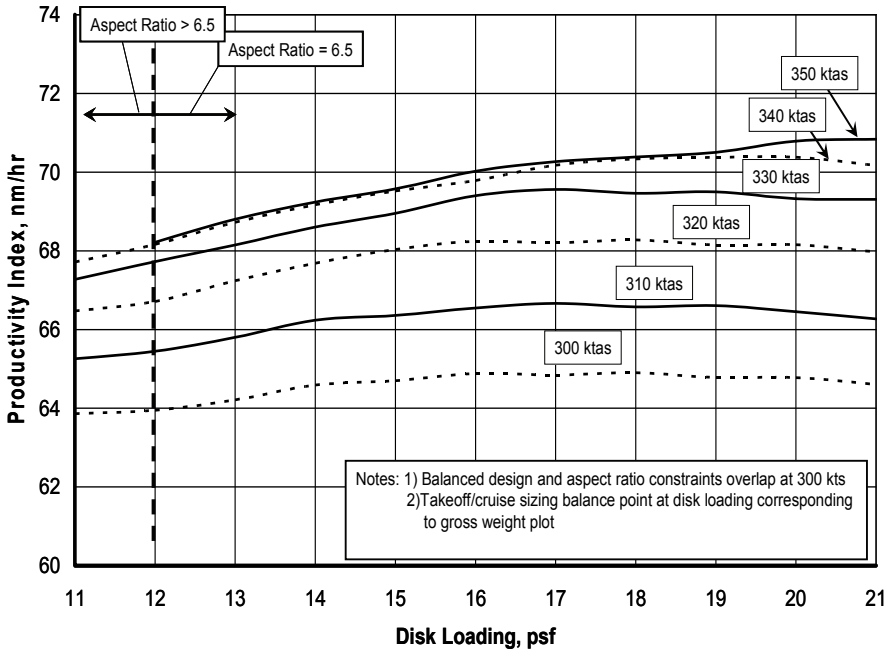

Figure 2-50. Impact of disk loading and design speed on productivity (30,000 feet).

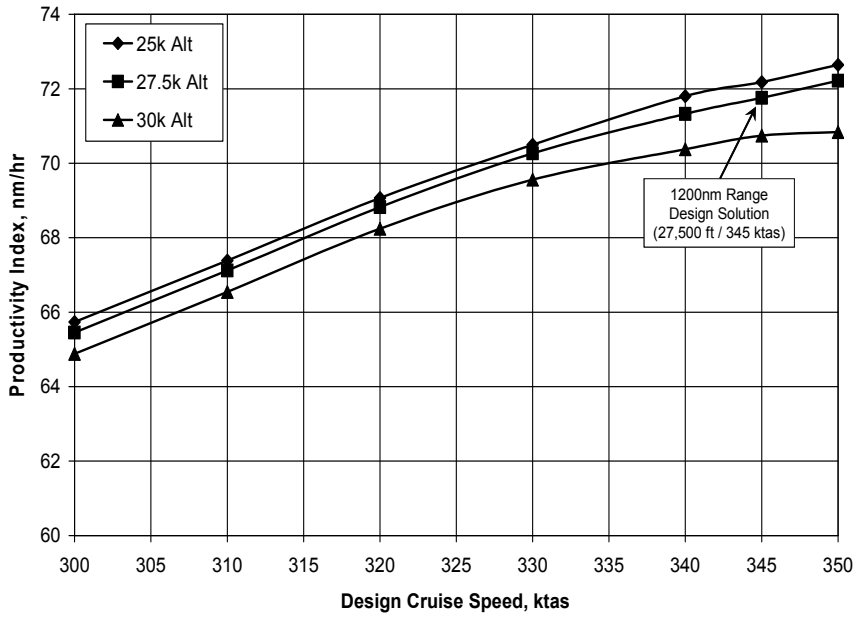

Figure 2-51. Productivity index for CTR120 with a design range of 1,200 nmi.

A productivity index plot similar to figure 2-39 was created for the 1,200-nmi range design. The results are shown in figure 2-51. The points used to define the curves are based on disk loadings that correspond to approximate minimum gross weight designs that very closely represent maximum productivity. Because there are only the discrete points from the sensitivity study and not exact solutions in terms of disk loading, there is some slight scatter in the curves. The general trends are similar to those in figure 2-39 in terms of airspeed.

Although a cruise altitude of 25,000 feet shows a slightly greater benefit in terms of productivity, the desire to cruise above that altitude with the best productivity possible resulted in selecting 27,500 feet. The best altitude and airspeed combination still appears to be close to the 27,500 feet and 345 KTAS, initially selected from the 1500-nmi-range study. Figure 2-51 does show that at 27,500 feet the productivity continued to climb an additional 0.6 percent between 345 and 350 KTAS; however, to increase the speed to 350 knots would require a push to a disk loading of 19 psf, and a 3-percent engine push.

Therefore, the sizing conditions for the final synthesis remained at the 27,500-foot cruise altitude and the 345-KTAS cruise speed selected from the 1500-nmi-range trade studies. The design disk loading is 18 psf.

2.6.7 Results

The following sections present the results of the CTR120 design process.

2.6.7.1 Design Description

A summary of the design characteristics of the CTR120 design is provided in table 2-8. The CTR120 weight empty breakdown is provided in the Industry Standard Group Weight Statement format and provided in table 2-9. The weight empty to design gross weight fraction for the CTR120 design is 0.67. The equivalent flat plate drag breakdown for the CTR120 is provided in table 2-10.

TABLE 2-8. SUMMARY OF CTR120 CONFIGURATION CHARACTERISTICS

Weights:		
Design Gross Weight, DGW	lb	147647
Maximum Gross Weight, MGW (Full Fuel & Payload)	lb	147647
Design Payload	lb	26400
Empty Weight + Trapped Fluids	lb	98737
Operating Load	lb	1070
Number of Crew	ND	5
Fuel System Capacity	lb	21441
Geometry:		
MR Radius	ft	36.1
Number of Blades per Rotor	ND	6
Thrust Equivalent Chord	in	34.4
Solidity	ND	
Wing Span	ft	100.4
Wing Chord	ft	15.4
Wing Area	sq ft	1550.9
Horizontal Span	ft	31.8
Horizontal Tail Area	sq ft	201.7
Tail Type	ND	T-tail
Vertical Span	ft	19.1
Vertical Tail Area	sq ft	273.4
Length Fuselage	ft	111.9
Fuselage Height	ft	12.0
Fuselage Width	ft	13.0
Nacelle Length (not including spinner)	ft	21.9
Nacelle Height	ft	10.2
Nacelle Width	ft	7.4
Engine/Xmsn:		
Number of Engines	ND	4
Engine Ratings, SLS, uninstalled		
2.5-min OEI Power	eshp	10900.0
Max Rated Power (10-min)	eshp	9372.0
Max Continuous Power	eshp	7198.0
MCP Xmsn rating @ mast (100%rpm)	hp	13063.0
Aero/Performance Related:		
Disk Loading at MGW	psf	18.0
Wing Loading at MGW	psf	95.2
Main Rotor Tip Speed (100% rpm)	fps	650
Main Rotor Tip Speed, A/P mode (70%rpm)	fps	455
Hover Download	%T	8.5
Flat Plate Drag (alpha=0)	sq ft	56.3
Oswald A/C efficiency "e"	ND	0.93
Incompressible Clmax (zero flaps)	ND	1.85
Design Cruise Altitude	ft	27500
Design Cruise Speed	ktas	345
Vlrc @ MGW/Std Day/Design Cruise Altitude	ktas	302
(Vlrc is speed at 0.99 best range speed)		
Vmcp @ MGW/Std Day/Design Cruise Altitude	ktas	345
(Vmcp is speed at 100% MCP available)		
Range (5k/ISA+20 deg C takeoff)		
@ max payload, max fuel & Vlrc)	nm	1331
@ max payload, max fuel & Vmcp	nm	1179

TABLE 2-9. SUMMARY OF CTR120 WEIGHTS

GROUP		PREDICTED WEIGHT (lbs)
WING GROUP - FORWARD		8989.0
ROTOR GROUP		16731.3
TAIL GROUP		1722.3
BODY GROUP		12836.3
LANDING GEAR GROUP		4198.1
NACELLE GROUP		3399.0
AIR INDUCTION GROUP		722.2
PROPULSION GROUP		21577.8
FUEL SYSTEM	1503.3	
DRIVE SYSTEM	14623.4	
FLIGHT CONTROLS GROUP		3755.7
APU SYSTEM GROUP		385.9
INSTRUMENTS GROUP		161.7
HYDRAULIC SYSTEM GROUP		3038.9
ELECTRICAL GROUP		3094.5
AVIONICS GROUP		420.5
FURNISHINGS & EQUIPMENT		9198.5
AIR CONDITIONING GROUP		1291.6
ANTI-ICING GROUP		2169.0
LOAD & HANDLING GROUP		192.1
WEIGHT EMPTY (Less Contingency		93884.1
CONTINGENCY		4694.2
WEIGHT EMPTY		98578.3
UNUSUABLE FLUIDS		158.7
WEIGHT EMPTY (w/ Unusable Fluids)		98737.0

TABLE 2-10. CTR120 DRAG BREAKDOWN

Component	feo
Fuselage	15.1
Wing	15.5
Sponson	4.2
Nacelle	11.8
Empennage	4.6
Clean Component Drag	51.2
Excrescence (10% of clean component drag	5.1
Total Drag (w/o cooling)	56.3

2.6.7.2 Three-View Drawings

The CTR120 3-view drawings for airplane and helicopter configurations are respectively shown in figures 2-52 and 2-53.

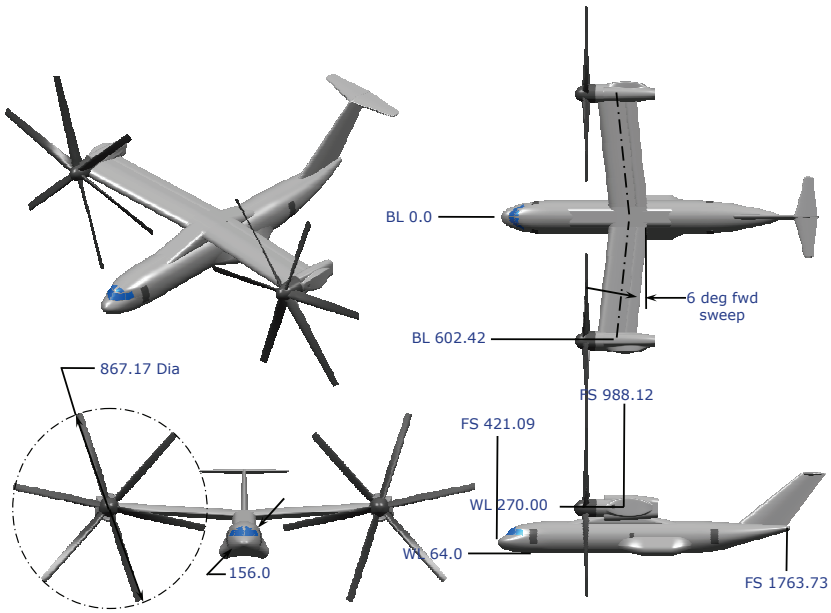

Figure 2-52. Three-view drawing of CTR120 configuration in airplane mode.

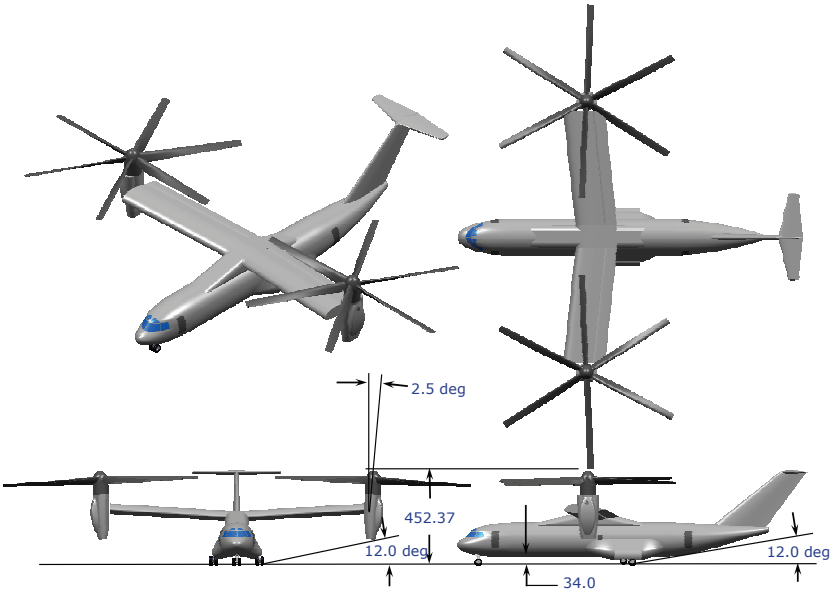

Figure 2-53. Three-view drawing of CTR120 configuration in helicopter mode.

2.6.7.3 Performance Characteristics

Isolated rotor Figure of Merit as a function of blade loading is shown in figure 2-54. It is based on the 5,000-foot, ISA+20°C design takeoff condition. Figure 2-54 includes the aircraft Figure of Merit as a function of the weight coefficient referred to rotor solidity.

Figures 2-55, 2-56, and 2-57 respectively provide a takeoff ceiling, speed-altitude envelope, and payload-range data for ISA and ISA+20°C ambient conditions. The table in figure 2-55 shows that the standard-day takeoff weight capability is significantly higher than the design gross weight; however, it cannot be used because it was assumed that the design gross weight would also be the maximum certified gross weight. A study was not conducted to determine the impact of defining the maximum certified weight to a maximum alternate weight rather than the design mission takeoff gross weight.

Because the CTR120 is designed to take off at 5k/ISA+20°C, by definition it is capable of a VTO (OEI) takeoff with maximum payload and full fuel. The VTO (OEI) takeoff capability is based on a power ratio of 0.85. This means that at the OEI condition the power available is 85 percent of that required to hover at the same gross weight.

The speed-altitude envelope was calculated at the design gross weight of 147,648 lbs. At standard-day conditions and the design cruise altitude of 27,500 feet, the long-range cruise speed is approximately 302 KTAS. The design mission profile was flown at 345 KTAS by definition and not long-range cruise speed. Figure 2-56 confirms that the maximum true airspeed at 100-percent MCP is approximately 345 knots.

The payload-range data in figure 2-57 confirms the design range of 1,200 nmi. This configuration has the option of both a VTO and STO takeoff depending on the design of the vertiport.

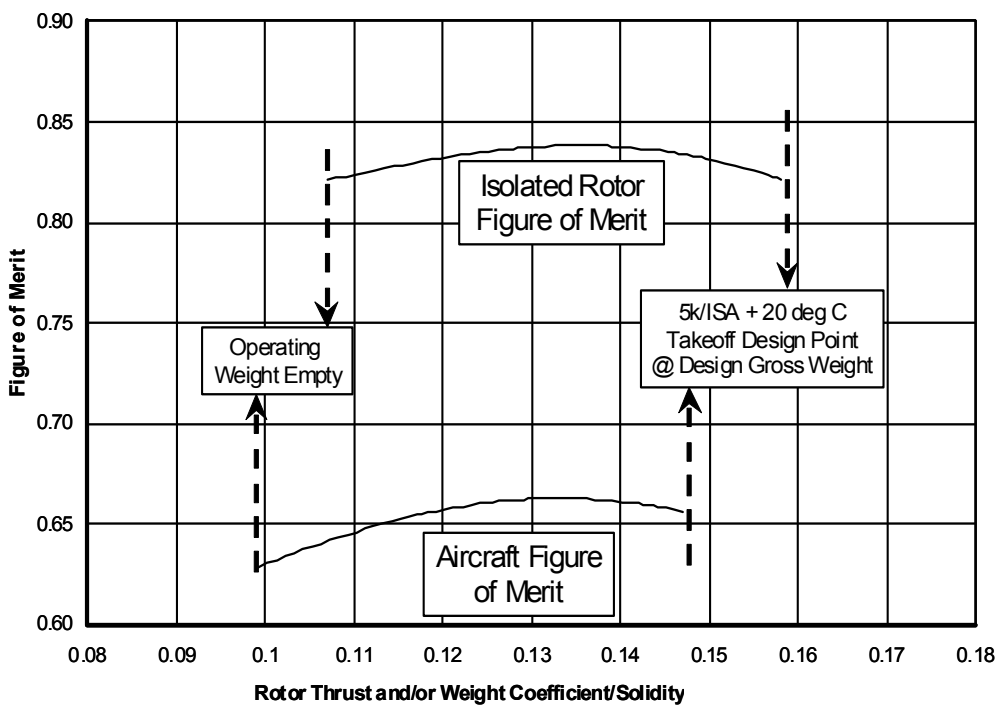

Figure 2-54. Installed rotor Figure of Merit for CTR120 design (5k/ISA+20°C).

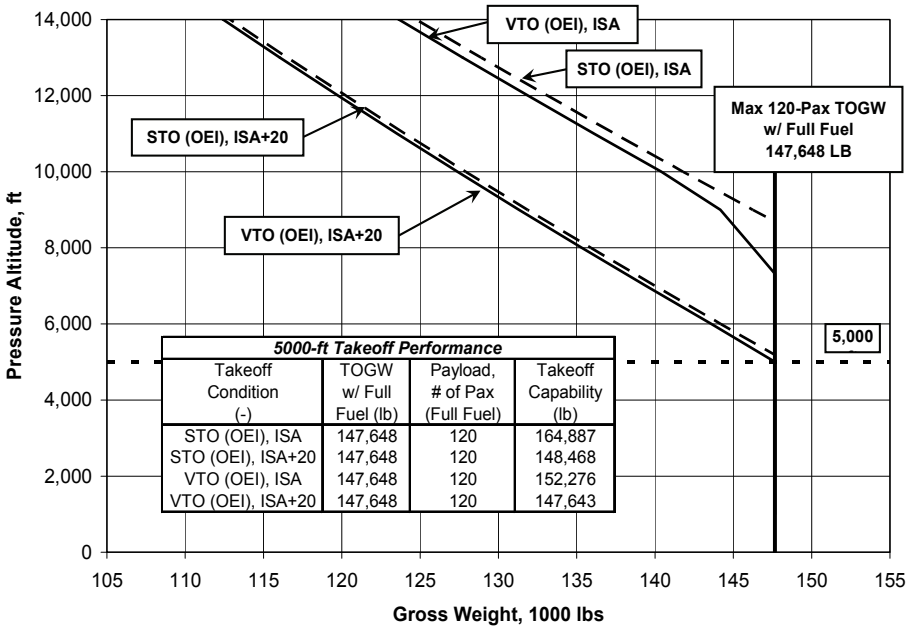

5000-ft Takeoff Performance			
Takeoff Condition (-)	TOGW w/ Full Fuel (lb)	Payload, # of Pax (Full Fuel)	Takeoff Capability (lb)
STO (OEI), ISA	147,648	120	164,887
STO (OEI), ISA+20	147,648	120	148,468
VTO (OEI), ISA	147,648	120	152,276
VTO (OEI), ISA+20	147,648	120	147,643

Figure 2-55. CTR120 OEI STO hover ceiling (ISA and ISA+20°C).

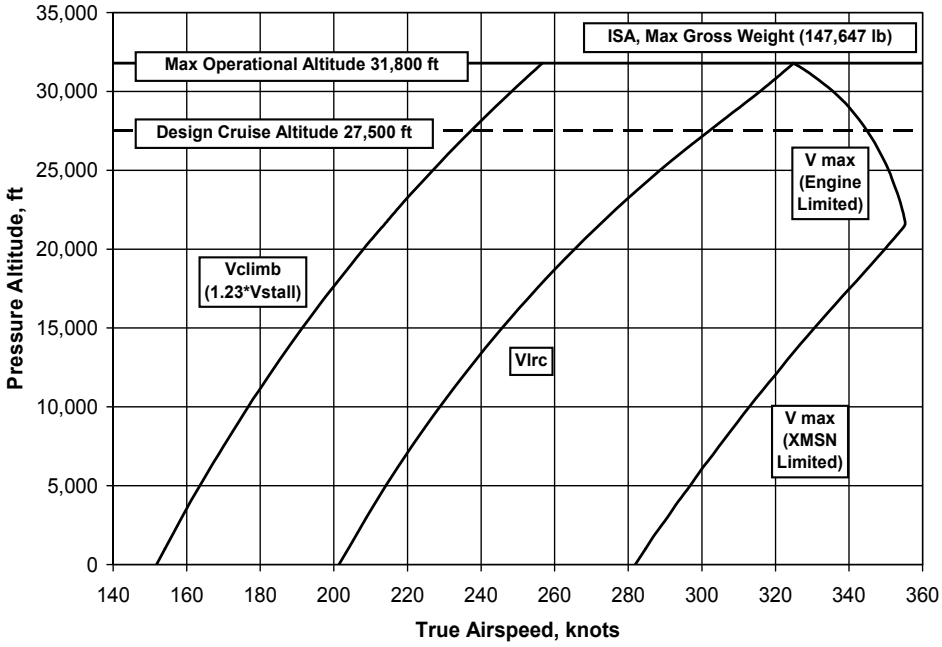

Figure 2-56. CTR120 partial speed-altitude envelope (ISA).

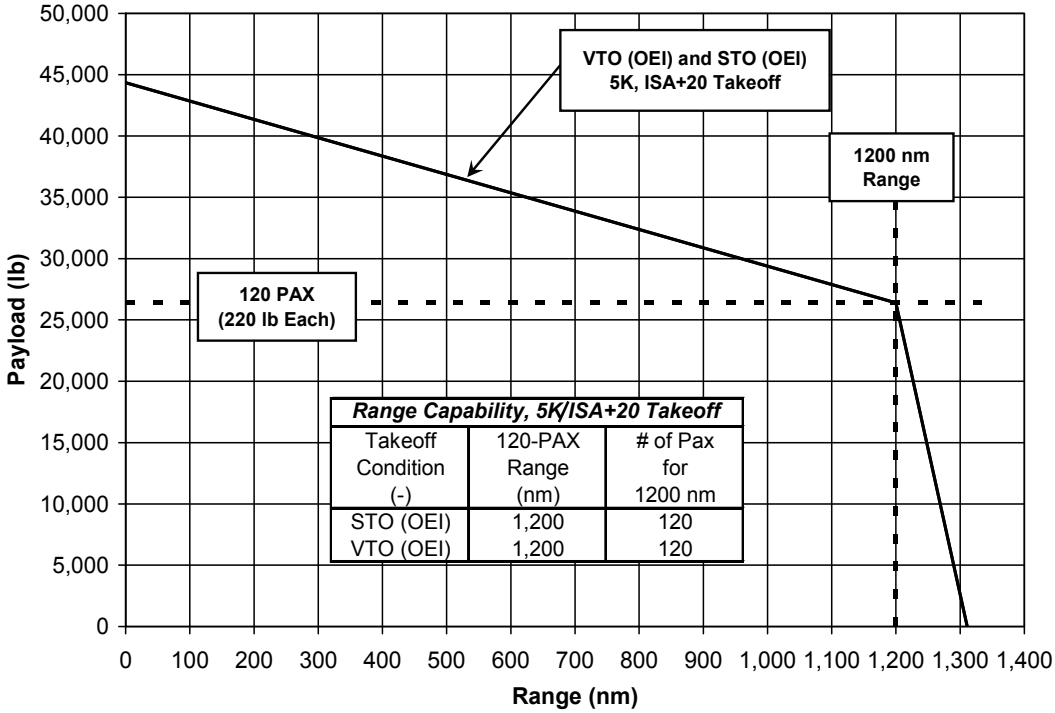

Range Capability, 5K/ISA+20 Takeoff		
Takeoff Condition (-)	120-PAX Range (nm)	# of Pax for 1200 nm
STO (OEI)	1,200	120
VTO (OEI)	1,200	120

Figure 2-57. CTR120 payload-range curve (ISA).

2.7 Design Recommendations

The following is a list of recommendations that have evolved from the Task I design effort of this study. These recommendations are made in the context of the objectives of this study and do not necessarily include technology recommendations for the sake of improving the design. Although some are not new and unique, they will hopefully serve to reinforce recommendations from other studies.

1) Conduct a study of the relationship between the operational modes described in section 2.1.1 and CTR size. This would help define not only commercial potential and viability but also alternate mission suitability for each CTR size.
2) Define the relationship between design goals such as range, speed, etc., and the impact on NextGen operations.
3) Define the potential benefit to the nation of long-range capability for disaster relief in terms of economic viability in NextGen.
4) Define operational altitude restrictions/desires, if any, in NextGen.
5) Conduct a detailed analysis of takeoff and landing profiles in the terminal area to assess engine rating structures and the impact on design. This should include the impact of water/alcohol injection.
6) Define the relative importance of operating out of terminal gates and whether practical solutions exist that could avoid a requirement for blade folding.
7) Conduct an in-depth configuration study.
8) Conduct a rigorous design study to define the benefit of noise reduction.
9) Define the relationship between cruise rpm and a balanced engine design.
10) Conduct trade studies to address the relationship between CTR design and emissions/noise requirements.

2.8 Generating Input Data for BADA

One of the requirements of this study was to provide data for the development of aircraft performance models for future evaluation of the CTR fleet in the NextGen environment. The performance models were developed by SAIC in the Base of Aircraft Data (BADA) format.

The CTR10, CTR30, and CTR120 design performance data was generated by the PRESTO program. A check on the ability of the BADA data to capture the mission-related performance of each configuration was made. In order to accomplish this objective, Bell provided a simple mission profile with only climb, cruise, and descent performance. This mission profile was then replicated using the BADA data. The results are discussed in section 3.0.

Performance data was generated for both airplane and conversion configurations. Because PRESTO was used to predict steady-state approach and takeoff performance, rather than the Bell Partial Task Simulator, a check of how well PRESTO correlates with the simulator was made. A steady-state 60-nacelle/110-KCAS time history from the simulator was analyzed in PRESTO. Relative to the simulator power required, PRESTO was 5-percent optimistic. This particular time history was flown before the simulation models were calibrated to the CTR10 and CTR30 configurations. A post-simulation comparison between PRESTO and the CTR10 and CTR30 configurations resulted in different answers. The CTR10 agreement was within 1 percent on fuel flow; however, the PRESTO prediction was 15-percent lower than the simulation of the CTR30 configuration. This is partially due to the fact that the simulation model could not be modified to be 100-percent representative of the PRESTO 30-passenger design.

Because of the format of the BADA model, a set of equivalent data was generated to represent the conversion mode. BADA effectively models a fixed-wing aircraft and requires drag, thrust, and fuel burn. In conversion mode the thrust vector is approximately aligned with the nacelle and not with the free-stream velocity vector. Consequently, the data was provided in an equivalent format to simulate the BADA airplane format. Power required was converted into an equivalent drag. As a result at very low speeds simulating approaches and takeoff conditions, the equivalent thrust forces became very large.

2.9 Noise Footprint

A pilot-in-the-loop (PITL) simulation was conducted using the Bell Helicopter Partial Task Simulator as described in section 4.4. The results of this effort provided time histories representative of takeoffs and landings in and out of Miami International Airport, where a high-definition visual database was available to support the VTOL and STOL piloted simulations. The following sections describe the process used to develop noise footprints representative of several takeoff and landings utilizing the simulation data.

2.9.1 Description of Task

Noise level contours were calculated for various flight conditions for three proposed civil tiltrotors. These were the CTR10, CTR30, and CTR120 NextGen designs at their respective maximum takeoff gross weights of 16,192 lbs, 46,430 lbs, and 147,647 lbs. The conditions include approaches at three different glide slopes (3, 6, and 9 degree) and two takeoffs (VTO and STO). The three aircraft configurations were each evaluated at these 5 flight conditions, resulting in a total of 15 noise contours.

2.9.2 Data

The noise data source used as a basis for these estimates were acoustic measurements taken during XV-15 flight tests in 1995–1999 in Waxahachie, TX. These flight tests were carried out jointly by Bell Helicopter and NASA, and the tests included measurements of flyovers and various terminal operations. For several of these flight conditions, the measured data was converted into sound hemispheres after completion of the tests. These sound hemispheres were used in this study as inputs to the sound propagation model, discussed below.

Sound hemispheres for flyover were used when sound hemispheres for takeoff did not exist. The aircraft configuration of the flyover sound hemispheres used to simulate the takeoff noise was similar to that which would have been used if takeoff hemispheres existed. Aircraft airspeed, rotor speed, and nacelle angle were the same or similar, therefore the rotor advancing tip Mach number is similar. The aircraft climb profile is modeled in the analysis, so the aircraft height and the slant ranges to the ground observer are identical whether takeoff or flyover hemispheres were used. Takeoff power would be higher than the power used during flyover at the same airspeed, which would result in a slightly louder sound hemisphere than the flyover hemispheres used. Considering the accuracy of the approximations used in the first-order analysis to estimate the various configurations, the effect that the higher power level might have on the result was considered to be of the same order of error, therefore no attempt was made to develop a power adjustment to account for the torque difference.

In addition to these noise inputs, flight profile time history data from the PITL simulations of the 15 flight conditions were used to create the flight tracks necessary for the noise propagation and ground contour analysis.

2.9.3 Data Processing

The sound hemispheres for various measured conditions were used as inputs to the Rotorcraft Noise Model (RNM) software from Wyle Laboratories. RNM takes into account the aircraft noise signatures (i.e., the hemispheres) for the specific conditions flown, the input flight track, atmospheric sound absorption, and the effects of ground reflections. The flight track is entered into an input data file that is read by RNM. Using this input file and the sound hemispheres propagates the noise to the ground and calculates overall noise levels on a distance-based grid. The output grid data can then be plotted as noise level contours. The noise level metric used in this analysis is A-weighted sound exposure level (SEL).

Because the three aircraft in this study had different design characteristics than the baseline XV-15 aircraft, some adjustments to the noise levels were required in order to account for differences in rotor blade tip speed and aircraft gross weight. The adjustments were calculated using the provided equations and applied to the calculated noise contour data generated using the XV-15 hemispheres. Other design differences were considered to have a secondary effect on noise levels and were excluded from this study.

The adjustment procedure used empirical corrections based on typical trends seen for helicopters. The tip speed adjustment was made using the following formula:

$$\Delta dB = 80*\log_{10}(M_{TIPdesired}/M_{TIPmeasured})$$

where M_{TIP} is rotor advancing blade tip Mach number.

TABLE 2-11. NOISE LEVEL ADJUSTMENTS

	Tip Speed Adjustment	Gross Weight Adjustment	Total Adjustment
CTR10	0.2 dB	0.7 dB	**0.9 dB**
CTR30	−3.3 dB	5.2 dB	**1.9 dB**
CTR120	–5.9 dB	10.3 dB	**4.4 dB**

The gross weight adjustment was made using the following formula:

$\Delta dB = 10*\log_{10}(GW_{desired}/GW_{measured})$

where GW is aircraft gross weight.

Applying the preceding formulas resulted in the following noise level adjustments for the CTR10, CTR30, and CTR120 cases as shown in table 2-11.

The preceding adjustments were applied to the output data. An SEL noise contour plot was then generated for each of the 15 conditions using a MATLAB plotting script.

The detailed process to generate each noise contour can be summarized as follows:

1) Acquire simulated flight profile time histories for the desired flight condition.
2) Plot the time histories of the variables pertinent to noise hemisphere selection. These variables are height, airspeed, and nacelle angle.
3) Based on the above plots, choose several break points in the time histories in order to identify linear flight track segments for the input files. (Each of the 15 flight profiles were defined to contain between 7 and 14 segments.)
4) Enter the flight track break point parameters into an input file to define the acoustical flight profile.
5) Run to generate the noise levels at the grid points specified in the input file.
6) Adjust the data in each output file for blade tip speed and gross weight according to the adjustments shown above.
7) Plot contours of equal SEL using the output data, down to a lower limit of 65 dBA SEL.

2.9.4 Results

The resulting contours are shown in figures 2-58 thru 2-72. Each figure shows east position on the X-axis and north position on the Y-axis. The X- and Y-spacing are the same on each plot, and similar conditions are plotted with identical axis limits to aid in visualization and comparison. The location of the landing/takeoff point is illustrated on each plot with a four-pointed star. The time histories for the parameters used to create the flight tracks are provided in appendix H. Since a flight simulation of the CTR120 design was beyond the scope of this study and the CTR10 and CTR30 profiles are very similar, the noise contours for the CTR120 design were developed using the CTR30 profiles. Because the CTR120 flight profiles match the CTR30 profiles exactly, they are not explicitly shown in appendix H.

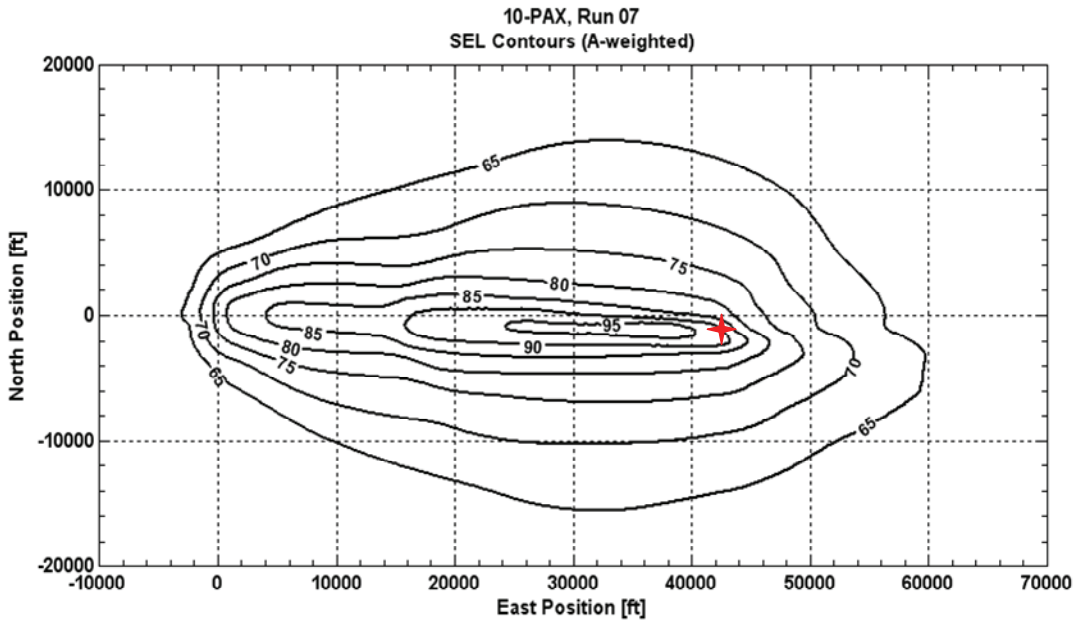

Figure 2-58. 10-passenger SEL noise contours for approach, 3-degree.
✦ Landing point (42709, –1597)

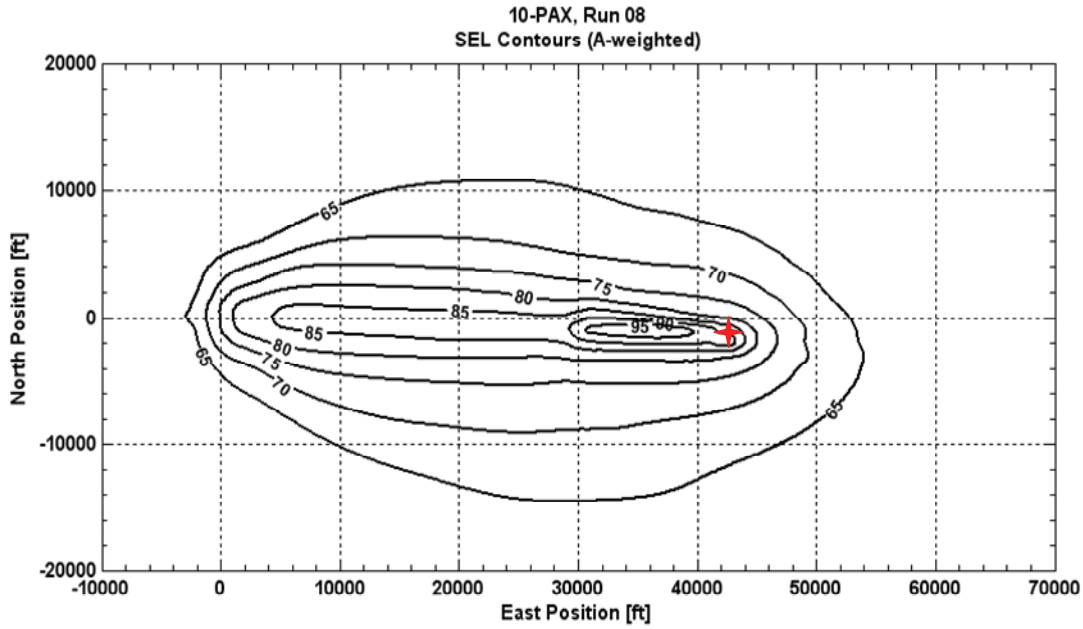

Figure 2-59. 10-passenger SEL noise contours for approach, 6-degree.
✦ Landing point (42725, –1611)

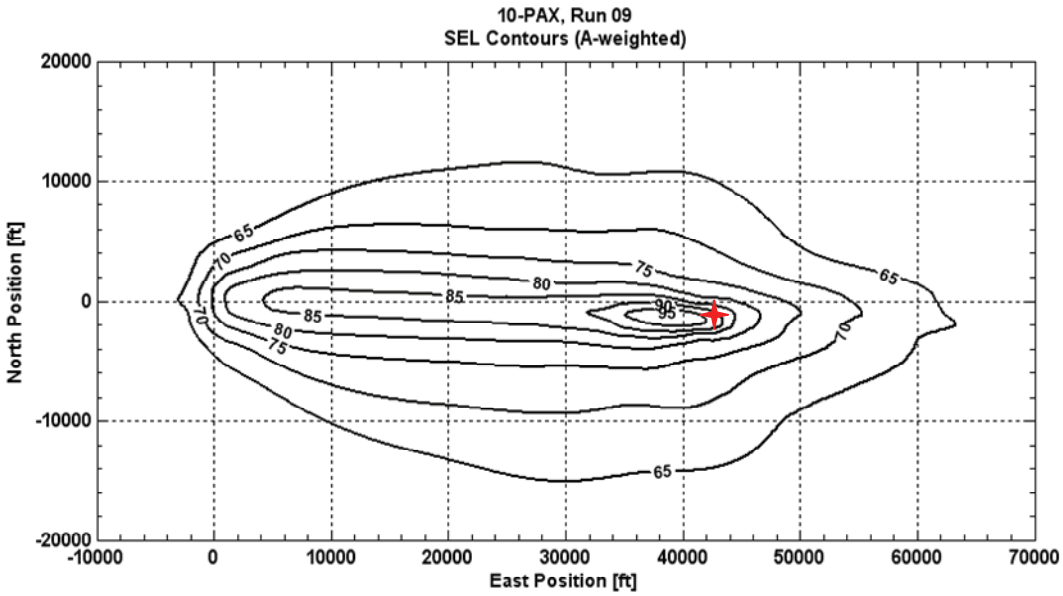

Figure 2-60. 10-passenger SEL noise contours for approach, 9-degree.
✦ Landing point (42745, –1616)

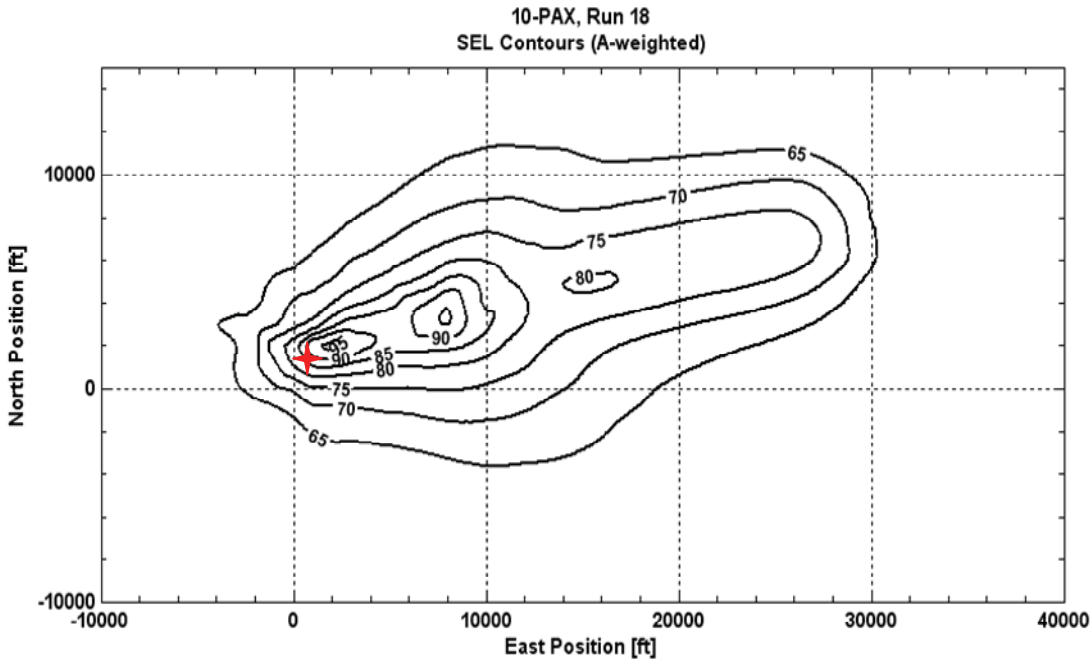

Figure 2-61. 10-passenger SEL noise contours for takeoff, VTO.
✦ Takeoff point (696, 1569)

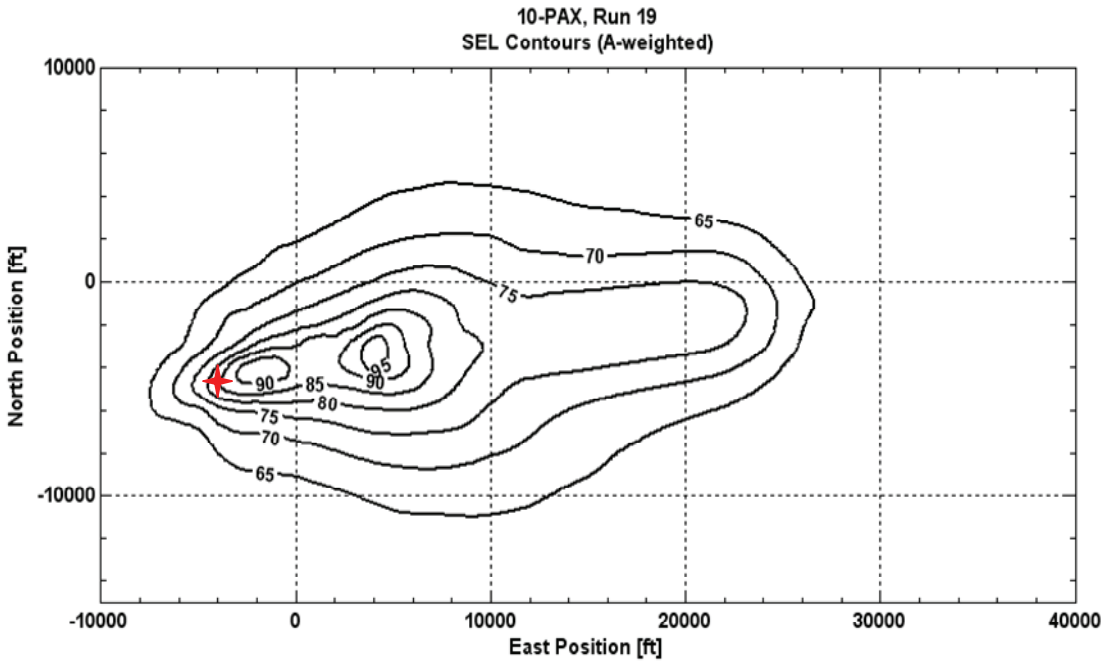

Figure 2-62. 10-passenger SEL noise contours for takeoff, STO.

✦ Takeoff point (–3976, –4611)

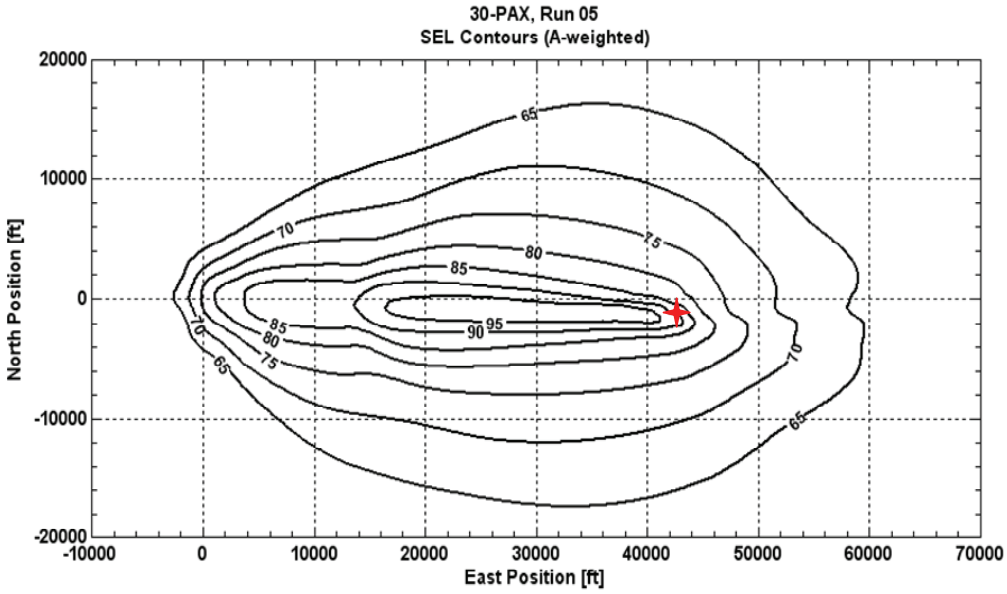

Figure 2-63. 30-passenger SEL noise contours for approach, 3-degree.

✦ Landing point (42748, –1594)

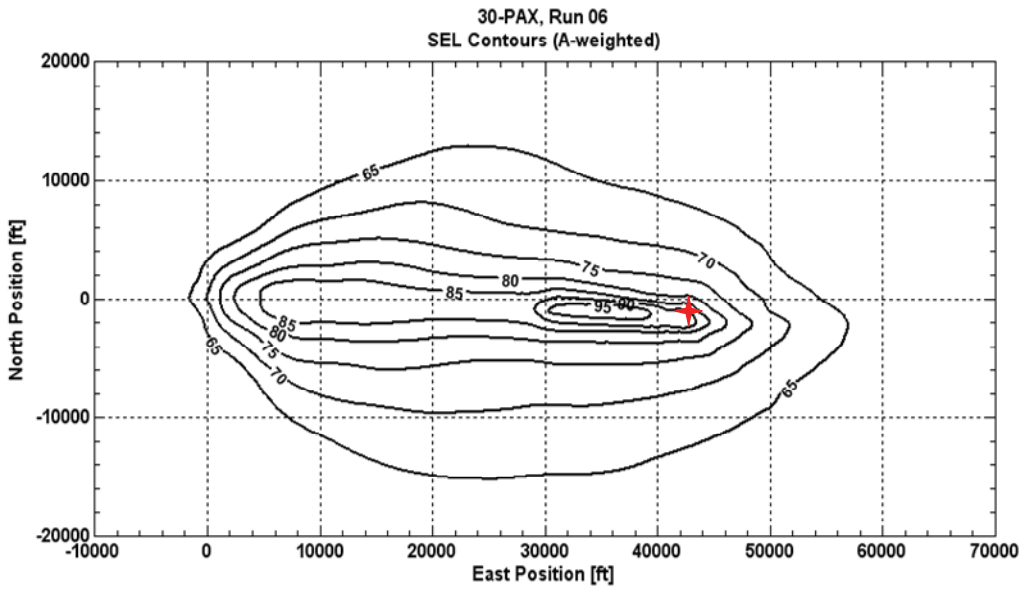

Figure 2-64. 30-passenger SEL noise contours for approach, 6-degree.
✦ Landing point (42754, –1594)

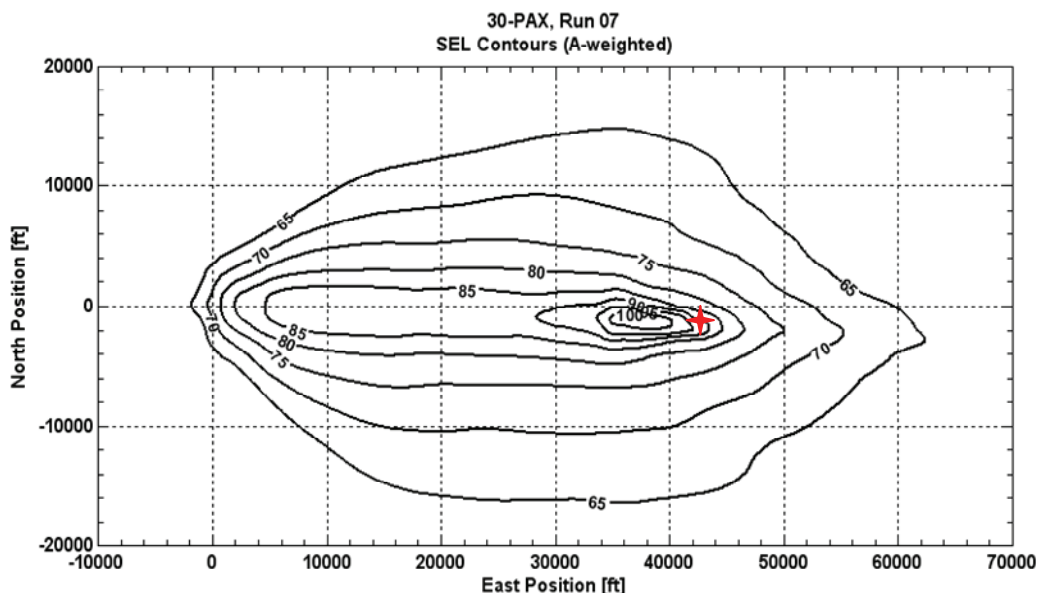

Figure 2-65. 30-passenger SEL noise contours for approach, 9-degree.
✦ Landing point (42738, –1601)

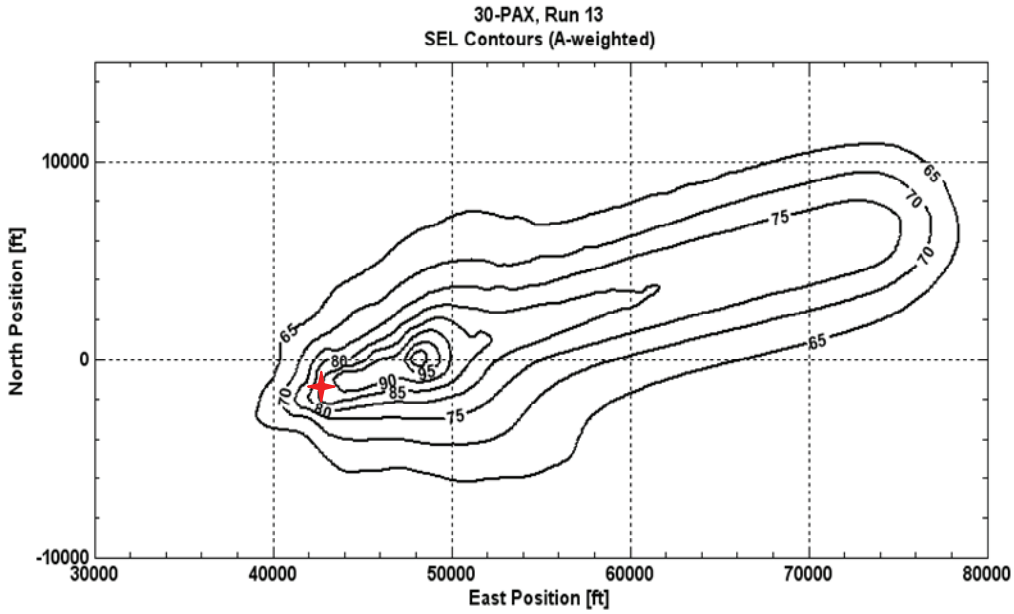

Figure 2-66. 30-passenger SEL noise contours for takeoff, VTO.
✦ Takeoff point (42810, –1594)

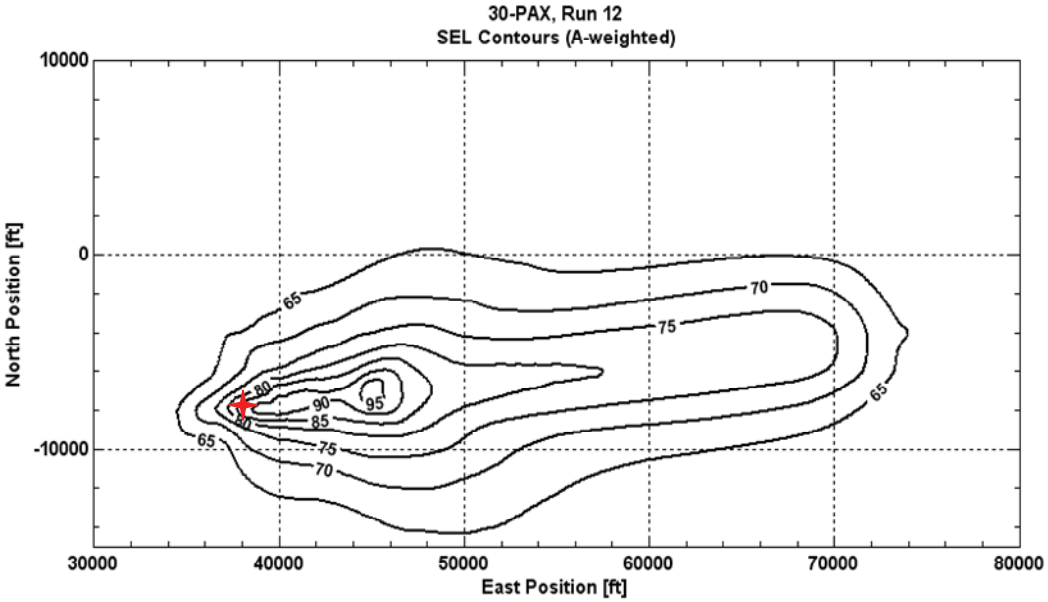

Figure 2-67. 30-passenger SEL noise contours for takeoff, STO.
✦ Takeoff point (38136, –7781)

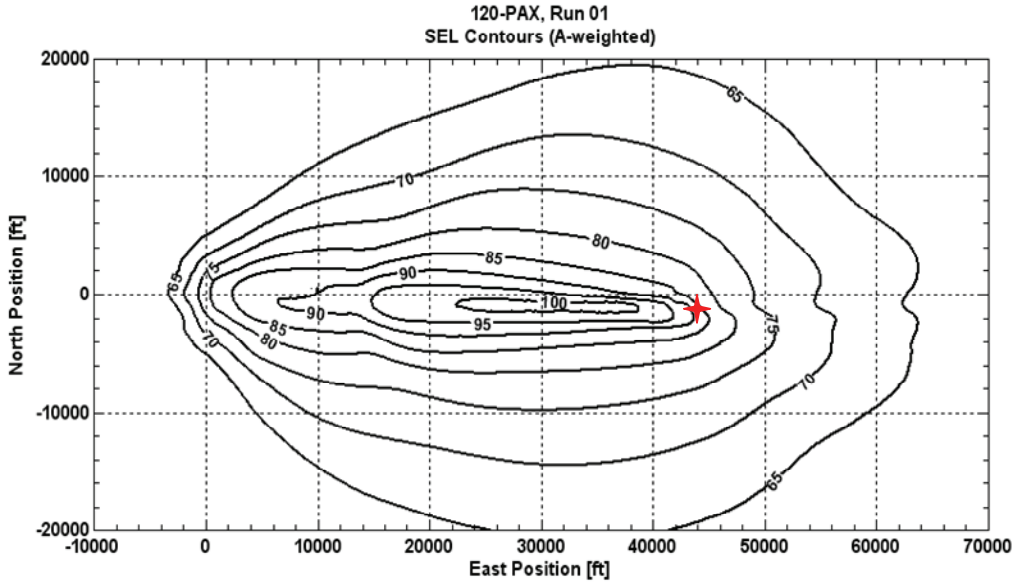

Figure 2-68. 120-passenger SEL noise contours for approach, 3-degree.
✦ Landing point (42754, –1594)

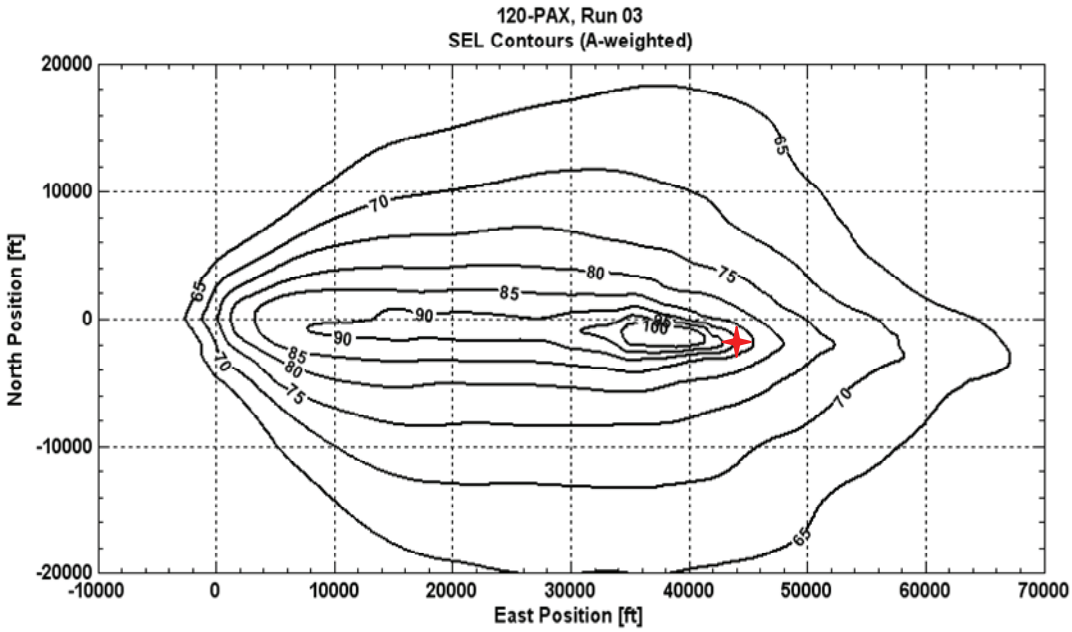

Figure 2-69. 120-passenger SEL noise contours for approach, 6-degree.
✦ Landing point (42738, –1601)

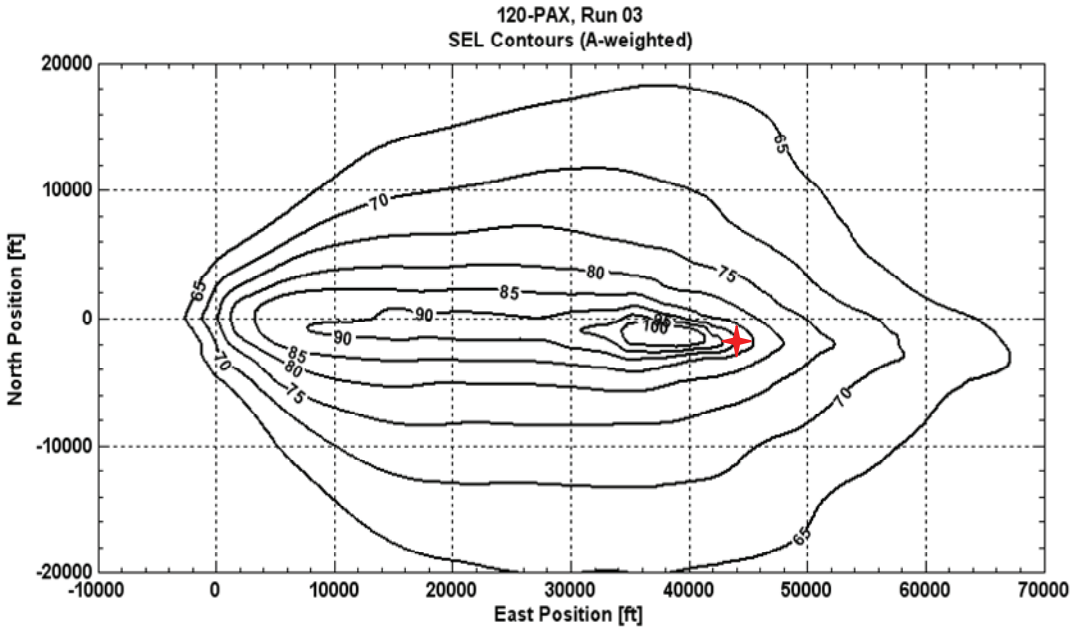

Figure 2-70. 120-passenger SEL noise contours for approach, 9-degree.
✦ Landing point (42748, –1594)

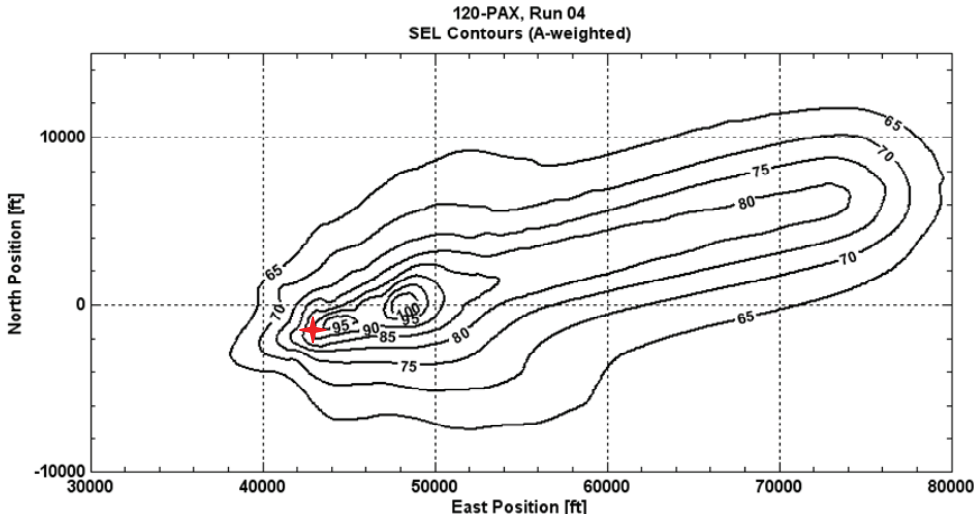

Figure 2-71. 120-passenger SEL noise contours for takeoff, VTO.
✦ Takeoff point (38136, –7781)

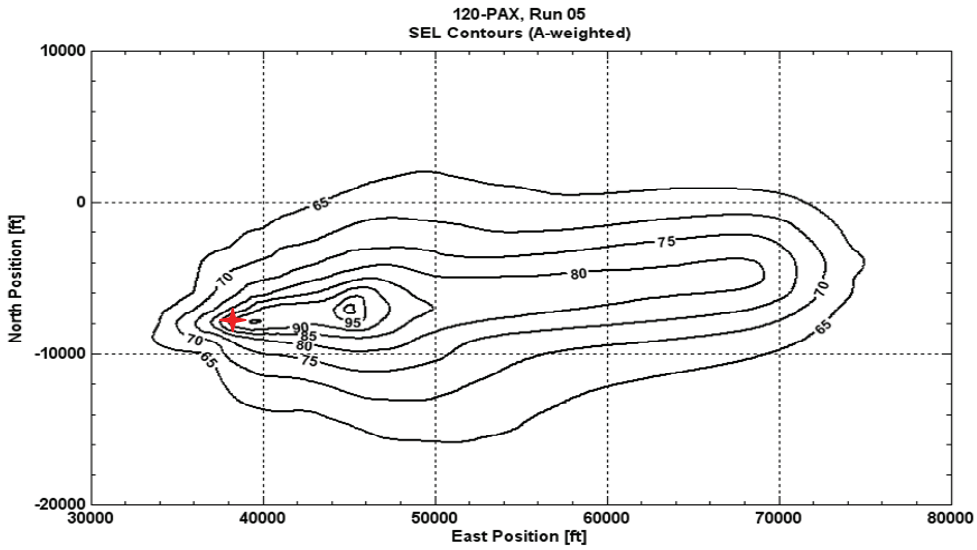

Figure 2-72. 120-passenger SEL noise contours for takeoff, STO.
✦ Takeoff point (42810, –1594)

3 CTR MODELING FOR NAS PERFORMANCE ANALYSIS

3.1 Introduction

The civilian tiltrotor (CTR) performance characteristics were captured such that transit performance and airspace throughput could be modeled using the Airspace Concept Evaluation System (ACES) for Next Generation Air Transportation System (NextGen) studies. The ACES software requires performance data to be supplied in the Base of Aircraft Data (BADA) format in support of Air Traffic Management (ATM) simulation studies. BADA is developed by the EUROCONTROL Experimental Center for use in ATM research.

The current version of BADA available publicly during this work was Version 3.6 (ref. 9); it produces nominal rate of climb/decent (ROCD) numbers within 100 fpm of actual aircraft data when in the nominal operations envelope. Further work by the BADA development team shows that predictive capability is not as robust at marginal ends of the envelope indicating error in excess of 300 fpm, as well as having significant effects on fuel consumption (ref. 10).

In support of the CTR in NextGen study a matrix of trim points was generated covering climb, cruise, and descent operations throughout the flight envelope. Bell performed design synthesis for the proposed CTR fleet and also generated the trim performance data for the CTR10, CTR30, and CTR120 variants. The CTR90 variant was sized based on the reduced BADA models for the CTR10, CTR30, and CTR120 variants. Pilot-in-the-loop (PITL) sessions were used to develop operational approach, landing, and takeoff profiles given the CTR10 and CTR30 variants.

3.2 BADA Performance Model Entries

This section outlines the performance and procedural terms that require definition for application of the BADA performance database. Some terms are directly reduced from the reference performance data given the CTR trim matrix. However, there are operational entries and maximum performance/safety envelope entries that are better identified as part of the overall CTR design specifications and/or direct result of the design synthesis process. These fall from the CTR mission requirements, as well as specifications on operational procedures that are not fully captured in a set of trim points. All required BADA entries are outlined in this section. Note that all coefficient definitions and equations outlined herein are also well defined in the BADA documentation (ref. 9). The BADA entries for the CTR10, CTR30, and CTR120 variants are based on Bell-supplied performance data. The CTR90 configuration was developed based on trends of the CTR10, CTR30, and CTR120 BADA models.

Each CTR airframe variant (CTR10, CTR30, CTR90, and CTR120) was described within the BADA framework based on entries in their own unique integral file types:

- Operations Performance File (.OPF)
- Airline Procedures File (.APF)
- Performance Table File (.PTF)

The following sections identify the BADA entries that populate these files for each CTR variant. A general overview of the BADA performance modeling theory is presented in appendix A for reference.

3.2.1 Aircraft Type

The BADA aircraft type entries for each CTR variant are shown in table 3-1. The models in BADA regarding engine types include jet-, turboprop-, and piston-style formulations. In the case of the CTR the turboprop entry is most relevant. However, the BADA performance file, as parsed by ACES, will only accommodate the jet-type engine model structure from BADA. Consequently, to ensure model compatibility, the BADA performance database was built on the jet engine model formulation to develop the equivalent system model. The wake category is a best estimate based on overall gross weight and/or comparison to like-size aircraft currently sized in the BADA database. Current airframes in the BADA library set the Airbus A318 (107 passenger) and A319 (124 passenger) in the medium wake category. According to the International Civil Aviation Organization (ICAO) (http://www.icao.int/) the XV-15 tiltrotor is listed as a light wake category airframe. Given this information the wake entries were defined as shown.

3.2.2 Airframe Geometry Data

Airframe geometry as required by BADA is defined in table 3-2. The entries are based on Bell design synthesis results.

3.2.3 Mass Characteristics

The BADA mass characteristics for each CTR variant are shown in table 3.3. These data are as supplied by Bell for each CTR variant.

TABLE 3-1. AIRFRAME TYPE CHARACTERISTICS

Parameter	Description (units)	CTR10	CTR30	CTR90	CTR120
Neng	Number of Engines	2*	2*	2*	2*
Engine Type	Jet, Turboprop, Piston	Jet	Jet	Jet	Jet
Wake Category	Heavy, Medium, Light	Light**	Light**	Medium**	Medium**

* For CTR, Neng is defined as number of rotors.
** Wake Category for CTR is defined in the airplane mode.

TABLE 3-2. AIRFRAME GEOMETRY CHARACTERISTICS

Parameter	Description (units)	CTR10	CTR30	CTR90	CTR120
b	Wingspan (m)	10.31	13.96	25.06	30.60
S	Wing Area (m^2)	17.03	35.49	103.28	144.08
l	Airframe Length (m)	13.41	18.79	30.52	34.09

TABLE 3-3. AIRFRAME MASS CHARACTERISTICS

Parameter	Description (units)	CTR10	CTR30	CTR90	CTR120
Mref	Reference Mass (kg)	7030.7	17916.9	45627.0	56699.0
Mmin	Minimum Mass (kg)	5302.0	14800.7	37388.8	45359.2
Mmax	Maximum Mass (kg)	7620.4	21060.3	54390.9	66972.0
Mpyld	Maximum Payload Mass (kg)	1184.33	3084.4	8981.1	11887.3

Where:

- Mref is an intermediate weight condition supplied by Bell for the CTR10, CTR30, and CTR120 variants and considered a reasonable mid-range loading.
- Mmin is selected as the operational empty weight. This is assumed to have crew aboard but no fuel or passengers.
- Mmax is selected as the maximum allowable takeoff mass.
- Mpyld = Mmax – Mmin – Max Fuel Load.

3.2.4 Flight Envelope Limitations

The BADA entries outlining the edge-of-the-envelope limitations for the CTR variants are shown in table 3-4. The maximum operating speeds (VMO, MMO) and altitude (hMO) are as provided in the Bell design synthesis per CTR. The remaining terms are determined given the provided Bell performance trim matrix data.

TABLE 3-4. FLIGHT ENVELOPE PARAMETERS

Parameter	Description (units)	CTR10	CTR30	CTR90	CTR120
VMO	Maximum Operating Speed (KCAS)	240	310	310	310
MMO	Maximum Operating Mach Number	0.48	0.6	0.6	0.6
hMO	Maximum Operating Altitude (ft)	38900	42118	44285	45368
hmax	Altitude at Maximum Takeoff Weight (MTOW) and ISA 300 fpm Residual Rate of Climb (ROC) (ft)	29870	32138	31819	31659
Gw	Weight Gradient on hmax (ft/kg)	3.2077	1.3679	0.7696	0.4705
Gt	Temperature Gradient on hmax (ft/°C)	–8.8235	–129.5	–139.65	–144.73

3.2.5 Flight Operations Schedule

The BADA entries outlining the flight operations airspeed schedules for the CTR airframes are shown in table 3-5. These terms are set based on provided Bell performance trim matrix data for climb, cruise, and descent, as well as background on how the CTR will be flown operationally in the passenger transport role.

3.2.6 Aerodynamics

The BADA aerodynamic characteristics for each CTR variant are shown in table 3-6 and were determined based on supplied performance trim data supplied by Bell. Values for STOL or VTOL configuration are identified in the tables, as well as the corresponding mapping with rate of climb (ROC) or glide slope (GS) angle operating conditions.

TABLE 3-5. FLIGHT OPERATIONS SCHEDULE PARAMETERS

Parameter	Description (units)	CTR10	CTR30	CTR90	CTR120
VCL1	Low Altitude Climb Speed (KCAS)	151	157	154	152
VCL2	High Altitude Climb Speed (KCAS)	155	161	156	153
MCL	Climb Mach Limit Above Transition Altitude	0.39	0.40	0.44	0.42
VCR1	Low Altitude Cruise Speed (KCAS)	193	206	201	198
VCR2	High Altitude Cruise Speed (KCAS)	184	200	197	197
MCR	Cruise Mach Limit Above Transition Altitude	0.44	0.48	0.54	0.54
VDES1	Low Altitude Descent Speed (KCAS)	230	244	244	244
VDES2	High Altitude Descent Speed (KCAS)	200	200	193	193
MDES	Descent Mach Limit Above Transition Altitude	0.44	0.43	0.44	0.44

TABLE 3-6. AIRFRAME AERODYNAMIC CHARACTERISTICS

Parameter	Description (units)	CTR10	CTR30	CTR90	CTR120
CD0,CR	Parasite Drag Coefficient in Cruise Configuration	0.05990	0.05849	0.04086	0.03204
CD2,CR	Induced Drag Coefficient in Cruise Configuration	0.04810	0.05289	0.04662	0.04348
CD0,IC	Parasite Drag Coefficient in Initial Climb Configuration	0.36349	0.42705	0.43646	0.33918
CD2,IC	Induced Drag Coefficient in Initial Climb Configuration	0.01598	0.021383	0.027139	0.024145
CD0,TO	Parasite Drag Coefficient in Takeoff Configuration 1,000 fpm ROC	STOL 0.32260 VTOL –12.35670	STOL 0.42396 VTOL 4.2404	STOL 0.47488 VTOL 18.0635	STOL 0.35794 VTOL 4.7414
CD2,TO	Induced Drag Coefficient in Takeoff Configuration	STOL 0.0098764 VTOL 0.0025598	STOL 0.018285 VTOL 0.0055689	STOL 0.025644 VTOL 0.008889	STOL 0.019272 VTOL 0.0073396
CD0,AP	Parasite Drag Coefficient in Approach Configuration –3/–6/–9 °GS	0.42436/ 0.57214/ 0.48485	0.436045/ 0.553336/ 0.484055	0.39973/ 0.46990/ 0.42846	0.34144/ 0.41299/ 0.37073
CD2,AP	Induced Drag Coefficient in Approach Configuration	0.02881	0.034666	0.040787	0.037409
CD0,LD	Parasite Drag Coefficient in Landing Configuration –3/–6/–9 °GS	STOL 2.77791/ 3.41753/ 4.06068 VTOL 12.76940/ 15.70459/ 18.67187	STOL 4.22332/ 4.82558/ 5.44787 VTOL 25.20372/ 28.37347/ 31.68655	STOL 4.77013/ 5.24222/ 5.74433 VTOL 32.17724/ 35.08876/ 38.21985	STOL 2.91198/ 3.30871/ 3.71849 VTOL 18.60385/ 20.84503/ 23.19928

TABLE 3-6. AIRFRAME AERODYNAMIC CHARACTERISTICS (concluded)

Parameter	Description (units)	CTR10	CTR30	CTR90	CTR120
CD2,LD	Induced Drag Coefficient in Landing Configuration	STOL 0.0077540 VTOL 0.0026077	STOL 0.015556 VTOL 0.0056728	STOL 0.023341 VTOL 0.0090598	STOL 0.018449 VTOL 0.0074862
CD0,DLDG	Parasite Drag Coefficient Due to Landing Gear Extended	0	0	0	0
CM16	Mach Drag Coefficient	0	0	0	0
VstallTO	Stall Speed Takeoff Configuration (KCAS)	STOL 76.9 VTOL 1	STOL 76.9 VTOL 1	STOL 76.9 VTOL 1	STOL 76.9 VTOL 1
VstallIC	Stall Speed Initial Climb Configuration (KCAS)	84.6	84.6	84.6	84.6
VstallCR	Stall Speed Cruise Configuration (KCAS)	122.1	121.9	116.4	113.6
VstallAP	Stall Speed Approach Configuration (KCAS)	38.5	38.5	38.5	38.5
VstallLD	Stall Speed Landing Configuration (KCAS)	STOL 30.8 VTOL 1	STOL 30.8 VTOL 1	STOL 30.8 VTOL 1	STOL 30.8 VTOL 1

The overall calculation of airframe drag within BADA for nominal cruise (CR) and initial climb (IC) conditions is formulated as follows:

$$C_D = C_{D0,CR} + C_{D2,CR} C_L^2 .$$

When in the defined approach configuration BADA quantifies overall airframe drag as follows as soon as the airframe descends below 8,000 feet above ground level (AGL) and speed falls below ($Vmin_{CR}$ + 10 kts):

$$C_D = C_{D0,AP} + C_{D2,AP} C_L^2$$

$$V_{\min CR} = 1.3 V_{stallCR} .$$

When in the defined landing configuration BADA quantifies overall airframe drag as follows as soon as the airframe descends below 3,000 feet AGL and speed falls below ($Vmin_{AP}$ + 10 kts):

$$C_D = C_{D0,LD} + C_{D0,DLDG} + C_{D2,LD} C_L^2$$

$$V_{\min AP} = 1.3 V_{stallAP} .$$

When in the defined takeoff configuration BADA quantifies overall airframe drag as follows:

$$C_D = C_{D0,TO} + C_{D2,TO} C_L^2 .$$

Overall drag (D) is formulated as follows:

$$D = \bar{q} S C_D .$$

The atmospheric model within BADA determines atmospheric density based on either ISA or non-ISA conditions for the computation of dynamic pressure above. The overall lift coefficient (C_L) within BADA is quantified under the assumption that the airframe flight path angle is always zero. A correction for bank angle (ϕ) is also included to account for turning flight:

$$C_L = \frac{2mg}{\rho V_{TAS}^2 S \cos\phi} .$$

Collected performance data for the CTR airframes was reduced to fit within this BADA structured format. Consequently, it was very important to consider the configurations that would be flown in proposed operation of the airframes for the takeoff (TO), initial climb (IC), cruise (CR), approach (AP), and landing (LD) phases. This would ensure the BADA performance dataset was consistent with proposed operational procedures for the CTR fleet. In addition, it provided equivalent system models linearized about the nominal operating conditions of the airframe.

3.2.7 Engine Thrust

The BADA propulsion model entries for each CTR variant are shown in table 3-7. Recall that BADA allows for a jet, turboprop, or piston model formulation. This particular study is best suited by the turboprop model. However, as noted previously, for compatibility with the ACES software a BADA jet propulsion model was required to develop the equivalent system model. All model formulations presented within this section are referenced from the BADA documentation and describe the general jet propulsion model configuration. Full details regarding BADA propulsion modeling techniques can be found in reference 9. A new entry (CTasc,to) was added for modeling takeoff thrust for ascent with details described below.

Overall, BADA models available thrust levels for the following phases of flight:

- Maximum power climb
- Reduced power climb
- Maximum cruise
- Descent

TABLE 3-7. PROPULSION SYSTEM THRUST CHARACTERISTICS.

Parameter	Description (units)	CTR10	CTR30	CTR90CTR	CTR120
CTc,1	1st Max Climb Thrust Coefficient (Newton)	14788.11	55348.78	114720.08	144405.73
CTc,2	2nd Max Climb Thrust Coefficient (ft)	110816.67	139329.60	137025.41	136592.64
CTc,3	3rd Max Climb Thrust Coefficient (1/ft^2)	–1.2E-10	–2.71E-10	–3.61E-10	–3.78E-10
CTc,4	1st Thrust Temperature Coefficient (°C)	0	0	0	0
CTc,5	2nd Thrust Temperature Coefficient (1/°C)	0.0014775	0.0019904	0.0036708	0.0045040
CTdes,low	Low Altitude Descent Thrust Coefficient	0.3780	0.2659	0.2276	0.2084
CTdes,high	High Altitude Descent Thrust Coefficient	0.2746	0.2369	0.2190	0.2101
hdes	Transition Altitude for Calculation of Descent Thrust (ft)	15,000	15,000	15,000	15,000
CTdes,app	Approach Thrust Coefficient –3/–6/–9 °GS	0.82196/ 0.71316/ 0.81748	0.62186/ 0.58945/ 0.95169	0.48439/ 0.48519/ 1.03470	0.67599/ 0.58317/ 0.89642
CTdes,ld	Landing Thrust Coefficient –3/–6/–9 °GS	STOL 1.15054/ 1.09349/ 1.03582 VTOL 1.46920/ 1.43873/ 1.40794	STOL 1.47841/ 1.40505/ 1.33088 VTOL 2.25627/ 2.21103/ 2.16530	STOL 1.80975/ 1.70667/ 1.60246 VTOL 3.12362/ 3.05423/ 2.98406	STOL 1.60850/ 1.50139/ 1.39309 VTOL 2.71699/ 2.64686/ 2.57595
CTasc,to	Takeoff Thrust Coefficient 1,000 fpm ROC	STOL 1.17356 VTOL 1.76048	STOL 0.92519 VTOL 2.67985	STOL 0.82419 VTOL 3.77222	STOL 1.13598 VTOL 3.38142

The maximum climb thrust generated at standard atmospheric conditions is formulated as follows:

$$\left(T_{\text{max climb}}\right)_{ISA} = C_{T,c1}\left(1 - \frac{h}{C_{T,c2}} + h^2 C_{T,c3}\right).$$

Nonstandard atmospheric conditions are accounted—given incremental temperature deviations from ISA— in the following way:

$$T_{\text{max climb}} = \left(T_{\text{max climb}}\right)_{ISA}\left(1 - C_{T,c5}\left(\Delta T_{ISA}\right)_{eff}\right)$$

$$\left(\Delta T_{ISA}\right)_{eff} = \Delta T_{ISA} - C_{T,c4}.$$

BADA models cruise configuration thrust such that it equals drag. However, it does implement a maximum available cruise thrust as a function of maximum available climb thrust:

$$\left(T_{cruise}\right)_{\max} = 0.95\left(T_{\text{max climb}}\right).$$

BADA models descent thrust in a similar fashion but allows for differentiation between altitude effects, approach, and landing configurations. The hdes term defines the threshold to differentiate between high and low altitude descent conditions as follows:

$$T_{des,high} = C_{Tdes,high} \times T_{\text{max climb}}$$

$$T_{des,low} = C_{Tdes,low} \times T_{\text{max climb}}.$$

When descending in approach or landing configuration, the descent thrust is modeled as follows:

$$T_{des,app} = C_{Tdes,app} \times T_{\text{max climb}}$$

$$T_{des,ld} = C_{Tdes,ld} \times T_{\text{max climb}}.$$

BADA does not specifically provide an entry to cater takeoff thrust per airframe. In order to support CTR terminal area operations, the modeling of takeoff thrust required must be known. An unused BADA entry was thus populated with a similar scale factor on maximum power climb thrust to model takeoff thrust levels. The new BADA scale factor ($C_{Tasc,to}$) modeling ascent takeoff thrust is presented below. ACES implementation must take this new parameter into consideration when preparing to operate the CTR in the terminal area.

$$T_{asc,to} = C_{Tasc,to} \times T_{\text{max climb}}.$$

Note that BADA allows for climb using lower power settings other than maximum climb power. The technique empirically reduces the power applied to the system and is outlined within the BADA documentation. Reduced power climbing is available in both the initial climb and standard climb phases of flight. The provided performance data for the CTR variants was reduced to fit within the general BADA model structure as outlined previously.

3.2.8 Fuel Flow

The BADA fuel flow model entries for each CTR variant are shown in table 3-8. Similar to thrust, BADA allows for the modeling of jet, turboprop, or piston engine performance in fuel flow. Although the Turboprop formulation is best suited to this application, the Jet fuel flow model was employed due to compatibility requirements for the ACES software. All model formulations presented within this section are referenced from the BADA documentation and describe the general jet propulsion model configuration. Full details regarding BADA fuel flow modeling techniques can be found in reference 9.

The following jet formulation for fuel flow is employed by BADA. The nominal fuel flow (in kg/min) is defined directly from overall thrust (T):

$$f_{nom} = \eta T$$

$$\eta = C_{f1}\left(1 + \frac{V_{TAS}}{C_{f2}}\right)$$

where V_{TAS} is true airspeed defined in knots. The preceding expressions are used during all flight phases excluding cruise, descent, and idle thrust conditions.

When in descent or idle thrust conditions BADA defines the minimum fuel flow (in kg/min) as a function of altitude above sea level (ft) where:

$$f_{\min} = C_{f3}\left(1 - \frac{h}{C_{f4}}\right).$$

TABLE 3-8. PROPULSION SYSTEM FUEL FLOW CHARACTERISTICS

Parameter	Description (units)	CTR10	CTR30	CTR90	CTR120
Cf1	Thrust Specific Fuel Consumption Coefficient (kg/min/kN)	0.28042	0.10985	0.088224	0.07741
Cf2	Thrust Specific Fuel Consumption Airspeed Term (KTAS)	275	65.96	51.66	44.78
Cf3	Descent Fuel Flow Coefficient (kg/min)	5.075	12.259	20.709	24.934
Cf4	Descent Fuel Flow Altitude Term (ft)	40932.93	48477.99	48483.18	48479.89
Cfcr	Cruise Fuel Flow Correction Coefficient	1.0767	1.0794	1.0961	1.1093

Under cruise conditions BADA calculates overall fuel flow as follows:

$$f_{CR} = \eta TC_{fCR} \,.$$

The provided performance data for the CTR fleet airframes was reduced to fit within the BADA model structure outlined above. The BADA performance model is defined in the most general way such that a multitude of airframes may be modeled given the same structure (refs. 9,10).

3.2.9 Ground Movement

Ground operational requirements as defined in BADA for each CTR variant are shown in table 3-9.

The values for takeoff and landing length depend on whether the airframe is in VTOL or STOL configuration, as well as the operational glide slope for final approach. VTOL implies a zero entry for TOL and LDL above, whereas run-on landings or short-field takeoffs imply non-zero entries. These entries are set to the nominal operational procedures defined for the CTR fleet based on PITL studies for the CTR10 and CTR30 airframes. Entries for the CTR90 and CTR120 airframes are extrapolated based on that data.

TABLE 3-9. AIRFRAME GROUND MOVEMENT CHARACTERISTICS

Parameter	Description (units)	CTR10	CTR30	CTR90	CTR120
TOL	Takeoff Length (m)	STOL 151.67 VTOL 0	STOL 179.22 VTOL 0	STOL 246.18 VTOL 0	STOL 271.45 VTOL 0
LDL	Landing Length –3/–6/–9 °GS (m)	STOL 40.84/ 47.55/ 46.33 VTOL 0/0/0	STOL 236.83/ 119.18/ 137.77 VTOL 0/0/0	STOL 713.08/ 293.25/ 359.97 VTOL 0/0/0	STOL 892.85/ 358.93/ 443.84 VTOL 0/0/0

3.3 Performance Data Collection

BADA model development targets the minimization of error between the performance model and full aircraft system in the areas of fuel consumption (f), thrust (T), and drag (D). Aircraft performance parameters relating to propulsive thrust, fuel flow, and aerodynamics are used to model each aircraft in the database. It is important to supply reference data for the nominal operational envelope of the aircraft at a minimum. Aircraft aerodynamic configuration is also important to capture, as equivalent system models are best developed around the nominal operating configurations. In the case of CTR modeling, nacelle (NAC) angle configuration is of importance.

In addition, it is critical to have an understanding of how the aircraft will be flown operationally to accomplish the mission. Figure 3-1 presents an overview of the CTR mission to transport passengers from origin to destination. The major phases are shown along with a mapping to the most relevant BADA aircraft configuration entry. The mission begins with a VTOL or STOL takeoff, followed by an initial climb-out. By 2,000 feet AGL the CTR is in full airplane mode (NAC 0 degrees) and climbs to cruise altitude at $1.23V_{stall}$. The CTR cruises at best-range velocity and descends from altitude, still in airplane mode, employing the Continuous Descent Arrival (CDA) technique. Upon reaching approximately1,500 feet AGL, the CTR begins conversion to approach and captures the glide slope while ending the mission with a VTOL or STOL landing.

For both VTOL and STOL missions the IC, CR, and AP aircraft configurations are identical. However, the TO and LD configurations will differ regarding NAC angle for these two modes of operations. Consequently, it was necessary to prepare two sets of BADA files per CTR variant. One set modeled STOL operations while the other modeled VTOL. Within the BADA framework this simply comes across as a STOL or VTOL variant for each size CTR.

The following sections describe the scope of the performance data collected, as well as the processes used to develop the BADA formatted equivalent system models.

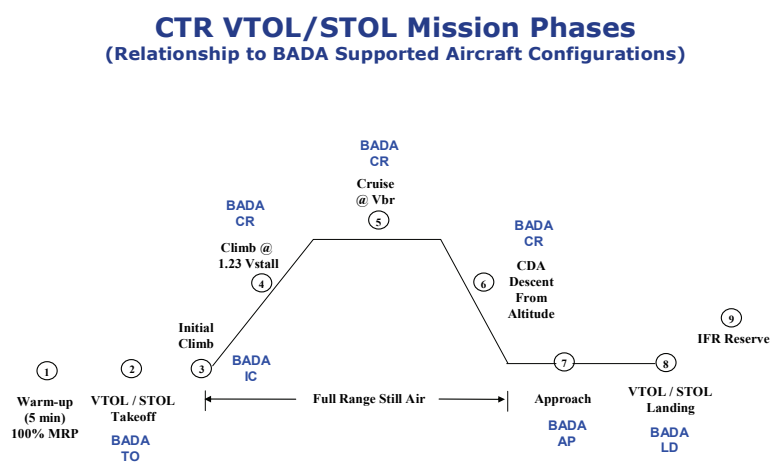

Figure 3-1. CTR VTOL/STOL mission phases mapped to BADA-supported configurations.

3.3.1 Trim Matrix Data

The following data was made available from Bell given the final products of the CTR design syntheses. Trim matrix data entries provided by Bell are at steady state, and unaccelerated flight conditions.

- Net forward propulsive force (including component of residual thrust)
- Net lift force
- Total drag force (including components of profile and induced drag)
- Total fuel flow rate
- Rate of climb/descent
- Trim airspeed (KCAS and KTAS)
- Dynamic pressure
- Mach
- Gross weight
- Nacelle angle
- Rotor rpm
- Pressure altitude
- Outside air temperature
- Flight path angle

The resulting BADA performance files were generated based on the supplied steady trim data.

BADA equations of motion assume the thrust line has a small angle of offset with respect to the airframe stability X-axis, and thus negligible. In the case of tiltrotor operations this is not a valid assumption depending on configuration. Thus, it requires the consolidation of overall lift due to *both* airframe aerodynamics and rotor thrust. Drag must also be considered in a similar fashion wherein *both* rotor drag and airframe aerodynamic drag are consolidated to properly account for the overall configuration of non-zero NAC angles.

3.3.2 Airplane Mode

Trim data throughout the flight envelope was captured for the following airplane modes of operations (NAC 0 degrees). These conditions were selected to efficiently populate the BADA data entries given the smallest trim set possible. Care was taken to ensure variation of the necessary model parameters such that a representative BADA model could be developed. Airplane mode is by far the dominant configuration with respect to time spent over a typical CTR mission. When above approximately 2,000 feet, the CTR variants are primarily in airplane mode for the climb, cruise, and descent.

- Maximum continuous power (MCP) cruise
- Long-range (LR) cruise power for level flight (PLF)
- MCP climb
- Idle power for descent (PFD)

- Absolute ceiling capture
- Service ceiling capture

A listing of airplane mode target trim points collected for BADA modeling purposes is presented in appendix B.

3.3.3 Conversion Mode

The remaining modes are AP, LD, TO, and IC. The approach configuration takes the CTR from initial conversion, post CDA completion at approximately 1,500 feet, down to acquisition of the decision altitude. Note that this mode has common NAC angle configuration for both VTOL and STOL. The landing phase, from decision altitude to touchdown, is best captured by two separate NAC angle configurations for VTOL and STOL. Likewise, the takeoff phase is best represented by two separate NAC angle configurations depending on VTOL or STOL operations. Based on Bell past tiltrotor experience it is known that, after takeoff, full airplane mode (NAC 0 degrees) is reached by approximately 2,000 feet AGL. In order to reduce the size of the trim matrix the IC performance can be set equivalent to either CR or STOL TO characteristics.

- Approach/ initial climb configuration PLF
- Approach configuration PFD (–3-, –6-, –9-degree glide slope)
- Landing configuration PLF
- Landing configuration PFD (–3-, –6-, –9-degree glide slope)
- Takeoff configuration PLF
- Takeoff configuration power for ascent (PFA) (250, 500, 750 fpm)

A listing of conversion mode target trim points collected for BADA modeling purposes is presented in appendix C.

3.4 BADA Model Determination

A repeatable process was developed to determine the BADA model parameters for all variants of the CTR airframes. Bell produced the airplane and conversion mode static trim point data using identical techniques for the CTR10, CTR30, and CTR120 variants and supplied the resulting performance data in a consistent format. This section outlines the analysis techniques used to process this static trim data for development of the final BADA-equivalent system models. Details are presented for the CTR10 variant within this section as an example. Additional supporting plots for the alternate variants such as CTR30 and CTR120 are presented in appendix D. Note that the CTR90 variant was not sized by Bell and, as such, performance data was not available for that variant. Consequently, the CTR90 BADA model was developed through examination of trends given the CTR10, CTR30, and CTR120 variants. The sizing of the CTR90 BADA model is presented in appendix E. A performance comparison of the linearly fitted CTR90 and an OEM designed 90-passenger CTR is presented in appendix F.

3.4.1 Aerodynamics

The overall calculation of airframe drag within BADA for CR conditions is formulated as follows:

$$C_D = C_{D0,CR} + C_{D2,CR} C_L^2 .$$

Trim data supplied for long-range cruise (LRC), maximum continuous power (MCP) cruise, MCP climb, and idle descent were binned together per CTR variant. Net lift and drag was included in this data and was then nondimensionalized as follows based on known wing planform area and dynamic pressure:

$$C_D = \frac{D}{\bar{q}S}$$

$$C_L = \frac{L}{\bar{q}S} .$$

This allowed for plotting of C_D versus C_L^2 and subsequent least-squares fitting of a line through the consolidated data to provide the best fit for the BADA drag equivalent system model in airplane mode. Including all data in the fit resulted in a drag performance equivalent system model for use over all mission segments. The resulting BADA model entries could then be calculated based on the best fit. The total drag for the CTR10 in airplane mode is shown in figure 3-2 along with the final best fit and resulting coefficient of determination (R^2). The coefficient of determination represents the proportion of variation in the source data that is explained by the model with a perfect fit having $R^2 = 1.0$.

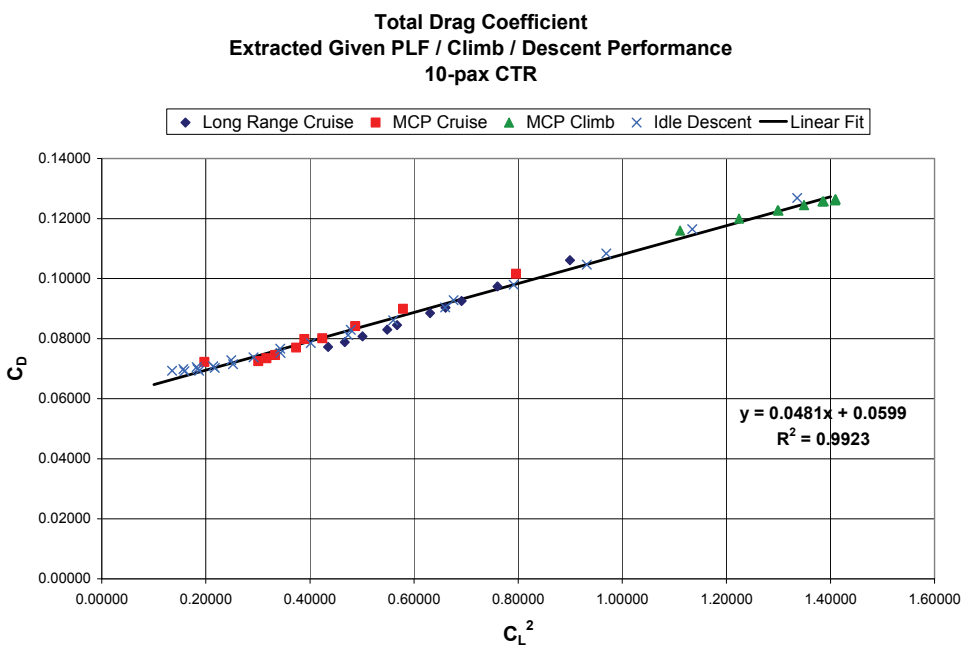

Figure 3-2. CTR10 airframe drag in airplane mode based on provided trim performance data.

TABLE 3-10. CTR10 CALCULATED STALL SPEED IN CR CONFIGURATION (NAC 0 DEGREES)

Altitude (ft)	Vstall @ MTOW (16,800 lbs) (KCAS)	Vstall @ MREF (15,500 lbs) (KCAS)
25,000	127.1	122.1
15,000	124.0	119.1
0	122.5	117.7

BADA requires the definition of a CR stall speed (VSTALLCR) for its operational logic as discussed previously. Although the event of stall is not modeled, the known stall speed is used in assigning lower limits on airspeed during operations. Operational speeds (such as stall speed) that are anchored to gross weight are defined within BADA about the known reference weight. Variations on that value based on actual gross weight are calculated within BADA as follows:

$$V = V_{ref}\sqrt{\frac{m}{m_{ref}}}\ .$$

The MCP climb trim points were captured across the altitude envelope of the airframe following a speed schedule of $1.23V_{stall}$ at MTOW. Results spanning the range of operational altitude were examined to yield the CR stall speeds as shown in table 3-10. The relation above was used to generate the stall speeds with respect to the nominal reference mass (MREF) as required by BADA.

Variations in stall speed across the envelope as shown previously can be caused by small changes in overall wing configuration such as those imparted by automatic wing flap schedules. As BADA only allows for a single entry, the more conservative value of 122.1 KCAS was selected for the CTR10 in airplane mode.

3.4.2 Propulsion

Maximum propulsion performance regarding thrust available is modeled in BADA based on maximum thrust in climb. The BADA formulation for this characteristic under standard atmospheric conditions (ISA) is a function of altitude as follows:

$$\left(T_{\max c\lim b}\right)_{ISA} = C_{T,c1}\left(1 - \frac{h}{C_{T,c2}} + h^2 C_{T,c3}\right).$$

Trim data was collected across the altitude envelope for the CTR variants under MCP climb conditions. Figure 3-3 presents the trim thrust for the CTR10 under MCP climb, MCP PLF, and LRC PLF conditions. The second-order least-squares fit for the MCP climb data results in the base maximum performance thrust model for the CTR10 variant.

The BADA-equivalent system model entries are calculated directly from the terms in the least-squares fit noted in the figure.

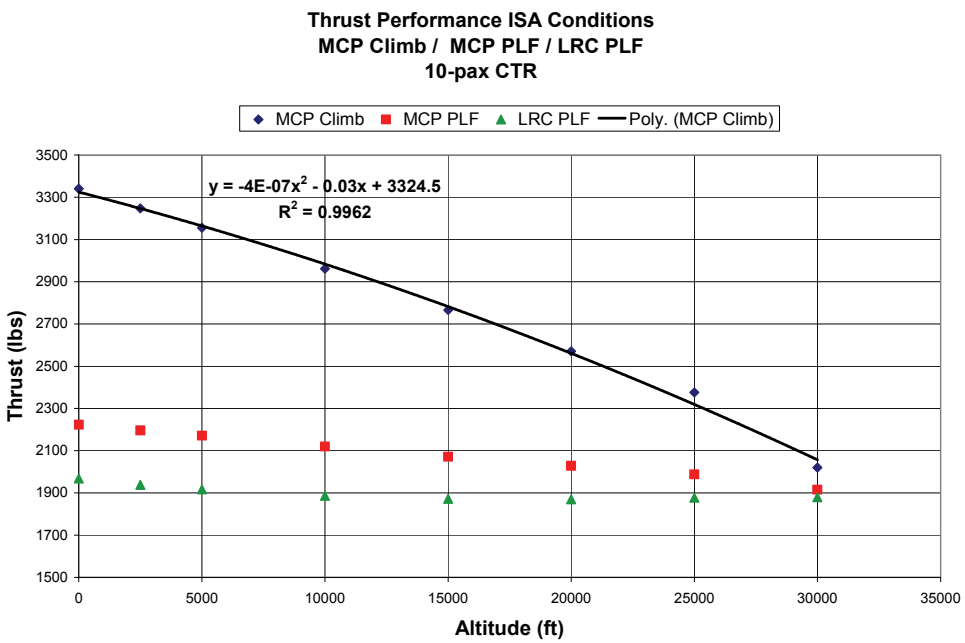

Figure 3-3. CTR10 thrust performance under various operating conditions.

The low-power-descent trim data was used for modeling the BADA descent thrust. The low, or idle, power setting thrust is modeled within BADA given the $C_{Tdes,low}$ and $C_{Tdes,high}$ coefficients shown below as a function of MCP climb thrust:

$$T_{des,high} = C_{Tdes,high} \times T_{\max\ climb}$$

$$T_{des,low} = C_{Tdes,low} \times T_{\max\ climb}\ .$$

The altitude h_{des} defines the threshold to differentiate between using high- or low-altitude descent conditions.

As an example, the CTR10 descent profiles were trimmed across the altitude envelope over a series of three constant true airspeeds. The descent thrust ratio ($T_{des}/T_{max\ climb}$) can be seen in figure 3-4 for the CTR10 as a function of altitude.

Given this information the value for h_{des} was selected to be 15k feet to split the altitude envelope equally. The final low-altitude value of $C_{Tdes,low}$ was determined by averaging all points available ≤15k feet. Likewise, the high-altitude value of $C_{Tdes,high}$ was determined by averaging all points ≥15k feet.

Nonstandard-day (non-ISA) effects on the propulsion system are modeled by BADA. The non-ISA effects on maximum thrust available in climb are modeled as follows:

$$\left(T_{\max\ climb}\right)_{Non-ISA} = \left(T_{\max\ climb}\right)_{ISA}\left(1 - C_{T,c5}\left(\Delta T_{ISA}\right)_{eff}\right)$$

$$\left(\Delta T_{ISA}\right)_{eff} = \Delta T_{ISA} - C_{T,c4}\ .$$

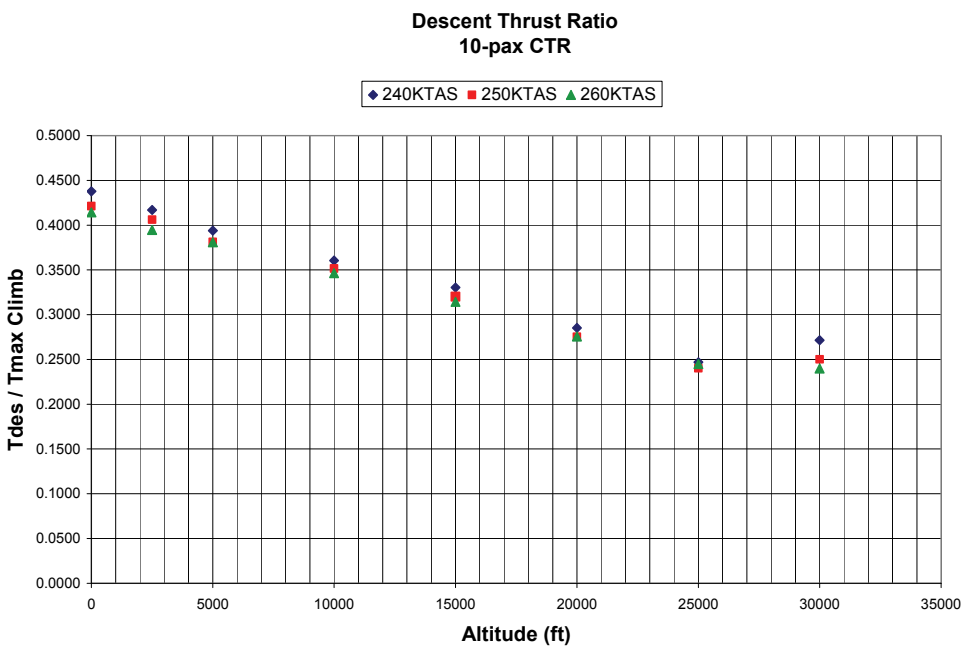

Figure 3-4. CTR10 descent thrust ratio across altitude envelope.

Simplifying this formulation $C_{T,c4}$ was set to zero for all CTR variants. Each CTR design was used to generate MCP climb trim data at 10k and 20k feet for ISA+20°C nonstandard-day conditions to capture this effect. This was in addition to the ISA condition trim points already collected at those altitudes. For the CTR10 the maximum climb thrust ratio of non-ISA to ISA conditions was 0.972 and 0.969 for the 10k and 20k foot points, respectively. Using an average value of the thrust ratio, a single value of $C_{T,c5}$ was determined as follows:

$$C_{T,c5} = \frac{\left(1 - \frac{\left(T_{\max c\lim b}\right)_{Non-ISA}}{\left(T_{\max c\lim b}\right)_{ISA}}\right)}{\left(\Delta T_{ISA}\right)_{eff}}.$$

Static trim data was also used to develop the fuel flow BADA model for each CTR variant. Fuel flow data for each variant was available under LR cruise, MCP cruise, MCP climb, and low-power-descent flight conditions. The nominal fuel flow (in kg/min) in BADA is defined directly from overall thrust (T):

$$f_{nom} = \eta T$$

$$\eta = C_{f1}\left(1 + \frac{V_{TAS}}{C_{f2}}\right)$$

where V_{TAS} is true airspeed defined in knots. The preceding expressions are used during all flight phases excluding cruise or descent under low-power/idle-thrust conditions. Consequently, the model above is built based on MCP climb fuel flow data. As an example, figure 3-5 presents values of η for the CTR10 variant for MCP climb, MCP cruise, and LR cruise conditions determined from provided trim data. The model for η was built given the linear fit (solid line) shown based on all available MCP climb data collected under ISA conditions.

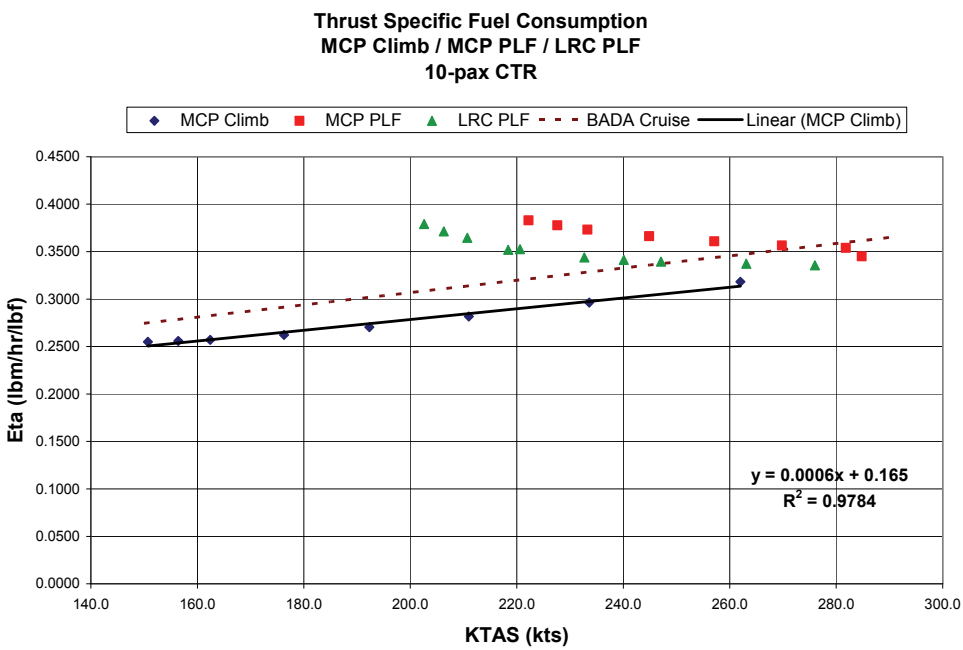

Figure 3-5. CTR10 descent thrust specific fuel consumption over various mission phases.

Under cruise conditions BADA calculates overall fuel flow as follows:

$$f_{CR} = \eta T C_{fCR} .$$

The scale factor C_{fCR} allows for better emulation of cruise fuel flow conditions. Using the MCP climb-based model shown in figure 3-5 would result in an overall shortfall in fuel burned over any given cruise mission segment. In order to determine this cruise fuel flow scale factor, only data points falling within the primary cruise altitude band for each CTR variant were considered. As an example, for the CTR10 the MCP cruise and LR cruise fuel flow points were considered over the 20–30k foot altitude envelope. This is considered a representative region of primary cruise flight for this CTR and serves to optimize the model for cruise fuel flow about the nominal region of operations for cruise. Each point examined resulted in a value for C_{fCR} with the average being selected as the final fuel flow scale factor. In the case of the CTR10 this resulted in a final value for C_{fCR} of 1.0767. The dashed line presented in figure 3-5 is the final cruise condition formulation of η to be used by the CTR10 BADA model.

When in low-power descent or idle-thrust conditions BADA defines the minimum fuel flow (in kg/min) as a function of altitude above sea level (ft) where:

$$f_{\min} = C_{f3}\left(1 - \frac{h}{C_{f4}}\right).$$

Performance trim data was collected in the descent configuration for each CTR variant over a series of three constant true airspeeds over the altitude envelope. This data was used to develop the low-power/idle-thrust model in the BADA formulation. As an example, the CTR10 descent thrust performance data is shown in figure 3-6. This performance data was used to build the low-power/idle-descent fuel flow model noted above with terms in the linear fit used to calculate C_{f3} and C_{f4}. The linear fit shown is based on the consolidated data set for 240, 250, and 260 KTAS points.

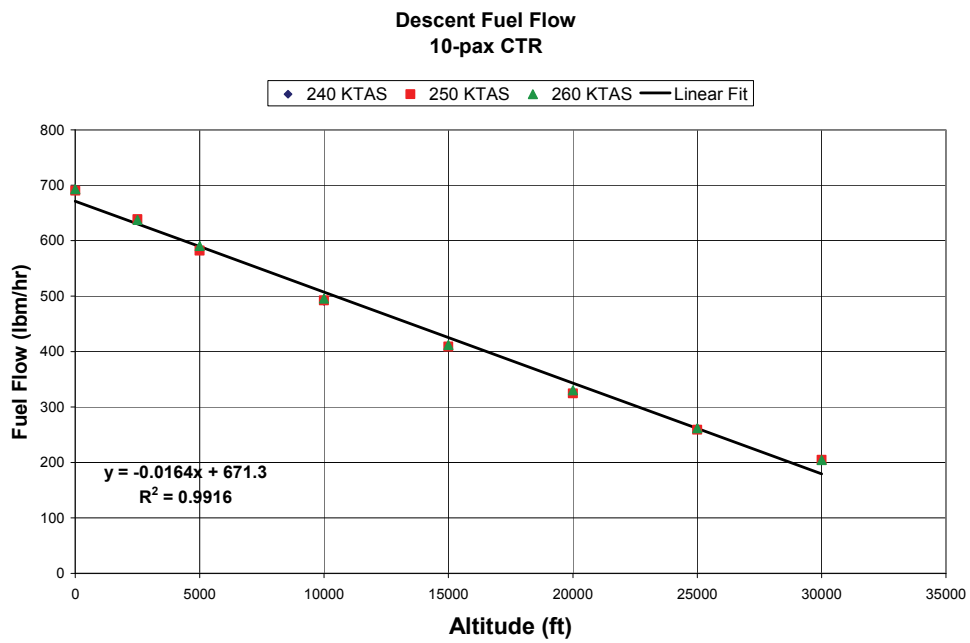

Figure 3-6. CTR10 low-power-descent fuel flow variant.

3.4.3 Flight Envelope Limitations

BADA provides several terms for specification of flight envelope limitations. Trim data collected from each CTR variant were used to identify various altitude limitations. BADA specifies the maximum operational altitude of an aircraft as follows:

$$h_{\max,\,actual} = \min\left(h_{MO}\,, h_{\max} + G_t\left(\Delta T_{ISA} - C_{Tc,4}\right) + G_w\left(m_{\max} - m_{actual}\right)\right).$$

Prior analysis set $C_{Tc,4}$ zero for all CTR variants. The value for h_{MO} denotes the absolute maximum operating altitude where the aircraft has no residual rate of climb available. This value was supplied as a direct result of a performance trim point for each CTR configured for minimum mass (M_{min}). In the case of the CTR10 this value was 38.9k feet.

A series of trim points configured for M_{min}, M_{ref}, and M_{max} for each CTR variant was also collected to determine the altitude under ISA conditions (h_{max}) where the CTR had a 300 fpm residual rate of climb available. These points result in the determination of terms h_{max} and G_w in the above formulation. The value for h_{max} denotes the altitude under MTOW conditions whereas G_w captures the effect of gross weight variation from MTOW. As an example, the necessary data to determine this characteristic for the CTR10 is shown in figure 3-7. The resulting CTR10 BADA entries for h_{max} and G_W were 29.87k feet and 3.2077 feet/kg based on the linear fit shown.

The effect of non-ISA conditions on h_{max} was also captured via a single trim point per CTR variant. The value of h_{max} was determined at MTOW for both ISA and ISA+20°C conditions. This performance information was suitable to determine the atmospheric temperature effect G_t. In the case of the CTR10 G_t was determined to be –8.8235 feet/deg C.

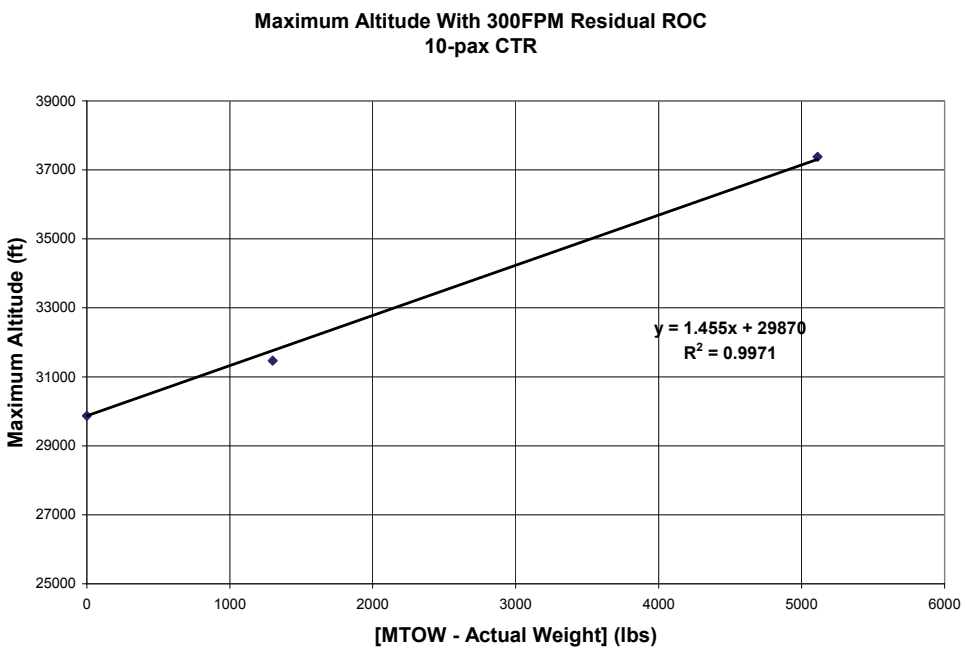

Figure 3-7. CTR10 effect of MTOW variation on maximum attainable altitude at 300-fpm residual ROC.

3.4.4 Flight Operations Schedule

As outlined in appendix A, BADA allows for limited customization of airspeed operational schedules for climb, cruise, and descent phases of the overall mission profile using a generic set of logic for all aircraft in the database.

Figure A-1 presents the airline climb speed schedule followed by all aircraft within the BADA environment based on operating altitude and a known reference stall speed. The analyst may specify two entries (V_{CL1} and V_{CL2}) for the schedule, as well as a constant Mach number schedule (M_{CL}) to capture once the transition altitude is met or exceeded. V_{CL1} defines the constant speed schedule for the region of 1.5k up to 10k feet. V_{CL2} defines the constant speed schedule from 10k feet up to the transition altitude. Thereafter M_{CL} is maintained by the aircraft.

The CTR climb schedule for all variants is fixed at 1.23 V_{stall} in airplane mode. The collected performance trim points for MCP climb supplied the airspeed schedule information required over the altitude envelope for each CTR to build the BADA climb schedule. The MCP climb trim points spanning the full altitude envelope were configured at MTOW.

As an example, consider the climb speed schedule resulting from available trim points for the CTR10 as shown in figure 3-8. The primary operating altitude range for the CTR10 is considered sea level to 25k feet. The low-altitude climb speed (V_{CL1}) was determined as the average of the schedule speeds covering the range of 0k to 10k ft. The high-altitude climb speed (V_{CL2}) was determined as the average of the schedule speeds covering the range of 10–25k feet. The Mach schedule (M_{CL}) was determined as the Mach number corresponding to the actual trim point climb speed at 25k feet. For the CTR10 this resulted in V_{CL1}, V_{CL2}, and M_{CL} of 151 KCAS, 155 KCAS, and 0.39, respectively.

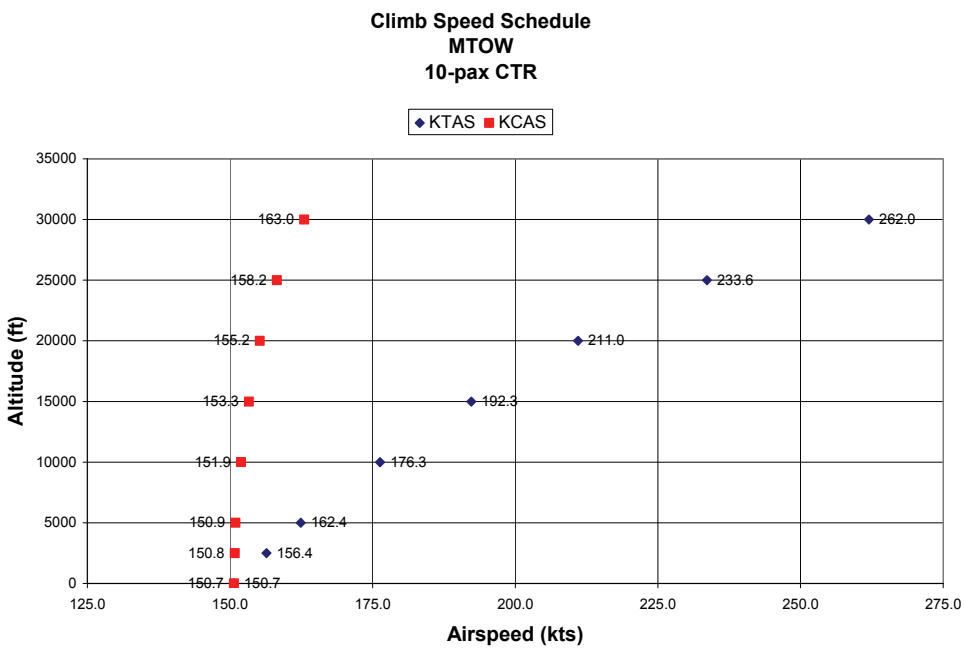

Figure 3-8. Climb schedule over the altitude envelope for the CTR10 at MTOW and airplane mode.

Similarly, figure A-2 presents the airline cruise speed schedule based on operating altitude. Two entries (V_{CR1} and V_{CR2}) may be specified, as well as a constant Mach number (M_{CR}), to capture once the transition altitude is met or exceeded. V_{CR1} defines the constant speed schedule for the region of 3k up to 10k feet. V_{CR2} defines the constant speed schedule from 10k feet up to the transition altitude. Thereafter, M_{CR} is maintained by the aircraft.

The collected performance trim points for LR cruise, or speed for best range, supplied the airspeed schedule information required over the altitude envelope for each CTR to build the BADA cruise schedule. These points spanned the full altitude envelope and were configured at MTOW.

As an example, consider the LR cruise speed schedule resulting from available trim points for the CTR10 shown in figure 3-9. The primary operating altitude range for the CTR10 is considered sea level to 25k feet. The low-altitude cruise speed (V_{CR1}) was determined as the average of the schedule speeds covering the range of 5–10k feet. The high altitude cruise speed (V_{CR2}) was determined as the average of the schedule speeds covering the range of 10–25k feet. The Mach schedule (M_{CR}) was determined as the Mach number corresponding to the actual trim point cruise speed at 25k feet. For the CTR10 this resulted in V_{CR1}, V_{CR2}, and M_{CR} of 193 KCAS, 184 KCAS, and 0.44, respectively.

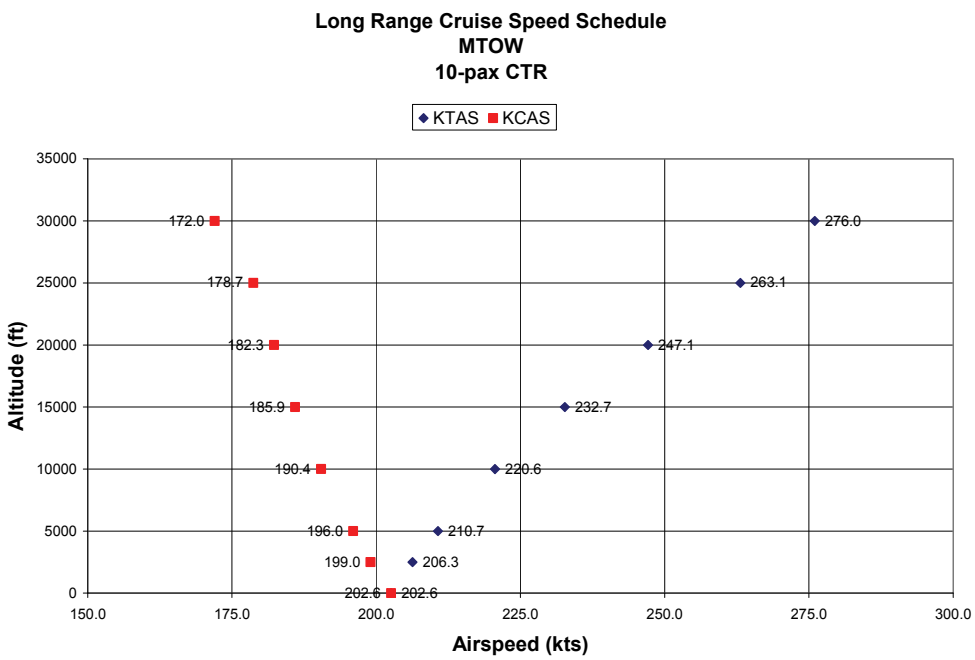

Figure 3-9. CTR10 LRC schedule over the altitude envelope in airplane mode at MTOW.

Finally, the airline descent schedule employed by BADA was shown in figure A-3 as a function of operating altitude and a known reference stall speed. Two airspeed entries (V_{DES1} and V_{DES2}), as well as a constant Mach number (M_{DES}), may be specified for the schedule. V_{DES1} defines the constant speed schedule for the region of 3k up to 10k feet. V_{DES2} defines the constant speed schedule from 10k feet up to the transition altitude. Thereafter, M_{DES} is maintained by the aircraft.

The collected performance trim points for descent supplied the airspeed schedule information required over the altitude envelope for each CTR to build the BADA descent schedule. These points spanned the full altitude envelope, were configured at MTOW, and were collected at constant true airspeeds of 240, 250, and 260 KTAS.

Consider the descent speed schedule resulting from available trim points for the CTR10 shown in figure 3-10. Operationally, it was assumed the CTR would be following a continuous descent arrival (CDA) profile. Consequently, the higher speed schedule of 260 KTAS was selected to model the descent profile for BADA. The primary operating altitude range for the CTR10 is considered sea level to 25k feet. The low-altitude descent speed V_{DES1} was determined as the average of the schedule speeds covering the range of 0–10k feet. The high-altitude descent speed V_{DES2} was determined as the average of the schedule speeds covering the range of 10–25k feet. The Mach schedule (M_{DES}) was determined as the Mach number corresponding to the actual trim point descent speed at 25k feet. For the CTR10 this resulted in V_{DES1}, V_{DES2}, and M_{DES} of 230 KCAS, 200 KCAS, and 0.44, respectively. It is important to note the average values for the low-altitude descent region (V_{DES1}) exceeded V_{MO} (240 KCAS). As a result, V_{DES1} was set at (V_{MO} – 10) KCAS to allow for an over-speed buffer for operations in BADA.

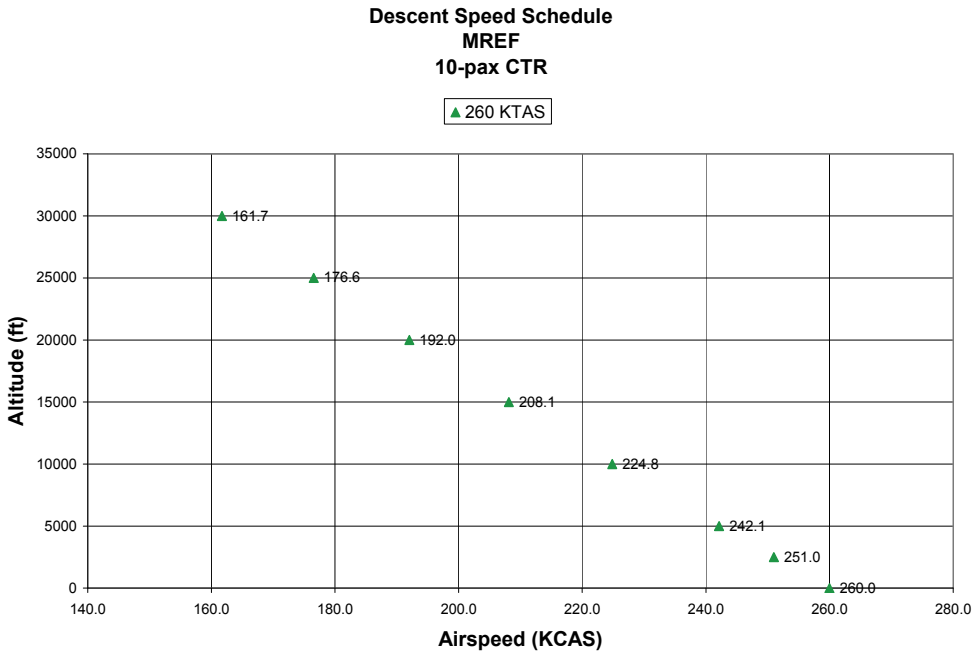

Figure 3-10. Descent schedule for the CTR10 at MREF and airplane mode.

The preceding methods were employed to develop the entries for climb, cruise, and descent operating airspeed schedules for the CTR variants. Note that BADA provides limited customization of the airspeed schedule as noted above. However, future CTR studies using ACES are projected to allow for waypoint-based airspeed and configuration schedules providing the freedom to define operating schedules with finer resolution. The entries above developed for BADA are considered a best representation given the allowable model structure.

3.4.5 Conversion Mode Modeling

Model development for this phase of flight operations was challenging in that the overall BADA framework was designed to support fixed-wing flight operations. This precludes the use of hover flight operations. In addition, this presents challenges in the capture of higher thrust levels required, over and above airplane mode maximum continuous power climb settings, for STOL and VTOL operations while also emulating fuel burn performance. The variable nacelle angle configurations of the CTR must be represented by mapping a fixed nacelle position to particular phases of flight. The BADA framework allows for the definition of aerodynamic properties for up to five aerodynamic settings as discussed in appendix A. Airplane mode for the CTR is defined by the CR configuration within BADA. The CTR conversion modes are defined by the four additional aerodynamic configurations available within the model structure. This includes TO, IC, AP, and LD. Dynamic nacelle transitions are not possible in this framework with conversion modes entered discontinuously. Due to the discrete limitations of nacelle angle modeling it was important to select configurations and flight conditions that best represented the flight operations schedule of the CTR fleet. This modeling task was being worked in parallel with planning for a future PITL study that would determine final ConOps for the airframes. However, Bell's past experience in tiltrotor design and operation allowed for the definition of representative nominal conditions on which to base the BADA conversion models. The trim performance data received from Bell for the CTR10, CTR30, and CTR120 variants were collected about the nominal flight configurations and conditions as outlined in appendix C.

The fixed-wing phase of operations for the CTR allowed for the emulation of aerodynamics, thrust, and fuel flow to match that of the Boeing-provided trim data. This CTR mode is the basis of CR aerodynamics, maximum thrust available, and nominal fuel flow. This is required due to the definition of the overall model structure and is intuitive in that the vast majority of any complete mission is flown in CR mode with conversion configuration limited to the airport terminal area only. The conversion modes of operation typically require much higher net thrust and much greater fuel flow than can be supported by the fixed-wing CR-based model available in BADA. With the least amount of operational time spent in these conversion modes, as well as the requirement to use the BADA framework, it was decided to target the Bell fuel flow numbers in the provided performance trim data while allowing thrust and aerodynamic drag performance to be fallouts. This would ensure higher fidelity fuel burn in the terminal area during conversion configuration.

The process for development of the BADA conversion model is identical for the CTR10, CTR30, and CTR120 variants. This section specifically references data for the CTR10 variant as an example. The supporting data for the CTR30 and CTR120 variants are presented in appendix D. The scaled CTR90 conversion mode modeling technique is presented in appendix E.

3.4.5.1 Conversion-Mode Propulsion

The nominal fuel flow model outlined in section 3.4.2 is rearranged as follows to specify conversion-mode thrust required to match the Bell-supplied fuel burn performance data:

$$T = \frac{f_{nom}}{\eta}.$$

Here f_{nom} is set to Bell-provided fuel burn performance data for a given trim point while η is populated with the current BADA-specific fuel consumption model output for the CTR variant under investigation. BADA defines the approach and landing thrust setting as a scaled value of the MCP climb thrust available at the given flight condition as shown:

$$T_{des,app} = C_{Tdes,app} \times T_{\text{max climb}}$$

$$T_{des,ld} = C_{Tdes,ld} \times T_{\text{max climb}} .$$

The CTR10 variant results for $C_{Tdes,app}$ and $C_{Tdes,ld}$ are presented in figure 3-11 as a function of glide slope angle. Determination of these parameters at the –3-, –6-, and –9-degree glide slope based on provided trim data allows for development of separate BADA files to emulate each operational approach angle. This provides a choice of operational approach angle when performing National Airspace studies in the future. Note that approach configuration is identical between STOL and VTOL operations down to the decision altitude. Upon reaching the decision altitude a significant distinction is made between STOL and VTOL performance given the different nacelle angle configurations. Each point in the plot is labeled with the corresponding C_{Tdes} value for reference.

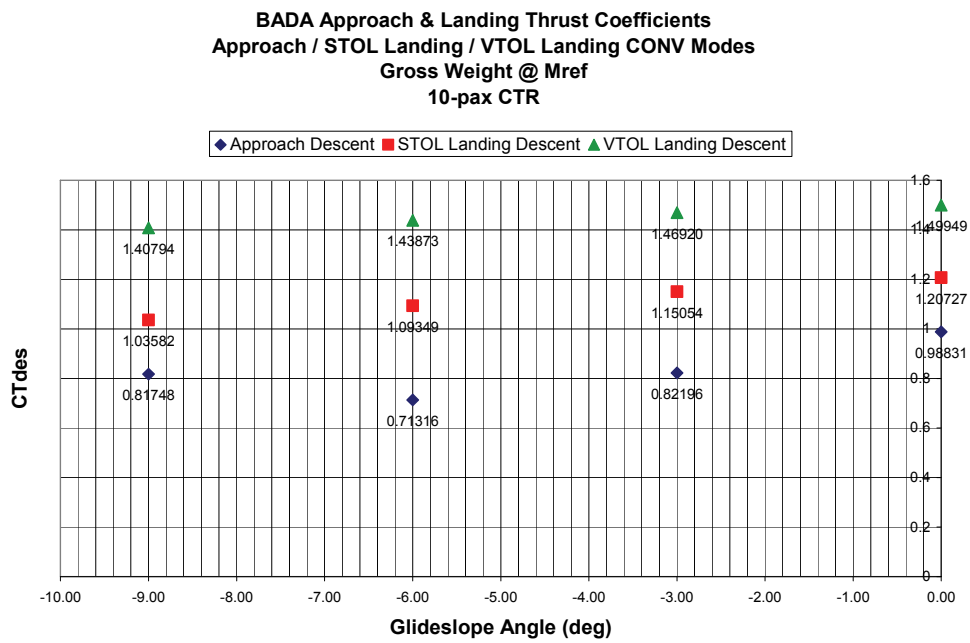

Figure 3-11. CTR10 approach and landing descent thrust scale factor.

Note that BADA does not support the specification of a takeoff thrust scale factor for ascent in the TO configuration. In order to accommodate the significant thrust increases required for takeoff operations in the STOL and VTOL CTR modes, a new scale factor ($C_{Tasc,to}$) was determined and populated in an unused entry location within each provided BADA file. This new takeoff term was developed in the same way as was the approach and landing thrust coefficients with the formulation noted below:

$$T_{asc,to} = C_{Tasc,to} \times T_{\max\ \text{climb}} .$$

The resulting TO thrust scale factor for the CTR10 as a function of steady rate of ascent is presented in figure 3-12. Original specifications for the trim matrices required points at 0-, 250-, 500-, and 750-feet/minute ascent rates. Operationally, it was decided the final CTR fleet would follow a 1,000-feet/minute ascent rate immediately following takeoff. Consequently, the linear fits presented in figure 3-12 were used to extrapolate the required thrust scaling coefficient for the 1,000-feet/minute takeoff ascent rate for use in the final BADA model. For the CTR10 this resulted in values of $C_{Tasc,to}$ of 1.1736 and 1.7605 for STOL and VTOL, respectively.

3.4.5.2 Conversion-Mode Aerodynamics

The calculated thrust outlined in section 3.4.5.1 was used to determine an equivalent system lift and drag for conversion mode aerodynamics using the following approximations for each trim point:

$$D = T - W\sin(\gamma)$$

$$L = W\cos(\gamma) .$$

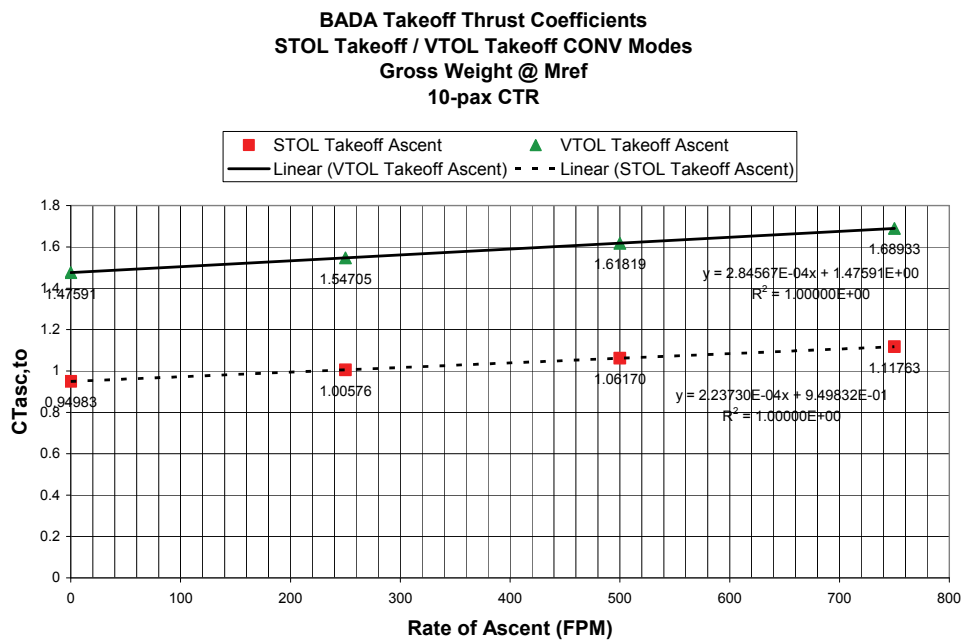

Figure 3-12. Takeoff thrust scale factor for the 10-passenger CTR.

The nondimensional lift (C_L) and drag (C_D) coefficients were then determined as outlined in section 3.4.1. Recall the general formulation of drag in the BADA model where:

$$C_D = C_{D0} + C_{D2} C_L^2 .$$

Plots of C_D versus C_L^2 resulted in linear least squares fits that were used in determining the aerodynamic coefficients C_{D0} and C_{D2} for each configuration (TO, IC, AP, and LD) for both STOL and VTOL operations. The least-squares fit shown in figure 3-13 was used to determine $C_{D0,IC}$ and $C_{D2,IC}$ for the CTR10 in IC mode under level flight conditions. Figure 3-14 presents aerodynamic drag for approach conversion mode formulated using data at –3-,–6-, and –9-degree glide slope angles. Similarly, this plot was used to generate the BADA entries for $C_{D0,AP}$ and $C_{D2,AP}$ for the CTR10.

Aerodynamics for the STOL and VTOL LD conversion modes of the CTR10 are shown in figure 3-15 and figure 3-16. Similar information is shown in figure 3-17 and figure 3-18 for the TO conversion mode of the CTR10. Each figure presents a linear least-squares fit given level flight condition data. Each figure also includes three points representing aerodynamic performance in either descending (–3-, –6-, –9-degree glide slope) or ascending flight (250, 500, 750 feet/minute). The least-squares fits were used to generate the BADA-equivalent system model coefficients for level flight conditions given each configuration (TO or LD) in STOL and VTOL modes. Assuming the C_{D2} drag model term remained constant, the C_{D0} term was biased for each configuration to target the descending or ascending data points. This allowed for development of a set of equivalent system BADA aerodynamic models for the TO and LD conversion modes in both STOL and VTOL flight. Consequently, BADA model files were developed to support STOL or VTOL operations with a combined AP and LD glide slope of –3, –6, or –9 degrees.

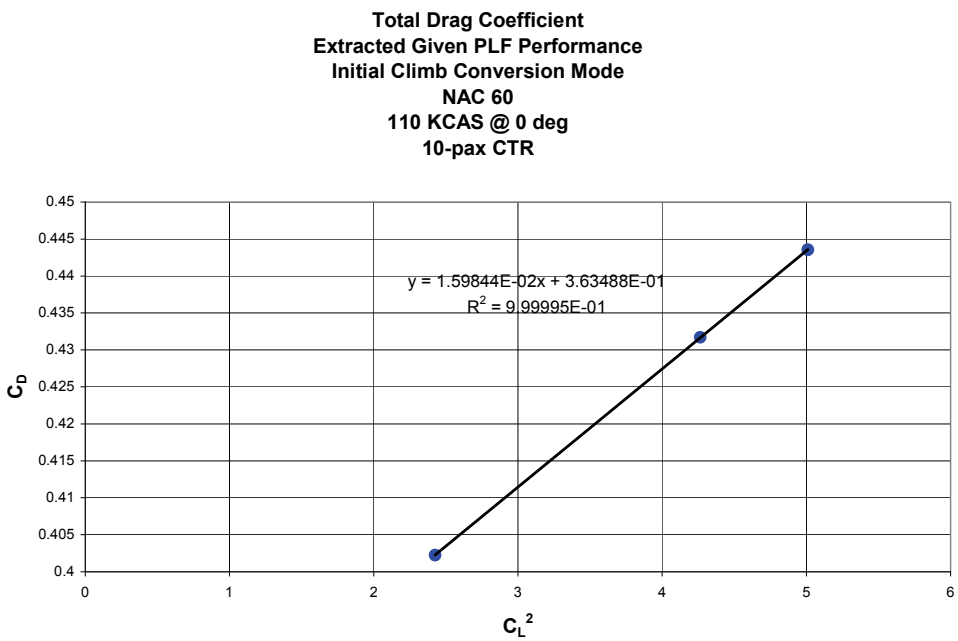

Figure 3-13. Aerodynamics for IC mode of the CTR10.

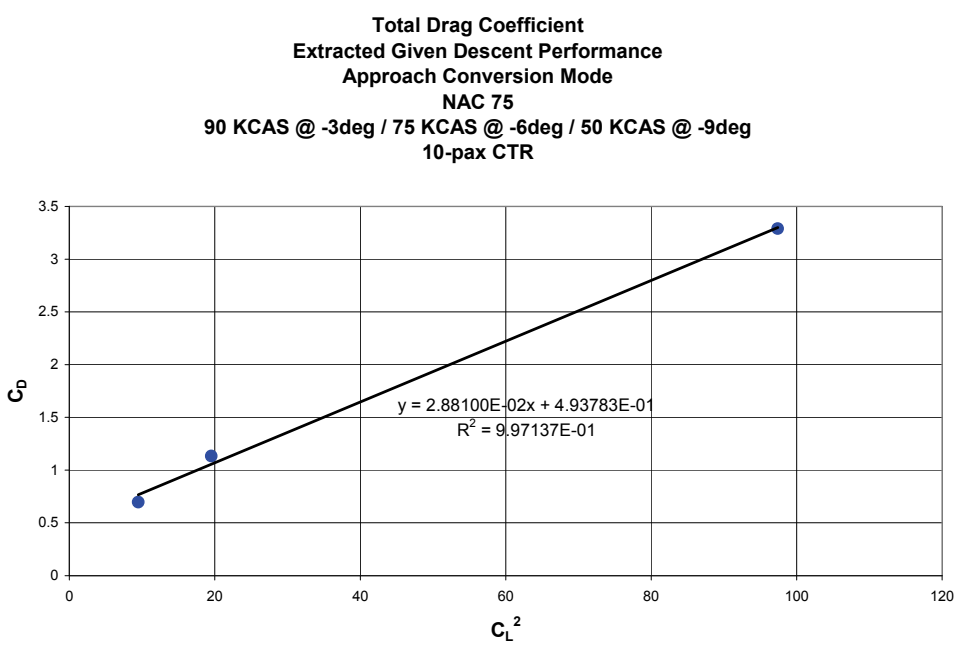

Figure 3-14. Aerodynamics for AP mode of the CTR10.

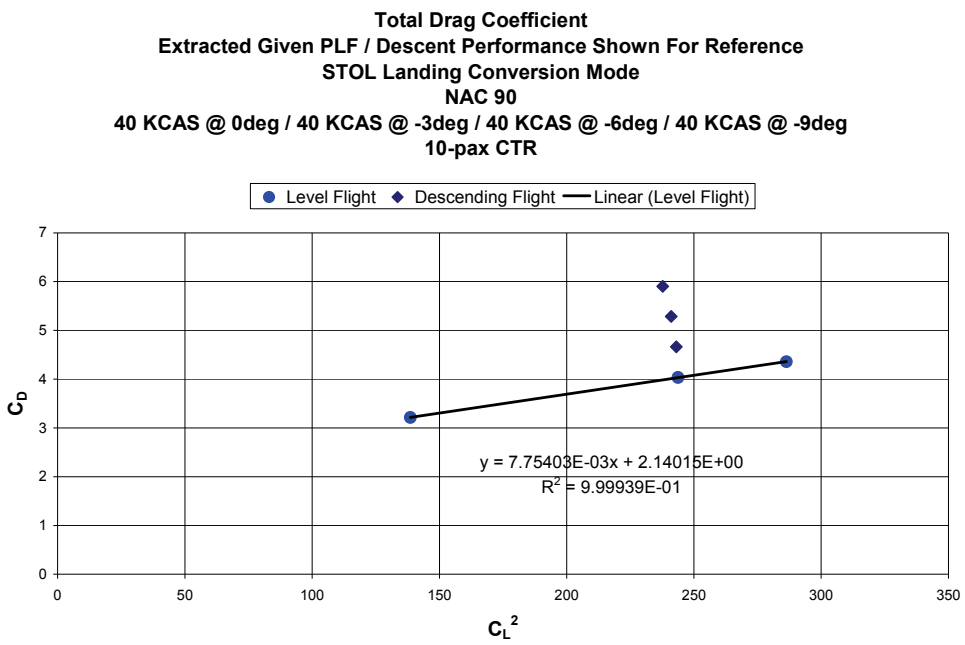

Figure 3-15. Aerodynamics for STOL LD mode of the CTR10.

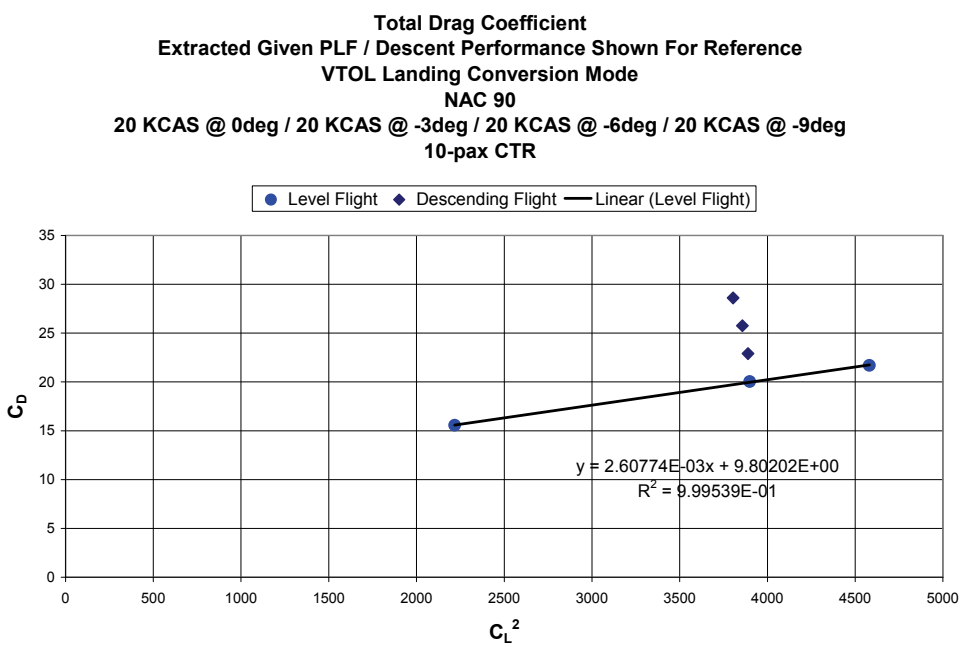

Figure 3-16. CTR10 aerodynamics for VTOL LD mode.

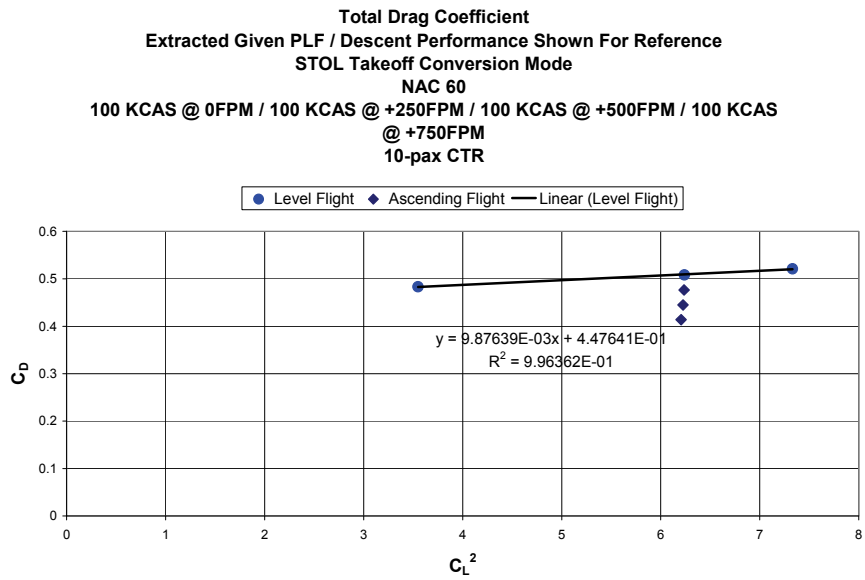

Figure 3-17. CTR10 aerodynamics for STOL TO mode.

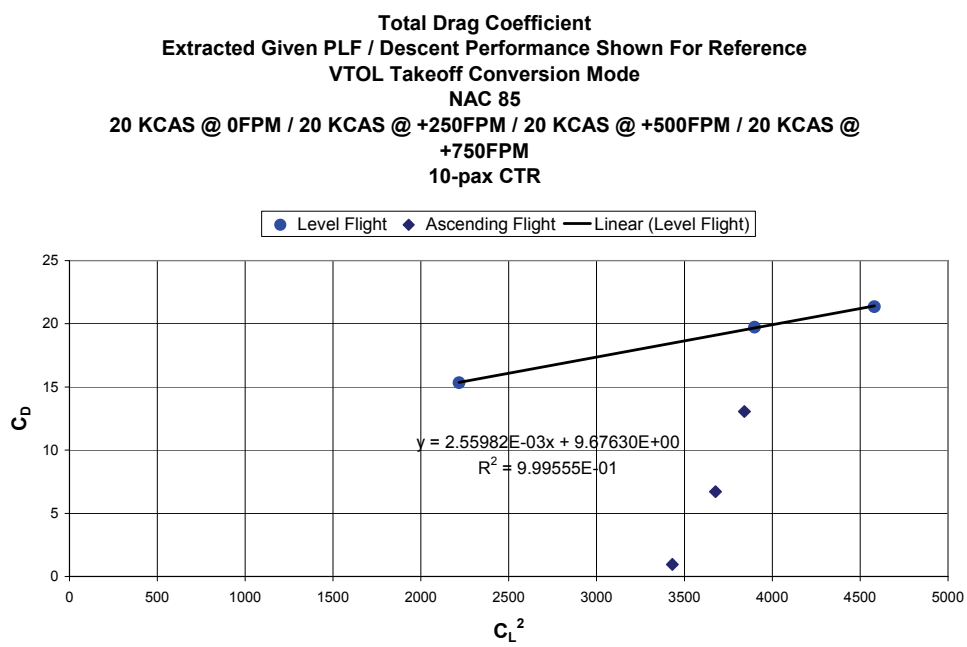

Figure 3-18. CTR10 Aerodynamics for VTOL TO mode.

Trim data was received to support TO ascending flight operations at 0, 250, 500, and 750 feet/minute. However, the selected fleet operations will have the CTR climbing out at TO targeting approximately 1,000 feet/minute. As a result, the C_{D0} terms for the 0-, 250-, 500-, and 750-feet/minute data points were used to generate a second-order least-squares fit as shown in figure 3-19 and figure 3-20. This fit was used to extrapolate the C_{D0} term for the 1,000-feet/minute flight condition to be used in the equivalent system BADA

model. For the CTR10 this resulted in a $C_{D0,TO}$ value of 0.3226 and –12.357 for STOL and VTOL, respectively. Note that the magnitudes, and even sign, of the C_{D0} terms can fallout unconventionally due to the equivalent system modeling technique used here. Thrust is back-calculated, given the fixed BADA thrust specific fuel consumption model for the CTR variant, such that Bell-provided fuel burn data is matched. Aerodynamic drag is determined such that it is consistent with calculated thrust to provide the necessary net buildup of forces. The C_{D2} drag model term is assumed constant given the level flight data for the conversion mode under investigation.

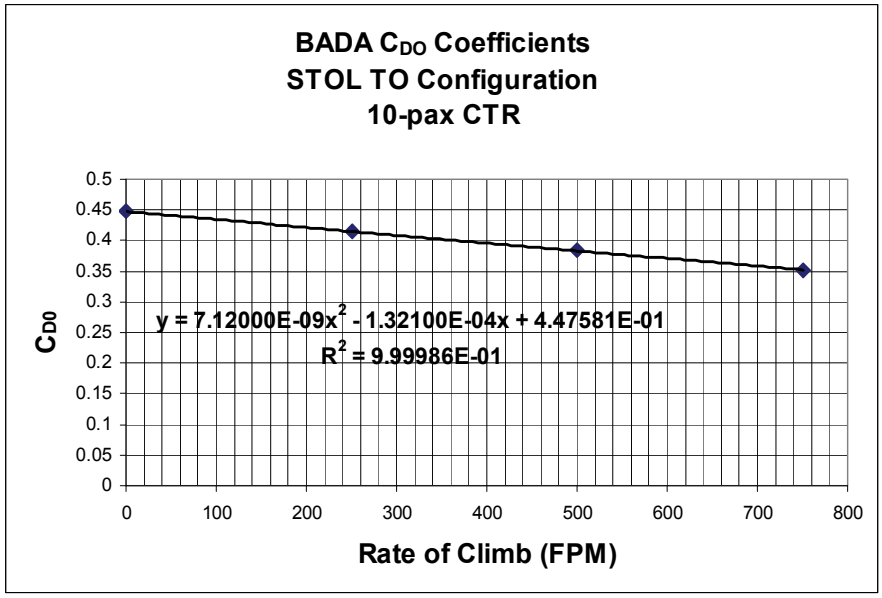

Figure 3-19. CTR10 STOL TO C_{DO} coefficients.

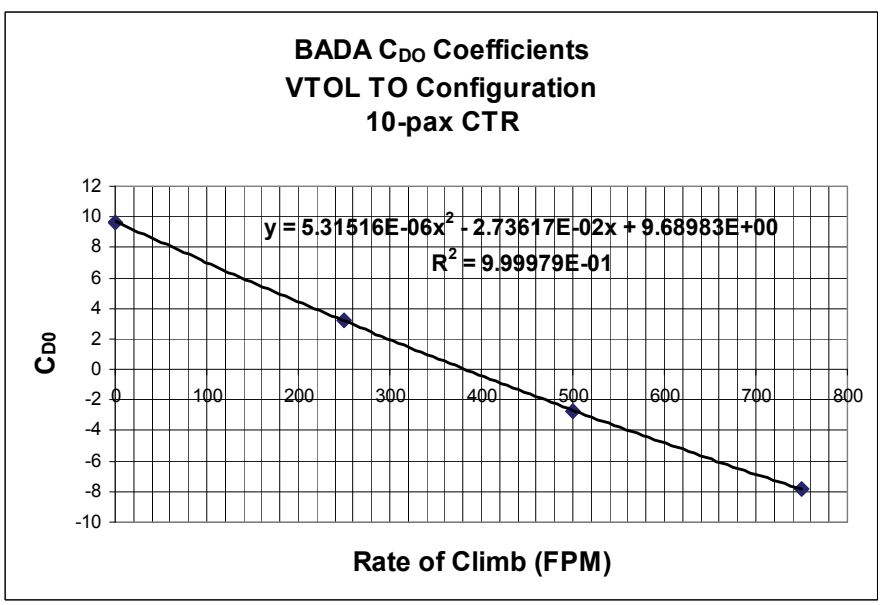

Figure 3-20. CTR10 VTOL TO C_{D0} coefficients.

BADA requires the definition of a TO, IC, AP, and LD stall speed for its operational logic as discussed in prior sections. Although the event of stall is not modeled, the known stall speed is used in assigning lower limits on airspeed during flight operations within BADA. Specific stall speed data was not available for the conversion modes in particular. In addition, when considering hover operations not supported by BADA, there is no stall speed to specify as an operational limit in the context of the fixed-wing BADA implementation. Consequently, an empirical technique was used to develop conversion-mode stall entries for BADA modeling of STOL and VTOL modes. Civil fixed-wing aircraft are typically bound to the requirement that operational approach speed must be at least 1.3 times the known stall speed for the configuration. The operational speeds for TO, IC, AP, and LD conversion modes were supplied in the Bell performance data. These speeds are identical for each CTR variant. For simplicity, the VTOL TO and VTOL LD stall speeds were set to 1 KCAS to avoid math modeling issues in the BADA framework. Recall this is a fixed-wing database with aerodynamic forces nondimensionalized with dynamic pressure. The lowest operational speeds provided by Bell in the trim data for the IC, AP, STOL LD, and STOL TO configurations were 110, 50, 40, and 100 KCAS respectively at the reference weight. The following approximation was then used to estimate stall speeds:

$$V_{Stall} = \frac{V_{Operational}}{1.3}.$$

This results in BADA stall speed entries of 84.6, 38.5, 30.8, and 76.9 KCAS for the IC, AP, STOL LD, and STOL TO configurations, respectively.

3.5 BADA Model Verification

A Performance Deck (PD) was developed that accepts the BADA model for each CTR variant. The deck can produce specific static trim point data or simulate mission segments of climb, cruise, and descent. Data such as fuel burned and time to transit mission segments is available for examination among other states. The model structure is built based on the BADA techniques used to generate the equivalent system performance models. The goal of this tool was to verify the final CTR BADA models and provide a measure of model accuracy prior to implementation into the ACES system.

Static trim points that were examined, spanning the altitude envelope for verification of each CTR variant, were as follows for airplane mode operation:

- Maximum continuous power climb
- Long-range cruise
- Maximum continuous power cruise
  - Following known maximum airspeed performance schedule
  - Following BADA-predicted maximum cruise thrust available with airspeed as a fallout

Simulation of mission segments has multiple techniques available. The most general technique models the climb speed, long-range cruise speed, and descent speed schedules of the CTR variants. The schedules are based on trim data provided for each variant on which the models were built. The mission simulator runs on the order of 10 Hz with fuel burn changing the mass of the CTR at each time step. The following information is specified for each total mission run:

- CTR variant (CTR10, CTR30, CTR90, CTR120)
- Initial gross weight

- Climb segment starting and ending altitude
- Cruise segment target altitude /climb segment ending altitude
- Cruise segment range to transit
- Descent segment ending altitude

The mission simulator provides inertial range transited, inertial altitude transited, fuel burned, and time-to-complete for each segment, as well as for the entire mission. Speed schedules for climb and cruise are dynamically updated based on gross weight.

The alternate technique for simulation of mission segments is designed to be consistent with the procedure used by the Bell PRESTO tool to produce the verification data. Each mission phase (climb, cruise, and descent) is broken into multiple segments. Over the entirety of each segment CTR airspeed, gross weight, and ROCD are held constant at average values for the overall determination of fuel burn and time to transit each segment. This alternate technique allows for direct comparison to mission profile verification data provided by Bell for each CTR variant. All the results discussed below regarding mission profile verification used this alternate simulation technique.

Two mission profile verification data sets were provided by Bell for each CTR variant. The overall design of the profiles was as follows:

- Profile 1
  - Climb from sea level to cruise altitude at 1.23 V_{stall}
  - Cruise at altitude for desired range at long-range cruise velocity
  - Descend from cruise altitude to sea level at 1,000 fpm
- Profile 2
  - Climb from sea level to cruise altitude at 1.23 V_{stall}
  - Cruise at altitude for desired range at MCP
  - Descend from cruise altitude to sea level at 2,000 fpm

In support of conversion mode verification, only static trim tests were available. These tests include the following conditions:

- Approach/initial climb configuration
  - Level flight
- Approach configuration
  - On glide slope of –3, –6, and –9 degrees
- STOL and VTOL landing configuration
  - Level flight
  - On glide slope of –3, –6, and –9 degrees
- STOL and VTOL takeoff configuration
  - Level flight
  - Rate of climb at 250, 500, and 750 fpm

3.5.1 CTR10 Verification

Verification of the CTR10 variant is discussed below. Topics include performance trim data and mission profile verification. The static trim comparisons offer an overview of the accuracy of the final BADA model across the altitude envelope. This provides guidance as to where in the envelope the model may be used with good predictive characteristics. The mission profile verification offers a measure of accuracy of the BADA model as applied to an operational scenario. This offers a good measure of end-to-end accuracy for a complete mission cycle. Verification results for the other CTR variants, i.e., CTR30, CTR90, and CTR120, are shown in appendix G.

3.5.1.1 Trim Verification

Verification results for the static trim points are shown in tables 3-11, 3-12, 3-13, and 3-14. The percent difference between the BADA model predicted and Bell design synthesis output are shown for airspeed, thrust, and fuel flow in all cases. These tables present the ability of the equivalent system model to recreate trim data supplied by Bell. An overestimation is indicated by a positive difference. Conversely, an underestimation is noted by a negative percent difference.

Tables 3-11, 3-12, and 3-13 indicate the ability of the BADA model to emulate aerodynamic drag with good accuracy given the low percent difference in thrust required over the majority of the cases. In addition, percent difference results for true airspeed serve to verify proper representation of the climb speed, long-range cruise speed, and known maximum airspeed schedules under MTOW conditions within the PD utility.

Table 3-11. CTR10 MCP CLIMB AT 1.23 V_{STALL} STATIC TRIM VERIFICATION RESULTS

Alt (k ft)	% Difference KTAS	% Difference Thrust	% Difference Fuel Flow
0	–0.13	–0.49	–0.38
2.5	0.06	–0.02	1.16
5	0.18	0.28	2.47
10	–0.06	0.76	3.99
15	–0.16	0.66	4.32
20	0.00	–0.21	3.30
25	0.13	–2.12	0.85
30	–0.04	2.25	3.47

TABLE 3-12. CTR10 LONG-RANGE CRUISE STATIC TRIM VERIFICATION RESULTS

Alt (k ft)	% Difference KTAS	% Difference Thrust	% Difference Fuel Flow
0	0.20	4.82	–14.61
2.5	–0.10	4.31	–12.74
5	–0.24	3.80	–10.77
10	0.00	3.11	–6.38
15	0.26	2.15	–2.50
20	0.16	0.73	0.13
25	–0.38	–1.16	1.71
30	0.14	–2.76	3.20

TABLE 3-13. CTR10 MCP CRUISE STATIC TRIM VERIFICATION BASED ON KNOWN MAXIMUM KTAS SCHEDULE

Alt (k ft)	% Difference KTAS	% Difference Thrust	% Difference Fuel Flow
0	0.27	2.87	–13.59
2.5	–0.18	1.96	–12.43
5	–0.34	1.39	–10.97
10	–0.04	0.94	–7.43
15	0.39	0.41	–4.15
20	0.22	–0.91	–2.07
25	–0.57	–2.94	–1.65
30	0.21	–3.35	1.44

MCP climb fuel flow accuracy is shown to vary from –0.38 percent to 4.32 percent difference over the entire altitude envelope. Overall, the MCP climb fuel flow is well predicted keeping in mind that climb operations steadily transit through the altitude envelope and do not dwell at any particular altitude for any significant amount of time. The LRC fuel flow is shown to best be emulated in the 15–30k foot altitude envelope with percent difference ranging from 0.13 to 3.2 percent. As altitude decreases below this band the prediction error significantly increases. Operationally, the CTR10 will cruise well above 15k feet and fuel flow is well predicted in that region. A similar result is seen in the MCP cruise fuel flow based on the known maximum performance true airspeed schedule. Note that this data, shown in table 3-13, is generated by setting the CTR airspeed within the deck utility to the known maximum possible true airspeed achievable by the CTR. Required thrust for level flight is then determined along with resulting fuel flow. Similarly, cruise fuel flow is found to be best predicted in the range of 15k to 30k feet with percent difference ranging from –1.44 to 4.15 percent. Again, the prediction error increases significantly as altitude decreases below this band.

TABLE 3-14. CTR10 MCP CRUISE STATIC TRIM VERIFICATION BASED ON BADA-PREDICTED MCP AVAILABLE

Alt (k ft)	% Difference KTAS	% Difference Thrust	% Difference Fuel Flow
0	25.16	42.07	32.59
2.5	24.96	40.47	34.39
5	24.56	38.48	35.53
10	23.52	33.76	36.26
15	21.70	27.72	34.47
20	18.90	20.13	29.67
25	14.76	11.11	21.36
30	10.11	2.45	12.93

Table 3-14 presents MCP cruise verification results based on using the BADA-model-predicted maximum cruise thrust available. The deck utility solves for a final true airspeed that provides overall aerodynamic drag equivalent to maximum cruise thrust available. Results indicate the BADA formulation is best employed when supplied with known airspeed operational schedules. In this case, the predicted maximum obtainable true airspeeds under MTOW conditions were found to be significantly overestimated by a difference of 10.11 to 25.16 percent, with error increasing as altitude decreases. Maximum available cruise thrust, and subsequently fuel flow, was also shown to be significantly overestimated by the BADA formulation. This is not surprising considering BADA predicts maximum available cruise thrust as 95 percent of MCP climb thrust across the operational envelope. Revisiting figure 3-3 it is clear to see how simply scaling the MCP climb thrust available by 0.95 will significantly overestimate MCP cruise thrust, with prediction error increasing as altitude decreases. This is a shortfall in the BADA model formulation that precludes use of this tool for predicting maximum speed performance with any real accuracy in this study.

3.5.1.2 Mission Profile Verification

Mission profile verification results are shown in table 3-15 and table 3-16. Long-range cruise mission results are presented in table 3-15. MCP cruise results are presented in table 3-16. Both tables present the inertial position transited, time to transit, and fuel burned over each mission phase of climb cruise and descent for both the BADA and Bell-provided verification data. In addition, the overall percent differences for these states are shown for each mission phase. Similar statistics are presented for the complete mission to provide a snapshot of the overall accuracy of the total mission cycle. A negative percent difference indicates underestimation while a positive percent difference denotes an overestimation of the BADA model.

The long-range cruise scenario of table 3-15 indicates good fuel burn prediction with an overall 1.65-percent difference for the entire mission cycle. Over the entire flight spanning a 1042.8-nmi range the BADA-formatted model overestimated fuel burned by only 41 lbs. Fuel burn was best modeled during the cruise segment (1.26 percent) with an overestimation of 25.6 lbs. The climb and descent segments indicate a 2.9- and 4.07-percent difference in fuel burn, respectively. This results in an overestimation of fuel burned of 7.81 lbs and 7.6 lbs for the climb and descent segments, respectively. Following the long-range cruise operational velocity schedule the CTR10 model is optimized for both long- and short-range flights. Note that

during short-range flights more overall mission time is spent in the climb and descent phases as the cruise segment becomes shorter.

The maximum continuous power cruise scenario of table 3-16 indicates good fuel burn prediction with an overall –2.19-percent difference for the entire mission cycle. Again in this test, the MCP cruise speed is set at the known maximum airspeed presented by the Bell design for the given gross weight. It was clear from prior static trim verification that the BADA-formulated model is best employed by supplying operational airspeeds. Over the entire flight spanning a 983.8-nmi range the BADA-formatted model underestimated fuel burned by only 54.23 lbs. Fuel burn was best modeled during the climb segment (2.9 percent) with an overestimation of 7.81 lbs. The cruise and descent segments indicate a –3.36 and 10.66-percent difference in fuel burn, respectively. This results in an underestimation of fuel burned of 71.4 lbs and an overestimation of 9.36 lbs for the cruise and descent segments, respectively.

TABLE 3-15. CTR10 LONG-RANGE CRUISE MISSION PROFILE VERIFICATION

	BADA Model			BELL Model			% Difference		
Mission Phase	**Dxpos (nmi)**	**Delta Time (min)**	**Fuel Burned (lbs)**	**Dxpos (nmi)**	**Delta Time (min)**	**Fuel Burned (lbs)**	**Dxpos**	**Delta Time**	**Fuel Burned**
MTOW Climb From SL to 25K at 1.23 V_{stall}	66.6	21.25	277.51	66.6	21.25	269.7	0.0	0.0	2.90
Cruise for 886.6 nmi at VLRC	886.6	208.09	2050.2	886.6	208.31	2024.6	0.0	–0.11	1.26
Descend to SL at 1,000 fpm	89.6	25.00	194.3	89.60	25.00	186.7	0.0	0.0	4.07
TOTALS:	1042.8	254.34	2522.01	1042.8	254.56	2481.00	0.0	–0.09	1.65

TABLE 3-16. CTR10 MCP CRUISE MISSION PROFILE

	BADA Model			BELL Model			% Difference		
Mission Phase	**Dxpos (nmi)**	**Delta Time (min)**	**Fuel Burned (lbs)**	**Dxpos (nmi)**	**Delta Time (min)**	**Fuel Burned (lbs)**	**Dxpos**	**Delta Time**	**Fuel Burned**
MTOW Climb From SL to 25K at 1.23 Vstall	66.6	21.25	277.51	66.6	21.25	269.7	0.0	0.0	2.9
Cruise for 865 nmi at MCP	865.0	181.11	2051.0	865	181.11	2122.4	0.0	0.0	–3.36
Descend to SL at 2,000 fpm	52.2	12.50	97.16	52.2	12.5	87.8	0.0	0.0	10.66
TOTALS:	983.8	214.86	2425.67	983.8	214.86	2479.9	0.0	0.0	–2.19

3.5.1.3 Conversion-Mode Verification

Static trim point verification results are shown in table 3-17 and table 3-18 for the CTR10. The percent difference between the BADA-model predicted and expected output are shown for thrust, drag, and fuel flow in all cases. These tables present the ability of the BADA-equivalent system model to recreate fuel flow trim data supplied by Bell, as well as the equivalent system thrust and drag formulated during BADA model development. An overestimation is indicated by a positive difference. Conversely, an underestimation is noted by a negative percent difference.

The level-flight trim point results in table 3-17 indicate good accuracy in the emulation of fuel flow, equivalent drag,, and equivalent thrust with the highest magnitude of error being 0.35 percent.

TABLE 3-17. CTR10 CONVERSION-MODE LEVEL-FLIGHT STATIC TRIM VERIFICATION

Conversion Mode	Flight Path Angle (deg)	% Difference Net Thrust	% Difference Total Drag	% Difference Fuel Flow
AP/IC LVL	0	0.01	0.01	0.01
AP/IC LVL	0	0.00	0.00	0.00
AP/IC LVL	0	0.02	0.02	0.02
STOL LD	0	0.08	0.08	0.08
STOL LD	0	–0.09	–0.09	–0.09
STOL LD	0	0.12	0.12	0.12
VTOL LD	0	0.17	0.17	0.18
VTOL LD	0	–0.35	–0.35	–0.34
VTOL LD	0	0.29	0.29	0.28
STOL TO	0	–0.07	–0.07	–0.07
STOL TO	0	0.27	0.27	0.26
STOL TO	0	–0.17	–0.17	–0.17
VTOL TO	0	0.17	0.17	0.17
VTOL TO	0	–0.34	–0.34	–0.34
VTOL TO	0	0.28	0.28	0.28

The ascending/descending static trim point results of table 3-18 indicate good overall accuracy. The conversion mode models are built to emulate Bell-supplied fuel burn performance; this is evident in the verification results. The thrust coefficient scale factors for the conversion modes also capture the scheduled equivalent thrust levels as expected. The drag model results indicate some variation as compared to the equivalent drag. It is clear that error increases with the magnitude of glide slope angle. Even so, for the majority of the cases the percent difference is much less than 1 percent. This trend is based on an inherent BADA model limitation wherein lift is always assumed to be that required for level flight operations, regardless of what flight phase the aircraft is transiting. The aircraft deviates from this assumption as the glide slope angle increases. The error accumulates through the induced drag component in the BADA aerodynamic model framework. The highest error is clearly seen in the VTOL takeoff verification cases due to the significant climb angles encountered during operation. BADA considers the takeoff phase to transit through approximately 400 feet. Very little time is spent in this region of operation when compared to an entire mission profile.

TABLE 3-18. CTR10 CONVERSION-MODE STATIC TRIM VERIFICATION

Conversion Mode	Flight Path Angle (deg)	% Difference Net Thrust	% Difference Total Drag	% Difference Fuel Flow
AP	–3	0.00	0.14	0.00
AP	–6	0.00	0.58	0.00
AP	–9	0.00	2.21	0.00
STOL LD	–3	0.00	0.14	0.00
STOL LD	–6	0.00	0.42	0.00
STOL LD	–9	0.00	0.81	0.00
VTOL LD	–3	0.00	0.15	0.00
VTOL LD	–6	0.00	0.46	0.00
VTOL LD	–9	0.00	0.90	0.00
STOL TO	1.4	0.00	0.02	0.00
STOL TO	2.8	0.00	0.04	0.00
STOL TO	4.2	0.00	0.09	0.00
VTOL TO	7.0	0.00	1.19	0.00
VTOL TO	13.8	0.00	8.57	0.00
VTOL TO	20.2	0.00	125.63	0.00

3.6 BADA Modeling for the Nacelle Conversion Operations

This section presents a consolidated set of lookup tables that define total fuel burned, distance transited, and time to transit for select phases of flight in the terminal area where the CTR fleet is running in conversion and the nacelle setting is greater than 0 degrees. These tables, combined with the PD that was developed for the airplane mode operations, form the Fuel Burn Post Processor (FBPP), a standalone software that generates fuel burn according to given flight trajectories. These tables are meant to be used in support of ACES/AvTerminal data post-processing where certain phases of flight, specifically the conversion mode where nacelle is operated between the airplane mode and helicopter mode, may not currently be available within those tools as described in sections 3.2–3.5 to model in a comparable fashion. All references to pilot-in-the-loop (PITL) data referenced in this section entail piloted simulation data collected in the effort described in section 4.4.

3.6.1 Flight Profile Defined

The general flight profile for the CTR is defined in figure 3-21. This figure presents the entire mission from departure to arrival. The phases of flight covered by data in this section include the following:

- Takeoff and climb up to 600 feet (Flight Profile Points 2–4)
- Airplane mode climb from 600 to 3,000 feet (Flight Profile Points 4–4.1)
- Airplane mode level flight at 1,500 feet during arrival (Flight Profile Points 8–8.1)
- Conversion from airplane mode at 1,500 feet, capture final approach fix, and descend on glide slope to touchdown (Flight Profile Points 8.1–12)

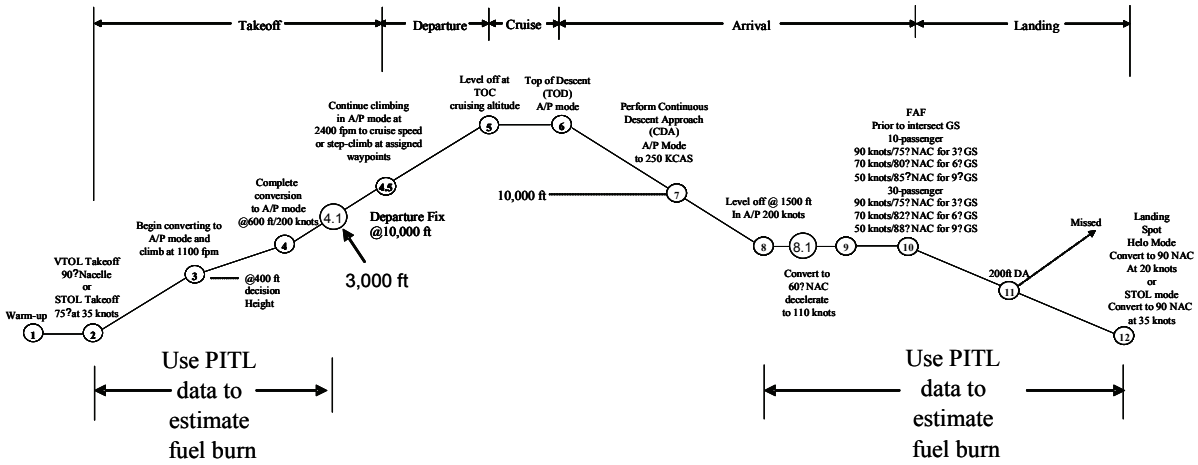

Figure 3-21. Overall CTR flight profile.

3.6.2 Using Pilot-in-the-Loop (PITL) Data

CTR PITL data collected for the CTR10 and CTR30 described in section 4.4 was examined to refine the conversion mode modeling. Segments of data were trimmed for both size airframes to cover the following profile mission points:

- Takeoff and climb up to 600 feet (Flight Profile Points 2–4)
- Conversion from airplane mode at 1,500 feet, capture final approach fix, and descend on glide slope to landing (Flight Profile Points 8.1–12)

Data was identified for both VTOL and STOL modes of operation. The takeoff segments (Points 2–4) were straightforward to parse. The arrival segments (Profile Points 8.1–12) were more challenging in that data from individual test points were consolidated together as necessary in order to model the final phases as a whole.

Data for time spent and inertial distance transited over each of the PITL segments was determined. Required PITL recorded airframe states such as rate of climb, altitude, and true airspeed, etc., were passed through the FBPP software to generate NextGen CTR airframe fuel burn numbers for each segment.

The CTR10 PITL data was used to generate CTR10 table entries. The CTR30 PITL data was used to generate CTR30 table entries. In addition, the CTR30 PITL data was used to generate table entries for the CTR90 and CTR120. For example, the CTR30 PITL data was used with the CTR90 performance FBPP model to determine the CTR90 fuel burn.

In all cases, while using the FBPP the closest representative BADA-model entries for aerodynamic configurations were used in an effort to be as comparable as possible. Note, however, that the CTR10 and CTR30 PITL models were not 100-percent representative of the PRESTO modeling by Bell as described in section 2.

3.6.3 Using the Performance Deck

The final flight profiles developed in appendix J were used to directly parse the inertial distance, time to transit, and fuel burned for Flight Profile Points 4–4.1. The history vector files parsed in this fashion were as follows:

- CTR_10pax_Tradeoff_1_BOS2PIT_history.mat
- CTR_30pax_Tradeoff_12_CTR_history.mat
- CTR_90pax_Tradeoff_12_CTR_bos2pit_history.mat
- CTR_120pax_Tradeoff_6_CTR_bpit_history.mat

These missions were run using Version 3.2.3 of the CTR Performance Deck (CTRPD), as described in appendix I, when CTR flight profiles were developed according to appendix J. These profiles model the BOS-to-PIT flight and include the airplane-mode portion of the flight only. The profiles begin at 600 feet and end at 1,500 feet. The total range in airplane mode transited is 420 nmi. As outlined in appendix I, an additional range of 10 nmi is allotted for conversion-mode operations to bring the total range to 430 nmi. This 10-nmi distance is important in that the level flight segment inertial distance to transit, while in airplane mode on the arrival, may be computed as follows:

$$(\text{Distance Pt 8 to 8.1}) = 10\ \text{nmi} - [(\text{Distance Pt 2 to 4}) + (\text{Distance Pt 8.1 to 12})].$$

TABLE 3-19. AIRPLANE MODE TIME TO TRANSIT AND FUEL BURN PER NMI AT 1,500 FEET LEVEL FLIGHT, 200 KTAS

CTR Size	Time to Transit 1 nmi at 200 KTAS (min)	Fuel Burn per nmi (lbm/nmi)
CTR10	0.3	3.67
CTR30	0.3	8.25
CTR90	0.3	16.21
CTR120	0.3	17.00

The ending gross weight of each history file above was noted and used to initialize the PD to obtain the fuel burn performance in airplane mode in level flight at 200 KTAS at 1,500 feet. This was used to generate fuel burn data spanning Flight Profile Points 8–8.1. The PD data for this segment is presented in table 3-19 in a per-nautical-mile basis and was used to generate the appropriate table entries found later in this section. Table 3-19 may be used in further support of NAS studies if this phase of flight must be lengthened or shortened due to obstacle avoidance or noise abatement requirements.

It is assumed that the segment defined by Flight Profile Points 8–8.1 can be lengthened or shortened as necessary to account for any special terminal area flight profile adjustments that might be specific to any given airport. This would specify that the CTR would remain in airplane mode at 1,500 feet to transit any additional space necessary until conversion and landing can begin. This assumes the segments after Flight Profile Point 8.1 are always the same length regarding inertial range, time to transit, and fuel burned.

3.6.4 Lookup Tables Defined

This section presents the lookup tables, tables 3-20 to 3-27, which define inertial distance transited, time to transit, and fuel burned for each of the phases of interest. Note that this data is made available for each CTR in both VTOL and STOL mode. In addition, this data is separated into glide slope (GS) angles of –3, –6, and –9 degrees for the approach and landing.

CTR10

TABLE 3-20. CTR10 TIME, DISTANCE, AND FUEL BURN PER FLIGHT PROFILE PHASE WITH STOL CONVERSION

10-pax STOL		Point 2 to 4	Point 4 to 4.1	Point 8 to 8.1	Point 8.1 to 12
GS –3 deg	Time (min)	0.590	2.397	0.186	5.670
	Distance (nmi)	0.482	8.183	0.618	8.900
	Fuel burn (lbs)	7.45	42.94	2.27	57.97
GS –6 deg	Time (min)	0.590	2.397	0.207	6.620
	Distance (nmi)	0.482	8.183	0.688	8.830
	Fuel burn (lbs)	7.45	42.94	2.53	62.56
GS –9 deg	Time (min)	0.590	2.397	0.213	7.230
	Distance (nmi)	0.482	8.183	0.708	8.810
	Fuel burn (lbs)	7.45	42.94	2.60	68.56

TABLE 3-21. CTR10 TIME, DISTANCE, AND FUEL BURN PER FLIGHT PROFILE PHASE WITH VTOL CONVERSION

CTR10 VTOL		Point 2 to 4	Point 4 to 4.1	Point 8 to 8.1	Point 8.1 to 12
GS –3 deg	Time (min)	0.500	2.397	0.259	5.750
	Distance (nmi)	0.376	8.183	0.864	8.760
	Fuel burn (lbs)	8.48	42.94	3.17	60.43
GS –6 deg	Time (min)	0.500	2.397	0.313	6.230
	Distance (nmi)	0.376	8.183	1.044	8.580
	Fuel burn (lbs)	8.48	42.94	3.83	60.15
GS –9 deg	Time (min)	0.500	2.397	0.307	7.010
	Distance (nmi)	0.376	8.183	1.024	8.600
	Fuel burn (lbs)	8.48	42.94	3.76	66.58

CTR30

TABLE 3-22. CTR30 TIME, DISTANCE, AND FUEL BURN PER FLIGHT PROFILE PHASE WITH STOL CONVERSION

CTR30 STOL		Point 2 to 4	Point 4 to 4.1	Point 8 to 8.1	Point 8.1 to 12
GS –3 deg	Time (min)	0.550	0.997	0.418	4.930
	Distance (nmi)	0.548	3.121	1.392	8.060
	Fuel burn (lbs)	15.67	58.03	11.49	125.32
GS –6 deg	Time (min)	0.550	0.997	0.637	5.180
	Distance (nmi)	0.548	3.121	2.122	7.330
	Fuel burn (lbs)	15.67	58.03	17.51	113.40
GS –9 deg	Time (min)	0.550	0.997	0.763	5.710
	Distance (nmi)	0.548	3.121	2.542	6.910
	Fuel burn (lbs)	15.67	58.03	20.97	131.05

TABLE 3-23. CTR30 TIME, DISTANCE, AND FUEL BURN PER FLIGHT PROFILE PHASE WITH VTOL CONVERSION

CTR30 VTOL		Point 2 to 4	Point 4 to 4.1	Point 8 to 8.1	Point 8.1 to 12
GS –3 deg	Time (min)	0.510	0.997	0.589	4.820
	Distance (nmi)	0.596	3.121	1.965	7.440
	Fuel burn (lbs)	34.96	58.03	16.21	136.51
GS –6 deg	Time (min)	0.510	0.997	0.526	5.790
	Distance (nmi)	0.596	3.121	1.755	7.650
	Fuel burn (lbs)	34.96	58.03	14.47	138.12
GS –9 deg	Time (min)	0.510	0.997	0.862	5.410
	Distance (nmi)	0.596	3.121	2.875	6.530
	Fuel burn (lbs)	34.96	58.03	23.71	132.45

CTR90

TABLE 3-24. CTR90 TIME, DISTANCE, AND FUEL BURN PER FLIGHT PROFILE PHASE WITH STOL CONVERSION

CTR90 STOL		Point 2 to 4	Point 4 to 4.1	Point 8 to 8.1	Point 8.1 to 12
GS –3 deg	Time (min)	0.550	1.088	0.418	4.930
	Distance (nmi)	0.548	3.816	1.392	8.060
	Fuel burn (lbs)	10.73	151.83	22.57	100.55
GS –6 deg	Time (min)	0.550	1.088	0.637	5.180
	Distance (nmi)	0.548	3.816	2.122	7.330
	Fuel burn (lbs)	10.73	151.83	34.40	90.64
GS –9 deg	Time (min)	0.550	1.088	0.763	5.710
	Distance (nmi)	0.548	3.816	2.542	6.910
	Fuel burn (lbs)	10.73	151.83	41.21	91.27

TABLE 3-25. CTR90 TIME, DISTANCE, AND FUEL BURN PER FLIGHT PROFILE PHASE WITH VTOL CONVERSION

CTR90 VTOL		Point 2 to 4	Point 4 to 4.1	Point 8 to 8.1	Point 8.1 to 12
GS –3 deg	Time (min)	0.510	1.088	0.589	4.820
	Distance (nmi)	0.596	3.816	1.965	7.440
	Fuel burn (lbs)	34.76	151.83	31.84	117.25
GS –6 deg	Time (min)	0.510	1.088	0.526	5.790
	Distance (nmi)	0.596	3.816	1.755	7.650
	Fuel burn (lbs)	34.76	151.83	28.44	112.53
GS –9 deg	Time (min)	0.510	1.088	0.862	5.410
	Distance (nmi)	0.596	3.816	2.875	6.530
	Fuel burn (lbs)	34.76	151.83	46.60	97.08

CTR120

TABLE 3-26. CTR120 TIME, DISTANCE, AND FUEL BURN PER FLIGHT PROFILE PHASE WITH STOL CONVERSION

CTR120 STOL		Point 2 to 4	Point 4 to 4.1	Point 8 to 8.1	Point 8.1 to 12
GS –3 deg	Time (min)	0.550	0.920	0.418	4.930
	Distance (nmi)	0.548	3.219	1.392	8.060
	Fuel burn (lbs)	12.92	162.33	23.68	115.19
GS –6 deg	Time (min)	0.550	0.920	0.637	5.180
	Distance (nmi)	0.548	3.219	2.122	7.330
	Fuel burn (lbs)	12.92	162.33	36.10	102.09
GS –9 deg	Time (min)	0.550	0.920	0.763	5.710
	Distance (nmi)	0.548	3.219	2.542	6.910
	Fuel burn (lbs)	12.92	162.33	43.24	101.42

TABLE 3-27. CTR120 TIME, DISTANCE, AND FUEL BURN PER FLIGHT PROFILE PHASE WITH VTOL CONVERSION

CTR120 VTOL		Point 2 to 4	Point 4 to 4.1	Point 8 to 8.1	Point 8.1 to 12
GS –3 deg	Time (min)	0.510	0.920	0.589	4.820
	Distance (nmi)	0.596	3.219	1.965	7.440
	Fuel burn (lbs)	30.54	162.33	33.42	125.31
GS –6 deg	Time (min)	0.510	0.920	0.526	5.790
	Distance (nmi)	0.596	3.219	1.755	7.650
	Fuel burn (lbs)	30.54	162.33	29.84	120.89
GS –9 deg	Time (min)	0.510	0.920	0.862	5.410
	Distance (nmi)	0.596	3.219	2.875	6.530
	Fuel burn (lbs)	30.54	162.33	48.90	103.44

3.6.5 Fuel Burn Comparison to PITL Recorded Data

The PITL simulation for the CTR10 and CTR30 did not have the full PRESTO-developed model installed. The overall performance of these PITL simulations was not identical to the PRESTO baseline for the CTR10 and CTR30 that was used to generate the BADA-formatted performance models. However, a comparison was made against PITL fuel burned, and the fuel burned as indicated by the FBPP software when presented with PITL aircraft states.

Figures 3-22 through 3-27 indicate a good match between the PITL and FBPP fuel burn data considering the model differences noted previously. The next section compares FBPP output data to verification data that was used to generate the fuel burn model. This serves as a more direct comparison to the CTR performance specified in the Bell-supplied trim data as described in section 2.

CTR10

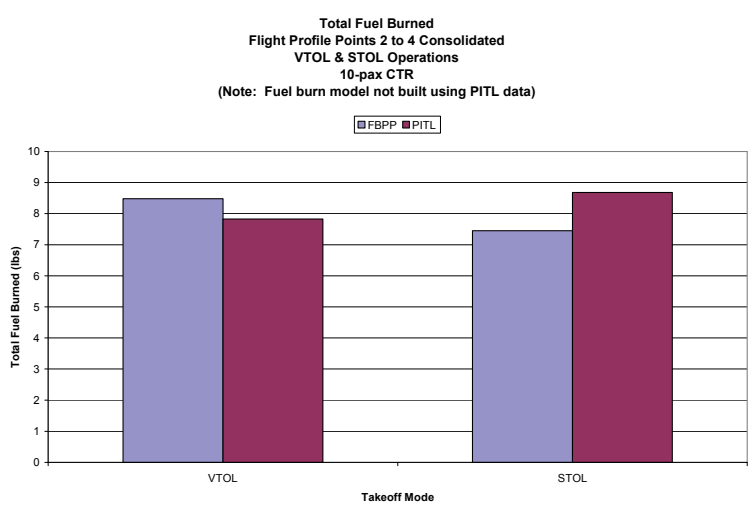

Figure 3-22. CTR10 fuel burn, Flight Profile Points 2 to 4 for STOL and VTOL operations.

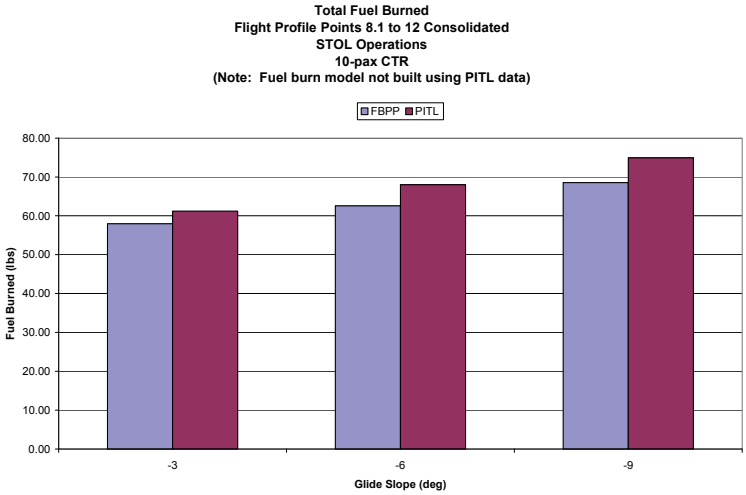

Figure 3-23. CTR10 fuel burn, Flight Profile Points 8.1 to 12, STOL operations at various GS angles.

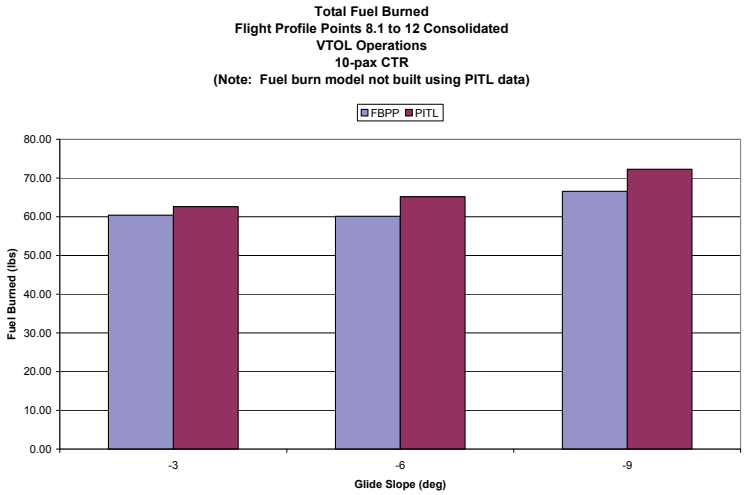

Figure 3-24. CTR10 fuel burn, Flight Profile Points 8.1 to 12, VTOL operations at various GS angles.

CTR30

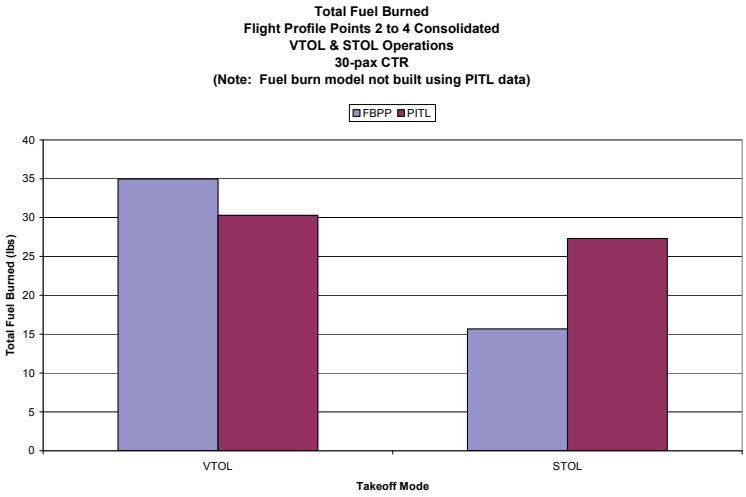

Figure 3-25. CTR30 fuel burn, Flight Profile Points 2 to 4, STOL and VTOL operations.

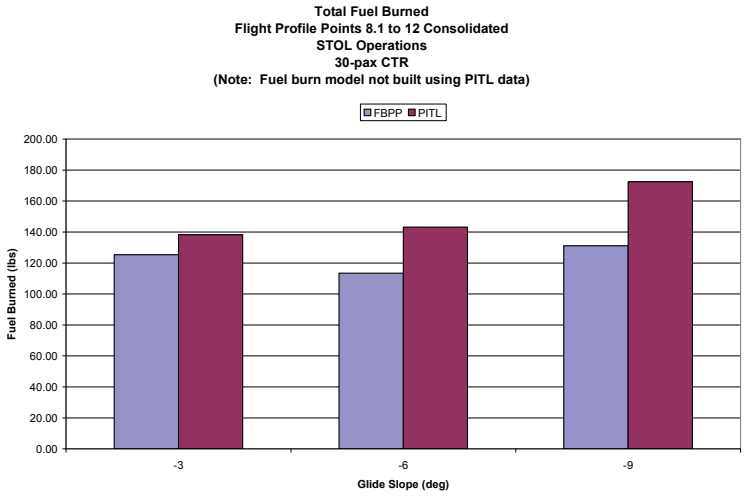

Figure 3-26. CTR30 fuel burn, Flight Profile Points 8.1 to 12, STOL operations at various GS angles.

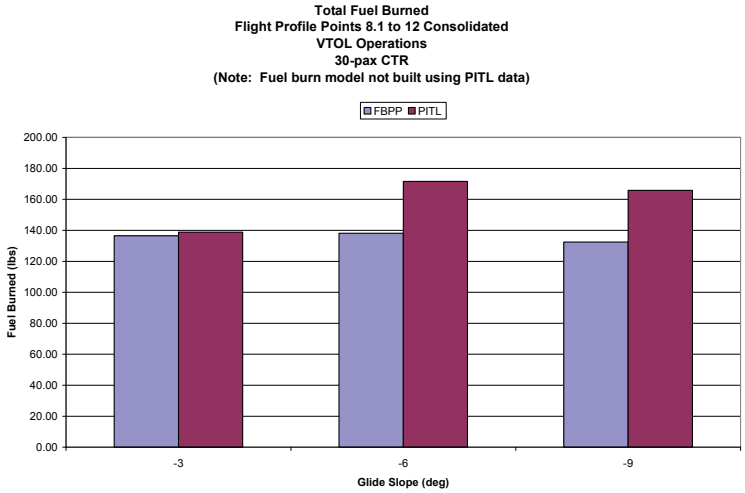

Figure 3-27. CTR30 fuel burn, Flight Profile Points 8.1 to 12, VTOL operations at various GS angles.

3.6.6 Fuel Burn Rate Comparison to Bell-Provided BADA Trim Data

As a final check of the conversion-mode fuel burn model a comparison was made against several of the Bell-provided trim points for BADA model development. The FBPP was trimmed at the given aircraft states in the trim point. The resulting fuel burn rate was compared to the static trim verification data. This test was run for the CTR10, CTR30, and CTR120, and it offers a more direct comparison of the FBPP fuel burn output versus data used to develop the fuel burn model.

Table 3-28 defines the configuration of each test case presented. Note that all test cases presented herein are at the defined BADA reference gross weight, an intermediate value, for each airframe. The midrange glide slope angle of –6 degrees was chosen along with the midrange takeoff rate of climb of 500 fpm. This is only a subset of cases available from the entire trim matrix. The full listing of available trim points is shown in appendix B.

TABLE 3-28. STATIC TRIM VERIFICATION CHECK CASE CONFIGURATIONS DEFINED

Test Case	Description
41	Initial climb configuration at level flight (NAC 60 deg)
49	Approach configuration at –6 deg GS (NAC 75 deg)
45A	STOL landing configuration at level flight (NAC 90 deg)
51A	STOL landing configuration at –6 deg GS (NAC 90 deg)
45B	VTOL landing configuration at level flight (NAC 90 deg)
51B	VTOL landing configuration at –6 deg GS (NAC 90 deg)
38A	STOL takeoff configuration at level flight (NAC 60 deg)
54A	STOL takeoff configuration at 500 fpm climb (NAC 60 deg)
38B	VTOL takeoff configuration at level flight (NAC 85 deg)
54B	VTOL takeoff configuration at 500 fpm climb (NAC 85 deg)

Figures 3-28, 3-29, and 3-30 presents the fuel burn comparison results for each test case. Overall the results indicate a good match between the FBPP software output and the Bell-provided performance trim data for the conversion mode cases investigated.

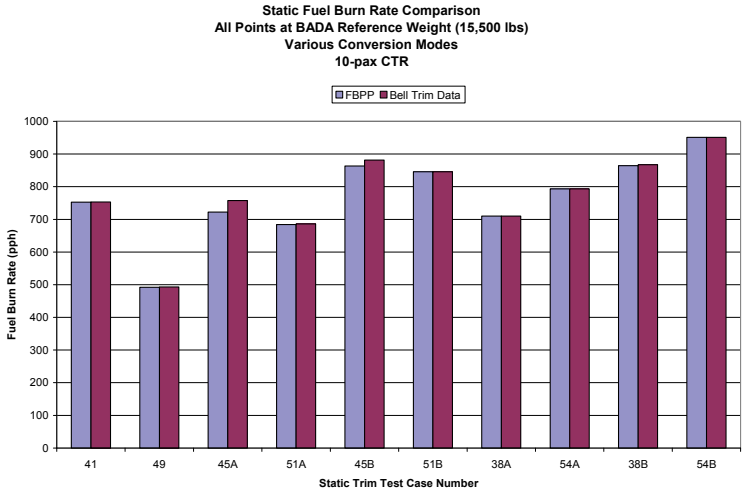

Figure 3-28. CTR10 conversion-mode static trim comparison data.

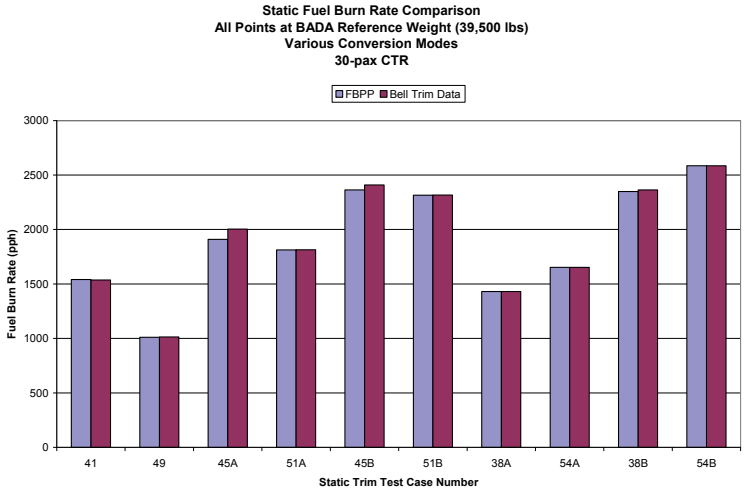

Figure 3-29. CTR30 conversion-mode static trim comparison data.

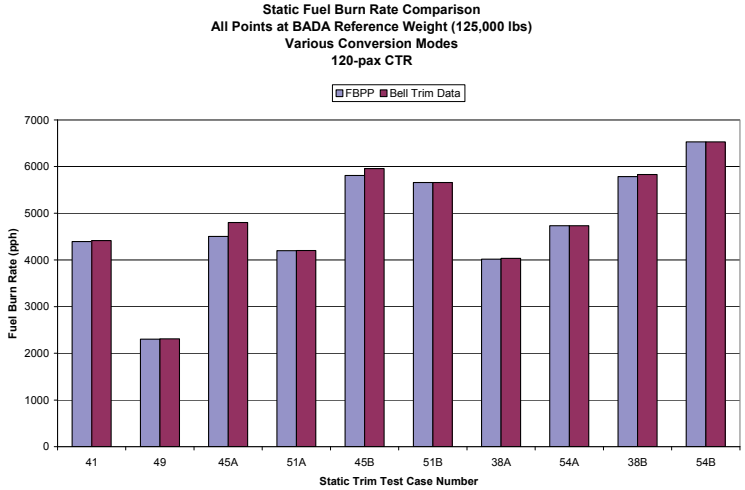

Figure 3-30. CTR120 conversion-mode static trim comparison data.

3.7 Verification of CTR Flight Performance Integrated Into the NAS Simulation Tools

Two NAS performance analysis tools were planned to be used to analyze the impact of the CTR fleet on NAS performance under NextGen. Airspace Concept Evaluation System (ACES) (ref. 19) was used to investigate NAS delay and capacity performance with a combination of CTR fleet mix and service regions such as North East Corridors, Atlanta, and Las Vegas, to assess the impact of the CTR fleet under NextGen. AvTerminal (ref. 20) was used to study the CTR fleet within the TRACON and terminal areas for flight time, track profile, noise, and fuel burn performance to support the environmental impact of the CTR fleet. Detail descriptions of these two NAS performance analysis tools are presented in section 6.2.

Both of these NAS performance analysis tools used the BADA modeling format to simulate flight performance of scheduled aircraft type and defined routes according to instrument flight rules (IFR) or visual flight rules (VFR). After integrating the BADA data parameters described in sections 3.2–3.5 into ACES, flight performance corresponding to the airplane mode of CTR flights for the CTR10, CTR30, CTR90, and CTR120 configurations were evaluated to ensure the accuracy of the integration process. A CTR Performance Deck (CTRPD), which was developed based on CTR static flight parameters derived from sections 3.2–3.4, was combined with the energy method to provide baseline pseudo flight dynamics for the flight characteristics of the CTR in airplane mode (i.e., 0-degree nacelle) described in appendix I.

3.7.1 Verification of CTR Flight Performance in ACES

ACES is primarily used to investigate NAS traffic delay and throughput capacity performance by simulating aircraft flight performance according to BADA modeling format for given aircraft types—based on given routes between the origin and destination pair cities at given speeds and altitudes. Flight time performance between the departure fix and arrival fix are calculated using BADA aircraft modeling methods. Flight time performance within the departure fixes and arrival fixes are estimated by averaging the speed between the fixes and threshold of the runway (ref. 19).

For CTR flight performance verification, efforts were focused on flight time performance between the pairing cities in the Northeast Corridors (NEC). Three representative city-pairs were selected (BOS-PHL, BOS-DCA, and BOS-PIT) for distances in the range of 200, 300, and 400 nmi, respectively. The CTR120 configuration was compared for all three city-pairs. CTR10, CTR30, and CTR90 configurations were compared for the BOS-DCA city-pair only.

The flight profiles for the CTR fleet were assumed in Great Circle (direct-to) routes as shown in figure 3-31. Since CTRPD was developed for the airplane mode only (flight segments 4.5–8 shown in figure 3-31), the CTR flight time performance in conversion mode from takeoff to 600 feet (flight segments 1–4.5), and approach and landing from 1,500 feet to touchdown (flight segments 8–12) was estimated using PITL simulation data described in section 4. Specific altitude and speed parameters were also developed using PITL simulation data. The flight time comparison between ACES and CTRPD is shown in table 3-29. Results show flight time generated by ACES compared satisfactorily with respect to the CTRPD results.

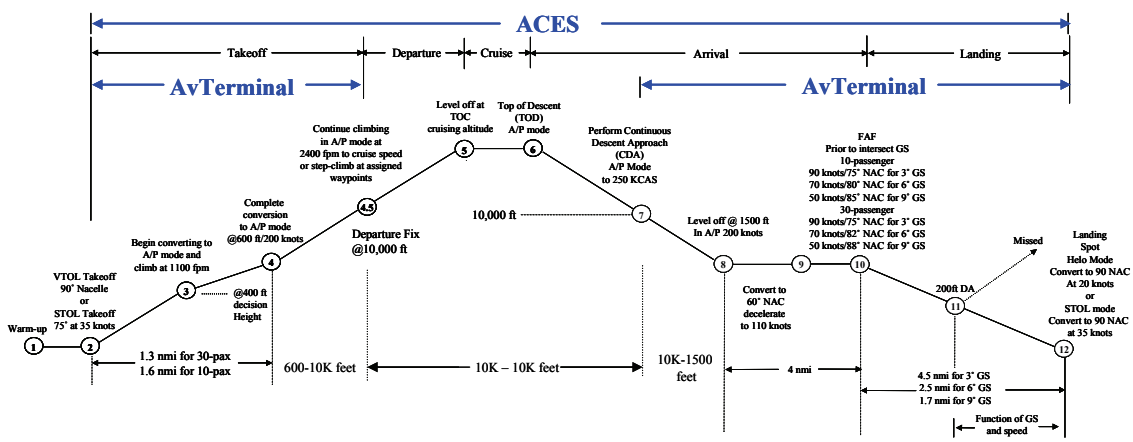

Figure 3-31. CTR10 VTOL TO C_{D0} coefficients.

TABLE 3-29. FLIGHT TIME PERFORMANCE COMPARISON BETWEEN ACES AND CTRPD

	Distance (nmi)	ACES (min)	CTRPD (min)	Error (%)
BOS-PHL	237			
120-pax		57	55.9	1.97
BOS-DCA	346			
10-pax		87	85.85	0.01
30-pax		72	74.66	-3.56
90-pax		77	74.27	3.68
120-pax		76	74.98	1.36
BOS-PIT	430			
120-pax		89	89.7	-0.78

3.7.2 Verification of CTR Flight Performance in AvTerminal

AvTerminal, a fast-time simulation modeling tool developed for terminal area capacity and delay analysis, can also use the same BADA data described in sections 3.2–3.4. Flight time and fuel burn data from CTR flight performances were checked with CTRPD in the airplane mode to ensure that the integration of the CTR BADA performance data into AvTerminal was consistent. A Great Circle route between BOS and EWR was chosen to check CTR climb, cruise, and descent performance in AvTerminal as shown in figure 3-31. Flight segments from 4.5–8 were flown by AvTerminal; the cruise segments (4.5–7) were also included for this verification by using the same flight algorithms as ACES and CTRPD to verify the BADA integration results.

Flight time and fuel burn performance for the AvTerminal CTR10, CTR30, CTR90, and CTR120 models were compared with those generated from CTRPD. Time response of altitude and true airspeed (TAS) are shown in figures 3-32 through 3-35 for the four CTR sizes. It should be noted that due to differences in setting up flying procedures the climb and descent rates could not be matched one-for-one, which contributed to differences as noted in tables 3-30 through 3-33 in those segments of flight. This is particularly true for the CTR120, where CTRPD took more than 10 nmi to descend from 10,000 feet to 1,500 feet because the decent rate in CTRPD was limited by achievable idle thrust, which produced larger flight time error at –27.23 percent and overall flight time error at –7.48 percent. However, other than this particular case, overall flight time and fuel burn responses are comparable as indicated in tables 3-30 through 3-33.

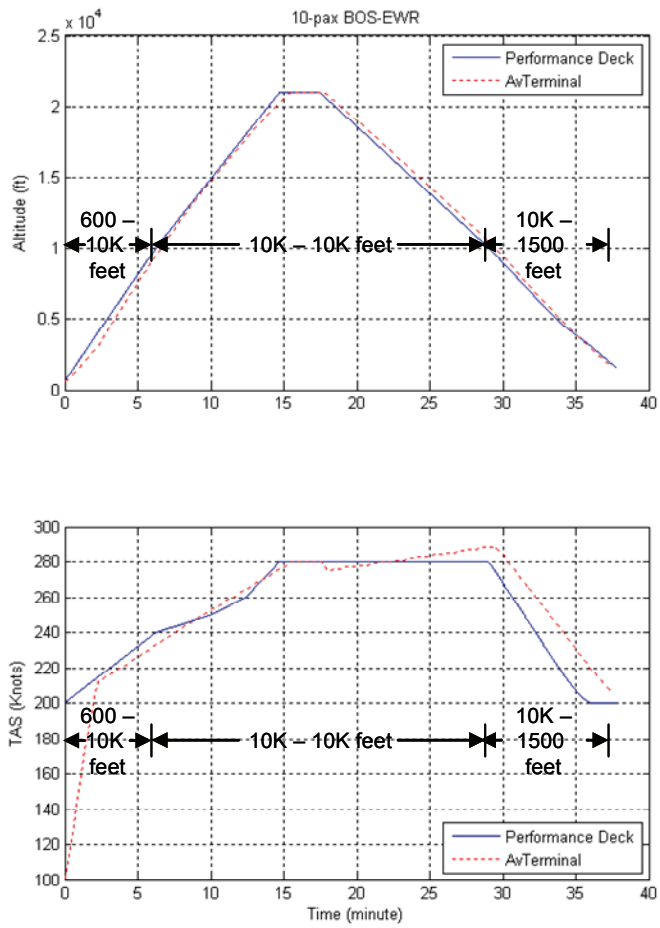

Figure 3-32. CTR10 altitude and TAS responses comparison.

TABLE 3-30. SUMMARY OF CTR10 FLIGHT TIME AND FUEL BURN COMPARISON BY FLIGHT SEGMENTS

	CTR Performance Deck (CTRPD)			AvTerminal				
	Distance	flight time	fuel burn	Distance	flight time	fuel burn	Flight time error wrt CTRPD	Fuel burn error wrt CTRPD
Flight Segment	nmi	min	lbs	nmi	min	lbs	%	%
600 - 10K feet	22.92	6.27	125.63	22.7	7	115	11.64	-8.46
10K-10K feet	102.7	22.8	335.78	104.6	22.75	342	-0.22	1.85
10K-1500 feet	33.55	8.79	84.52	33.5	8	94	-8.99	11.22
TOTAL	159.17	37.86	545.93	160.8	37.75	551	-0.29	0.93

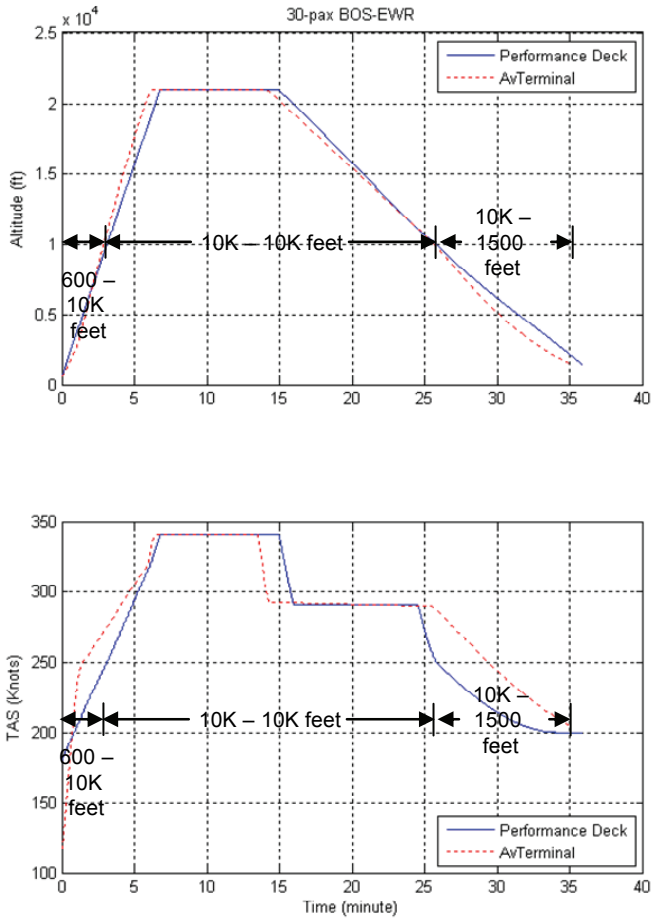

Figure 3-33. CTR30 altitude and TAS responses comparison.

TABLE 3-31. SUMMARY OF CTR30 FLIGHT TIME AND FUEL BURN COMPARISON BY FLIGHT SEGMENTS

	CTR Performance Deck (CTRPD)			AvTerminal				
	Distance	flight time	fuel burn	Distance	flight time	fuel burn	Flight time error wrt CTRPD	Fuel burn error wrt CTRPD
Flight Segment	nmi	min	lbs	nmi	min	lbs	%	%
600 - 10K	11.19	3.13	217.95	11.5	3.5	214	11.82	-1.81
10K-10K	116.5	22.71	969.36	116.39	22.75	974	0.18	0.48
10K-1500	36.01	10.06	199.63	37.4	8	240	-20.48	20.22
Total	163.7	35.9	1386.94	165.29	34.25	1428	-4.60	2.96

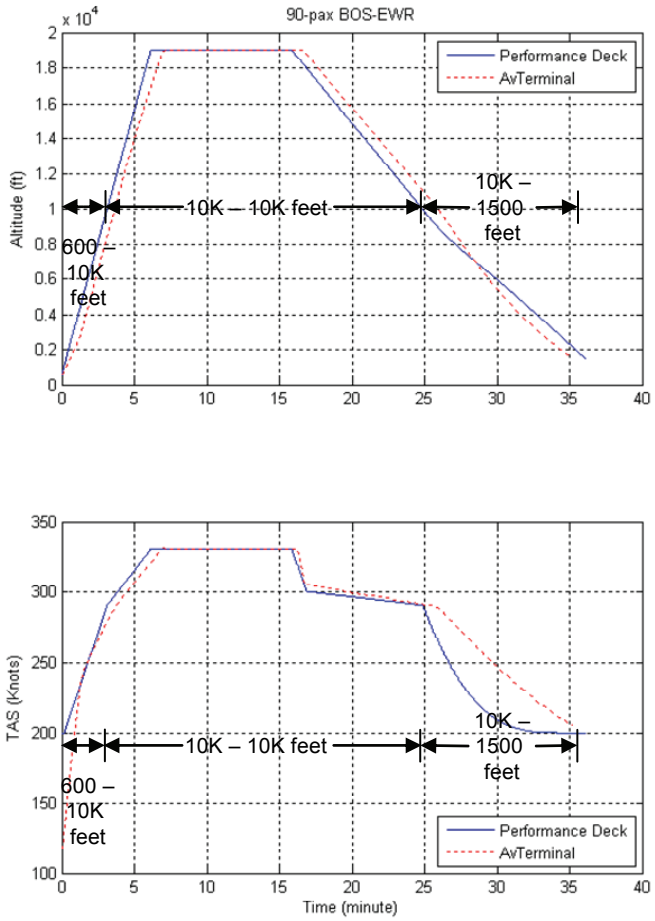

Figure 3-34. CTR90 altitude and TAS responses comparison.

TABLE 3-32. SUMMARY OF CTR90 FLIGHT TIME AND FUEL BURN COMPARISON BY FLIGHT SEGMENT

	CTR Performance Deck (CTRPD)			AvTerminal				
	Distance	flight time	Fuel burn	Distance	Flight time	Fuel burn	Flight time error wrt CTRPD	Fuel burn error wrt CTRPD
Flight Segment	nmi	min	lbs	nmi	min	lbs	%	%
600 - 10K	12.58	3.14	549.01	13.12	4	556	27.39	1.27
10K-10K	113.57	21.74	1988.18	113.7	22	1915	1.20	-3.68
10K-1500	41.19	11.26	398.6	38.69	9.5	474	-15.63	18.92
Total	167.34	36.14	2935.79	165.51	35.5	2945	-1.77	0.31

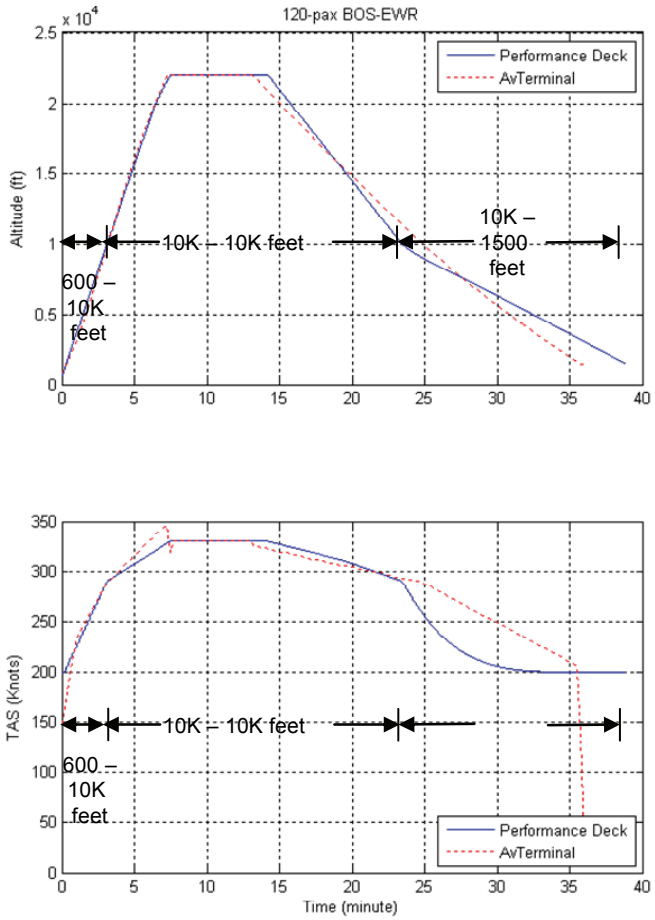

Figure 3-35. CTR120 altitude and TAS responses comparison.

TABLE 3-33. SUMMARY OF CTR120 FLIGHT TIME AND FUEL BURN COMPARISON BY FLIGHT SEGMENT

	CTR Performance Deck (CTRPD)			AvTerminal				
	Distance	flight time	Fuel burn	Distance	Flight time	Fuel burn	Flight time error wrt CTRPD	Fuel burn error wrt CTRPD
Flight Segment	nmi	min	lbs	nmi	min	lbs	%	%
600 - 10K	12.58	3.14	631.57	12.966	3.25	607	3.50	-3.89
10K-10K	107.3	20.31	1974.64	107.26	21.5	2111	5.86	6.91
10K-1500	55.53	15.46	610.09	44.957	11.25	594	-27.23	-2.64
Total	175.41	38.91	3216.3	165.183	36	3312	-7.48	2.98

3.7.3 Estimated CTR Taxi Fuel Flow

CTR fuel flow during ground taxi operations was estimated using hover fuel flow and idle descent fuel flow as references. Table 3-34 shows the estimates that were used in this study.

The taxi fuel flow estimates provided here are preliminary and are intended to support the analyses in section 6. Further refinement of these estimates is needed in future studies.

TABLE 3-34. ESTIMATED CTR TAXI FUEL FLOW

Taxi Fuel Flow	CTR10	CTR30	CTR90	CTR120
lbs/hour	495	1,210	2,200	2,650
lbs/minute	8.3	20.1	36.7	44.2

4 CTR CONCEPT OF OPERATIONS

The civil tiltrotor (CTR), which is a type of aircraft in the powered lift category, maintains a unique thrust vectoring capability via wing-tip-mounted prop-rotors that can rotate through a 90-degree arc. This capability results in an aircraft that has the cruise performance of a fixed-wing turboprop combined with the vertical lift ability of a rotorcraft. A recent study found that, "Half the country's routes are less than 500 miles and the busiest corridors are between metropolitan air travel centers" (ref. 21). The operational capability to perform VTOL and STOL landings and takeoffs allows great flexibility in expanding access to major airports without interfering or adding congestion to fixed-wing aircraft operating on congested runways. The most effective benefit of a CTR fleet is realized via the operational use of Runway-Independent Operations (RIO). While the RIO concept has varied applications such as independent arrivals/landings on parallel runways, in this instance it is the capability to perform these operations either without a runway, or with the use of a vertiport, a taxiway, or an uncongested runway. However, RIO is limited by runway configuration, available STOL runways, and available vertiports at each airport. The implementation of RIO is dependent on the development and implementation of NextGen and Area Navigation/Required Navigation Performance (RNAV/RNP) to achieve reduced safe separation minimum.

Using RIO, CTRs increase overall airport operations without increasing operations on highly congested runways or reducing the number of "short haul" turboprops on those same runways. This will result in opening up additional slots for other "long haul" aircraft. Travelers can fly directly from high-density hubs to city centers or small-city uncongested airports. This type of operation suggests a design cruising range under 250 miles (ref. 10). A 1994 MITRE Corporation study of the Northeast Corridor (NEC) looked at CTR operational range for feeder airports within 500 miles of a corridor airport (ref. 22). In a 1995 report to Congress, the Civil Tiltrotor Development Advisory Committee (CTRDAC) suggested CTR short-haul markets in the range of 100–600 miles (ref. 3).

NextGen proposes a new NAS ConOps with new capabilities and technologies to transform the current NAS into one that is capable of supporting the expected increase of traffic volume without compromising flight safety. Those parts of the NextGen ConOps that will have an impact on CTR fleet operations are the Optimized Profile Descent (OPD) that allow continuous descent approach (CDA), RNAV, RNP, and Four-Dimensional Trajectory (4DT)-Based Operation.

4.1 STOL and VTOL

The need for long runways that can handle airplanes that approach the runway at a 3-degree glide slope (GS) has been the predominant requirement for decades. As airplanes have increased in size and passenger capacity, so has runway length. The result is that "pouring concrete" to extend or build new runway capacity is an extremely complex, costly, and time-consuming process. Due to the CTR conventional cruise and VTOL/STOL unique characteristics, the ConOps of the fleet needs to take full advantage of its V/STOL capabilities in increasing NAS capacity while mitigating any potential negative effects (e.g., noise, flight in icing, etc.) of this technology.

The unique V/STOL attributes of the CTR provide flexibility in expanding access to major airports without interfering with fixed-wing aircraft operating at congested runways. VTOL, as defined for a CTR takeoff and landing operation, uses nacelles at approximately 90 degrees for vertical takeoff and landing at vertiports or on a runway/taxiway. STOL, as defined for CTR operations, uses nacelles at a preset angle (e.g., 60 degrees for takeoff and 75 degrees for landing) to operate on conventional runways. To achieve the optimal benefit of deploying the CTR fleet, STOL operation is assumed to be applied to airports with STOL-capable runways or underutilized runways.

4.1.1 STOL Runway Sizing

Previous work estimated the runway requirements for a 40-passenger CTR STOL operation to be a minimum of 800 feet supporting touchdown weight and 1,000 feet total planned length (ref. 4). In a separate study, runway length for a 40-passenger CTR takeoff and landing under STOL configuration was estimated at 100 feet in STOL configuration (ref. 23). The 1995 report (ref. 3) from the CTRDAC suggested a runway length of 400 feet for a 40-passenger CTR operation. Required STOL runway length for the CTR10, CTR30, CTR90, and CTR120 variants will be developed based on approach flight path, noise footprint, and takeoff in one-engine-inoperative (OEI) mode. The assumption for runway or vertiport surface in most past studies was found to be concrete (refs. 2-4,24).

Required STOL runway length is determined by FAA safety requirements. For example, in STOL mode, under nominal operation and a given set of ambient conditions, the MTOW loading requires the longest runway length. However, if balanced field length requirements are in effect for the CTR, then required runway length can be set via the accelerate-stop condition. Under these circumstances, the CTR accelerates to maximum STOL abort speed with braking and aft nacelle applied to roll to a complete stop. Alternatively, the accelerate-takeoff requirement assumes engine failure at the abort speed with takeoff operations still carried through. Details regarding these techniques can be found in FAA Advisory Circular (AC) 150/5325-4B (ref. 23) for fixed-wing aircraft.

4.1.2 VTOL Pad Sizing

Selecting airport real estate at a well-established fixed-wing airport to host a suitable vertiport can be a challenge. This is particularly true under the assumption that currently existing real estate surfaces must be used. In order to establish a ground footprint for a landing zone suitable for the CTR variants in this study, FAA AC 150/5390-3 (ref. 25) titled “Vertiport Design” was consulted for guidance. This AC recommends geometry for the following vertiport landing site components:

- Touchdown and Lift-Off Area (TLOF)
  - The prepared (hard/paved) landing surface
- Final Approach and Takeoff Area (FATO)
  - Area where final approach transitions to hover for landing
  - Area where takeoff maneuver is commenced

These areas must be clear of obstacles to provide a clear VTOL landing pad. Note that these requirements deal only with the landing pad dimensions and, as outlined in figure 4-1, were specified for a tiltrotor aircraft with an effective rotor span (RS) of 100 feet. Scaling of these dimensions based on actual CTR RS was used, as recommended in the AC, to develop a suitable footprint requirement based on the CTR10, CTR30, CTR90, and CTR120 variants in this study. The resulting VTOL landing site dimensions were determined assuming the more stringent IFR conditions for TLOF sizing:

- CTR120: Assume RS 191 feet, given current Bell design synthesis 1500-nmi range
  - FATO: 478 feet x 478 feet
  - TLOF: 287 feet x 287 feet
- CTR90: Assume RS 142 feet, given NASA LCTR design paper as reference 5
  - FATO: 355 feet x 355 feet
  - TLOF: 213 feet x 213 feet

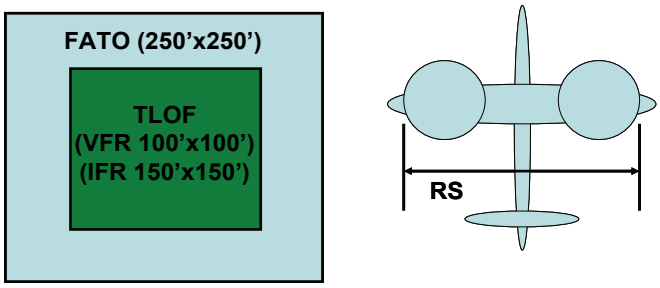

Figure 4-1. VTOL landing pad dimensions with a 100-foot-effective RS.

- CTR30: Assume RS 84.58 feet, given V-22 specifications outlined on their website (http://www.bellhelicopter.com/en/aircraft/military/pdf/V-22_64214_pGuide.pdf)
  - FATO: 212 feet x 212 feet
  - TLOF: 127 feet x 127 feet
- CTR10: Assume RS 60 feet, given Bell BA609 specifications outlined on Bell helicopter website (http://www.bellagusta.com/air_ba_main.cfm)
  - FATO: 150 feet x 150 feet
  - TLOF: 90 feet x 90 feet

This AC also suggests that the center of any TLOF must be at least 700 feet from any fixed-wing active runway under VFR conditions. In addition, IFR conditions require that only one TLOF can be placed within any FATO. Having an established set of criteria for the VTOL landing pad area was important in the overall process of surveying an airport for candidate vertiport sites.

4.2 Runway-Independent Operations

When runway-independent operations (RIO) and STOL are assumed, it is estimated that the CTR could remove approximately 10 percent of the operations nationally based on a 40-passenger seating capacity (ref. 4). In another airspace study of the NEC—also based on a 40-seat CTR and simultaneous noninterference (SNI) operations with the existing traffic—technical delay and effective delay at airports were reduced when the CTR fleet replaced existing fixed-wing airplanes at various market capture rates (ref. 2). SNI is a concept of airspace traffic flow management using simultaneous, converging instrument approaches to Instrument Meteorological Condition (IMC) minima RNP routes with separated FATOs to separate TLOF areas. Potential business cases for the CTR fleet have been suggested (refs. 1-3).

- Urban area to urban area, or city center to city center: Flows of business travel movement drive the need of shuttle services.
- The "spine" network service: Connects two or more city centers or high-density travel concentrations such as city center to uncongested hub airport or small city to small city.
- Hub feeder: Small city to high-density hub airport.

The proposed business case matrix for the CTR fleet under NextGen is shown in table 4-1.

TABLE 4-1. PROPOSED CTR FLEET OPERATIONAL MODELS IN NEXTGEN

Passenger Capacity	Metroplex Usage				
	City Center Vertiport to City Center Vertiport	City Center Vertiport to Airport Vertiport	Airport Vertiport to Airport Vertiport	Airport Vertiport to Uncongested Runway	Runway to Runway*
CTR10	√	√	√	√	No
CTR30	√	√	√	√	No
CTR90	No	No	√	√	No
CTR120	No	No	√	√	No

*Runway to runway may be considered for small cities and/or uncongested airports.

A city center vertiport is defined as an existing vertiport being used by helicopter operations at city centers where vertical landing and noise issues have already been addressed. The CTR90 and CTR120 aircraft will not be able to operate in this environment due to size and weight issues.

An airport vertiport is defined as a CTR operational space at or near an existing runway such that RIO can be performed without interfering with existing traffic flow. Assumptions can be made that a number of existing major airports are suitable to support the CTR fleet under RIO (ref. 4). The city-center-to-vertiport scenario will operate under these assumptions as well to shuttle travelers between city centers and major hubs under RIO. Note that RIO is only needed at congested airports, many of which have been identified by the FAA in its list of Operations Network (OPSNET) 45 airports (ref. 26).

The airport-vertiport-to-uncongested-runway scenario is also a feasible business case to shuttle travelers between major hubs and uncongested airports using existing runways with available slots, which will help increase the NAS capacity.

In the runway-to-runway scenario, runway is defined as a congested major airport asset. Flying the CTR fleet from runway to runway is considered not having any positive benefit to the NAS performance under these conditions. For a congested airport, there is no immediate benefit to replacing turboprop slots with CTR since the cost to build, operate, and maintain these aircraft is considered higher than similar-seating-capacity turboprops (ref. 2). In addition, the large rotors of the CTR may create stronger wake than conventional turboprop and thus require larger separation between airplanes.

4.3 Noninterference Operations

The immediate benefit of the CTR fleet is its ability to follow trajectories within the terminal area that are decoupled from those of fixed-wing aircraft. The ability to fly Noninterference Operations (NIO) is critical to the success of the CTR fleet. The CTR can be deployed to take advantage of underutilized or unused real estate at currently existing airports with its VTOL/STOL capability. If some of the turboprop fleet roles can be shifted to the CTR, this would vacate more slots from the existing traffic, making them available to the larger capacity jets, thus increasing the conventional traffic capacity. Furthermore, the CTR fleet can ferry passengers into hub airports from underutilized airfields, city centers, etc., in a more efficient manner. The overall effect is to increase throughput in the airspace system and/or reduce congestion.

NextGen ConOps that will have an impact on CTR fleet NIO are the CDA, RNAV, and RNP, as well as 4DT.

4.3.1 Optimized Profile Descent (Formerly Continuous Descent Approach)

Present-day conventional or fixed-wing approaches are built around a series of stair-step descents with altitude maintained between descent segments. This standard technique suffers from higher fuel consumption due to higher thrust requirements throughout the approach with multiple throttle excursions. In addition, they introduce elevated noise and emissions within the environment. Widespread use of Optimized Profile Descent (OPD) is assumed in the NextGen airspace environment. The OPD is built on a gradual descent, at idle or near-idle thrust, along the approach path and discards the present-day segmented (sometimes called dive and drive) technique. Consequently, this implies the aircraft is higher in altitude at any given point along the approach when compared to present-day operations. Overall, the OPD requires less thrust and thus less fuel consumption, resulting in higher efficiency across the approach profile and less emissions. The lower thrust requirements and higher altitude at any given point along the approach reduce the environmental noise experienced on the ground in surrounding communities.

4.3.2 Area Navigation and Requirement Navigation Performance

RNAV and RNP are two performance-based navigation capabilities currently being implemented in the NAS and are part of NextGen ConOps. RNAV enables aircraft to fly a desired flight path within the coverage of ground- or space-based navigation aids, within the limits of the capability of the self-contained systems, or a combination of both capabilities. As such, RNAV operations remove the requirement for a direct link between aircraft navigation and a particular navigational aid (NAVAID), allowing aircraft to have better access and flexibility for point-to-point operations. RNP operations are RNAV with the introduction of a requirement for onboard performance monitoring and alerting. The defining characteristic of RNP is the ability of the aircraft navigation system to monitor the navigation performance it achieves and to inform the crew if the requirement is not met during that operation. The possible benefits of RNAV/RNP operations are:

- Reduced route separation resulting in increased airspace capacity and efficiency
- Improved obstacle clearance limits
- Lower landing weather minimums
- Reduced pilot and controller workload
- More “fly direct to” capability and capacity

4.3.3 Four-Dimensional Trajectory-Based Operation

Four-Dimensional Trajectory (4DT)-Based Operation offers operators and service providers spatial and time-based information about the aircraft and traffic in a specific airspace. 4DT can be used to achieve optimal spacing and merging while maintaining safe separation within a given airspace. With 4DT, the direct benefit is that airspace can be used more effectively without compromising the safety of the flying public.

4.4 Developing CTR flight profiles via Pilot-in-the-Loop Simulation

The main objective of the CTR Pilot-in-the-Loop (PITL) testing was to develop a set of baseline flight profiles to help optimize CTR flight operations at the terminal area. CTR fleet performance data for CTR10, CTR30, CTR90, and CTR120 aircraft were developed in Base of Aircraft Data (BADA) format, which will be used to support Airspace Concept Evaluation System (ACES) NAS performance analysis. However, the ConOps of CTR in the terminal area, specifically in takeoff, departure, and approach and landing, which involve nacelle conversion, will be in gross approximation of aerodynamic and rotor thrust contributions, and

might not be adequately captured by the BADA/ACES modeling process. It was therefore desirable to consider PITL simulation to establish acceptable flight profiles, and compare time- and fuel-based performance generated by the BADA/ACES modeling approach. It was the intent of this test to examine factors that may affect CTR ConOps and flight profiles in the terminal area, and lay the groundwork for selecting most likely scenarios in developing the baseline flight profiles for testing.

The ability to convert between a fixed-wing and VTOL/STOL configuration gives the CTR its great flexibility to adapt to various operational environments. Although the CTR operations from point to point will be performed in a cruise airplane mode (0-degree nacelle angle), conversion modes and processes were determined for the approach, landing, takeoff, and climb-out phases of flight for both VTOL and STOL operations.

Conversion between operational modes can be a high-workload piloting task more easily completed while in straight and level flight operations. However, with the implementation of CDA profiles, conversion may need to occur while in descent or climb-out conditions. Performing conversion during these flight phases may increase pilot workload. PITL studies worked toward selecting an acceptable process to complete conversion. Past work has shown the use of advanced technology, such as a flight director system, can greatly alleviate pilot workload in the conversion phases of flight (ref. 27).

4.4.1 Flight Profile Optimization

In general there are several variables that can be used to classify an approach profile as optimal through minimization of:

- Fuel burn and emissions
- Environmental noise
- Pilot workload and feasibility
- Time spent within terminal area

These are a few of the parameters that could be considered. In this PITL study the main interest is developing terminal area procedures that are deemed acceptable by the aircrew regarding workload and feasibility. In addition, these procedures should be specified such that they would be decoupled from fixed-wing traffic sharing the terminal area airspace, ideally allowing straight-in approaches and straight-out departures, subject to the desirability of upwind approaches. This, in turn, serves to maximize throughput at any given airport. Care must be taken to select approach profiles and procedures that could be generalized as much as possible to different airport terminal airspace environments. However, it is understood that the airspace environment of each airport may have localized geographic differences and/or traffic patterns that may require special attention during future air traffic analysis studies.

Approach profiles designed and flown using the PITL simulation will not be optimized regarding environmental noise. However, estimated noise levels along the approach will be provided given the final flight profiles collected from the PITL studies. There has been past work regarding noise data collection for tiltrotor aircraft. In particular, ground noise measurements were taken during an XV-15 flight test program (ref. 28). The goal of this past work was to discern the effects of approach conditions and configurations on noise levels at various points along the approach path, as well as laterally dispersed from the path. Studies indicated the following variables pertinent in defining a good noise abatement approach and descent profile:

- Nacelle angle schedule
- Airspeed schedule
- Glide slope schedule

This past work for XV-15 recommends maintaining the nacelle angles as low as possible (60-degree nacelle rotation or less) over the duration of the approach until operationally necessary to perform further conversion.

CTR procedural techniques required in the event of emergency must be considered when designing standard flight operations. In the event of missed approach, aborted takeoff, or other more pressing issues such as engine failure, the recovery trajectory must not interfere with regular fixed-wing traffic in the immediate vicinity. Of course, rejoining fixed-wing traffic to recover the aircraft is expected as needed. In addition, it is important to decouple the nominal CTR operational envelope from the off-nominal fixed-wing trajectories in the event that those aircraft must follow through with off-nominal recovery procedures such as a missed approach.

The impact of CTR operations through emissions is also of note. Clearly, selecting operational profiles that limit thrust required throughout the approach and departure are pertinent in minimizing propulsion system emissions. Operational procedures such as the CDA noted previously help to alleviate the environmental impact. Minimizing time spent in VTOL mode when designing operational procedures also plays a role in reducing this environmental impact.

4.4.2 Baseline Flight Profile Development

The Miami International Airport (MIA) as shown in figure 4-2 was selected as the major airport to be used for the terminal area traffic simulation since there is an existing high-definition visual database of that airport within Bell Helicopter simulation. The 4DTs at this airport were selected and a methodology developed to document commonalities and differences in developing approach profiles between the MIA and North East Corridor airports, e.g., LaGuardia Airport (LGA). Specific issues need to be investigated are underlined in the following subsections.

4.4.2.1 VTOL/STOL Landing Locations at MIA

An analysis was done to determine the available locations at MIA where a vertiport and a STOL runway could be located that would allow for vertical takeoffs and landings of CTR10, CTR30, CTR90, and CTR120 aircraft. To narrow down the possible locations, the following assumptions were made for the analysis:

1) Winds are typically from the east at MIA. Under this wind condition, fixed-wing arrival traffic typically uses runways 9 and 8L, and departing traffic typically uses 12 and 8R. These traffic patterns were assumed for the analysis.
2) Spots chosen for VTOL and STOL were assumed to be available to use as such and could be made to be structurally capable of handling landings.

An initial look at possible vertiport locations was performed based on the size requirements for each of the CTR variants as defined in Advisory Circular No. 150/5390-3, “Vertiport Design,” FAA, May 31, 1991. Since all existing runways are currently used by fixed-wing traffic, existing taxiways were examined for the STOL runway. These possible locations were then evaluated for approach, landing, departure, and missed approach flight segments. The following evaluation criteria were used:

1) Interference with existing fixed-wing traffic was avoided.
2) Upwind approach, landing, and departures were preferred.
3) Approaches and departures parallel to existing fixed-wing traffic patterns were preferred.
4) Buildings/structures in close vicinity to landing zone were avoided.

5) Low flight over neighborhoods, highways, taxiways, and runways was avoided.

6) Distance from existing terminal infrastructure for handling passengers and luggage was minimized.

The vertiport location was chosen at Spot 2 on the north side of the airport, and Taxiway S at the south end of the airport was selected as the STOL runway. Figure 4-2 shows the selected landing locations as well as the assumed fixed-wing traffic. However, during the initial assessment of Spot 2 in the simulator, it was determined that not enough visual cues were available at the open parking area from the visual database for the pilot to perform a precision vertical landing. Spot 2a, which nears Spot 2 as shown in figure 4-2, was chosen instead to provide adequate visual cues from the near hanger and ground texture for the pilot to assess speed and position for an approach and landing in VTOL mode. Spot 2a has the space to fit a vertiport for the CTR10, CTR30, CTR90, and CTR120 aircraft as defined in figure 4-1. Spot 2a offers an approach from the west and a departure to the east with the least amount of existing structure along the flight path. It is also parallel to existing fixed-wing traffic and avoids flight over existing runways and taxiways.

Taxiway S, at the bottom of Spot 8 in figure 4-2, offers the most lateral separation from existing runways. In addition, since Runway 9 is used for arriving traffic, the first half of Taxiway S would not be needed for fixed-wing traffic. Missed approaches and takeoff will take the CTR over existing runways and taxiways, however, the CTR should be at a sufficient altitude to avoid interference. During the PITL, it took 2,300 feet for the CTR30 using short takeoff configuration to climb to 1500 feet, which should leave enough separation to turn and clear Runway 12 for departing fixed-wing traffic.

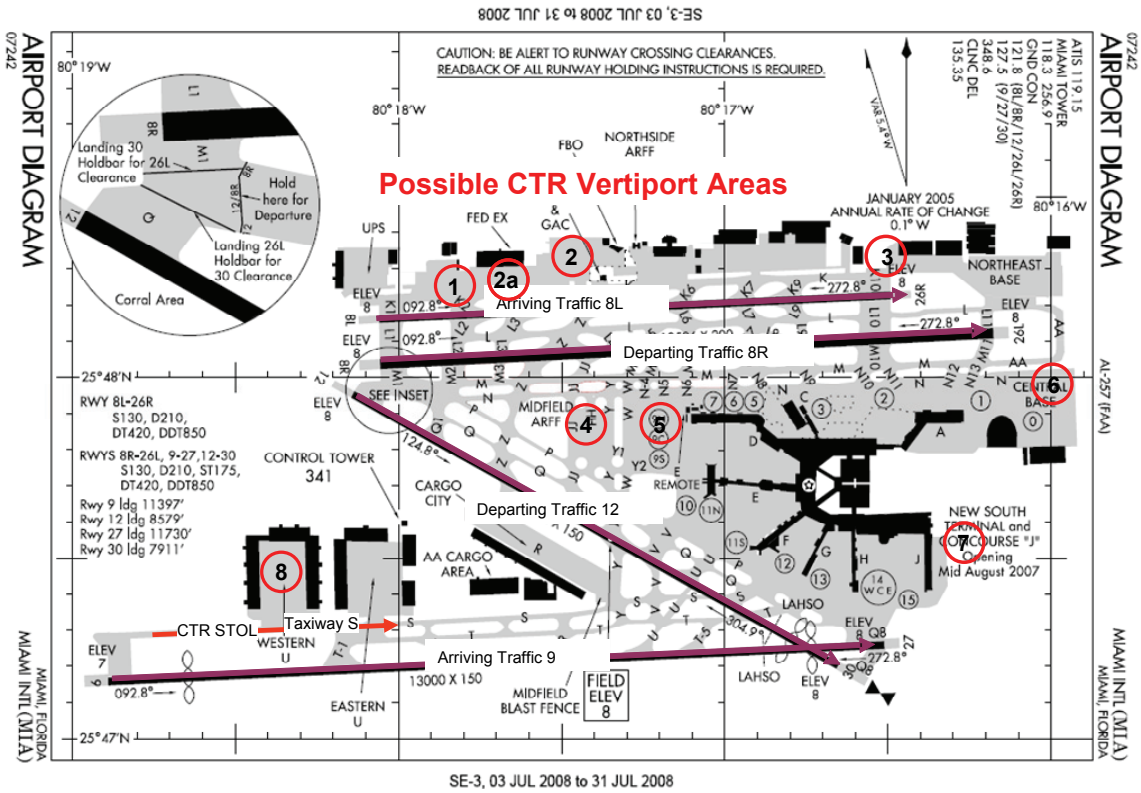

Figure 4-2. VTOL and STOL landing areas at MIA.

4.4.2.2 CTR Approach and Landing Flight Profiles

The Instrument Approach Procedure (IAP) into MIA will be a Lateral Navigation with Precision Vertical Guidance (LPV) Wide Area Augmentation System (WAAS) approach. A Decision Altitude (DA) of 200 feet was chosen to correspond to the Category 1 ILS approach minimum decision altitude. The visibility minimum for this approach will be determined based in-part on the results of the PITL testing. The proposed approach profile is shown in figure 4-3; the following description of the approach profile refers to this figure. The approach into MIA began at the top of descent (TOD) which is where transition from the cruise flight segment begins and is labeled as point 6 in figure 4-3. Descent speed needs to be evaluated at the PITL simulation. The TOD was chosen to be 25k feet mean sea level (MSL), which corresponds to the maximum cruise ceiling for the CTR10. From the TOD, the CTR enters the OPD segment of the flight for a continuous descent. The OPD consists of a low-power descent from the TOD to the terminal area. OPDs of 3, 6, and 9 degrees are investigated in the PITL tests. The OPD segment is indicated as point 7 in figure 4-3. The estimated rates of descent at a constant ground speed (assumed zero wind), as well as the distance of the OPD, are displayed in figure 4-3.

At point 8 in figure 4-3, the CTR would level off at 1,500 feet AGL, perform a conversion to 60-degree nacelle, and slow to 110 knots. An additional conversion would take place to acquire desired nacelle setting and speed prior to Final Approach Fix (FAF) of point 10. The purpose of this segment is to put the CTR into a stable configuration to shoot the approach. In existing tiltrotors (V-22, BA609) it is difficult for the pilot to manually fly a glide slope while converting the nacelles. There is no auto-nacelle/auto-pilot function in the PITL simulations used for this testing so the pilots will have to fly the approaches manually. If the capability exists in the future for auto-conversion, this segment of the flight can be eliminated and the OPD can transition directly to the glide slope where the conversion to helicopter mode can occur.

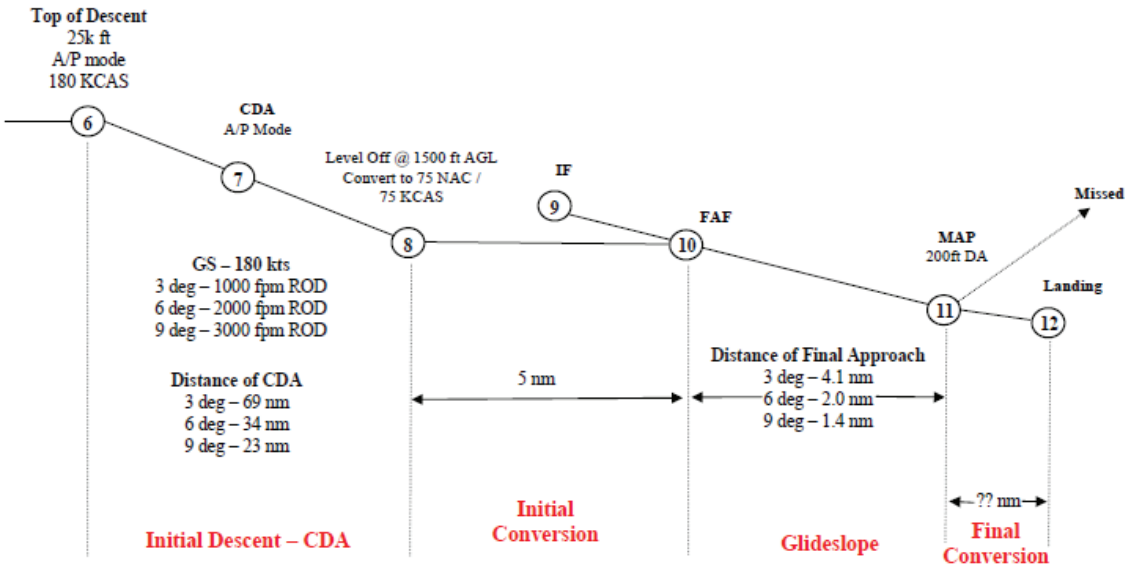

Figure 4-3. Initial CTR approach profile.

After the initial conversion, the CTR, in landing configuration (i.e., gear down and in landing flap setting), will intersect the glide slope at the FAF labeled as point 10 in figure 4-3. The CTR will follow the glide slope to the DA, labeled as point 11. At this point, a visual reference to the landing point must be obtained to continue the approach. If a visual reference to the landing point is not obtained at the DA, a Missed Approach procedure must be executed. This point is called the Missed Approach Point or MAP. Point 12 in figure 4-3 represents the vertiport for a VTOL landing or the touchdown point on the STOL runway.

The distance between the MAP and the landing or touchdown point would be determined in the PITL simulation tests. The distance for the STOL and VTOL may be different and will be investigated in the PITL simulation. For VTOL, the distance must be enough that the pilot will have suitable time to transition to helicopter mode and perform a hover landing. For STOL, the distance must be enough so that the pilot has suitable time to transition for a run-on landing. This distance will factor into determining the minimum visibility requirements for this approach.

The visual approach from the MAP to a vertical landing will be accomplished by a slow conversion from 75-degree nacelle and 75 KCAS (appropriate nacelle and speed at MAP, pt 11, would be investigated at the PITL simulation) to helicopter mode, and a deceleration to a hover over the landing spot. At this point, a normal hover landing will be performed.

During the visual approach to a STOL landing, the pilot will convert from 75-degree nacelle and 75 KCAS to 85-degree nacelle and <60 KCAS before the touchdown point. After touchdown the power will be reduced, the nacelles will be converted to full aft, and brakes will be applied.

The missed approach will consist of a straight-ahead climb to 2k feet MSL. At the MAP the CTR will be at 75-degree nacelle and 75 knots. The pilot will apply full power and once positive rate of climb has been established, the pilot should transition to 60-degree nacelle and accelerate to 110 KCAS.

For the PITL testing, this initial climb and transition is the key part of the procedure. The full missed-approach procedure is still being developed and will have to be integrated with the existing fixed-wing departure, missed approach, and approach procedures into MIA. In the final design of the missed-approach procedure, after reaching 2,000 feet MSL the pilot will transition to airplane mode and initiate a turn to be vectored back to the initial fix (IF).

4.4.2.3 Takeoff and Departure Profile Design

The vertical takeoff will be made to a hover of 10 feet. The nacelles will be slowly rotated forward and the CTR will begin to accelerate and climb. The nacelle transition and acceleration should continue until airplane mode. The BA609 takeoff profile was be reviewed, and specific takeoff procedures (taking Category A performance into account) were investigated in the PITL simulation.

For short takeoff, the nacelles were set to 60 degrees (or 75 degrees) on the ground and power advanced slowly as needed until full power was reached. Once the desired climb rate was obtained, a slow transition to airplane mode was achieved. Again the BA609 short takeoff procedure was reviewed, and specific procedures were investigated in the PITL simulation to consider possible engine failure scenarios.

Departure Procedures (DPs) are still being developed and will have to be integrated with existing fixed-wing DPs and missed approaches.

4.4.2.4 One Engine Inoperative Considerations

One Engine Inoperative (OEI) performance for the CTRs is assumed to be able to meet the certification standards set forth in the BA609 Draft Proposed Airworthiness Standards document dated 9/18/07. Full evaluation of OEI performance and the impact on the landing areas at MIA are ongoing.

4.4.3 Simulation Facility Descriptions

PITL testing was performed using Bell-provided CTR simulation and flight simulator facility and resources to investigate optimal flight trajectories under the NextGen and CTR ConOps. PITL provided the assessment of human-dependent operational procedures, nacelle conversion schedule, and constraints in the operational characteristics of the CTR and the environment.

4.4.3.1 PITL Simulation Math Model

The CTR10 and CTR30 were simulated in the PITL test. The CTR math models use a generic CTR simulation framework. The CTR10 and CTR30 performance parameters, including aerodynamics and propulsive characteristics, were drawn from design results described in section 2 for all flight phases of the CTRs, which include takeoff, climb, cruise, descent, and approach and landing. VTOL and STOL characteristics including nacelle conversion were modeled according to designed performance.

4.4.3.2 Simulation Facility

The simulator used was the high-fidelity BA609 simulator cab within the Bell Partial Task Simulator (PTS). The PTS, as shown in figure 4-4, contains a 3-channel visual system with a field-of-view of 148 degrees x 52 degrees (azimuth x elevation) at a frame rate of 50 Hz, and is capable of running practically any simulation scenario in the simulation lab databases. Figure 4-5 shows an inside view of the BA609 Simulator cab while flying in the Terminal Area Traffic Simulation. This figure also demonstrates the third-person view capability that can be used by the pilots/engineers within the Bell Helicopter Simulation Lab to pan the view point around as needed to better observe the interactions of the piloted ownship with other aircraft within the air and/or ground traffic pattern. The control loader was developed to have representative force-feel characteristics of the CTR10 and CTR30 aircraft.

Figure 4-4. The Bell Helicopter Partial Task Simulator (PTS).

Figure 4-5. BA609 cockpit with the third-person view.

4.4.3.3 Visual database

The terminal area traffic real-time database of MIA is a database used to store updated navigation information for discrete Standard Terminal Arrival Routes (STARS), Standard Instrument Departures (SIDs), missed approaches, and holding patterns. This database is used during real-time simulations to provide the required aircraft latitude (LAT), longitude (LON), altitude, and heading values at specific waypoints along a particular route. Approach profiles were developed based on reconfigured traffic flow to support a noninterfering CTR operation with respect to conventional traffic flow. Location for VTOL and/or STOL were identified according to existing MIA infrastructure to create a runway-independent operation yet provide adequate visual cues to the pilot for approach and landing maneuvers.

4.4.4 PITL Test Matrix Specification

The Bell piloted simulator flew a minimum of four separate flight profiles to include VTOL landings and takeoffs, as well as STOL for the CTR10 and CTR30 configurations. The flight profiles were selected to emphasize the unique characteristics of the CTR. The use of piloted simulation is crucial to confirm that the profiles have acceptable workload and performance margins for passenger route use. The flight simulator time history data were recorded and used to validate the BADA models created in section 3.

For PITL testing the TOD point was assumed to be at 4,500 feet AGL to minimize time in the simulator. One descent flight was made to evaluate the descent profile and level-off altitude and speed before the initial nacelle conversion as shown in the first test case in table 4-2. Subsequent approach and landing runs were started at 110 knots with 60-degeree nacelle at 1,500 feet. The following number of runs was planned for the CTR10 and CTR30 tests:

- From FAF to DA
  - Three approach paths (3, 6, and 9 degrees) for VTOL
  - Three approach paths (3, 6, and 9 degrees) for STOL
- MAP
  - Three approach paths (3, 6, and 9 degrees)
- Takeoff in VTO and STO

Note that one run per glide slope is needed from FAF to DA to investigate requirements for the DA. A DA of 200 feet was selected for the PITL simulation.

4.4.5 PITL Test Results

The two-day PITL simulation test evaluated CTR10 and CTR30 flight procedures in the terminal area according to the test matrix. The main objectives of the PITL simulation were to develop realistic CTR flight profiles and conversion schedule in approach and landing, and takeoff in the terminal area based on CTR design characteristics described in section 2 to evaluate pilot workload, and to identify required control augmentation and navigation aids. Based on the test results, the CTR takeoff profile for the CTR10 and CTR30 is summarized in figure 4-6. The CTR approach and landing profiles for CTR10 and CTR30 are summarized in figure 4-7. The distance from Point 6 (TOD) and Point 8 (the final level-off before FAF in figure 4-7) to Point 11, the landing spot, was determined by the CTR NIO traffic flow layout relative to the fixed-wing traffic flow to the existing runways.

Specific takeoff runway lengths until clearing the 50 feet altitude from the PITL simulation are summarized in table 4-3. Time history of CTR10 and CTR30 PITL test results for VTOL and STOL operations of 3-, 6-, and 9-degree approach paths are shown in appendix H.

Several issues underlined in previous sections are addressed below.

One of the concerns in taking off from Taxiway S eastbound is whether CTR can clear Runway 12, which is used for fixed-wing departure traffic. From the PITL data, a STO from Taxiway S cleared 1,000 feet altitude at 8,000 feet distance from the rolling start. The distance from the rolling start to where the taxiway intersects Runway 12 is 9,000 feet. There is enough separation for the departing CTR to clear the Runway 12 traffic.

TABLE 4-2. PLANNED PITL TEST MATRIX

		Conversion and Intercept Glide Slope at FAF	**Fly Glide Slope to DA**	
1	Trim to 250 knots airplane mode at 4,500 feet	Descent to 1500 ft, level off at 200 knots, and convert to 100 knots/60˚ nacelle	TBD	Descent and level off
2	Trim to 110 knots/ 60˚ nacelle at 1,500 feet	Convert to 90 knots/ 75˚ nacelle	3˚	Vertical landing
3	| |	Convert to 70 knots/ 85˚ nacelle	6˚	Vertical landing
4	| |	Convert to 50 knots/ 88˚ nacelle	9˚	Vertical landing
5	| |	Convert to 90 knots/ 75˚ nacelle	3˚	STOL
6	| |	Convert to 70 knots/ 85˚ nacelle	6˚	STOL
7	| |	Convert to 50 knots/ 88˚ nacelle	9˚	STOL
8	| |	Convert to 90 knots/ 75˚ nacelle	3˚	Missed approach
9	| |	Convert to 70 knots/ 85˚ nacelle	6˚	Missed approach
10	| V	Convert to 50 knots/ 88˚ nacelle	9˚	Missed approach
	Takeoff	Nacelle and speed	Climb speed (fpm)	Level off altitude (ft) and speed (knots)
11	VTO	TBD	TBD	TBD
12	STO	60˚ with decision speed TBD	TBD	TBD

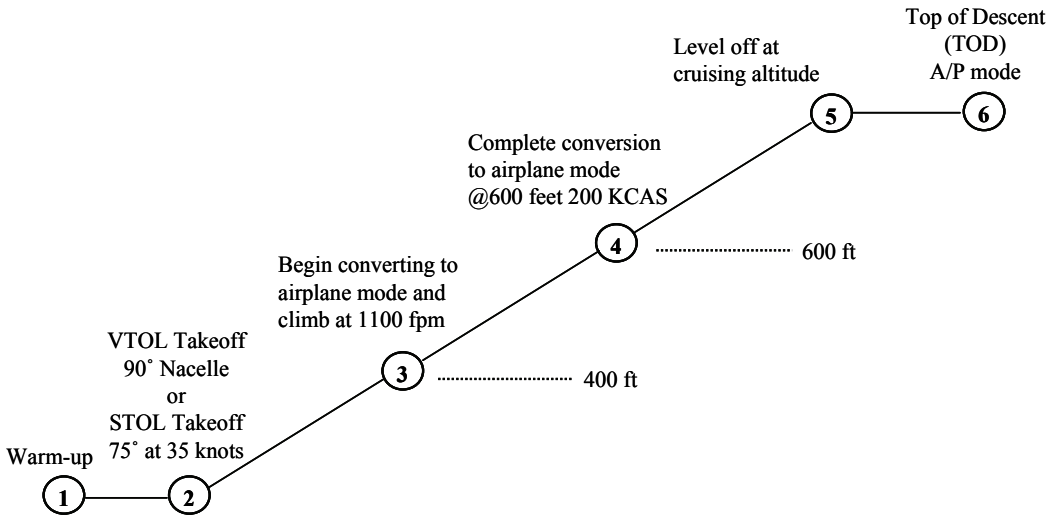

Figure 4-6. CTR takeoff profile from PITL experiment.

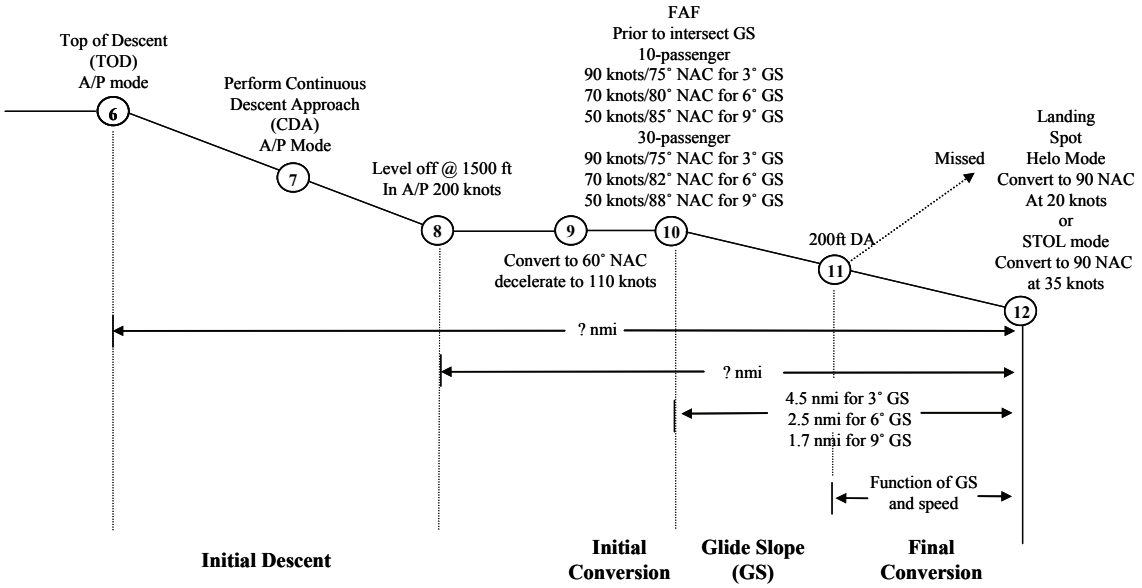

Figure 4-7. CTR approach profile from the PITL experiment.

TABLE 4-3. TAKEOFF AND LANDING RUNWAY LENGTH REQUIREMENTS UNDER STOL CONFIGURATION

CTR10 With a Reference Weight of 16,191 Lbs	
Takeoff length (from start to clear 50-ft obstacle)	497.6 ft
Landing length (from touchdown to a full stop)	
3˚ glide slope	134 ft
6˚ glide slope	156 ft
9˚ glide slope	152 ft
CTR30 With a Reference Weight of 46,430 Lbs	
Takeoff length (from start to clear 50-ft obstacle)	588 ft
Landing length (from touchdown to a full stop)	
3˚ glide slope	777 ft
6˚ glide slope	391 ft
9˚ glide slope	452 ft

From the PITL, one run was made by descending from 4,500 feet to 1,500 feet at an initial speed of 250 knots. The pilot descended at 1,600 fpm and leveled off at 200 knots. This confirmed the CTR can descend from a higher speed at the TOD.

Specific nacelle conversion and speed schedule for CTR10 and CTR30 at three glide slopes were investigated and summarized in table 4-4 and table 4-5.

Issues regarding takeoff procedures and one engine out are discussed in section 4.4.6 Pilot Comments.

4.4.6 Pilot Comments

A NextGen Simulation was conducted in the BHTI Sim Lab on 10 and 11 November 2009. The main purpose of the simulation was to demonstrate an initial set of baseline flight profiles developed to help optimize CTR flight operations at the terminal area. The session on 10 Nov was dedicated to the CTR10 tiltrotor design utilizing the BA-609 cab and control laws. On the 11th the CTR30 design was flown utilizing the CV-22 cab and control laws. The BA-609 does not have a Flight Director or coupled modes available while the CV-22 has a Flight Director that can be coupled to fly the aircraft. Although the BA609 and CV-22 cabs and control laws were used, the simulation models were modified to reflect the airframe weight, aerodynamics, and engine fuel flow characteristics respectively of both the CTR10 and CTR30 NextGen CTR designs.

The profiles flown in both aircraft designs included 3-, 6-, and 9-degree glide slope precision approaches to a hover and to a rolling landing. Missed approaches from the three glide slopes were flown as were takeoffs from a hover and a STO. Some additional data points were flown: a level-off from a descent, deceleration, and reconvert to approach configuration. Also flown was a spiral descent at various airspeeds and descent

rates to measure diameter of spiral and normal load factor, Nz. One case was flown from 10,000 feet to 1,500 feet followed by reconversion and a full ILS approach flown to the hover spot. This last point was accomplished in the CTR30 design and used the Flight Director coupled mode.

The approaches were flown in IMC to a breakout of 200 feet after which the approach was terminated visually to either a hover or to a rolling landing. In the CTR10 design, only raw data was available while in the CTR30 design the Flight Director could be used. Having the Flight Director reduced the pilot workload somewhat.

The nacelle/airspeed combinations in approach and landing are shown in table 4-4 for the CTR10 and in table 4-5 for the CTR30.

The aircraft was initially at 75 degrees/90 knots (CTR10) and 60 degrees/110 knots (CTR30), and the above configurations were established prior to glide slope intercept. There was no real effort to minimize total time for the approach—just to be well stabilized at the conditions prior to intercepting glide slope and descending. There was some discussion as to using the data gathered (that would show time/distance for the reconfiguration) to optimize the approach. Flight Director cues could be developed to prompt the pilot to make the changes based on distance from approach termination.

To precisely fly an approach at these slow airspeeds it is necessary to have excellent handling qualities. This will require control law development that includes particular testing at these slow speeds along with an airspeed indicating system that is accurate to less than 40 knots. Tests included flying at a minimum speed of 50 knots but for the 9-degree glide slope some further testing should be conducted to look at 35–40 knot approaches. This may help with workload on the glide slope and will reduce the vertical velocity as well.

Another requirement to fly these type of approaches is to have a Flight Director who is well tuned to handle the steep glide slope angles, such as 6 and 9 degree, as well as the slow speeds. The Flight Director in the CTR30 design, which was tuned to a 3-degree glide slope, was helpful at the higher 6- and 9-degree glide slopes, but the lateral guidance was very active/nervous while on the approach, which was distracting. The vertical guidance for glide slope maintenance was not accurate for the 6- and 9-degree glide slopes. For those approaches, pilot used raw data. A well-tuned Flight Director for the higher glide slope angles is a must to fly these approaches precisely.

TABLE 4-4. CTR10 NACELLE AND AIRSPEED SETTINGS

Glide Slope Angle	Nacelle Angle (°)	Airspeed (KCAS)
3	75	90
6	80	70
9	85	50

TABLE 4-5. CTR30 NACELLE AND AIRSPEED SETTINGS

Glide Slope Angle	Nacelle Angle (°)	Airspeed (KCAS)
3	75	90
6	82	70
9	88	50

The 3-degree glide slope approach was easily flown with both machines. The 6-degree approach was slightly more challenging, while the 9-degree approach required significant pilot inputs to maintain glide slope and airspeed. No Handling Qualities Ratings (HQRs) were taken for the individual approaches.

For the approaches to the spot, breaking out at 200 feet above ground level was a challenge for the 6- and 9-degree glide slopes in that the time from break-out until hover was on the order of 5–6 seconds. It was somewhat artificial in the testing as pilot knew he was going to break out at 200 feet; once pilot achieved breakout the visibility was unrestricted and pilot was very familiar with the expected sight picture. Further testing may be needed to determine best decision height for the steeper glide slope approaches.

For the approaches to the taxiway, the glide slope was set to essentially take the aircraft to the end of the STOL runway. For 3 degree, this was no problem when breaking out at 200 feet as there was sufficient distance to transition and touchdown in the first quarter of the runway. As the glide slope steepened, the distance obviously decreases, the time to transition is reduced, and the touchdown moves down the runway. Further testing should be done to determine optimal decision height and also optimal location of the glide slope transmitter to allow full use of the runway for the steeper glide slopes.

A cursory examination of One Engine Inoperative (OEI) was made during development of the approaches. An engine failure was simulated just prior to glide slope intercept as pilot flew the approach to landing. The power required is low during the approach and no difficulties were noted in flying the approach, but the arrestment of the sink rate was a challenge in the approach to a spot with the models we were flying. It was basically a no-hover landing and would have been quite hard. The rolling landings were accomplished easily, keeping the airspeed above translational lift. Further testing should be done with accurate power available modeled for the given designs.

The takeoffs were quite easily flown as were the missed approaches. Having a Flight Director to provide cues was helpful in the CTR30, although pilot was trying to adjust the Flight Director and fly simultaneously. If there is a developed departure and go-around in the Flight Director that includes alterable en-route and final conditions (airspeed, heading, altitude, etc.) the workload would be minimized.

The spiral descent was easily flown in the CTR30 design. Pilot was able to use the Flight Director to cue for airspeed and descent rate while the bank angle was held by the attitude loop. We flew bank angles to provide standard-rate and half-standard-rate turns. Airspeeds flown were 200, 220, 240, and 250 knots at descent rates of 1,500 and 2,000 fpm.

On the last spiral descent data run, the Flight Director was coupled and was used to fly the descent and level off by the pilot. Once leveled off and headed in the general direction of the airport, a heading was commanded to intercept the ILS approach, reconfigured to approach configuration, capture the localizer which it did and flew to 200 feet where the approach was completed visually to a hover. Auto-Nacelle feature was engaged which automates the nacelle movement—only a speed needed to be selected and the Flight Director commanded the nacelle position for that airspeed. This demonstrates the necessity of having a Flight Director that will precisely fly the profiles commanded—resulting in a reduced pilot workload.

4.4.6.1 Summary of Pilot Comments

Several key comments to improve future CTR flight operations were identified during the PITL:

1) A well-tuned Flight Director to fly steep approach profiles is a must.
2) Having a Flight Director that will precisely fly the profiles in a coupled-mode to reduce pilot workload is recommended.
3) If a slower approach speed at intercepting the glide slope is required than was established during the PITL, improved handling qualities with advanced flight control law are recommended to maintain the precision needed for the task.
4) OEI was evaluated. No difficulties in approach but would be landed hard in hover mode. No issue with rolling landing. Further testing with a more accurate propulsion model is recommended.
5) Established flight profile can be extended to CTR90 and CTR120 models.

4.5 Developing Desired Flight Parameters for the CTR Fleet for the NextGen Performance Analysis

Flight profiles developed from the PITL simulations described in section 4.4.5 are adjusted to include the departure fix at 10,000 feet, Point 4.5 in figure 4-7, and arrival fix also at 10,000 feet, Point 7, for the climb phase and descend phase of the flight respectively. Since the CTR Performance Deck (CTRPD) was developed for the CTR in airplane mode, flight segments in airplane mode as shown in figure 4-7, or Point 4 to Point 8, were used to investigate the tradeoff between cruise speed and cruise altitude based on Productivity Index, as shown below to determine the optimal cruise speed and cruise altitude for the given service range based on the flight time and fuel burn.

$$\textbf{\textit{Productivity Index (PI)}} = \frac{Payload \times Range}{(Weight \quad Empty + Block \quad Fuel) \times Block \quad Time}$$

For any given origin-destination city-pair (OD-pair), e.g., BOS-DCA, the distance for the airplane mode is first estimated from the distance when CTR converts to the airplane mode during the takeoff, i.e., from Points 1–4 in figure 4-7, and when CTR converts from the airplane mode to conversion mode for an approach and landing, i.e., from Points 8–12 in figure 4-7, based on the PITL results. Using this estimated distance in airplane configuration, cruise speed and cruise altitude were then perturbed, while climb rates were bounded by the maximum available thrust during the climb segments, and descend rates were bounded by the achievable descend rate during the descent segments for each passenger size of the CTR fleet. Speeds at departure fix and arrival fix were kept at 250 KCAS, and at below 250 KCAS for altitude below 10,000 feet, while meeting the speed target shown in figure 4-7 at lower-altitude segments to comply with FAA flight procedures.

A detail approach to develop the tradeoff is described in appendix J. Final results for typical OD-pairs in the NEC region are shown in figure 4-8 and summarized in table 4-6. Distances in parentheses in table 4-6 are estimated distance flown in airplane mode for the given OD-pair. These cruise speeds and cruise altitudes were applied to OD-pairs for similar distances during the NAS performance analysis in other regions, as discussed in section 6.

TABLE 4-6. ORIGIN-DESTINATION CITY-PAIR CRUISE SPEED AND CRUISE ALTITUDE DEVELOPED BASED ON PRODUCTIVITY INDEX

		10-passenger		30-passenger		90-passenger		120-passenger	
City-pair	Distance	Cruise speed (knots)	Cruise Altitude (feet)	Cruise speed (knots)	Cruise Altitude (feet)	Cruise speed (knots)	Cruise Altitude (feet)	Cruise speed (knots)	Cruise Altitude (feet)
BOS-PIT	430(420)	280	25000	340	23000	340	27500	345	27500
BOS-DCA	346(336)	280	25000	340	21000	340	27500	345	27500
BOS-PHL	237(227)	280	25000	340	21000	340	27500	345	27500
BOS-EWR	174(164)	280	21000	340	21000	320	19000	330	22000
PHL-IAD	117(107)	230	8000	280	8000	320	12000	320	12000
PHL-BWI	78(68)	230	8000	280	8000	270	6000	270	6000

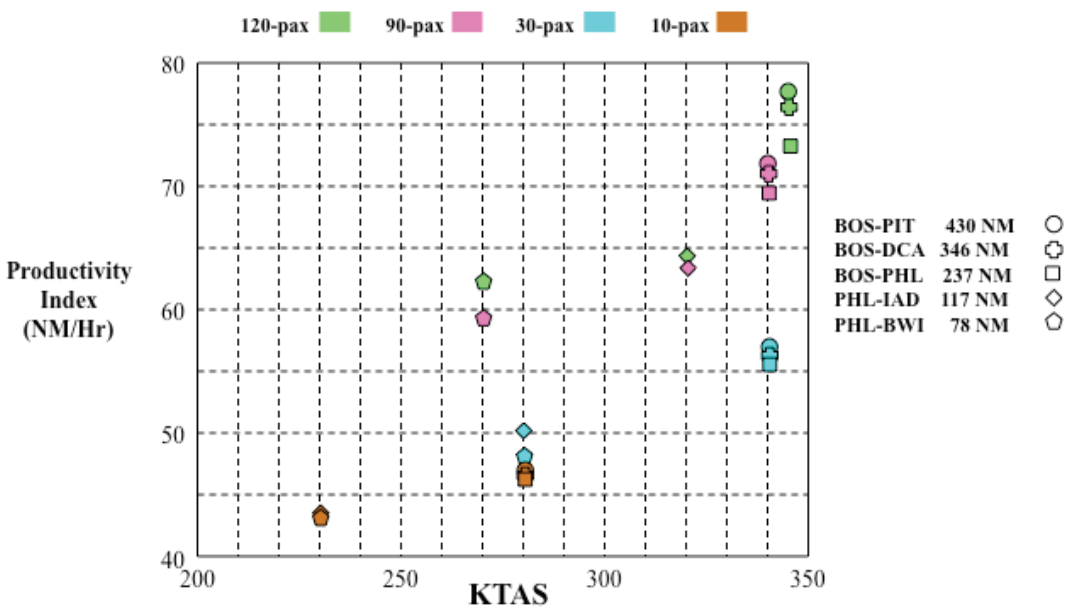

Figure 4-8. Productivity index for the CTR fleet in selected origin-destination city-pairs.

4.6 Potential Certification and Safety Issues

The CTR is an example of a new category of aircraft known as Powered Lift Aircraft (PLA). PLA are heavier-than-air aircraft that are capable of vertical takeoff and landing and low-speed flight that depends principally on engine-driven lift devices or engine thrust for lift during these flight regimes, and on nonrotating airfoil(s) for lift during horizontal flight. Examples include the Bell/Boeing V-22, Boeing (formerly Harrier) AV-8, and Bell/Augusta BA-609. The V-22 and Harrier are military aircraft and the BA-609, currently undergoing certification, is a multi-turbine-engine powered lift category, tiltrotor class aircraft. Using the BA-609 as a baseline, this study reviews potential type certification and safety issues unique to operational implementation of CTRs into the NAS. Since Airworthiness Requirements for CTRs have not been finalized, these issues are based on the current proposed requirements and a technical evaluation of the unique design characteristics of CTRs.

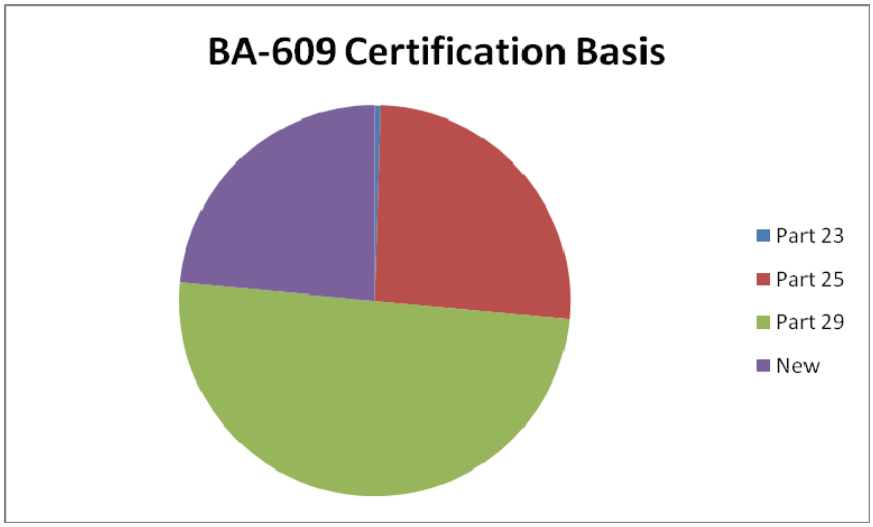

Figure 4-9. Regulations over BA-609 certification.

The BA-609 has been in the development process for over 15 years, and the recent estimates suggest late 2010 or early 2011 for concurrent certification by both the U.S Federal Aviation Administration (FAA) and the European Aviation Safety Agency (EASA). The Bell and Augusta partners are currently discussing the certification schedule and other issues; the certification basis is shown graphically in figure 4-9.

The applicant for the BA-609 submitted a type certification request to include the applicable requirements of Title 14 Code of Federal Regulations (CFR), Part 23 (Normal, Utility, Acrobatic, and Commuter Category Airplanes), Part 25 (Transport Category Airplanes), and Part 29 (Transport Category Rotorcraft) found to be appropriate by the FAA, as well as any additional airworthiness criteria determined by the FAA. The FAA first proposed airworthiness standards for the BA-609 in September 2007, under the provisions of Federal Aviation Regulation 21.17 (b), designation of applicable regulations for special classes of aircraft for which airworthiness standards have not been issued. The "special class" category for aircraft was created for nonconventional aircraft for which airworthiness standards have not been issued and provides a means for applicants to propose airworthiness standards for their particular special class aircraft.

The Certification Basis, when completed, will consist of the following:

Certification Basis = Part 23 + Part 25 + Part 29 + New Tiltrotor unique requirements (TR)

The Part 23 requirements relate only to composite structures. Depending on publication data this may replace by a proposed change to Part 29, damage tolerance and fatigue evaluation composite requirements.

4.6.1 Process for NAS Operational Approval

While this study looks at CTR10, CTR30, CTR90, and CTR120 variants, which go beyond the BA-609 design, the airworthiness requirements for that aircraft are important because they will set the tone for certification of future aircraft in that class.

To avoid confusion concerning the relationship between obtaining a Type Certificate (TC) and its relationship to safety, several concepts must be defined:

Safety

The state in which the risk to harm to persons or of property damage is reduced to, and maintained at or below an acceptable level through a continuing process of hazard identification and risk management.

Risk

Risk is the assessed potential for adverse consequences resulting from a hazard.

Type Certificate (TC)

A TC is issued by the FAA when an applicant demonstrates that the type design of a product meets all the applicable airworthiness requirements.

Production Certificate (PC)

A PC represents FAA approval of the quality control system for the production of an aircraft. This ensures that when a product is produced it conforms to the type design.

Airworthiness Certificate (AC)

An AC is issued to each aircraft to document that it conforms to an approved type design and is in a condition for safe operation. An AC is needed to register and operate an aircraft in the U.S.

Operational Approval

Operational Approval is the process the FAA uses to approve that a type-certificated aircraft can be operated in the NAS. For each air carrier and/or commercial operator this occurs when the FAA approves its aircraft operating specification.

To summarize:

$$NAS\ Operations = TC + PC + AC + Operation\ Specification$$

4.6.2 Design-Driven Certification Issues

The unique design/operational features of the CTRs under review in this study will influence the development of new tiltrotor unique airworthiness standards. The following is not an exhaustive list but is illustrative of certain critical issues.

From a transport category rotorcraft perspective the BA-609 will be the first civil rotorcraft that has a fully fly-by-wire (FBW) flight control system (FCS), a pressurized cabin, is certified for dual pilot IFR/flight into known icing conditions, and has a composite structure and rudderless “T” tail configuration. Follow-on CTRs will baseline their airworthiness requirements from this design point.

This study looks at four CTR versions (CTR10, CTR30, CTR90, and CTR120) with corresponding changes in airframe geometry and mass as shown in table 4-7.

TABLE 4-7. CTR IN NEXTGEN DESIGN, DIMENSION, AND MASS PROPERTIES

Description (units)	CTR10	CTR30	CTR90	CTR120
Wingspan (m)	10.31	13.96	25.06	30.60
Wing Area (m^2)	17.03	35.49	103.28	144.08
Airframe Length (m)	13.41	18.79	30.52	34.09
Reference Mass (kg)	7030.7	17916.9	45627.0	56699.0
Minimum Mass (kg)	5302.0	14800.7	37388.8	45359.2
Maximum Mass (kg)	7620.4	21060.3	54390.9	66972.0

The following type certification issues are identified due to unique CTR features:

1) Aircraft icing, both ground de-icing and in-flight icing. Currently it is proposed that CTRs comply with the provisions of FAR Part 25.929, "propeller de-icing," Part 25.1419, "ice protection," Part 29.1093, "induction system icing protection," and special tiltrotor requirement (TR) TR.1416 concerning pneumatic de-icing boot systems. It is critical, during the type certification process, for an applicant to demonstrate through test, simulation, and analysis that a CTR can operate safely throughout its declared icing operating envelope in airplane mode, helicopter mode, and during conversion. One example is a rotorcraft hovering in blowing snow and then transitioning to takeoff. Snow may accumulate on or in the engine inlet area during hover and then be dislodged and ingested into the inlet. Another example would be changes to aircraft flutter characteristics due to ice accretion on critical surfaces. The FARs require that no person may takeoff in an aircraft when frost or snow is adhering to the wings, control surfaces, propellers, engine inlets, etc., with references to 14 CFR Sections 91.527, 121.629(b), and 135.227(a). Therefore, flight crews must check their aircraft before flight when there is icing. There are several FAA Advisory Circulars (ACs) (refs. 23,29-32) that provide information on de-icing and anti-icing of aircraft before takeoff. Failure to develop and implement these procedures as part of an air carrier operating specification could lead to aircraft operational limitations, in icing, in order to minimize a safety-of-flight issue.

2) Since the CTR operates in both helicopter and airplane modes, demonstration of crashworthiness requirements is a certification issue. The proposed standards for the BA-609 are a mix of Part 29, 25, and Special TRs. For example, the fuselage door standards are a mix of FAR Parts 25.783, 29.783, and a new TR.783. In performing a safety analysis to define the criteria for a "survivable" crash, prop-rotors failing "fixed" in airplane mode and helicopter mode, as well as a critical angle during conversion, must be considered. The resulting crash loads affect the design of such items as seats, overhead storage compartments and fuel tanks. As this aircraft grows in size and number of passengers, certain requirements can change. Above 19 passengers, the air carrier operating requirements for flight attendants change as well certain cabin equipment requirements (see 14 CFR sections 121.305, 121.309, and 121.344(a) for examples.)

3) The BA-609, as well as future CTRs, will be fully FBW aircraft with advanced flight management systems (FMS) and FCS. Showing compliance with the requirements of TR.1309, for the BA-609, or the provisions of Part 25.1309, for other CTR designs, will be difficult. For example, consider the effect of

turbulence on a CTR barbell like mass distribution. Having engine masses positioned at the aircraft wingtips is a unique configuration with impacts on the aircraft structural stability under varying aerodynamics loads (aeroelasticity). Current FCS designs build in filters to the feedback loops to dampen oscillation and ensure adequate stability margins when the aircraft enters turbulence (whether clear air turbulence or wake vortex). To meet DO-178, level "A" verification, and validation certification standards for both the basic FCS code and aeroelastic algorithms will be difficult. There is limited aeroelasticity data on a basic BA-609 configuration, not to mention larger CTRs. Besides the above, under the provisions of the Safety Management System, the applicant must demonstrate that any potential catastrophic impact resulting from in-flight events such as lightning strikes, wake vortex encounter, and exposure to HIRF are extremely remote.

4) Flight crew training is another potential safety issue. In 1997 the FAA changed 14 CFR Section 61 (see 14 CFT Sections 121.305, 121.309, and 121.344(a) for examples) to incorporate requirements for a powered-lift pilot license. During helicopter-mode flight operations there are certain pilot actions that may be required to maintain safe operation, but these may seem counter-intuitive to a fixed-wing pilot. In airplane mode the same may be true for an experienced helicopter pilot. An example can be found in the discussion of a V-22 accident in April 2000 that took the lives of all 19 persons on-board the aircraft (ref. 33). In summary, the data showed the aircraft in a high rate of descent at a very low forward airspeed. These conditions lead to a condition known as power settling or vortex ring state. When an aircraft descends so quickly, a pilot's natural tendency is to add power to slow the descent. In a vortex ring state, adding power results in an increased sink rate. Helicopter pilots are aware of this and trained to reduce power and increase airspeed to fly out of the condition. The pilots of the V-22 were not aware they were in this condition. For tiltrotor training it is imperative that pilots be able to identify off-nominal conditions when they occur and mentally select the proper response in a timely manner.

5) A follow-on to the pilot licensing/training safety issue is the design and certification of a human-factor-based flight deck for a dual-pilot/IFR-rated CTR aircraft. The questions of what type of data and how it is displayed on the flight deck need to be addressed. With a CTR flight envelope cycling from VTOL, conversion, to airplane mode and then back again, a particular flight mode drives the issue of how the man-machine interface functions will be evaluated and eventually distributed, and the flight deck be designed to present timely, accurate, and clear information to the crew. This is critical to safety of flight especially during off-nominal conditions.

6) Part of the Operational Approval process will look at such things as whether special maintenance requirements for CTRs are needed. Data for this will be generated during the certification process FAA maintenance steering group deliberations.

7) There are additional criteria for air carrier operations for extended twin-engine operations (ETOPS); they could apply to the CTRs depending on proposed route structures.

8) One final issue remains: noise certification. Currently, 14 CFR Part 36 does not contain noise requirements for CTRs. International Civil Aviation Organization (ICAO) adopted tiltrotor noise guidelines in Annex 16, Volume 1, Attachment F, Amendment 7, dated March 21, 2002. The FAA cannot "accept" the ICAO requirements and will need to promulgate noise standards under FAR 36. The FAA has not indicated if they will propose the ICAO standard or something different.

The preceding is not an exhaustive list of potential certification and safety issues but those considered critical at this time. Any NAS operational issues that need to be developed as NextGen requirements are defined for such concepts as arrival/departure corridors, self separation, and trajectory-based operations (TBOs).

5 CTR OPERATIONS IN NEXTGEN

Recent NASA research led by Sensis Corporation on "Integration of Advanced Concepts and Vehicles into the Next Generation Air Transportation System" (refs. 34,35) (New Vehicle Integration NASA Research Announcement (NVI NRA)) found that civil rotorcraft have the potential to relieve air traffic congestion by utilizing runway independent, vertical terminal operations and providing point-to-point travel. However, that research cautioned that meaningful integration of this potential capability into NextGen presumed overcoming limits of current rotorcraft technologies. Enhanced throughput capability (higher speed, longer range, and more payload capability), and operational and environmental (especially noise) acceptance were considered to be the key drivers towards the air transportation system level operation of rotorcraft. In the late 1980s, the Boeing company showed that a large civilian tiltrotor fleet derived from the V-22 Osprey technology could partially fulfill these challenges in an economically viable manner (ref. 1). NASA's comparative research for future heavy lift rotorcraft systems concluded that "Large Civil Tiltrotor had the best cruise efficiency, hence the lowest weight and cost and were economically competitive, with the potential for substantial impact on the air transportation system" (ref. 6).

The current study builds on and extends the NVI NRA study with respect to vehicle design, pilot-in-the-loop (PITL) simulation, and operational concepts. The NVI NRA study considered five specific types of future advanced vehicles:

- Cruise-efficient short takeoff and landing (CESTOL) vehicles
- Large civilian tiltrotor aircraft (LCTR)
- Unmanned aircraft systems (UAS)
- Very light jets (VLJs)
- Supersonic transports (SST)

The NVI NRA study selected a NASA reference design, current at the time of the study, for a large civil tiltrotor (LCTR2) as the baseline rotorcraft. The LCTR2 was designed for the short-haul regional market with entry into service of 2018 or later; had the capacity to carry 90 passengers for 1,000 nmi at 300-knots cruise speed, and was designed to operate from underutilized vertiports. The choice of this particular vehicle concept was based on vehicle characteristics that reflected the need to compare a middle ground, high-speed, long-range rotorcraft alongside four other advanced air vehicles in a future scenario.

The NVI NRA study considered five advanced vehicle concepts, and included an analysis of the business case for operation of the representative air vehicles. The CTR concept studied was NASA's LCTR2, a short-haul regional transport with an assumed initial service date of 2018. The LCTR2 was designed to transport up to 90 passengers (at 32-inch seat pitch with single class 2-2 seating) to the maximum range of 1,200 nmi at 300 knots cruise speed. The LCTR2 design used a wing spanning 107 feet, employing a blade folding mechanism, with assumed weight penalty of 1,000 lbs for each rotor blade. Four advanced 7,500-lb class turbo-shaft engines would drive two 65-foot-diameter prop-rotors.

The study concluded that, combined with precise independent approach/departure paths and new landing pads at congested hubs, the LCTR would have the ability to serve busy short-haul city-to-city routes. However, the drawbacks—increased operating costs, safety, and environmental concerns—were comparatively more pronounced for the LCTR than the CESTOL study vehicle. The study cautioned that if NextGen succeeded in adding significantly capacity and predictability for conventional operations, then the LCTR business model as described in the NVI NRA study seemed unlikely to succeed. However, if NextGen failed to enable reliable service for conventional aircraft then LCTRs had the potential for more viability.

The NVI NRA study conclusions with respect to the LCTR are summarized in this paragraph. Acquiring and maintaining a fleet of 90-passenger LCTRs would be more costly compared to 90-passenger fixed-wing aircraft. Operators of LCTRs would have to charge passengers more per seat. The LCTR business model assumed that travelers would pay a premium for more reliable and predictable on-time service between popular city-pairs. Using vertiports separate from main airport runways, combined with precise independent approach and departure paths and new landing pads at congested hubs, the LCTR would have the capacity to handle the busiest short-haul city-to-city routes. LCTRs would be able to get into and out of heavily congested airports more reliably and with less delay than fixed-wing aircraft. Passengers traveling on LCTRs could reliably leave for a remote city in the morning and reliably return home the same evening. For the LCTR demand set, flights between high traffic city-pairs within the range of a typical shuttle operation (500 nmi) were identified in the baseline demand set and replaced with LCTRs. The NVI NRA study concluded that a 2025 scenario would require 300 LCTRs, growing to 800 by 2040.

Building on the NVI NRA, the current study shares the premise that, regardless of the technology, it remains true that airport and NAS capacity will be increased through the operation of any vehicle capable of taking off and landing using a very short (600 feet or less) runway or vertiport, and capable of flying arrival, departure, and en route segments that are independent from those of conventional aircraft.

The objective of the current study is to investigate the impact that a CTR fleet may have under NextGen. For that purpose, the study evaluated NextGen requirements to identify relevant technology and ConOps applicable to CTR operations such as performance-based services (e.g., Area Navigation/Required Navigation Performance (RNAV/RNP) and Four-Dimensional Trajectory (4DT)-Based Operations).

The current study extends work done under the NVI NRA in four main respects:

- The current study developed three separate CTR configurations (with seat configurations of 10, 30, and 120 passengers), using major Original Equipment Manufacturer (OEM) design practices to assess the case for CTR operations in the NAS based on performance, market demand, and NAS capacity. Flight performance of the three CTR configurations is evaluated based on mission requirements and tiltrotor manufacturing technology such as airframe, engine, rotor, and manufacturing materials, assuming an in-service date of 2025. The flight performance of a fourth CTR configuration (with a seat configuration of 90 passengers), was scaled from the performance of the other three CTRs, and checked against published reports, to complete the fleet mix for a NAS performance analysis.
- The current study took a high-fidelity approach to analyzing the flight performance of a CTR fleet in evaluating NAS performance. Flight profiles for four different CTR sizes were developed using a fixed-based high-fidelity PITL flight simulation experiment to investigate the runway-independent operations (RIO) issues at a major airport, man-machine interface issues at various flight phases, and operational issues associated with the conversion characteristics at the takeoff and approach and landing phases. Established flight profiles were later used to determine optimal cruise speed and altitude for the CTR fleet. Procedures for establishing a noninterfering CTR operation and RIO for a terminal area are developed based on a sample airport (Miami International), and evaluated via the PITL simulation for the CTR10 and CTR30. Flight profiles for approach and landing and takeoff were evaluated based on CTR flight characteristics in conversion mode, pilot workload, approach and landing cueing requirements, and one-engine-inoperative (OEI) requirements for VTOL and STOL operations.
- Flight performance based on weight, speed, and altitude was then translated to conform to the Base of Aircraft Data (BADA) aircraft performance model taking into account the CTR's unique nacelle conversion and a range of cruise, takeoff, and approach and landing profiles. The enhanced BADA data were then applied to a NAS performance analysis to evaluate the impact of the CTR fleet in the NextGen. The CTR fleet ConOps assumes noninterference operations (NIO) and runway-independent operations (RIO) capabilities, since these unique capabilities of the CTR can offer potential improvements to the performance of NAS (i.e., increased capacity and reduced delay while meeting required safety standards).

- NAS performance in terms of throughput, delays, and capacities was evaluated using Airspace Concept Evaluation System (ACES), a distributed, agent-based simulation of the NAS consisting of NAS models and simulation control and assessment tools. The future effects of a fleet of 30-, 90-, and 120-passenger aircraft (CTR30, CTR90, and CTR120) were first evaluated in the Atlanta, Las Vegas, and North East Corridor regions, using current projections of passenger growth and capacity through 2025 consistent with those of the FAA and Joint Planning and Development Office (JPDO). The selection of these three regional scenarios resulted from the projection of significant 2025 delays in these regions, and the estimated effect on NAS delay reduction of substituting CTR service for conventional scheduled service on routes under 500 statute miles. A preliminary investigation of a CTR10 fleet was considered in a notional business model. Environmental effects such as noise and emission were also considered.

Additional background on the current study and its scope is contained in a paper describing the study presented in 2010 (ref. 36).

5.1 NextGen Concept of Operations

Recognizing that new technology and processes are necessary to meet the need for greater capacity and efficiency in the National Airspace System, the JPDO compiles and communicates planning information through three foundational documents: The NextGen Concept of Operations (ConOps), Enterprise Architecture (EA), and Integrated Work Plan (IWP). These three documents describe what the NextGen end-state will be, how it will operate, when NextGen capabilities and potential improvements will be introduced, and who will be responsible for implementing the capabilities and improvements.

The JPDO supports collaborative planning through its announced intent to publish annual updates to these documents. The JPDO NextGen ConOps has evolved through several versions, with the first mature version (2.0) released in 2007 (ref. 11). On September 30, 2010, JPDO released its ConOps for NextGen (Version 3.2) (ref. 37), Integrated Work Plan for the NextGen System (Version FY13) (ref. 38), and Enterprise Architecture (Version FY13) (ref. 39).

The current NextGen ConOps (Version 3.2) states the most fundamental requirement of NextGen is to safely accommodate significantly increased traffic and to do this in airspace that is already congested such as between heavily traveled city-pairs (Washington, DC and Chicago). This requirement leads to the development and implementation of High-Performance Trajectory-Based Operations (HP-TBO) in high-density airspace. Using HP-TBO 4DTs allows the Air Navigation Service Provider (ANSP) to precisely schedule traffic through congested airspace, especially as aircraft start to merge approaching a major airport. It is safe to assume these capabilities will apply to CTR operations at vertiports since two of NextGen's major goals are to "…accommodate a broader range of aircraft capabilities and performance characteristics" and "Meet the needs of flight operators…for access, efficiency, and predictability in executing their operations and missions."

A NextGen ConOps concept applicable to CTR operations on vertiport-to-vertiport routes is that of "flow corridors" for separation-capable aircraft with similar performance traveling in the same direction on very similar routes. The JPDO NextGen ConOps defines flow corridors as long tubes or "bundles" of near-parallel 4DT routings which support very high traffic throughput, while allowing traffic to shift as necessary to enable weather avoidance, reduce congestion, and meet defense and security requirements. The airspace for aircraft (including CTRs) operating in flow corridors is protected as aircraft not part of the flow do not penetrate the corridor. It is likely that specific flow corridors will be set up for CTR operations, since these operations will, for the most part, operate on high-traffic-density origin-destination (O-D) pairs.

The 4DT assignments in a flow corridor will not ensure that conflicts never occur but will ensure that any conflicts are easily resolved with small speed or trajectory adjustments even with the high traffic density. The

corridor is large enough for aircraft to use their separation capabilities for entering and leaving the corridors, as well as for overtaking other aircraft in that corridor, all of which are accomplished with well-defined procedures to ensure safety. CTRs are assumed to operate under Automatic Dependent Surveillance-Broadcast (ADS-B) (In) with Cockpit Display of Traffic Information (CDTI), so that delegated self-separation capability will be an option to supplement ground controller responsibility for separation.

Aircraft operating in flow corridors are procedurally separated from other traffic not in the corridor. The high traffic density achieved in corridors and the separation of aircraft with different performance increases airspace available to other traffic and reduces the need for traffic management initiatives; thus the flow corridor is implemented along the optimum routes and altitudes. The corridor may be dynamically shifted to avoid severe weather or take advantage of favorable winds. Procedures exist to allow aircraft to safely exit the corridor in the event of a declared emergency. Under the current NextGen ConOps, for scalability and affordability, the ANSP could delegate separation tasks to capable aircraft whenever this benefits the aircraft involved, overall operations, or ANSP productivity. Some airspace would be designated as self-separation airspace where self-separation operations are authorized for properly equipped aircraft. CTRs in flow corridors would be likely candidates for delegated self-separation, since CTRs would operate in-trail along defined routings, in a manner similar to the delegated separation now used for visual approaches.

Flow corridors for CTR operations are not explicitly considered in the NextGen ConOps. Under the ConOps, aircraft would typically be assigned final 4DT arrival profiles at the top of descent (TOD). CTRs and other traffic operating outside flow corridors in airspace serving trajectory-based traffic, including aircraft arrivals and departures from complex and dense en route airspace, would be ANSP-managed, with traffic management and surface management functions supported by advanced automation. Arrival/departure area and airport surface management would be integrated to ensure arrival flows matched projected airport capacity for improved overall throughput and efficient flight trajectories that would eliminate current low-altitude path-stretching and holding.

The NextGen ConOps also does not explicitly consider airborne merging and spacing procedures that would apply for CTRs and fixed-wing aircraft, in particular for operations using multiple vertiports at the same location. Rotorcraft and other “runway-independent” aircraft needing access to trajectory-based arrival/ departure corridors would be coordinated with fixed-wing flows (presumably to include noninterference operations) to avoid congestion and improve overall flow of both types of aircraft. The NVI NRA study developed a notional airspace redesign for the New York Metroplex that supported noninterfering arrival/departure routings based on RNP 0.3 procedures, but it did not consider the increased complexity of 4DT procedures for CTR operations at multiple colocated vertiports. The NextGen ConOps discussion of 4DT procedures does include delegated separation, airborne merging and spacing, airborne self-separation, low-visibility approaches and departures, high-density arrivals and departures, and surface procedures. Design of flow corridors and arrival/departure corridors for all-weather CTR operations will require extensive design, analysis, and rulemaking before 4DTs can be operationally introduced for both conventional fixed-wing and CTR aircraft. The requirement for development of a CTR-specific NextGen ConOps is discussed in more detail in section 6.

The development of quieter aircraft, coupled with widespread implementation of low-noise approaches, would ease restrictions currently imposed for noise abatement at many airports.

5.2 NextGen Capabilities Applied to CTR Operations

One of the most critical issues in achieving CTR operational success is to ensure the CTR fleet is appropriately equipped to take advantage of NextGen infrastructure improvements. A critical assumption is that this equipment (avionics) is approved and available for installation at the time of CTR service entry. The JPDO NextGen Avionics Roadmap, version 1.0 (ref. 24), dated October 24, 2008, communicates how the infrastructure improvements correlate to aircraft capabilities and functions, and how these capabilities/functions evolve over time. Avionics derived from three NextGen technologies (i.e., data communications, RNAV/RNP, and ADS-B) will enhance operator benefits and airspace capability.

5.2.1 Performance-Based Services

The following performance-based services are developed by the FAA to allow the NextGen infrastructure to support JPDO visions and plans.

Automatic Dependent Surveillance-Broadcast (ADS-B), both In and Out, is available. Real-time air situational awareness is provided by integrating cooperative and non-cooperative surveillance data from all air vehicles.

- ADS-B (In) provides information to the cockpit of properly equipped aircraft that can be used for multiple applications.
- ADS-B (Out) provides high-accuracy and frequent aircraft position reports that can be used by Air Traffic Control (ATC) to provide radar-like separation in non-radar areas.

Cockpit Display of Traffic Information (CDTI) provides graphical display of air traffic to improve situational awareness. Relative guidance, predominantly based on speed control, to maintain spacing can be located on the CDTI.

Digital Data Communications are used for clearance delivery, frequency changes, uplink of RNAV/RNP procedures, and negotiated Continuous Descent Arrivals (CDAs) and Required Time of Arrivals (RTAs).

Electronic Flight Bags (EFBs) are used to provide the flight crew with charts, manuals and weather data. One application is ADS-B (In) information displayed on a moving map that has own-ship location to improve surface movement safety.

Flight Information Services-Broadcast (FIS-B) are used for aircraft not having weather radar.

Equivalent Visual Operations are supported by Synthetic Vision Systems/Enhanced Vision Systems (SVS/EVS).

Traffic Information Services-Broadcast (TIS-B) and Automatic Dependent Surveillance-Rebroadcast (ADS-R) are used to provide traffic information when equipped to receive surveillance information from the ANSP. For aircraft that operate on different links, ADS-R service is a component of TIS-B to rebroadcast ADS-B data across the different links to ensure that aircraft operating on one link can receive ADS-B information from aircraft on the other datalink frequency.

5.2.2 Trajectory-Based Operations

The following trajectory-based services are developed by the FAA to provide the NextGen procedures to support JPDO visions and plans.

Four-Dimensional Trajectory (4DT)-Based Operation is available for super density airspace and congested airports.

RNP procedures along with ADS-B (In) and CDTI are used for closely spaced parallel approaches.

RNP coupled with RTA and ADS-B (In) are used for aircraft spacing for optimized runway throughput.

Optimized Profile Descents/Continuous Descent Approaches are available for use in CTR operations when required (e.g., minimizing fuel consumption, noise, or emissions).

Airborne Merging and Spacing using ADS-B, RNP, and Traffic Collision Avoidance System (TCAS) is available within CTR flow corridors.

5.3 NextGen ConOps Applied to CTR Operations

5.3.1 Net-Centric Operations

At the heart of the NextGen concept is the information sharing component known as net-centric operations (NCO). NCO allows NextGen to adapt to growing operations as well as shifts in demand, making NextGen a scalable system. NCO also provides the foundation for robust, efficient, secure, and timely transport of information to and from a broad community of users and individual subscribers. The result is a system that minimizes duplication, achieves integration, and facilitates the concepts of distributed decision making by ensuring that all decision elements have exactly the same information on which to base a decision, independent of when or where the decision is made. Specifically, when CTRs operate in the STOL mode, the NCO will improve situational awareness and help manage the flow of aircraft to and from the ramp control area, which may be used as a staging area for CTR operations. Controllers will be able to more efficiently manage the use of taxiways and runways, which will mean fewer radio transmissions (crew workload), shorter wait times, and fewer departure delays (less fuel burn and lower emissions). In VTOL operation the shared situational awareness will provide increased coordination and improved capacity when CTR arrival/departures are integrated with conventional aircraft. This will be especially true when considering separation for off-nominal conditions such as missed approach procedures. The result will be a better balance of arrivals and departure flows, especially for airports in close proximity such as the New York Metroplex.

Since CTR operations require transition and conversion in and out of airplane mode, and since those transitions/conversions occur in the terminal area and involve differences in maneuverability between CTRs and conventional aircraft, there will be a need for CTR-specific NextGen ConOps, especially during merging and OPD/CDA. NCO and CTR NextGen ConOps will use shared situational awareness to ensure that each flight has no potential flight plan conflicts and allows for efficient CTR arrival while maintaining overall efficiency of the airspace operation.

5.3.2 Shared Situational Awareness

Shared Situational Awareness (SSA) is fundamental to the NextGen vision for providing integrated information sharing, air domain awareness, and weather information. Integrated information sharing depends on availability of SSA information services. Authorized subscribers can access the information desired in an automated and virtual fashion, where subscribers produce a standing request for information using established protocols and standards.

SSA services offer a suite of tools and information designed to provide NextGen participants with real-time aeronautical and geospatial information that is communicated and interpreted between machines without the need for human intervention. A reliable, common weather picture provides data and automatic updates to a wide range of users, aiding optimal air transportation decision making. Positioning, navigation, and timing (PNT) services reduce dependence on costly ground-based navigational aids by providing users with current location and any corrections such as course, orientation, and speed necessary to achieve the desired destination.

Integrated information capability provides shared situational awareness and enables authorized stakeholders to provide, discover, and consume timely and accurate NextGen relevant information (e.g., weather, surveillance, PNT, aeronautical, and geospatial) in a decentralized, distributed, and coordinated environment. Through available enterprise services provided by NCO, an environment is available where trusted aviation stakeholder partnerships, and aligned data policies and standards (which include data conflict resolution) can enhance decision making by dramatically shortening decision cycle times and improving situational awareness. Providing pilots and controllers with better situational awareness, such as aircraft operational intent, will result in the reduction of flight path anomalies.

5.3.3 Distributed Decision Making

NextGen capabilities emphasize distributed decision making, system flexibility, scalability, robustness, and resiliency. They also stress the importance of providing information to users while reducing the need for ANSP control.

These NextGen capabilities will fundamentally change the approach to air transportation operations in 2025. Capacity, flow management, and efficiency are increased with the transformation from clearance-based operations to TBO, as required by demand and complexity. Advancements in aircraft capabilities allow for reduced separation and support the transition from rules-based operations to performance-based operations. In addition, the transition of separation responsibility from the controller to the flight crew in some areas allows controllers to focus on overall flow management instead of individual flight management. Self separation enables maximum user flexibility in exchange for high capability aircraft equipage and associated crew training. Recent introduction of Precision Runway Monitor-Alternative (PRM-A) approaches to Closely-Spaced Parallel Runway (CSPR) approaches provides an example of the application of accurate surveillance (based on multilateration) and precision conformance monitoring for ATC separation assurance of aircraft flying 3,000 feet apart. The combination of accurate ground-based surveillance and ground conformance monitoring, with independent accurate relative position indication in the cockpit, suggests that the future ConOps for CTR operations may support delegated separation responsibility for CTR operations within procedurally-separated CTR flow corridors.

5.3.4 Integrated Safety Management System

CTR design and operations are assumed to be consistent with the three NextGen safety goals of safer management practices; safer aviation system technologies; and worldwide standards, regulations, and procedures. Improved safety operations ensure safety considerations must be fully integrated throughout the air transportation system by increased collaboration and information sharing, improved automation (e.g., decision support systems), prognostic safety risk analysis, and enhanced safety promotion and assurance methods.

5.3.5 Human and Automation Capabilities

The NextGen ATM system capitalizes on human and automation capabilities. It employs complementary air and ground technologies in a distributed manner. Both humans and automation play important and well-defined roles, which take advantage of the types of functions each can best perform. Although new technology is critical to implementing the NextGen ATM system, ensuring that both service providers and flight operators are given appropriate roles is equally critical.

Automation supports the migration from tactical to strategic decision making by assimilating data and supplying information, as well as by performing many routine tasks. Ultimately, the determination of when to fully automate and when to provide decision support is made to optimize overall system performance and ensure that service providers and flight operators perform well and can respond to off-nominal and emergency events when required. Increased reliance on automation is coupled with fail-safe modes that do not require full reliance on humans as a backup for automation failures. In addition, backup functions are distributed throughout the system, and there are layers of protection to allow for graceful degradation of services in the event of automation failures.

Automation is particularly critical to the CTR fleet with its unique nacelle-tilting characteristics during the takeoff, and approach and landing flight phases, which naturally demands higher pilot workload. Automation in flight control, flight director, and guidance displays has been specifically called out during the PITL experiment in section 4. Such requirements from a handling-qualities prospective, coupled with NextGen performance-based flight rules, will likely be a challenging research topic.

5.3.6 Integrated Arrival/Departure Operations

Integrated arrival and departure airspace management allows terminal transition areas to extend into current en route airspace, allowing reduced separation standards. Reduced separation standards will permit a greater number of RNAV and RNP procedures to be flown within the transition airspace, increasing throughput for both the conventional fleet as well as the CTR fleet. These improvements will also allow greater flexibility for aircraft reroutes around severe weather or other disruptions.

In addition, capacity and runway throughput are increased through the reduction of lateral separation requirements. With the use of precision navigation, on-board displays, and alerting technology, independent converging approaches are conducted while maintaining Visual Meteorological Condition (VMC) arrival rates in Instrument Meteorological Condition (IMC).

While dedicated CTR flow corridors offer potential for noninterference between CTR and fixed-wing traffic by procedurally separating CTR and conventional traffic, achieving complete independence of operations at airports may be limited by wake vortex separation requirements. This may require integration of arrival and departure times for both types of traffic under closely-separated conditions.

5.3.7 Flexible Airspace Management

Flexible airspace management is supported by automation that allows reallocation of trajectory information, surveillance, communications, and display information to different positions or different facilities, enabling increased flexibility to modify or change sector boundaries and airspace volume definitions in accordance with predefined configurations. The ability of the ANSP to reconfigure airspace and services in response to changing demand will improve NAS efficiency and reduce congestion and delay.

Weather and traffic volume will continue to require adaptive airspace configuration. CTR operation on short flight segments and at lower speeds and altitudes than conventional traffic will involve greater need for weather-dependent routings. The CTR ConOps, therefore, will need to include provisions for reconfigurable 4D flow corridors to minimize adverse impact of local weather and atmospheric conditions on CTR operations. Provision for aircraft de-icing requirements includes both procedures on how a CTR will be de-iced, as well as the icing dwell time (the time between when a CTR is de-iced until it must either takeoff or be de-iced again). Real-time knowledge of surface winds, blowing snow, and rainfall will be critical for CTR operations especially in the VTOL mode.

6 CTR FLEET PERFORMANCE ANALYSIS UNDER NEXTGEN

Three regional CTR scenarios were evaluated—Atlanta, Las Vegas, and a Northeast Corridor (NEC) scenario based on service at nine major airports. Effects of a fleet of CTR30 (30-seat), CTR90 (90-seat), or CTR120 (120-seat) aircraft operating in 2025 were initially evaluated in the NEC, using projections based on FAA and JPDO assumptions. After reviewing high ACES delays for the NAS conventional fleet in 2025, two additional scenarios were evaluated. The two scenarios, covering the Atlanta and Las Vegas regions, were projected to experience significant delays; introduction of RIO/NIO operations was shown to offer significant reductions in NAS-wide delays. Effects of the CTR10 fleet in a notional business model were also evaluated. Environmental effects such as noise and emission due to the CTR fleet were also investigated.

The three regions were selected by reviewing ACES NAS-wide simulations of projected airport delays in 2025, and picking those major airports or airport groups with the highest projected delays. The schedules and capacity assumptions used were those developed by JPDO that were available at the time the earlier NASA New Vehicle Integration NRA (ref. 34) (NVI NRA) study was conducted. Figure 6-1 is a map developed for the NVI NRA, showing projected 2025 delays for high-delay airports (each stack level in a column represents 10 minutes average delay as measured in ACES).

The results of NVI NRA study suggest that three of the major airports with projected capacity shortages are those serving Atlanta, Las Vegas, and Philadelphia. The three regional scenarios chosen for evaluation in the current study followed from the results of the earlier study. The Atlanta region represents a connections-based air traffic hub. The Las Vegas region represents a hub supporting origin-destination traffic. The NEC region represents a regional network supported by 9 major airports (Boston Logan International Airport (BOS), Baltimore Washington International Airport (BWI), Ronald Regan Washington National Airport (DCA), Newark Liberty International Airport (EWR), Dulles International Airport (IAD), John F. Kennedy International Airport (JFK), New York LaGuardia International Airport (LGA), Philadelphia International Airport (PHL), and Pittsburg International Airport (PIT), with linking the 9 airports, as well as service between each of the 9 airports and other airports less than 500 miles distant.

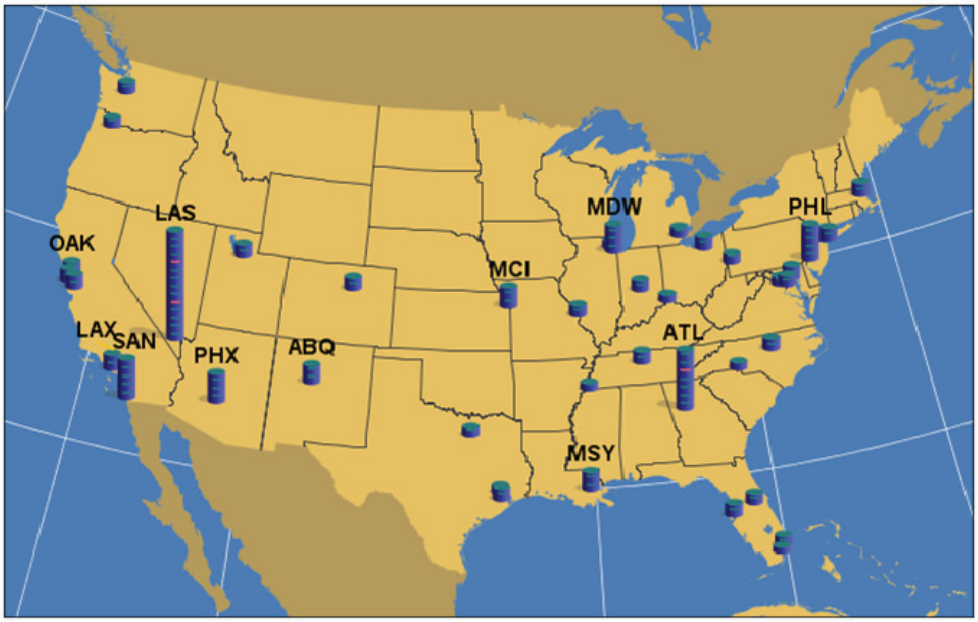

Figure 6-1. NVI NRA major U.S. airport delay projections for 2025.

When updated JPDO schedules and capacity estimates for 2025 were evaluated in the current study, the overall conclusions about airport capacity shortages did not change significantly. Figure 6-2 shows the average delays projected by ACES using current projections.

Airport capacity shortages are still projected for the Atlanta and Las Vegas metropolitan areas. Philadelphia no longer appears in the list of cities facing serious capacity challenges. Chicago-Midway, San Diego, New York, and Washington, D.C. have been added to the list. The three regional scenarios selected for evaluating the outcome of using CTRs to replace conventional fixed-wing schedules allow the potential effects of CTRs for replacement service on short-haul regional air routes to be evaluated using ACES. The evaluation is performed in this study in terms of both delays at the current airports and NAS-wide delays. Future studies can extend the analysis to other metropolitan regions in comparable future baseline demand and capacity projections.

The approach in this study, confined to the three selected regional scenarios, was to consider conventional flights operated on under-500-mile routes in the 2025 ACES schedule as eligible for replacement using CTR service. Flights in the baseline 2025 schedule assigned to be operated by small- and medium-size airliners (15-seat commuter aircraft up to A321 aircraft) were assumed to be replaced by CTR30, CTR90, or CTR120 aircraft.

For the purposes of this study, the three regional scenarios were assigned names of ATL500, LAS500, and NEC500, indicating only flights less than 500 miles are being considered. Figure 6-3 shows the route networks for the three regional scenarios.

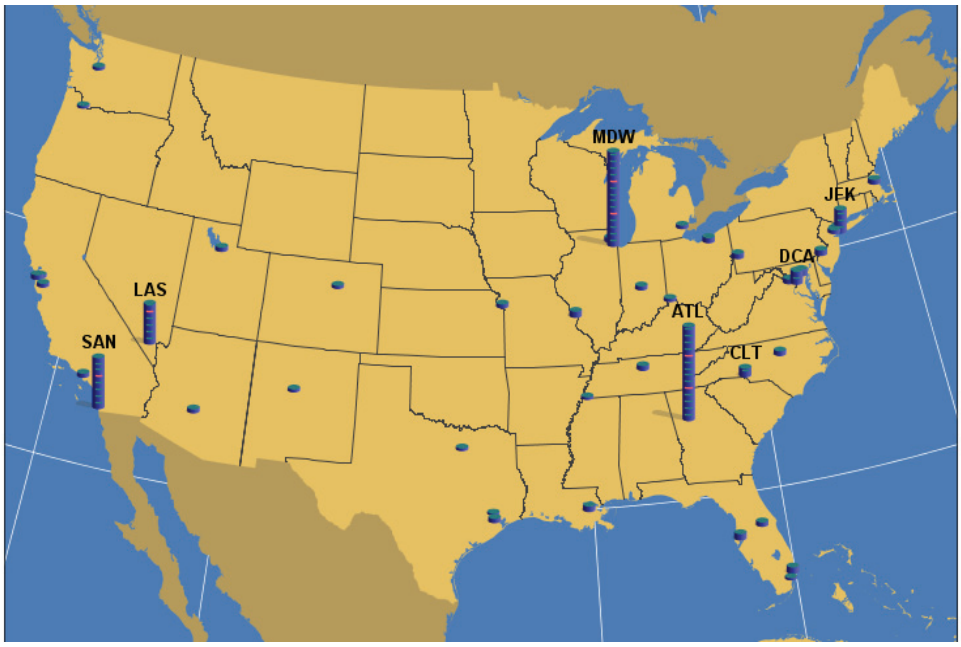

Figure 6-2. Current baseline major U.S. airport delay projections for 2025.

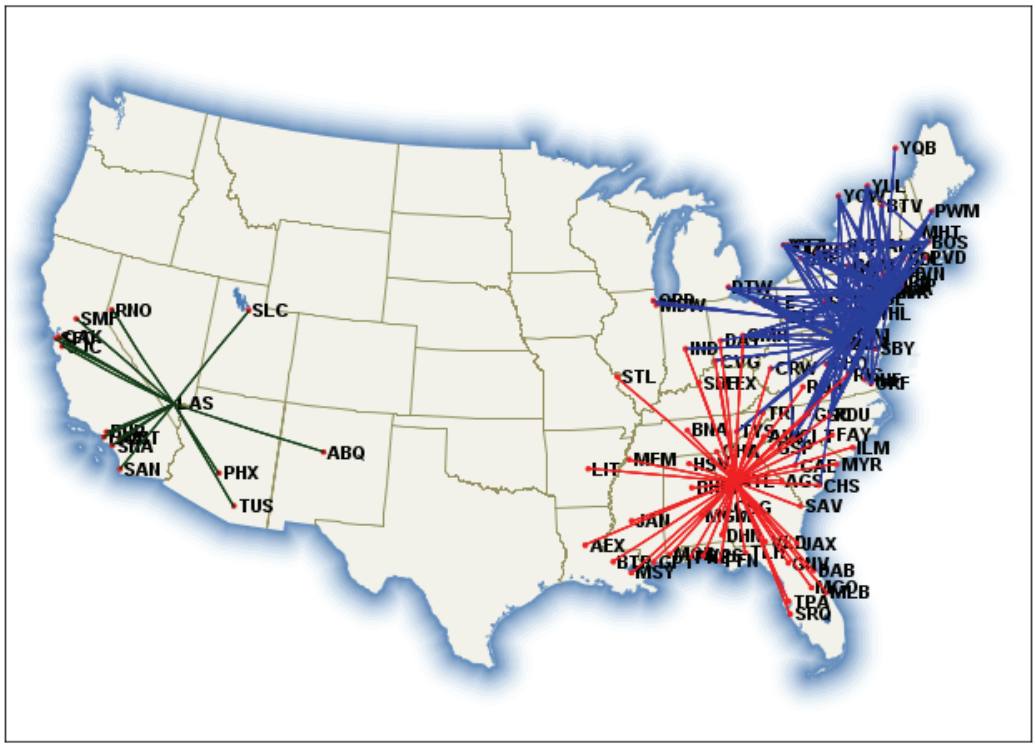

Figure 6-3. CTR regional networks.

The CTR variant assigned to any city-pair market was determined by the number of total scheduled seats offered in that market. CTR capacity was assigned to replace conventional capacity in the ACES 2025 schedule, under an assumption that the number of replacement CTR seats on any route segment would closely match the number of conventional seats replaced, as summarized in table 6-1.

TABLE 6-1. SUMMARY OF DEPARTURES AND SEATS BY REGION

	Replaced Conventional		Substituted CTR	
Region	**Daily Departures**	**Daily Seats**	**Daily Departures**	**Daily Seats**
ATL500	1,374	114,817	1,066	114,600
LAS500	622	82,689	692	83,040
NEC500	3,307	239,965	2,654	240,420
Total	5,303	437,471	4,412	438,060

Source: ACES 2025 schedule with CTR matching seat replacement.

6.1 NextGen Performance Metrics for CTR

This section develops a set of metrics to assess the impact of new CTR operational procedures on operations in NextGen, including but not limited to capacity, delay, and safety under normal and off-normal conditions (such as weather and Special Activity Airspace).

6.1.1 Approach to Development of Performance Metrics

The Sensis *Advanced Vehicle Concepts and Implications for NextGen* (NVI NRA) report (ref. 34) included a comprehensive discussion of metrics, including definitions of over 100 individual metrics. The approach presented in this technical note focuses on a limited number of fundamental performance metrics necessary for comparing scenarios with and without CTR substitution (CTR, Conventional, and Mixed CTR-Conventional Operations). These metrics can be considered to be a subset of the NVI NRA metrics, focusing on operational and service performance. The proposed metrics are designed to allow aggregation to support overall comparisons.

Performance metrics relate to both operational performance and service performance, and involve comparison of mixed CTR-conventional operations with pure conventional operations. Operational performance metrics apply to aircraft ground and flight operations, while service performance metrics apply to the trip experience as perceived by travelers.

Most performance comparisons will use time, distance, fuel consumed, or emissions as measures. The measures may be absolute or comparative. The measures may be expressed as central tendency (e.g., average or median values), and may involve dispersion (e.g., variability, uncertainty, or probability distributions). Performance measures support efficiency comparisons. The Operational Performance and Service Performance metrics are illustrated in figure 6-4 and are addressed separately in the following paragraphs.

High-level metrics are the result of aggregating lower-level metrics. The approach proposed here is to develop metrics which can either be estimated for each defined operational phase (with estimates derived from prior tasks in this project or through explicit assumptions about 2025 ConOps), or which can be allocated to individual operations through system simulations such as ACES (ref. 19).

In addition to performance metrics, cost and safety metrics are relevant in comparing CTR, and conventional and mixed CTR-conventional operations.

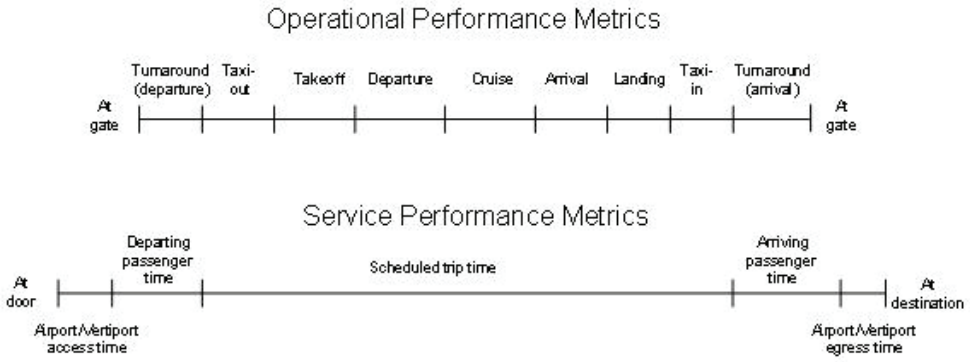

Figure 6-4. Operational and service performance metrics.

6.1.2 Operational Performance Metrics

Operational performance metrics apply to the discrete phases of aircraft ground and flight operations. The notional approach is to define time, distance, fuel-burn, and emissions metrics to each operational phase for every conventional and CTR operation. The concept will be to consider differences between conventional and CTR operations relative to estimates of delay versus unimpeded or planned time, and relative to excess distance travelled relative to direct distance ("circuity").

An all-purpose generic listing of flight phases does not exist. The current FAA NextGen Implementation Plan (NGIP) (ref. 40) describes in its text the following flight phases for NextGen midterm (2018) operations: flight planning; push back, taxi, and departure; climb and cruise; descent and approach; landing, and taxi and arrival. In a chart illustrating the phases of flight, the NGIP uses the following different set of flight phases: flight planning; push back/taxi/takeoff; domestic/oceanic cruise; and descent/final approach/landing.

A similar International Civil Aviation Organization (ICAO) listing of flight phases includes the following: planning, ramp, surface departure, departure, dispersion, cruise, collection, approach, surface arrival, and ramp (ref. 41).

Eight flight phases may be considered in order to support comparison of CTR and conventional operations:

1) Turnaround: gate-in to gate-out; unloading, loading, and negotiating clearance
2) Taxi-out: from gate or loading stand to start of takeoff
3) Takeoff: from start of takeoff to departure fix
4) Departure: from departure fix to TOC
5) Cruise: en route from TOC to TOD
6) Arrival: from TOD to final approach fix
7) Landing: from final approach fix to touchdown
8) Taxi-in: from touchdown to gate or unloading stand

The following metrics are proposed within each of the above phases for comparison of CTR, Conventional, and Mixed CTR-Conventional operations:

- Unimpeded or free-flow time
- Delay
- Fuel burn
- Emissions
- Departure and arrival noise impact
- Direct (Great Circle) distance toward destination
- Excess distance (circuity)

These metrics are suggested as the basis for comparing conventional, CTR, and mixed operations in the current project. For the most part, these metrics build on the analysis presented in sections 4 and 5. Table 6-2 shows the application of operational performance metrics to the eight flight phases.

TABLE 6-2. OPERATIONAL PERFORMANCE METRICS

	Unimpeded Time	Delay	Fuel Burn	Emissions	Surface Noise	Direct Distance	Excess Distance
Flight Phases:							
o Turnaround	x	x	x	x			
o Taxi-out	x	x	x	x	x		
o Takeoff	x	x	x	x	x		
o Departure	x	x	x	x	x	x	x
o Cruise	x	x	x	x		x	x
o Arrival	x	x	x	x	x	x	x
o Landing	x	x	x	x	x		
o Taxi-in	x	x	x	x	x		

6.1.3 Service Performance Metrics

Service performance metrics apply to the trip experience as perceived by travelers. The following is a list of service performance categories that can be considered for comparison of CTR, Conventional, and Mixed CTR-Conventional operations:

- Airport/Vertiport access time: from trip origin to airport/vertiport entry
- Departing passenger time: from airport/vertiport entry to flight departure (gate-out)
- Scheduled trip time: gate-to-gate trip time published in air carrier schedules
- Arriving passenger time: from flight arrival (gate-in) to airport/vertiport exit
- Airport/Vertiport egress time: from airport/vertiport exit to trip destination

Two metrics apply to these categories:

- Planned time: median time allowance to complete under normal conditions
- Buffer time: excess time allowance for 90-percent on-time arrival confidence level

Table 6-3 shows the application of service performance metrics to the service performance categories.

For CTR operations at existing airports, the assumption will likely be that airport access and egress times will not differ for conventional and CTR operations.

Additional analysis and discussion is required to develop comparisons of scheduled block times and actual block times for conventional and CTR operations in 2025, given that differing estimates of delay will likely be associated with RIO/NIO and conventional operations. Expected delay and delay variability are both anticipated to differ between CTR and conventional operations.

TABLE 6-3. SERVICE PERFORMANCE METRICS

	Planned Time	Buffer Time
Airport/vertiport access time	x	x
Departing passenger time	x	x
Scheduled trip time	x	x
Arriving passenger time	x	x
Airport/vertiport egress time	x	x

The scheduled trip time metric represents the time that an air carrier publishes in its schedule and shows in a computer reservation system. This is the time that an air carrier presents to the public as the time necessary to complete a scheduled flight. In practice, this time is determined by the expected time to perform a flight plus a buffer time. Figure 6-5 shows the composition of scheduled trip times.

An air carrier determines the appropriate level of buffer time to include in its schedules. Buffer times are set to the level needed to maintain an airline's on-time performance and to absorb delay. There is no Department of Transportation (DOT) or FAA on-time performance standard, nor are there DOT or FAA policy standards as to what constitutes acceptable delay. The Operational Data Reporting Requirements of the FAA specify reportable delays as delays to instrument flight rules (IFR) traffic of 15 minutes or more.

What follows from figure 6-5 is that a NextGen objective should be to improve schedule predictability by reducing trip time variance. Historically, U.S. domestic scheduled airline trip times have been characterized by growing levels of delay and variability that have required increasing buffer times. Between 1995 and 2005, U.S. major airlines as a group reported annual 85th percentile arrival delays between 17 and 28 minutes (after scheduled arrival, with 15 minutes or more after schedule being defined as late). Under the current ATM system, 85 percent of flights arriving within 15 minutes of schedule could be considered to be a good level of reported on-time performance. Performance under NextGen should improve on this; a reasonable NextGen 2025 performance target would be 90 percent of arrivals within 15 minutes of scheduled arrival time.

Scheduled Trip Time =
Taxi-out + Takeoff + Departure
+ Cruise
+ Arrival + Landing + Taxi-in

Planned Trip Time

+ Buffer

Adding buffer time assures a high percentage of reported on-time arrivals, particularly when trip time variance is high.

Reported on-time performance can be improved in two ways:

- Reducing trip time variance (i.e. better schedule predictability)
- Inflating the buffer time (i.e. increasing "schedule padding")

Figure 6-5. Composition of scheduled trip times.

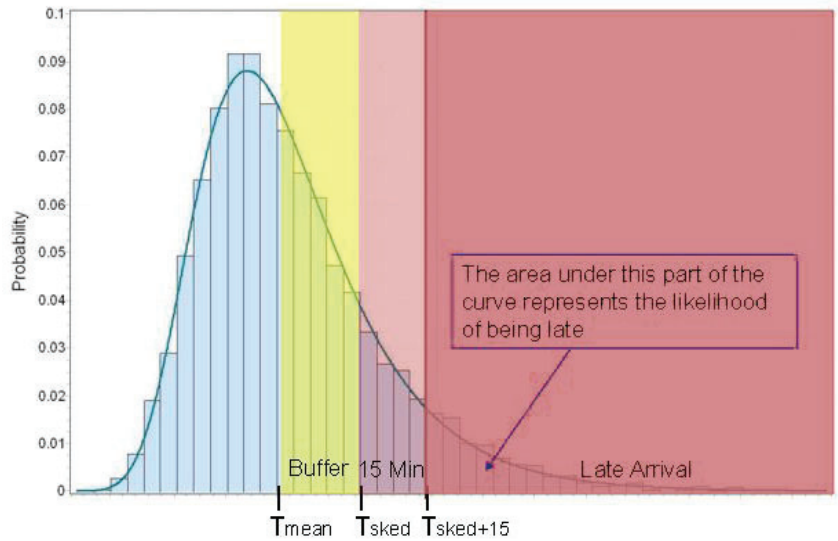

Figure 6-6. Arrival time distribution and 15-minute standard.

Note that scheduled trip times are assigned to flights and do not include turnaround times either prior to or subsequent to the flight. Scheduled trip times also do not include any propagated delay from previous flights. Thus, scheduled trip time as a metric does not capture delays due to turnaround and accumulated delays.

Figure 6-6 shows graphically how the buffer time and 15-minute tolerances are added to expected (mean) trip times to control the likelihood of late flight arrivals. The time shown in figure 6-6 as $T_{sked+15}$ is considered to be on time.

Service performance metrics are important in planning and measuring NextGen performance. The ability to effectively employ Four-Dimensional Trajectory (4DT) for scheduled operations will enable reduced trip time variability. Reduced trip time variability will be a goal for both CTR and conventional scheduled airline service, and this will translate directly into reduced trip times and higher quality of service.

A predictability objective for future CTR service should be to eliminate the need for a schedule buffer. This implies a scheduled time equal to the mean time, and managing variation under NextGen so that 90 percent of flights arrive within 15 minutes of the mean time.

6.1.4 Cost Metrics

Operating costs may be considered as a metric. For the purposes of this study, relative operating costs of CTR and conventional operations were not considered. Delay, fuel burn, and carbon-dioxide emissions were considered as costs, to the extent that replacing conventional operations with RIO/NIO operations reduces congestion and avoids excessive fuel consumption for delayed flights.

6.1.5 Safety Metrics

Safety metrics are considered to be an absolute (rather than relative) study metric. The performance objective is that there should be no degradation in safety.

6.1.6 Off-Normal Conditions

Differences between CTR and conventional operations in ability to accommodate representative off-normal scenarios need to be considered. A suggested approach is to consider several different off-normal scenarios and compare operational procedures that will likely apply to CTR and conventional operation.

6.1.7 Aggregation of Metrics

The proposed performance metrics are designed to support scenario-wide aggregation. This requires estimation of attributes for both conventional and CTR types of operations in the NEC scenario region in 2025, as well as the Atlanta and Las Vegas regions, which were later included in this study.

An initial appraisal is that an approach such as that proposed would complement ACES as a NAS-wide simulator. However, the proposed approach requires assumptions to be both clearly stated and reasonable for both conventional and CTR operations.

6.1.8 Relationship Between Performance Metrics and Performance Targets

Performance targets represent the expected expectations of air transportation service providers. The development of 2025 scenarios in this study and the estimation of performance metrics requires consideration of performance targets and performance gaps between operational capabilities and performance targets.

One factor in determining the attractiveness of scenarios involving CTR operations is CTR ability to close performance gaps. This requires agreement on whether or not conventional operations can meet desired 2025 capability and performance targets, and the extent to which, and at what cost, mixed conventional-CTR operations can close 2025 performance gaps.

An assumption will need to be made later about conventional fleet composition and equipage in 2025, together with an analysis of the sensitivity of the results to different equipage levels.

6.1.9 Definition of Selected Terms

6.1.9.1 Four-Dimensional Trajectory (4DT)

A 4DT represents the “centerline” of a path plus the positioning uncertainty, including waypoint. Positioning uncertainty includes lateral, longitudinal, and vertical positioning uncertainty. Some waypoints within a 4DT may be defined with controlled time of arrivals (CTAs), which constrains the uncertainty for planning purposes. The required level of specificity of the 4DT depends on the operating environment in which the flight is flown. Associated with a 4DT is the separation zone around an aircraft and the aircraft intent information, which provides near-term information on the expected flight path (ref. 38).

6.1.9.2 Flow Corridors

A flow corridor is a long “tube” of airspace that encloses groups of flights flying along the same path in one direction. It is airspace procedurally separated from surrounding traffic and special-use airspace, and it is reserved for aircraft in that group. There is a minimum distance that traffic within the corridor must maintain from the edge of the corridor (i.e., “the corridor walls have some thickness”) (ref. 38). A depiction of a flow corridor is shown in figure 6-7.

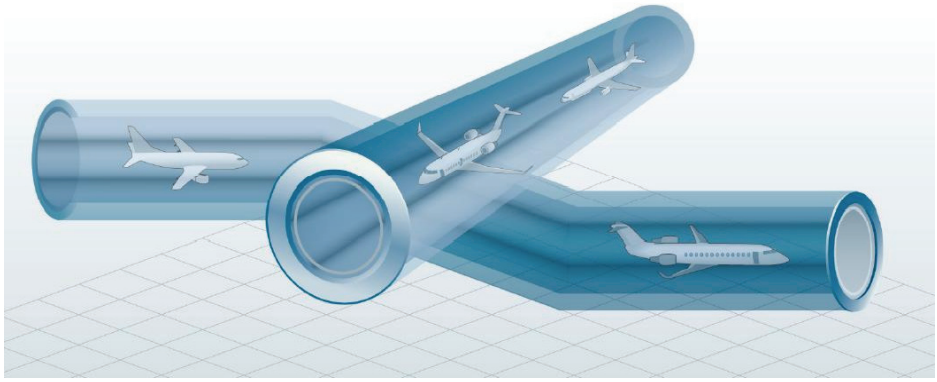

Figure 6-7. Flow corridors.

6.1.9.3 Unimpeded Time

Unimpeded time is representative of the time needed to complete an operation in a period of low traffic (free-flow conditions with no delays) (ref. 37).

6.1.9.4 Optimized Profile Descent (OPD)

An OPD is an arrival procedure designed to eliminate level segments flown below cruise altitude, thus minimizing fuel burn, emissions, and noise (ref. 42). Figure 6-8 graphically portrays an OPD.

6.1.9.5 Circuity (Excess Distance)

Circuity is a measure of flight efficiency and represents the excess distance traveled with respect to the shortest distance between the total trip origin and destination, under zero-wind conditions. The efficiency calculation for each flight phase can be calculated as the difference between the track distance (A) and the distance component in the direction of the Great Circle route between the origin and destination airports or vertiports (G).

Thus: $Circuity = A - G$ for each flight phase

Total trip circuity (Σ Circuity) is the sum of the circuity values for all flight phases, and the total trip track distances (Σ A) and Great Circle distances (Σ G) are the sums of individual flight phase track distances and Great Circle distances, respectively. Total trip circuity is illustrated in figure 6-9. Figure 6-10 shows an example of circuitous routings between Boston and Philadelphia in July 2007 (ref. 42).

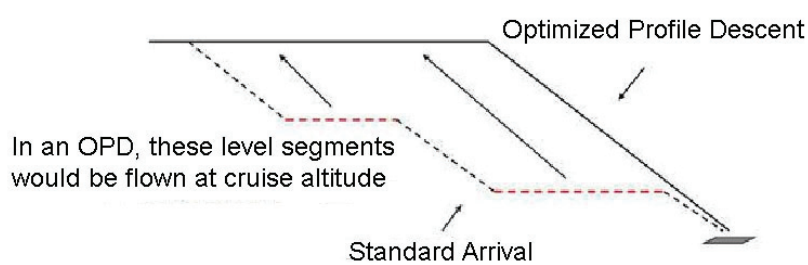

Figure 6-8. Optimized Profile Descent.

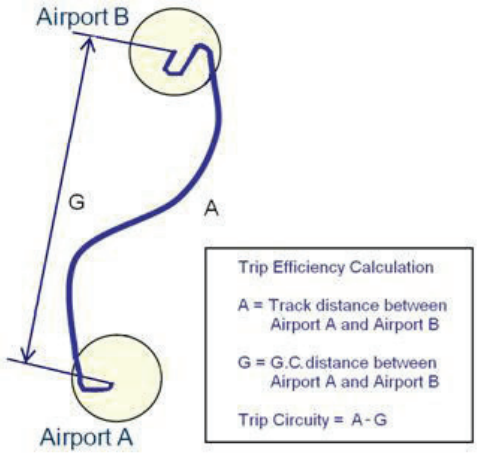

Figure 6-9. Trip circuity.

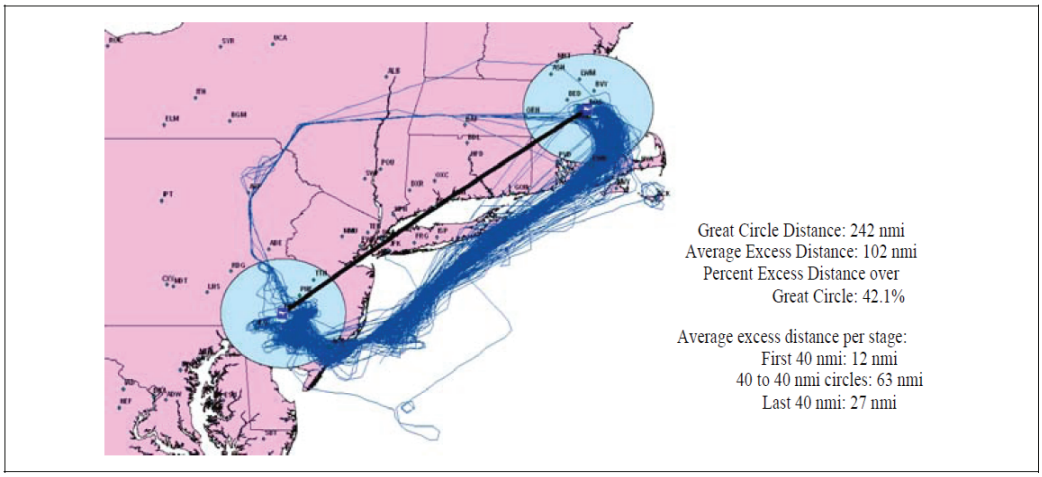

Figure 6-10. Circuity in practice.

6.2 NextGen Performance Analysis Tools

This section summarizes surveyed simulation tools with respect to CTR NAS-wide and terminal analysis. The tools investigated are listed below along with a brief description of their capabilities. Table 6-4 summarizes the capabilities of simulation platforms investigated in this study.

ACES: The Airspace Concept Evaluation System (ACES) is a distributed, agent-based simulation of the National Airspace System (NAS) consisting of NAS models and simulation control and assessment tools. The MPAST trajectory generated was implemented from arrival to departure fixes, based on EUROCONTROL BADA approaches.

AvTerminal: AvTerminal is a tool for evaluating aerospace concepts and algorithms in the terminal area. AvTerminal uses 3-degree of freedom (DOF) point-mass modeling to simulate 4DT in the terminal airspace and runway system. It also has Traffic Flow Management (TFM) and ATC modules that can apply separation rules and spacing restrictions, and analyze impacts of mixed operations. It has the ability to evaluate the effect of new arrival/departure procedures and separation requirement, and support post-processing analysis by providing track, aircraft state, airport capacity, and runway delay data.

SIMMOD: SIMMOD is a "free" discrete-event simulation engine that is owned by the FAA. Due to the complex nature of the data inputs and outputs from SIMMOD, several third-party vendors offer data preparation tools which can ease SIMMOD study creation tasks. Instead of a 4D or 3D trajectory model, SIMMOD uses a "node-link" model of trajectory, which is based on a deconstruction of airspace into a set of nodes and links (with different node restrictions). Aircraft move from node to node along the links and the track data is obtained through linear interpolation.

AvDemand: AvDemand is a demand generating tool that can simplify time-consuming steps in the demand generation process by providing tools to support automated creation and tailoring of NAS-wide flight schedule and flight plan data. AvDemand contains three major functions: demand generation, demand input/output, and demand analysis. However, AvDemand proliferates a baseline based on a growth assumption, and it cannot create a new schedule conformed to a demand or fleet requirement.

TABLE 6-4. CAPABILITIES OF SIMULATION PLATFORMS INVESTIGATED

Tool	Application	Type	4DT	Delegated Separation	Merging and Spacing	Self Separation	Source
ACES	ConOps Evaluation	NAS-wide Fast Time	Y	Y	Y	Y	NASA
AvTerminal	ConOps Evaluation	Terminal Area Fast Time	Y	NA	Y	Y	Sensis
SIMMOD	ConOps Evaluation	Terminal area Fast Time	N	Unknown	Unknown	Unknown	FAA
AvDemand	Demand Generation	NAS-wide	NA	NA	NA	NA	Sensis
AEDT	Noise and Emission	NAS-wide and Terminal Area	NA	NA	NA	NA	FAA
KTG	ConOps Evaluation	Terminal Area Fast Time	Y	Unknown	Unknown	Unknown	NASA

AEDT: Aviation Environmental Design Tool (AEDT) can be used to analyze the impacts of emission and noise. The complete track data are used as input by AEDT to compute the fuel burn and the full complement of emissions results, including CO2, CO, NOx, and particulate matter, as well as noise contours in the vicinity of the airports. Airspace delays (implicitly indicated by the track data) can also be captured for the fuel burn and emissions calculations.

KTG: KTG is a terminal area evaluation tool that is built based on a kinematic trajectory generator. It belongs to a third party and there is limited publicly available information regarding the capability of the tool.

6.3 Assumptions for NextGen Performance Analysis

The replacement of short-haul conventional airline flights by CTRs represents a key assumption in this study, and the use of ACES to evaluate the consequent reduction in delay is a key conclusion that follows.

Table 6-5 shows the number of city-pair markets considered for CTR substitute service. Service connecting two cities is considered to be a single market, regardless of flight direction, e.g. the Las Vegas-McCarran International Airport (LAS)–Los Angeles International Airport (LAX) market includes both LAS-LAX and LAX-LAS flights.

Table 6-6 shows the number of daily flight departures considered for CTR substitute service, by region and CTR type.

Table 6-7 shows calculated unimpeded block hours in each region by CTR type assigned to individual markets.

Table 6-8 represents an estimate of the number of CTR airframes required to support each regional network assuming that each airframe could be operated 8.6 unimpeded block hours per day.

TABLE 6-5. CTR MARKETS

Region	CTR 30	CTR 90	CTR 120	CTR Total
ATL500	3	21	27	51
LAS500			14	14
NEC500	38	71	54	163
Total	41	92	95	228

TABLE 6-6. CTR DEPARTURES

Region	CTR 30	CTR 90	CTR 120	CTR Total
ATL500	54	282	730	1,066
LAS500			692	692
NEC500	604	790	1,260	2,654
Total	658	1,072	2,682	4,412

TABLE 6-7. CTR UNIMPEDED BLOCK HOURS

Region	CTR 30	CTR 90	CTR 120	CTR Total
ATL500	52	337	947	1,336
LAS500			870	870
NEC500	638	964	1,581	3,183
Total	690	1,302	3,398	5,390

TABLE 6-8. CTR AIRFRAMES AT 8.6 BLOCK HOURS PER DAY

Region	CTR 30	CTR 90	CTR 120	CTR Total
ATL500	6	39	110	155
LAS500			101	101
NEC500	74	112	184	370
Total	80	151	395	626

The 8.6 unimpeded block hours per day number was derived by analyzing the number of flight segments that CTR aircraft would operate during the hours of 0630 to 2230 local time, and allowing for 45-minutes average turnaround time between flights and for 10 percent of aircraft not assigned to service (i.e., in maintenance or serving as spares or backup aircraft).

Figure 6-11 shows the relationship between expected CTR delay per operation and daily operations at a single vertiport, assuming the operation of a fleet of CTR90 and CTR120 aircraft. In order to keep average delay at a vertiport at a not-to-exceed value of 4 minutes, the maximum number of operations per vertiport was capped at 200 (representing an upper limit of 100 departures and 100 arrivals). This was achieved by adding additional vertiports at an airport location. Vertiports were assumed to operate independently at a maximum VTOL capacity of 12/12/20 arrivals/departures/operations per hour.

A total of 11 cities in the study were configured with multiple vertiports for the ACES simulations. Atlanta led the list with six vertiports, followed by Las Vegas with five, Philadelphia with four, and Washington Dulles with three. Seven other cities were configured with two vertiports: Boston, Baltimore–Washington, New York–Newark, New York–LaGuardia, New York–Kennedy, Washington–National, and Pittsburgh.

At airports with multiple vertiports, operations per vertiport averaged 135 per day, with ACES delay per operation averaging 3.24 minutes. At airports with a single vertiport, operations per vertiport averaged 37 per day, with average delay per operation at 3.16 minutes.

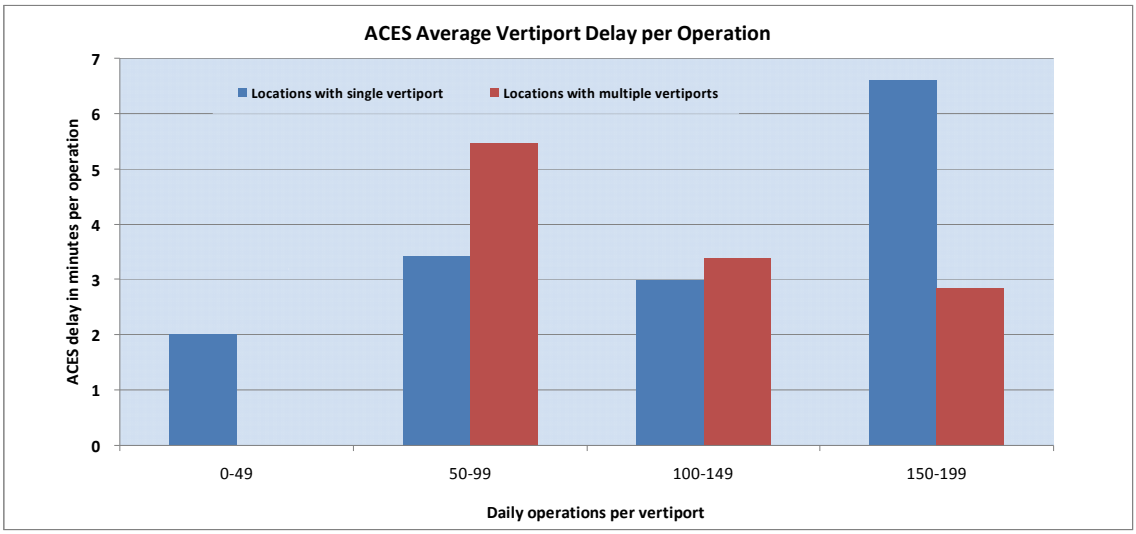

Figure 6-11. ACES vertiport relationship between average delay and daily operations.

Note that in the initial assignment flights to multiple vertiports, the focus was on balancing daily capacity at each vertiport. No attempt was made to coordinate arrival and departure slots throughout the day to achieve level operations at individual vertiports. However, flight-by-flight ACES delays were reviewed. This review led to several iterations in which CTR flight schedules were moved away from peak times, with the result that the average ACES delay was reduced to less than one minute without adding additional vertiports.

Table 6-9 summarizes results generated by ACES for a fleet of CTR90 and CTR120 mixed fleet (Test Point 2.4 in Test Matrix, as presented in section 6.4.5) at airports with more than 150 daily operations, which is a subset of results shown in figure 6-11.

Determination of the number of required vertiports was based on CTR90 and CTR120 mixed fleet (Test Point 2.4) operational requirements, and produced an ACES estimate of 3.2-minutes average delay per operation. If CTR30 operations are assumed to be added (Test Point 3.4 in the Test Matrix, as presented in section 6.4.5) without adding vertiports, then the average delay per operation increases from the 3.2 minutes per operation in Test Point 2.4 to an average of about 4 minutes per operation.

Two iterations of delay analysis were performed. Table 6-9 and figure 6-11 show the results of the first iteration (the iteration used to determine the required number of vertiports at any airport location). As an exercise to test the sensitivity of delay to scheduling assumptions, two additional iterations were conducted using "de-peaking" to limit the number of operations in any 10-minute period. This was accomplished through limiting the frequency of successive takeoffs or landings to one every 10 minutes (i.e., 12 operations per hour). This had the effect of reducing average delay for the CTR90 and CTR120 mixed fleet to 0.7 minutes per operation. Further investigation of scheduling operations and assignment of vertiports exclusively to either takeoffs or landings was beyond the scope of this study.

The ACES-simulated delays derived from the second iteration of delay analysis were selected for use in the analysis of CTR fleet operations in this study. These were considered achievable if fully coordinated operations (matching operations to vertiport capacity) were permitted.

TABLE 6-9. CTR OPERATIONS AND AVERAGE DELAY PER AIRPORT/VERTIPORT

	Daily Operations by Vertiport (no.)								
Airport	**1**	**2**	**3**	**4**	**5**	**6**	**Total Operations Per Day**	**Operations Per Vertiport**	**Average Delay Per Operation**
ATL	170	170	168	168	168	168	1,012	169	1.88
LAS	136	130	136	160	130		692	138	1.69
PHL	124	124	124	122			494	124	2.93
IAD	104	102	102				308	103	3.47
BOS	162	144					306	153	1.98
LGA	154	150					304	152	5.24
JFK	176	120					296	148	5.19
BWI	154	140					294	147	5.31
EWR	120	104					224	112	4.51
DCA	102	118					220	110	5.31
PIT	90	90					180	90	5.46
CLT	198						198	198	6.48
RDU	192						192	192	6.71

6.3.1 Major Assumptions—Conventional Aircraft

The analysis of conventional aircraft performance in this study pertains to the aircraft operating the 5,303 flights which are eligible for replacement by CTRs. The most important assumptions involve the handling of flight delays, fuel burn, trip time, and seat capacity. The primary source for these assumptions is the Sensis analysis of airline monthly and quarterly reports to DOT.

Delay was applied to all conventional flights in a uniform manner. ACES develops delay values for each individual flight. In this study, delay values of up to 15 minutes are assumed to be taken at the departure gate, with no fuel burn impact. The next 10 minutes of delay (up to a delay value of 25 minutes) are taken in taxi-out, and the next 5 minutes above that (up to a delay value of 30 minutes for an individual flight) are assumed to be taken in flight.

Table 6-10 shows the basic assumptions used for analysis of conventional aircraft fuel burn, airborne time, and seating capacity. Additional assumptions, including estimates of unimpeded airport taxi times, were obtained from analysis of airline monthly on-time reports to DOT.

Note that conventional fuel and performance data are based on estimates reported in current aircraft operations, and do not make any allowance for improved fuel burn performance in 2025. Historically, between 1995 and 2009, average annual U.S. airline fuel efficiency improvement has been about 1.25 percent for small narrow-body aircraft (ref. 43).

Detailed assumptions in the analysis of conventional aircraft operations are contained in appendix N.

TABLE 6-10. CONVENTIONAL AIRCRAFT PERFORMANCE ASSUMPTIONS

Aircraft Type	Aircraft	Taxi lb per min	Fuel lb per LTO Cycle	Fuel lb per airborne minute	airborne min per track NM	ACES Enroute TAS KT	Nominal Seats
Airbus A319	A319	29	1676	78	0.148	406	123
Airbus A320	A320	34	2039	83	0.148	410	149
Airbus A321	A321	30	1789	103	0.148	442	170
Boeing 717-200	B712	25	1426	66	0.148	409	117
Boeing 727-100	B721	51	2765	133	0.148	474	110
Boeing 727-200	B722	51	2765	133	0.148	416	148
Boeing 737-300	B733	29	1663	75	0.148	416	132
Boeing 737-400	B734	30	1789	80	0.148	397	142
Boeing 737-500	B735	26	1531	73	0.148	417	111
Boeing 737-700	B737	29	1874	70	0.148	402	134
Boeing 737-800	B738	30	1940	83	0.148	417	152
Boeing 737-900	B739	28	1888	87	0.148	446	170
Beechcraft Airliner	BE99	7	340	6	0.287	209	15
Canadair Regional Jet CRJ-100	CRJ1	12	700	49	0.148	380	52
Canadair Regional Jet CRJ-200	CRJ2	12	700	49	0.148	367	49
Canadair Regional Jet CRJ-700	CRJ7	13	840	53	0.148	392	68
Canadair Regional Jet CRJ-900	CRJ9	16	920	58	0.148	405	86
McDonnell Douglas DC-9-30	DC93	34	1841	79	0.148	403	100
McDonnell Douglas DC-9-40	DC94	38	2125	79	0.148	398	110
McDonnell Douglas DC-9-50	DC95	38	2125	86	0.148	400	124
de Havilland Dash 8-100	DH8A	8	400	8	0.185	245	37
de Havilland Dash 8-200	DH8B	8	400	8	0.185	250	37
de Havilland Dash 8-300	DH8C	8	488	10	0.185	260	50
de Havilland Dash 8-400	DH8D	8	488	10	0.185	323	70
Embraer ERJ-135	E135	13	700	39	0.148	393	37
Embraer ERJ-145	E145	13	686	38	0.148	386	50
Embraer 175	E170	16	964	45	0.148	394	72
Embraer ERJ-190	E190	17	1069	66	0.148	405	100
Embraer EMB-145XR	E45X	12	700	49	0.148	411	50
McDonnell Douglas MD-82	MD82	33	2100	80	0.148	416	125
McDonnell Douglas MD-83	MD83	33	2100	80	0.148	417	125
McDonnell Douglas MD-88	MD88	33	2100	80	0.148	419	130
McDonnell Douglas MD-90	MD90	35	2145	82	0.148	430	149
Saab 340	SF34	8	488	10	0.233	257	33
Fairchild SA-227DC Metro	SW4	6	360	6	0.260	240	19

During the 37th ICAO General Assembly held in Montreal in October 2010, ICAO member states adopted a resolution setting a goal of 2-percent annual average aviation fuel efficiency improvement up to the year 2050, together with capping CO_2 emissions as of 2020.

The aviation industry had proposed a 1.5-percent average annual improvement through 2020. After ICAO adopted the recent resolution, the aviation industry supported the 2-percent annual target, with the reservation that the amount over 1.5 percent would need to be achieved through system operational improvements. A goal proposed for discussion by the FAA is to "improve NAS energy efficiency (fuel burned per miles flown) by at least 2 percent annually" as a performance metric for 2018 (ref. 44).

Overall required improvement between 2010 and 2025 is of the order of 25 percent (assuming a 1.5-percent annual improvement rate), and 35 percent (assuming a 2-percent annual rate).

6.3.2 Major Assumptions—CTR Aircraft

Detailed assumptions in the analysis of CTR aircraft operations are contained in appendix O.

All CTR flights are assumed to operate on Great Circle direct routings and operate in VTOL mode. Appendix O details estimates of CTR time, distance, and fuel burn for each phase of flight. These estimates have been extensively validated against results from the Fuel Burn Post Processor (FBPP), as described in section 3.6. The CTR baseline assumptions can be modified to provide results for each route. CTR configurations can be analyzed for either VTOL or STOL conversion, for any configuration specified in section 3.6.4, tables 3-20 through 3-27.

In order to analyze CTR operations over the full range of routes and CTR sizes in the Test Matrix (discussed in section 6.4.5) and regional scenarios (sections 6.6 through 6.8), CTR fuel burn and flight time performance was fitted to FBPP (discussed in section 3.6) test points, using an iterative approach to minimizing least-squares residual differences. The goodness-of-fit results for the model used in section 6 for flight time and fuel burn for all individual CTR configurations, as measured by the coefficients of determination (R^2), ranged from 0.998556 to 0.999943.

The fuel burn difference between STOL and VTOL was found to be less than one percent (section 6.10).

6.4 Descriptions of the NAS Analysis Test Matrix

The current study followed the process used in the NASA NVI NRA study (ref. 40). The NVI NRA study used baseline demand sets that were created by the JPDO's Interagency Portfolio and System Analysis (IPSA) group in 2008. One demand set was for the year 2025. The airframes in the JPDO demand set were, for the most part, the same as today, except for the A380 and B-787.

The schedules that JPDO created, using the FAA Terminal Area Forecast (TAF), were based on relatively unconstrained consumer demand. In general, they did not account for the finite capacities of airports or airspace (there are some limits on a few major congested airports). When the schedules are flown using ACES, or any other NAS simulator, the delays that result are much longer than would be tolerable in practice. In the NVI NRA, in order to obtain schedules with reasonable delays, flights were removed from the unconstrained schedules using a process known as trimming. In the current study there was no trimming. Instead, conventional flights in under-500-statute-mile markets were replaced by CTR services.

The 2025 baseline conventional schedules were the most recent available. The current study used March 19, 2009, as the "seed day" for the purpose of ACES simulation. The JPDO grows seed-day schedules using

expected passenger growth rates that are published annually in the FAA TAF (ref. 45). These growth rates extend 15 to 20 years into the future and are based on factors such as expected growth rates for population and income. The JPDO also developed estimates of future airport capacities. In the current study, three different airport and NAS capacity projections were developed, representing three different scenarios. The scenarios represent a refinement of the FAA "*Capacity Needs in the National Airspace System 2007–2025*" report (FACT 2 report) (ref. 46).

The 2025 baseline ACES simulation results for both the NVI NRA and current studies showed extremely high levels of delay. These delays were driven to a large extent by projected demand growth exceeding projected capacity growth at two airports—Atlanta and Las Vegas. In a NAS-wide simulation like ACES, delays at major airports act as choke points. Reducing the demand on limited runway capacity at airports with extreme delays served to reduced NAS-wide delays.

The NAS analysis test matrix was designed to include test points covering the three different projected 2025 NAS capacity scenarios.

6.4.1 2025 Baseline Runway

The 2020 Baseline Runway is a "runways only" baseline, assuming no technology improvements. The runway assumes concrete will be poured according to the current NGIP (ref. 40), but there will be no other improvements. Some airports will show improved capacity due to the new runways, but other airports have the same capacity as today, and terminal/en route capacities are the same as today.

6.4.2 2025 Baseline Technology

The 2025 Baseline Technology is an estimate of the technology-based capacity improvements planned by the FAA. This capacity set also includes new runways that are in the current NGIP (ref. 40), which are more or less those to be built out by the 2018 to 2020 time frame. This capacity set also includes the impact of technology on all domains (airport capacity, terminal, en route). The bulk of these are also part of the FAA NGIP, but there are some additional ones that are considered reasonable for the 2020–2025 time frame (since this is essentially a 2025 capacity and the NGIP ends in 2020). Note, however, that technology (as opposed to runways) is frozen at 2020.

6.4.3 2025 Most Likely

2025 Most Likely is a projection of what 2025 will look like if plans and programs underway today continue in a manner similar to past plans and programs. It is probably best described as similar to the 2025 Baseline Technology above, except technology is not frozen at 2020. This assumes that additional technology-based improvements are implemented between 2020 and 2025. The capacities are a small step above the 2025 Baseline Technology case.

6.4.4 ACES Delay Metric

ACES assigns delay to individual flights in each simulation. There are many different options for summarizing and expressing delay. The most familiar delay metric is average delay per flight, for arriving flights and for departing flights. For individual airports, average flight arrival delay and flight departure delay is a useful and accepted comparative delay metric.

However, what works for individual airports does not necessarily work for the NAS as a whole. The issue is that flight delays are driven by flights serving major airports, and the NAS covers a wide range of airports, large and small. Table 6-11 shows various measures of average delay in minutes for the baseline 2025 ACES simulation (no CTR substitution, 70-percent direct routings).

Three regional CTR replacement scenarios were evaluated—Atlanta, Las Vegas, and the NEC. Given the most recent 2025 demand and schedule projections available to the study team, together with current estimates of 2025 NextGen capacity at U.S. major airports, these three regional scenarios offered an appropriate context in which to test the effects of removing conventional aircraft capacity from the system through the use of CTR air vehicles.

This study focuses on the delay metric associated with OPSNET 45 airports, an FAA-defined group of leading US airports (http://aspmhelp.faa.gov/index.php/OPSNET_45). From table 6-12, it is apparent that average delays at smaller airports (those not included in the OPSNET 45 group) are lower than those in the OPSNET 45 group. This is especially true when combined delays (arrivals and departures averaging 21.6 minutes) at OPSNET 45 airports are compared to delays at other airports (averaging 1.0 minute for flights that neither depart from, nor arrive at, OPSNET 45 airports).

TABLE 6-11. DELAY METRIC SELECTION

Delay Metric	Average Delay (Minutes)
NAS Wide	16.5
OPSNET 45 Airports Arrive	27.3
OPSNET 45 Airports Depart	20.3
OPSNET 45 Airports (Arrive and Depart)	21.6
NEC9 Airports Arrive	14.7
NEC9 Airports Depart	21.9
Intra NEC9 Airports	21.8
Atlanta Arrive	182.0
Atlanta Depart	36.7
LAS Arrive	73.7
LAS Depart	33.7

TABLE 6-12. DELAY METRIC FOR OPSNET 45 AIRPORTS

Average Delay (Minutes)	OPSNET 45 Airports	Other Non-OPSNET 45 Airports	NAS All Airports
Arrival	27.3	4.9	16.6
Departure	20.3	12.4	16.6
Combined	21.6	1.0	16.6

6.4.5 Test Matrix

The test matrix design is shown in table 6-13. The average delays shown for the designated test points represent metrics for conventional fleet operations using combined OPSNET 45 delay minutes obtained from ACES runs. The delays for NIO/RIO CTR operations are initially assumed to be maintained at a design level not-to-exceed 4-minutes average through the provision of sufficient vertiports at each location to support that design-delay level.

The following approach was used in the design of the Test Matrix:

1) Test Points 0.0 and 0.1 are used for baselining ACES simulations of NAS performance of the conventional fleet in 2025. Test Point 0.0 (the "mixed-equipage" option) was selected as the baseline assuming 70-percent fleet equipage for NextGen, defined for ACES purposes as capable of flying direct routes, with 30 percent assumed to follow ACES-generated fix-based routes. Test Point 0.1 (the "fix-based" option) was a baseline variation that assumed all conventional flights followed fix-based routes. In the baselines, flights followed fix-based routes or direct-to routes, with the same number of flights in both cases.
2) Test Points 1.1–1.4 evaluate the use of CTR120 aircraft to replace conventional aircraft on routes that could support larger aircraft. Replacement of conventional schedule capacity was done on a seat-for-seat basis, i.e., for each seat of conventional capacity removed, one CTR seat was substituted. The baseline for Test Points 1.1–1.4 was the Test Point 0.0 (mixed-equipage).
3) Test Points 2.1–2.4 assume the same CTR120 replacement as Test Points 1.1–1.4, combined with CTR90 aircraft replacing conventional aircraft in additional city-pair markets with lower levels of seats offered.
4) Test Points 3.1–3.4 expand the replacement to markets with sufficient seats to justify CTR30 aircraft, while maintaining the same levels of CTR90 and CTR120 aircraft schedules.
5) Test Point 4.0 is a variation on Test Point 1.4, assuming CTR120 replacement, compared to Test Point 0.1 fix-based.
6) Test Point 5.0 represents a CTR10 scenario.
7) Test Point 6.0 represents VTOL/STOL operational comparisons.
8) Test Point 7.0 is designed to show the sensitivity to a higher CTR load-factor. This is done by assuming the replacement of CTR120 aircraft in Test Point 2.4 with CTR90 aircraft, resulting in an all-CTR90 fleet.
9) Test Point 8.0 is designed to show the sensitivity to different taxi-time assumptions.

In replacing conventional scheduled flights with CTRs, seat equivalence was maintained. An added assumption was that average load-factors in replacement-eligible markets was uniformly 60 percent. The result is that the number of passengers assigned to CTR replacement operations is the same as on replaced conventional flights. The passenger counts are illustrative, and are simply the result of applying a 60-percent load factor to an equivalent number of seats.

ACES test scenario setup is summarized in appendix K.

TABLE 6-13. TEST MATRIX

Test Point	2025 Capacity Scenario Description		Baseline Technology Average Delay (minutes)	Baseline Runways Average Delay (minutes)	Projected Average Delay (minutes)
0.0	Conventional Fleet, Mixed Equipage[1]		21.8	22.0	21.6
0.1	Conventional Fleet, Fix-Based Routing		28.3	28.5	21.5
1.1	CTR120 Fleet	Northeast Region			20.4
1.2		Atlanta Region			12.7
1.3		Las Vegas Region			18.6
1.4		Combined Scenario (NE, ATL, LAS)	10.2		8.1
2.1	CTR90 and CTR120	Northeast Region			20.3
2.2	Mixed Fleet	Atlanta Region			11.9
2.3		Las Vegas Region			18.6
2.4		Combined Scenario (NE, ATL, LAS)	7.8		7.2
3.1	CTR30, CTR90, and CTR120	Northeast Region			20.5
3.2	Mixed Fleet	Atlanta Region			11.9
3.3		Las Vegas Region			18.6
3.4		Combined Scenario (NE, ATL, LAS)	7.8		7.2
4.0	CTR120 Fleet	Combined Scenario, Conventional Fleet with Fix-Based Routing			8.2 est
5.0	CTR10 Scenario				√
6.0	VTOL/STOL Operational Comparisons[2]				√
7.0	Sensitivity to CTR Load Factor Assumptions[3]				√
8.0	Sensitivity to CTR Taxi Time Assumptions				√

Notes:
1. Mixed-equipage indicates that 70% of conventional fleet in 2025 are assumed to operate GC direct routes.
2. Nominal CTR case assumes STOL operations.
3. Nominal CTR case assumes 60% load factor, alternate case 80% percent (replace CTR120 with CTR90).

6.5 Results From the Baseline (Test Points 0.0, 0.1)

Test Point 0.0 from table 6-13 is the reference test point in this study, as it represents the baseline case for conventional aircraft operations without CTR replacement in 2025. The effect of 2025 capacity improvements in three different assumptions, i.e., Baseline Technology, Baseline Runway, and Projected as discussed in sections 6.4.1–6.4.3, did not show significant differences in Average Delay as shown in table 6-13.

Table 6-14 shows results for baseline Test Point 0.0, Conventional Fleet with mixed equipage (i.e., 70 percent of the conventional fleet is capable to operate Great Circle direct routes as discussed in section 6.4.5). Carbon Dioxide emission is converted from weight of the fuel burn using the standard jet fuel density, 6.7 pounds/gallon, and 9.57 kilograms Carbon Dioxide per gallon, per U.S. Energy Administration, "Voluntary Reporting of Greenhouse Gases Program, Fuel Carbon Dioxide Emission Coefficients," http://www.eia.doe.gov/oiaf/1605/coefficients.html.

A variation of the baseline was considered for Test Point 0.1. This test point assumes conventional operations, without CTR replacement, with operations over fix-based routings. Table 6-15 shows results for Test Point 0.1 Conventional Fleet, Fix-Based Routes.

The main differences between Test Points 0.0 and 0.1 are in circuity, which drives block fuel, and in the differences in delay results in the two ACES simulation runs. Note that ACES delay results show relatively small differences in delays between the two test points. In the case of the ATL500 region, and for the combined regions, the total fix-based delay result is lower than the comparable mixed-equipage case. This difference, driven by extreme delays created by a 2025 ACES demand capacity imbalance in Atlanta, should not be considered to be significant. While mixed-equipage routings produce shorter routings and associated fuel savings, the mixed-equipage assumption does not affect system capacity in a significant way.

TABLE 6-14. TEST POINT 0.0, CONVENTIONAL FLEET WITH MIXED EQUIPAGE

Test Point 0.0	**Region**			**Combined**
Mixed Equipage	**ATL500**	**LAS500**	**NEC500**	
Daily Departures	1,374	622	3,307	5,303
Taxi Out, minutes	14,485	6,150	36,813	57,448
Taxi In, minutes	6,999	2,447	15,558	25,004
Track Distance, nmi	382,337	177,285	890,394	1,450,016
GC Distance, nmi	363,496	169,340	859,822	1,392,659
Circuity, nmi	18,841	7,944	30,572	57,357
Unimpeded Block Time, minutes	81,801	36,481	197,733	316,015
OPSNET 45 Delay Before Substitution, minutes	198,378	46,972	48,793	294,143
Average Delay Per Flight	144	76	15	55
2009 Block Fuel, lbs (current level)	6,087,000	3,709,600	11,389,900	21,186,500
2025 Block Fuel, lbs (25% improvement)	4,565,300	2,782,200	8,542,500	15,890,000
Carbon Dioxide, metric tons	8,690	5,280	16,236	30,206
Carbon Dioxide, metric tons (25% improvement)	6,490	3,960	12,166	22,616
Passengers	68,890	49,613	143,979	262,482
Daily Seats	114,817	82,689	239,965	437,471
Load Factor	60%	60%	60%	60%

TABLE 6-15. TEST POINT 0.1, CONVENTIONAL FLEET WITH FIX-BASED ROUTES

Test Point 0.1	**Region**			**Combined**
Fix-Based Routing	**ATL500**	**LAS500**	**NEC500**	
Daily Departures	1,374	622	3,307	5,303
Taxi Out, minutes	14,485	6,150	36,813	57,448
Taxi In, minutes	6,999	2,447	15,558	25,004
Track Distance, nmi	426,021	197,918	962,613	1,586,552
GC Distance, nmi	363,496	169,340	859,822	1,392,659
Circuity, nmi	62,525	28,578	102,791	193,893
Unimpeded Block Time, minutes	88,202	39,508	208,713	336,423
OPSNET 45 Delay Before Substitution, minutes	187,283	47,088	50,229	284,600
Average Delay Per Flight	136	76	15	54
2009 Block Fuel, lbs (current level)	6,488,300	3,948,400	11,948,600	22,385,300
2025 Block Fuel, lbs (25% improvement)	4,866,100	2,961,300	8,961,500	16,788,900
Carbon Dioxide, metric tons	9,240	5,632	17,028	31,900
Carbon Dioxide, metric tons (25% improvement)	6,930	4,224	12,760	23,914
Passengers	68,890	49,613	143,979	262,482
Daily Seats	114,817	82,689	239,965	437,471
Load Factor	60%	60%	60%	60%

6.6 Results From the CTR120 Fleet (Test Points 1.1–1.4)

Figure 6-12 shows the three CTR120 fleet regional networks, i.e., Atlanta, Las Vegas, and the NEC, as discussed in section 6.4.4. Conventional flights in under-500-statute-mile markets were replaced by CTR services for flights anchored in Atlanta, Las Vegas, and nine NEC airports respectively.

The following tables summarize NAS delay performance analysis of the CTR120 fleet, conventional fleet replaced by the CTR120 fleet, and performance comparisons.

Table 6-16 shows the results for CTR operations with a single type CTR120 operation.

Table 6-17 shows the results for the mixed-equipage (70 percent in NextGen equipage or capable to fly Great Circle or direct-to routes) conventional flights replaced as a result of CTR120 fleet operations.

Table 6-18 shows the relative differences comparing the mixed-equipage conventional fleet operations (table 6-17) with the CTR120 operations (table 6-16). In this table, positive numbers represent lower CTR values, and negative numbers (in parentheses) represent higher CTR values.

Table 6-19 shows fix-based conventional flights (100-percent current-day avionics equipage, or not capable of flying Great Circle or direct-to routes) replaced by CTR120 aircraft.

Table 6-20 shows the relative differences comparing the fix-based conventional fleet operations (table 6-19) with the CTR120 operations (table 6-16). In this table, positive numbers represent lower CTR values, and negative numbers (in parentheses) represent higher CTR values.

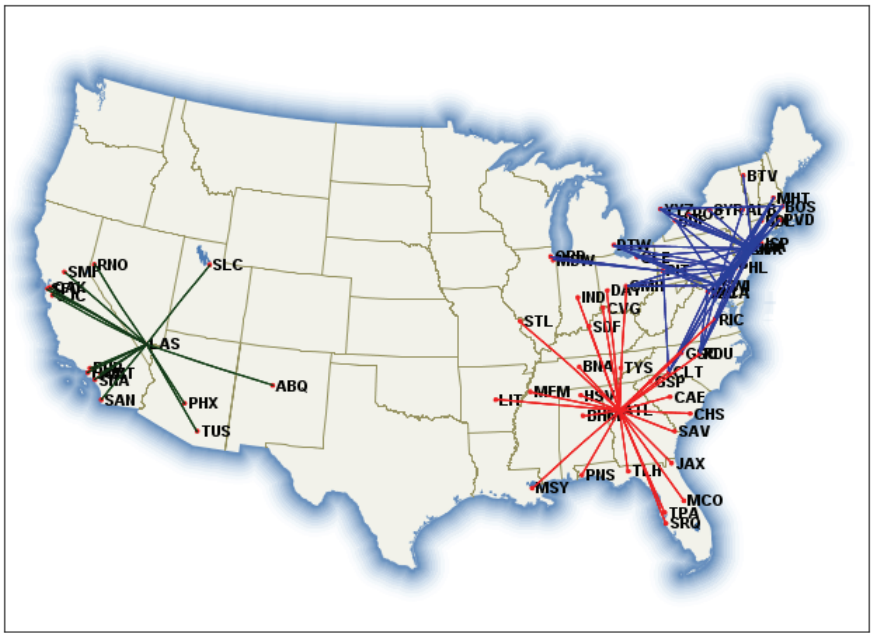

Figure 6-12. CTR120 fleet regional networks.

TABLE 6-16. CTR 120-PASSENGER FLEET OPERATIONS

Test Point 1.4	**Region**			**Combined**
CTR120	**ATL500**	**LAS500**	**NEC500**	
Daily Departures	730	692	1,260	2,682
Taxi Out, minutes	5,840	5,536	10,080	21,456
Taxi In, minutes	4,380	4,152	7,560	16,092
Track Distance, nmi	208,953	188,314	342,160	739,427
GC Distance, nmi	208,953	188,314	342,160	739,427
Circuity, nmi	0	0	0	0
Unimpeded Block Time, minutes	55,888	51,298	93,258	200,445
OPSNET 45 Delay Before Substitution, minutes	400	73	1,131	1,604
Average Delay Per Flight	0.5	0.1	0.9	0.6
2025 Block Fuel, lbs	3,967,729	3,629,694	6,585,289	14,182,713
2025 Carbon Dioxide, metric tons	5,654	5,172	9,385	20,211
Passengers	52,560	49,824	90,720	193,104
Daily Seats	87,600	83,040	151,200	321,840
Load Factor	60%	60%	60%	60%

TABLE 6-17. CONVENTIONAL FLEET FLIGHTS WITH MIXED EQUIPAGE REPLACED BY CTR120 FLEET

Test Point 0.0 Mixed-Equipage Conventional Fleet **Conventional Flights Replaced by CTR-120 Option**	**Region**			**Combined**
	ATL500	**LAS500**	**NEC500**	
Daily Departures	898	622	1,659	3,179
Taxi Out, minutes	9,805	6,150	18,729	34,684
Taxi In, minutes	4,633	2,447	7,919	14,999
Track Distance, nmi	258,909	177,285	470,150	906,343
GC Distance, nmi	247,008	169,340	454,298	870,646
Circuity, nmi	11,901	7,944	15,851	35,697
Unimpeded Block Time, minutes	55,247	36,481	100,648	192,376
OPSNET 45 Delay Before Substitution, minutes	124,621	46,972	32,130	203,723
Average Delay Per Flight	139	76	19	64
2009 Block Fuel, lbs (current level)	4,471,600	3,709,600	7,102,300	15,283,500
2025 Block Fuel, lbs (25% improvement)	3,353,700	2,782,200	5,326,800	11,462,700
Carbon Dioxide, metric tons	6,380	5,280	10,120	21,780
Carbon Dioxide, metric tons (25% improvement)	4,774	3,960	7,590	16,324
Passengers	52,636	49,613	90,688	192,937
Daily Seats	87,726	82,689	151,146	321,561
Load Factor	60%	60%	60%	60%

TABLE 6-18. SAVINGS OF CTR120 FLEET (TABLE 6-16) OVER CONVENTIONAL MIXED EQUIPAGE FLEET (TABLE 6-17)

Test Point 0.0 Mixed-Equipage Conventional vs. Test Point 1.4 CTR120 **Conventional (Mixed-Equipage) and CTR Differences (table 6-17 subtracted from table 6-16)**	**Region**			**Combined**
	ATL500	**LAS500**	**NEC500**	
Daily Departures	168	(70)	399	497
Taxi Out, minutes	3,965	614	8,649	13,228
Taxi In, minutes	253	(1,705)	359	(1,093)
Track Distance, nmi	49,956	(11,029)	127,990	166,916
GC Distance, nmi	38,055	(18,974)	112,138	131,220
Circuity, nmi	11,901	7,944	15,851	35,697
Unimpeded Block Time, minutes	(641)	(14,817)	7,390	(8,069)
OPSNET 45 Delay Before Substitution, minutes	124,221	46,899	30,999	202,119
Average Delay Per Flight	138	75	18	63
2009 Block Fuel, lbs (current level)	503,871	79,906	517,011	1,100,787
2025 Block Fuel, lbs (25% improvement)	(614,029)	(847,494)	(1,258,489)	(2,720,013)
2009 Carbon Dioxide, metric tons	726	108	735	1,569
Carbon Dioxide, metric tons (25% improvement)	(880)	(1,212)	(1,795)	(3,887)
Passengers	76	(211)	(32)	(167)
Daily Seats	126	(351)	(54)	(279)
Load Factor	0%	0%	0%	0%

In this table, positive numbers represent lower CTR values, and negative numbers (in parentheses) represent higher CTR values.

TABLE 6-19. CONVENTIONAL FIX-BASED FLIGHTS REPLACED BY CTR 120-PASSENGER FLEET OPERATIONS

Test Point 0.1 Fix-Based Conventional Fleet **Fix-Based Conventional Flights Replaced by CTR120**	**Region**			**Combined**
	ATL500	**LAS500**	**NEC500**	
Daily Departures	898	622	1,659	3,179
Taxi Out, minutes	9,805	6,150	18,729	34,684
Taxi In, minutes	4,633	2,447	7,919	14,999
Track Distance, nmi	289,832	197,918	508,143	995,893
GC Distance, nmi	247,008	169,340	454,298	870,646
Circuity, nmi	42,825	28,578	53,844	125,247
Unimpeded Block Time, minutes	59,761	39,508	106,259	205,528
OPSNET 45 Delay Before Substitution, minutes	118,542	47,088	32,509	198,139
Average Delay Per Flight	132	76	20	62
2009 Block Fuel, lbs (current level)	4,773,700	3,948,400	7,447,500	16,169,600
2025 Block Fuel, lbs (25% improvement)	3,580,300	2,961,300	5,585,700	12,127,300
2009 Carbon Dioxide, metric tons	6,798	5,632	10,604	23,034
Carbon Dioxide, metric tons (25% improvement)	5,104	4,224	7,964	17,292
Passengers	52,636	49,613	90,688	192,937
Daily Seats	87,726	82,689	151,146	321,561
Load Factor	60%	60%	60%	60%

TABLE 6-20. SAVINGS OF CTR120 FLEET (TABLE 6-16) OVER CONVENTIONAL FIX-BASED FLEET (TABLE 6-19)

Test Point 0.1 Fix-Based Conventional vs. Test Point 1.4 CTR120 **Conventional (Fix-Based) and CTR Differences (table 6-16 subtracted from table 6-19)**	**Region**			**Combined**
	ATL500	**LAS500**	**NEC500**	
Daily Departures	168	(70)	399	497
Taxi Out, minutes	3,965	614	8,649	13,228
Taxi In, minutes	253	(1,705)	359	(1,093)
Track Distance, nmi	80,880	9,604	165,983	256,466
GC Distance, nmi	38,055	(18,974)	112,138	131,220
Circuity, nmi	42,825	28,578	53,844	125,247
Unimpeded Block Time, minutes	3,873	(11,790)	13,001	5,083
OPSNET 45 Delay Before Substitution, minutes	118,142	47,015	31,378	196,535
Average Delay Per Flight	131	76	19	62
2009 Block Fuel, lbs (current level)	805,971	318,706	862,211	1,986,887
2025 Block Fuel, lbs (25% improvement)	(387,429)	(668,394)	(999,589)	(2,055,413)
2009 Carbon Dioxide, metric tons	1,144	460	1,219	2,823
Carbon Dioxide, metric tons (25% improvement)	(550)	(948)	(1,421)	(2,919)
Passengers	76	(211)	(32)	(167)
Daily Seats	126	(351)	(54)	(279)
Load Factor	0%	0%	0%	0%

In this table, positive numbers represent lower CTR values, and negative numbers (in parentheses) represent higher CTR values.

In brief summary, the CTR120 shows reduced average delay compared to the conventional fleet with mixed-equipage or with fix-based avionics. At the same time, the CTR120 fleet also uses less fuel than the conventional fleet with mixed-equipage or with fix-based avionics based on the 2009 fuel burn performance of the conventional fleet. However, when compared with the 2025 projected fuel burn performance of the conventional fleet, the CTR120 fleet does not performed as well since the CTR120 is designed with 2017 engine technology based on a service entry of 2025 according to the OEM technology insertion practice described in section 2.2.2. A further discussion on fuel burn performance is presented in appendix I.

The main differences between tables 6-18 and 6-20 are in the values for circuitry, fuel burn, and delay due to equipage of the conventional fleet. The improved efficiency of the mixed-equipage case (Test Point 0.0) than the fix-based case (Test Point 0.1) is apparent when comparing the two tables.

6.7 Results From CTR90 and CTR120 Mixed CTR Fleet (Test Points 2.1–2.4)

Figure 6-13 shows the mixed CTR 90 and CTR120 fleet network as described in section 6.6, i.e., Atlanta, Las Vegas, and the NEC, and conventional flights in under-500-statute-mile markets that were replaced by CTR services for flights anchored in Atlanta, Las Vegas, and nine NEC airports respectively.

Table 6-21 shows the results for a mixed CTR90 and CTR120 fleet. Table 6-22 shows the results for the mixed-equipage conventional flights (70 percent NextGen equipage operating on direct-to routings) replaced as a result of CTR90 and CTR120 operations. Table 6-23 shows the relative differences comparing the CTR90 and CTR120 fleet operations (table 6-21) with the mixed-equipage conventional fleet operations that they replaced (table 6-22). In this table, positive numbers represent lower CTR values, and negative numbers (in parentheses) represent higher CTR values.

Results show the mixed CTR90 and CTR120 fleet could reduce average delay per flight from the conventional flights they replaced. However, the fuel burn by the CTR fleet would not match the projected 2025 fuel burn performance of the conventional fleet, which is discussed in section 7.3

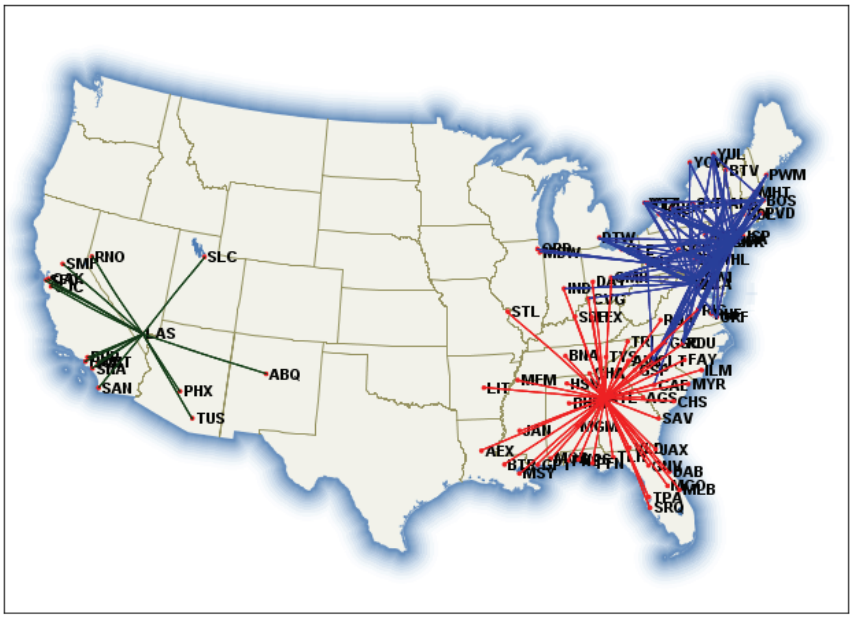

Figure 6-13. CTR90 and CTR120 mixed fleet regional networks.

TABLE 6-21. CTR90 AND CTR120 MIXED FLEET OPERATIONS

Test Point 2.4 **CTR90 and CTR120 Mixed Fleet**	**Region**			**Combined**
	ATL500	**LAS500**	**NEC500**	
Daily Departures	1,012	692	2,050	3,754
Taxi Out, minutes	8,096	5,536	16,400	30,032
Taxi In, minutes	6,072	4,152	12,300	22,524
Track Distance, nmi	281,847	188,314	552,823	1,022,984
GC Distance, nmi	281,847	188,314	552,823	1,022,984
Circuity, nmi	0	0	0	0
Unimpeded Block Time, minutes	75,960	51,298	150,625	277,883
OPSNET 45 Delay Before Substitution, minutes	492	73	1,867	2,433
Average Delay Per Flight	0.5	0.1	0.9	0.6
2025 Block Fuel, lbs	5,262,500	3,629,694	10,305,336	19,197,530
2025 Carbon Dioxide, metric tons	7,500	5,172	14,687	27,359
Passengers	67,788	49,824	133,380	250,992
Daily Seats	112,980	83,040	222,300	418,320
Load Factor	60%	60%	60%	60%

TABLE 6-22. CONVENTIONAL MIXED-EQUIPAGE FLIGHTS REPLACED BY CTR90 AND CTR120 OPERATIONS

Test Point 2.4 Mixed Equipage **Conventional Flights Replaced by CTR90 and CTR120**	**Region**			**Combined**
	ATL500	**LAS500**	**NEC500**	
Daily Departures	1,341	622	2,904	4,867
Taxi Out, minutes	14,179	6,150	32,615	52,944
Taxi In, minutes	6,846	2,447	13,795	23,088
Track Distance, nmi	375,815	177,285	803,928	1,357,027
GC Distance, nmi	357,599	169,340	777,568	1,304,508
Circuity, nmi	18,215	7,944	26,359	52,519
Unimpeded Block Time, minutes	80,303	36,481	175,797	292,581
OPSNET 45 Delay Before Substitution, minutes	80,303	36,481	175,797	292,581
Average Delay Per Flight	60	59	61	60
2009 Block Fuel, lbs (current level)	5,999,264	3,709,600	10,602,532	20,311,396
2025 Block Fuel, lbs (25% improvement)	4,499,448	2,782,200	7,951,899	15,233,547
2009 Carbon Dioxide, metric tons	8,558	5,280	15,114	28,952
Carbon Dioxide, metric tons (25% improvement)	6,402	3,960	11,330	21,692
Passengers	67,920	49,613	133,115	250,648
Daily Seats	113,200	82,689	221,858	417,747
Load Factor	60%	60%	60%	60%

TABLE 6-23. SAVINGS OF CTR90/120 MIXED FLEET (TABLE 6-21) OVER CONVENTIONAL MIXED-EQUIPAGE FLIGHTS (TABLE 6-22)

Mixed-Equipage Conventional vs. Test Point 2.4 CTR90 and CTR120 **Mixed-Equipage Conventional and CTR Differences (table 6-21 subtracted from table 6-22)**	**Region**			**Combined**
	ATL500	**LAS500**	**NEC500**	
Daily Departures	329	(70)	854	1,113
Taxi Out, minutes	6,083	614	16,215	22,912
Taxi In, minutes	774	(1,705)	1,495	564
Track Distance, nmi	93,968	(11,029)	251,104	334,043
GC Distance, nmi	75,752	(18,974)	224,745	281,524
Circuity, nmi	18,215	7,944	26,359	52,519
Unimpeded Block Time, minutes	4,343	(14,817)	25,172	14,698
OPSNET 45 Delay Before Substitution, minutes	79,811	36,408	173,930	290,148
Average Delay Per Flight	59	59	60	59
2009 Block Fuel, lbs (current level)	736,764	79,906	297,196	1,113,866
2025 Block Fuel, lbs (25% improvement)	(763,052)	(847,494)	(2,353,437)	(3,963,983)
2009 Carbon Dioxide, metric tons	1,058	108	427	1,593
Carbon Dioxide, metric tons (25% improvement)	(1,098)	(1,212)	(3,357)	(5,667)
Passengers	132	(211)	(265)	(344)
Daily Seats	220	(351)	(442)	(573)
Load Factor	0%	0%	0%	0%

In this table, positive numbers represent lower CTR values, and negative numbers (in parentheses) represent higher CTR values.

6.8 CTR30, CTR90, and CTR120 Mixed Fleet Results (Test Points 3.1–3.4)

Figure 6-14 shows the mixed CTR30, CTR90, and CTR120 network as described in section 6.6, i.e., Atlanta, Las Vegas, and the NEC, and conventional flights in under-500-statute-mile markets that were replaced by CTR services for flights anchored in Atlanta, Las Vegas, and nine NEC airports respectively.

Table 6-24 shows the results for a mixed CTR30, CTR90, and CTR120 fleet. Table 6-25 shows the results for the mixed-equipage conventional flights (70 percent NextGen equipage operating on direct-to routings) replaced as a result of CTR30, CTR90, and CTR120 operations. Note that this table is the same as table 6-14, but is repeated here to support comparison with tables 6-24 and 6-26. Table 6-26 shows the relative differences comparing the CTR30, CTR90, and CTR120 fleet operations (table 6-24) with the mixed-equipage conventional fleet operations that they replaced (table 6-25). In this table, positive numbers represent lower CTR values, and negative numbers (in parentheses) represent higher CTR values.

Results show the mixed CTR30, CTR90, and CTR120 fleet could reduce average delay per flight from the conventional flights they replaced. However, the fuel burn by the CTR fleet would not match the targeted 2025 fuel performance of the conventional fleet, which is discussed in section 7.3.

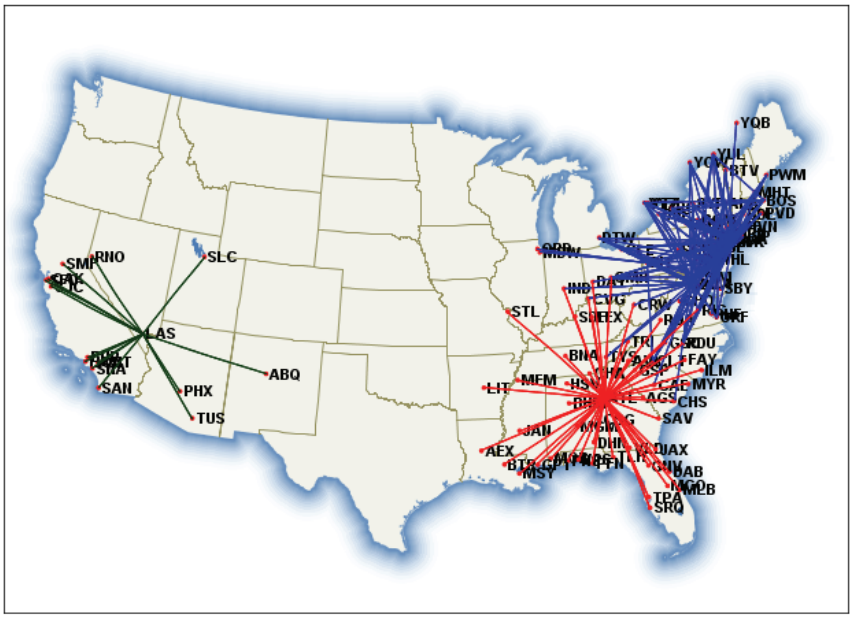

Figure 6-14. CTR30, CTR90, and CTR120 mixed fleet regional networks.

TABLE 6-24. CTR30, CTR90, AND CTR120 FLEET OPERATIONS

Test Point 3.4 **CTR30, CTR90, and CTR120 Mixed Fleet**	**Region**			**Combined**
	ATL500	**LAS500**	**NEC500**	
Daily Departures	1,066	692	2,654	4,412
Taxi Out, minutes	8,528	5,536	21,232	35,296
Taxi In, minutes	6,396	4,152	15,924	26,472
Track Distance, nmi	291,497	188,314	679,323	1,159,133
GC Distance, nmi	291,497	188,314	679,323	1,159,133
Circuity, nmi	0	0	0	0
Unimpeded Block Time, minutes	79,064	51,298	188,660	319,022
OPSNET 45 Delay Before Substitution, minutes	734	73	6,331	7,137
Average Delay Per Flight	0.7	0.1	2.4	1.6
2025 Block Fuel, lbs	5,361,262	3,629,694	11,547,208	20,538,165
2025 Carbon Dioxide, metric tons	7,641	5,172	16,456	29,269
Passengers	68,760	49,824	144,252	262,836
Daily Seats	114,600	83,040	240,420	438,060
Load Factor	60%	60%	60%	60%

TABLE 6-25. CONVENTIONAL MIXED-EQUIPAGE FLIGHTS REPLACED BY CTR30, CTR90, AND CTR120 OPERATIONS

Test Point 0.0 **Mixed-Equipage Conventional Fleet** **Conventional Flights Replaced by CTR30/90/120**	**Region**			**Combined**
	ATL500	**LAS500**	**NEC500**	
Daily Departures	1,374	622	3,307	5,303
Taxi Out, minutes	14,485	6,150	36,813	57,448
Taxi In, minutes	6,999	2,447	15,558	25,004
Track Distance, nmi	382,337	177,285	890,394	1,450,016
GC Distance, nmi	363,496	169,340	859,822	1,392,659
Circuity, nmi	18,841	7,944	30,572	57,357
Unimpeded Block Time, minutes	81,801	36,481	197,733	316,015
OPSNET 45 Delay Before Substitution, minutes	198,378	46,972	48,793	294,143
Average Delay Per Flight	144	76	15	55
2009 Block Fuel, lbs (current level)	6,087,000	3,709,600	11,389,900	21,186,500
2025 Block Fuel, lbs (25% improvement)	4,565,300	2,782,200	8,542,500	15,890,000
2009 Carbon Dioxide, metric tons	8,690	5,280	16,236	30,206
Carbon Dioxide, metric tons (25% improvement)	6,490	3,960	12,166	22,616
Passengers	68,890	49,613	143,979	262,482
Daily Seats	114,817	82,689	239,965	437,471
Load Factor	60%	60%	60%	60%

TABLE 6-26. SAVINGS OF CTR30/90/120 MIXED-FLEET (TABLE 6-24) OVER CONVENTIONAL MIXED-EQUIPAGE FLIGHTS (TABLE 6-25)

Mixed-Equipage Conventional vs. Test Point 3.4 CTR30, CTR90, and CTR120 **Mixed-Equipage Conventional and CTR Differences (table 6-24 subtracted from table 6-25)**	**Region**			**Combined**
	ATL500	**LAS500**	**NEC500**	
Daily Departures	308	(70)	653	891
Taxi Out, minutes	5,957	614	15,581	22,152
Taxi In, minutes	603	(1,705)	(366)	(1,468)
Track Distance, nmi	90,841	(11,029)	211,071	290,883
GC Distance, nmi	72,000	(18,974)	180,500	233,526
Circuity, nmi	18,841	7,944	30,572	57,357
Unimpeded Block Time, minutes	2,737	(14,817)	9,073	(3,007)
OPSNET 45 Delay Before Substitution, minutes	197,644	46,899	42,462	287,006
Average Delay Per Flight	144	75	12	54
2009 Block Fuel, lbs (current level)	725,738	79,906	(157,308)	648,335
2025 Block Fuel, lbs (25% improvement)	(795,962)	(847,494)	(3,004,708)	(4,648,165)
2009 Carbon Dioxide, metric tons	1,049	108	(220)	937
Carbon Dioxide, metric tons (25% improvement)	(1,151)	(1,212)	(4,290)	(6,653)
Passengers	130	(211)	(273)	(353)
Daily Seats	217	(351)	(455)	(589)
Load Factor	0%	0%	0%	0%

In this table, positive numbers represent lower CTR values, and negative numbers (in parentheses) represent higher CTR values.

6.9 Results From the CTR10 Fleet Scenarios (Test Point 5.0)

The notional concept for 10-seat CTR operations is an on-demand service for passengers traveling between metropolitan airports and between airports and city center or suburban heliports. In this study an assumption was made that there would not be a demand for regularly scheduled service with 10-seat CTRs.

There may be potential in a 2025 study period for innovative applications for smaller CTR aircraft on routes served by larger aircraft. For example, the original NEC shuttle services offered a no-reservation service with what was, in effect, a guaranteed seat. If the scheduled 8 a.m. Boston to New York shuttle was filled, the airline guaranteed that there would be a backup aircraft available to accommodate any additional passengers (even in the case of a single passenger). This eventually evolved into a service where the 8 a.m. flight would leave early when it was filled, and the backup aircraft would wait until it was filled.

The CTR-10 might potentially fill a role enabling regular service with larger CTR aircraft to operate at higher load factors, with consequent higher probability of oversold seats on regular services. Smaller CTRs would, in effect, serve as insurance against "involuntary denied boarding" of passengers. Smaller CTRs could absorb overflow demand on regular routes, or could reroute passengers between nearby metropolitan airports to make connections or accommodations on less highly booked flights.

The innovation that would likely need to occur would be the ability to coordinate the operation of smaller CTRs with regular, scheduled large CTR service, while at the same time having the flexibility to offer on-demand small CTR service and local inter-vertiport service.

6.10 Results of VTOL/STOL CTR Operations (Test Point 6.0)

All of the previous CTR fleet operations in section 6 were assumed to be in VTOL conversion mode. An assessment of the fuel burn effects due to STOL operations was made in Test Point 6.0. Table 6-27 applies the number of daily departures by CTR type and region to the takeoff and landing fuel consumption from the tables in section 3.6.4. Table 6-27, which uses the same number of flights as Test Point 3.4 (table 6-24), shows the effect of VTOL takeoff and landing operations on fuel consumption relative to the STOL operations. If the VTOL results from Test Point 3.4 (CTR30, CTR90, and CTR120 fleet operations, as shown in table 6-24) were generated using STOL conversion mode for all takeoffs and landings, the net effect would show a fuel savings of 177,283 lbs (table 6-27) from a base of 20,538,165 lbs (table 6-24), a reduction in CTR fleet-wide fuel burn of 0.86 percent.

6.11 Sensitivity Analysis of CTR Load Factor (Test Point 7.0)

The effect of operations at a higher load factor was evaluated by downsizing CTR120 fleet operations relative to Test Point 2.4 (table 6-21). Table 6-28 shows the effect of modifying Test Point 2.4 (mixed CTR90 and CTR120 fleet at a 60-percent load factor) by replacing all CTR120 flights with CTR90 aircraft. Since there was no change to the number of flights, there is no effect on average delay. With reduced capacity, under the assumption that the same number of passengers can be accommodated, the result is to increase the average load factor from 60 percent (Test Point 2.4) to a combined 74 percent for all three regions, as shown in table 6-28 (Test Point 7.0). Fuel burn decreases from 19,197,530 (table 6-21) to 17,999,669 lb (table 6-28), a reduction of 6.2 percent.

TABLE 6-27. FUEL BURN COMPARISON BETWEEN CTR VTOL AND STOL OPERATIONS

	CT12 ATL500	CT12 LAS500	CT12 NEC500	CT09 ATL500	CT09 NEC500	CT03 ATL500	CT03 NEC500	Total
Daily departures	730	692	1,260	282	790	54	604	4,412
STOL Operation								
Fuel lbs per departure	175.25	175.25	175.25	162.56	162.56	73.70	73.70	
Fuel lbs per arrival	138.87	138.87	138.87	123.12	123.12	136.81	136.81	
Fuel per landing and takeoff (LTO) cycle	314.12	314.12	314.12	285.68	285.68	210.51	210.51	
Daily Totals								
Departure fuel lbs	127,933	121,273	220,815	45,842	128,422	3,980	44,515	692,779
Arrival fuel lbs	101,375	96,098	174,976	34,720	97,265	7,388	82,633	594,455
Total fuel lbs	229,308	217,371	395,791	80,562	225,687	11,368	127,148	1,287,234
VTOL Operation								
Fuel lbs per departure	192.87	192.87	192.87	186.59	186.59	92.99	92.99	
Fuel lbs per arrival	158.73	158.73	158.73	149.09	149.09	152.72	152.72	
Fuel per LTO cycle	351.60	351.60	351.60	335.68	335.68	245.71	245.71	
Daily Totals								
Departure fuel lbs	140,795	133,466	243,016	52,618	147,406	5,021	56,166	778,489
Arrival fuel lbs	115,873	109,841	200,000	42,043	117,781	8,247	92,243	686,028
Total fuel lbs	256,668	243,307	443,016	94,662	265,187	13,268	148,409	1,464,517
VTOL Excess Above STOL Operation								
Fuel lbs per departure	17.62	17.62	17.62	24.03	24.03	19.29	19.29	
Fuel lbs per arrival	19.86	19.86	19.86	25.97	25.97	15.91	15.91	
Fuel per LTO cycle	37.48	37.48	37.48	50.00	50.00	35.20	35.20	
Daily Totals								
Departure fuel lbs	12,863	12,193	22,201	6,776	18,984	1,042	11,651	85,710
Arrival fuel lbs	14,498	13,743	25,024	7,324	20,516	859	9,610	91,573
Total fuel lbs	27,360	25,936	47,225	14,100	39,500	1,901	21,261	177,283

TABLE 6-28. HIGH LOAD FACTOR OPTION: USE OF CTR90 TO REPLACE CTR120 IN TEST POINT 2.4 (MIXED CTR90 AND CTR120 FLEET)

Test Point 7.0	**Region**			**Combined**
All-CTR90 High Load Factor Option	**ATL500**	**LAS500**	**NEC500**	
Daily Departures	1,012	692	2,050	3,754
Taxi Out, minutes	8,096	5,536	16,400	30,032
Taxi In, minutes	6,072	4,152	12,300	22,524
Track Distance, nmi	281,847	188,314	552,823	1,022,984
GC Distance, nmi	281,847	188,314	552,823	1,022,984
Circuity, nmi	0	0	0	0
Unimpeded Block Time, minutes	75,577	50,938	149,965	276,479
OPSNET 45 Delay Before Substitution, minutes	492	73	1,867	2,433
Average Delay Per Flight	0.5	0.1	0.9	0.6
2025 Block Fuel, lbs	4,926,754	3,323,210	9,749,705	17,999,669
2025 Carbon Dioxide, metric tons	7,020	4,737	13,895	25,652
Passengers	67,788	49,824	133,380	250,992
Daily Seats	91,080	62,280	184,500	337,860
Load Factor	74%	80%	72%	74%

TABLE 6-29. EFFECT OF ONE ADDITIONAL MINUTE OF TAXI TIME PER FLIGHT ON DAILY FUEL CONSUMPTION

	CTR120 ATL500	CTR120 LAS500	CTR120 NEC500	CTR90 ATL500	CTR90 NEC500	CTR30 ATL500	CTR30 NEC500	Total
Daily departures	790	692	1,260	282	790	54	604	
Taxi fuel per minute (lbs)	44.17	44.17	44.17	37.67	37.67	20.17	20.17	
Daily fuel impact of 1 minute added taxi time per operation (lbs)	34,894	30,566	55,654	10,341	28,969	1,089	12,183	173,696

6.12 Results of Sensitivity Study of Taxi-Out/Taxi-In Time (Test Point 8.0)

The CTR fleet taxi-out and taxi-in assumptions for vertiport operations are 8 minutes and 6 minutes respectively, as discussed in appendix L. These assumptions are based on the time needed to perform the start-up check list and taxi out to the vertiport, and the time necessary to allow for engine cool-down and for the rotors to come to a complete stop. Table 6-29 shows the estimated daily effect on fuel burn of one additional minute of either taxi-out or taxi-in time.

6.13 CTR NAS Performance Under NextGen Analysis Summary

From ACES simulations reported in sections 6.3 through 6.8, the cumulative impact of CTR replacement can be derived, as illustrated in table 6.30 and figures 6-15 and 6-16. Table 6-30 shows the cumulative delay impact of adding test points, relative to conventional mixed-equipage operations. The difference between test point delays shown in table 6-13 and those in table 6-30 is that table 6-13 shows average delay for each test point on its own.

TABLE 6-30. CUMULATIVE DELAY REDUCTION FROM CTR REPLACEMENT

NAS-Wide OPSNET 45 Delay Minutes			
Description	**Test Point**	**Total**	**Average**
Baseline 0.0	0.0	939,461	21.6
ATL CTR120	1.2	544,461	12.7
LAS CTR120	1.3	407,278	9.5
NEC CTR120	1.0	329,884	8.1
ATL CTR90	2.2	290,132	7.3
NEC CTR90	2.1	279,582	7.2
NEC CTR30	3.1	279,179	7.2
ATL CTR30	3.2	278,590	7.2

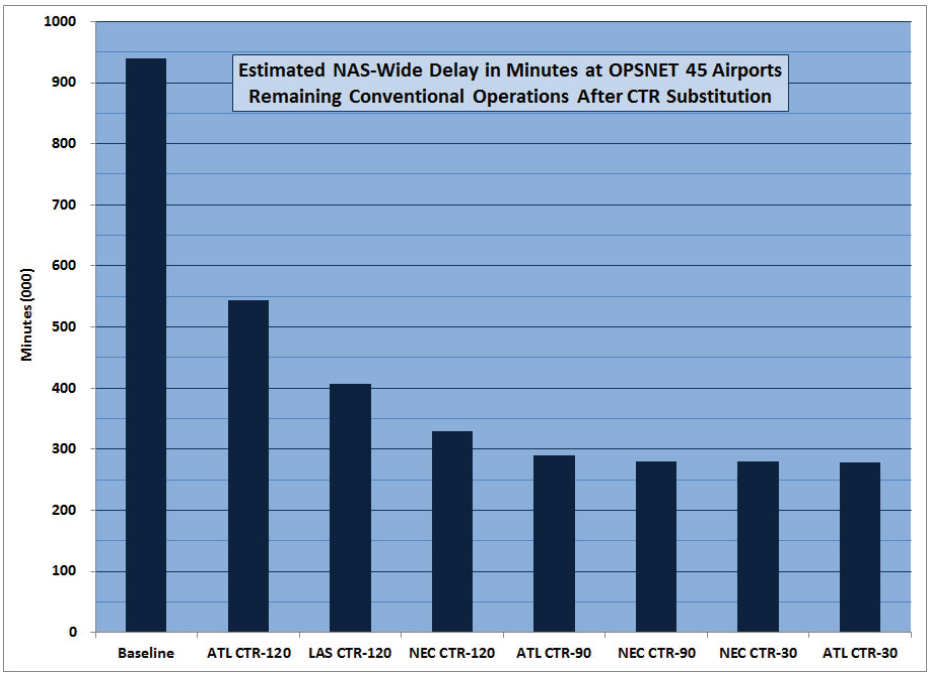

Figure 6-15. Cumulative total delay reduction from CTR substitution.

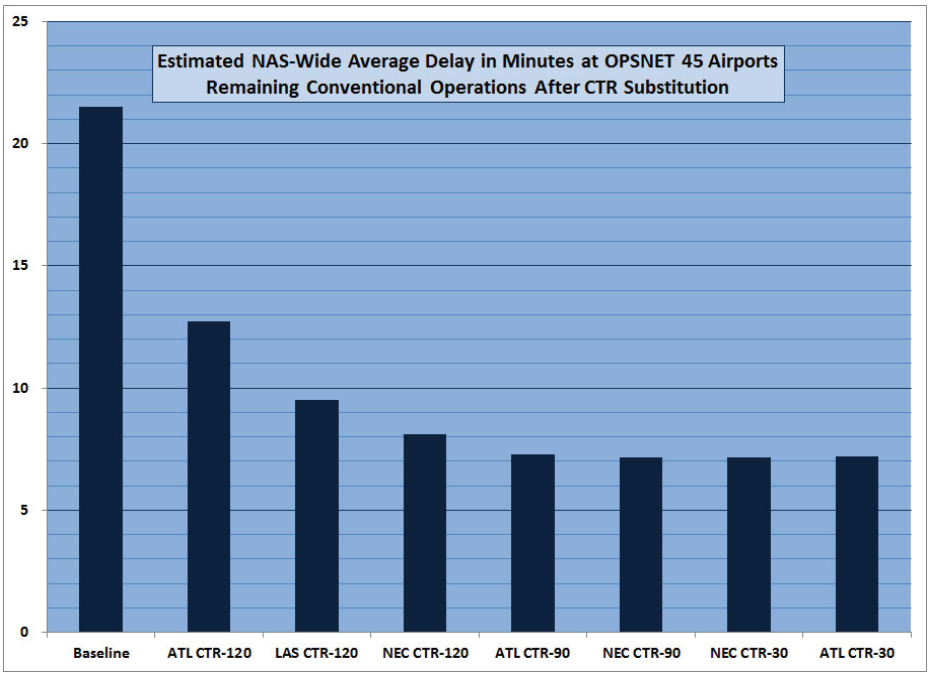

Figure 6-16. Cumulative average delay reduction from CTR substitution.

Table 6-30 shows that using an ACES simulation to replace conventional flights with CTR120 aircraft in the Atlanta region reduces total NAS-wide delay at OPSNET 45 airports from 939,000 minutes to 544,000 minutes (corresponding to average delays of 21.6 minutes and 12.7 minutes, respectively). Further replacement of conventional aircraft continues to reduce total and average delay levels, until CTR90 aircraft are introduced in the Atlanta and NEC regions, when delays stabilize at a level of about 280,000 minutes and at an average of 7.2 minutes delay per operation at OPSNET 45 airports. The results of the ACES simulation runs are shown graphically in figures 6-15 and 6-16.

While they cannot be considered conclusive, the results of the ACES and supporting analyses in this study suggest that replacing short-haul (in this study considered to be under 500 statute mile) air service with runway-independent and network-independent air service may be beneficial. The benefit is mainly to relieve a severe demand/capacity imbalance at major airports through the assignment of CTRs to replace conventional aircraft on denser short-haul routes. In this study, when the routes replaced thinned to a density that could be served with CTR30 aircraft, the marginal reduction in total and average delay decreased to a point where it is difficult to justify development and introduction of small CTR aircraft on the basis of delay reduction.

The study leaves open the possibility that small CTRs (CTR10 and CTR30 aircraft) may have a supplemental role in a hybrid business case model that combines scheduled and adaptive (demand/responsive) service. It is difficult to justify such a secondary role for smaller CTRs, however, without a firm prospect for development of larger CTR aircraft.

The study reaches no conclusion about whether the CTR90 or the CTR120 is the most appropriate size of aircraft to provide replacement short-haul service. Continued evolution of the technology and understanding of the economics of CTR operations is needed, together with a greater understanding of the environmental impacts and the tradeoffs between capacity gains through additional runways or additional runway-independent operation.

7 ENVIRONMENTAL IMPACT OF THE CTR FLEET

Two environmental impact topics, i.e., noise and emission, are investigated for the CTR fleet under the NextGen. Noise could be a critical factor if adjacent communities around the location where the CTR fleet is deployed accept the CTR operations (refs. 4,5). Using scaled CTR noise contours based on CTR fleet passenger configurations, noise impact at Newark Liberty International Airport (EWR) was analyzed. In support of prior NASA airspace systems analysis, EWR operations had been extensively analyzed as part of a technology and operational concept analysis for Extreme Short Takeoff and Landing (ESTOL) aircraft (refs. 19,47). In the current study, the emission impact of a CTR fleet was conducted using the fuel burn as the measuring metric, and was compared with the conventional fleet. Results of these investigations are described in the following sections.

7.1 Noise Impact at EWR

During the CTR performance design effort discussed in section 2, noise footprints for the CTR10, CTR30, and CTR120 NextGen designs were developed using representative takeoff and landing time histories developed from pilot-in-the-loop (PITL) studies by Bell Helicopter, processed noise data from XV-15 flight tests, and Rotorcraft Noise Model (RNM) software (ref. 48). The procedures and results are documented in section 2.9.

The results from section 2 were used in the assessment of the initial noise impact for CTR operations in the Northeast Corridor (NEC) into and out of EWR. To achieve this goal, the following subtasks were developed:

- Verify the noise footprint results from section 2.9 using the latest version of the RNM software.
- Generate input data needed for Integrated Noise Model (INM) (ref. 49) using RNM.
- Compare the results of RNM and INM, and document the differences.
- Generate the initial noise impact at EWR using INM.

The Aviation Environmental Design Tool (AEDT) (ref. 50) is being developed as the next-generation aviation environmental consequence tool replacing INM, and several other tools, but it is not yet ready for production work.

7.1.1 CTR Noise Contours in RNM

The development of the noise footprints in Sound Exposure Level (SEL) as described in section 2.9 was conducted using RNM version 3 and Bell's in-house XV-15 data set obtained during the flight tests of 1995–1999 (see section 2.9.2). The current version of RNM distributed by the NASA Langley Research Center is 7.2.2. Before proceeding further, it was deemed appropriate to verify the results from section 2.9 using the current version of RNM and the XV-15 noise data set obtained directly from NASA Langley. This data set was developed from the same set of flight tests, but is significantly smaller (49 hemispheres versus 122 hemispheres for the Bell in-house data set). Two representative cases were chosen for comparison: the CTR30 vertical takeoff (figure 2-67) and 3-degree approach (figure 2-63).

7.1.1.1 Procedure

Using RNM Version 7.2.2, October 2009 (ref. 48), the procedures described in section 2.9.3 were followed:

- Develop a flight profile for the RNM input file from the simulated flight profile histories (appendix H).
- Run RNM to generate the SEL over a uniform grid.
- Adjust the output for blade tip speed and gross weight using the factors listed in table 2-11.
- Over-plot the new results from RNM 7 with the previous results of RNM 3 (section 2.9.4).

7.1.1.2 Results

The results of the CTR30 vertical takeoff test case are shown in figure 7-1. This corresponds to Run 13 of the PITL studies. The data from figure 2-67 (black, generated using RNM 3) are over-plotted with the results from RNM 7 (red). The blue line represents the approximate ground track from the takeoff point until the run ended. While not identical, the match is good. It is believed that the differences can be attributed to small algorithmic/computational updates between RNM 3 and RNM 7, with the largest differences occurring during the initial climb when the nacelles are transitioning. The more steady-state flight during the climb and level out at 1,500 feet (upper right corner of the figure) shows an excellent match.

The results of the CTR30 3-degree approach test case are shown in figure 7-2. This corresponds to Run 05 of the PITL studies. The data from figure 2-63 (black, generated using RNM 3) are over-plotted with the current results from RNM 7 (red). The blue line represents the approximate ground track from the initial condition at 1,500 feet with nacelles at 60 degrees until the landing point.

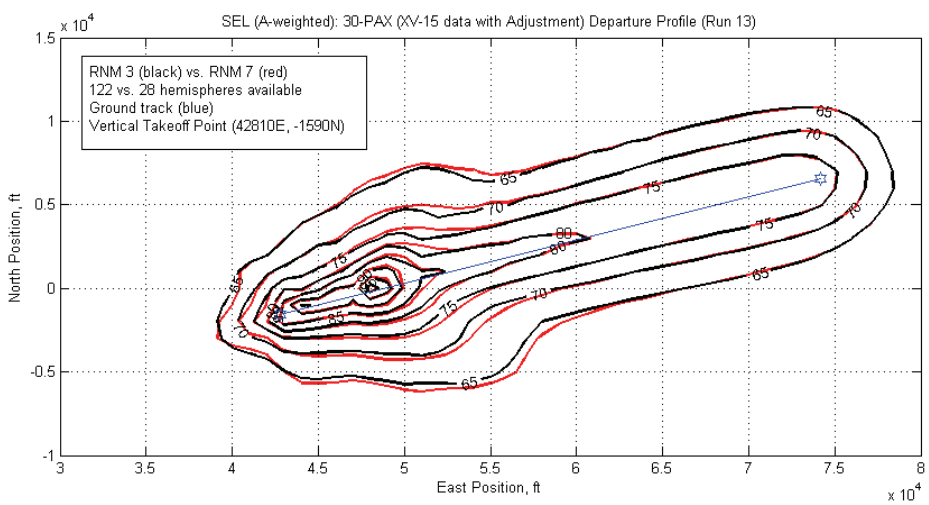

Figure 7-1. CTR30 vertical takeoff (VTO) departure comparison, Run 13, SEL (A-weighted) contours.

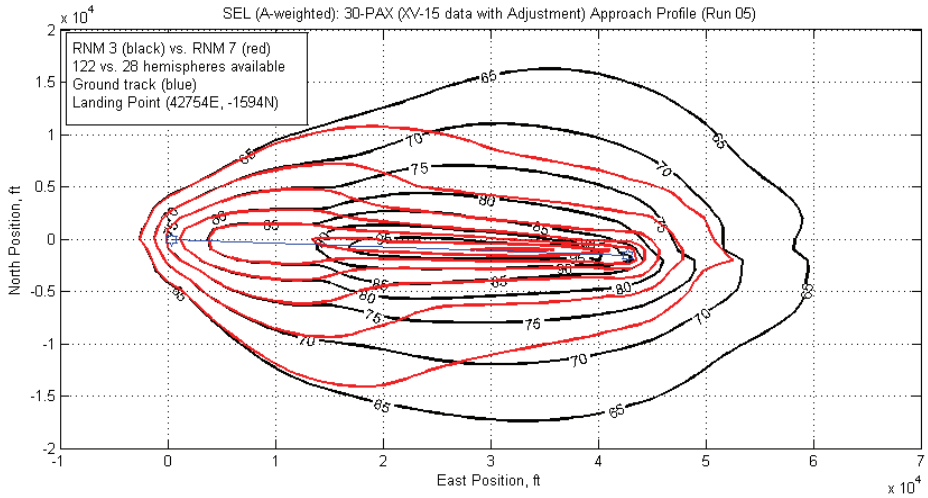

Figure 7-2. CTR30 3-degree-approach comparison, Run 05, SEL (A-weighted) contours.

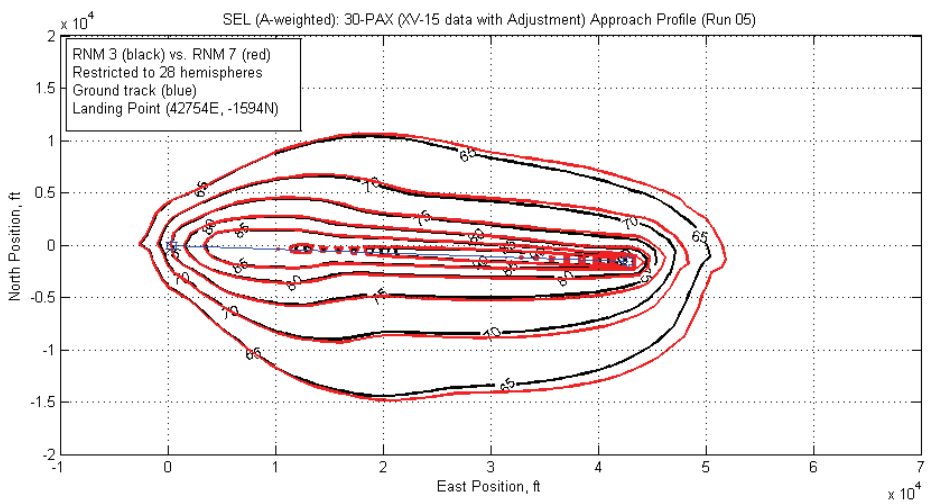

Figure 7-3. CTR30 3-degree approach, RNM 3 vs. RNM 7 with restricted hemisphere set.

The match on the left side of the figure is excellent during level flight. As the nacelles begin to transition and the descent begins, the match deteriorates. After some testing with both RNM 3 and RNM 7, it was determined that the differences between the plots could be almost entirely attributed to extra source noise data not available to RNM 7. As mentioned previously, the tests done in section 2.9 were conducted using the Bell in-house set of XV-15 sound hemispheres. This data set contains 122 hemispheres representing different airspeeds, flight path angles, and nacelle angles. The data set distributed by NASA Langley for use with RNM 7 contains only 48 sound hemispheres, and due to a structural change in the way RNM 7 uses sound hemispheres, only 28 of those 48 hemispheres are available during any one run. For this particular run, RNM 3 uses 10 sound hemispheres while RNM 7 uses only 7 hemispheres. Even more significantly, there are only 4 common hemispheres between the two sets (at 60- and 70-degree nacelle, and then at 90 degrees near touchdown). If RNM 3 is allowed to use only the 28 sound hemispheres available to RNM 7, the noise footprints are almost identical. This is shown in figure 7-3. Any remaining differences are attributed to minor changes in computational algorithms.

Due to the more general availability of the XV-15 hemisphere set from NASA Langley for this study and the status of RNM 7 as the current version of the tool, all further computations will be conducted with these data and tool.

7.1.1.3 Additional Discussion

During the investigations, two additional important factors related to RNM operation were discovered that should be noted clearly here. First, neither version of RNM interpolates on nacelle angle. This can introduce significant changes in output for what seem to be insignificant changes in input. Second, as mentioned in the previous section, a change in the hemisphere input interpolation was introduced in RNM 7 that limits the available hemispheres for computation.

As described in section 2.5.1, the RNM program (ref. 48) uses a hemisphere selection and interpolation algorithm to determine noise characteristics. At each point along the flight trajectory, sound hemispheres are first selected based on a nacelle angle, using a nearest-neighbor technique. When the flight trajectory nacelle angles fall exactly between hemisphere values, the hemispheres with the larger nacelle angle are chosen under the assumption that these will generate higher noise levels below the vehicle. No interpolation is done on nacelle angle. After the appropriate subset of hemispheres with appropriate nacelle angles is determined, additional selection based on airspeed and flight path angle is performed, and two-dimensional linear interpolations of the remaining hemispheres are conducted.

While the specific flight paths and hemispheres used to generate figure 7-1 have been controlled, other tests showed that similar large differences between noise contours could be generated with very tiny changes in nacelle angle. Because no interpolation is done on nacelle angle, the granularity of the source data becomes important. In this case, the database has hemispheres for nacelle angles of 70 degrees and 80 degrees. When the input file set the nacelle angle to 74.8 degrees based on one interpretation of the simulated flight profiles, the 70-degree hemispheres were used by RNM. When a different interpretation set the nacelle angle to 75 degrees, the 80-degree hemispheres where used by RNM. With all other factors held constant, large differences such as those seen in figure 7-2 were evident.

The other important factor was a change in RNM 7 in which the set of input hemispheres used in a particular test must all have the same dimensions for the two input angles that describe the angular position of the test point with respect to the aircraft. The XV-15 data set, as described previously, was generated over a series of different flight tests. As a result, many of the sound hemisphere data files have slightly different dimensions for these two angles. It was decided by the RNM developers that it was not appropriate to extrapolate to unknown or missing data points when the different hemispheres do not have identical dimensions. RNM 7 does have a method to skip over fictitious or sentinel values installed in sound hemispheres as place-fillers, but it was not deemed appropriate for the current study to modify the XV-15 database in such a manner.

It is clear that these two factors in the current implementation of RNM mean that the source database and the particular flight paths need to be carefully controlled. The results of this investigation will be relayed back to NASA Langley and the developers of RNM, along with recommendations on nacelle interpolation and array size implementations, in the hopes of providing useful input to future updates.

7.1.2 CTR Noise Contours in INM

INM is provided with a large database of Noise Power-Distance (NPD) data files for fixed-wing aircraft and a smaller, but still significant, database of NPD data files for helicopters. While INM has incorporated methods for handling helicopters, these methods are slightly less comprehensive than the methods used for fixed-wing aircraft. In particular, power settings are assumed constant for particular flight segments. Most significantly for this study, INM does not directly handle the noise changes associated with nacelle position in a tiltrotor

aircraft. While it does include additional asymmetric noise patterns associated with helicopter operation, these are insufficient in themselves to handle tiltrotor operation.

The first step in using INM for an analysis of the NextGen tiltrotor fleet is to attempt to replicate the results of the RNM tests from section 2.9 for single departures and arrivals. To replicate the results, NPD data must be developed for the vehicles.

7.1.2.1 Generating NPD data for INM from RNM

The input source data for RNM are sound hemispheres that describe the sound level at different frequencies for a constant radius, half-sphere below the aircraft. The input source data for INM are NPD data as described by Society of Automotive Engineers (SAE) AIR 1845 (ref. 51). The SEL noise levels in the NPD files record the accumulated noise level (N) for a fixed power setting (P) at ten distinct altitudes (D) as an aircraft proceeds along a straight flight path, parallel to the ground, and of infinite length. INM does appropriate computations to adjust for conditions different from those.

To generate the needed NPD files for INM, a series of level over-flights are conducted in RNM at the appropriate altitudes. The SEL value is recorded at ground level, and the value is stored in the NPD file. To best represent the XV-15 data set, the conditions representing single hemispheres are converted to NPD data sets as shown in table 7-1.

The flight profiles for both RNM and INM are described by a series of line segments and curves with prescribed altitudes and airspeeds. It is not a true simulation in the sense that the movement is not restricted by RNM or INM to the detailed capabilities of the aircraft and power plant. To generate the needed NPD data, the aircraft is set to "fly" straight and level, but use the desired noise hemisphere, even if that hemisphere was developed with a flight path angle of –3 degrees.

TABLE 7-1. OVER-FLIGHT CONDITIONS USED TO GENERATE NPD DATA

Hemisphere Number	True Airspeed (KTS)	Flight Path Angle (deg)	Nacelle Angle (deg)
016	190	0	0
112	107	0	60
006	106	0	80
012	69	–3	80
002	42	0	80
011	69	–3	90
010	63	–3	90

For helicopters, INM does not specify a power setting for each NPD data set, but rather an operational mode. Each mode is assumed to be at a single power setting with no "interpolation" between modes. There are 14 operation modes defined:

- Approach at constant speed (APPR)
- Depart at constant speed (TO)
- Level flyover at constant speed (LFLO)
- Ground idle (GIDLE)
- Flight idle (FIDLE)
- Hover in ground effect (HIGE)
- Hover out of ground effect (HOGE)
- Vertical ascent in ground effect (VASC)
- Approach with horizontal deceleration (DCLH)
- Approach with descending deceleration (DCLD)
- Depart with horizontal acceleration (ACLH)
- Depart with climbing acceleration (ACLC)
- Taxi at constant speed (TAXI)

There are two important notes about helicopter operation modes and how they are used in INM. First, if separate NPD data are not provided for each operation type, INM will substitute appropriately, with some subsequent loss of accuracy. For example, INM will use the "departure at constant speed" NPD data for a departure segment with acceleration if the "depart with climbing acceleration" NPD is not available (ref. 52). INM will make the appropriate speed adjustments during the acceleration though. Second, each operation mode has a single NPD data set associated with it, thus implying a single power setting and noise signature. Of the 14 operation modes, half are associated with either ground operations or hover/vertical operations. While important in general, these aren't dominant modes generating community noise for these studies. Of the remaining seven operation modes, three are for departure, three are for approach, and one is level flight. These are all that can be used for a single aircraft. These modes are not sufficient to represent the typical approach or departure profile for a CTR with varying nacelle angles in addition to power settings.

7.1.2.2 Procedure

The basic procedure for developing a noise contour plot for a single operation in INM is outlined below.

Step 1: Develop a straight-line approximation of the vertical flight profile and horizontal ground track. For these studies, the horizontal ground track is assumed to be a single straight line. Departure and approach vertical profiles must begin or end on the ground, respectively. It is not possible to do a partial profile as can be done in RNM.

Step 2: Select or input the vehicle types and associated noise characteristics.

Step 3: Set the number of each type of flight operation.

Step 4: Run the given configurations to generate the noise data.

Step 5: Plot the noise contour.

The INM input profile is over-plotted on the original approach history in figure 7-4 for the CTR30, 3-degree approach. The underlying simulated flight data is the same as found in figure H-6a (Run 05) from PITL simulation. A similar input profile was developed for the CTR30 VTO departure from figure H-10a (Run 13). Following the recommendation of section 2.9.4, the 90-passenger and 120-passenger operations will use these same two vertical profiles for these noise studies in INM.

To generate the noise footprint for a single fixed-wing aircraft or helicopter, the vehicle type and a single operation into the desired airport are set in INM. For the current study, Newark Liberty International Airport (EWR) is selected in INM (altitude approximately 18 feet ASL). Although no terrain data are introduced (i.e., all approach and departure directions are identical subject only to a rotation of the coordinate system for single operations), a vertiport was created near the end of Runway 11 to simulate the desired system.

Given the limitations of the helicopter operation modes in INM described in the previous section when applied to CTR profiles, an augmented method was employed to generate noise contours in INM. Rather than a single aircraft generating the noise of a single approach or departure, the output of two or more aircraft operations are combined to create the equivalent of a single operation. Each of these Piece-Wise-NPD (PWN) aircraft have valid NPD data sets for one or two of the INM helicopter operation modes, while they have mathematically insignificant values (INM does not allow zero noise data) for the other modes. Due to the cumulative nature of the SEL noise measurement, an appropriate summation of the PWN aircraft gives identical results to a single aircraft with the appropriate NPD values in for all operation modes. All results in this and the following section use PWN aircraft.

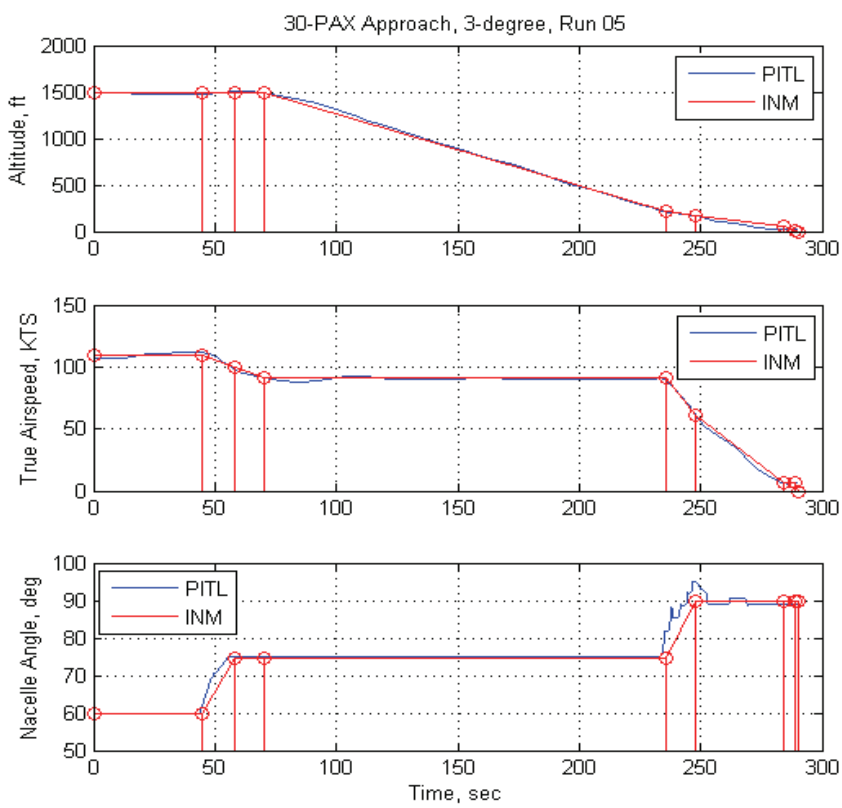

Figure 7-4. CTR30 3-degree-approach profile for INM input.

As discussed in section 2.9.3, when using the XV-15 noise data the output contours from RNM are adjusted to account for the gross weight and rotor tip speed differences between the XV-15 and the various CTR sizes. The adjustments for CTR10, CTR30, and CTR120 are shown in table 2-11 as 0.9 dB, 1.9 dB, and 4.4 dB, respectively. For the current study, an interpolated adjustment of 3.4 dB will be used for the 90-passenger CTR.

7.1.2.3 Results

The SEL noise footprint for the CTR30 approach developed in INM (equivalent to the RNM footprints in figure 7-1) is shown in figure 7-5. The RNM footprint using the restricted set of hemispheres is included for comparison. While the match is poor at the beginning (around [0, 0] when the aircraft is at 1,500 feet, 110 knots), it improves considerably near the touchdown point.

Investigating further leads to the conclusion that the mismatch in figure 7-5 is primarily due to what might be called start-up transients. The approach starts somewhat at 1,500 feet and 110 knots with a 60-degree nacelle angle followed soon after by the final approach. It appears that the RNM and INM handle this point in the sky differently. Extending the length of the level flight segment at 1,500 feet in both RNM and INM gives the results shown in figure 7-6; there is much better agreement of noise contours.

The approach footprints for the CTR90 and CTR120 are shown in figures 7-7 and 7-8, respectively. As previously discussed, the CTR30, CTR90, and CTR120 plots are all developed from the XV-15 data set using an adjustment in dB level of the SEL output plots from RNM and INM. As such, the shapes of the curves are identical, given the same input flight profile.

The noise footprint for the CTR30 takeoff developed in INM (equivalent to the RNM footprints in figure 7-1) is shown in figure 7-9. The RNM footprint using the restricted set of 28 hemispheres is included for comparison; the match is good. The differences are mostly attributable to the takeoff and nacelle transition region. This is the weakest point of the modeling method in INM. Additional adjustment of NPD data sets might increase the match, but with very little benefit to the overall analysis.

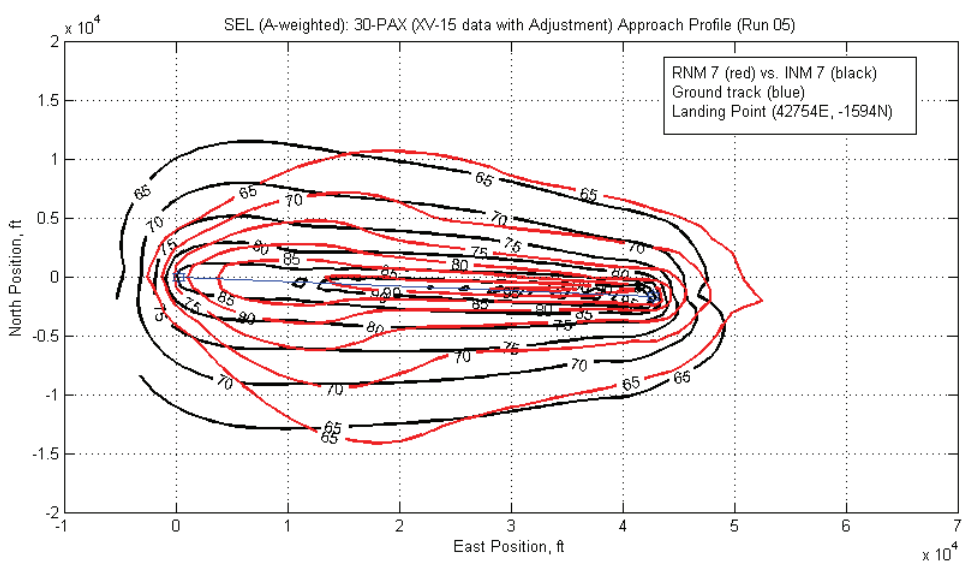

Figure 7-5. SEL noise footprint of a CTR30 3-degree final approach: RNM vs. INM.

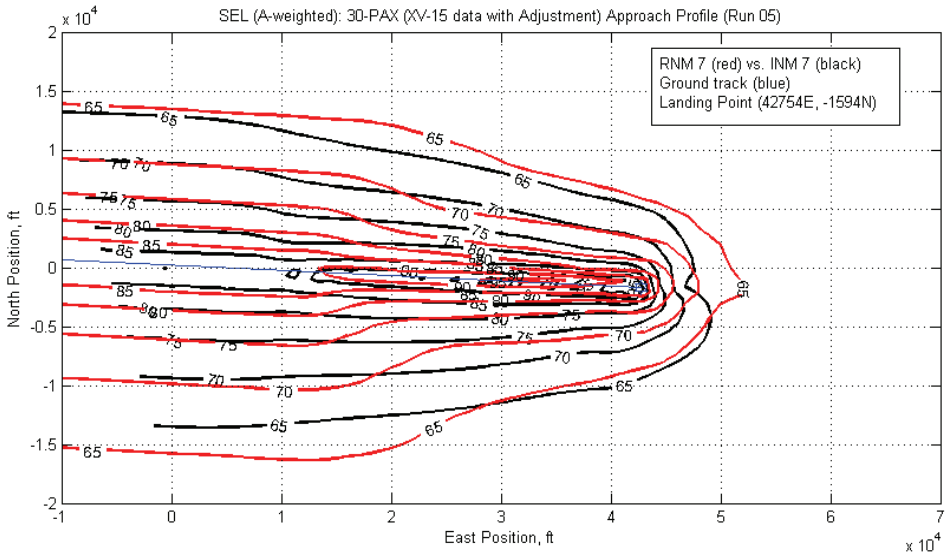

Figure 7-6. SEL noise footprint of a CTR30 3-degree extended approach.

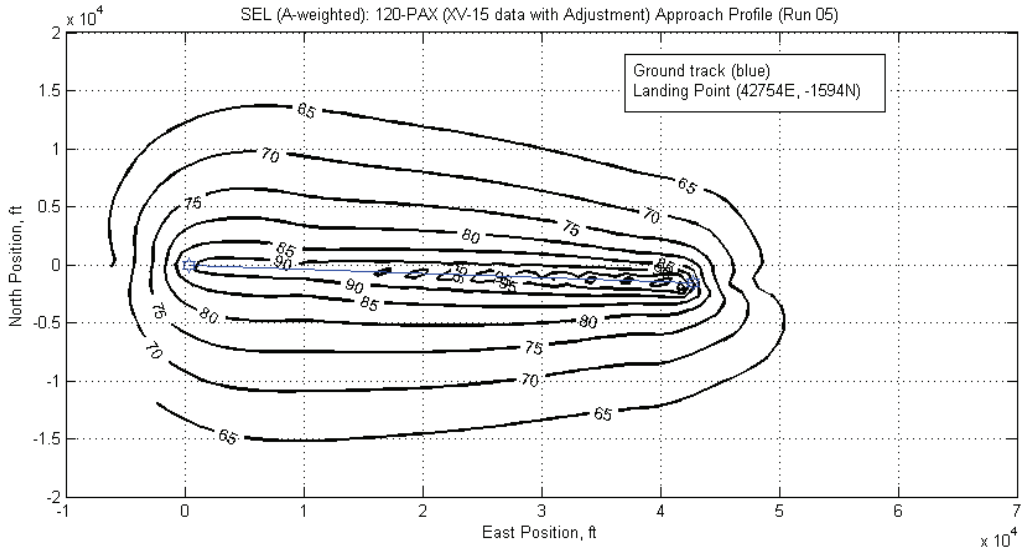

Figure 7-7. SEL noise footprint of a CTR120 3-degree approach.

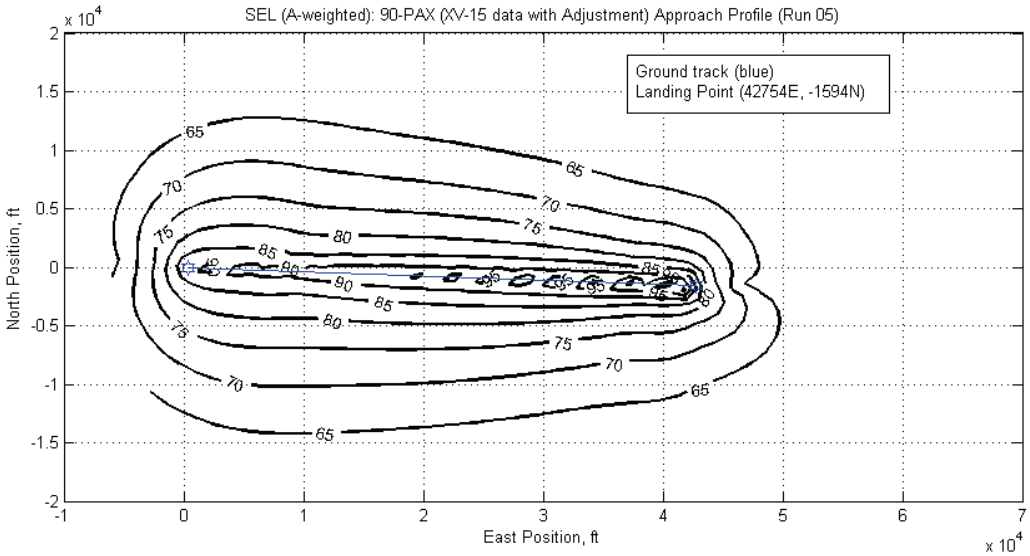

Figure 7-8. SEL noise footprint of a CTR90 3-degree approach.

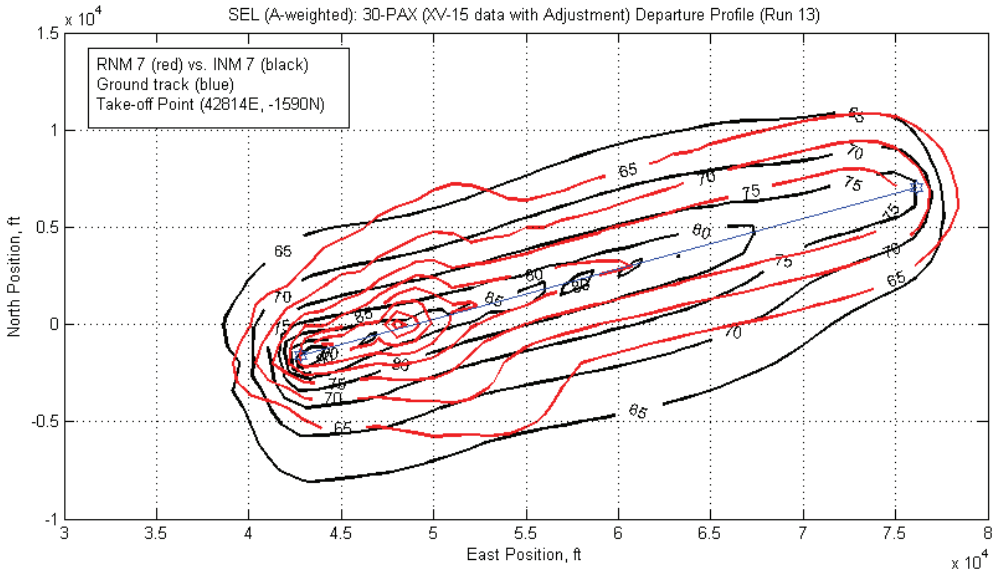

Figure 7-9. SEL noise footprint of a CTR30 VTO departure from EWR.

7.1.3 CTR Noise Impact at EWR

The final area of investigation is the cumulative effect of all CTR operations on a single airport. Using the PWN aircraft technique developed in the previous section, the SEL footprints for inbound, outbound, and combined CTR operations at EWR for the NEC are documented.

7.1.3.1 Noise Footprint Results for Outbound Flights

Table 7-2 lists the NEC outbound flights used for NAS performance analysis of a CTR30, CTR90, and CTR120 mixed fleet as described in section 6-8. Possible vertiport sites for the CTR mixed fleet at EWR are shown in figure 7-10 and discussed in appendix L. The noise footprint for the NEC outbound flights listed in table 7-2 is shown in figure 7-11; the noise results depict a mixed fleet and a single vertiport at spot no. 5 near the end of runway 11 at EWR (shown in figure 7-10). The CTR noise contours were laid over the population distribution at EWR based on the 2000 Census Bureau data shown in figure 7-12. The height of the red dots indicates the size of the population at that location.

7.1.3.2 Noise Results for Inbound Flights

Table 7-3 lists the NEC inbound flights scheduled for the CTR fleet at EWR. The noise footprint for the NEC inbound flights listed in table 7-3 is shown in figure 7-13; the noise results depict a mixed fleet and a single vertiport at spot no. 5 near the end of runway 11 at EWR (shown in figure 7-10). Figure 7-14, overlaying the CTR noise contours on the population distribution at EWR based on the 2000 Census Bureau data, shows the inbound CTR traffic noise footprint with the given schedules.

TABLE 7-2. OUTBOUND FLIGHTS SCHEDULED FOR THE CTR FLEET AT EWR

Destination	Departure Angle (deg)	CTR Passenger Configuration	Number of Daily Departures
BOS	55	120	13
PHL	225	90	6
DCA	230	90	6
BWI	231	30	7
IAD	235	90	7
PIT	268	90	6

TABLE 7-3. INBOUND FLIGHTS SCHEDULED FOR THE CTR FLEET AT EWR

Origin	Approach Angle (deg)	CTR Passenger Configuration	Number of Daily Approaches
BOS	235	120	13
PHL	45	90	6
DCA	50	90	6
BWI	51	30	7
IAD	55	90	7
PIT	88	90	6

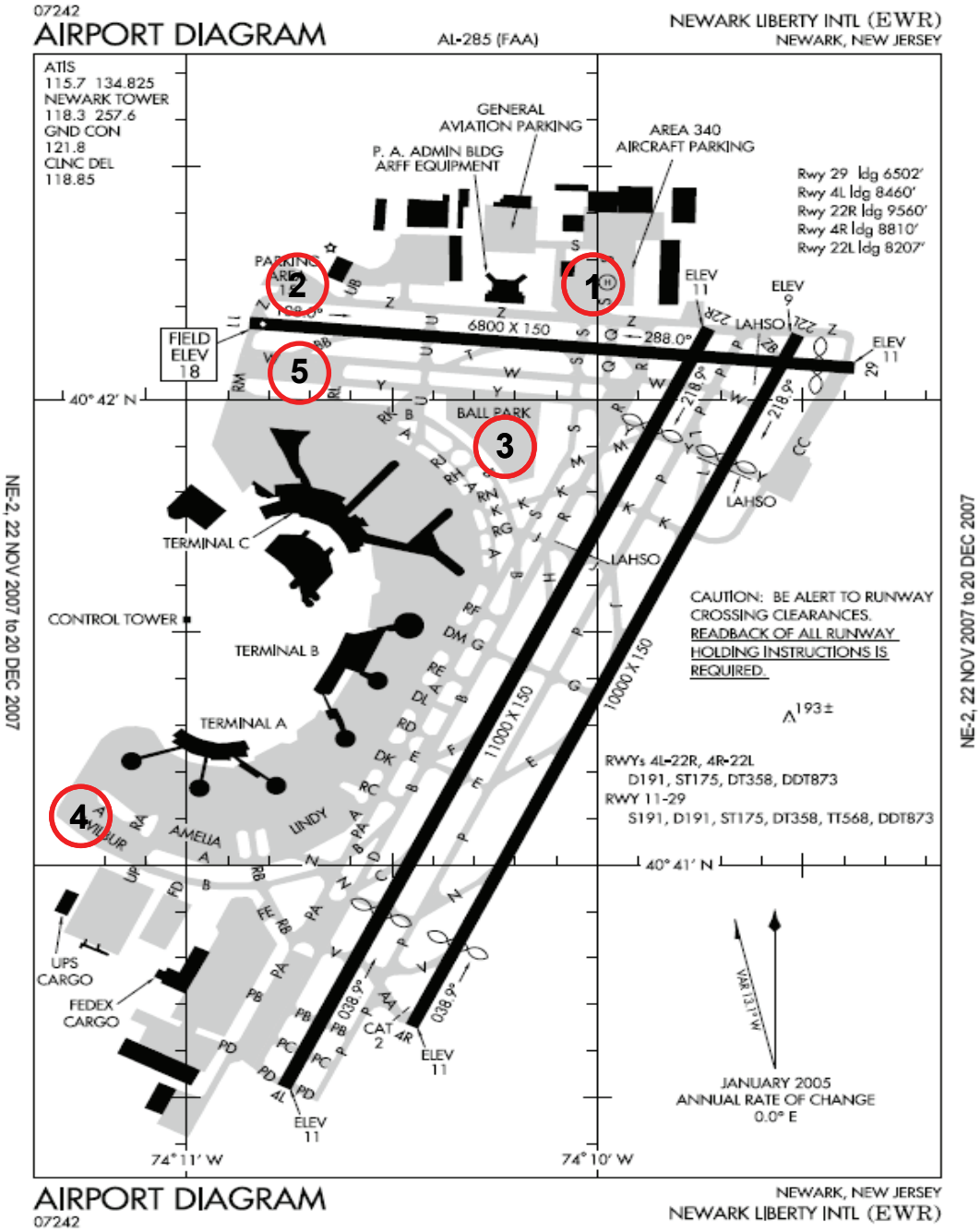

Figure 7-10. Possible vertiport sites for the CTR fleet at EWR.

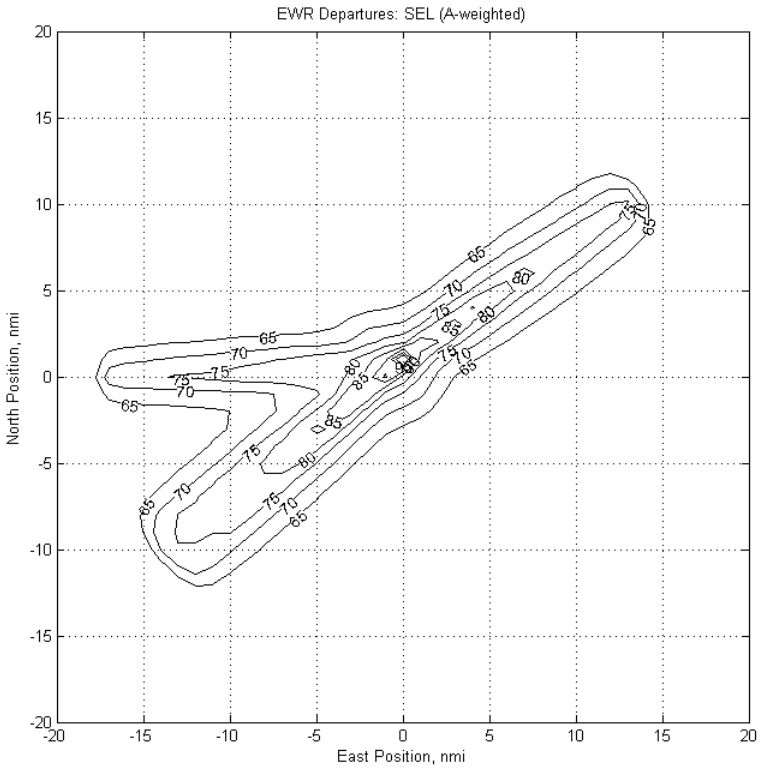

Figure 7-11. SEL noise footprint for outbound NEC EWR flights.

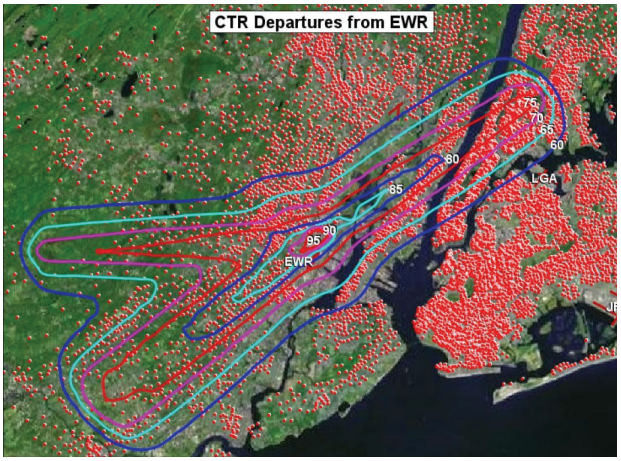

Figure 7-12. SEL noise footprint for outbound NEC EWR flights (background image courtesy of Google Earth).

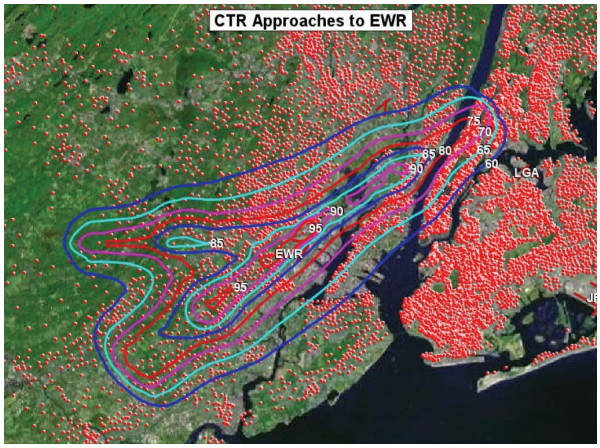

Figure 7-13. SEL noise footprint for inbound NEC EWR flights (background image courtesy of Google Earth).

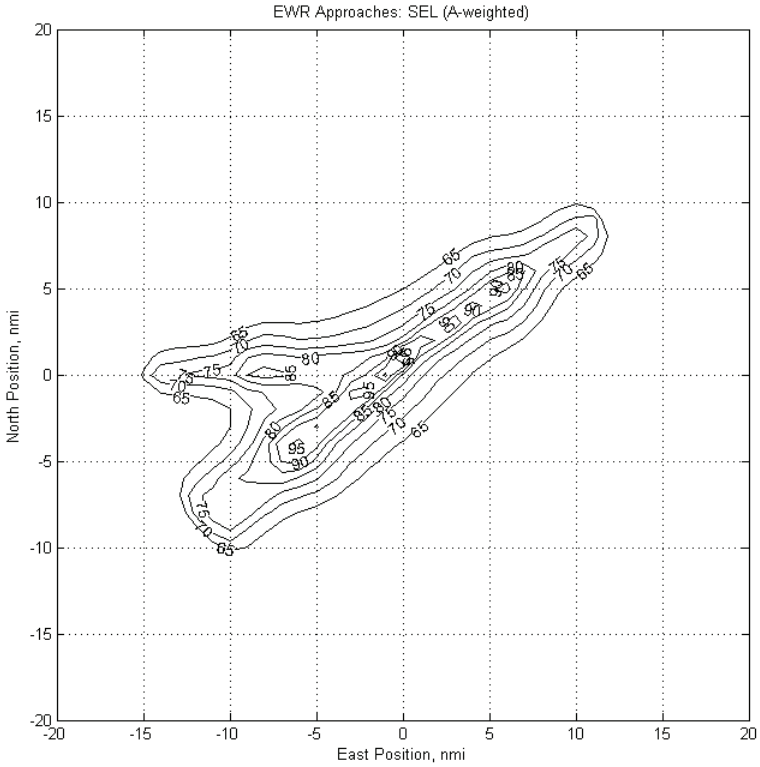

Figure 7-14. SEL noise footprint for inbound NEC EWR flights.

7.1.3.3 Combined Noise Results for All Flights

Combining the results of the previous two sections, the SEL noise footprint for all CTR operations into and out of EWR for the NEC origins and destinations is shown in figure 7-15. Figure 7-16, overlaying the CTR SEL noise contours on the population distribution at EWR based on the 2000 Census Bureau data, shows the combined inbound and outbound noise footprint with the given schedules.

7.1.4 DNL Noise Impact at EWR

Instead of using A-weighted SEL, which is a normalized cumulative statistic to 1 second, Day-Night Average Sound Level (DNL) of a 24-hour period is the standard noise measurement statistic used by the FAA to examine the community noise impact due to aircraft operations at an airport. In particular, DNL levels less than 65 dB are said to be compatible with residential land use. During a previous NASA NVI NRA study (ref. 34), the year 2040 DNL noise contours at EWR were calculated for 1,491 flights including standard aircraft, cruise-efficient short takeoff and landing (CESTOL), and large civilian tiltrotor aircraft (LCTR) operations. The 60-dB contour area was 19.0 square miles.

As an attempt to compare to the NASA NVI NRA results, the DNL is calculated for NEC operations at EWR using the same distribution of origins/distributions as in section 7.1.3, but increasing the number of operations as shown in table 7-4 to match the number of flights estimated in NASA NVI NRA study at 1,491 flights at EWR.

The DNL noise footprint for these 1,491 CTR operations at EWR is shown in figure 7-17. This noise footprint is overlaid onto the population distributions by Sensis as shown in figure 7-18 based on the Census Bureau data. The 60 dB contour area for CTR operations is 14.0 square miles compare to 19.0 square miles from the NASA NVI NRA study. The results are essentially equivalent given the level of detail in the comparisons.

TABLE 7-4. ASSUMED MIXED CTR FLIGHTS AT EWR FOR DNL COMPARISON

Airport	Departures	Arrivals	Total
BOS	215	216	431
DCA	100	100	200
IAD	116	116	232
PHL	99	99	198
PIT	99	99	198
BWI	116	116	232
Total	745	746	1491

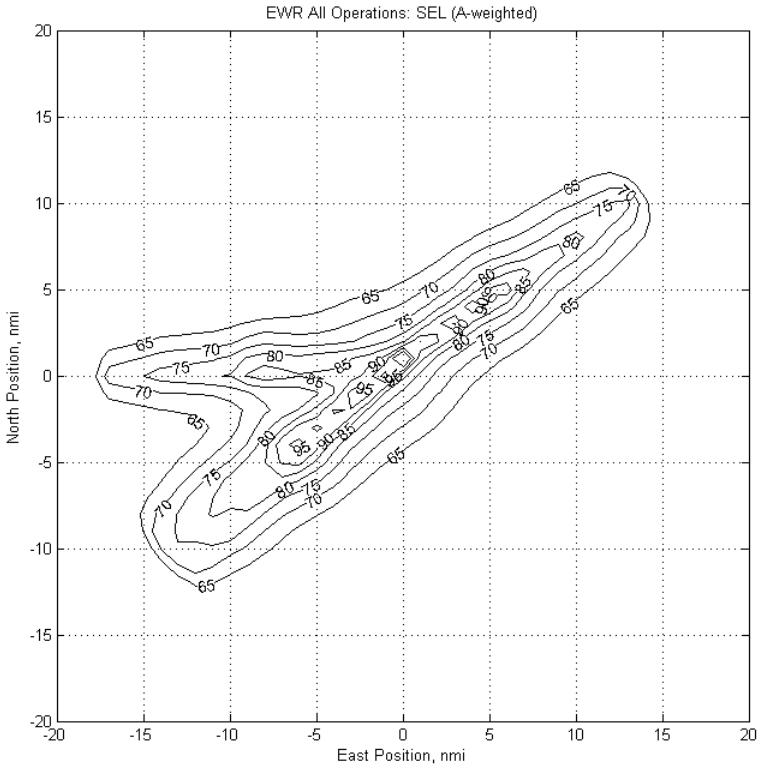

Figure 7-15. SEL noise footprint for all NEC EWR flights.

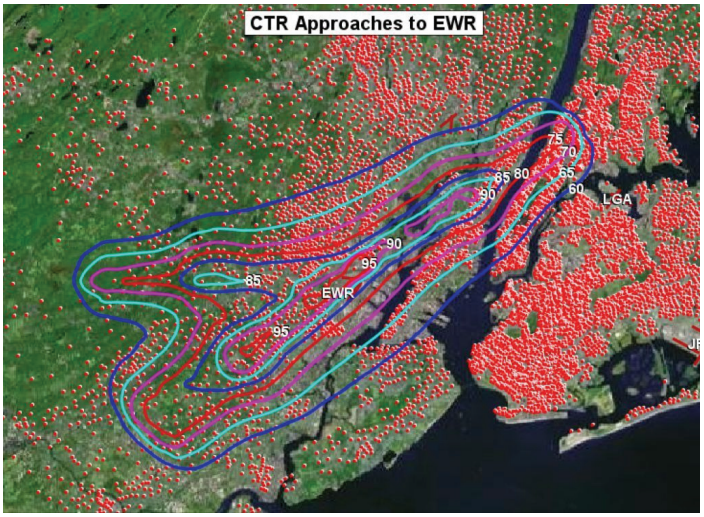

Figure 7-16. SEL noise footprint for all NEC EWR operations (background image courtesy of Google Earth).

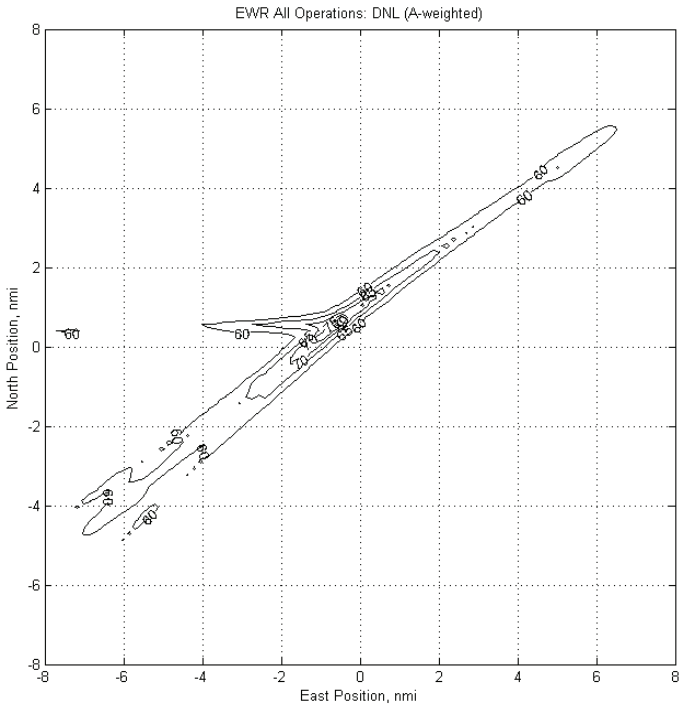

Figure 7-17. DNL noise footprint for assumed all CTR NEC EWR operations.

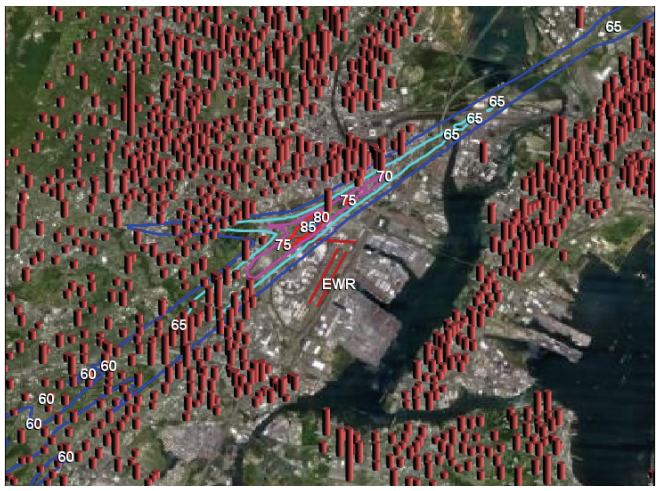

Figure 7-18. DNL noise footprint for assumed all CTR NEC EWR flights over population distributions (background image courtesy of Google Earth).

7.1.4.1 Improving Noise Footprint Using DNL Information

From figure 7-18, communities in the southwest corner and northeast of the vertiport would likely be exposed to the approach and departure noise of the CTR fleet since the community is under the CTR DNL noise footprint. This information could be use to design the CTR flight procedures, and/or redesign the flight routes to alleviate the noise impact to the community. A simple adjustment to the CTR flight procedure is demonstrated here to show the application of such a process. It was shown in section 4 that the CTR is capable of flying a 9-degree approach profile. Assuming all flights in table 7-4 change from a 3-degree approach to a 9-degree approach, the resulting DNL noise contours from INM are shown in figure 7-19. The results show a reduced noise footprint for the 9-degree approach, which should improve the negative noise impact to the surrounding communities. The top two photos in figure 7-20 show a comparison of the 3-degree approach versus the 9-degree approach when overlaying respected noise contours over the population distribution at EWR. The 9-degree approach shows the improved noise impact to the neighborhood with the exception of one population concentration zone. An additional iteration by rerouting the BOS to EWR approach, as shown in the bottom photo of figure 7-20, shows further improvement of the noise impact to the neighborhood. However, the impact due to the rerouting, such as maintaining safe separation from the conventional traffic to and from runways 4R and 4L, will need to be addressed. The process demonstrated here shows that the CTR noise database can be applied with the INM as a tool to help assess noise impact to the community in selected vertiport locations, as well as assist in route planning to improve the noise impact to the community around the vertiport.

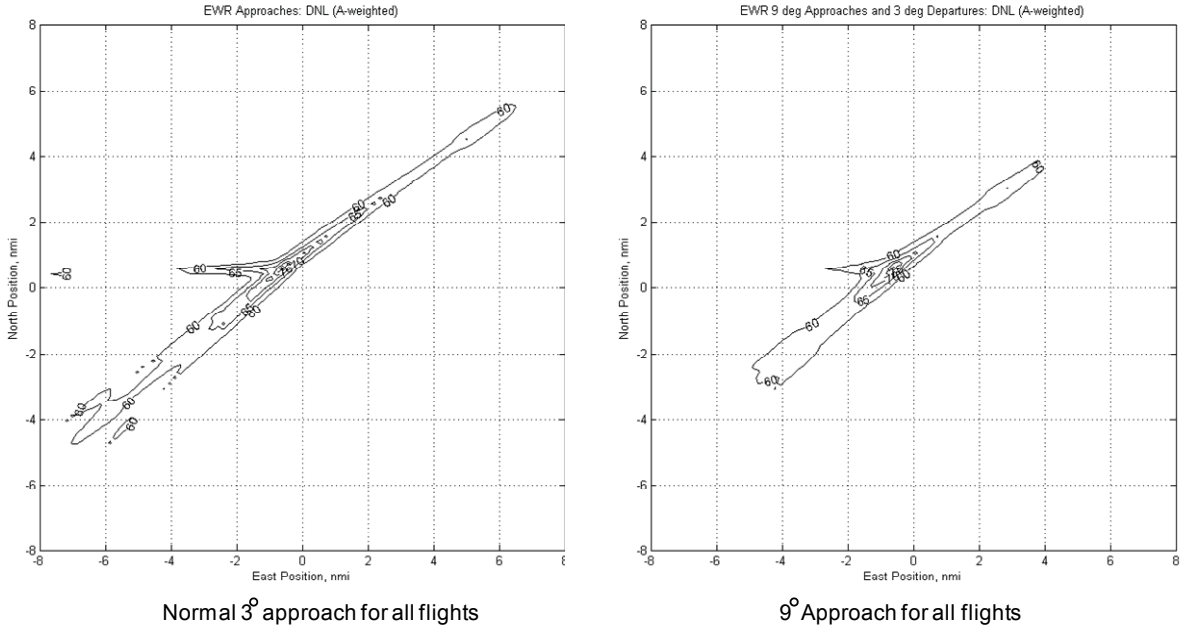

Figure 7-19. DNL noise footprint comparison for a 3-degree (left) and a 9-degree (right) approach at EWR.

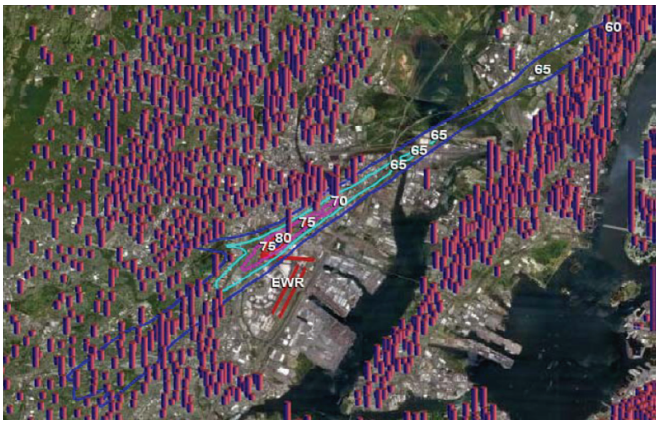

3-deg approach for all flights (Figure 7-18)

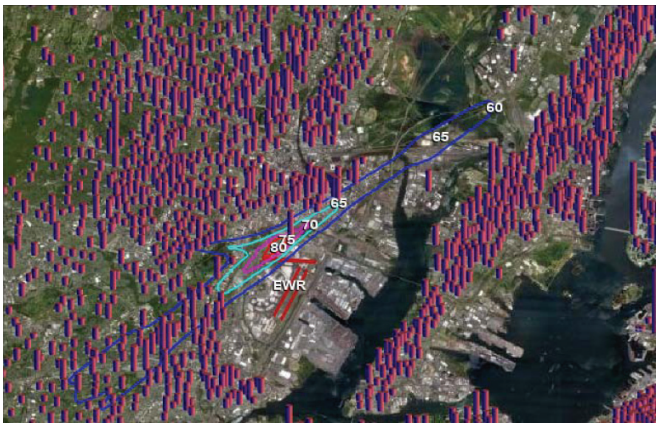

9-deg approach for all flights

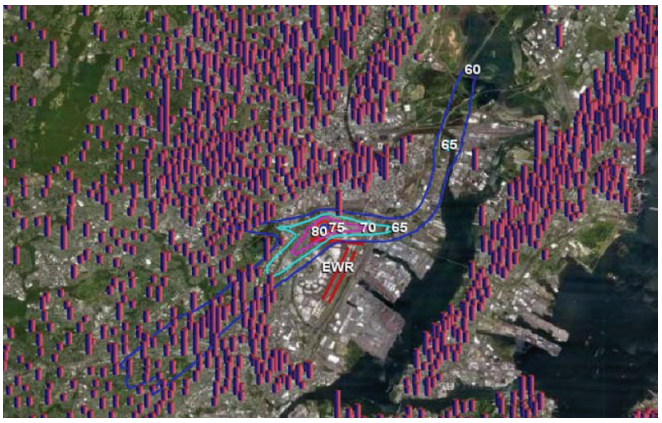

9-deg approach for all flights plus re-routing BOW-EWR approach

Figure 7-20. DNL noise footprint comparison for 3-degree (top), 9-degree (middle), and rerouted 9-degree (bottom) approach at EWR (background images courtesy of Google Earth).

7.1.5 Recommendations for future CTR Noise Impact studies

An initial evaluation of the results in section 7.1.3 suggests that route assumptions made for this study (i.e., assuming 55/235 type of takeoff and arrival routes for Boston, etc.) are not optimal with respect to community noise impact. Further optimization taking into account all traffic into and out of EWR and the population distribution is required.

The DNL results of section 7.1.4 support the data and methodologies developed here, so the next steps would be to generate additional DNL contour plots using INM (or AEDT as it becomes available) for a fully representative set of operations at EWR and compare those results with those developed by the NASA NVI study with similar traffic volumes to determine the impact of the CTR fleet at EWR.

7.2 Overview of the Emission Impact of a CTR Fleet

In the NASA NVI NRA study (ref. 34) system-wide climate impact assessments were conducted for scenarios with the new vehicle technology candidates. Each of the new vehicle scenarios was found to cause greater damage to the global climate relative to the relevant baseline scenario in terms of both time-integrated surface temperature change and monetized damages due to the higher fuel burn and emissions. The 90-seat tiltrotor was noted to be detrimental due to fuel burn levels greater than the baseline case.

In the NASA NVI NRA study, a metroplex-scale air quality analysis was performed over the New York City (NYC) region, for the conventional current airspace as well as for the NextGen airspace. The NextGen scenario produced fewer emissions from the airspace activity compared to the conventional airspace, and the effects of this reduction in emissions manifest themselves in an overall decrease in particulate matter (PM) concentrations in the NYC region. In particular, the reduction in PM Ammonium was observed far beyond the local NYC metroplex area, extending further along the coast and inland. The reduction in PM due to the NextGen airspace has the greatest effect close to the airports, the decrease becoming less pronounced as the distance from the datum increases.

During the course of the environmental analysis, the Advanced Vehicle Concepts research team identified a few potentially valuable areas of research for follow-on work. The scope of the current study did not allow these to be investigated, but the comments made in the earlier study remain valid. With regard to the air quality analysis, it would be valuable to refine the grid to 4 km instead of 12 km to provide better resolution over the NYC metroplex. While the Advanced Vehicle Concepts report only presented regional assessments for air quality and noise, Aviation Environmental Portfolio Management Tool (APMT)-Impact software (ref. 53) is capable of conducting system-wide analyses in these domains. Given the required input data, the research team could analyze the impact of each of the new vehicles in terms of system-wide noise and air quality in a similar manner to the analysis of global climate change.

In the current study, the evaluation was limited to an estimate of relative carbon dioxide emissions resulting from CTR substitution for conventional aircraft. The main inputs to the model were fuel burn and CO_2 emissions (which scale directly from fuel burn).The results are reflected in tables 6-14 through 6-28, and are summarized in table 7-5.

TABLE 7-5. CTR EMISSIONS SUMMARY

Conventional Mixed Equipage	**CT12 ATL500**	**CT12 LAS500**	**CT12 NEC500**	**CT09 ATL500**	**CT09 NEC500**	**CT03 ATL500**	**CT03 NEC500**
2009 block fuel in lbs (current level)	4,471,600	3,709,600	7,102,300	1,527,664	3,500,282	87,736	787,318
2025 block fuel in lbs (25% improvement)	3,353,700	2,782,200	5,326,800	1,145,748	2,645,099	65,852	570,601
2009 CO_2 in metric tons	6,380	5,280	10,120	2,178	4,994	132	1,122
2025 CO_2 in metric tons (25% improvement)	4,774	3,960	7,590	1,628	3,740	88	836

Source: Derived from tables 6-17, 6-22, and 6-25.

CTR Fleet

2009 block fuel in lbs (current level)							
2025 block fuel in lbs (25% improvement)	3,967,729	3,629,694	6,585,289	1,294,770	3,720,047	98,762	1,241,872
2009 CO_2 in metric tons	NA	NA	NA	NA	NA	NA	NA
2025 CO_2 in metric tons (25% improvement)	5,654	5,172	9,385	1,846	5,302	141	1,769

Source: Derived from tables 6-16, 6-21, and 6-24.

CTR 2025 Excess Above Conventional

2009 block fuel in lbs (current level)	(503,871)	(79,906)	(517,011)	(232,894)	219,765	11,026	454,554
2025 block fuel in lbs (25% improvement)	614,029	847,494	1,258,489	149,022	1,074,948	32,910	671,271
2009 CO_2 in metric tons	(726)	(108)	(735)	(332)	308	9	647
2025 CO_2 in metric tons (25% improvement)	880	1,212	1,795	218	1,562	53	933

7.3 Summary

7.3.1 Noise

Using INM or AEDT (when released), the process described in section 7.1 has established and demonstrated a credible methodology to evaluate the noise impact at selected airport locations for CTR aircraft operations. This methodology was developed to generate CTR NPD data for the INM using the XV-15 noise database and verify the results between the RNM and INM. This provides a methodology for future NAS stakeholders to evaluate the location of vertiports and to develop RIO routes at the airport and/or city-center for CTR operations to mitigate the noise impact to the community. The initial assessment of the CTR fleet noise level using DNL is that it is approximately equivalent to that of a commercial conventional fixed-wing fleet.

7.3.2 Fuel Burn

Comparison of CTR fuel burn performance for different test points relative to conventional aircraft performance for 2025 is shown in tables 6-18, 6-20, 6-23, 6-26, and 7-5. The comparisons are based on an equivalent number of seats in each case, and show CTR fuel burn relative to conventional aircraft operating at equivalent capacity over the same route structure.

Figure 7-21 compares block-to-block fuel burn per seat for the three CTR variants against the conventional fleet as a function of stage length. The scatter points in the graph represent the range of fuel burn for the different types of conventional aircraft assumed in the ACES schedule analyzed in this study. The dark green (2025 technology) and yellow (2009 technology) lines in the chart represent a linear fit for the conventional fleet. The inference that can be drawn from figure 7-21 is that the CTR90 and CTR120 aircraft are estimated to have comparable efficiency (in terms of fuel burn per seat) compared to conventional aircraft at short ranges (around 100 nmi), but lose this advantage as stage lengths increase.

As shown in figure 7-21, CTR120 fuel efficiency at the level assumed in this study falls between conventional 2009 and 2025 levels. It should be noted that the CTR fuel burn performance in this study was developed based on 2017 engine technology for a 2025 service milestone, following OEM technology insertion practice as indicated in section 2.2.2. Therefore a fuel burn performance comparison between the CTR120 and a 2017 conventional fleet is warranted.

Comparing conventional fleet performance at projected 2017 levels with CTR technology at 2017 levels—assuming an annual 1.5-percent fuel burn improvement through 2017 for conventional aircraft—and following a methodology consistent with the one taken in this study, total fuel consumption for the conventional fleet would drop from 15,283,500 lbs (at the 2009 level shown in table 6-17) to 13,449,480 lbs (a 12-percent improvement) versus 11,462,700 lbs (a 25-percent improvement projected for 2025 in table 6-17).

Thus the difference between the CTR120 fuel burn performance (i.e., the total fuel burn of 14,182,713 lbs from table 6-16), would be 5.4 percent higher than conventional fleet performance based on 2017 technology at 13,449,480 lbs. This leads to a conclusion that for CTR aircraft to be competitive from a fuel efficiency point of view, other system improvements, such as aerodynamic design to reduce the drag and manufacturing technology to reduce the weight, are needed to improve fuel burn performance.

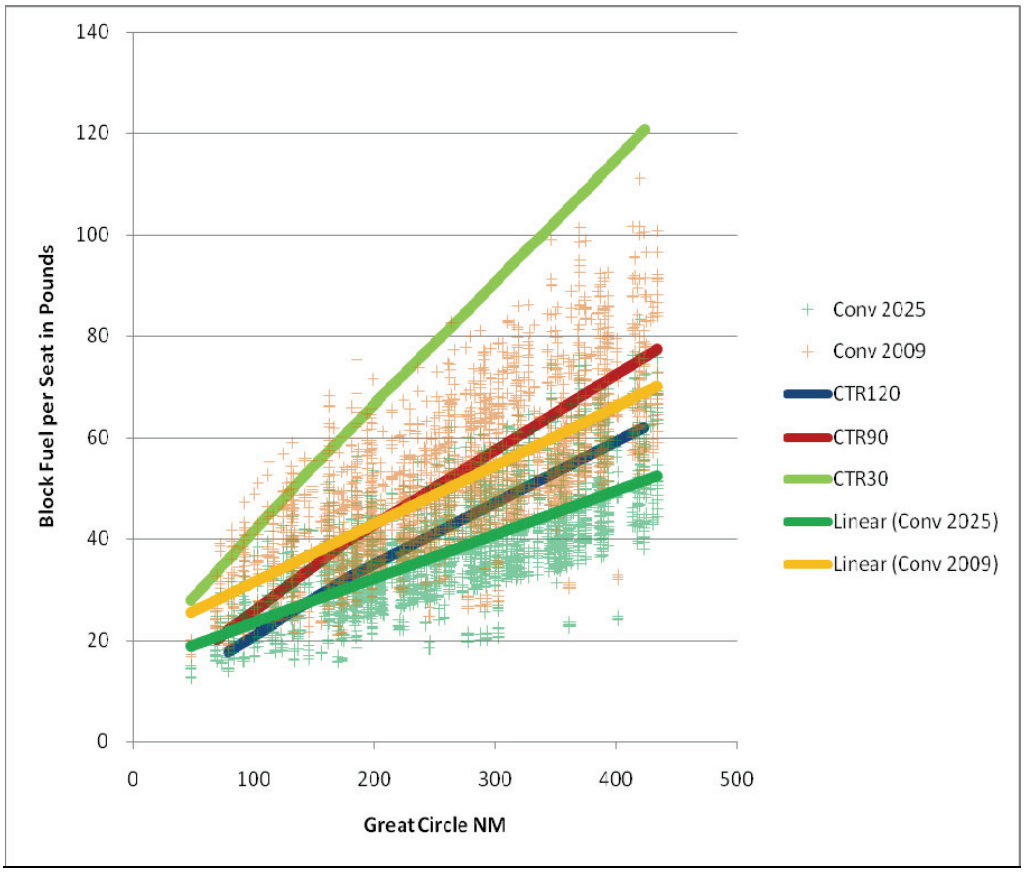

Figure 7-21. CTR and conventional block fuel per seat vs. distance.

8 SUMMARY AND RECOMMENDATIONS

A systems' study of CTR in NextGen was developed to assess the potential impact of a CTR fleet under NextGen, and investigate technology, concept of operations (ConOps) of a fleet of CTR, and analysis tools required to support future CTR research under NextGen based on a complete start-to-end analysis approach. This systems study began by developing a performance design of a CTR fleet via OEM design methodology and then using that CTR fleet performance data to 1) develop operational profiles in the terminal area for VTOL and STOL operations with a pilot-in-the-loop (PITL) simulation; 2) translate the developed CTR performance into BADA modeling format, which was then used directly by NASA-developed NAS performance analysis tools such as ACES to analyze the potential impact of the CTR fleet on NAS performance in 2025; and 3) evaluate the environmental impact of a CTR fleet.

This effort specifically looks for issues in areas related to the CTR operations in NextGen from the systems' prospective listed below. These findings and recommendations are summarized in the sections 8.1 through 8.4:

1) CTR design technology based on findings from the CTR ConOps during the NAS performance analysis.
2) Modeling requirements in support of future CTR NAS performance analysis.
3) NextGen ConOps needed to support the CTR operations and impact of the CTR fleet on current NextGen ConOps.
4) ConOps for CTR operations in NAS.

8.1 CTR Technology

One of the main objectives of this study is to develop performance data for a fleet of CTR in 10-, 30-, 90-, and 120-passenger configurations. Performance for all phases of flight, which include takeoff, climb, cruise, descent, and approach and landing are developed following OEM design process. Major areas that can benefit from additional analysis are listed below.

8.1.1 CTR Design

1) CTR design is highly dependent on the missions, which drive the design goals, such as weight, range, speed, and cruising altitude. Direct assessment of mission requirements from NextGen is desired.
2) A detail analysis of takeoff and landing profiles in the terminal area to assess engine rating structures and the impact on design is recommended.
3) Fuel burn performance developed based on the CTR propulsion technology in this study could not match the targeted 2025 fuel burn performance of the conventional fixed-wing fleet. Reviewing airframe aerodynamic design technology is recommended for CTR to gain additional fuel efficiency.
4) A rigorous design study to define the benefit of noise reduction and emission requirements is recommended.
5) The relationship between cruise rpm and a balanced engine design needs to be investigated.

8.2 BADA and NAS Simulation

One of the major efforts of this study is to translate CTR performance data into BADA modeling format so that a NAS performance analysis can be developed to study tradeoffs of a fleet of CTR under the NextGen using NASA-developed Airspaces Concept Evaluation System (ACES).

1) BADA is strictly a fixed-wing performance and operations database. Strict VTOL hover operations are not possible, but the aircraft can transit to a very slow speed where the maneuver can be considered completed.
2) Modeling of the unique conversion modes allowed by the CTR airframe requires their performance be fit into a predetermined fixed-wing aircraft performance model structure.
3) Fuel flow in airplane mode can be modeled well for cruise and climb/descent as outlined in the verification tables data.
4) The BADA model is best used to set operating conditions at known ConOps values where the performance model was identified via trim data. BADA model formulation should NOT be used to extrapolate performance by any means. This was made clear in the airplane mode verification results; BADA model formulation is best used by targeting a specific altitude, at a specific airspeed, per a known operational schedule. No attempt should be made to apply maximum power to a BADA formulation to see what maximum airspeed can be reached, as an example.
5) Optimization of the CTR model within the BADA framework does not guarantee that the same fidelity will be obtained once rolled into ACES. For example, there are some standard BADA model entry coefficients for fuel flow, etc., that are not imported by ACES from the BADA formatted files.
6) The current CTR BADA files will make possible use of currently unused BADA model entries, which will require parsing from the BADA files for proper accuracy along with implementation in the ACES model.
7) ACES requires the use of the jet engine performance model for propulsion and fuel flow modeling. Thus the CTR performance, specifically for the conversion mode, needs to follow the model structure for BADA development for compatibility.
8) Future ACES might best be updated to accommodate CTR by adding the ability to tilt the known thrust angle (or nacelle angle).
9) Terminal area operations are critical to CTR operations especially for NIO and RIO operations. A NAS performance analysis simulation, which includes en route, terminal, and vertiport, to fully evaluate CTR NAS performance is recommended.

8.3 NextGen ConOps

NextGen ConOps cover a wide range of concepts and capabilities envisioned for 2025. Key NextGen ConOps that will have direct impact to the operations of a fleet of CTR are:

1) RNAV/RNP, which provides performance-based navigation procedures for the CTR fleet to operate in a narrowly developed airspace in the terminal area, with precision navigation to conduct NIO and RIO while maintaining safety.
2) 4DT, which will provide four-dimensional flight plans to both the operator and ANSP with uncertainties. 4DT will enhance the separation assurance as well as the capacity performance of the NAS. The CTR fleet will benefit from 4DT by optimizing the flight plans according to the current state of traffic and weather conditions at the terminal or desired destination.

3) Datalink Communication, which is a centerpiece of NextGen's net-centric operations, will provide surveillance, situation awareness, and communications between the cockpit and ATC service providers on the ground. Datalink communication will help CTR pilots manage the workload during the most demanding critical flight phases, i.e., takeoff and approach and landing. Pilots can also use Datalink to negotiate enhanced flight profiles with ANSP to effectively operate the CTR fleet.

Areas where NextGen needs to make adjustments to adopt a fleet of CTR are listed below:

1) Procedurally separated CTR flow corridors will be required to support NIO.
2) Takeoff and approach and landing procedures, and separation assurance performance requirements (e.g., RNP) that can support a CTR fleet that might share a common area or airspace with existing fixed-wing traffic.
3) Approach and landing procedures to accommodate a range of descent profiles.
4) To support RIO operations, separate takeoff and approach profiles for the CTR fleet will have to be developed according to location of vertiports. Maintaining safe separation from fixed-wing flight routes, and expected general aviation and helicopter traffic, while minimizing noise impact within limited airspace in the airport terminal area will be a challenge as demonstrated in this study.

8.4 CTR ConOps

The study suggests that there is a benefit to fielding a fleet of CTR based on the NIO and RIO assumptions. However, there are operational issues such as location of the vertiports, the number of vertiports, detail design of the RIO and NIO routes at the terminals, and transition from en-route airspace to the terminal areas. To fully maximize the potential of the CTR fleet in NAS, NIO and RIO are key operational concepts that have to be adopted under the NextGen. NASA's New Vehicle and System Integration project has demonstrated new traffic flow patterns in the Northeast Corridor (NEC). These assumptions will be carried into a follow-on effort in developing specific traffic flow, helipads/vertiports, and stub runways for the NAS performance analysis.

This study made a gross assumption regarding the RIO of the CTR fleet. Only taxi time to and from gate and vertiport was considered for the NAS performance analysis, and it was found that this taxi time did impact the delay performance of the CTR operations. However, how to operate the CTR out of terminal gates with consideration of rotor downwash and safety of the ground crew, and requirements for blade folding design if needed to mitigate passenger jet-way operations, were not considered. More efforts will be needed to address this segment of the flight operations.

Specific lessons learned from PITL simulation regarding CTR ConOps are listed below.

8.4.1 Lessons From PITL simulation

1) Traffic flow patterns for each CTR operating location (i.e., runway, taxiway, helipad, or vertiport), will need to be examined individually to account for existing fixed-wing traffic pattern, wind direction, clearance from ground structures, and noise abatement.
2) From past CTR studies and the PITL simulation, it is highly desired to have an augmented flight control system with auto flap and nacelle schedule to reduce pilot workload during the conversion mode, especially for a higher than normal glide slope angle approach, such as 6 or 9 degrees. Control law development in low speed is recommended to enhance the handling qualities in a high-precision and

high-workload environment. Flight deck automation, coupled with NextGen flight rules in support of RIO, will need to be addressed.

3) From past CTR studies and the PITL simulation, it is highly desired to have a well-tuned flight director to provide coupled navigation cues according to specific flight operations such as takeoff and approach and landing, especially for the steep descent profiles.

4) A decision altitude of 200 feet on approach and landing needs to be investigated, especially for the steep descent profiles. Due to higher descent rate, the pilot's workload to arrest the descent rate while making nacelle transitions under limited ground cues, and whether there is enough time to respond to off-nominal situation, should be addressed.

9 REFERENCES

1 Anon.: Civil Tiltrotor Missions and Applications: A Research Study. Boeing Commercial Airplane Co., Bell Textron, Inc., Boeing Vertol, NASA CR-177451, Nov. 1987.

2 Anon.: Civil Tiltrotor Missions and Applications: Phase II—The Commercial Passenger Market, Summary Final Report. Boeing Commercial Airplane Co., Bell Helicopter Textron, Inc., Boeing Helicopters, NASA CR-177576, Feb. 1991.

3 Anon. (Civil Tiltrotor Development Advisory Committee): Report to Congress in accordance with PL1-0-581, vol. 1, Final Report, Dec. 1995.

4 Johnson, J.; Stouffer, V.; Long, D.; and Gribko, J.: Evaluation of the National Throughput Benefits of the Civil Tiltrotor. NASA CR-2001-211055, Sept. 2001.

5 Stouffer, V.; Johnson, J.; and Gribko, J.: Civil Tiltrotor Feasibility Study for the New York and Washington Terminal Areas. NASA CR-2001-210659, Jan. 2001.

6 Johnson, W.; Yamauchi, G. K.; and Watts, M. E.: NASA Heavy Lift Rotorcraft Systems Studies. NASA/TP-2005-213467, Dec. 2005.

7 Acree, C. W., Jr.; Yeo, H.; and Sinsay, J. D.: Performance Optimization of the NASA Large Civil Tiltrotor. International Powered Lift Conference, London, UK, July 22–24, 2008.

8 Spivey, D.: Runway Independent Aircraft—Increasing the Capacity of Existing Airports. AIAA Paper 2002-5958, AIAA International Powered Lift Conference, Williamsburg, VA, Nov. 5–7, 2002.

9 Anon. (European Organization for the Safety of Air Navigation, Brussels, Belgium): User Manual for the Base of Aircraft Data (BADA)—Revision 3.6. EUROCONTROL Experimental Center (EEC) Note no. 10/04, July 2004.

10 Nuic, A.; Poinsot, C.; and Iagaru, M. G.: Advanced Aircraft Performance Modeling for ATM: Enhancements to the BADA Model. IEEE/AIAA 24th Digital Avionics System Conference, Washington D.C., Oct. 30–Nov. 3, 2005.

11 Anon. (Joint Planning and Development Office (JPDO), Washington, D.C.): Concept of Operations for the Next Generation Air Transportation System, Version 2.0, July 13, 2007.

12 Smith, D. E.; Wilkerson, J.; Montoro, G. J.; Coy, J.; and Zuk, J.: Technology Development for Runway Independent Aircraft. American Helicopter Society 39th Annual Forum, Phoenix, AZ, May 2003.

13 Wilkerson, Joseph B. and Smith, Roger L.: Aircraft System Analysis of Technology Benefits to Civil Transport Rotorcraft. NASA CR-2009-214594, June 2009.

14 Editorial Staff: Aviation Week, Aerospace Source Book 2006, The McGraw-Hill Companies, Jan. 16, 2006.

15 Trept, Ted; Sigl, David; and Robertson, D.: Development and Application of the PRESTO Air Vehicle Predesign Synthesis Methodology. American Helicopter Society 51st Annual Forum, Fort Worth, TX, May 9–11, 1995.

16 Magee, John P.: Design of the Bell 609 Civil Tiltrotor Aircraft. International Powered Lift Conference, London, UK, Sept. 2–4, 1998.

17 Rosenstein, H. and Clark, R.: Aerodynamic Development of the V-22 Tilt Rotor. AIAA/AHS/ASEE Aircraft Systems, Design, and Technology Meeting, Dayton, OH, Oct. 20–22, 1986.

18 Kingston, L. and DeTore, J.: Tilt Rotor V/STOL Aircraft Technology. Second European Rotorcraft and Powered Lift Aircraft Forum, Bueckeburg, Federal Republic of Germany, Sept. 20–22, 1976.

19 Couluris, G. J.; Phillips, J.; Hange, C. E.; and Wardwell, D. A.: CESTOL Impact on U.S. Airport Network Operations: Preliminary Analysis. International Power Lift Conference, London, UK, July 2008.

20 Phillips, J. D.: An Accurate and Flexible Trajectory Analysis. Society of Automotive Engineers (SAE) Paper 975599, World Aviation Congress and Exposition, Anaheim, CA, Oct. 1997.

21 Puentes, R. and Tomer, A.: Expect Delays: An Analysis of Air Travel Trends in the United States. Metropolitan Infrastructure Initiative Series No. 6, The Brookings Institution, Washington, D.C., Oct. 2009.

22 Trigeiro, W. W.; Szebrat, X. P.; and Fraser, S. B.: Effects of Civil Tiltrotor Service in the Northeast Corridor on En Route Airspace Loads. DOT/FAA/AOR-100/94/008, The MITRE Corporation, Bedford, MA, and McLean, VA, Oct. 1994.

23 Anon. (Federal Aviation Administration, U.S. Dept. of Transportation, Washington, D.C.): Runway Length Requirements for Airport Design. Advisory Circular 150/5325-4B, July 1, 2005.

24 Anon. (Joint Planning and Development Office (JPDO), Washington D.C.): NextGen Avionics Roadmap, Version 1.0., Oct. 24, 2008.

25 Anon. (Federal Aviation Administration, U.S. Dept. of Transportation, Washington, D.C.): Vertiport Design. Advisory Circular 150/5390-3, May 31, 1991.

26 Anon.: Research and Innovative Technology Administration, Bureau of Transportation Statistics, http://www.bts.gov/publications/journal_of_transportation_and_statistics/volume_07_number_01/html/paper_06/appendix_06_a.html. Accessed Dec. 2010.

27 Decker, W.A.: Evaluation of Two Cockpit Display Concepts for Civil Tiltrotor Instrument Operations on Steep Approaches. Piloting Vertical Flight Aircraft: A Conference on Flying Qualities and Human Factors, July 1, 1993, pp. 433–452.

28 Smith, D. E.; Wilkerson, J.; Montoro, G. J.; Coy, J.; and Zuk, J.: Technology Development for Runway Independent Aircraft. American Helicopter Society 39th Annual Forum, Phoenix, AZ, May 2003.

29 Anon. (Federal Aviation Administration, U.S. Dept. of Transportation, Washington, D.C.): Airport Winter Safety Operations. Advisory Circular 150/5200-30C, Dec 9, 2008.

30 Anon. (Federal Aviation Administration, U.S. Dept. of Transportation, Washington, D.C.): Design of Aircraft Deicing Facilities. Advisory Circular 150/5300-14B, Feb. 5, 2008.

31 Anon. (Federal Aviation Administration, U.S. Dept. of Transportation, Washington, D.C.): Ground Deicing and Anti-icing Program. Advisory Circular 120-60B, Dec. 20, 2004.

32 Anon. (Federal Aviation Administration, U.S. Dept. of Transportation, Washington, D.C.) Pilot Guide–Large Aircraft Deicing. Advisory Circular 120-58, Sept. 30, 1992.

33 Whittle, Richard: The Dream Machine: The Untold History of the Notorious V-22 Osprey. Simon & Schuster, New York City, NY, April 2010.

34 Blake, M. et al.: Advanced Vehicle Concepts and Implications for NextGen. Sensis Document No. 840-023053, Sensis Corporation, Syracuse, NY, submitted to NASA, Jan. 2010.

35 Blake, M.; Young, R.; Smith, J.; Wright, K.; Mediavilla, R.; and Wieland, F.: Advanced Vehicle Concepts in the Next Generation Air Transportation System. AIAA Paper 2009-7121, 9th AIAA Aviation Technology, Integration, and Operations Conference, Hilton Head, SC, Sept. 2009.

36 Young, L. A.; Chung, W. W.; Paris, A.; Salvano, D.; Young, R.; Gao, H.; Wright., K.; Miller, D.; and Cheng, V.: A Study of Civil Tiltrotor Aircraft in NextGen Airspace. AIAA Paper 2010-9106, 10th AIAA Aviation Technology, Integration, and Operations Conference, Fort Worth, TX, Sept. 2010.

37 Anon. (Joint Planning and Development Office (JPDO), Washington, D.C.): Concept of Operations for the Next Generation Air Transportation System, Version 3.2., Sept. 30, 2010.

38 Anon. (Joint Planning and Development Office (JPDO), Washington D.C.): Integrated Work Plan for the Next Generation Air Transportation System, Executive Summary, FY13. Oct. 1, 2010.

39 Anon. (Joint Planning and Development Office (JPDO), Washington D.C.): Next Generation Air Transportation System Enterprise Architecture (EA), Overview and Summary Information (AV-1), Sept. 30, 2010.

40 Anon. (Federal Aviation Administration, Dept. of Transportation, Washington, D.C.): NextGen Implementation Plan. http://www.faa.gov/nextgen/media/ng2010_implementation_plan.pdf, Mar. 2010. Accessed Oct. 2011.

41 Anon. (International Civil Aviation Organization, Montreal, Canada): Global Air Traffic Management Operational Concept, First Ed., 2005.

42 Anon. (EUROCONTROL Performance Review Commission and Federal Aviation Administration ATO Strategy and Performance Business Unit): U.S./Europe Comparison of ATM-Related Operational Performance. http://www.eurocontrol.int/prc/gallery/content/public/Docs/US_Europe_Comparison_of_ATM_Related_operational_performance.pdf, Oct. 2009. Accessed Oct. 2011.

43 Anon. (Massachusetts Institute of Technology, Cambridge, MA): MIT Airline Data Project. http://airlinedataproject.mit.edu. Accessed Oct. 2011.

44 Anon. (Federal Aviation Administration, Washington, D.C.): Destination 2025. http://www.faa.gov/about/plans_reports/media/Destination2025.pdf. Accessed Dec. 2010.

45 Anon. (Federal Aviation Administration, Dept. of Transportation, Washington, D.C.): Terminal Area Forecast (TAF). http://aspm.faa.gov/main/taf.asp/. Accessed Dec. 2010.

46 Anon. (Federal Aviation Administration, Washington, D.C.): Capacity Needs in the National Airspace System, 2007–2025: An Analysis of Airports and Metropolitan Area Demand and Operational Capacity in the Future, May 2007. http://www.faa.gov/airports/resources/publications/reports/media/fact_2.pdf. Accessed Dec. 2010.

47 Couluris, G. J.; Hange, C. E.; Wardwell, D. A.; Signor, D.; and Phillips, J.: A Potential Impact Analysis of ESTOL Aircraft on Newark Airport Operations. AIAA Paper AIAA-2007-6700, AIAA Modeling and Simulation Technologies Conference and Exhibit, Hilton Head, SC, Aug. 2007.

48 Anon. (Wyle Laboratories, Inc., Arlington, VA): Rotorcraft Noise Model, Technical Reference and User Manual (V7.2), Wyle Report WR 08-04, Oct. 2009. Revised April 2010.

49 Anon. (Federal Aviation Administration, Washington, D.C.): Integrated Noise Model (INM), Version 7.0, Technical Manual, FAA-AEE-08-01, Jan. 2008.

50 Anon. (Federal Aviation Administration, Washington, D.C.): Aviation Environmental Design Tool (AEDT) User Guide: Beta1c., Oct. 2010.

51 Anon. (Society of Automotive Engineers (SAE)): Procedure for the Calculation of Aircraft Noise in the Vicinity of Airports. SAE Aerospace Information Report (SAE AIR) 1845, SAE Committee A-21, Aircraft Noise, 1986.

52 Anon. (Federal Aviation Administration, Washington, D.C.): Integrated Noise Model (INM), Version 7.0, User's Guide, FAA-AEE-07-04, April 2007.

53 Anon. (Massachusetts Institute of Technology, Cambridge, MA): Aviation Environmental Portfolio Management Tool (APMT). http://web.mit.edu/aeroastro/partner/apmt/airimpact.html. Accessed Oct. 2011.

APPENDIX A. BADA OVERVIEW

This section summarizes the techniques employed by BADA for overall point mass simulation used in support of airspace studies. This includes equations of motion, theory of operation, and definition of aircraft operations logic. This particular study employs only the performance database format outlined in BADA, with final airspace ATM simulations taking place using the ACES software. However, a general background in the operation of the complete BADA software environment is beneficial to gain a good understanding of how the BADA models for the CTR aircraft were developed. Further detail regarding BADA theory and design is available (refs. A-1 and A-2).

A-1 BADA Equations of Motion and Theory of Operation

BADA uses a Total Energy Model (TEM) to emulate aircraft translation through the airspace taking into account:

- Aerodynamics—lift and drag
- Propulsive Thrust—including propulsive efficiency and fuel flow
- Gravitational Effects—through aircraft weight and burned fuel

Note that this utility is built around fixed-wing capabilities and operations. The overall state equation of the TEM uses a mass-varying kinetic approach:

$$(T-D)\,V_{TAS} = mg\dot{h} + mV_{TAS}\dot{V}_{TAS}\,.$$

where m, h, and V_{TAS} are airframe mass, inertial altitude and true airspeed parallel to the velocity vector. The technique models the rate of work acting on the aircraft via forces to rates of increase in potential and kinetic energy.

Rearrangement of this relation provides the following state equation used directly by BADA:

$$\dot{h} = \left(\frac{T-D}{mg}\right)V_{TAS}(ESF)\,.$$

ESF is the Energy Share Factor in this equation:

$$ESF = \left(1 + \frac{V_{TAS}}{g}\frac{dV_{TAS}}{dh}\right)^{-1}.$$

A fuel consumption model within BADA accounts for the change in aircraft mass over time as follows:

$$\dot{m} = -F\,.$$

Horizontal velocity is modeled in BADA with the following state equation:

$$V_H = V_{TAS}\cos(\gamma).$$

BADA allows the aircraft translational dynamics to be calculated in one of three modes:

- Speed and Throttle Controlled—Rate of climb/descent (ROCD) is calculated (most commonly used)
- ROCD and Throttle Controlled—Speed is calculated
- Speed and ROCD Controlled—Thrust is calculated

Note that for the tiltrotor, speed, power, and ROCD can be independent given the ability to control the engine nacelle (NAC) angle. Consequently, it was important to capture NAC angle as a configuration variable. In order to reduce the size of the required reference data trim matrix, the NAC configurations were limited to representative settings to be used under nominal operational conditions. Note that this does not allow for robust performance extrapolation for the BADA utility if alternate NAC configurations are simulated in the ATM scenarios.

The overall structure of the BADA utility contains the following major elements:

- Aircraft Specific—performance numbers (lift/drag/thrust and fuel flow/geometry)
- Operations—models aircrew/airframe procedural specifics ((CAS) schedules, etc.)
- Limitations—such as speed/altitude/propulsion limitations of safe operation
- Actions—calculation of the aerodynamic/propulsive/gravitational effects
- Motion—the TEM equations of motion

Atmospheric conditions are modeled within BADA allowing for both standard (International Standard Atmosphere (ISA)) and nonstandard conditions. Nonstandard conditions are emulated through alteration of sea level conditions with the atmospheric model propagated to the flight altitude.

A-2 BADA Flight Operations Defined

The airline procedures for climb, cruise, and descent phases are defined in the BADA Airline Procedure File (BADA.APF). This section presents the methodology used by BADA to generalize these phases of flight over the many aircraft entries in the performance database. The BADA airline procedures outlining velocity schedules for climb, cruise, and descent phases are shown in figures A-1through A-3 with generic variables shown that are customizable per airframe. Again, BADA is a fixed-wing performance database with a generic operations schedule built around that premise.

It is important to note that these schedules are presented for reference given the BADA performance data. ACES has an integrated system for defining altitude and airspeed schedules based on way-point specification, and that is what will be used in the final ACES implementation to best match the proposed flight operations of the CTR variants. The BADA operational formulation is presented in this appendix simply to document the complete set of entries found in the CTR variant BADA files and to provide necessary background to gain an understanding of how the CTR BADA entries were developed.

Figure A-1 presents the airline climb speed schedule followed by all aircraft within the BADA environment based on operating altitude and a known reference stall speed. The analyst may specify two entries (V_{CL1} and V_{CL2}) for the schedule, as well as a constant Mach number schedule (M_{CL}) to capture once the transition altitude is met or exceeded.

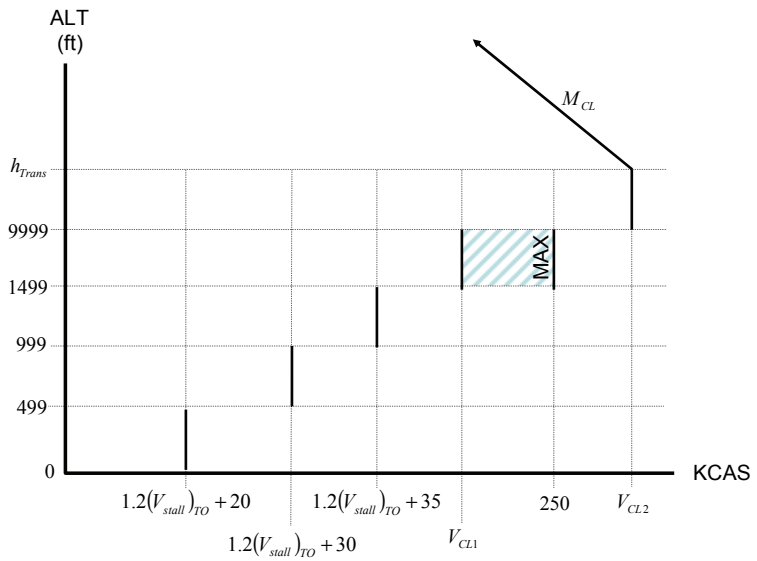

Figure A-1. BADA airline procedure KCAS schedule in climb.

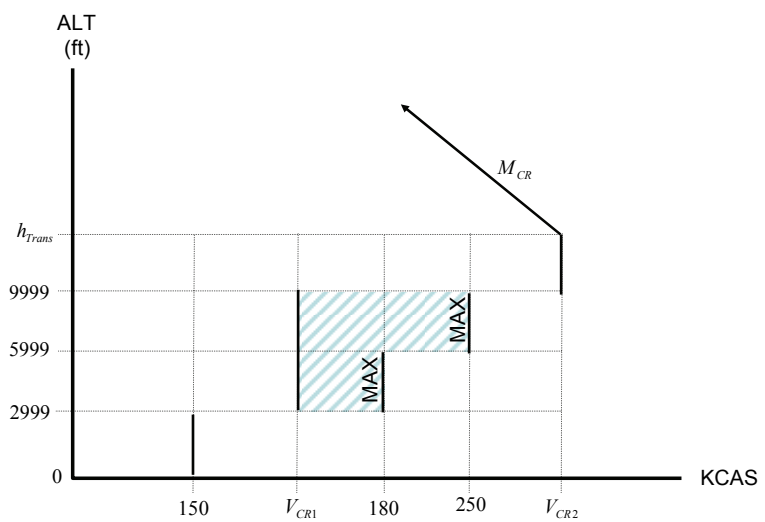

Figure A-2. BADA airline procedure KCAS schedule in cruise.

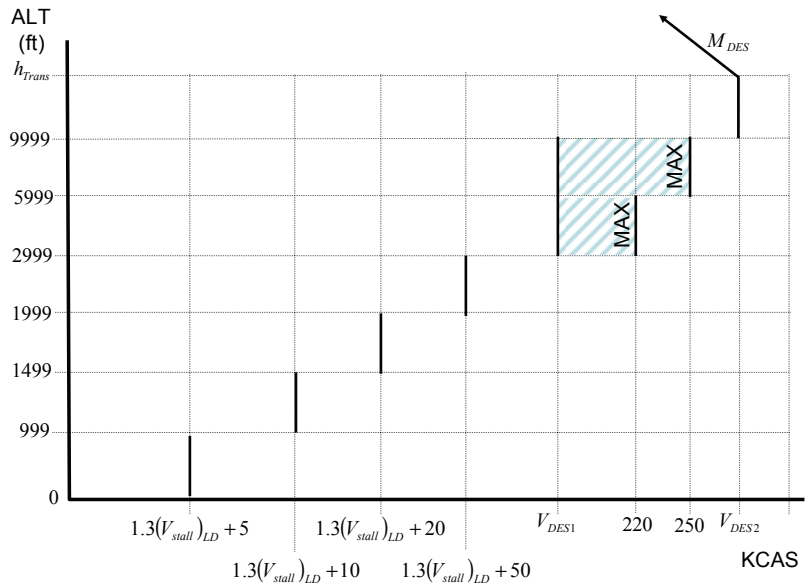

Figure A-3. BADA airline procedure KCAS schedule in descent.

Similarly, figure A-2 presents the airline cruise speed schedule based on operating altitude. Two entries (V_{CR1} and V_{CR2}) may be specified, as well as a constant Mach number (M_{CR}) to capture once the transition altitude is met or exceeded.

As an example of how to interpret the profiles, consider the climb KCAS schedule in figure A-1. This figure denotes that below 500 feet the airframe maintains ($1.2(V_{stall})_{TO} + 20$) KCAS, etc. Upon reaching 1,500 feet the airframe targets MIN(V_{CL1},250) KCAS. The remainder of the velocity schedules can be interpreted in a similar way. These schedule entries are configured to match those of the CTR variants as closely as possible given the limited customization available.

The airline descent schedule employed by BADA is shown in figure A-3 and can be interpreted in a similar fashion. All BADA airline operational procedure logic is well defined in the BADA documentation (ref. A-1).

A-3 BADA Airframe Configurations Defined

BADA allows for the definition of five discrete aerodynamic configurations for use throughout the operational envelope. These configurations are takeoff (TO), initial climb (IC), cruise (CR), approach (AP), and landing (LD). BADA uses an operations schedule that *automatically* defines whether the airframe is in the TO, IC, CR, AP, or LD configuration based on altitude, airspeed, and rate of climb or descent. These thresholds are currently defined in the BADA General Parameters File (BADA.GPF). The overall logic BADA uses to set the airframe aerodynamic configuration is shown in figure A-4. The primary altitude thresholds are as follows:

- Maximum TO configuration (H_{maxTO})—400 feet AGL
- Maximum IC configuration (H_{maxIC})—2,000 feet AGL
- Maximum AP configuration (H_{maxAP})—8,000 feet AGL
- Maximum LD configuration (H_{maxLD})—3,000 feet AGL

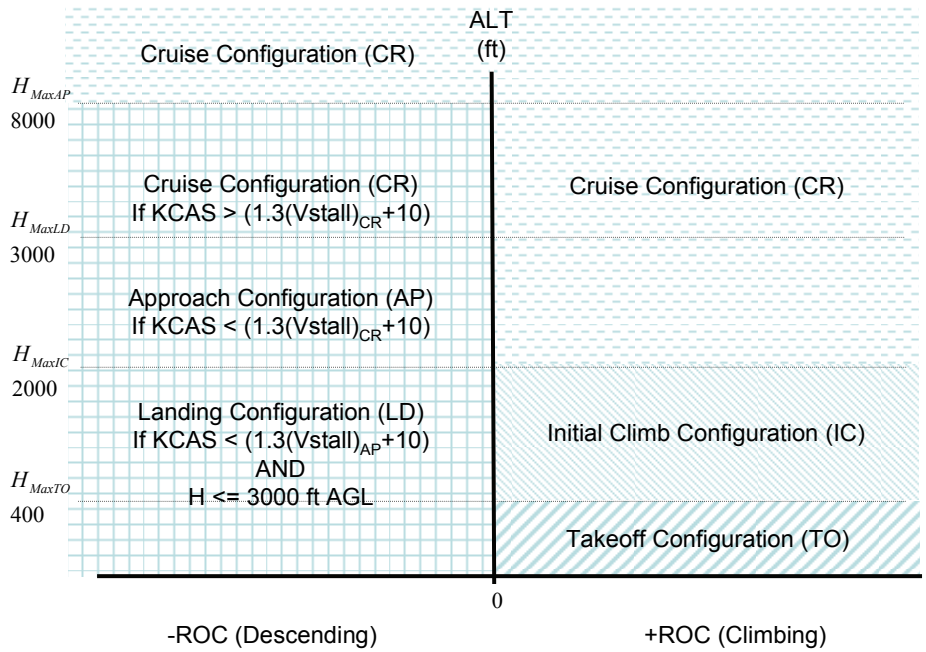

Figure A-4. BADA-defined airframe configurations based on ROCD and altitude above ground level (AGL).

Figure A-4 denotes rate of climb or descent on the X-axis and altitude AGL on the Y-axis. In level or climbing flight it indicates the airframe is in TO configuration up to 400 feet AGL with a transition to IC until 2,000 feet AGL is obtained. Beyond that the airframe enters the CR configuration. When in descent, the airframe remains in CR above 8,000 feet AGL but changes its aerodynamic configuration based on airspeed as shown.

Again, this information is shown for reference regarding how BADA defines airframe operations as generically as possible. In this study, ACES has an integrated user interface that allows for definition of waypoints, airframe configuration settings, and flight condition targets that are used in support of NextGen airspace simulations.

A-4 References

A-1. Nuic, A.: User Manual for the Base of Aircraft Data (BADA)—Revision 3.6. EUROCONTROL Experimental Center (EEC) Note No. 10/04, European Organization for the Safety of Air Navigation Brussels, Belgium, July 2004.

A-2. Nuic, A.; Poinsot, C.; and Iagaru, M. G.: Advanced Aircraft Performance Modeling for ATM: Enhancements to the BADA Model. IEEE/AIAA 24th Digital Avionics System Conference, Washington D.C., Oct. 30–Nov. 3, 2005.

APPENDIX B. AIRPLANE MODE PERFORMANCE TRIM MATRIX

Configuration: Cruise

Operations: Long-Range Cruise Power for Level Flight (PLF)

Purpose: Capture CR aerodynamics as well as propulsion performance across envelope. Mass variation required as indicated to capture parasite and induced drag effects. Long-range cruise velocity (VLRC) is set at velocity schedule for best range.

Case	Altitude (ft)	Weight (lbs)	KCAS	Power Setting	Landing Gear	Glide Slope (deg)	Atmosphere	NAC
1	0	MTOW	VLRC	PLF	Up	0	ISA	0
2	2,500	MTOW	VLRC	PLF	Up	0	ISA	0
3	5,000	MTOW	VLRC	PLF	Up	0	ISA	0
4	10,000	MTOW	VLRC	PLF	Up	0	ISA	0
5	15,000	MTOW	VLRC	PLF	Up	0	ISA	0
6	20,000	MMIN	VLRC	PLF	Up	0	ISA	0
7	20,000	MREF	VLRC	PLF	Up	0	ISA	0
8	20,000	MTOW	VLRC	PLF	Up	0	ISA	0
9	25,000	MTOW	VLRC	PLF	Up	0	ISA	0
10	30,000	MTOW	VLRC	PLF	Up	0	ISA	0

Configuration: Cruise

Operations: Maximum Continuous Power (MCP) Cruise at Level Flight

Purpose: Capture CR aerodynamics as well as propulsion performance across envelope. Mass variation required as indicated to capture parasite and induced drag effects. Identify MCP propulsion performance.

Case	Altitude (ft)	Weight (lbs)	KCAS	Power Setting	Landing Gear	Glide Slope (deg)	Atmosphere	NAC
1A	0	MTOW	Fallout	MCP	Up	0	ISA	0
2A	2,500	MTOW	Fallout	MCP	Up	0	ISA	0
3A	5,000	MTOW	Fallout	MCP	Up	0	ISA	0
4A	10,000	MTOW	Fallout	MCP	Up	0	ISA	0
5A	15,000	MTOW	Fallout	MCP	Up	0	ISA	0
6A	20,000	MMIN	Fallout	MCP	Up	0	ISA	0
7A	20,000	MREF	Fallout	MCP	Up	0	ISA	0
8A	20,000	MTOW	Fallout	MCP	Up	0	ISA	0
9A	25,000	MTOW	Fallout	MCP	Up	0	ISA	0
10A	30,000	MTOW	Fallout	MCP	Up	0	ISA	0

Configuration: Cruise

Operations: Maximum Continuous Power (MCP) Climb

Purpose: Capture propulsion performance across envelope for maximum power climb capability. Variation in atmospheric conditions captures the effect on propulsion performance at altitude. VCL is set at standard climb velocity schedule of 1.23 Vstall.

Case	Altitude (ft)	Weight (lbs)	KCAS	Power Setting	Landing Gear	Glide Slope (deg)	Atmosphere	NAC
11	0	MTOW	VCL	MCP	Up	Fallout	ISA	0
12	2,500	MTOW	VCL	MCP	Up	Fallout	ISA	0
13	5,000	MTOW	VCL	MCP	Up	Fallout	ISA	0
14	10,000	MTOW	VCL	MCP	Up	Fallout	ISA	0
15	10,000	MTOW	VCL	MCP	Up	Fallout	ISA+20	0
16	15,000	MTOW	VCL	MCP	Up	Fallout	ISA	0
17	20,000	MTOW	VCL	MCP	Up	Fallout	ISA	0
18	20,000	MTOW	VCL	MCP	Up	Fallout	ISA+20	0
19	25,000	MTOW	VCL	MCP	Up	Fallout	ISA	0
20	30,000	MTOW	VCL	MCP	Up	Fallout	ISA	0

Configuration: Cruise

Operations: Power for Descent (PFD—Idle/Low Power)

Purpose: Capture cruise descent thrust across the envelope. Each case captures three true airspeeds for variation.

Case	Altitude (ft)	Weight (lbs)	KCAS	Power Setting	Landing Gear	Glide Slope (deg)	Atmosphere	NAC
21	0	MREF	VDES1,2,3	PFD	Up	Fallout	ISA	0
22	2,500	MREF	VDES1,2,3	PFD	Up	Fallout	ISA	0
23	5,000	MREF	VDES1,2,3	PFD	Up	Fallout	ISA	0
24	10,000	MREF	VDES1,2,3	PFD	Up	Fallout	ISA	0
25	15,000	MREF	VDES1,2,3	PFD	Up	Fallout	ISA	0
26	20,000	MREF	VDES1,2,3	PFD	Up	Fallout	ISA	0
27	25,000	MREF	VDES1,2,3	PFD	Up	Fallout	ISA	0
28	30,000	MREF	VDES1,2,3	PFD	Up	Fallout	ISA	0

Configuration: Cruise

Operations: Maximum Continuous Power (MCP) Climb

Purpose: Capture maximum altitude at which aircraft no longer has the ability to climb. This point is defined as the maximum operational altitude of the aircraft.

Case	Altitude (ft)	Weight (lbs)	KCAS	Power Setting	Landing Gear	Glide Slope (deg)	Atmosphere	NAC
29	Fallout	MMIN	VCL	MCP	UP	0	ISA	0

Configuration: Cruise

Operations: Maximum Continuous Power (MCP) Climb

Purpose: Capture maximum altitude at which aircraft has a 300 fpm residual rate of climb available. Variation on weight and atmospheric conditions captures effect of those terms. These points gather the information necessary to define the service ceiling of the aircraft.

Case	Altitude (ft)	Weight (lbs)	KCAS	Power Setting	Landing Gear	Glide Slope (deg)	Atmosphere	NAC
30	Fallout	MMIN	VCL	MCP	Up	Fallout	ISA	0
31	Fallout	MREF	VCL	MCP	Up	Fallout	ISA	0
32	Fallout	MTOW	VCL	MCP	Up	Fallout	ISA	0
33	Fallout	MTOW	VCL	MCP	Up	Fallout	ISA	0

APPENDIX C. CONVERSION MODE PERFORMANCE MATRIX

VTOL/STOL APPROACH

Configuration: Approach/ Initial Climb (IC) (NAC set for approach)

Operations: VTOL/STOL Power for Level Flight (PLF)

Purpose: Capture AP/IC aerodynamics as well as propulsion performance. Mass variation required as indicated to capture parasite and induced drag effects.

Case	Altitude (ft)	Weight (lbs)	KCAS	Power Setting	Landing Gear	Glide Slope (deg)	Atmosphere	NAC
40	1,500	MMIN	110	PLF	Up	0	ISA	60
41	1,500	MREF	110	PLF	Up	0	ISA	60
42	1,500	MTOW	110	PLF	Up	0	ISA	60

Configuration: Approach (NAC set for approach)

Operations: VTOL/STOL Power for Descent (PFD)

Purpose: Capture AP aerodynamics as well as propulsion performance. These points capture performance over a range of glide slope angles.

Case	Altitude (ft)	Weight (lbs)	KCAS	Power Setting	Landing Gear	Glide Slope (deg)	Atmosphere	NAC
43	1,500	MREF	90	PFD	Up	–3	ISA	75
49	1,500	MREF	75	PFD	Up	–6	ISA	75
50	1,500	MREF	50	PFD	Up	–9	ISA	75

STOL LANDING

Configuration: STOL Landing (NAC set for STOL landing)

Operations: STOL Power for Level Flight (PLF)

Purpose: Capture STOL LD aerodynamics as well as propulsion performance. Mass variation required as indicated to capture parasite and induced drag effects.

Case	Altitude (ft)	Weight (lbs)	KCAS	Power Setting	Landing Gear	Glide Slope (deg)	Atmosphere	NAC
44A	200	MMIN	40	PLF	Up	0	ISA	90
45A	200	MREF	40	PLF	Up	0	ISA	90
47A	200	MTOW	40	PLF	Up	0	ISA	90

Configuration: STOL Landing (NAC set for STOL landing)

Operations: STOL Power for Descent (PFD)

Purpose: Capture STOL LD aerodynamics as well as propulsion performance. These points capture performance over a range of glide slope angles.

Case	Altitude (ft)	Weight (lbs)	KCAS	Power Setting	Landing Gear	Glide Slope (deg)	Atmosphere	NAC
48A	200	MREF	40	PFD	Up	–3	ISA	90
51A	200	MREF	40	PFD	Up	–6	ISA	90
52A	200	MREF	40	PFD	Up	–9	ISA	90

VTOL LANDING

Configuration: VTOL Landing (NAC set for VTOL landing)

Operations: VTOL Power for Level Flight (PLF)

Purpose: Capture VTOL LD aerodynamics as well as propulsion performance. Mass variation required as indicated to capture parasite and induced drag effects.

Case	Altitude (ft)	Weight (lbs)	KCAS	Power Setting	Landing Gear	Glide Slope (deg)	Atmosphere	NAC
44B	200	MMIN	20	PLF	Up	0	ISA	90
45B	200	MREF	20	PLF	Up	0	ISA	90
47B	200	MTOW	20	PLF	Up	0	ISA	90

Configuration: VTOL Landing (NAC set for VTOL landing)

Operations: VTOL Power for Descent (PFD)

Purpose: Capture VTOL LD aerodynamics as well as propulsion performance. These points capture performance over a range of glide slope angles.

Case	Altitude (ft)	Weight (lbs)	KCAS	Power Setting	Landing Gear	Glide Slope (deg)	Atmosphere	NAC
48B	200	MREF	20	PFD	Up	–3	ISA	90
51B	200	MREF	20	PFD	Up	–6	ISA	90
52B	200	MREF	20	PFD	Up	–9	ISA	90

STOL TAKEOFF

Configuration: STOL Takeoff (NAC set for STOL Takeoff)

Operations: STOL Power for Level Flight (PLF)

Purpose: Capture STOL TO aerodynamics as well as propulsion performance. Mass variation required as indicated to capture parasite and induced drag effects.

Case	Altitude (ft)	Weight (lbs)	KCAS	Power Setting	Landing Gear	Rate of Climb (fpm)	Atmosphere	NAC
37A	200	MMIN	100	PLF	Up	0	ISA	60
38A	200	MREF	100	PLF	Up	0	ISA	60
39A	200	MTOW	100	PLF	Up	0	ISA	60

Configuration: STOL Takeoff (NAC set for STOL Takeoff)

Operations: STOL Power for Ascent (PFA)

Purpose: Capture STOL TO aerodynamics as well as propulsion performance. These points capture performance over a rate of climb range.

Case	Altitude (ft)	Weight (lbs)	KCAS	Power Setting	Landing Gear	Rate of Climb (fpm)	Atmosphere	NAC
53A	200	MREF	100	PFA	Up	250 fpm	ISA	60
54A	200	MREF	100	PFA	Up	500 fpm	ISA	60
55A	200	MREF	100	PFA	Up	750 fpm	ISA	60

VTOL TAKEOFF

Configuration: VTOL Takeoff (NAC set for VTOL Takeoff)

Operations: VTOL Power for Level Flight (PLF)

Purpose: Capture VTOL TO aerodynamics as well as propulsion performance. Mass variation required as indicated to capture parasite and induced drag effects.

Case	Altitude (ft)	Weight (lbs)	KCAS	Power Setting	Landing Gear	Rate of Climb (fpm)	Atmosphere	NAC
37B	200	MMIN	20	PLF	Up	0	ISA	85
38B	200	MREF	20	PLF	Up	0	ISA	85
39B	200	MTOW	20	PLF	Up	0	ISA	85

Configuration: VTOL Takeoff (NAC set for VTOL Takeoff)

Operations: VTOL Power for Ascent (PFA)

Purpose: Capture VTOL TO aerodynamics as well as propulsion performance. These points capture performance over a rate of climb range.

Case	Altitude (ft)	Weight (lbs)	KCAS	Power Setting	Landing Gear	Rate of Climb (fpm)	Atmosphere	NAC
53B	200	MREF	20	PFA	UP	250 fpm	ISA	85
54B	200	MREF	20	PFA	UP	500 fpm	ISA	85
55B	200	MREF	20	PFA	UP	750 fpm	ISA	85

APPENDIX D. CTR30 AND CTR120 BADA MODEL DETERMINATION

D-1 CTR30 and CTR120 CTR BADA Model Determination

The process for developing the airplane mode BADA model given the performance data provided by Bell Helicopter was outlined in detail in section 3. The repeatable process was presented for the 10-passenger CTR vehicle. This appendix documents the supporting plots for the alternate CTR30 and CTR120 vehicles that were used in development of the corresponding airplane mode BADA models. Identical procedures were used as presented in section 3.4 for the CTR10.

D-1.1 Aerodynamics

This section presents plots of C_D versus C_L^2 and least-squares fit of a line through the consolidated data to provide the BADA drag equivalent system model in airplane mode. Combining all data in the fit provides a drag performance equivalent system model for use over all mission segments. Note that compressibility issues required the exclusion of the MCP cruise data points from the overall CTR30 drag model. The CTR120, built upon a complete design synthesis by Bell, did not encounter compressibility effects and made use of all trim data available. The total drag for the CTR30 and CTR120 in airplane mode is shown in figure D-1 and figure D-2 along with the final best fit and resulting coefficient of determination (R^2).

The MCP climb trim points were captured across the altitude envelope of the airframe following a speed schedule of 1.23 Vstall at MTOW. Results spanning the range of operational altitude were examined to yield the CR stall speeds as shown in tables D-1 and D-2.

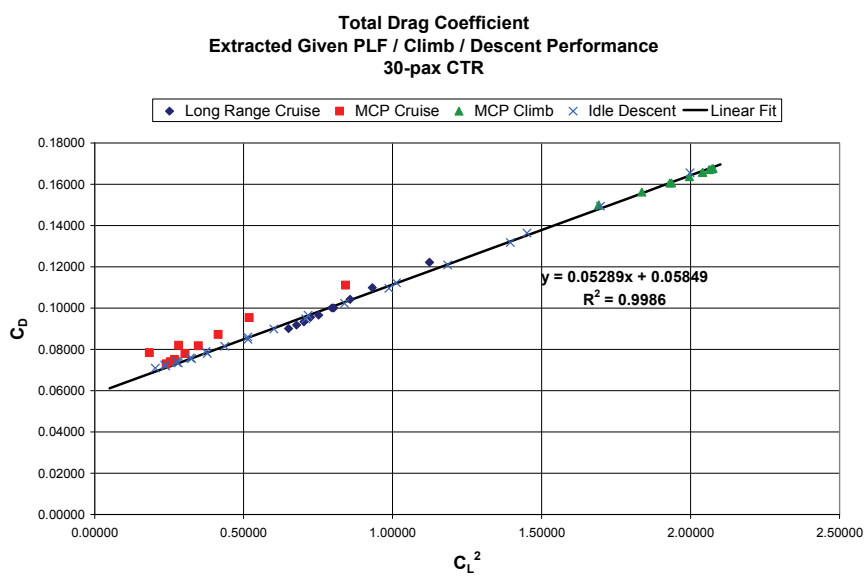

Figure D-1. Total airframe drag for the CTR30 in airplane mode (NAC 0 degrees) based on provided trim performance data.

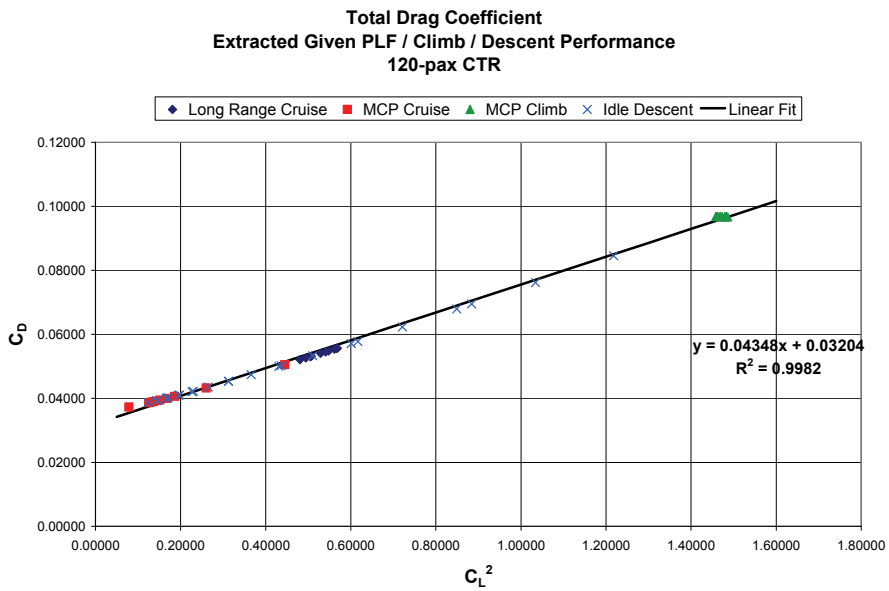

Figure D-2. Total airframe drag for the CTR120 in airplane mode (NAC 0 degrees) based on provided trim performance data.

TABLE D-1. CTR30 CALCULATED STALL SPEED IN CR CONFIGURATION (NAC 0 DEGREES)

Altitude (ft)	Vstall @ MTOW (46,430 lbs) (KCAS)	Vstall @ MREF (39,500 lbs) (KCAS)
25,000	132.2	121.9
15,000	129.2	119.2
0	127.6	117.7

TABLE D-2. CTR120 CALCULATED STALL SPEED IN CR CONFIGURATION (NAC 0 DEGREES)

Altitude (ft)	Vstall @ MTOW (147,648 lbs) (KCAS)	Vstall @ MREF (125,000 lbs) (KCAS)
30,000	123.5	113.6
25,000	123.5	113.6
15,000	123.4	113.6
0	123.4	113.6

Variations in stall speed across the envelope can be caused by small changes in overall wing configuration such as those imparted by automatic wing flap schedules. As BADA only allows for a single entry, the more conservative value of 121.9 KCAS was selected for the CTR30 in airplane mode. The entry of 113.6 KCAS was selected for the CTR120 airframe in airplane mode.

D-1.2 Propulsion

Trim data was collected across the altitude envelope for the CTR vehicles under various steady conditions. Figures D-3 and D-4 present the trim thrust for the CTR30 and CTR120 respectively, under MCP climb, MCP PLF, and LRC PLF conditions. The second-order least-squares fit for the MCP climb data results in the base maximum performance thrust model for the CTR vehicles.

As for the 10-passenger CTR, the BADA equivalent system model entries are calculated directly from the terms in the least-squares fit noted in figures D-3 and D4.

Low-power-descent trim data was used for modeling BADA descent thrust. The CTR30 and CTR120 descent profiles were trimmed across the altitude envelope over a series of three constant true airspeeds. The descent thrust ratio ($T_{des}/T_{max\ climb}$) is shown in figures D-5 and D-6 for the CTR30 and CTR120, respectively.

Given this information, 15k feet was the value selected for h_{des} to split the altitude envelope equally for both airframes. The final low-altitude value of $C_{Tdes,low}$ was determined by averaging all points available ≤15k feet. Likewise, the high-altitude value of $C_{Tdes,high}$ was determined by averaging all points ≥15k feet.

Nonstandard day (non-ISA) effects on the propulsion system are also modeled by BADA. Simplifying this formulation, $C_{T,c4}$ was set to zero for all CTR vehicles. Each CTR design was used to generate MCP climb trim data at 10k and 20k feet for ISA+20°C nonstandard day conditions to capture this effect. This was in addition to the ISA condition trim points already collected at those altitudes. For the CTR30 the maximum climb thrust ratio of non-ISA to ISA conditions was 0.9703 and 0.9501 for the 10k and 20k foot points, respectively. Similarly, for the CTR120 the maximum climb thrust ratio of non-ISA to ISA conditions was 0.9680 and 0.8518. Using an average value of the thrust ratio for each airframe, a single value of $C_{T,c5}$ was determined per CTR based on procedures outlined previously for the 10-passenger vehicle.

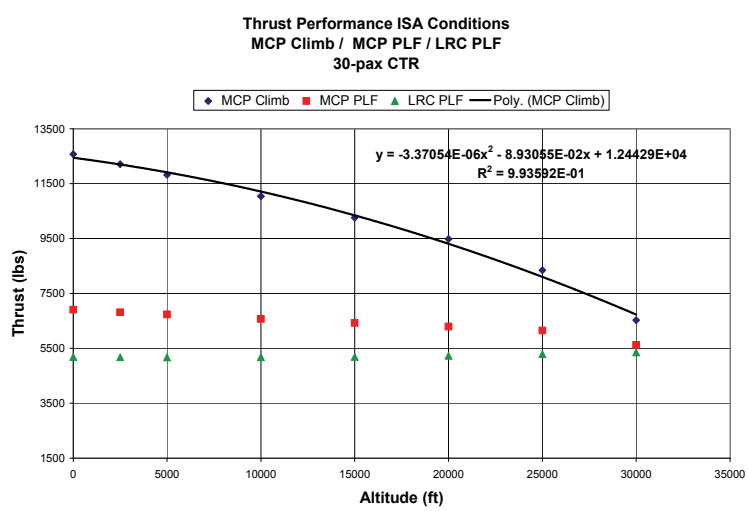

Figure D-3. Thrust performance for the CTR30 under various operating conditions.

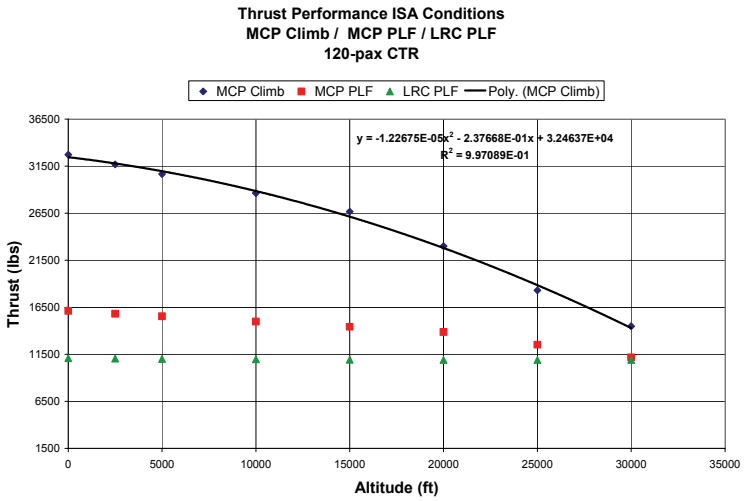

Figure D-4. Thrust performance for the CTR120 under various operating conditions.

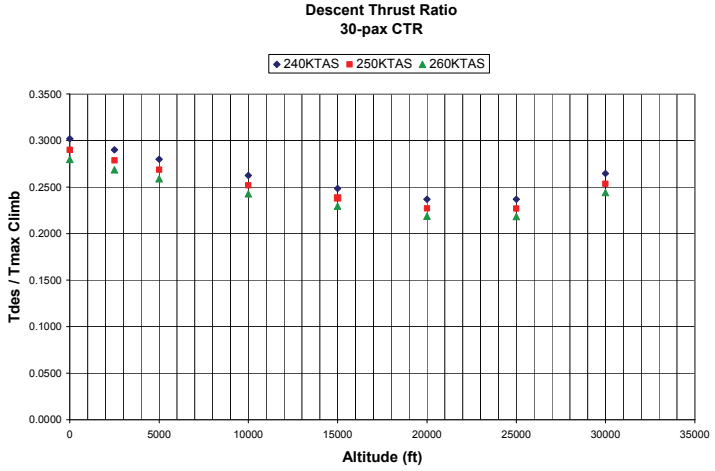

Figure D-5. Descent thrust ratio across altitude envelope for the CTR30.

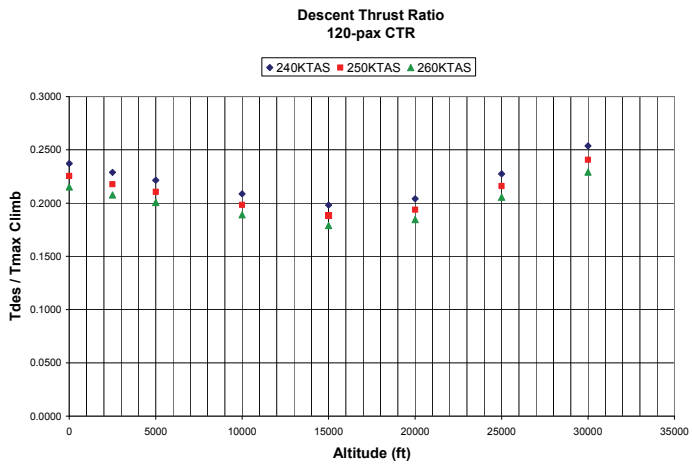

Figure D-6. Descent thrust ratio across altitude envelope for the CTR120.

Static trim data was also used to develop the fuel flow BADA model for each CTR vehicle. Fuel flow data for each vehicle was available under LR cruise, MCP cruise, MCP climb, and low-power-descent flight conditions. Figures D-7 and D-8 present values of η for the CTR30 and CTR120 vehicles for MCP climb, MCP cruise, and LR cruise conditions determined from provided trim data. The model for η was built given the linear fit (solid line) shown based on all available MCP climb data collected under ISA conditions.

The BADA scale factor C_{fCR} allows for better emulation of cruise fuel flow conditions. Using the MCP climb-based models shown in figures D-7 and D-8 results in an overall shortfall in fuel burned over any given cruise mission segment. This is consistent with findings for the 10-passenger airframe.

In the case of the CTR30 a final value for C_{fCR} of 1.0794 was determined for the cruise fuel flow scaling adjustment. The 120-passenger airframe uses a value of 1.1093. The dashed line presented in figures D-7 and D-8 is the final cruise condition formulation of η used by the CTR30 and CTR120 BADA model, respectively.

Performance trim data was collected in the descent configuration for each CTR variant over a series of three constant true airspeeds across the altitude envelope. This data was used to develop the low-power/idle thrust model in the BADA formulation. The CTR30 and CTR120 descent thrust performance data is shown in Figures D-9 and D-10. This performance data was used to build the low-power/idle-descent fuel flow model with terms in the linear fit used to calculate C_{f3} and C_{f4}. The linear fit shown is based on the consolidated data set for 240, 250, and 260 KTAS points.

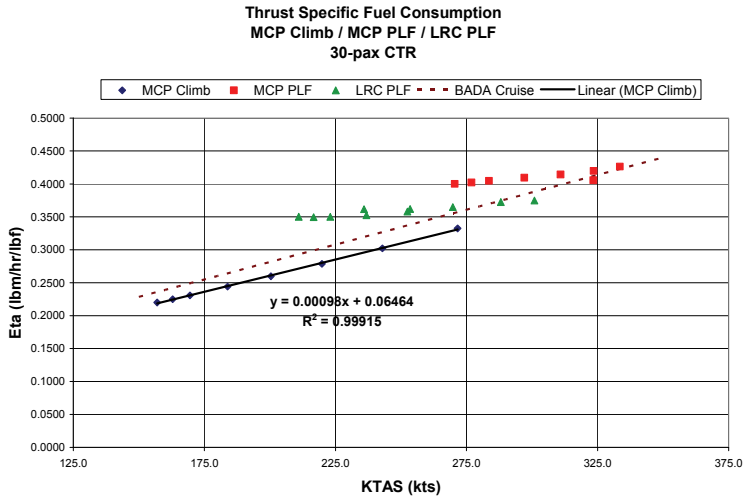

Figure D-7. TSFC for the CTR30 over various mission phases.

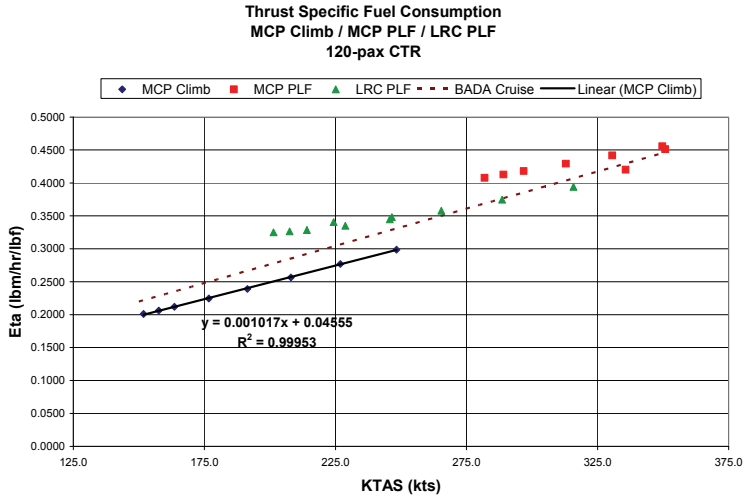

Figure D-8. TSFC for the CTR120 over various mission phases.

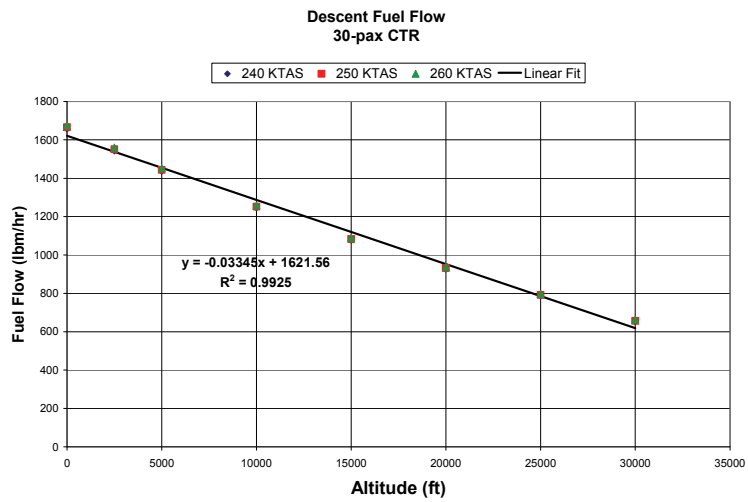

Figure D-9. Low-power-descent fuel flow for the CTR30 vehicle.

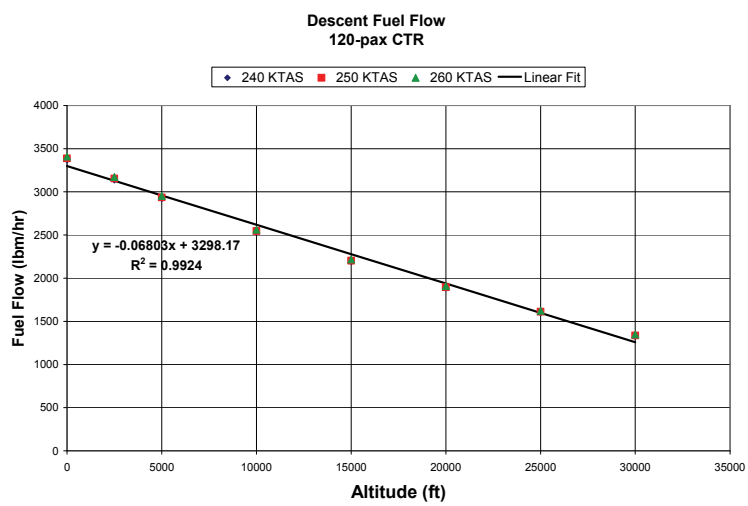

Figure D-10. Low-power-descent fuel flow for the CTR120 vehicle.

D-1.3 Flight Envelope Limitations

BADA provides several terms for specification of flight envelope limitations. Trim data collected from each CTR variant were used to identify various altitude limitations. The value for h_{MO} denotes the absolute maximum operating altitude when the aircraft has no residual rate of climb available. This value was supplied as a direct result of a performance trim point for each CTR configured for minimum mass (M_{min}). In the case of the CTR30 this value was 42,118 feet. The CTR120 has an absolute ceiling of 45,368 feet.

A series of trim points configured for M_{min}, M_{ref}, and M_{max} for each CTR variant was also collected to determine the altitude under ISA conditions (h_{max}) where the CTR has a 300-fpm residual rate of climb available. These points result in the determination of terms h_{max} and G_w. The value for h_{max} denotes the altitude under MTOW conditions whereas G_w captures the effect of gross weight variation from MTOW. The

necessary data to determine this characteristic for the CTR30 is shown in figure D-11, and data for the CTR120 is presented in figure D-12. The resulting CTR30 BADA entries for h_{max} and G_W are 32,138 feet and 1.3679 feet/kg based on the linear fit shown. The 120-passenger BADA entries for h_{max} and G_W are 31,659 feet and 0.4705 feet/kg.

The effect of non-ISA conditions on h_{max} was also captured via a single trim point per CTR vehicle. The value of h_{max} was determined at MTOW for both ISA and ISA+20°C conditions. This performance information was suitable to determine the atmospheric temperature effect G_t. In the case of the CTR30, G_t was determined to be –129.5 feet/degree C. In the case of the CTR120, G_t was determined to be –144.7 feet/degree C.

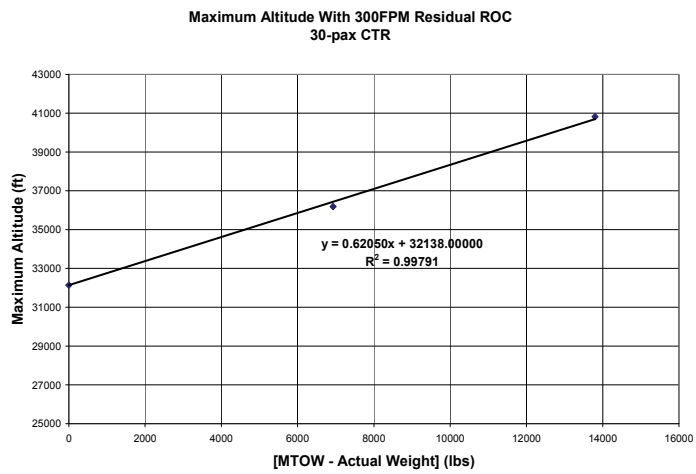

Figure D-11. Effect of gross weight variation from MTOW on maximum obtainable altitude with 300-fpm residual ROC available for the CTR30.

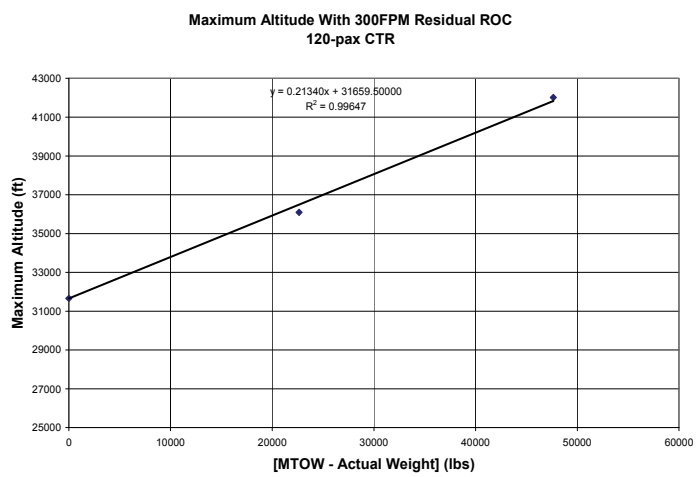

Figure D-12. Effect of gross weight variation from MTOW on maximum obtainable altitude with 300-fpm residual ROC available for the CTR120.

D-1.4 Flight Operations Schedule

As outlined in appendix A, BADA allows for limited customization of airspeed operational schedules for climb, cruise, and descent phases of the overall mission profile using a generic set of logic for all aircraft in the database.

The primary operating altitude range for the CTR30 is considered sea level to 25k feet while that of the CTR120 is sea level to 30k feet. Consider the climb speed schedule resulting from available trim points for the 30- and 120-passenger vehicles as shown in figures D-13 and D-14. The low-altitude climb speed V_{CL1} was determined as the average of the schedule speeds covering the range of 0k to 10k feet for both vehicles. The high-altitude climb speed V_{CL2} was determined as the average of the schedule speeds covering the range of 10k to 25k feet for the CTR 30- and 10k to 30k feet for the 120-passenger vehicles. The Mach schedule (M_{CL}) was determined as the Mach number corresponding to the actual trim point climb speed at 25k feet for the CTR30 and 30k feet for the CTR120. For the CTR30, this resulted in V_{CL1}, V_{CL2}, and M_{CL} of 157 KCAS, 161 KCAS, and 0.40 respectively. The CTR120 resulted in V_{CL1}, V_{CL2}, and M_{CL} of 152 KCAS, 153 KCAS, and 0.42 respectively.

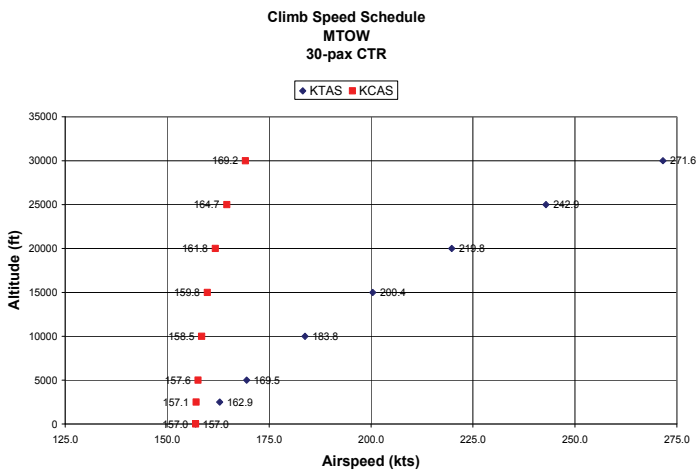

Figure D-13. Climb schedule over the altitude envelope for the CTR30 at MTOW and airplane mode.

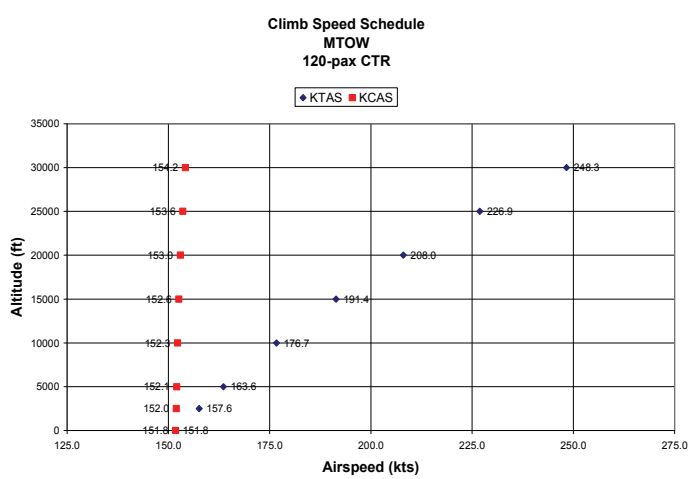

Figure D-14. Climb schedule over the altitude envelope for the CTR120 at MTOW and airplane mode.

Similarly, appendix A presented the airline cruise speed schedule based on operating altitude. Two entries (V_{CR1} and V_{CR2}) may be specified, as well as a constant Mach number (M_{CR}) to capture once the transition altitude is met or exceeded. V_{CR1} defines the constant speed schedule for the region of 3k up to 10k feet. V_{CR2} defines the constant speed schedule from 10k feet up to the transition altitude. Thereafter, M_{CR} is maintained by the aircraft.

The collected performance trim points for LR cruise, or speed for best range, supplied the airspeed schedule information required over the altitude envelope for each CTR to build the BADA cruise schedule. These points spanned the full altitude envelope and were configured at MTOW.

The LR cruise speed schedule for the CTR30 and CTR120 are shown in figures D-15 and D-16. The primary operating altitude range for the CTR30 is considered sea level to 25k feet while that of the 120-passenger is up to 30k feet. The low-altitude cruise speed V_{CR1} was determined as the average of the schedule speeds covering the range of 5k to 10k feet for both airframes. The high-altitude cruise speed V_{CR2} was determined as the average of the schedule speeds covering the range of 10k to 25k feet for the CTR30 and 10k to 30k feet for the CTR120. The Mach schedule (M_{CR}) was determined as the Mach number corresponding to the actual trim point cruise speed at 25k feet and 30k feet for the 30- and 120-passenger vehicles, respectively. For the CTR30, this resulted in V_{CR1}, V_{CR2}, and M_{CR} of 206 KCAS, 200 KCAS, and 0.48 respectively. The CTR120 resulted in V_{CR1}, V_{CR2}, and M_{CR} of 198 KCAS, 197 KCAS, and 0.54 respectively.

Finally, the airline descent schedule employed by BADA was shown in appendix A as a function of operating altitude and a known reference stall speed. Two airspeed entries (V_{DES1} and V_{DES2}), as well as a constant Mach number (M_{DES}), may be specified for the schedule. V_{DES1} defines the constant speed schedule for the region of 3k up to 10k feet. V_{DES2} defines the constant speed schedule from 10k feet up to the transition altitude. Thereafter, M_{DES} is maintained by the aircraft.

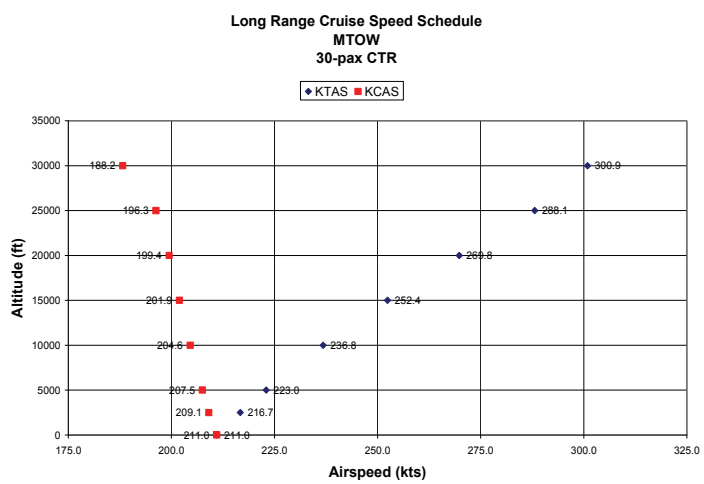

Figure D-15. Long-range cruise schedule over the altitude envelope for the CTR30 at MTOW and airplane mode.

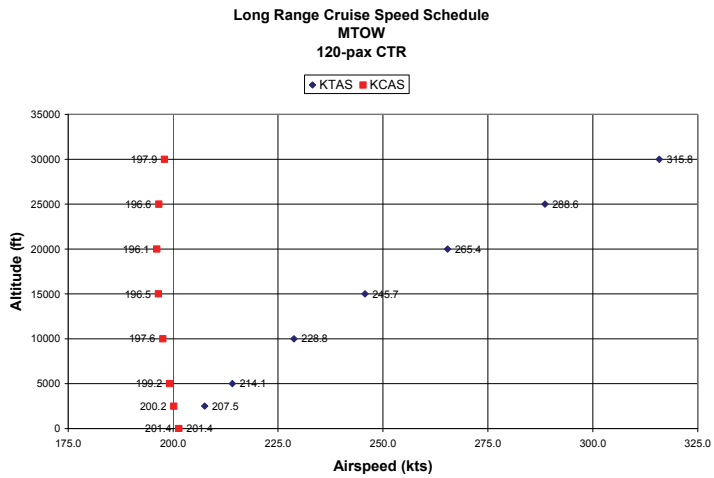

Figure D-16. Long-range cruise schedule over the altitude envelope for the CTR120 at MTOW and airplane mode.

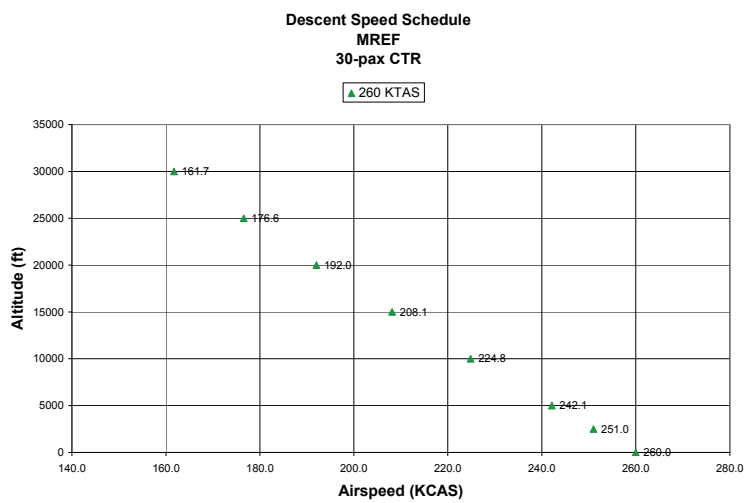

Figure D-17. Descent schedule for the CTR30 at MREF and airplane mode.

The collected performance trim points for descent supplied the airspeed schedule information required over the altitude envelope for each CTR to build the BADA descent schedule. These points spanned the full altitude envelope, were configured at MTOW, and were collected at constant true airspeeds of 240, 250, and 260 KTAS.

The descent speed schedule for the CTR30 and CTR120 are shown in figures D-17 and D-18. As for the 10-passenger vehicle, it was assumed the CTR will be following a continuous descent arrival (CDA) profile. Consequently, the higher speed schedule of 260 KTAS was selected to model the descent profile for BADA. The low-altitude descent speed V_{DES1} was determined as the average of the schedule speeds covering the range of 0k to 10k feet for both airframes. The high-altitude descent speed V_{DES2} was determined as the average of the schedule speeds covering the range of 10k to 25k feet for the CTR30 and 10k to 30k feet for the CTR120. The Mach schedule (M_{DES}) was determined as the Mach number corresponding to the actual trim point descent speed at 25k feet for the CTR30 and 30k feet for the 120-passenger vehicle. For the CTR30, this resulted in V_{DES1}, V_{DES2}, and M_{DES} of 244 KCAS, 200 KCAS, and 0.43 respectively. The 120-passenger vehicle resulted in V_{DES1}, V_{DES2}, and M_{DES} of 244 KCAS, 193 KCAS, and 0.44 respectively.

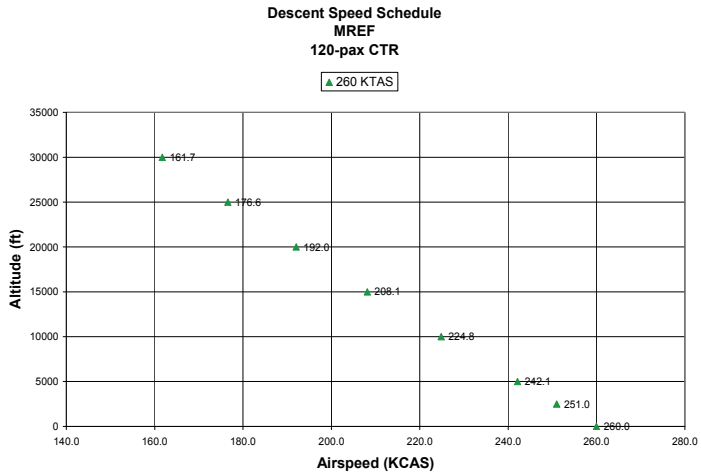

Figure D-18. Descent schedule for the CTR120 at MREF and airplane mode.

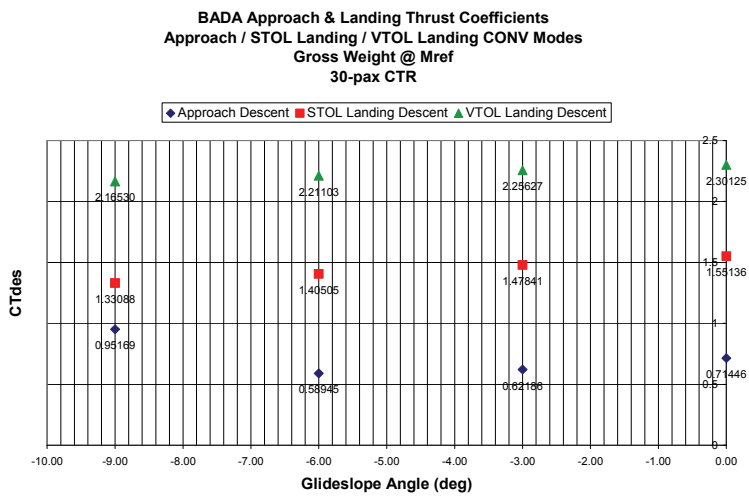

Figure D-19. Approach and landing descent thrust scale factor for the CTR30.

D-1.5 Conversion Mode Modeling

The process for development of the BADA conversion model is identical for the CTR10, CTR30, and CTR120. Section 3.4.5 outlined the details regarding development of the BADA conversion mode models using the 10-passenger CTR vehicle as an example. This section presents the supporting data for the 30- and 120-passenger vehicles. Consequently, the underlying analysis procedures for model development are identical to those described in section 3.4.5.

D-1.5.1 Conversion Mode Propulsion

The 30- and 120-passenger vehicle results for $C_{Tdes,app}$ and $C_{Tdes,ld}$ are shown in figures D-19 and D-20 as a function of glide slope angle. Determination of these parameters at the –3-, –6-, and –9-degree glide slope based on provided trim data allows for development of separate BADA files to emulate each operational approach angle. Each point in the plot is labeled with the corresponding C_{Tdes} value for reference.

The TO thrust scale factor for the CTR30 and CTR120 as a function of steady rate of ascent is shown in figures D-21 and D-22. The linear fits presented in these figures were used to extrapolate the required thrust scaling coefficient for the 1000 feet/minute takeoff ascent rate for use in the final BADA model. For the CTR30 this resulted in values of $C_{Tasc,to}$ of 0.9252 and 2.6798 for STOL and VTOL respectively. The CTR120 resulted in values of $C_{Tasc,to}$ of 1.1359 and 3.3814 for STOL and VTOL respectively.

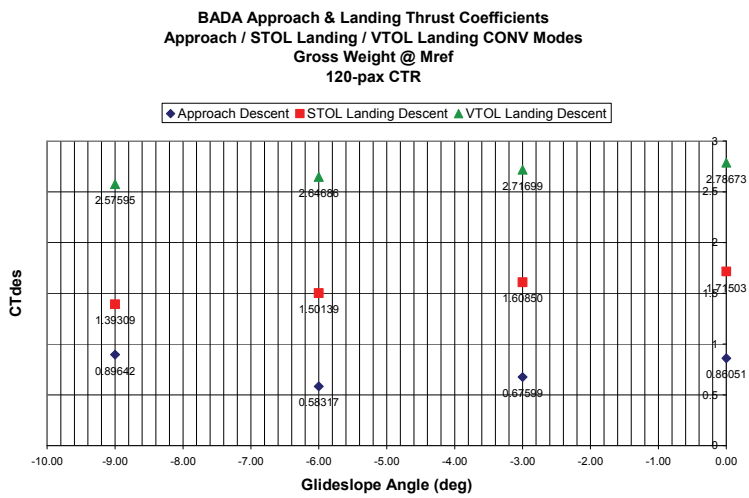

Figure D-20. Approach and landing descent thrust scale factor for the CTR120.

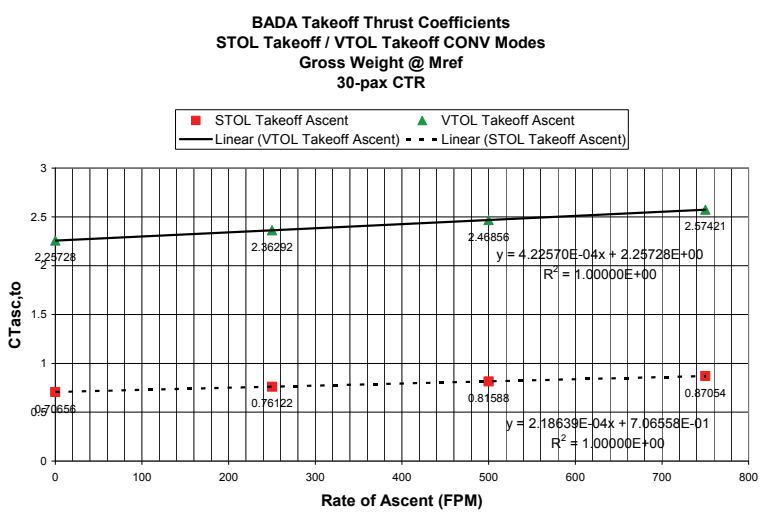

Figure D-21. Takeoff ascent thrust scale factor for the CTR30.

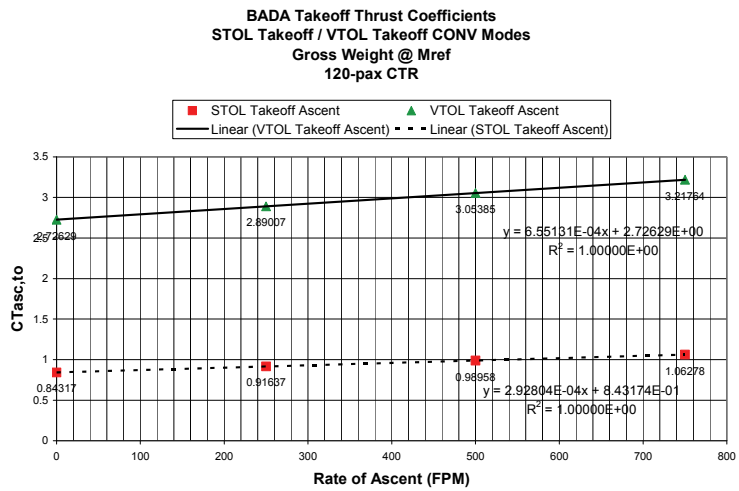

Figure D-22. Takeoff ascent thrust scale factor for the CTR120.

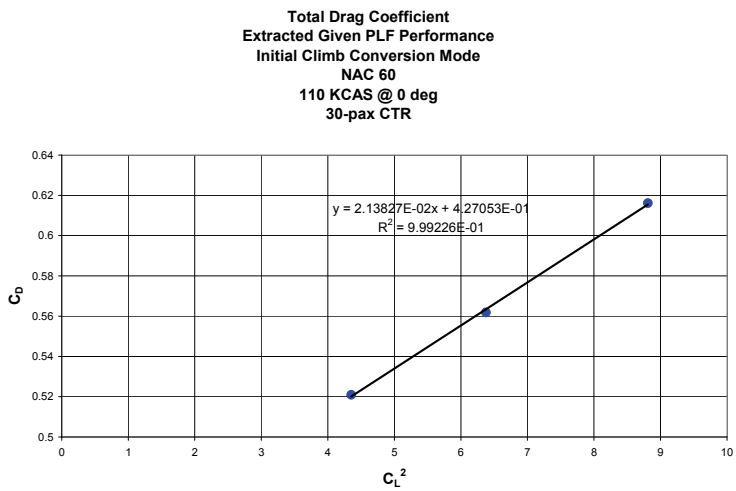

Figure D-23. Aerodynamics for IC mode of the CTR30.

D-1.5.2 Conversion Mode Aerodynamics

Figure D-23 was used to determine $C_{D0,IC}$ and $C_{D2,IC}$ for the CTR30 in IC mode under level flight conditions. Figure D-24 presents aerodynamic drag for approach conversion mode formulated using data at –3-, –6-, and –9-degree glide slope angles. Similarly, this plot was used to generate the BADA entries for $C_{D0,AP}$ and $C_{D2,AP}$ for the CTR30.

The least-squares fit shown in figure D-25 was used to determine $C_{D0,IC}$ and $C_{D2,IC}$ for the CTR120 in IC mode under level flight conditions. Figure D-26 presents aerodynamic drag for approach conversion mode formulated using data at –3-, –6-, and –9-degree glide slope angles. Similarly, this plot was used to generate the BADA entries for $C_{D0,AP}$ and $C_{D2,AP}$ for the CTR120.

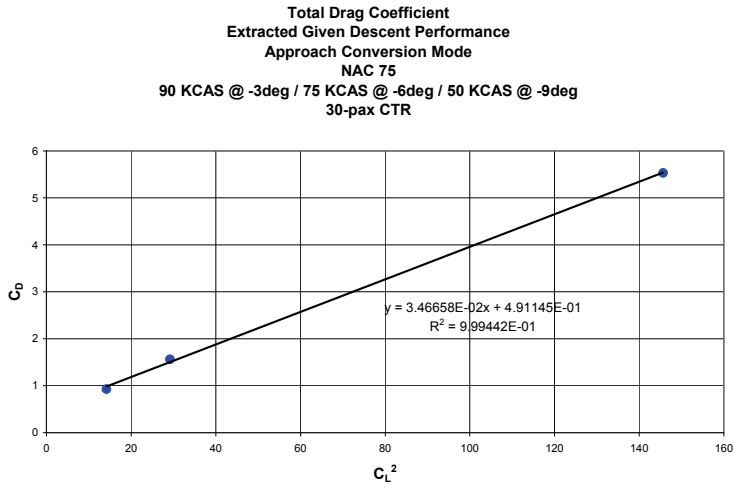

Figure D-24. Aerodynamics for AP mode of the CTR30.

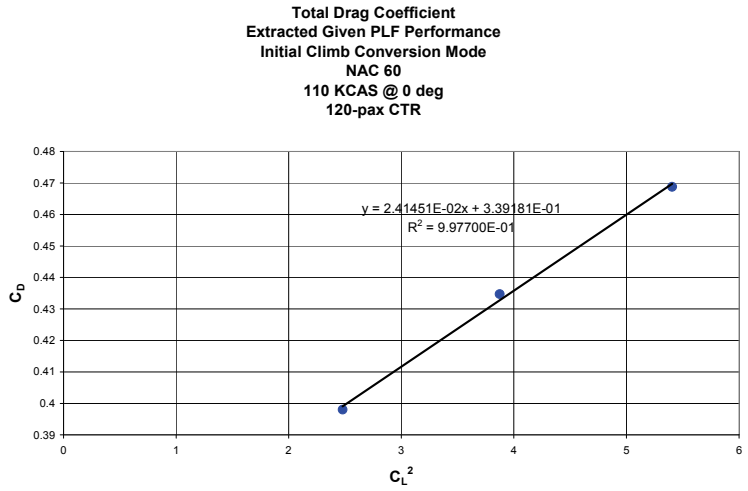

Figure D-25. Aerodynamics for IC mode of the CTR120.

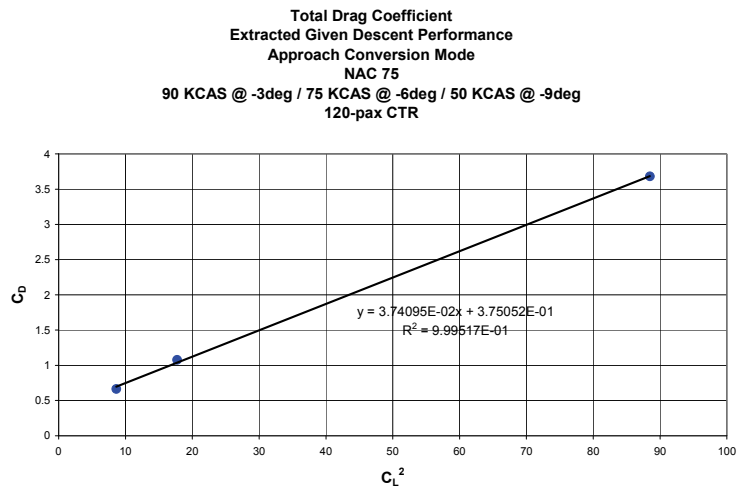

Figure D-26. Aerodynamics for AP mode of the CTR120.

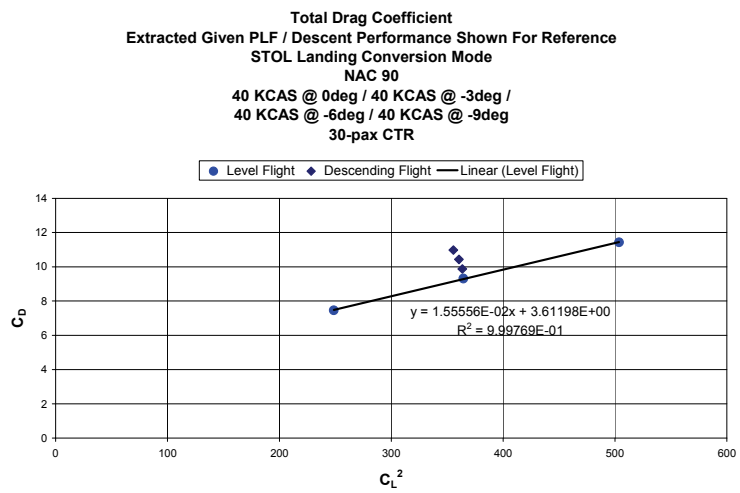

Figure D-27. Aerodynamics for STOL LD mode of the CTR30.

Aerodynamics for the STOL and VTOL LD conversion modes of the CTR30 are shown in figures D-27 and D-28. Similar information is shown in figures D-29 and D-30 for the TO conversion mode of the CTR30. The second-order least-squares fit as shown in figures D-31 and D-32 was used to extrapolate the C_{D0} term for the 1,000 feet/minute flight condition. The overall analysis is identical to that outlined for the 10-passenger vehicle in section 3.4.5.2.

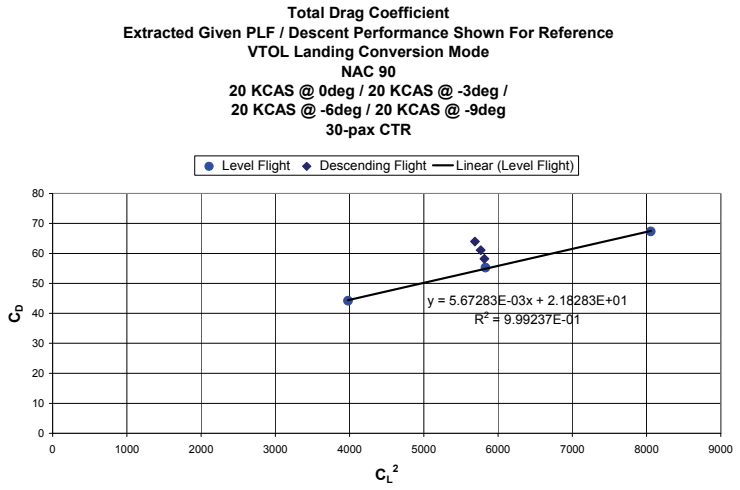

Figure D-28. Aerodynamics for VTOL LD mode of the CTR30.

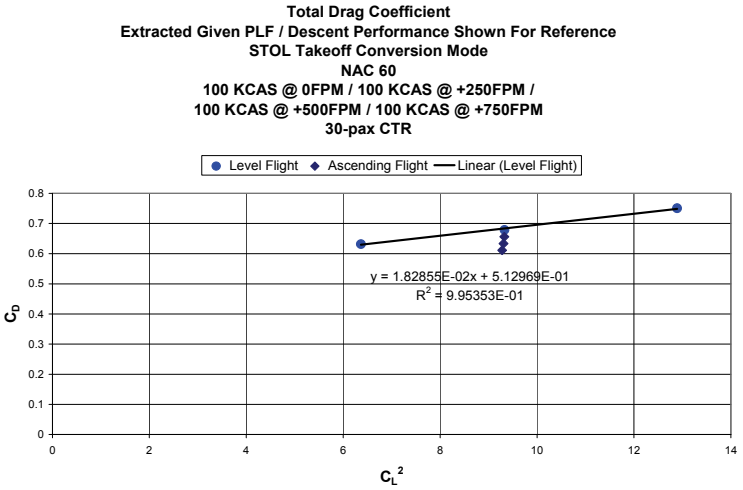

Figure D-29. Aerodynamics for STOL TO mode of the CTR30.

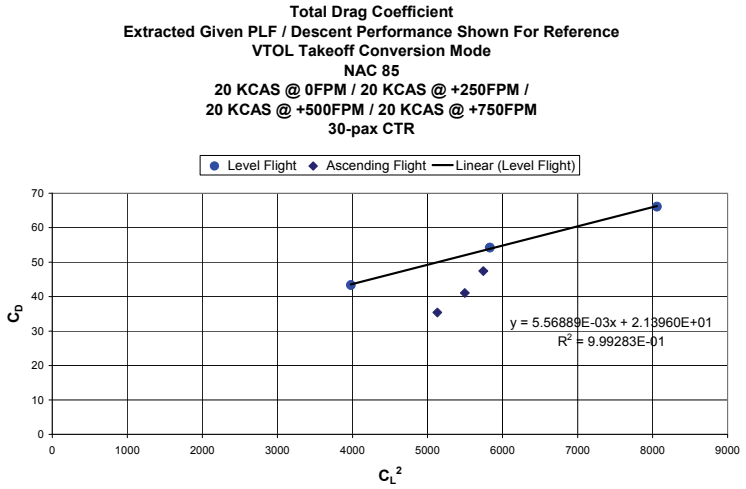

Figure D-30. Aerodynamics for VTOL TO mode of the CTR30.

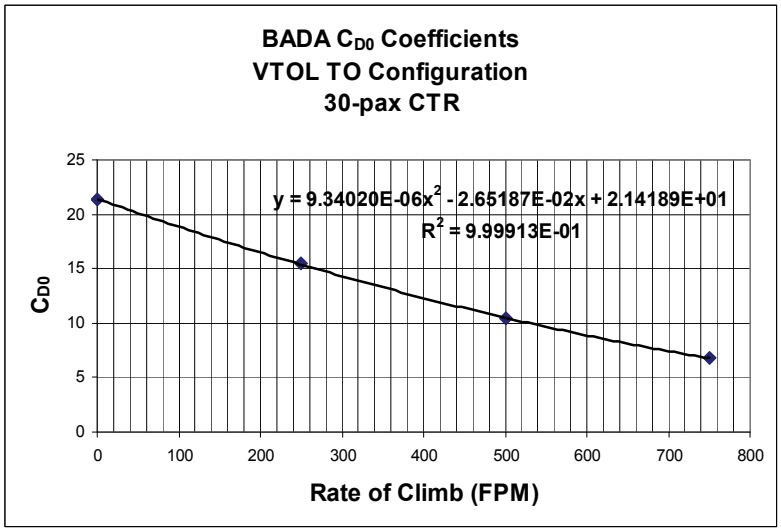

Figure D-31. Aerodynamics for VTOL TO mode of the CTR30.

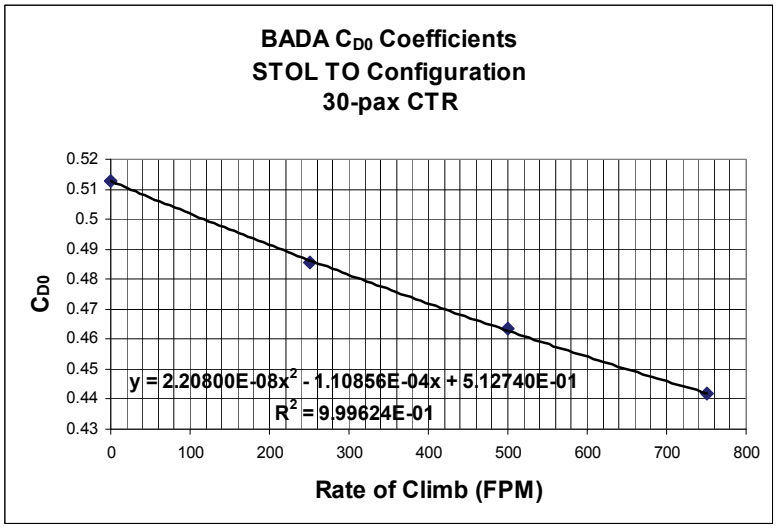

Figure D-32. STOL TO C_{DO} coefficients for the CTR30.

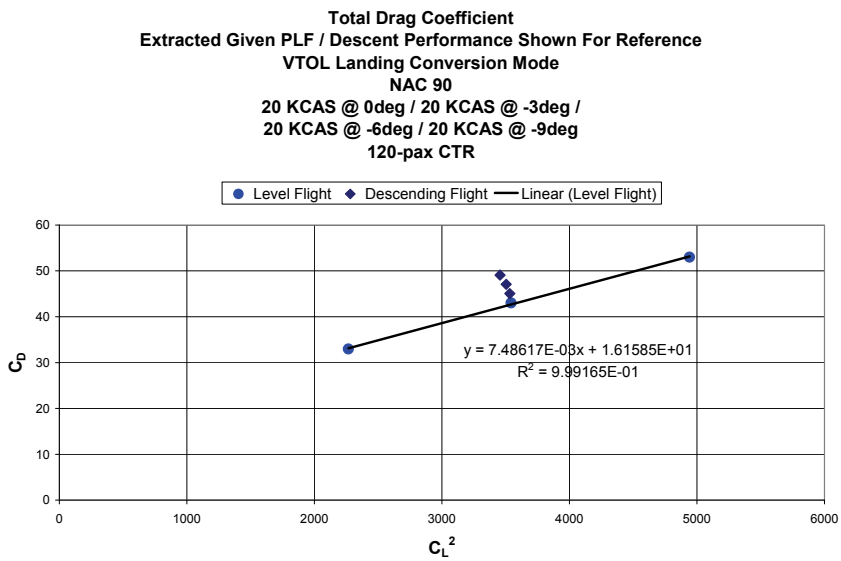

Figure D-33. Aerodynamics for VTOL LD mode of the CTR120.

Aerodynamics for the STOL and VTOL LD conversion modes of the CTR120 are shown in figures D-33 and D-34. Similar information is shown in figures D-35 and D-36 for the TO conversion mode of the CTR120. The second-order least-squares fit as shown in figure D-37 and D-38 was used to extrapolate the C_{D0} term for the 1000 feet/minute flight condition. The overall analysis is identical to that outlined for the 10-passenger vehicle in section 3.4.5.2.

The conversion mode stall characteristics for the 30- and CTR120 are identical to that specified for the 10-passenger CTR in section 3.4.5.2.

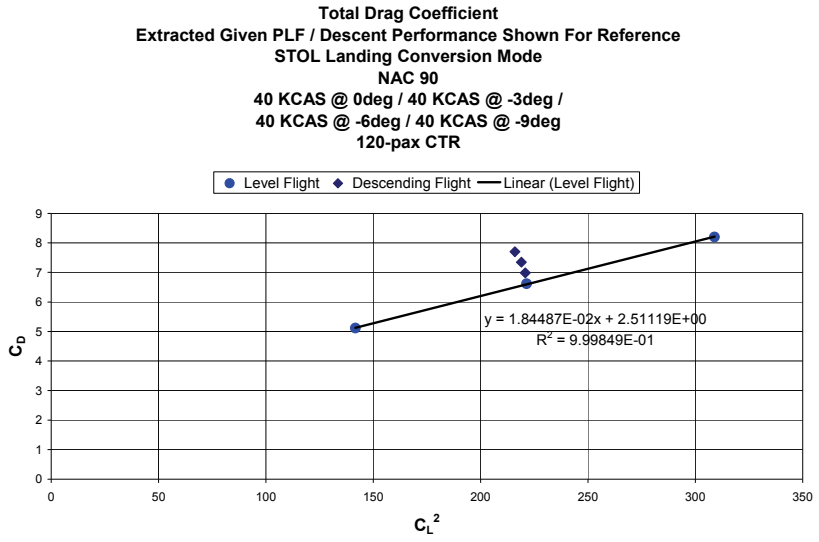

Figure D-34. Aerodynamics for STOL LD mode of the CTR120.

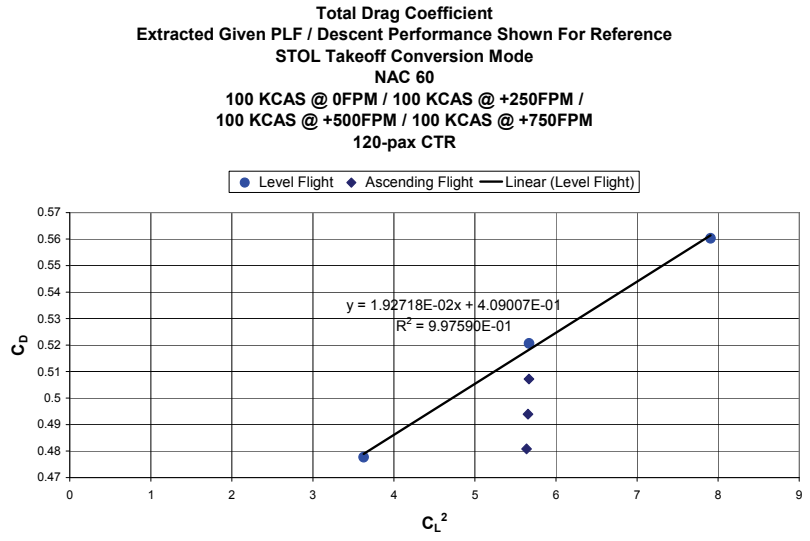

Figure D-35. Aerodynamics for STOL TO mode of the CTR120.

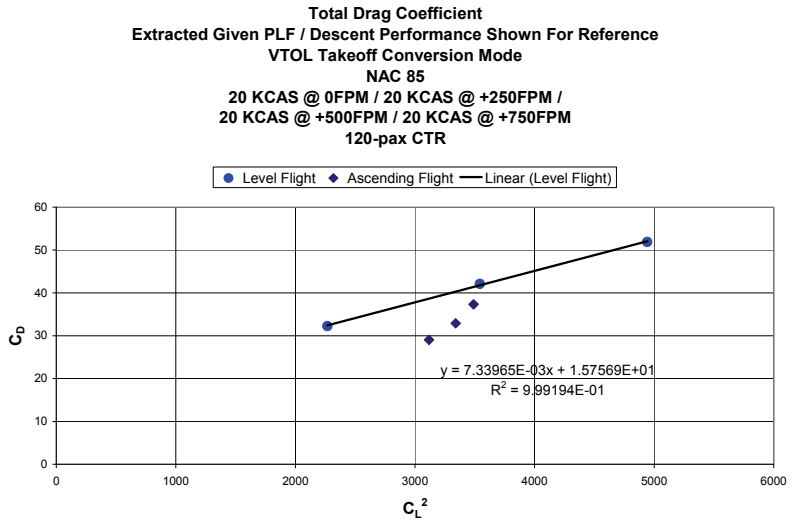

Figure D-36. Aerodynamics for VTOL TO mode of the CTR120.

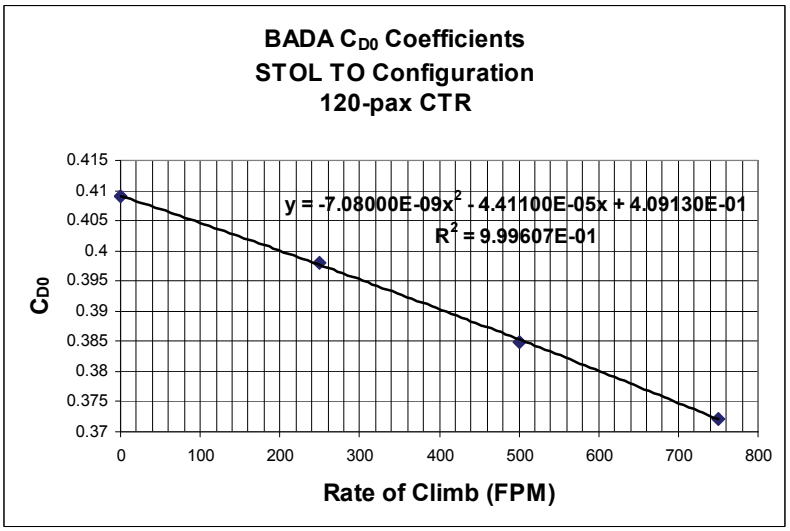

Figure D-37. STOL TO C_{DO} coefficients for the CTR120.

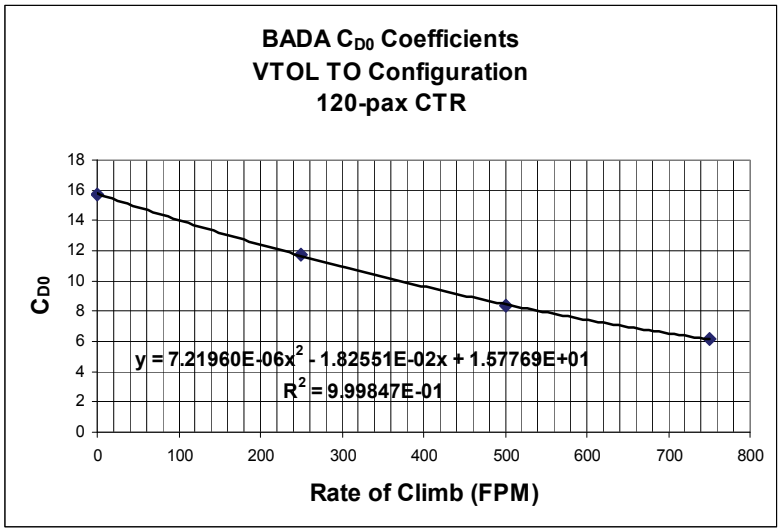

Figure D-38. VTOL TO C_{DO} coefficients for the CTR120.

APPENDIX E. CTR90 BADA MODEL LINEAR SIZING

E-1 Introduction

In support of the CTR in NextGen project, Science Applications International Corporation (SAIC) developed a CTR90 BADA model based on the BADA models generated for the CTR10, CTR30, and CTR120 airframes. The CTR10, CTR30, and CTR120 airframe BADA models were developed based on performance data supplied by Bell.

Overall, the 90-passenger BADA model is based on a scaling technique given the known BADA models and performance data of the other three airframes. The resulting 90-passenger BADA model may be employed in NAS NextGen studies in the second year of this project. References made herein regarding linear scaling of the CTR90 imply passenger capacity as the independent variable unless otherwise specified. Final BADA model coefficients for the CTR90 are presented in section 3 alongside data describing the other CTR vehicles.

Comparisons are made between the LCTR2 (90-passenger) CTR design developed by NASA Ames Research Center and the 90-passenger scaled model of this effort when data is available.

E-2 Geometry

The geometry of the CTR90, as used by BADA, was sized based on trends indicated using the 10-, 30-, and 120-passenger design data provided by Bell. Similar geometry data available for the NASA Ames LCTR2 (90-passenger) airframe was included when available.

The pertinent design geometry for use with BADA for the CTR10, CTR30, and CTR120 vehicles from section 2 are shown below in table E-1.

The following plots (figures E-1 through E-7) present this information in addition to a data point based on the NASA Ames LCTR2 (90-passenger) CTR vehicle for comparison. In most cases both a linear and second-order polynomial fit is presented for the CTR10, CTR30, and CTR120 data.

TABLE E-1. CTR10, CTR30, AND CTR120 SPECIFICATIONS FOR USE IN SIZING THE CTR90

Passenger Size	OWE (Mmin lbm)	Wingspan (ft)	Fuselage Length (ft)	Wing Area (ft^2)	MTOW (Mmax lbm)	Mref (lbm)	Mpayload (lbm)	Max Fuel (lbm)
10	11689	33.83	44	183.3	16800	15500	2611	2500
30	32630	45.8	61.667	382	46430	39500	6800	7000
120	100000	100.4	111.833	1550.9	147648	125000	26207	21441

E-2.1 Operational Weight Empty (OWE)

The scaled CTR90 uses the second-order fit below to estimate OWE with the fit anchored to the known CTR10, CTR30, and CTR120 data points. A comparison point is shown for the NASA LCTR2 reference design.

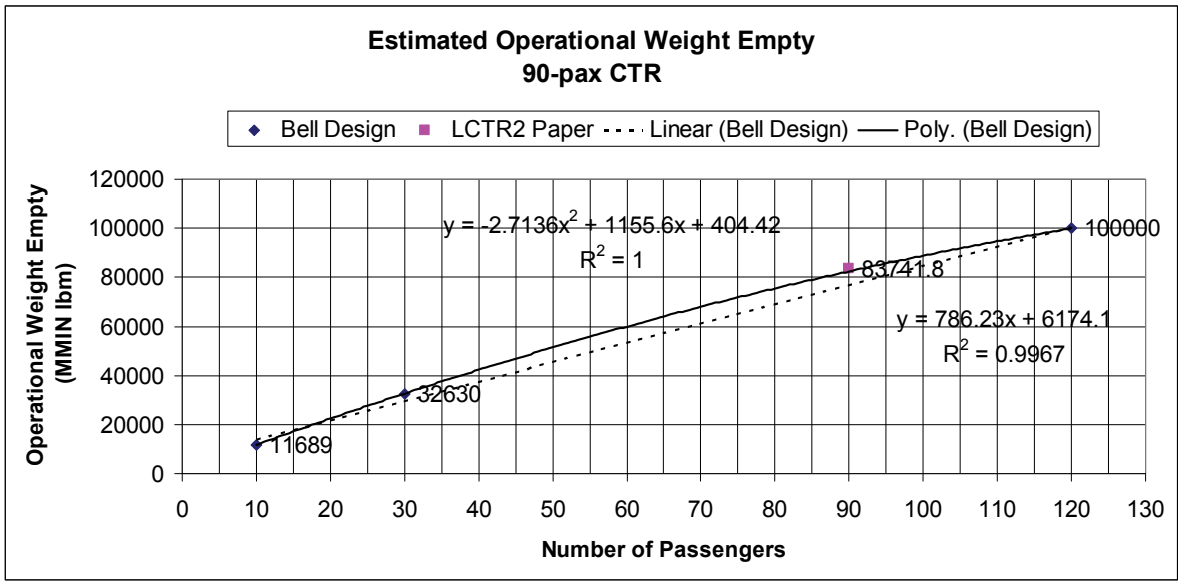

Figure E-1. Sizing the CTR90 OWE.

E-2.2 Wingspan

The scaled CTR90 uses the linear fit below to estimate wingspan. A comparison point is shown for the NASA LCTR2 design.

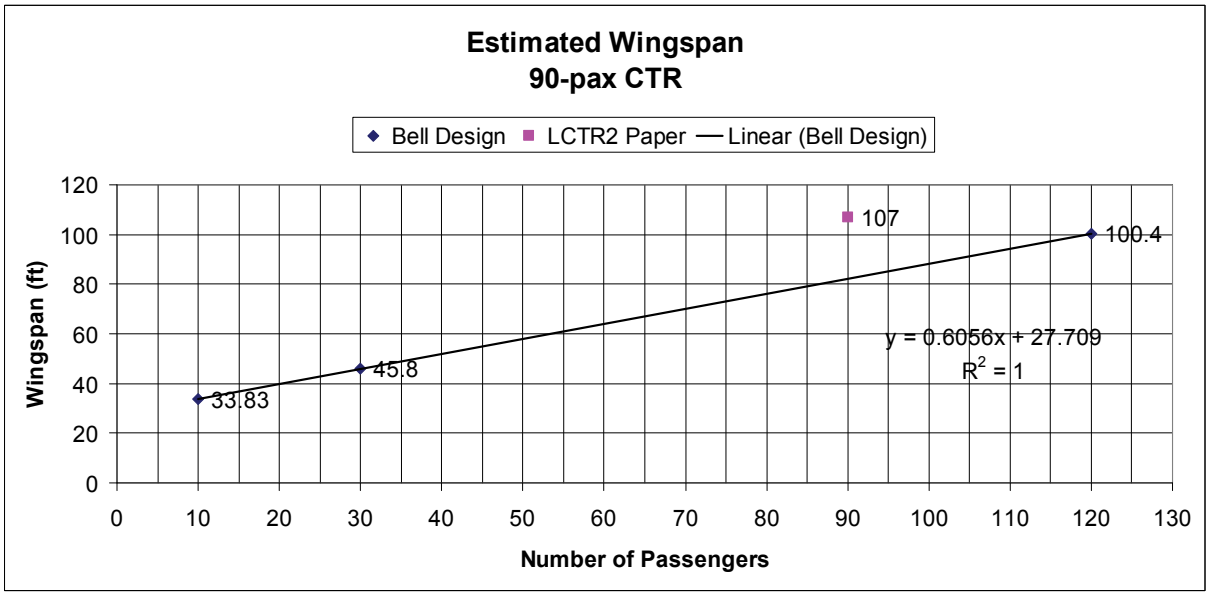

Figure E-2. Sizing the CTR90 wingspan.

A note regarding the NASA Ames LCTR2 CTR90 wingspan data point: The NASA design team added extended wing panel sections outboard of the engine nacelles. It is interesting that the "inner" wing span of the NASA Ames LCTR2 is 77 feet. This denotes the span of the wing panels out to the engine nacelles. The Bell-designed CTR vehicles have engine nacelles placed at the tip of the wing span with no outboard wing panels.

E-2.3 Fuselage Length

The scaled CTR90 uses the second-order fit below to estimate fuselage length with the fit anchored to the known CTR10, CTR30, and CTR120 data points. A comparison point is shown for the NASA LCTR2 design.

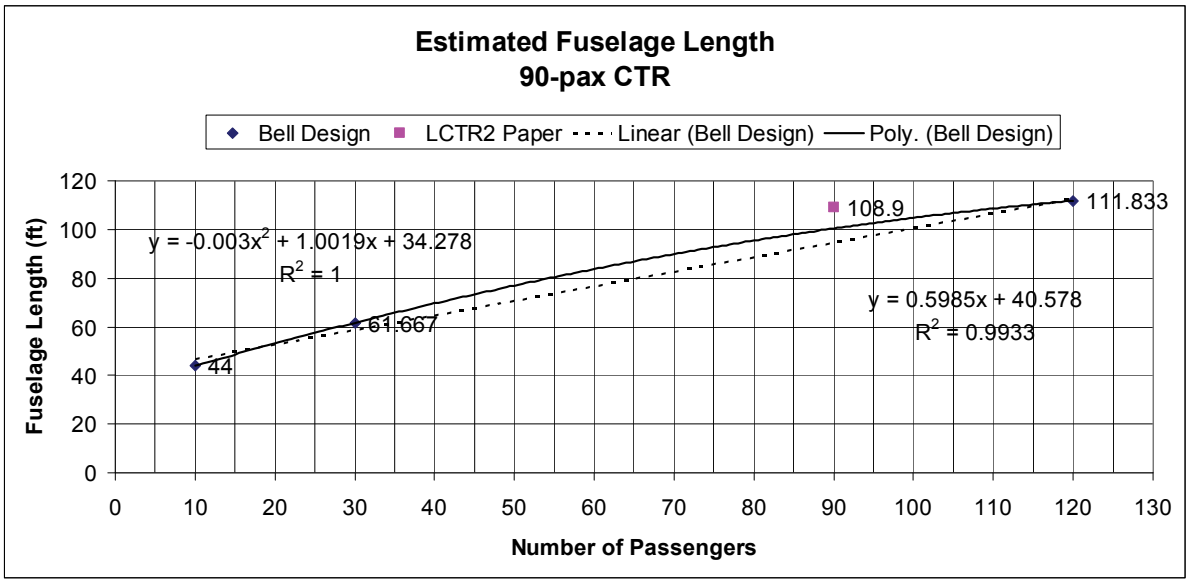

Figure E-3. Sizing the CTR90 fuselage length.

E-2.4 Wing Area

The scaled CTR90 uses the second-order fit below to estimate total wing area with the fit anchored to the known CTR10, CTR30, and CTR120 data points. A comparison point is shown for the NASA LCTR2 design.

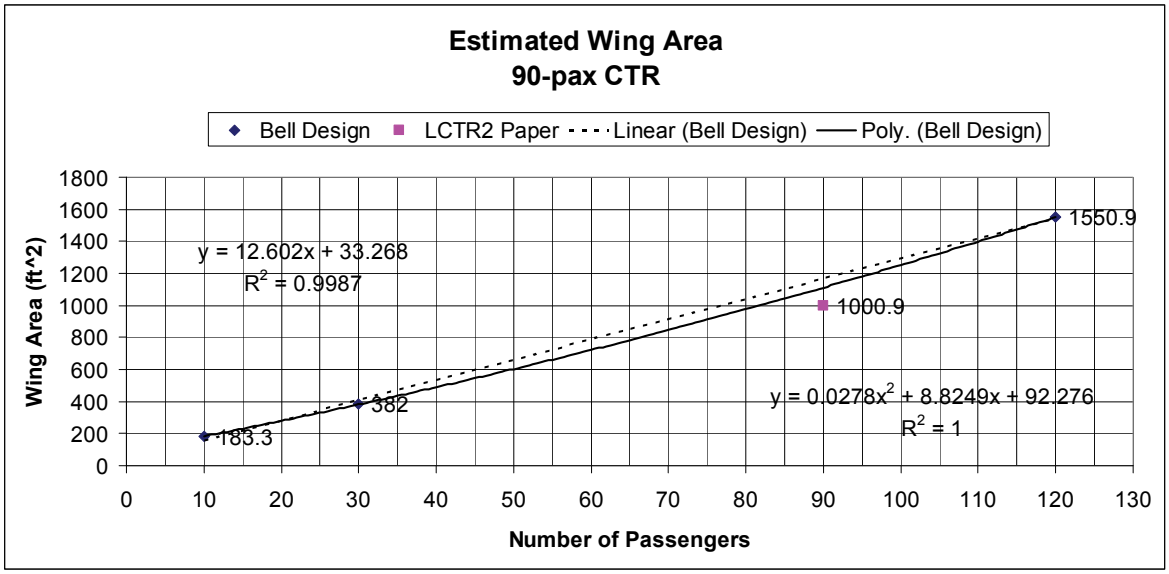

Figure E-4. Sizing the CTR90 wing area.

E-2.5 Maximum Takeoff Weight (MTOW)

The scaled CTR90 uses the second-order fit below to estimate total wing area with the fit anchored to the known CTR10, CTR30, and CTR120 data points. A comparison point is shown for the NASA LCTR2 design.

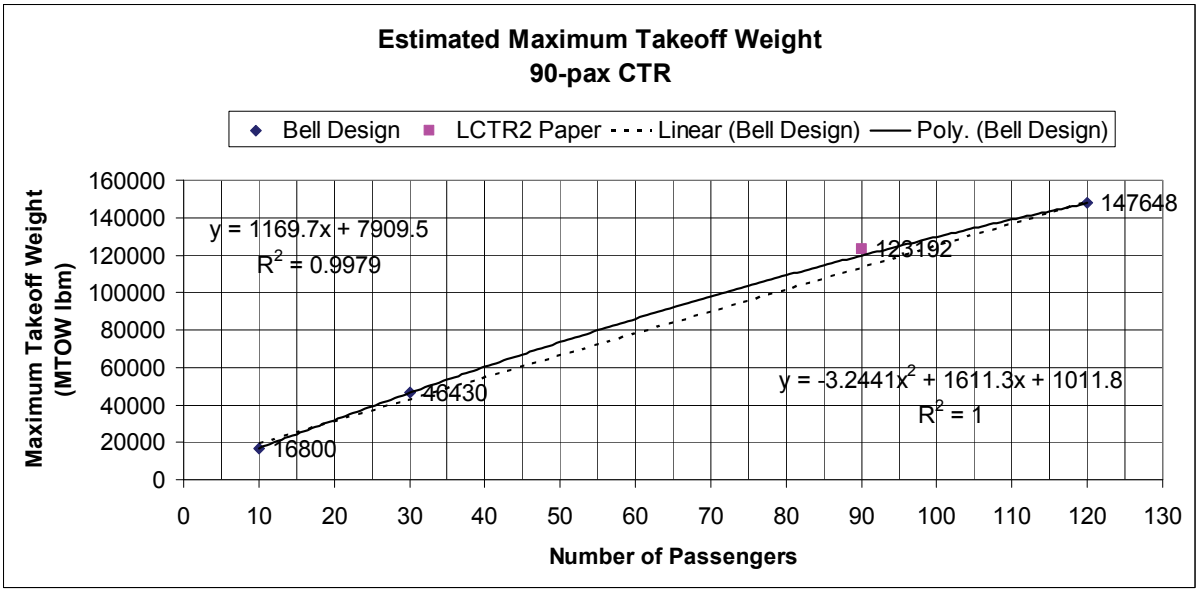

Figure E-5. Sizing the CTR90 MTOW.

E-2.6 Reference Weight

The scaled CTR90 uses the second-order fit below to estimate a reference weight with the fit anchored to the known CTR10, CTR30, and CTR120 data points. The reference weight is intended to be a middle range loading for use by BADA.

E-2.7 Maximum Payload Weight

In this study the payload weight is meant to indicate passengers and accompanying baggage weight. This amount does not include fuel. It is simply defined here as 220 lbs per passenger resulting in a maximum payload weight of 19,800 lbs for the CTR90. This is identical to the NASA LCTR2 design.

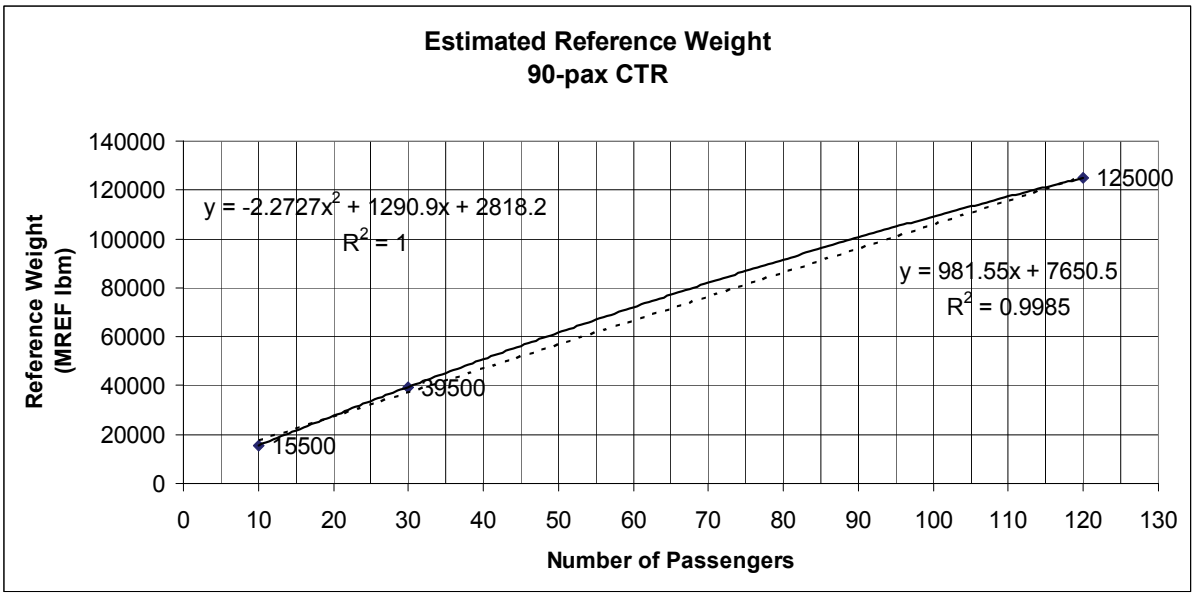

Figure E-6. Sizing the CTR90 reference weight.

E-2.8 Maximum Fuel Capacity

The scaled CTR90 uses the second-order fit below to estimate maximum fuel capacity with the fit anchored to the known CTR10, CTR30, and CTR120 data points. A comparison point is shown for the NASA LCTR2 design.

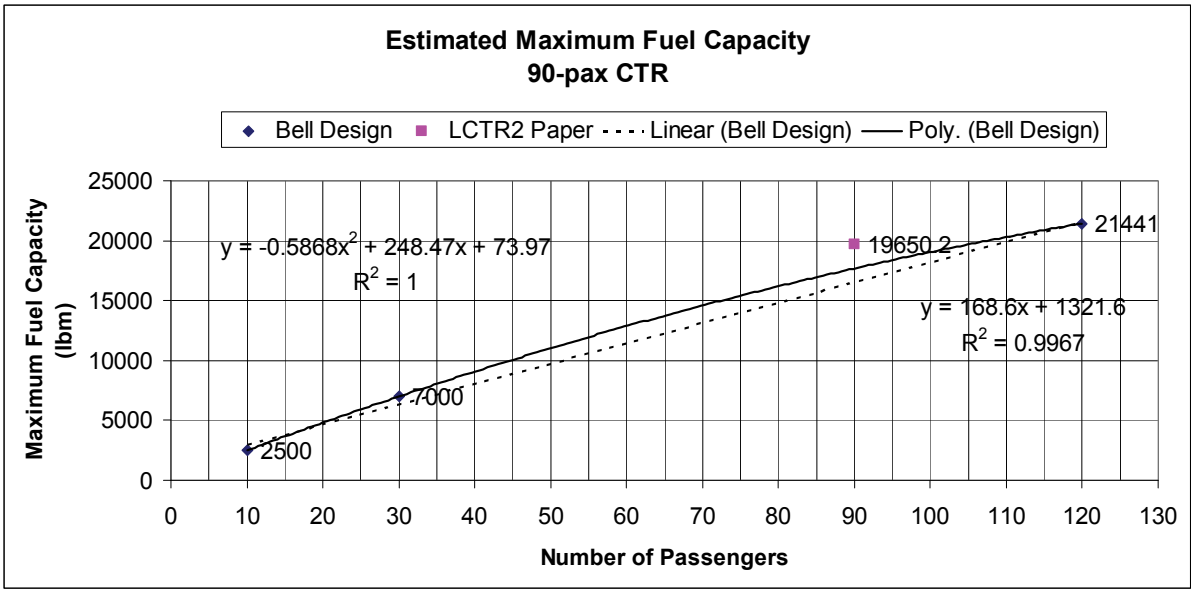

Figure E-7. Sizing the CTR90 maximum fuel capacity.

E-2.9 CTR90 Geometry Summary

Table E-2 summarizes the BADA relevant geometry for the SAIC sized CTR90 and shows the geometry of the NASA Ames LCTR2 design for comparison.

TABLE E-2. GEOMETRY SUMMARY OF THE RESULTING CTR90 COMPARED TO THE NASA AMES LCTR2 DESIGN

90-Pax Design	OWE (lbs)	Wingspan (ft)	Fuselage Length (ft)	Wing Area (ft^2)	MTOW (lbs)	Mref (lbs)	Mpayload (lbs)	Fuel Capacity (lbs)
SAIC Sizing	82,428.3	82.21	100.15	1,111.7	119,911.5	100,590.3	19,800	17,683.2
NASA LCTR2	83,741.8	107 (inner span 77)	108.9	1,000.9	123,192	N/A	19,800	19,650.2

E-3 Aerodynamics

The aerodynamic drag as represented in the BADA model for the CTR10, CTR30, and CTR120 airframe is outlined in table E-3 below. The airplane mode stall velocity for the known reference weight (Mref) within BADA is presented as well. Note that the stall velocity and aerodynamic drag model formulation for the SAIC sized CTR90 is simply a linear prediction based on the 30- and 120-passenger data. This formulation uses passenger capacity as the independent variable for sizing purposes.

The plot of nondimensional drag coefficient versus lift coefficient is shown in figure E-8 for the CTR10, CTR30, and CTR120, and sized CTR90 vehicles.

TABLE E-3. BADA ENTRIES FOR STALL SPEED, PARASITE DRAG, AND INDUCED DRAG PRESENTED FOR ALL CTR VEHICLES USED IN SIZING THE CTR90 CHARACTERISTICS

Passenger Size	Vstall @ Mref (KCAS)	BADA Parasite Drag Coefficient	BADA Induced Drag Coefficient
10	122.1	0.0599	0.0481
30	121.93	0.058489	0.052892
SAIC Sized 90	116.39	0.040859	0.04662
120	113.62	0.032044	0.043484

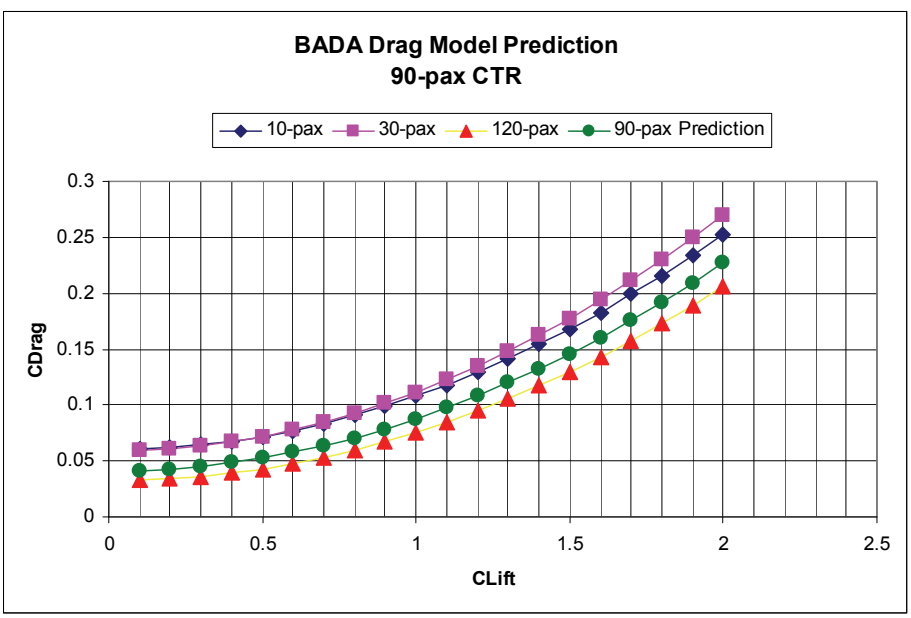

Figure E-8. Sizing the CTR90 drag characteristics.

E-4 Propulsion

This section describes the sizing of the CTR90 propulsion model for BADA formulation.

E-4.1 Maximum Continuous Power (MCP) Climb

The CTR90 thrust model for the MCP climb phase is based on a linear scaling of the thrust versus altitude formulation between the CTR30 and CTR120 vehicles. The plot shown in figure E-9 presents the thrust at altitude for MCP climb conditions for the CTR10, CTR30, sized CTR90, and CTR120 vehicles. This data is for ISA conditions with the second-order fit being the source of the MCP climb thrust coefficients for the 90-passenger BADA model.

Non-ISA effects on this model are based on a linear sizing of the BADA temperature effect coefficient (CTc5) shown in figure E-10. The linear fit below was used to generate the non-ISA effect for the CTR90 with the results indicated in table E-4.

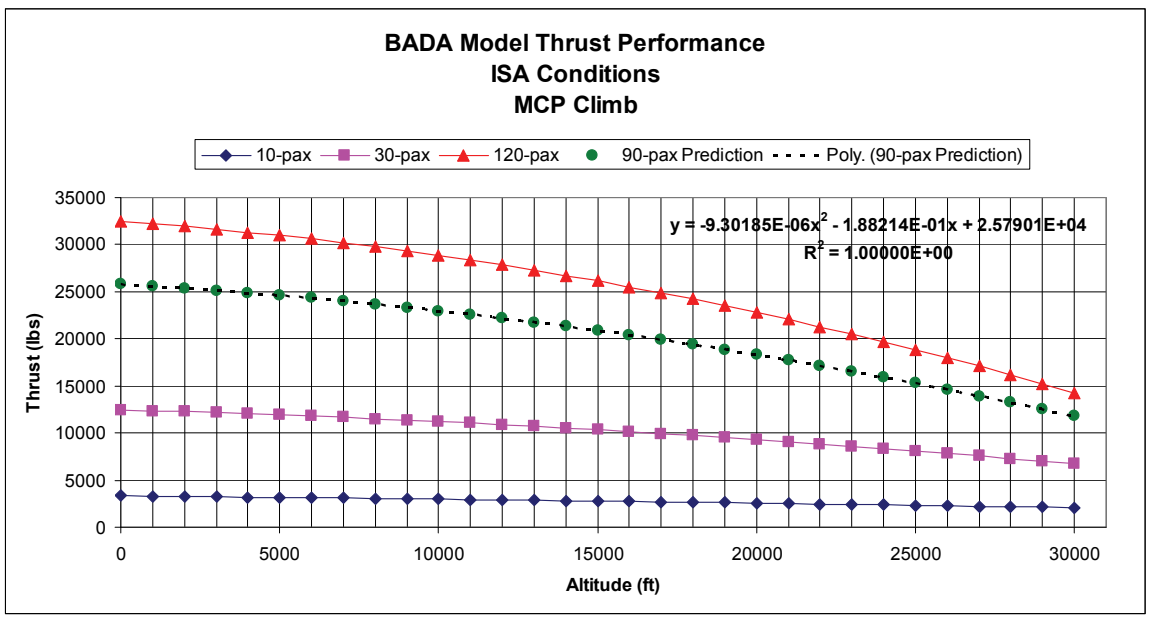

Figure E-9. Sizing the CTR90 MCP climb thrust performance.

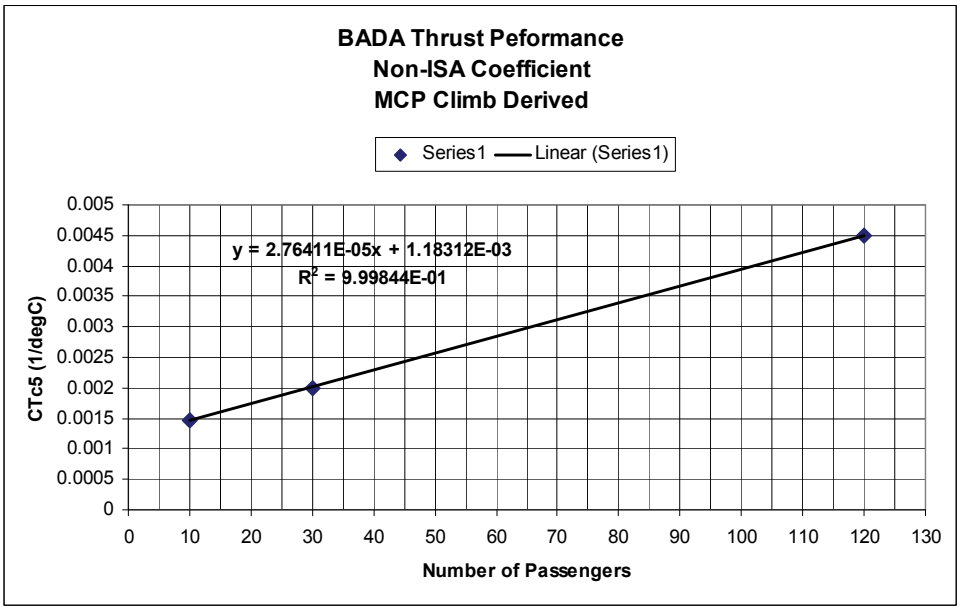

Figure E-10. Sizing the CTR90 MCP climb non-ISA temperature effect on thrust performance.

TABLE E-4. SIZING THE CTR90 NON-ISA TEMPERATURE EFFECT COEFFICIENT AS APPLIED TO MCP CLIMB THRUST

CTR	BADA Non-ISA Effect C_{Tc5} (1/degC)
10	0.0014775
30	0.0019904
SAIC Sized 90	0.003670819
120	0.00450405

E-4.2 Maximum Continuous Power Level Cruise

The CTR90 thrust model for the MCP cruise phase is based on a linear scaling of the thrust versus altitude formulation between the CTR30 and CTR120 vehicles. The plot shown in figure E-11 presents the thrust at altitude for MCP cruise conditions for the 10-, 30-, sized 90-, and 120-passenger CTR vehicles. This data is for ISA conditions.

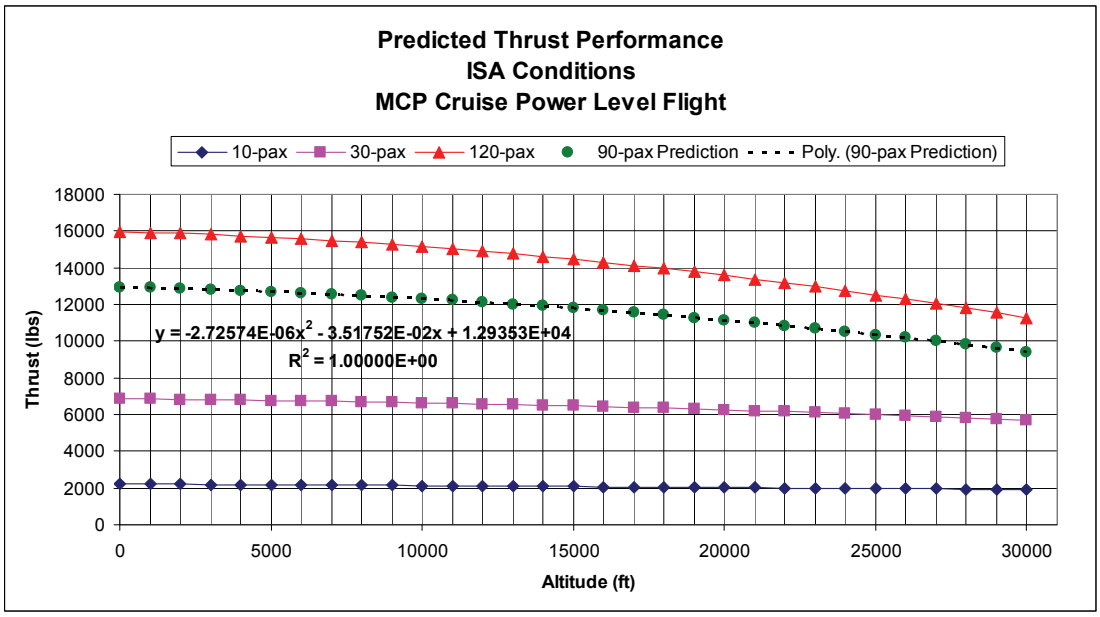

Figure E-11. Sizing the CTR90 MCP cruise thrust performance.

E-4.3 Descent Thrust

The descent thrust scale factor for the BADA model formulation of the CTR90 was sized linearly based on the known trends for $C_{Tdes,low}$ and $C_{Tdes,high}$ for the 30- and 120-passenger vehicles. The altitude at which the BADA formulation switches between the low- or high-altitude scaling coefficients is set consistently with the other vehicles. Results are shown in table E-5 and figure E-12.

TABLE E-5. THE CTR90 DESCENT THRUST COEFFICIENTS PRESENTED WITH DATA FROM AVAILABLE VEHICLES

CTR	CTdes,low	CTdes,high	hdes (ft)
10	0.378	0.2746	15,000
30	0.2659	0.2369	15,000
SAIC Sized 90	0.2276	0.2190	15,000
120	0.20844	0.21008	15,000

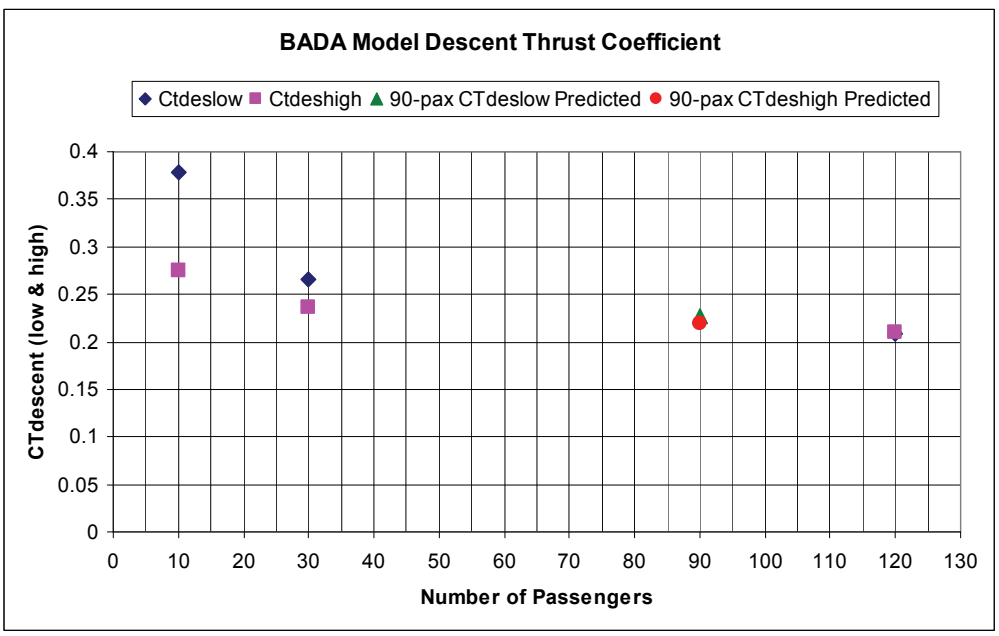

Figure E-12. Sizing the CTR90 high- and low-altitude-descent thrust coefficients.

E-5 Flight Envelopes

The envelope limitations used in BADA for the CTR90 are sized based on known BADA performance data for the 10-, 30-, and 120-passenger vehicles. The resulting envelope terms are outlined in table E-6 with details as follows:

- Mass Gradient Gw: This BADA term describes the effect of gross weight on the altitude at which the airframe has 300-fpm rate of climb available. It alters the value of Hmax based on gross weight. This parameter for the CTR90 is a linear scaling between the 30- and 120-passenger BADA entries for Gw.
- Vmo: The never exceed speed. The 90-passenger entry is held constant to the 30- and 120-passenger entries.
- Mmo: The never exceed Mach number. The 90-passenger entry is held constant to the 30- and 120-passenger entries.
- Hmo: The absolute ceiling for the airframe at minimum gross weight where no residual rate of climb is available. This parameter for the CTR90 is a linear scaling between the 30- and 120-passenger BADA entries for Hmo.
- Hmax: The altitude wherein the airframe has 300-fpm rate of climb available under ISA and MTOW conditions. This parameter for the CTR90 is a linear scaling between the 30- and 120-passenger BADA entries for Hmax.
- Gt: The BADA non-ISA effect of temperature on the ability to obtain the 300-fpm rate of climb. It alters the value of Hmax based on non-ISA conditions. This parameter for the CTR90 is a linear scaling between the 30- and 120-passenger BADA entries for Gt.

TABLE E-6. THE CTR90 FLIGHT ENVELOPE LIMITATIONS PRESENTED WITH DATA FROM AVAILABLE VEHICLES

CTR	Mass Gradient Gw (ft/lbm)	Vmo (KCAS)	Mmo	Hmo (ft)	Hmax (ft)	Gt (ft/deg C)
10	1.455	240	0.48	38900	29870	–8.8235
30	0.6205	310	0.6	42118	32138	–129.5
SAIC Sized 90	0.3491	310	0.6	44285	31819	–139.65
120	0.2134	310	0.6	45368	31659	–144.725

E-6 Fuel Consumption

The CTR90 fuel consumption model for the MCP climb phase is based on a linear scaling of the BADA thrust specific fuel consumption (TSFC) η versus true airspeed formulation between the CTR30 and CTR120 vehicles. The plot shown in figure E-13 presents η at various airspeeds for MCP climb conditions for the CTR10, CTR30, sized CTR90, and CTR120 vehicles. This data is for ISA conditions with linear fit being the source of the BADA TSFC model for the 90-passenger BADA model.

Similarly, the BADA descent minimum fuel flow model for the CTR90 is sized linearly based on the known data for the 30- and 120-passenger vehicles. The plot shown in figure E-14 presents the BADA descent minimum fuel flow for the CTR10, CTR30, sized CTR90, and CTR120 vehicles. The linear fit as shown is the basis of the 90-passenger BADA model coefficients for this characteristic.

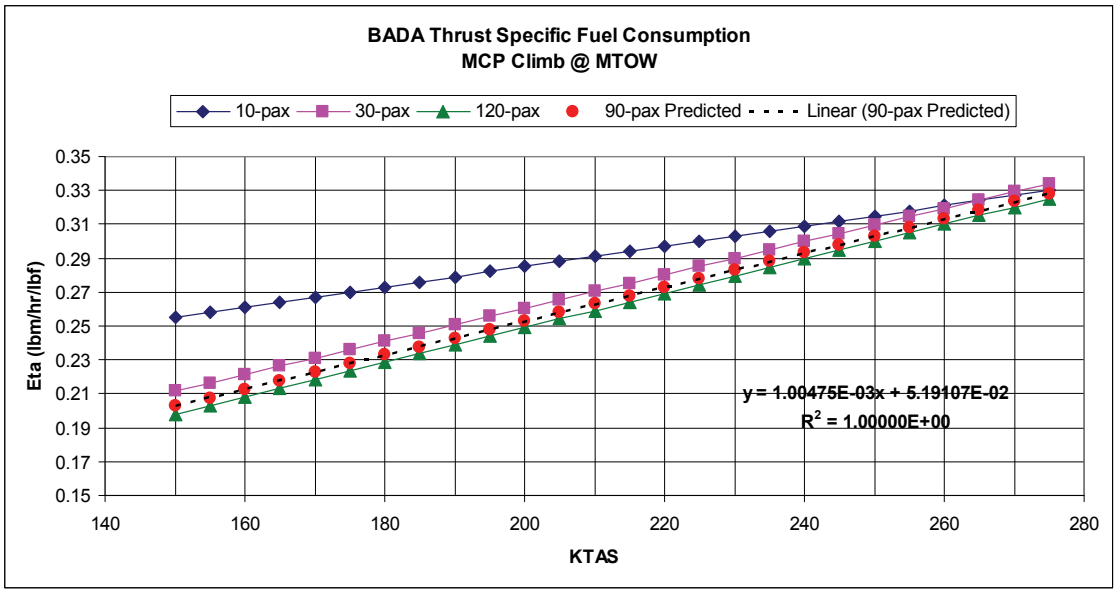

Figure E-13. Sizing the CTR90 MCP climb TSFC.

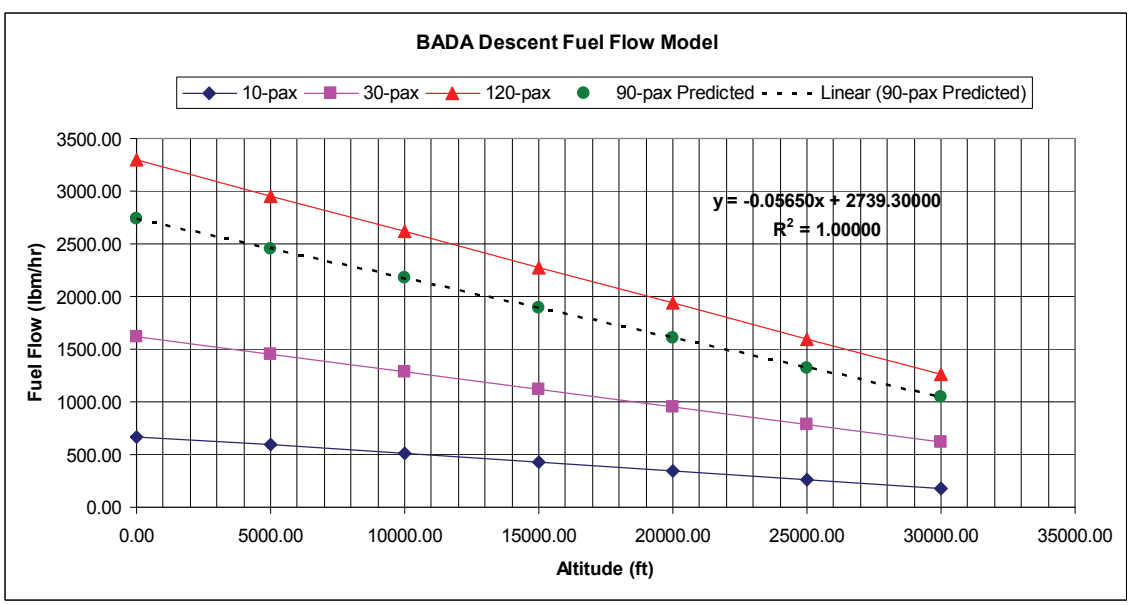

Figure E-14. Sizing the CTR90 descent phase fuel flow.

The BADA level flight cruise fuel flow scale factor (Cfcr) is tasked with adjusting the MCP climb fuel flow model to adapt to level flight conditions (see figure E-15). The CTR90 BADA entry for this term was scaled based on the second-order fit of the known CTR10, CTR30, and CTR120 vehicle values. Table E-7 below outlines the BADA Cfcr entries for each CTR.

TABLE E-7. THE CTR90 CRUISE FUEL FLOW SCALE FACTOR PRESENTED WITH DATA FROM AVAILABLE VEHICLES

CTR	Cfcr
10	1.07676
30	1.07943
SAIC Sized 90	1.09612
120	1.10935

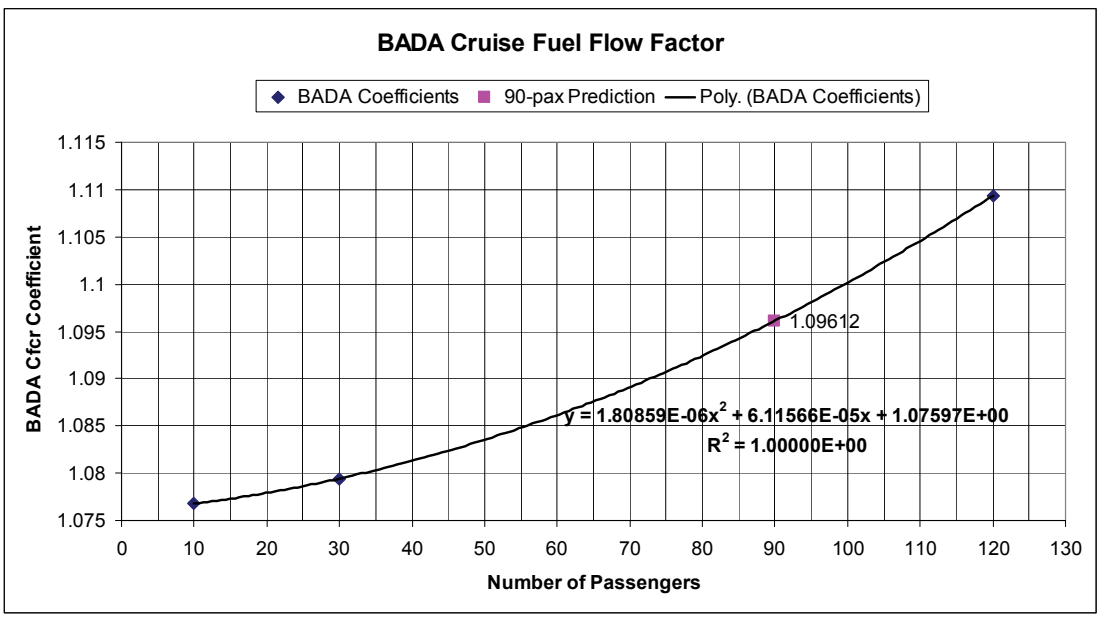

Figure E-15. Sizing the CTR90 cruise fuel flow scale factor.

E-7 Operational Speed Schedules

The CTR90 operational climb and long-range cruise velocity schedules, both at MTOW configuration, are based on a linear scaling between the 30- and 120-passenger known performance data. The plots shown in figures E-16 and E-17 indicate the climb and long-range cruise velocity schedules at MTOW for the CTR10, CTR30, sized CTR90, and CTR120 vehicles. The airspeed/altitude climb and long-range cruise schedules as shown were used to populate the BADA flight operation entries using the identical technique employed for the 10-, 30-, and 120-passenger vehicles. The CTR90 descent speed schedule is set identical to that of the 30- and 120-passenger vehicles.

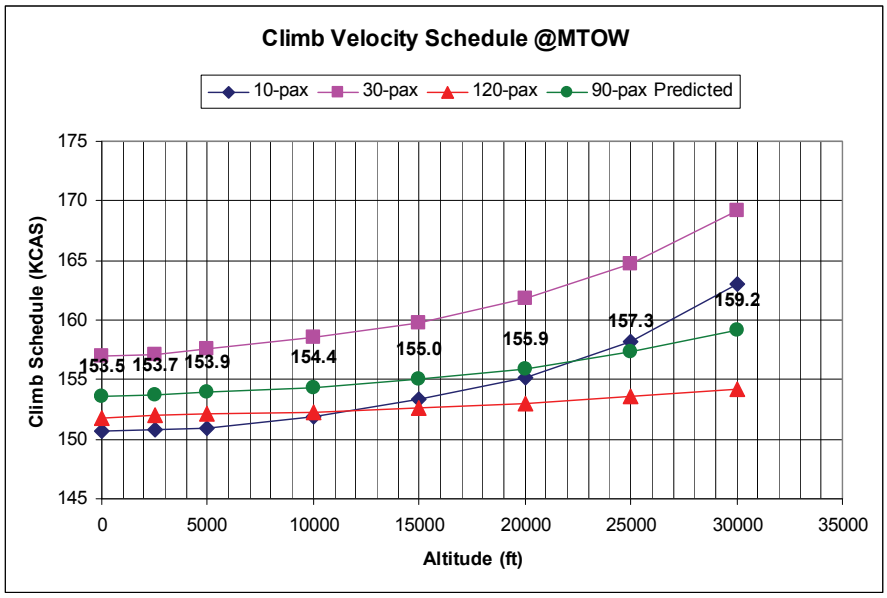

Figure E-16. Sizing the CTR90 MTOW climb velocity schedule.

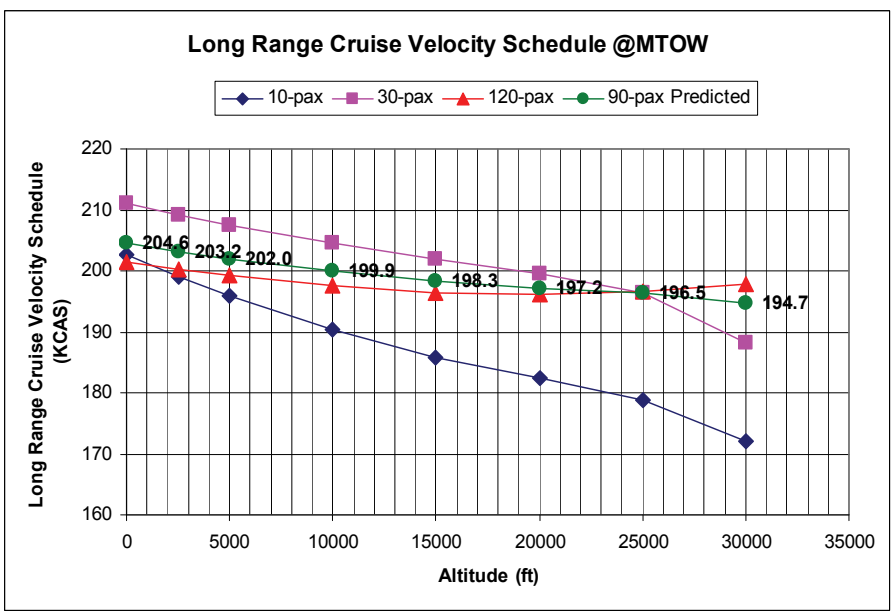

Figure E-17. Sizing the CTR90 long-range cruise velocity schedule.

E-8 Mission Comparisons

Verification data for the CTR10, CTR30, and CTR120 vehicles, in the form of simulated mission profiles, was supplied by Bell for comparison to the SAIC-developed BADA models. The SAIC sized CTR90 BADA model was also used to generate a similar mission to see how overall performance compares with the CTR fleet as a whole.

The mission profiles examined in this comparison are as follows:

- CTR10 and CTR30 (supplied Bell mission profiles)
  - Climb from sea level to 25k feet at 1.23 Vstall
  - Cruise at long-range cruise speed
  - Descend to sea level at 1000 fpm
- CTR90 (SAIC-generated mission profile based on BADA model)
  - Climb from sea level to 27.5k feet at 1.23 Vstall
  - Cruise at long-range cruise speed
  - Descend to sea level at 1000 fpm
- CTR120 (supplied Bell mission profile)
  - Climb from sea level to 27.5k feet at 1.23 Vstall
  - Cruise at long-range cruise speed
  - Descend to sea level at 1000 fpm

The mission profiles, as defined above, were flown to consume all useable fuel to a dry tank. Table E-8 outlines the total range, total fuel burned, and total time to perform the climb, cruise, and descent segments in whole for each CTR. Similar data is shown for the cruise mission segment alone for each CTR as well.

TABLE E-8. SUMMARY OF RANGE, FUEL BURN, AND COMPLETION TIME FOR AN ENTIRE MISSION, AS WELL AS THE CRUISE PHASE ONLY, FOR ALL CTR VEHICLES

CTR	Total Range (nmi)	Total Fuel Burn (lbs)	Total Time (minutes)	Cruise Phase Range (nmi)	Cruise Phase Fuel Burn (lbs)	Cruise Phase Time (minutes)
10	1042.8	2481	254.56	886.6	2024.6	208.31
30	1060.9	6998.5	236.4	932.6	6003	200.14
90	1364	17681	292.45	1197.5	15075	244.07
120	1598.3	21439.4	338.9	1431.8	18729	295.8

The plots shown in figures E-18 through E-21 outline the total mission range, which includes the climb, cruise, and descent phase, as well as the cruise phase segment alone. Similar data is shown for fuel burned. The sized CTR90 falls within the trends of the CTR10, CTR30, and CTR120 vehicles designed by Bell.

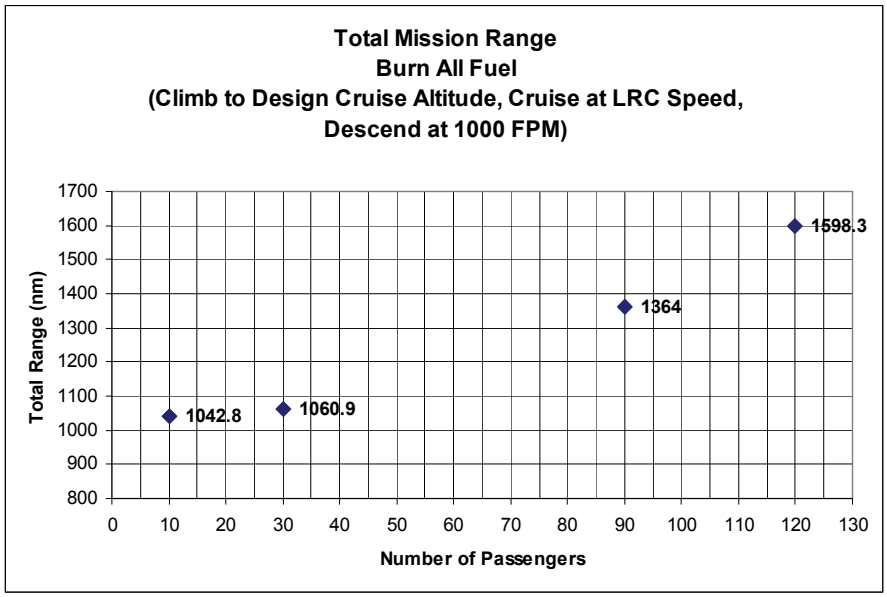

Figure E-18. Summary of total mission range for all CTR vehicles including climb from sea level to altitude, cruise at altitude, and descent to sea level.

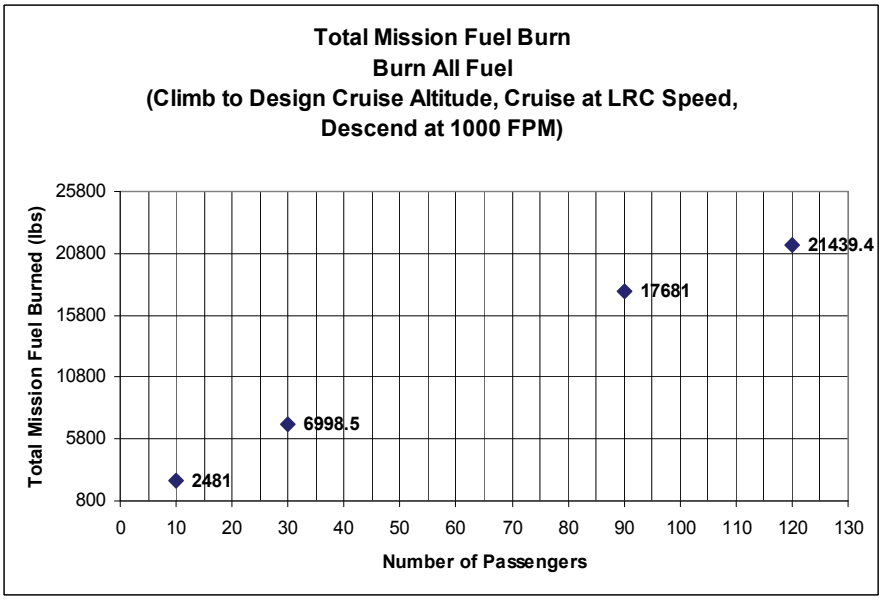

Figure E-19. Summary of total mission fuel burned for all CTR vehicles including climb from sea level to altitude, cruise at altitude, and descent to sea level.

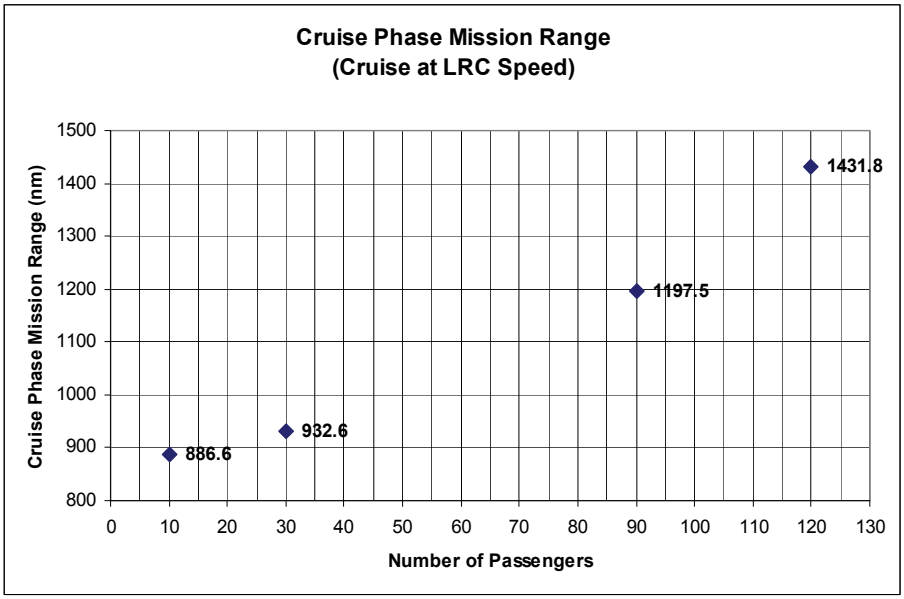

Figure E-20. Summary of cruise phase mission range for all CTR vehicles.

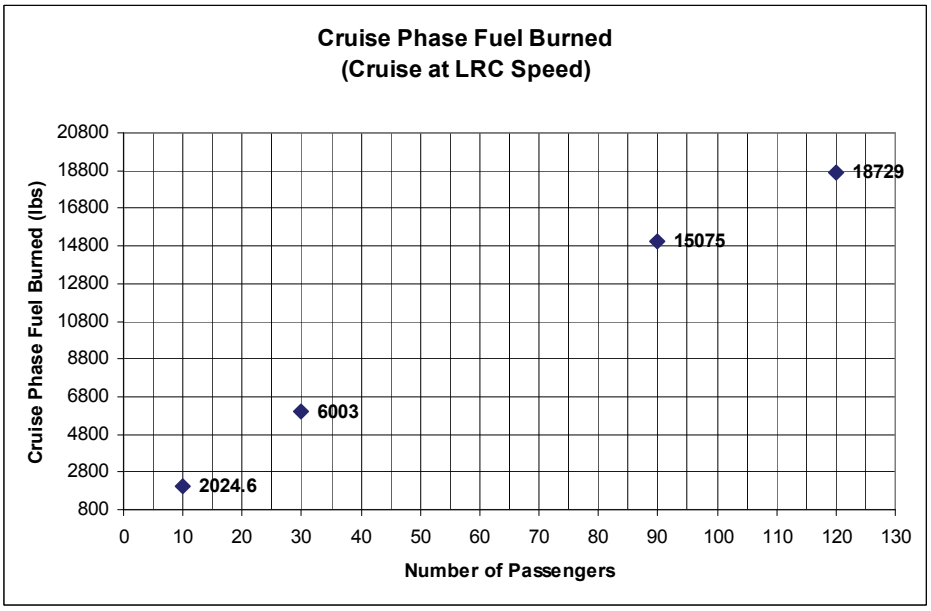

Figure E-21. Summary of cruise phase fuel burned for all CTR vehicles.

E-9 Conversion Modes

The CTR90 conversion mode aerodynamics and propulsion characteristics within the BADA framework are based on trend sizing given known models for the other three vehicles. This section provides an overview of the supporting graphs used for sizing the 90-passenger BADA entries. The final BADA entries are shown in section 3.2.

As in airplane mode, the conversion mode sizing examines trends of pertinent parameters against passenger capacity. Least-squares fit of the data for the CTR10, CTR30, and CTR120 provide a means to estimate the parameters under investigation for the CTR90.

The conversion mode stall characteristics for the CTR90 are identical to those specified for the other CTR vehicles.

E-9.1 Initial Climb Conversion Mode

This section presents the second-order least-squares fits resulting in the BADA parasite and induced drag for the initial climb (IC) conversion mode (figures E-22 and E-23). Note that this mode is valid for use in two phases of flight—one being the intermediate mode of nacelle transition during the climb-out following takeoff on the way to airplane mode, and the other being the level flight segment planned at the bottom of descent from altitude wherein an intermediate nacelle angle is set prior to final transition to the STOL or VTOL approach and landing phase. This configuration is common to both STOL and VTOL operations.

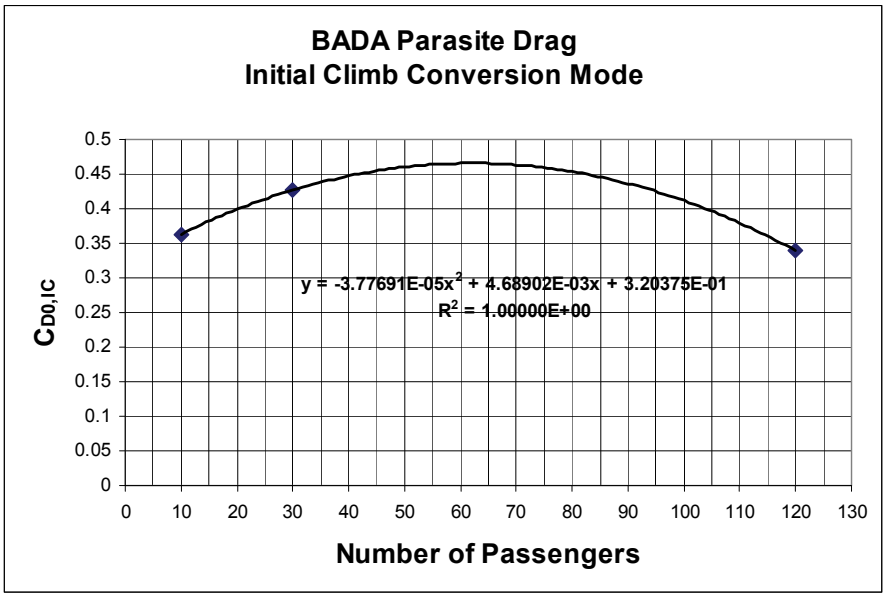

Figure E-22. Sizing the IC parasite drag for the CTR90.

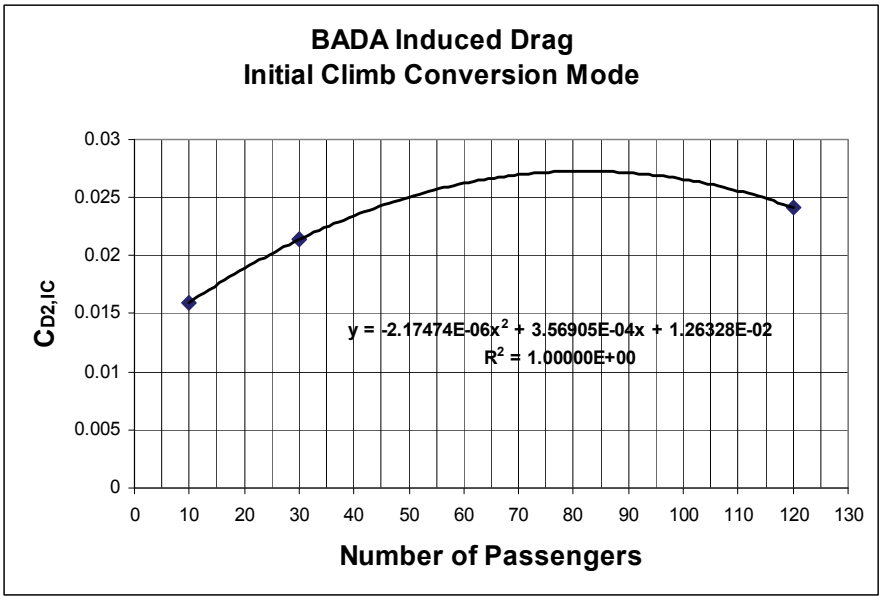

Figure E-23. Sizing the IC induced drag for the CTR90.

E-9.2 Approach Conversion Mode

This section presents the second-order least-squares fits resulting in the BADA parasite and induced drag for the approach (AP) conversion mode. This mode of flight is common between STOL and VTOL operations until reaching the decision altitude. Note that the parasite drag (figure E-24) in the equivalent system model varies with targeted glide slope angle (–3, –6, or –9 degrees) while induced drag (figure E-25) is held constant.

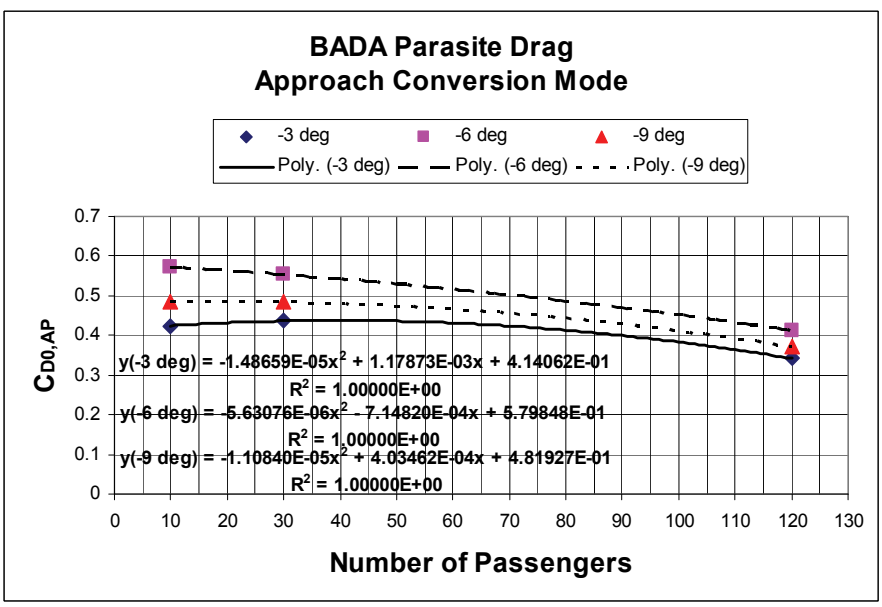

Figure E-24. Sizing the AP parasite drag for the CTR90 based on glide slope angle.

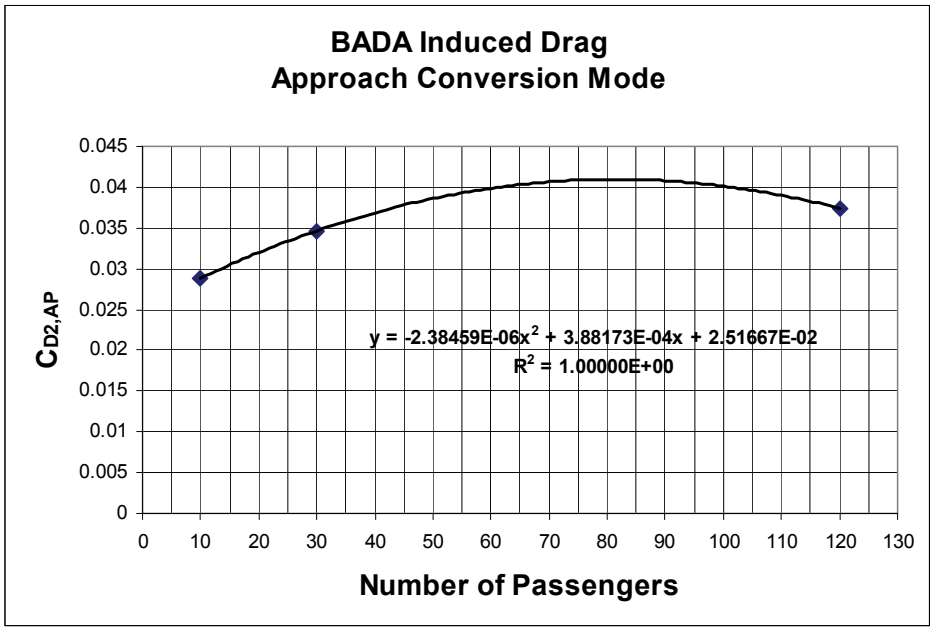

Figure E-25. Sizing the AP induced drag for the CTR90.

E-9.3 STOL Takeoff Conversion Mode

This section presents the second-order least-squares fits resulting in the BADA parasite and induced drag for the STOL takeoff (TO) conversion mode. Note that the parasite drag (figure E-26) in the equivalent system model varies with targeted rate of climb (0, 250, 500, or 750 fpm) while induced drag (figure E-27) is held constant.

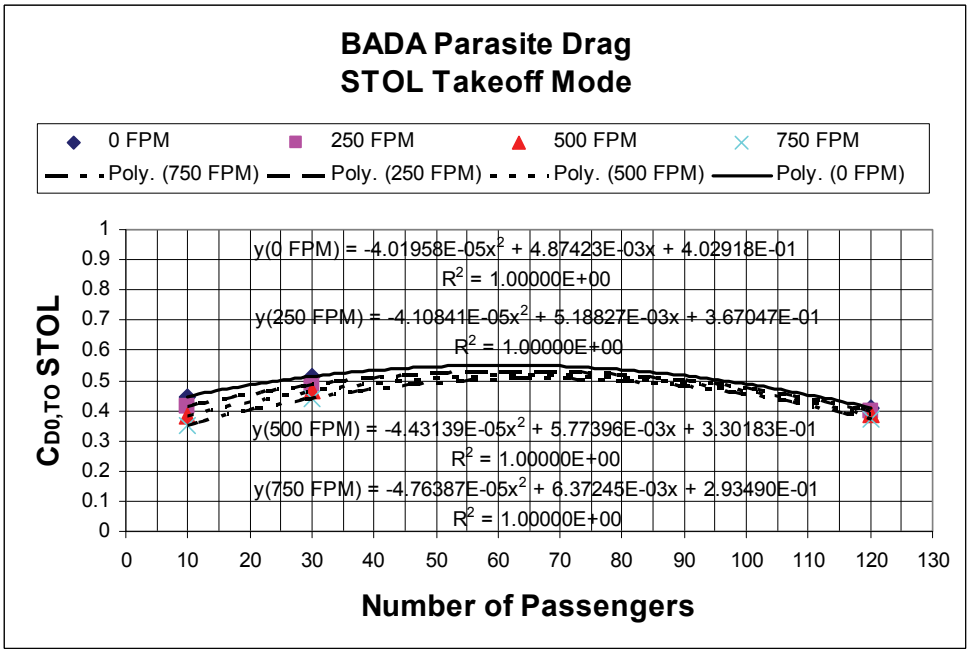

Figure E-26. Sizing the STOL TO parasite drag for the CTR90 based on ROC.

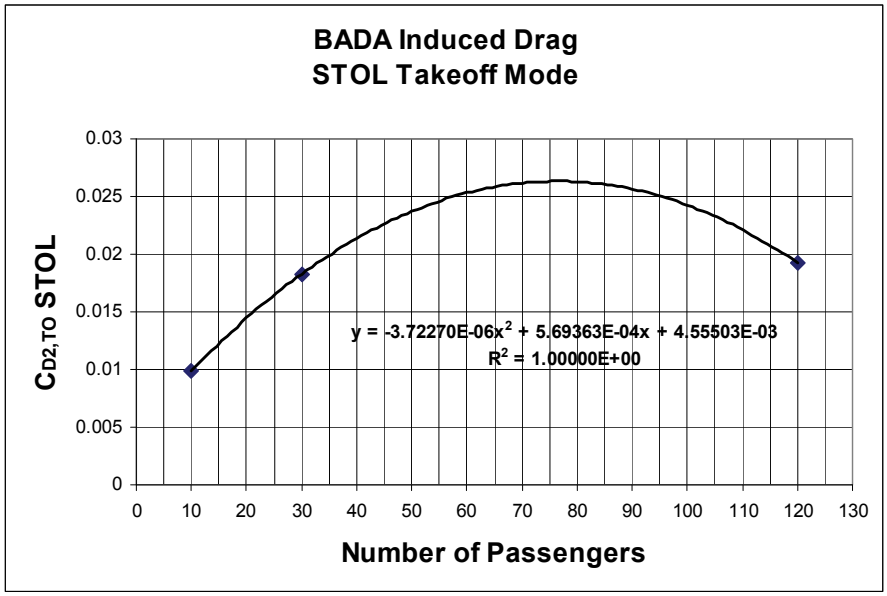

Figure E-27. Sizing the STOL TO induced drag for the CTR90.

E-9.4 VTOL Takeoff Conversion Mode

This section presents the second-order least-squares fits resulting in the BADA parasite and induced drag for the VTOL takeoff (TO) conversion mode. Note that the parasite drag (figure E-28) in the equivalent system model varies with targeted rate of climb (0, 250, 500, or 750 fpm) while induced drag (figure E-29) is held constant.

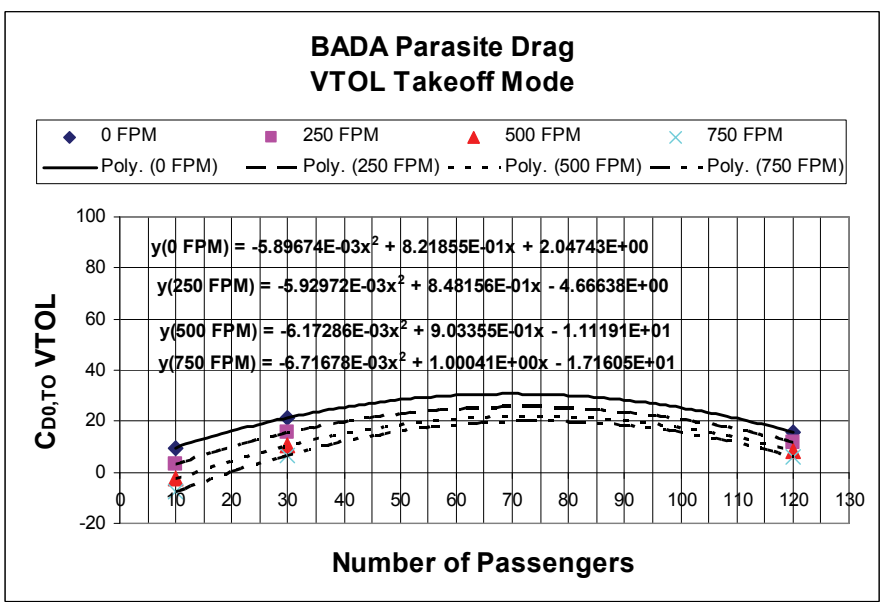

Figure E-28. Sizing the VTOL TO parasite drag for the CTR90 based on ROC.

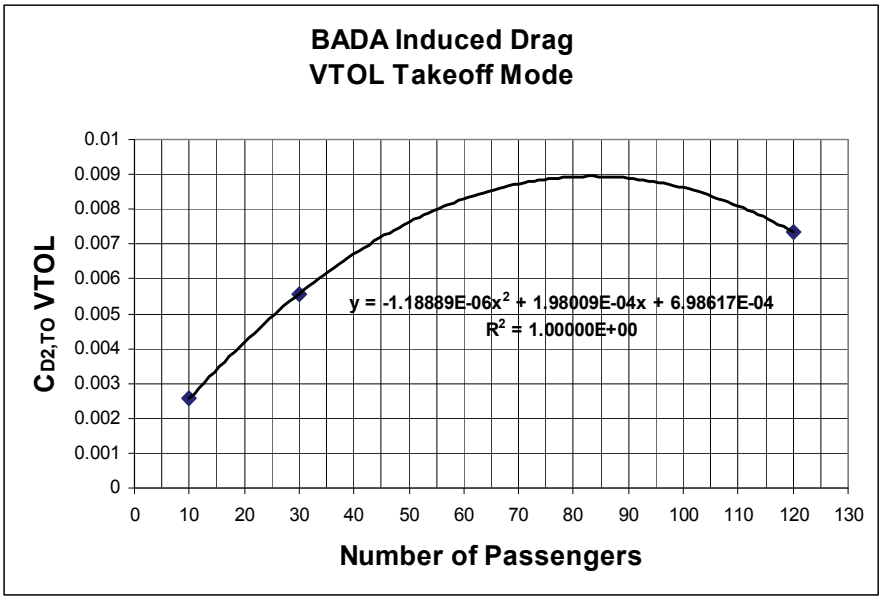

Figure E-29. Sizing the VTOL TO induced drag for the CTR90.

E-9.5 STOL Landing Conversion Mode

This section presents the second-order least-squares fits resulting in the BADA parasite and induced drag for the STOL landing (LD) conversion mode. Note that the parasite drag (figure E-30) in the equivalent system model varies with targeted glide slope angle (–3, –6, or –9 degrees) while induced drag (figure E-31) is held constant.

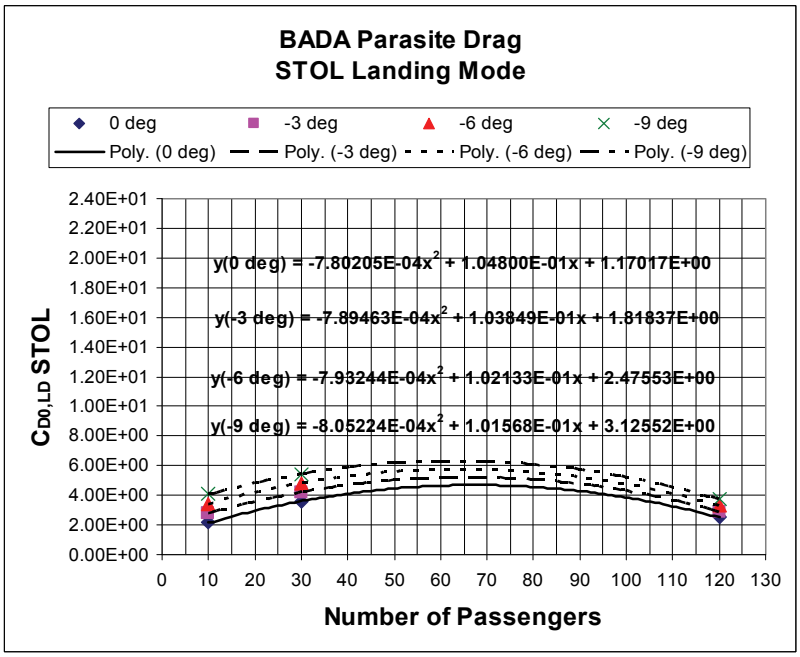

Figure E-30. Sizing the STOL LD parasite drag for the CTR90 based on glide slope angle.

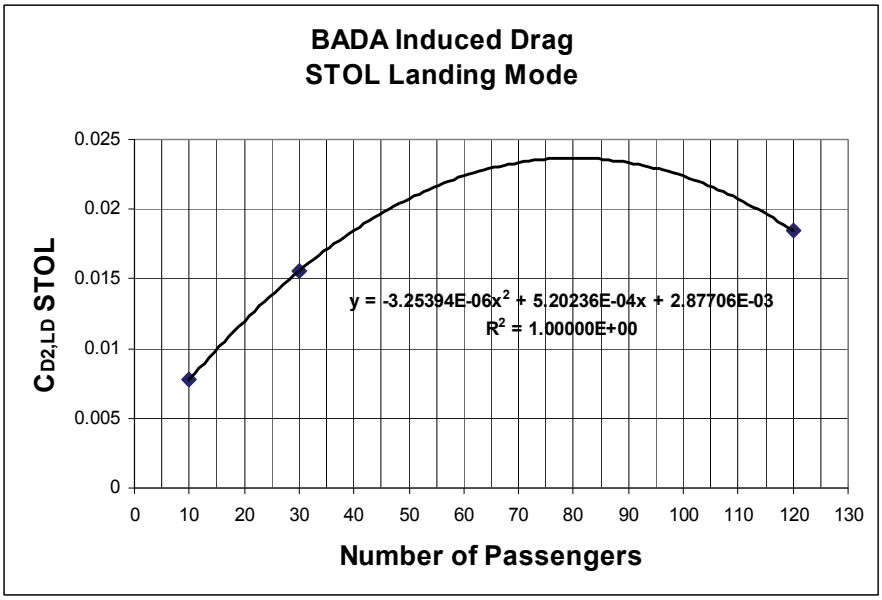

Figure E-31. Sizing the STOL LD induced drag for the CTR90.

E-9.6 VTOL Landing Conversion Mode

This section presents the second-order least-squares fits resulting in the BADA parasite and induced drag for the VTOL landing (LD) conversion mode. Note that the parasite drag (figure E-32) in the equivalent system model varies with targeted glide slope angle (–3, –6, or –9 degrees) while induced drag (figure E-33) is held constant.

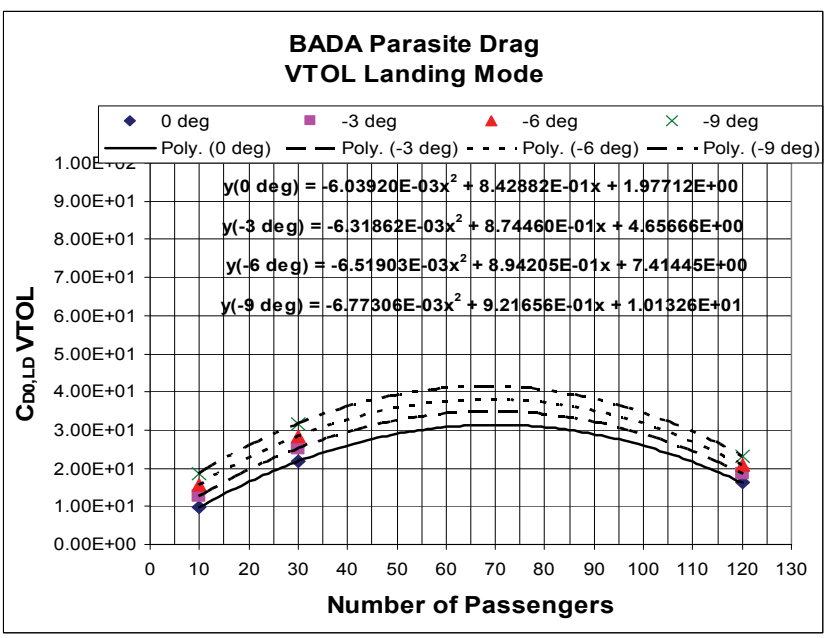

Figure E-32. Sizing the VTOL LD parasite drag for the CTR90 based on glide slope angle.

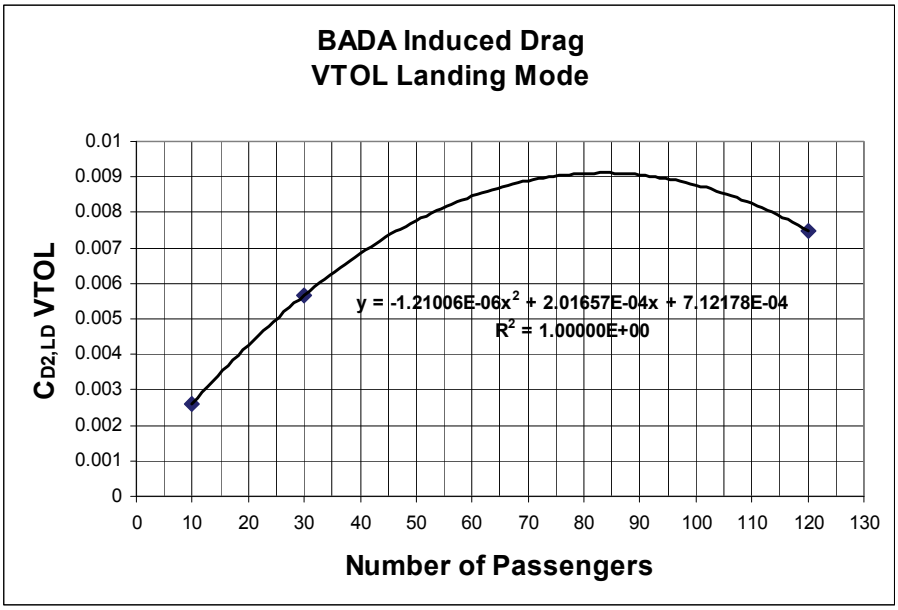

Figure E-33. Sizing the VTOL LD induced drag for the CTR90.

E-9.7 Conversion Mode Thrust Coefficients

This section presents the second-order least-squares fits resulting in the BADA thrust coefficients for approach (AP) (figure E-34), landing (LD) (figures E-35 and E-36), and takeoff (TO) (figures E-37 and E-38) conversion modes. Note that the AP and LD thrust coefficients are a function of targeted glide slope angle (–3, –6, or –9 degrees). The takeoff ascent thrust coefficients are a function of targeted rate of climb (0, 250, 500, 750, or 1,000 fpm). In addition, these terms vary based on STOL or VTOL modes.

Note that the takeoff ascent thrust coefficient has been added to support CTR operations in that the base BADA model formulation does not include this term. In order to support the significantly greater thrust levels required for STOL and VTOL takeoff operations, the CTasc,to term was added to the BADA formatted files in a previously unused data slot. Future users of the CTR BADA files must be sure to make use of these new terms as outlined in section 3.

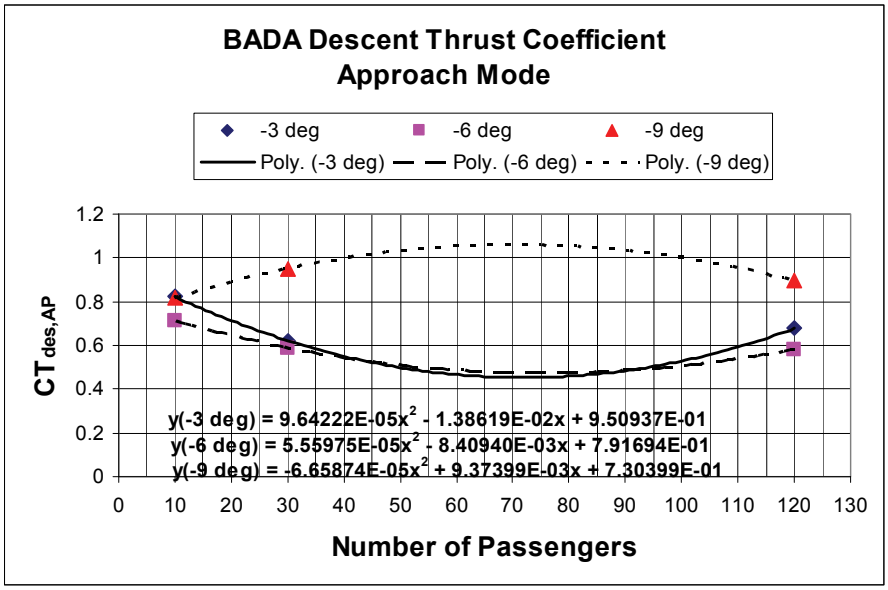

Figure E-34. Sizing the AP mode descent thrust coefficient for the CTR90.

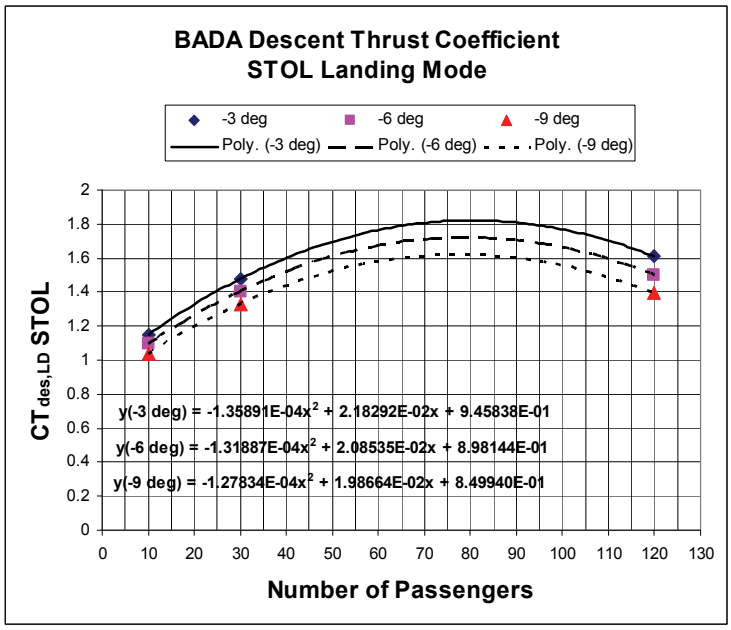

Figure E-35. Sizing the STOL LD mode descent thrust coefficient for the CTR90.

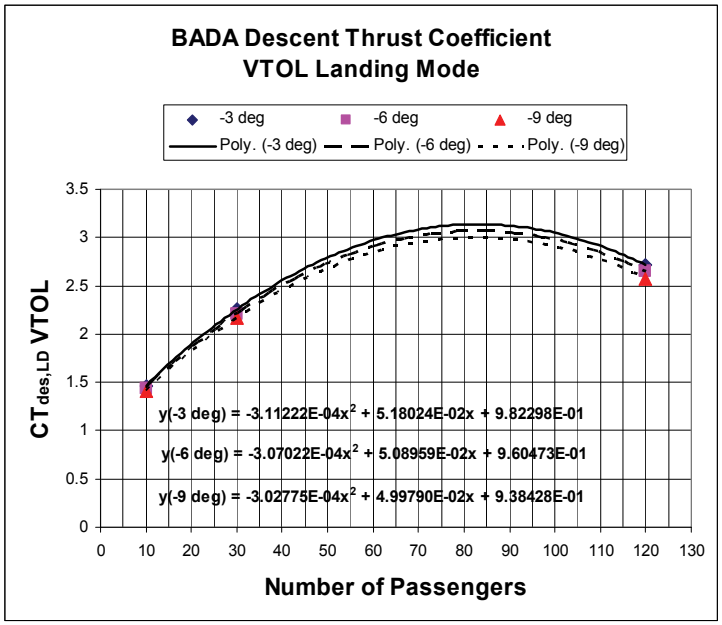

Figure E-36. Sizing the VTOL LD mode descent thrust coefficient for the CTR90.

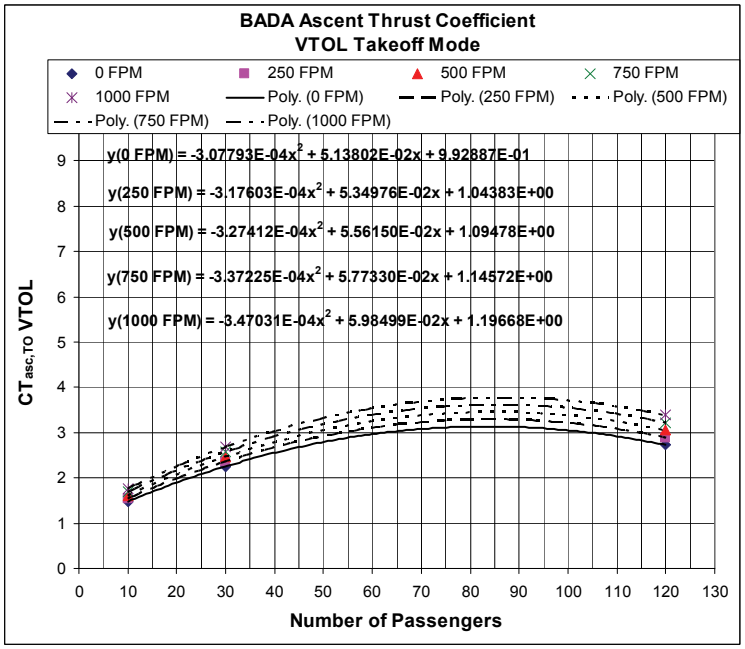

Figure E-37. Sizing the VTOL TO mode ascent thrust coefficient for the CTR90.

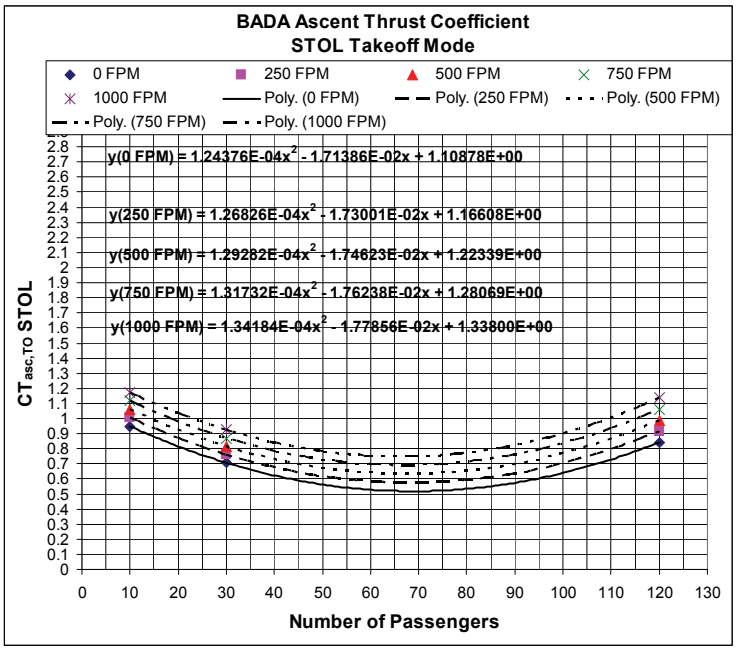

Figure E-38. Sizing the STOL TO mode ascent thrust coefficient for the CTR90.

APPENDIX F. CTR90 BADA PERFORMANCE MODEL COMPARISON

F-1 Introduction

In section 2, Bell Helicopter designed a fleet of civil tiltrotor (CTR) aircraft and provided the subsequent performance data required to develop BADA-based performance models. Data was supplied for CTR10, CTR30, and CTR120 configurations. In order to fill out the fleet a CTR90 was sized by Science Applications International Corporation (SAIC) based on regression analysis of BADA model characteristics outlined in section 2 for the 10-, 30-, and 120-passenger vehicles.

An independent task was assigned to Bell Helicopter by NASA to officially design a CTR90 vehicle (ref. F-1) and provide the same performance data as was delivered for the other three vehicles described in section 2. This appendix compares notable airplane mode performance characteristics between the linear-scaled CTR90 model and the Bell designed model.

Details of the scaled CTR90 sizing can be found in appendix E. The final Bell-provided design can be found in the corresponding Bell Task Order document (ref. F-1). It is important to note that currently only the scaled CTR90 has been formatted into a set of BADA files supporting the CTR in NextGen studies.

F-2 Geometry Comparison

The main airframe geometry and characteristic terms used by BADA are compared to the final Bell design in table F-1.

TABLE F-1. COMPARISON OF AIRFRAME GEOMETRY AND MASS

Parameter	Scaled Model	Bell Design	% Difference
Mmin OWE (lbs)	82428.3	80000	3.04
Mref (lbs)	100590.3	97500	3.17
Mmax MTOW (lbs)	119911.5	114818	4.44
Fuselage Length (ft)	100.15	98.6	1.57
Wingspan (ft)	82.21	88.1	–6.69
Wing Area (ft^2)	1111.7	1195	–6.97
Fuel Capacity (lbs)	17683.2	14885	18.80
Payload Weight (lbs)	19800	19800	0.00

F-3 Envelope Performance Comparison

The comparison of absolute ceiling (Hmo) and maximum ceiling with 300-fpm residual rate of climb available (Hmax @ MTOW loading) is shown in table F-2. The maximum continuous power (MCP) climb speed schedule comparison for 1.23 Vstall at MTOW conditions is shown in table F-3. The long-range cruise level flight speed schedule comparison at MTOW conditions is shown in table F-4. The MCP level flight cruise speed schedule comparison at MTOW conditions is shown in table F-5.

TABLE F-2. COMPARISON OF AIRFRAME ALTITUDE ENVELOPE

Parameter (ft)	Scaled Model	Bell Design	% Difference
Hmo	44285	44218	0.15
Hmax	31819	31556	0.83

TABLE F-3. COMPARISON OF MCP CLIMB SPEED SCHEDULE AT 1.23 VSTALL AND MTOW LOADING

Altitude (ft)	Scaled Model KCAS	Bell Design KCAS	% Difference
0	153.5	152.6	0.61
2,500	153.7	152.7	0.65
5,000	153.9	152.7	0.81
10,000	154.4	153.0	0.89
15,000	155.0	153.3	1.11
20,000	155.9	153.7	1.45
25,000	157.3	154.3	1.94
30,000	159.2	154.9	2.78

TABLE F-4. COMPARISON OF LONG-RANGE CRUISE SPEED SCHEDULE AT MTOW CONDITIONS

Altitude (ft)	Scaled Model KCAS	Bell Design KCAS	% Difference
0	204.6	199.2	2.71
2,500	203.2	198.1	2.56
5,000	202.0	196.9	2.57
10,000	199.9	195.4	2.32
15,000	198.3	194.4	2.01
20,000	197.2	194.0	1.65
25,000	196.5	194.4	1.08
30,000	194.7	195.7	–0.53

TABLE F-5. COMPARISON OF MCP LEVEL FLIGHT CRUISE SPEED SCHEDULE AT MTOW CONDITIONS

Altitude (ft)	Scaled Model KCAS	Bell Design KCAS	% Difference
0	277.0	278.8	–0.66
2,500	274.8	276.3	–0.53
5,000	272.3	273.6	–0.48
10,000	265.8	268.3	–0.92
15,000	257.3	263.1	–2.21
20,000	246.0	257.7	–4.52
25,000	230.7	237.4	–2.82
30,000	205.4	207.4	–0.95

F-4 Propulsion Performance Comparison

The MCP climb thrust comparison for 1.23 Vstall at MTOW conditions is shown in table F-6. The MCP level flight cruise thrust comparison at MTOW conditions is shown in table F-7.

TABLE F-6. COMPARISION OF MCP CLIMB THRUST FOR 1.23 VSTALL AT MTOW CONDITIONS

Altitude (ft)	Scaled Model (lbf)	Bell Design (lbf)	% Difference
0	25790.1	26004	–0.82
2,500	25261.4	25184	0.31
5,000	24616.5	24374	0.99
10,000	22977.8	22772	0.90
15,000	20874.0	21217	–1.62
20,000	18305.1	18271	0.19
25,000	15271.1	14557	4.91
30,000	11772.0	11542	1.99

TABLE F-7. COMPARISON OF MCP LEVEL FLIGHT CRUISE THRUST AT MTOW CONDITIONS

Altitude (ft)	Scaled Model (lbf)	Bell Design (lbf)	% Difference
0	12935.3	13275	–2.56
2,500	12830.3	13042	–1.62
5,000	12691.3	12802	–0.86
10,000	12311.0	12326	–0.12
15,000	11794.4	11879	–0.71
20,000	11141.5	11432	–2.54
25,000	10352.3	10264	0.86
30,000	9426.9	9152	3.00

F-5 Fuel-burn Performance Comparison

The BADA MCP climb thrust specific fuel consumption (TSFC) comparison for the 1.23 Vstall, MTOW condition is shown in table F-8. Bell design values are determined directly from the supplemental Bell report. The scaled model values are determined by applying the Bell design climb trim true airspeeds, for the given altitude at MTOW and 1.23 Vstall, to the scaled 90-pax TSFC MCP climb fuel consumption model. This BADA model, outlined in detail in section 3, is a linear function of true airspeed. This technique serves to produce a direct comparison of the TSFC model without including effects of gross weight or stall speed schedule, differences affecting overall trim thrust in the scaled model.

TABLE F-8. MCP CLIMB TSFC COMPARISON

Altitude (ft)	Scaled Model (lbm/hr/lbf)	Bell Design (lbm/hr/lbf)	% Difference
0	0.2052	0.2014	1.91
2,500	0.2110	0.2067	2.07
5,000	0.2170	0.2123	2.20
10,000	0.2303	0.2250	2.35
15,000	0.2451	0.2394	2.40
20,000	0.2619	0.2568	1.99
25,000	0.2809	0.2771	1.36
30,000	0.3025	0.2984	1.38

The BADA MCP level flight cruise TSFC comparison for the MTOW condition is shown in table F-9. Bell design values are determined directly from the supplemental Bell report. The scaled model values are determined by trimming the 90-pax SAIC-developed performance deck at MCP level flight cruise under the scaled model MTOW loading and MCP level flight cruise thrust limits. Differences between the Bell design and the scaled model MTOW and MCP thrust limits will affect these results. With this in mind, the percent difference results remain low. The scaled model MTOW was estimated high by ~4.4 percent while the MCP level flight thrust limits of the scaled model were generally slightly lower than the Bell design.

The BADA low-power-descent fuel flow rate comparison for the MREF loading condition is shown in table F-10. Bell design values are taken directly from the supplemental Bell report. Differences between the Bell design and scaled model MREF will affect these results as the scale model MREF is ~3.2 percent higher than that of the final Bell design. This difference contributes to a higher required thrust, and thus fuel flow, for any given altitude to trim at the 250 KTAS descent speed trim point.

TABLE F-9. MCP LEVEL FLIGHT CRUISE TSFC COMPARISON

Altitude (ft)	Scaled Model (lbm/hr/lbf)	Bell Design (lbm/hr/lbf)	% Difference
0	0.4051	0.3943	2.74
2,500	0.4092	0.3989	2.57
5,000	0.4138	0.4042	2.39
10,000	0.4234	0.4153	1.95
15,000	0.4329	0.4271	1.36
20,000	0.4407	0.4407	0.00
25,000	0.4426	0.4351	1.73
30,000	0.4209	0.4057	3.74

TABLE F-10. LOW-POWER-DESCENT FUEL CONSUMPTION COMPARISON

Altitude (ft)	Scaled Model (lbm/hr)	Bell Design (lbm/hr)	% Difference
0	2739.3	2694	1.68
2,500	2598.05	2508	3.59
5,000	2456.8	2335	5.22
10,000	2174.3	2024	7.43
15,000	1891.8	1752	7.98
20,000	1609.3	1507	6.79
25,000	1326.8	1281	3.58
30,000	1044.3	1062	–1.67

F-6 Conclusions

Overall the scaled CTR90, based on BADA data for the other three vehicles, has been shown to have similar performance and geometry/mass characteristics to the Bell-designed 90-pax CTR. Only airplane mode performance has been investigated. The details of the scaled sizing of CTR90 are outlined in the section 3 and appendix E.

When given a set of performance data spanning various airframe passenger capacities, and thus size, it is reasonable to follow the simple sizing/scaling technique outlined within this appendix to generate a representative BADA performance model with the accuracy shown above. Keep in mind that this is based on the assumption that the same manufacturer has provided designs for various capacity airframes of the same type. In addition, the same sizing algorithms and design basis were used by the manufacturer to develop all vehicles for which performance trim data was supplied. In general, this allowed for a quick and simple sizing for a BADA model to capture an intermediate airframe size for fleet capacity distribution studies. If initial airspace simulations indicate a major positive impact given the new intermediate size, then a more thorough physics-based design could be completed to more accurately characterize the proposed vehicle.

F-7 References

F-**1**. Trept, T., Regnier, B., and Wood, T.: Design of 90-Passenger Civil Tiltrotor. Bell Helicopter Report No. 699-099-880, Dec. 9, 2009 (to be published).

APPENDIX G. CTR30, CTR90, AND CTR120 BADA MODEL VERIFICATION

Verification of CTR30, CTR90, and CTR120 is discussed below. Topics include performance trim data and mission profile verification. The static trim comparisons offer an overview of the accuracy of the final BADA model across the altitude envelope. This provides guidance as to where in the envelope the model may be used with good predictive characteristics. The mission profile verification offers a measure of accuracy of the BADA model as applied to an operational scenario. This offers a good measure of end-to-end accuracy for a complete mission cycle. Similar to the CTR10 verification discussed in section 3.5.1, all CTR30 and CTR120 testing compares the developed BADA model against verification data supplied by Bell Helicopter. Since the CTR90 was developed by linearly scaling from the CTR10, CTR30, and CTR120 performance, the performance of the 90-passenger BADA model is verified against a NASA 90-passenger design (ref. G-1).

G-1 CTR30 Verification

G-1.1 Trim Verification

Verification results for the static trim points are shown in tables G-1 to G-4. The percent difference between the BADA model predicted and the Bell design synthesis output are shown for airspeed, thrust, and fuel flow in all cases. These tables present the ability of the equivalent system model to recreate trim data supplied by Bell. An overestimation is indicated by a positive difference. Conversely, an underestimation is noted by a negative percent difference.

Overall results indicate the ability of the BADA model to emulate aerodynamic drag with good accuracy given the low percent difference in thrust required over the majority of the cases for climb and long-range cruise. In addition, percent difference results for true airspeed serve to verify proper representation of the climb speed, long-range cruise speed, and known maximum airspeed schedules under MTOW conditions within the performance deck utility. Note that the maximum continuous power (MCP) cruise points of table G-3 indicate a significant underestimation of thrust required, and thus fuel burn, when on the known KTAS schedule. This is as expected due to the compressibility effects encountered by the CTR30 design under MCP conditions. The 30-passenger vehicle did not include the MCP cruise data in the overall aerodynamic model buildup due to this issue as the allowable BADA model structure does not support its implementation.

The MCP climb fuel flow is well predicted. The long-range cruise (LRC) fuel flow is shown to best be emulated in the 15k- to 30k-foot altitude envelope. As altitude decreases below this band the prediction error significantly increases. Operationally, the CTR30 will cruise well above 15k feet, and fuel flow is well predicted in that region. The MCP cruise fuel flow based on the known maximum performance true airspeed schedule does not have a similar result due to the inability to account for aerodynamic compressibility effects. Note that this data, shown in table G-3, is generated by setting the CTR airspeed within the deck utility to the known maximum possible true airspeed achievable by the CTR. Required thrust for level flight is then determined along with resulting fuel flow. In the typical cruise altitude envelope the 30-passenger BADA model significantly underestimates MCP thrust and fuel flow.

Table G-4 shows MCP cruise verification results based on using the BADA model predicted maximum cruise thrust available. In these cases the deck utility solves for a final true airspeed that provides overall aerodynamic drag equivalent to maximum cruise thrust available. Results indicate that the BADA formulation is best employed when supplied with known airspeed operational schedules. In this case the predicted maximum obtainable true airspeeds under MTOW conditions were found to be significantly overestimated by 31.0- to 42.8-percent difference, with error increasing as altitude decreases. Maximum available cruise thrust, and subsequently fuel flow, is also shown to be significantly overestimated by the BADA formulation. This is

not surprising considering BADA predicts maximum available cruise thrust as being 95 percent of MCP climb thrust across the operational envelope. Revisiting figure D-3 it is clear to see how simply scaling the MCP climb thrust available by 0.95 will significantly overestimate MCP cruise thrust with prediction error increasing as altitude decreases. This is a shortfall in the BADA model formulation that precludes use of this tool as predicting maximum speed performance with any real accuracy.

TABLE G-1. MCP CLIMB AT 1.23 V_{STALL} STATIC TRIM VERIFICATION RESULTS FOR THE CTR30

Alt (k ft)	% Difference KTAS	% Difference Thrust	% Difference Fuel Flow
0	0.51	–1.05	–1.36
2.5	0.00	–0.05	–0.34
5	–0.41	0.79	0.51
10	–0.44	1.58	1.54
15	–0.10	0.83	1.22
20	0.36	–1.85	–1.09
25	0.45	–2.90	–2.39
30	–0.37	3.11	2.28

TABLE G-2. LONG-RANGE CRUISE STATIC TRIM VERIFICATION RESULTS FOR THE CTR30

Alt (k ft)	% Difference KTAS	% Difference Thrust	% Difference Fuel Flow
0	0.24	3.27	–13.46
2.5	–0.14	2.76	–12.19
5	–0.27	2.36	–10.77
10	–0.04	1.72	–7.61
15	0.28	0.96	–4.81
20	0.19	–0.31	–2.83
25	–0.45	–2.00	–1.80
30	0.17	–3.46	0.12

TABLE G-3. MCP CRUISE STATIC TRIM VERIFICATION RESULTS BASED ON KNOWN MAXIMUM KTAS SCHEDULE FOR THE CTR30

Alt (k ft)	% Difference KTAS	% Difference Thrust	% Difference Fuel Flow
0	–0.15	–2.57	–13.42
2.5	0.22	–2.55	–11.98
5	0.07	–3.15	–11.45
10	–0.24	–4.60	–10.70
15	–0.10	–5.96	–9.62
20	0.37	–7.54	–8.98
25	–0.27	–10.11	–11.13
30	0.06	–7.26	–5.74

TABLE G-4. MCP CRUISE STATIC TRIM VERIFICATION RESULTS BASED ON BADA-PREDICTED MAXIMUM CRUISE THRUST AVAILABLE FOR THE CTR30

Alt (k ft)	% Difference KTAS	% Difference Thrust	% Difference Fuel Flow
0	42.40	71.16	104.20
2.5	42.76	70.02	106.28
5	42.81	68.06	106.93
10	42.31	62.15	104.71
15	40.62	52.88	96.31
20	37.84	40.51	81.21
25	33.37	25.17	58.60
30	31.05	13.70	45.28

G-1.2 Mission Profile Verification

Mission profile verification results are shown in tables G-5 and G-6. LRC mission results are presented in table G-5. Maximum continuous power (MCP) cruise results are presented in table G-6. Both tables present the inertial position transited, time to transit, and fuel burned over each mission phase of climb cruise and descent for both the BADA and Bell-provided verification data. In addition, the overall percent differences for these states are shown for each mission phase. Similar statistics are presented for the complete mission to provide a snapshot of the overall accuracy of the total mission cycle. A negative percent difference indicates underestimation while a positive percent difference denotes an overestimation by the BADA model.

The LRC scenario of table G-5 indicates good fuel burn prediction with an overall –2.15-percent difference for the entire mission cycle. Over the entire flight spanning a 1060.9-nmi range the BADA-formatted model

underestimated fuel burned by 150.2 lbs. Fuel burn was best modeled during the climb segment (–0.34 percent) with an underestimation of 1.7 lbs. The cruise and descent segments indicate a –2.62-percent and 1.76-percent difference in fuel burn, respectively. This results in an underestimation of fuel burned of 157.2 lbs in cruise and overestimation of 8.7 lbs for the descent segment. Following the LRC operational velocity schedule the CTR30 model is optimized for both long- and short-range flights. Note that during short-range flights more overall mission time is spent in the climb and descent phases as the cruise segment becomes shorter.

TABLE G-5. LRC MISSION VERIFICATION FOR THE CTR30

	BADA Model			BELL Model			% Difference		
Mission Phase	**Dxpos (nmi)**	**Delta Time (min)**	**Fuel Burned (lbs)**	**Dxpos (nmi)**	**Delta Time (min)**	**Fuel Burned (lbs)**	**Dxpos**	**Delta Time**	**Fuel Burned**
MTOW Climb from SL to 25K at 1.23 V_{stall}	36.70	11.26	500.98	36.70	11.26	502.70	0.00	0.00	–0.34
Cruise for 932.6 nm at VLRC	932.60	200.16	5845.80	932.60	200.14	6003.00	0.00	0.01	–2.62
Descend to SL at 1000 fpm	91.60	25.00	501.47	91.60	25.00	492.80	0.00	0.00	1.76
TOTALS:	1060.90	236.42	6848.25	1060.9	236.40	6998.50	0.00	0.01	–2.15

TABLE G-6. MAXIMUM CONTINUOUS POWER CRUISE MISSION VERIFICATION FOR THE CTR30

	BADA Model			BELL Model			% Difference		
Mission Phase	**Dxpos (nmi)**	**Delta Time (min)**	**Fuel Burned (lbs)**	**Dxpos (nmi)**	**Delta Time (min)**	**Fuel Burned (lbs)**	**Dxpos**	**Delta Time**	**Fuel Burned**
MTOW Climb from SL to 25K at 1.23 Vstall	36.70	11.26	500.98	36.7	11.26	502.7	0.00	0.00	–0.34
Cruise for 801.2 nm at MCP	801.20	142.83	5390.70	801.2	142.94	6243.9	0.00	–0.08	–13.66
Descend to SL at 2000 fpm	54.90	12.50	250.75	54.8	12.5	248.1	0.18	0.00	1.07
TOTALS:	892.80	166.59	6142.43	892.7	166.7	6994.7	0.01	–0.07	–12.18

The MCP cruise scenario of table G-6 indicates significant underestimation in fuel burn with an overall –12.18-percent difference for the entire mission cycle. Again, in this test the MCP cruise speed is set at the known maximum airspeed presented by the Bell design for the given gross weight. It was clear from prior static trim verification that the BADA-formulated model is best employed by supplying operational airspeeds. This result is consistent with static trim verification testing noted in section G-1.1 at MCP cruise conditions.

Over the entire flight spanning a 892.8-nmi range the BADA-formatted model underestimated fuel burned by 852.3 lbs. Fuel burn was best modeled during the climb segment (–0.34 percent) with an underestimation of 1.7 lbs. The cruise and descent segments indicate a –13.66-percent and 1.07-percent difference in fuel burn, respectively. This results in an underestimation of fuel burned of 853.2 lbs and overestimation of 2.7 lbs for the cruise and descent segments, respectively.

G-1.3 Conversion Mode Verification

Static trim point verification results are shown in tables G-7 and G-8 for the CTR30. The percent difference between the BADA model predicted and expected output are shown for thrust, drag, and fuel flow in all cases. These tables present the ability of the BADA equivalent system model to recreate fuel flow trim data supplied by Bell, as well as the equivalent system thrust and drag formulated during BADA model development. An overestimation is indicated by a positive difference. Conversely, an underestimation is noted by a negative percent difference.

The level flight trim point results in table G-7 indicate good accuracy in the emulation of fuel flow, equivalent drag, and equivalent thrust with the highest magnitude of error being 0.71 percent.

The ascending/descending static trim point results of table G-8 indicate good overall accuracy. The conversion mode models are built to emulate Bell-supplied fuel burn performance. This is evident in the verification results. The thrust coefficient scale factors for the conversion modes also capture the scheduled equivalent thrust levels as expected. The drag model results indicate some variation as compared to the equivalent drag. It is clear that error increases with the magnitude of glide slope angle. In most cases the difference is much less than 2 percent. Results are similar to those seen in the 10-passenger verification testing.

TABLE G-7. CONVERSION MODE LEVEL FLIGHT STATIC TRIM VERIFICATION FOR THE CTR30

Conversion Mode	Flight Path Angle (deg)	% Difference Net Thrust	% Difference Total Drag	% Difference Fuel Flow
AP/IC LVL	0	–0.15	–0.15	–0.15
AP/IC LVL	0	0.29	0.29	0.29
AP/IC LVL	0	–0.09	–0.09	–0.10
STOL LD	0	0.29	0.29	0.30
STOL LD	0	–0.34	–0.34	–0.33
STOL LD	0	0.18	0.18	0.18
VTOL LD	0	0.49	0.49	0.49
VTOL LD	0	–0.63	–0.63	–0.63
VTOL LD	0	0.29	0.29	0.29
STOL TO	0	–0.39	–0.39	–0.39
STOL TO	0	0.71	0.71	0.71
STOL TO	0	–0.26	–0.26	–0.26
VTOL TO	0	0.48	0.48	0.48
VTOL TO	0	–0.61	–0.61	–0.61
VTOL TO	0	0.28	0.28	0.28

TABLE G-8. CONVERSION MODE STATIC TRIM VERIFICATION FOR THE CTR30

Conversion Mode	Flight Path Angle (deg)	% Difference Net Thrust	% Difference Total Drag	% Difference Fuel Flow
AP	–3	0.00	0.18	0.00
AP	–6	0.00	0.76	0.00
AP	–9	0.00	2.36	0.00
STOL LD	–3	0.00	0.19	0.00
STOL LD	–6	0.00	0.63	0.00
STOL LD	–9	0.00	1.30	0.00
VTOL LD	–3	0.00	0.19	0.00
VTOL LD	–6	0.00	0.63	0.00
VTOL LD	–9	0.00	1.30	0.00
STOL TO	1.4	0.00	0.03	0.00
STOL TO	2.8	0.00	0.08	0.00
STOL TO	4.2	0.00	0.17	0.00
VTOL TO	7.0	0.00	1.06	0.00
VTOL TO	13.8	0.00	4.56	0.00
VTOL TO	20.2	0.00	11.06	0.00

G-2 CTR120 Verification

G-2.1 Trim Verification

Verification results for the static trim points are shown in tables G-9 to G-12. The percent difference between the BADA model predicted and Bell design synthesis output are shown for airspeed, thrust, and fuel flow in all cases. These tables present the ability of the equivalent system model to recreate trim data supplied by Bell. An overestimation is indicated by a positive difference. Conversely, an underestimation is noted by a negative percent difference.

Overall results indicate the ability of the BADA model to emulate aerodynamic drag with good accuracy given the low percent difference in thrust required over the majority of the cases for climb, long- range cruise, and MCP cruise following the known KTAS schedule. In addition, percent difference results for true airspeed serve to verify proper representation of the climb speed, long-range cruise speed, and known maximum airspeed schedules under MTOW conditions within the performance deck utility.

The MCP climb fuel flow is well predicted. The LRC fuel flow is shown to best be emulated in the 15k to 30k foot altitude envelope. As altitude decreases below this band the prediction error steadily increases. Operationally the CTR120 will cruise well above 15k feet and fuel flow is well predicted in that region. The MCP cruise fuel flow based on the known maximum performance true airspeed schedule indicates the same result. Note that this data, shown in table G-11, is generated by setting the CTR airspeed within the deck utility to the known maximum possible true airspeed achievable by the CTR. Required thrust for level flight is then determined along with resulting fuel flow.

Table G-12 presents MCP cruise verification results based on using the BADA model predicted maximum cruise thrust available. In these cases the deck utility solves for a final true airspeed that provides overall aerodynamic drag equivalent to maximum cruise thrust available. Results here indicate the BADA formulation is best employed when supplied with known airspeed operational schedules. In this case the predicted maximum obtainable true airspeeds under MTOW conditions were found to be significantly overestimated by 23.15-percent to 49.43-percent difference with error increasing as altitude decreases. Maximum available cruise thrust, and subsequently fuel flow, is also shown to be significantly overestimated by the BADA formulation. This is not surprising considering BADA predicts maximum available cruise thrust as being 95 percent of MCP climb thrust across the operational envelope. Revisiting figure D-4 it is clear to see how simply scaling the MCP climb thrust available by 0.95 will significantly overestimate MCP cruise thrust with prediction error increasing as altitude decreases. This is a shortfall in the BADA model formulation that precludes use of this tool for predicting maximum speed performance with any real accuracy.

TABLE G-9. MCP CLIMB AT 1.23 V_{STALL} STATIC TRIM VERIFICATION RESULTS FOR THE CTR120

Alt (k ft)	% Difference KTAS	% Difference Thrust	% Difference Fuel Flow
0	0.26	–0.80	–1.10
2.5	–0.06	0.34	0.10
5	–0.18	1.00	0.88
10	–0.17	0.77	0.94
15	0.00	–2.03	–1.53
20	0.14	–0.81	–0.45
25	0.13	3.01	2.89
30	–0.12	–1.37	–1.65

TABLE G-10. LONG-RANGE CRUISE STATIC TRIM VERIFICATION RESULTS FOR THE CTR120

Alt (k ft)	% Difference KTAS	% Difference Thrust	% Difference Fuel Flow
0	0.30	1.80	–12.78
2.5	–0.05	1.77	–11.26
5	–0.23	1.75	–9.66
10	–0.26	1.79	–6.35
15	0.00	1.98	–3.06
20	0.23	2.07	0.02
25	0.21	2.08	2.70
30	–0.19	1.94	5.06

TABLE G-11. MCP CRUISE STATIC TRIM VERIFICATION RESULTS BASED ON KNOWN MAXIMUM KTAS SCHEDULE FOR THE CTR120

Alt (k ft)	% Difference KTAS	% Difference Thrust	% Difference Fuel Flow
0	0.50	–2.27	–11.25
2.5	–0.42	–3.29	–12.02
5	–0.61	–3.31	–11.31
10	0.26	–1.73	–7.37
15	0.82	–0.57	–3.99
20	–0.60	–1.80	–4.58
25	–0.06	0.21	–0.93
30	0.12	1.80	4.14

TABLE G-12. MCP CRUISE STATIC TRIM VERIFICATION RESULTS BASED ON BADA-PREDICTED MAXIMUM CRUISE THRUST AVAILABLE FOR THE CTR120

Alt (k ft)	% Difference KTAS	% Difference Thrust	% Difference Fuel Flow
0	49.34	91.28	146.57
2.5	49.43	90.90	148.84
5	48.99	89.30	148.86
10	46.95	83.15	142.97
15	42.65	72.16	127.07
20	35.60	56.03	100.55
25	31.41	43.10	80.97
30	23.15	21.41	49.40

G-2.2 Mission Profile Verification

Mission profile verification results are shown in tables G-13 and G-14. LRC mission results are presented in table G-13. MCP cruise results are presented in table G-14. Both tables present the inertial position transited, time to transit, and fuel burned over each mission phase of climb cruise and descent for both the BADA and Bell-provided verification data. In addition, the overall percent differences for these states are shown for each mission phase. Similar statistics are presented for the complete mission to provide a snapshot of the overall accuracy of the total mission cycle. A negative percent difference indicates underestimation while a positive percent difference denotes an overestimation by the BADA model.

The long-range cruise scenario of table G-13 indicates good fuel burn prediction with an overall 1.71-percent difference for the entire mission cycle. Over the entire flight spanning a 1431.8-nmi range the BADA-formatted model overestimated fuel burned by 366.5 lbs. Fuel burn was best modeled during the climb segment (–0.96 percent) with an underestimation of 15.1 lbs. The cruise and descent segments indicate a 2.37-percent and –5.37-percent difference in fuel burn, respectively. This results in an overestimation of fuel burned of 443.0 lbs in cruise and underestimation of 61.4 lbs for the descent segment. Following the long-range cruise operational velocity schedule the CTR120 model is optimized for both long- and short-range flights. Note that during short-range flights more overall mission time is spent in the climb and descent phases as the cruise segment becomes shorter.

The maximum continuous power cruise scenario of table G-14 indicates an underestimation in fuel burn with an overall –0.88-percent difference for the entire mission cycle. Again, in this test the MCP cruise speed is set at the known maximum airspeed presented by the Bell design for the given gross weight. It was clear from prior static trim verification that the BADA-formulated model is best employed by supplying operational airspeeds. This result is consistent with static trim verification testing noted previously in section G-2.1 at MCP cruise conditions.

TABLE G-13. LRC MISSION VERIFICATION FOR THE CTR120

	BADA Model			BELL Model			% Difference		
Mission Phase	**Dxpos (nmi)**	**Delta Time (min)**	**Fuel Burned (lbs)**	**Dxpos (nmi)**	**Delta Time (min)**	**Fuel Burned (lbs)**	**Dxpos**	**Delta Time**	**Fuel Burned**
MTOW Climb from SL to 25K at 1.23 V_{stall}	49.7	15.6	1550.9	50.2	15.6	1566.0	–1.0	0.0	–0.96
Cruise for 1431.8 nm at VLRC	1431.8	295.8	19172.0	1431.8	295.8	18729.0	0.0	0.0	2.37
Descend to SL at 1000 fpm	116.31	27.5	1083.0	116.3	27.5	1144.4	0.01	0.0	–5.37
TOTALS:	1597.81	338.9	21805.9	1598.3	338.9	21439.4	–0.03	0.0	1.71

TABLE G-14. MCP CRUISE MISSION VERIFICATION FOR THE CTR120

	BADA Model			BELL Model			% Difference		
Mission Phase	**Dxpos (nmi)**	**Delta Time (min)**	**Fuel Burned (lbs)**	**Dxpos (nmi)**	**Delta Time (min)**	**Fuel Burned (lbs)**	**Dxpos**	**Delta Time**	**Fuel Burned**
MTOW Climb from SL to 25K at 1.23 Vstall	49.7	15.6	1550.9	50.2	15.6	1566	–1.0	0.0	–0.96
Cruise for 1305.8 nm at MCP	1305.8	223.7	19158.0	1305.8	223.7	19376.9	0.0	0.0	–1.13
Descend to SL at 2000 fpm	67.9	13.75	541.53	67.9	13.75	497.2	0.0	0.0	8.92
TOTALS:	1423.4	253.05	21250.43	1423.9	253.05	21440.1	–0.04	0.0	–0.88

Over the entire flight spanning a 1305.8-nmi range the BADA-formatted model underestimated fuel burned by 189.7 lbs. Fuel burn was best modeled during the climb segment (–0.96 percent) with an underestimation of 15.1 lbs. The cruise and descent segments indicate a –1.13-percent and 8.92-percent difference in fuel burn, respectively. This results in an underestimation of fuel burned of 218.9 lbs and an overestimation of 44.3 lbs for the cruise and descent segments, respectively.

G-2.3 Conversion Mode Verification

Static trim point verification results are shown in tables G-15 and G-16 for the CTR120. The percent difference between the BADA model predicted and expected output are shown for thrust, drag, and fuel flow in all cases. These tables present the ability of the BADA equivalent system model to recreate fuel flow trim data supplied by Bell, as well as the equivalent system thrust and drag formulated during BADA model development. An overestimation is indicated by a positive difference. Conversely, an underestimation is noted by a negative percent difference. The level flight trim point results in table G-15 indicate good accuracy in the emulation of fuel flow, equivalent drag, and equivalent thrust with the highest magnitude of error being 0.74 percent.

The ascending/descending static trim point results from table G-16 indicate good overall accuracy. The conversion mode models are built to emulate Bell-supplied fuel burn performance. This is evident in the verification results. The thrust coefficient scale factors for the conversion modes also capture the scheduled equivalent thrust levels as expected. The drag model results indicate some variation as compared to the equivalent drag. It is clear that error increases with the magnitude of glide slope angle. In most cases the difference is much less than 2 percent. Results are similar to those seen in the 10-passenger verification testing.

TABLE G-15. CONVERSION MODE LEVEL FLIGHT STATIC TRIM VERIFICATION FOR THE CTR120

Conversion Mode	Flight Path Angle (deg)	% Difference Net Thrust	% Difference Total Drag	% Difference Fuel Flow
AP/IC LVL	0	0.27	0.27	0.26
AP/IC LVL	0	–0.44	–0.44	–0.44
AP/IC LVL	0	0.22	0.22	0.22
STOL LD	0	0.26	0.26	0.26
STOL LD	0	–0.29	–0.29	–0.29
STOL LD	0	0.17	0.17	0.17
VTOL LD	0	0.57	0.57	0.57
VTOL LD	0	–0.74	–0.74	–0.74
VTOL LD	0	0.34	0.34	0.34
STOL TO	0	0.27	0.27	0.27
STOL TO	0	–0.43	–0.43	–0.44
STOL TO	0	0.22	0.22	0.22
VTOL TO	0	0.56	0.56	0.56
VTOL TO	0	–0.73	–0.73	–0.72
VTOL TO	0	0.34	0.34	0.34

TABLE G-16. CONVERSION MODE STATIC TRIM VERIFICATION FOR THE CTR120

Conversion Mode	Flight Path Angle (deg)	% Difference Net Thrust	% Difference Total Drag	% Difference Fuel Flow
AP	–3	0.00	0.17	0.00
AP	–6	0.00	0.72	0.00
AP	–9	0.00	2.33	0.00
STOL LD	–3	0.00	0.20	0.00
STOL LD	–6	0.00	0.64	0.00
STOL LD	–9	0.00	1.33	0.00
VTOL LD	–3	0.00	0.20	0.00
VTOL LD	–6	0.00	0.65	0.00
VTOL LD	–9	0.00	1.36	0.00
STOL TO	1.4	0.00	0.03	0.00
STOL TO	2.8	0.00	0.07	0.00
STOL TO	4.2	0.00	0.14	0.00
VTOL TO	7.0	0.00	1.08	0.00
VTOL TO	13.8	0.00	4.56	0.00
VTOL TO	20.2	0.00	10.79	0.00

G-3 CTR90 Verification

Section 2 described the design of a fleet of civil tiltrotor (CTR) aircraft (i.e., CTR10, CTR30, and CTR120), and provided the subsequent performance data required to develop BADA-based performance models. In order to fill out the fleet a CTR90 was sized based on linear scaling of BADA model entries as outlined in section 2 and described in appendix E.

Bell Helicopter, under NASA sponsorship, concurrently developed a 90-passenger CTR design (ref. G-1). This appendix compares notable airplane mode performance characteristics between the sized/scaled 90-passenger CTR model described in appendix E and the Bell CTR design (ref. G-1). It is important to note that currently only the sized/scaled 90-passenger CTR model (appendix E) has been formatted into a set of BADA files supporting the CTR in NextGen studies.

G-3.1 Geometry Comparison

The main airframe geometry and characteristic terms used by BADA are compared to the final Bell design (ref. G-1) shown in table G-17.

TABLE G-17. AIRFRAME GEOMETRY AND MASS COMPARISON

Parameter	Sized/Scaled Model	Bell Design	% Difference
Mmin OWE (lbs)	82428.3	80000	3.04
Mref (lbs)	100590.3	97500	3.17
Mmax MTOW (lbs)	119911.5	114818	4.44
Fuselage Length (ft)	100.15	98.6	1.57
Wingspan (ft)	82.21	88.1	–6.69
Wing Area (ft^2)	1111.7	1195	–6.97
Fuel Capacity (lbs)	17683.2	14885	18.80
Payload Weight (lbs)	19800	19800	0.00

G-3.2 Envelope Performance Comparison

The comparison of absolute ceiling (Hmo) and maximum ceiling with a 300-fpm residual rate of climb available (Hmax @ MTOW loading) is shown in table G-18.

TABLE G-18. AIRFRAME ALTITUDE ENVELOPE COMPARISON

Parameter	Sized/Scaled Model	Bell Design	% Difference
Hmo (ft)	44285	44218	0.15
Hmax (ft)	31819	31556	0.83

The MCP climb speed schedule comparison for 1.23 Vstall at MTOW conditions is shown in table G-19. The long-range cruise level flight speed schedule comparison at MTOW conditions is shown in table G-20. The MCP level flight cruise speed schedule comparison at MTOW conditions is shown in table G-21.

TABLE G-19. COMPARISON OF MCP CLIMB SPEED SCHEDULE AT 1.23 VSTALL AND MTOW LOADING

Altitude (ft)	Sized/Scaled Model KCAS	Bell Design KCAS	% Difference
0	153.5	152.6	0.61
2,500	153.7	152.7	0.65
5,000	153.9	152.7	0.81
10,000	154.4	153.0	0.89
15,000	155.0	153.3	1.11
20,000	155.9	153.7	1.45
25,000	157.3	154.3	1.94
30,000	159.2	154.9	2.78

TABLE G-20. COMPARISON OF LONG-RANGE CRUISE SPEED SCHEDULE AT MTOW CONDITIONS

Altitude (ft)	Sized/Scaled Model KCAS	Bell Design KCAS	% Difference
0	204.6	199.2	2.71
2,500	203.2	198.1	2.56
5,000	202.0	196.9	2.57
10,000	199.9	195.4	2.32
15,000	198.3	194.4	2.01
20,000	197.2	194.0	1.65
25,000	196.5	194.4	1.08
30,000	194.7	195.7	–0.53

TABLE G-21. COMPARISON OF MCP LEVEL FLIGHT CRUISE SPEED SCHEDULE AT MTOW CONDITIONS

Altitude (ft)	Sized/Scaled Model KCAS	Bell Design KCAS	% Difference
0	277.0	278.8	–0.66
2,500	274.8	276.3	–0.53
5,000	272.3	273.6	–0.48
10,000	265.8	268.3	–0.92
15,000	257.3	263.1	–2.21
20,000	246.0	257.7	–4.52
25,000	230.7	237.4	–2.82
30,000	205.4	207.4	–0.95

G-3.3 Propulsion Performance Comparison

The MCP climb thrust comparison for 1.23 Vstall at MTOW conditions is shown in table G-22. The maximum continuous power level flight cruise thrust comparison at MTOW conditions is shown in table G-23.

TABLE G-22. COMPARISON OF MCP CLIMB THRUST FOR 1.23 VSTALL AT MTOW CONDITIONS

Altitude (ft)	Sized/Scaled Model (lbf)	Bell Design (lbf)	% Difference
0	25790.1	26004	–0.82
2,500	25261.4	25184	0.31
5,000	24616.5	24374	0.99
10,000	22977.8	22772	0.90
15,000	20874.0	21217	–1.62
20,000	18305.1	18271	0.19
25,000	15271.1	14557	4.91
30,000	11772.0	11542	1.99

TABLE G-23. MCP LEVEL FLIGHT CRUISE THRUST AT MTOW CONDITIONS COMPARISON

Altitude (ft)	Sized/Scaled Model (lbf)	Bell Design (lbf)	% Difference
0	12935.3	13275	–2.56
2,500	12830.3	13042	–1.62
5,000	12691.3	12802	–0.86
10,000	12311.0	12326	–0.12
15,000	11794.4	11879	–0.71
20,000	11141.5	11432	–2.54
25,000	10352.3	10264	0.86
30,000	9426.9	9152	3.00

G-3.4 Fuel-burn Performance Comparison

The BADA MCP climb thrust specific fuel consumption (TSFC) comparison for the 1.23 Vstall, MTOW condition is shown in table G-24. Bell design values are determined directly from ref. G-1. The sized/scaled model values are determined by applying the Bell design climb trim true airspeeds, for the given altitude at MTOW and 1.23 Vstall, to the scaled 90-passenger TSFC MCP climb fuel consumption model. This BADA model, outlined in detail in appendix E, is a linear function of true airspeed. This technique serves to produce a direct comparison of the TSFC model without including effects of gross weight or stall speed schedule, differences affecting overall trim thrust in the scaled model.

The BADA MCP level flight cruise TSFC comparison for the MTOW condition is shown in table G-25. Bell design values are determined directly from the supplemental Bell report (ref. G-1). The scaled model values are determined by trimming the 90-passenger SAIC-developed performance deck at MCP level flight cruise under the scaled model MTOW loading and MCP level flight cruise thrust limits. Differences between the Bell design and the scaled model MTOW and MCP thrust limits will affect these results. With this in mind, the percent difference results remain low. The scaled model MTOW was estimated high by ~4.4 percent while the MCP level flight thrust limits of the scaled model were generally slightly lower than the Bell design.

TABLE G-24. MCP CLIMB TSFC COMPARISON

Altitude (ft)	Sized/Scaled Model (lbm/hr/lbf)	Bell Design (lbm/hr/lbf)	% Difference
0	0.2052	0.2014	1.91
2,500	0.2110	0.2067	2.07
5,000	0.2170	0.2123	2.20
10,000	0.2303	0.2250	2.35
15,000	0.2451	0.2394	2.40
20,000	0.2619	0.2568	1.99
25,000	0.2809	0.2771	1.36
30,000	0.3025	0.2984	1.38

TABLE G-25. MCP LEVEL FLIGHT CRUISE TSFC COMPARISON

Altitude (ft)	Sized/Scaled Model (lbm/hr/lbf)	Bell Design (lbm/hr/lbf)	% Difference
0	0.4051	0.3943	2.74
2,500	0.4092	0.3989	2.57
5,000	0.4138	0.4042	2.39
10,000	0.4234	0.4153	1.95
15,000	0.4329	0.4271	1.36
20,000	0.4407	0.4407	0.00
25,000	0.4426	0.4351	1.73
30,000	0.4209	0.4057	3.74

TABLE G-26. LOW-POWER-DESCENT FUEL CONSUMPTION COMPARISON

Altitude (ft)	Sized/Scaled Model (lbm/hr)	Bell Design (lbm/hr)	% Difference
0	2739.3	2694	1.68
2,500	2598.05	2508	3.59
5,000	2456.8	2335	5.22
10,000	2174.3	2024	7.43
15,000	1891.8	1752	7.98
20,000	1609.3	1507	6.79
25,000	1326.8	1281	3.58
30,000	1044.3	1062	–1.67

The BADA low-power-descent fuel flow rate comparison for the MREF loading condition is shown in table G-26. Bell design values are taken directly from ref. G-1. Differences between the Bell design and scaled model MREF will affect these results as the scale model MREF is approximately 3.2 percent higher than that of the final Bell design. This difference contributes to a higher required thrust, and thus fuel flow, for any given altitude to trim at the 250-KTAS descent speed trim point.

G-3.5 Conclusions

Overall the scaled CTR90, based on BADA data for the other three airframes, has been shown to have similar performance and geometry/mass characteristics to the Bell-designed 90-passenger CTR. Only airplane mode performance has been investigated. The details of the scaled sizing of the CTR90 are outlined in the Year-1 report.

When given a set of performance data spanning various airframe passenger capacities, and thus size, it is reasonable to follow the simple sizing technique outlined within the Year-1 report to get a representative BADA performance model with the accuracy shown above. Keep in mind that this is based on the assumption that the same manufacturer has provided designs for various capacity airframes of the same type. In addition, the same sizing algorithms and design basis were used by the manufacturer to develop all airframes for which performance trim data was supplied. In general, this allowed for a quick and simple sizing for a BADA model to capture an intermediate airframe size for fleet capacity distribution studies. If initial airspace simulations indicate a major positive impact given the new intermediate size, then a more thorough physics-based design could be completed to more accurately characterize the proposed vehicle.

G-4 References

G-1. Trept, T., Regnier, B. and Wood, T.: Design of 90-Passenger Civil Tiltrotor. Bell Helicopter Report No. 699-099-880, Dec. 9, 2009 (to be published).

APPENDIX H. PILOT-IN-THE-LOOP FLIGHT SIMULATION RESULTS

Select runs representative of approaches and takeoffs for both the 10- and 30-passenger designs are presented in this section. Figures H-1, H-2, and H-3 respectively present time histories for 3-, 6-, and 9-degree glide slope approaches for the 10-passenger CTR. Figures H-4 and H-5 respectively present VTO and STO takeoff time histories for the 10-passenger CTR. The 10-passenger profiles were developed based on a gross weight corresponding to the maximum fuel load and payload weight of 16,192 lbs.

Figures H-6, H-7, and H-8 respectively present time histories for 3-, 6-, and 9-degree glide slope approaches for the CTR30. Figures H-9 and H-10 respectively present VTO and STO takeoff time histories for the CTR30. The 30-passenger profiles were developed based on a gross weight corresponding to the maximum fuel load and payload weight of 46,430 lbs.

The above time histories also correspond to those for which the noise footprints were developed and presented in section 2.9.4. Note that each time history includes markers that identify the data range used for the noise analysis. The start and end times are shown by a double vertical line, delineating the portion of the time history selected for the acoustical flight track input to rotorcraft noise model (RNM).

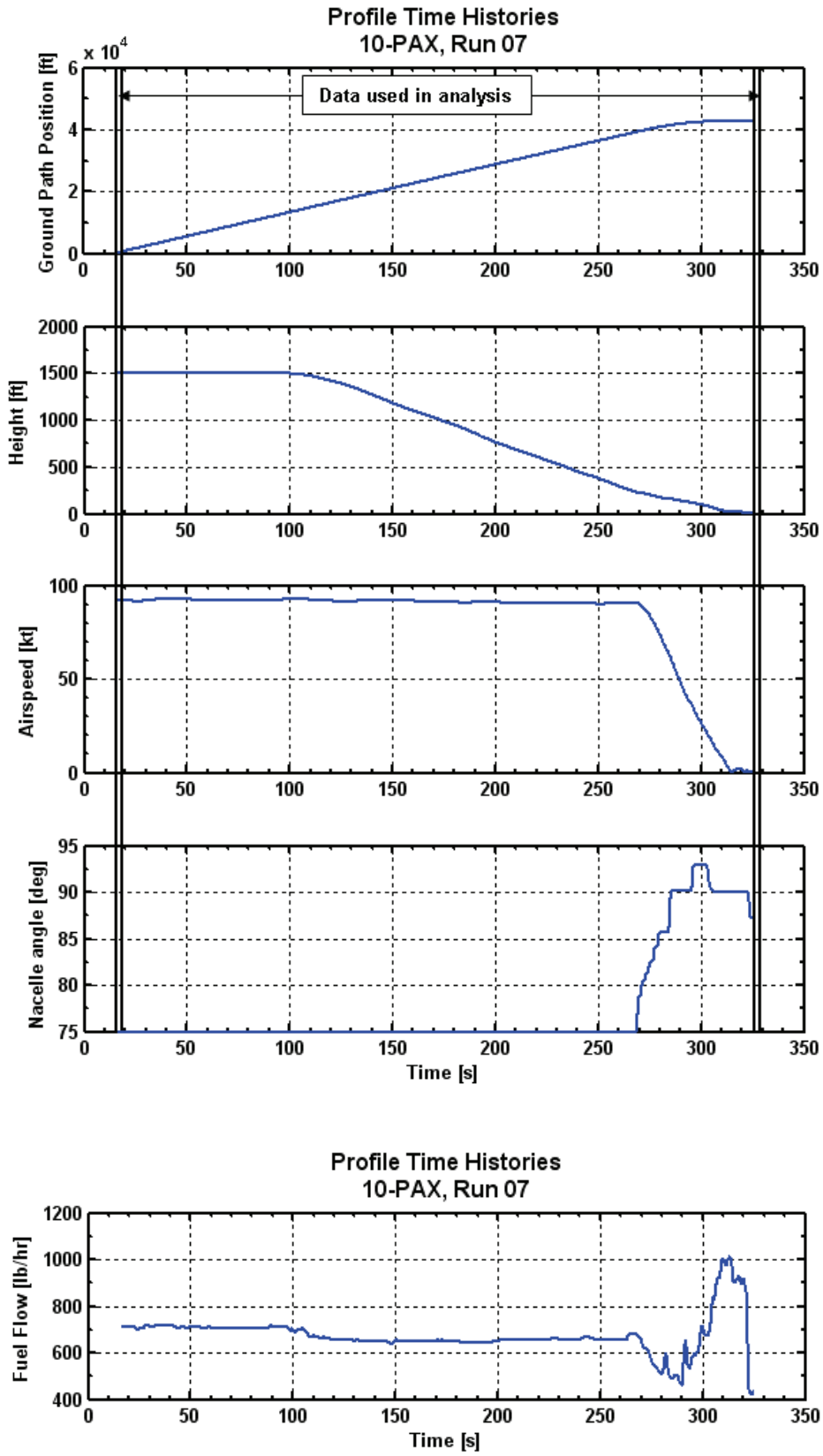

Figure H-1. 10-passenger approach time history, 3 degrees.

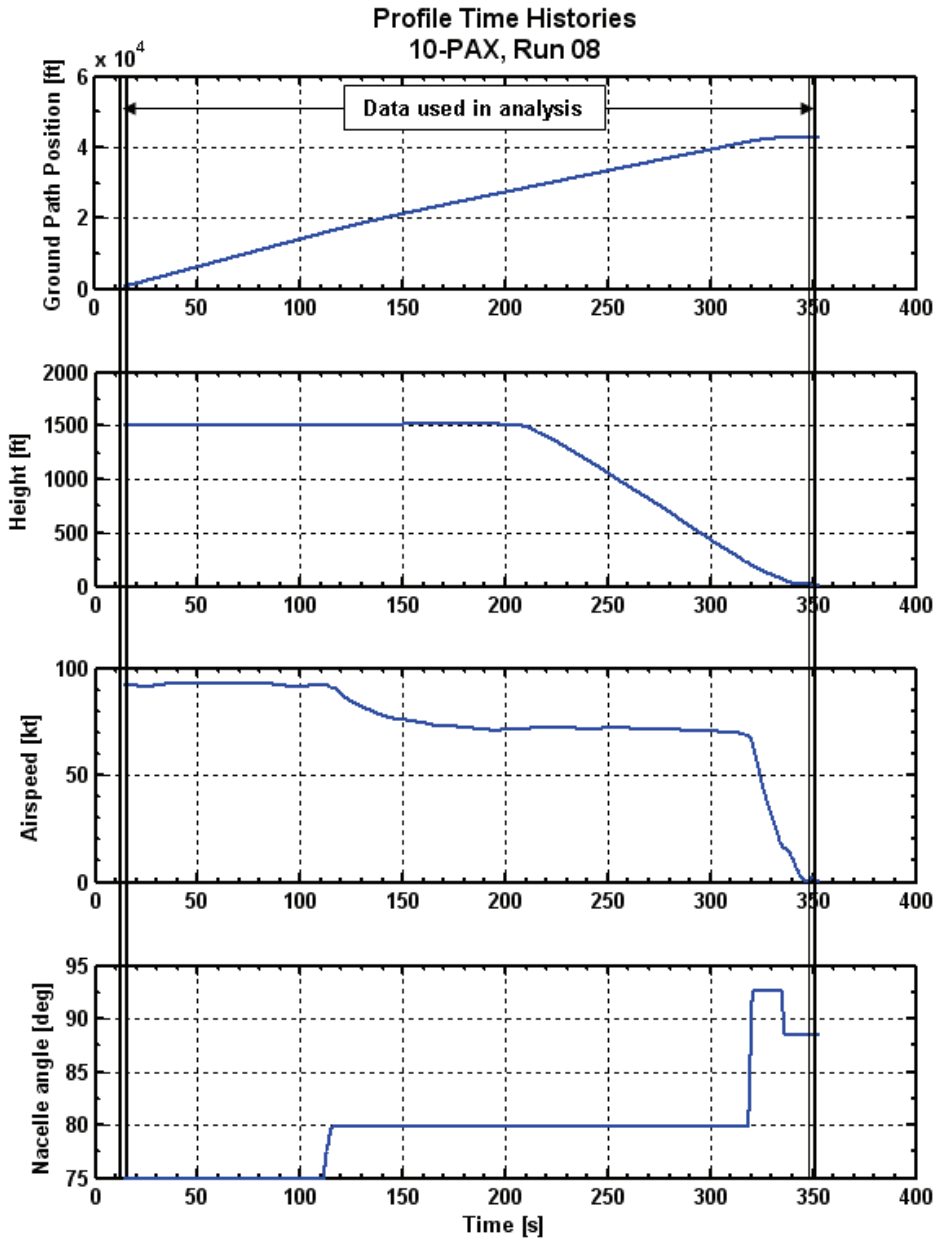

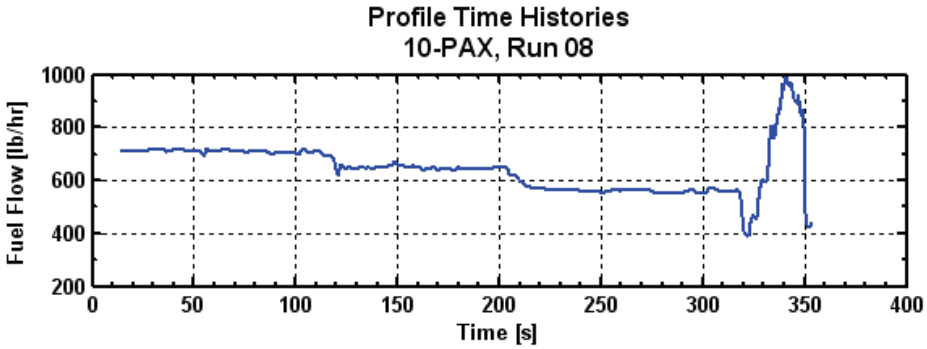

Figure H-2. 10-passenger approach time history, 6 degrees.

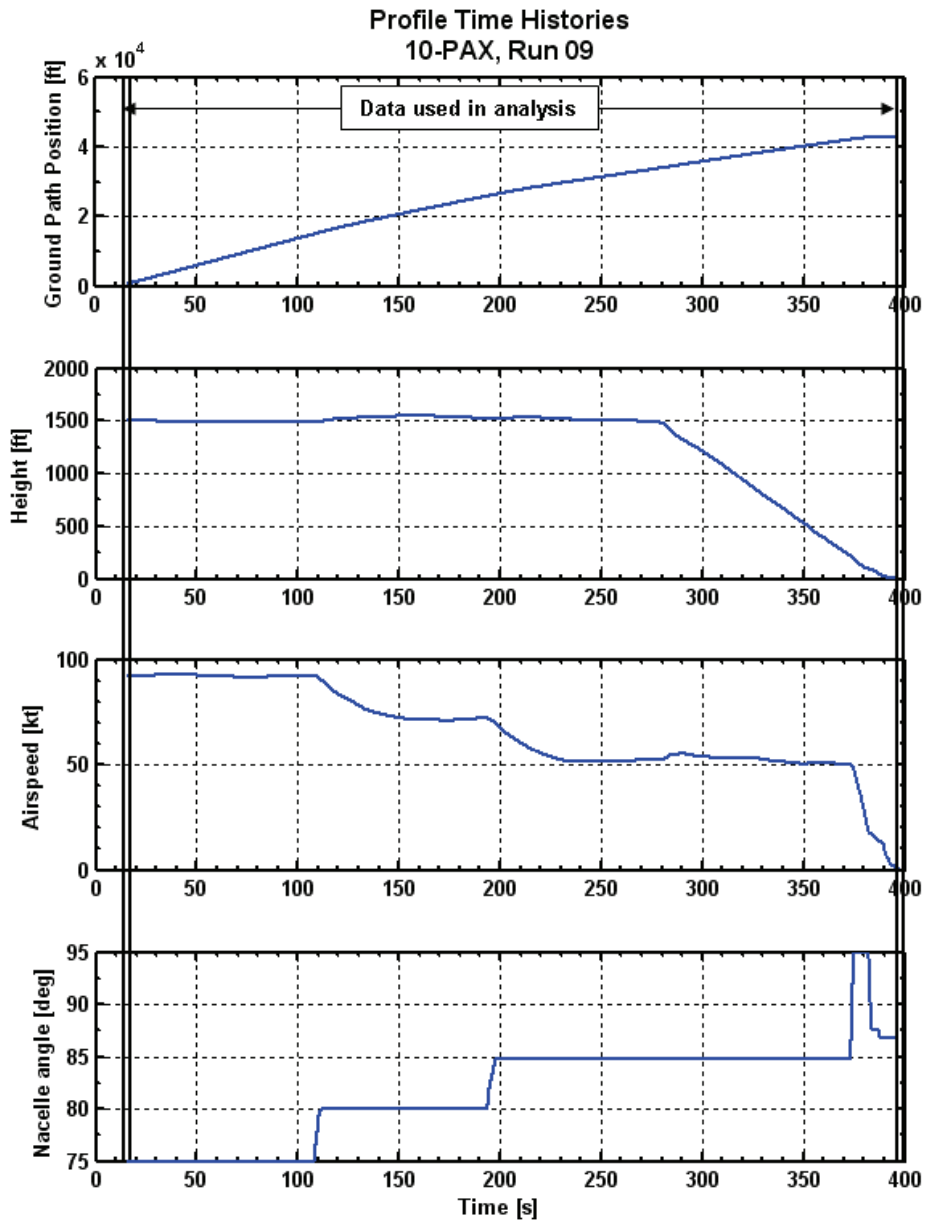

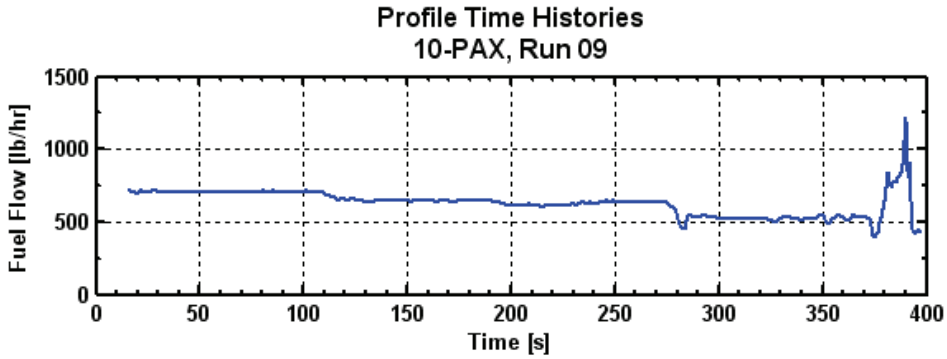

Figure H-3. 10-passenger approach time history, 9 degrees.

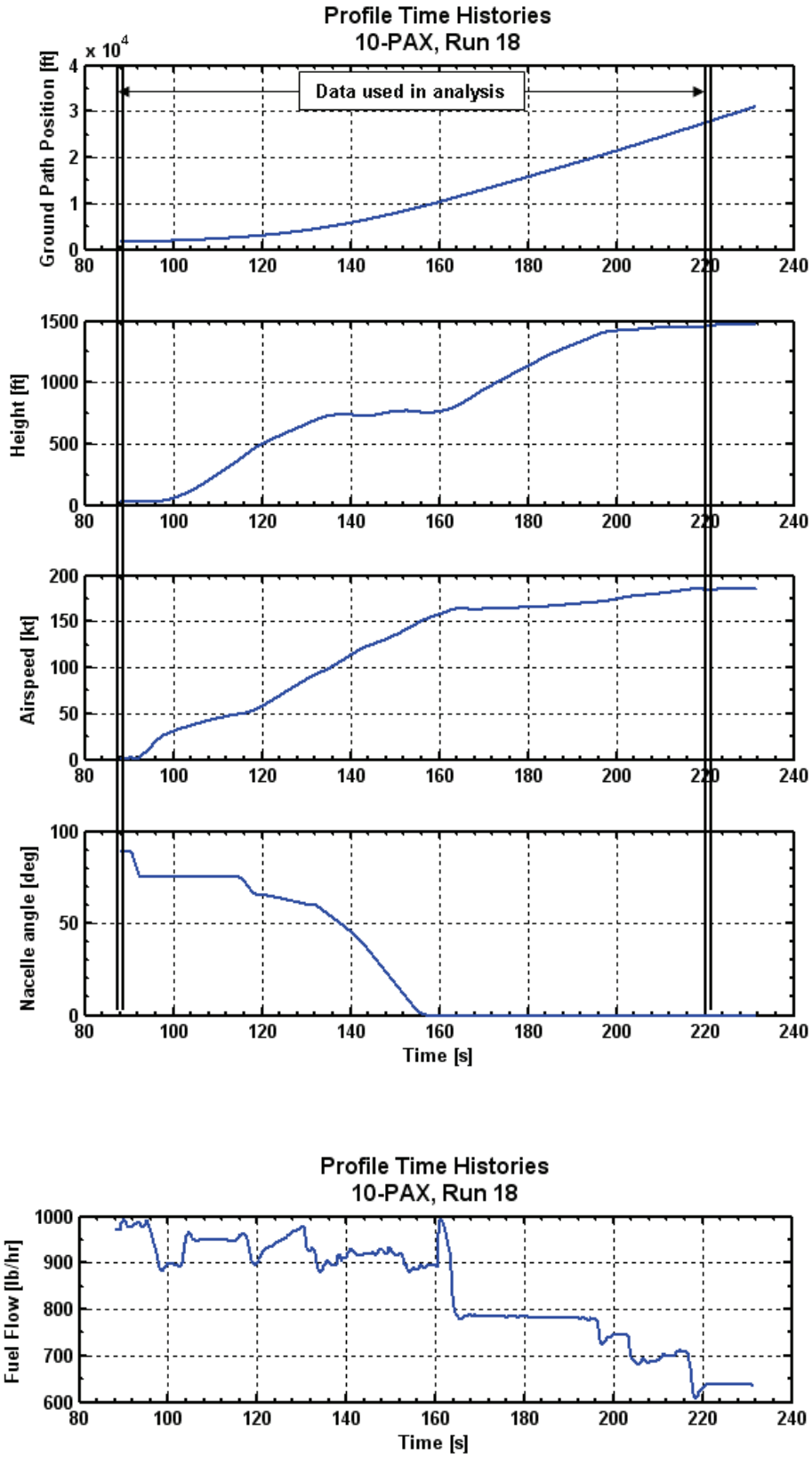

Figure H-4. 10-passenger takeoff time history, VTO.

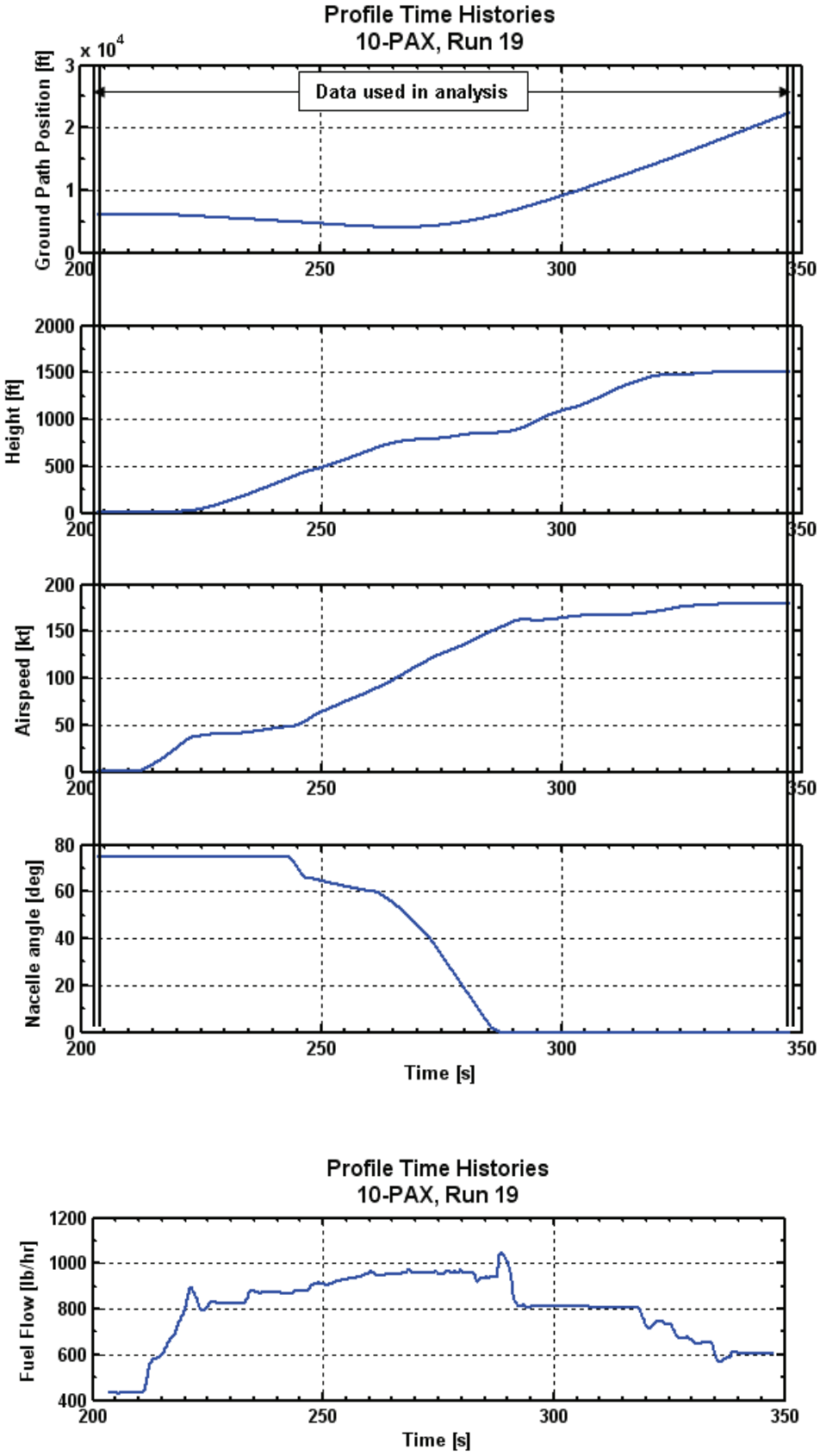

Figure H-5. 10-passenger takeoff time history, STO.

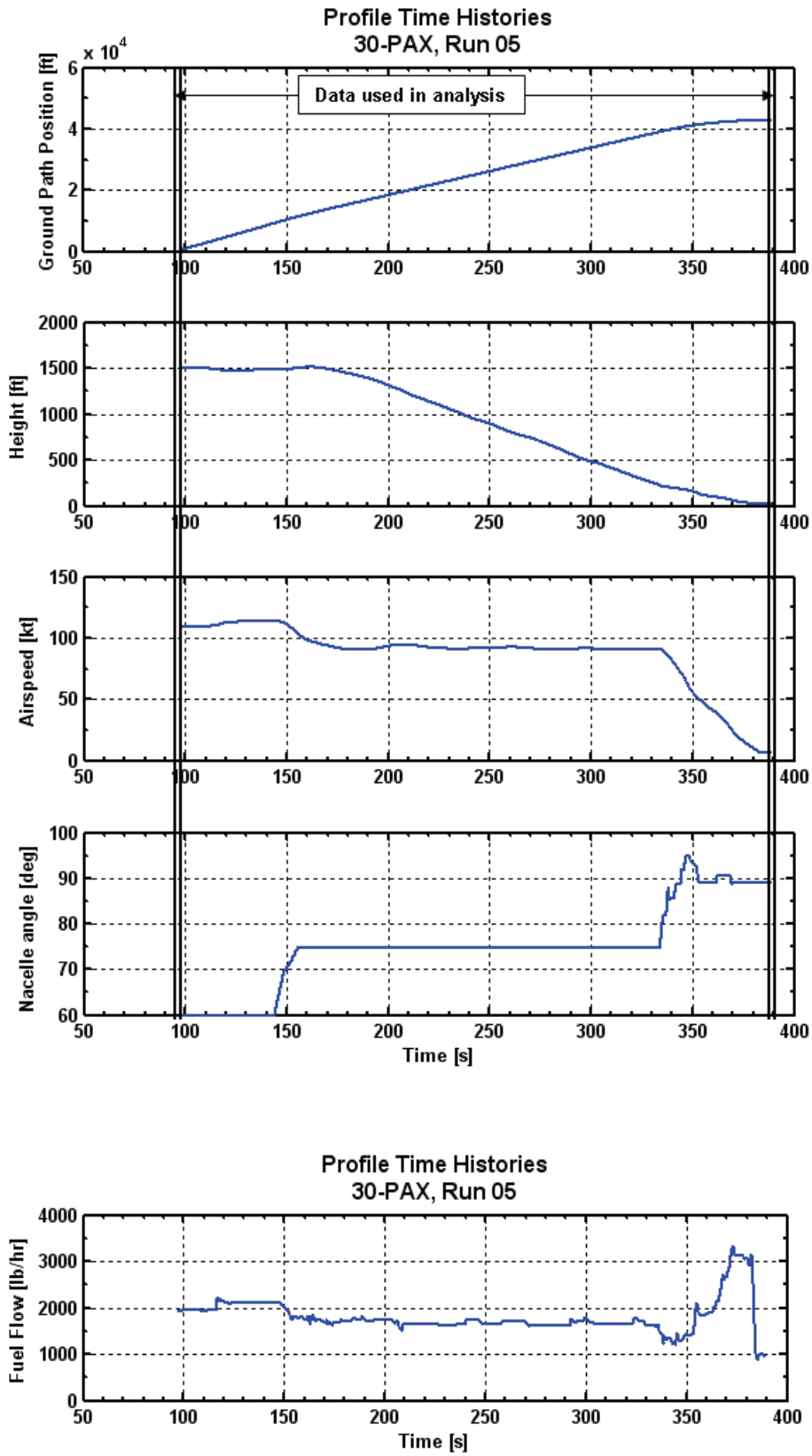

Figure H-6. 30-passenger approach time history, 3 degrees.

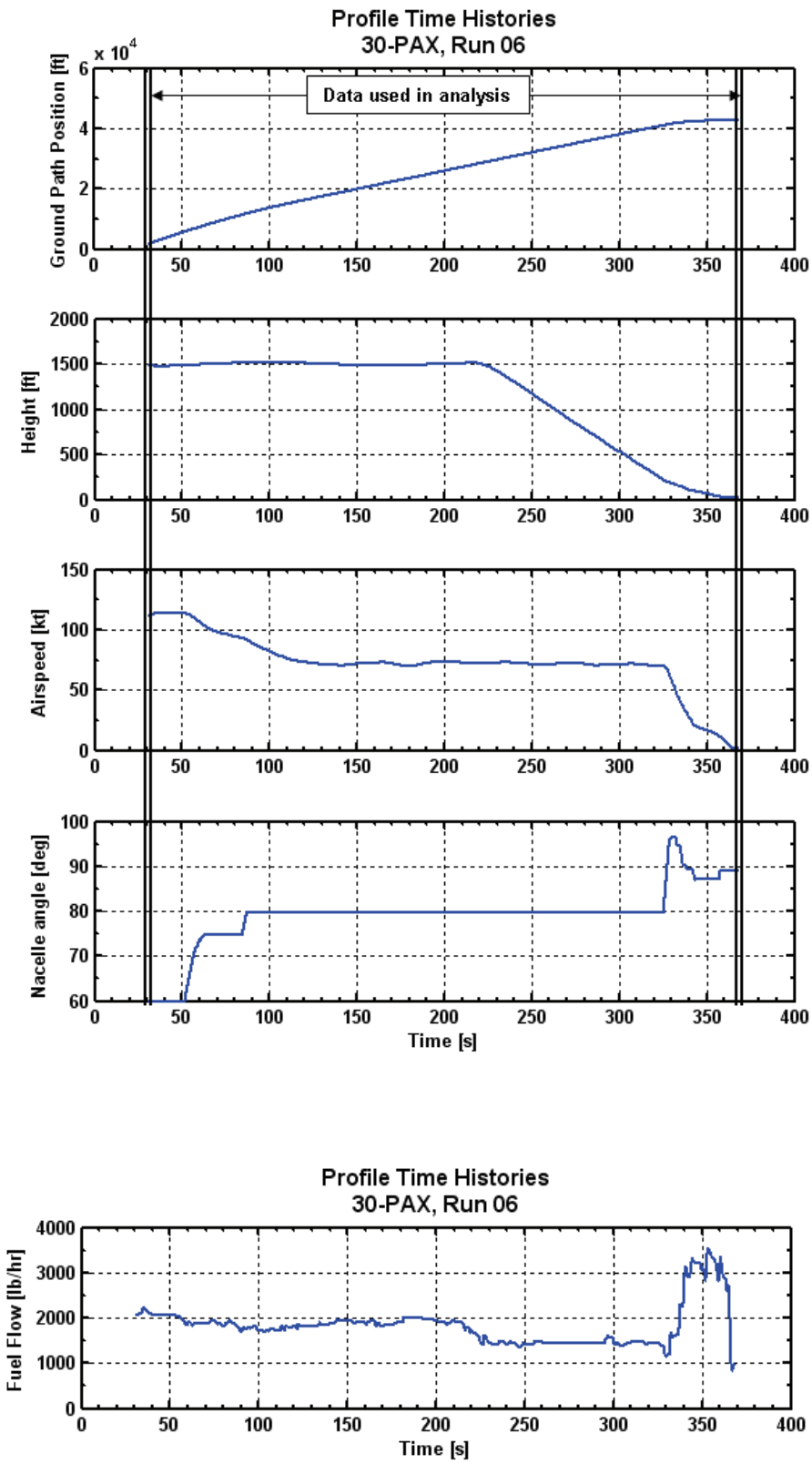

Figure H-7. 30-passenger approach time history, 6 degrees.

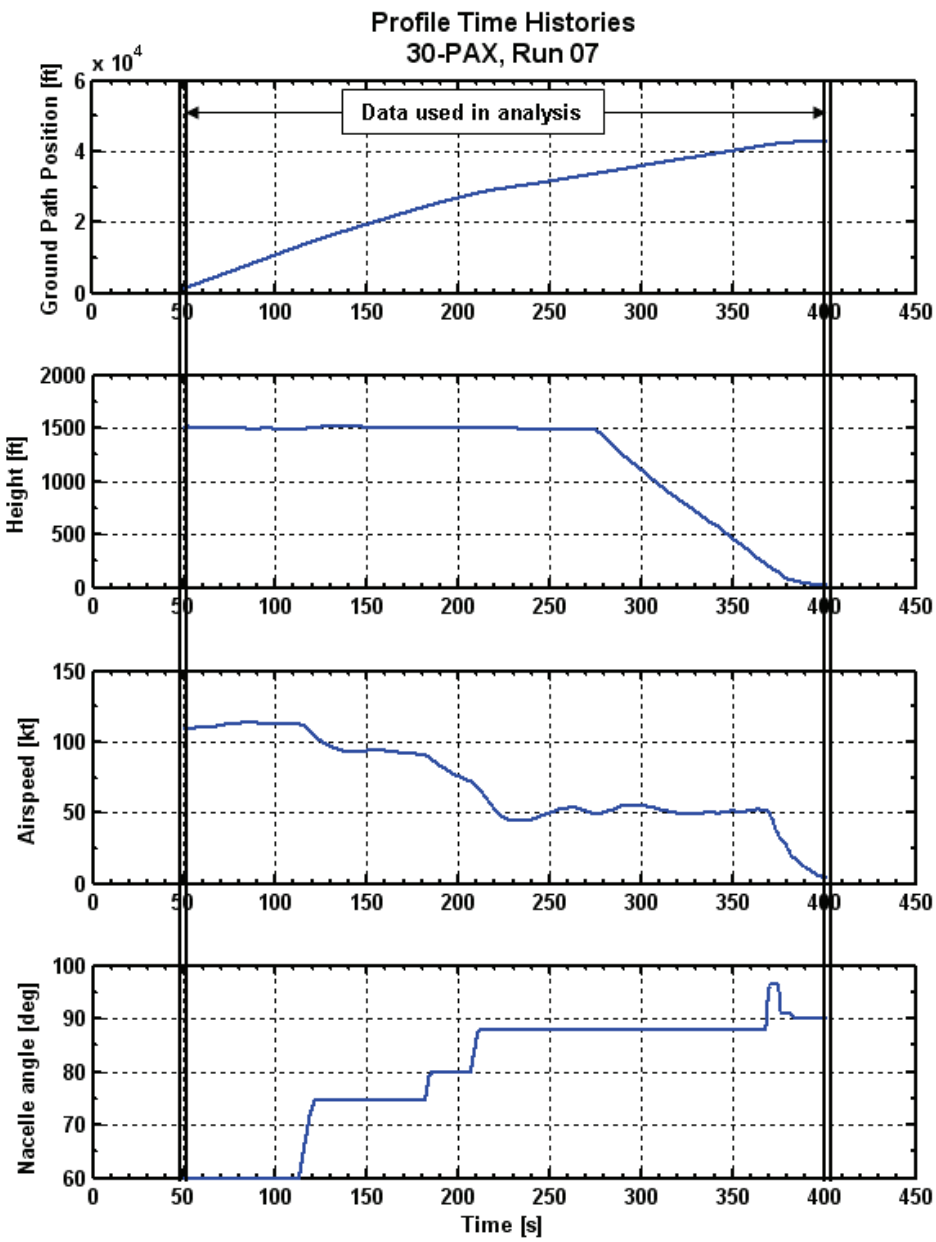

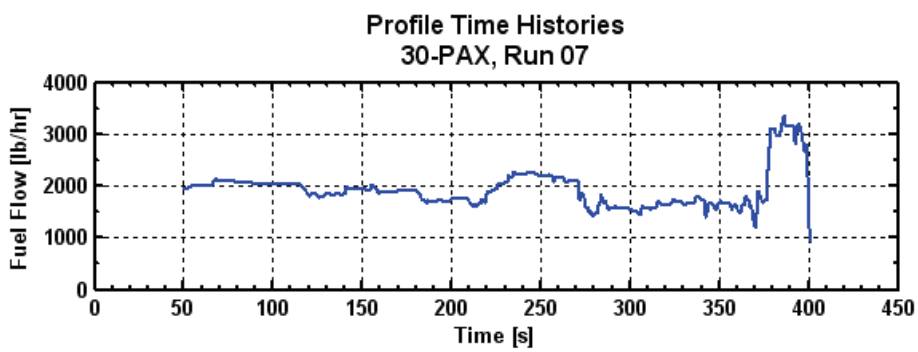

Figure H-8. 30-passenger approach time history, 9 degrees.

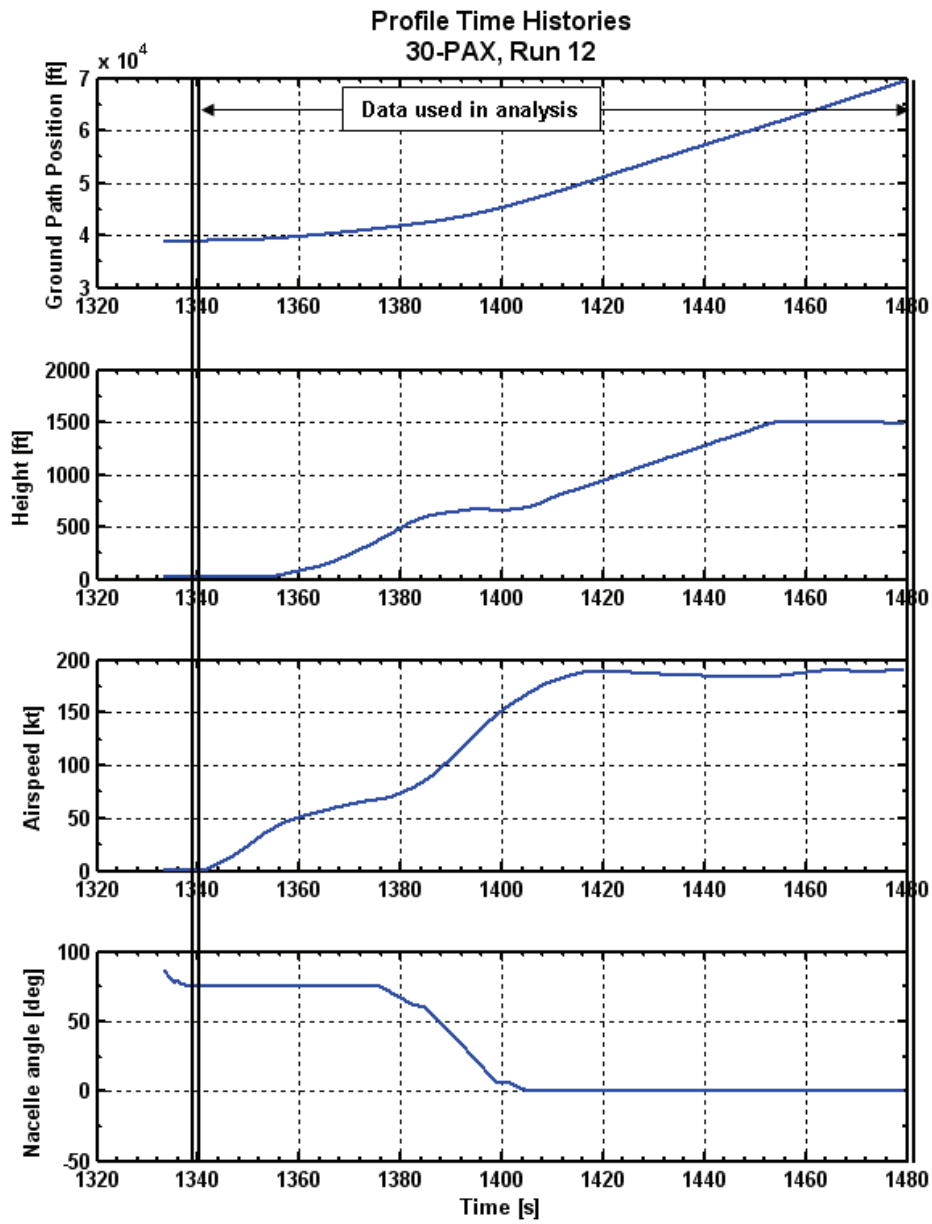

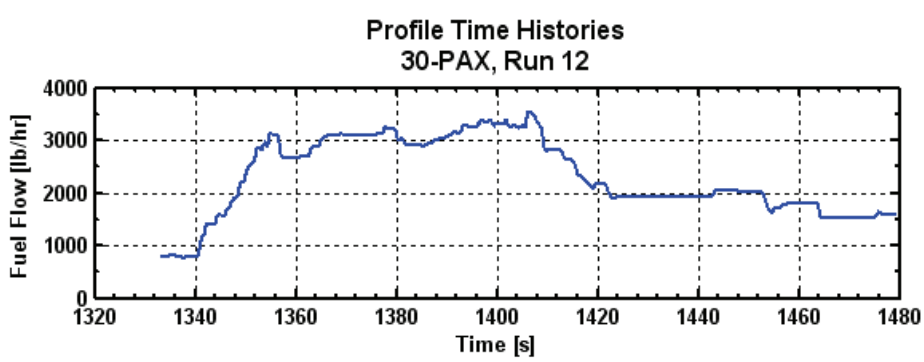

Figure H-9. 30-passenger takeoff time history, STO.

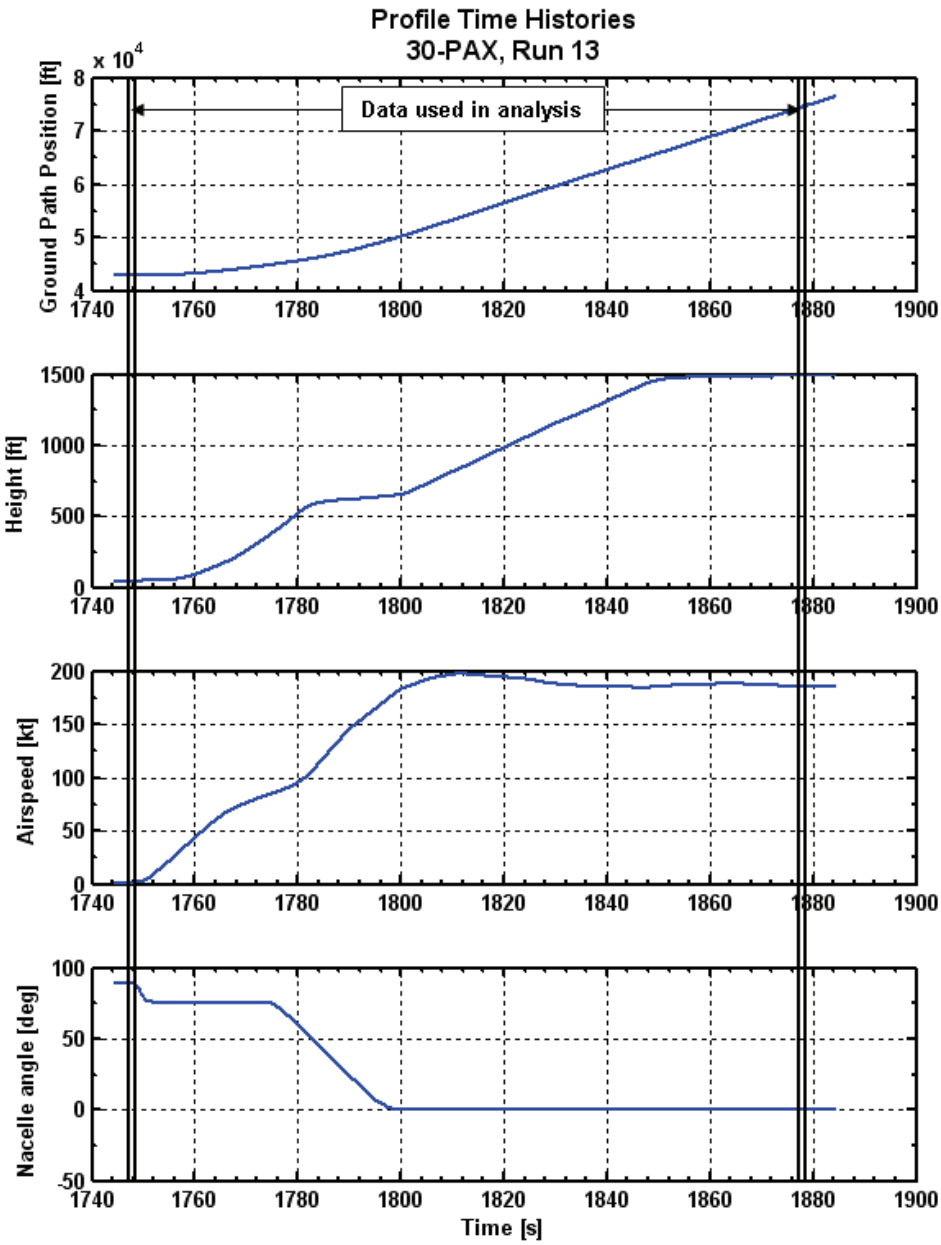

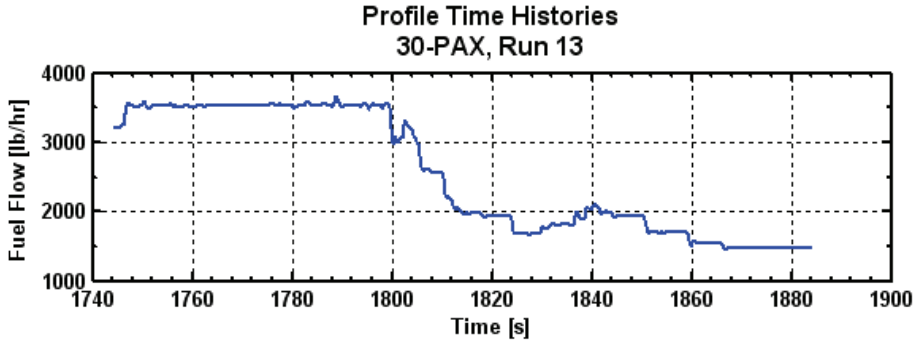

Figure H-10. 30-passenger takeoff time history, VTO.

A qualitative assessment was made to evaluate what the characteristics of the takeoff and approach profiles of the larger CTRs such as the 90- and 120-passenger design might be. This was accomplished by comparing the altitude time histories of the 10- and 30-passenger designs. Figures H-11, H-12 and H-13 respectively show a comparison of the 10- and 30-passenger approach profiles for 3-, 6- and 9-degree glide slopes. As expected the profiles are essentially identical. The apparent differences in time are the result of speed and nacelle variations; however, a check of the distance traveled from start to finish is the same. These variations would be negated if the pilot had consistent cues on approach to the landing spot. The approach to a landing spot is not a power available issue; therefore, it can be concluded that the approach profile of the 90- and 120-passenger designs would be the same as those for the 10- and 30-passenger designs. The 30-passenger approach flight profiles were used to generate the 120-passenger approach noise contours in section 2.0

Takeoff profile comparisons of the 10- and 30-passenger design were made next. The results are presented for the VTO and STO takeoffs respectively in figure H-14 and H-15. The results are very similar. Pilot technique and takeoff requirements are factors in the profiles developed. For each configuration and for both takeoff conditions the pilot started transition at approximately the same time and altitude to convert to the "en route" configuration by 1,500 feet AGL which is a tiltrotor requirement (based on BA609 certification basis).

The takeoff profiles are more prone to variations when considering One Engine Inoperative (OEI) requirements, design disk loading, power-to-weight ratios and engine rating structure difference between CTR designs. However, for the AEO conditions simulated it is believed that the larger CTR takeoff profiles would be similar. The 30-passenger takeoff flight profiles were used to generate the 120-passenger takeoff noise contours in section 2.0.

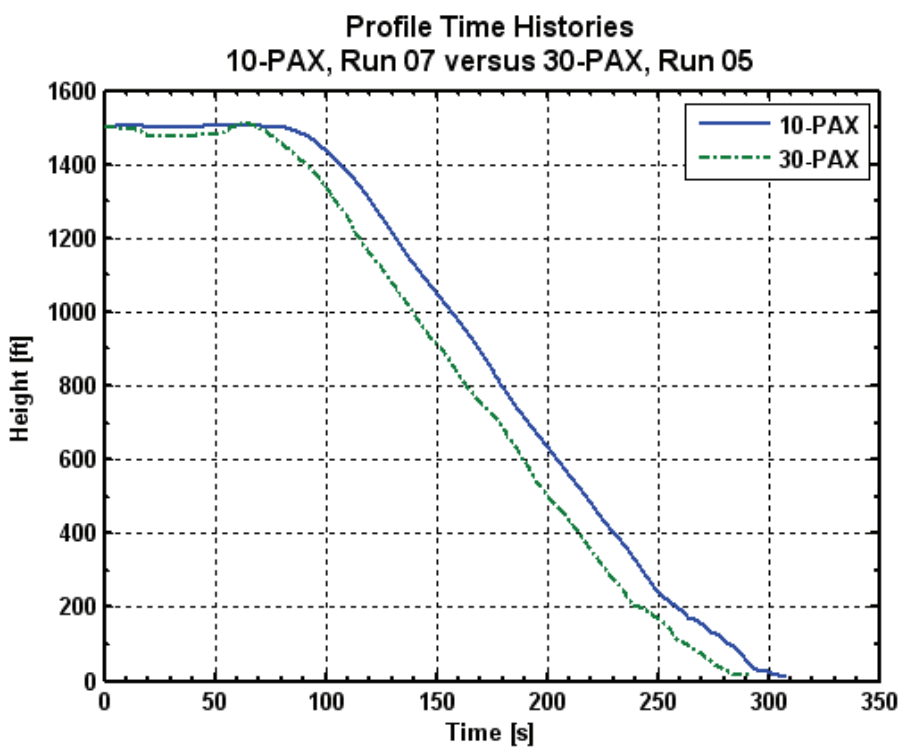

Figure H-11. Approach, 3 degrees.

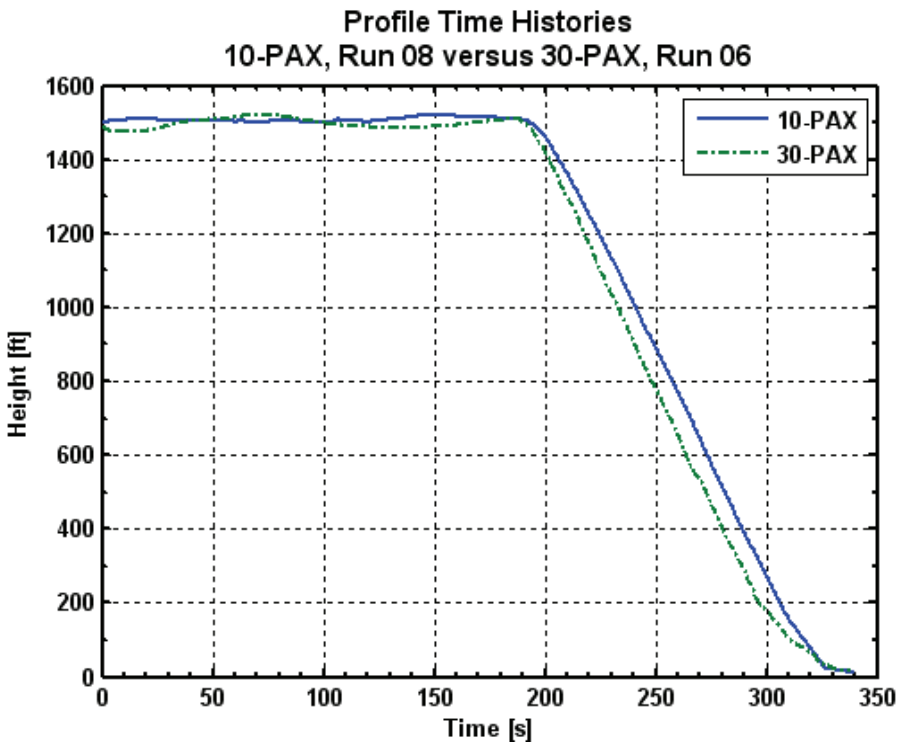

Figure H-12. Approach, 6 degrees.

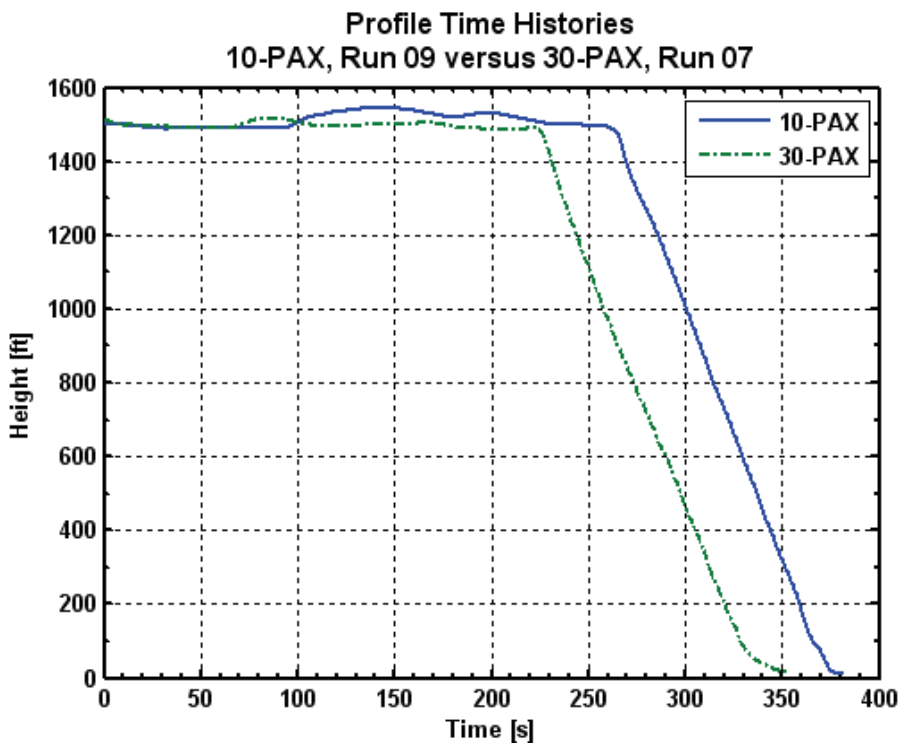

Figure H-13. Approach, 9 degrees.

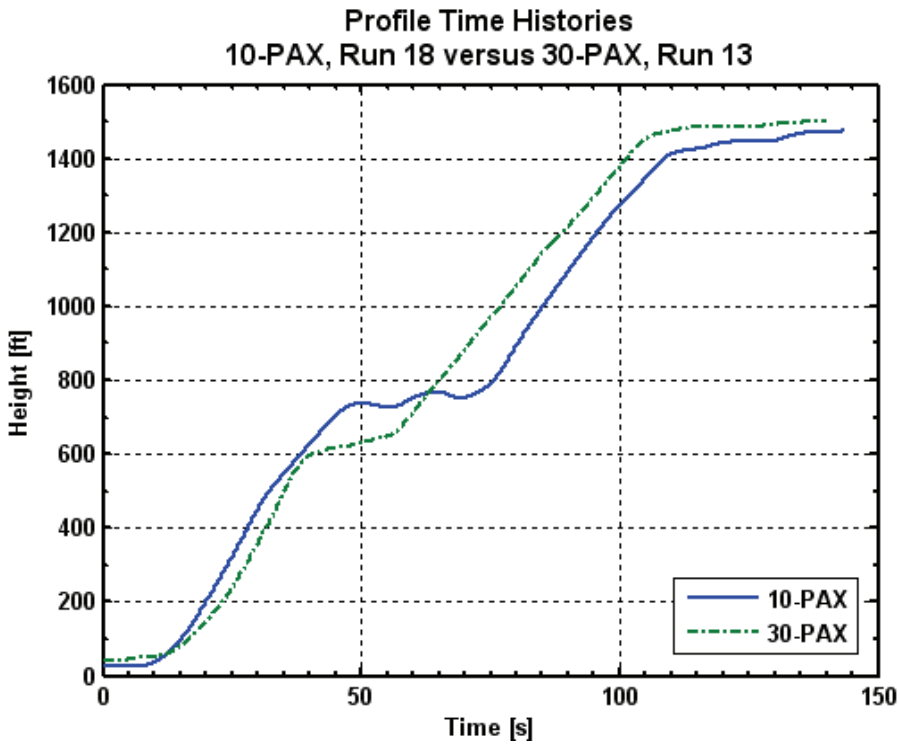

Figure H-14. Takeoff, VTO.

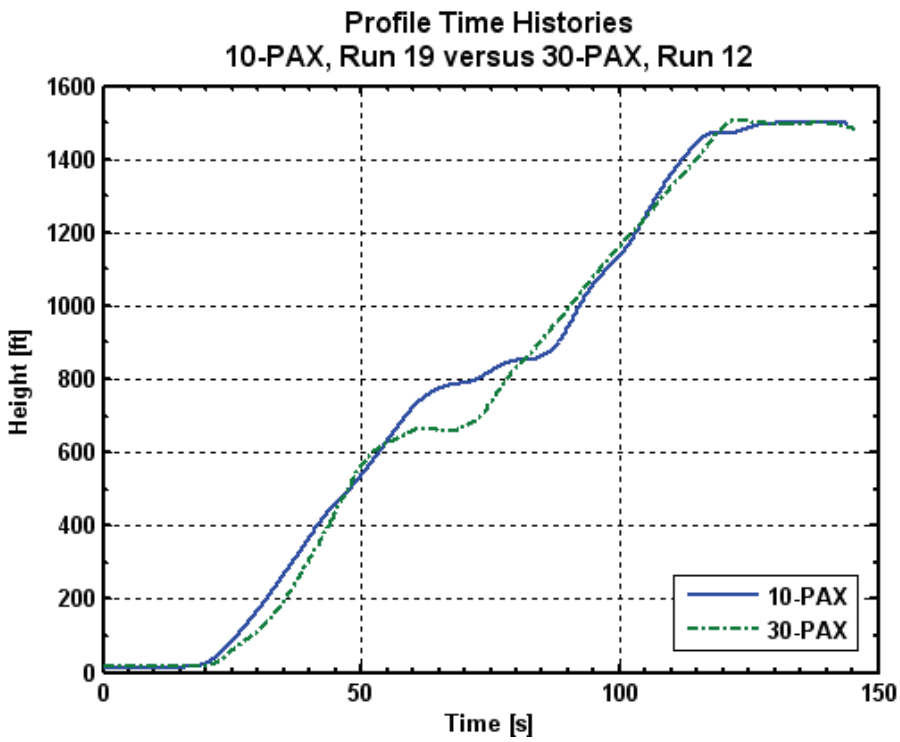

Figure H-15. Takeoff, STO.

APPENDIX I. CTR PERFORMANCE DECK

I-1 Introduction

A performance deck (PD) for the civil tiltrotor (CTR) fleet was built by Science Applications International Corporation (SAIC) based on data supplied by Bell Helicopter in support of BADA model development. Overall, the performance deck (PD) models the climb, cruise, and descent modes of flight, currently limited to airplane mode, for the CTR10, CTR30, CTR90, and CTR120. This utility was developed as an aid in shaping suitable mission flight profiles in airplane mode for various city-pairs. The PD is written in the MATLAB framework, and missions are flown in a batch environment wherein a configuration file is supplied for each test case. The PD tool does not model atmospheric winds nor does it support nonstandard day atmospheric conditions.

The goal of this appendix is to describe the underlying design behind the PD. A PD user's guide (ref. I-1) may be referenced regarding how to operate the PD software. Past work outlined in ref. I-2 was used to verify the PD tool against Bell Helicopter-supplied sample mission flights generated using their PRESTO software.

I-2 Model Basis

The underlying basis of the CTR BADA-formatted performance models for all the CTR aircraft is documented in section 3 of the report. Note that the current build of the CTR PD (Version 3.2.3) supports airplane-mode-only flight performance. The initial development of this utility was to support design of the airplane mode mission segment planning which entails the majority of the flight. This utility supported flight profile design in this mode for all CTR airframe models (CTR10, CTR30, CTR90, and CTR120).

Overall the BADA-formatted models resulting from section 3 are the basis of the performance characteristics for each CTR in the PD. This includes airplane mode aerodynamics, mass, fuel burn, and propulsion system performance characteristics. The CTR PD utility was developed in the MATLAB programming language allowing for additional expansion of performance model capability to better support the CTR research efforts. This expansion of the PD tool was limited to available performance data that was collected from the Bell Helicopter CTR conceptual design and PITL efforts. Areas expanded on over the basic BADA formulation include calculation of overall lift coefficient, fuel burn characteristics, and propulsion system thrust performance. These model improvements are discussed in following sections. Note that these updates were limited to currently existing CTR performance data described in section 2 so the best fidelity is limited by the data on hand. The available data also mandates the selected model structure updates and implementation as the collection of additional trim data was not part of the Year-2 effort.

I-2.1 Total Energy Method

The theory behind modeling flight profiles within the PD is based on the total energy method. This method entails distributing the overall airframe energy between potential and kinetic energy. In general, the total system energy is defined as follows:

$$(T - D)V = mg\frac{dh}{dt} + mV\frac{dV}{dt}.$$

For climb, cruise, or descent flight profile segments the thrust required is determined as follows by the PD:

$$T = D + \left(mg\frac{dh}{dt} + mV\frac{dV}{dt} \right)\left(\frac{1}{V} \right).$$

From the PD user's guide a desired rate of climb, velocity, and acceleration is known for each segment of the total mission. As described in the user's guide adjoining flight profile segments of differing target speeds enact an acceleration/deceleration schedule that is distributed over the current segment with the goal of obtaining the new speed at the start of the next segment. The atmospheric conditions are known at each point given the ISA atmospheric model and fuel burn results in the known CTR mass as the simulation propagates through time. Solving the preceding equation given these known targets results in the total thrust required. If required thrust does not exceed total thrust available then the condition can be met and simulation propagation continues. However, if thrust required exceeds thrust available then a CTR performance limit has been reached, and the resulting effect is captured differently whether in climb/descent or cruise conditions.

Under cruise conditions, if a CTR is commanded to achieve a condition that exceeds total maximum thrust available, then total thrust is capped at the available value and the following deceleration is applied to the airframe with simulation propagation continuing. This is an effective way of modeling the upper limit to level flight speed for the airframe. Clearly, under level cruise flight dh/dt = 0.

$$\frac{dV}{dt} = \left((T - D)\frac{1}{m} \right) - \frac{g}{V}\frac{dh}{dt}.$$

Under climb/descent conditions, the fallout rate of climb/descent is calculated as follows:

$$\frac{dh}{dt} = \left((T - D)\frac{V}{mg} \right) - \frac{V}{g}\frac{dV}{dt}.$$

Consequently, hitting maximum thrust available and/or commanding acceleration will reduce the energy available to obtain the desired rate of climb. The relation above provides the rate of climb/descent achievable at any time when in either climb or descent. If unable to hit the desired target rate of climb/descent, the simulation propagation continues based on what output is achievable.

I-2.2 Atmospheric Model

The atmospheric model within the PD supports ISA conditions only. In addition, it only provides support for the first gradient layer (from sea level to 11 km) and the first isothermal layer (11 km to 25 km) of the atmosphere. This model provides the dynamic pressure, calibrated airspeed, and Mach number for the CTR airframes as the simulation propagates.

I-2.3 Aerodynamic Model

Overall the aerodynamic model remains intact given the BADA-formatted CTR performance data from the Year-1 effort. Consequently, the same logic is employed in the PD to determine overall airframe lift and drag. The original BADA formulation determined the required lift coefficient based on the assumption that level flight was only considered. The original assumption that wings-level flight is only being considered is still in place. To expand utility to support climb and descent segments with higher fidelity, this calculation is now approximated as a function of flight path angle as follows:

$$C_L = \frac{2mg\cos(\gamma)}{\rho V_{TAS}^2 S\cos\phi}.$$

I-2.4 Propulsion Model

Updates were made within the PD to expand on maximum continuous power (MCP) thrust in cruise, as well as the thrust specific fuel consumption (TSFC) model structure throughout the entire flight envelope. The following sections provide a summary of these updates.

I-2.4.1 Thrust Model Enhancements

The maximum climb thrust formulation, as well as flight idle thrust approximation, remains the same as the original CTR BADA model formulation. However, an improvement has been made within the PD regarding maximum thrust available in level flight. The original BADA formulation simply defines maximum thrust available in level flight as follows:

$$\left(T_{cruise}\right)_{\max} = 0.95\left(T_{\max c\lim b}\right).$$

This was found to be insufficient in modeling the upper limits of level flight performance for the CTR across the flight envelope. The preceding approximation resulted in an overestimation of maximum thrust available under cruise conditions. Consequently, the known maximum available level flight cruise thrust was modeled in a fashion identical to that of the maximum climb thrust with altitude. These level cruise performance limits were fit based on the performance trim data described in section 3. Each CTR now has a nonlinear fit polynomial to describe maximum cruise thrust as a function of altitude. The actual trim data points for each CTR that were used to produce the new maximum thrust for level flight performance limitations can be referenced in section 3. The final fits for each CTR used within the PD are shown in figure I-1 for airplane mode operations.

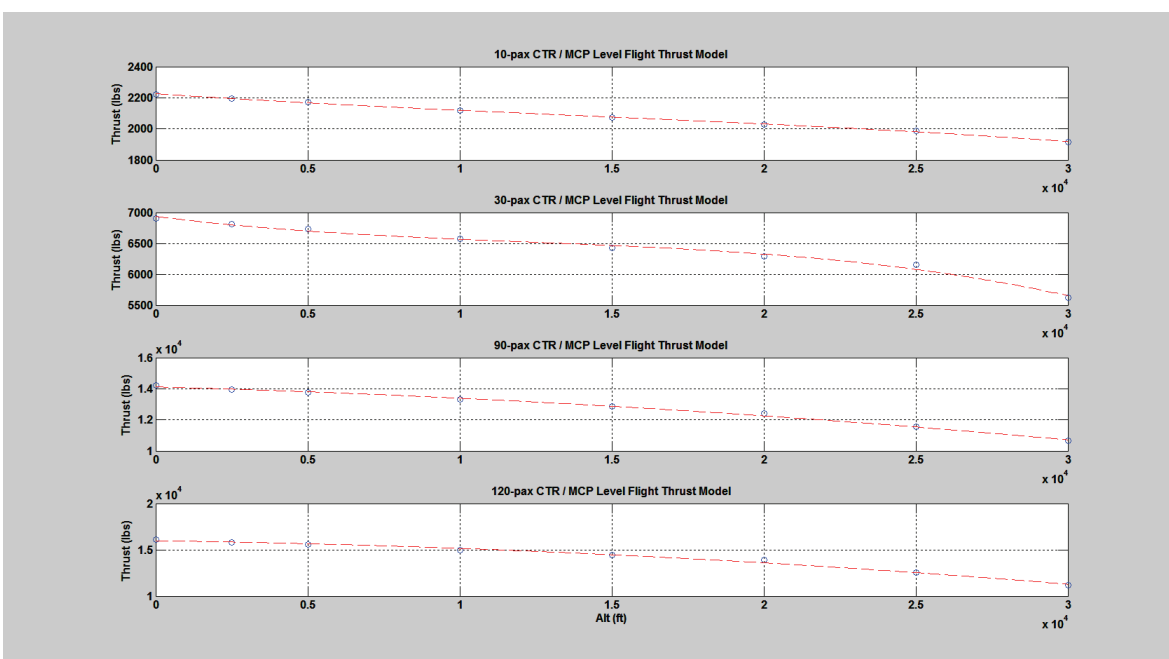

Figure I-1. MCP thrust available in level flight for each CTR airframe based on trim data from appendix B. The model representations used in the PD are displayed as dashed red lines.

I-2.4.2 Fuel Burn Model Enhancements

Updates have also been made to the fuel consumption model to support more generality, as opposed to the strict link to certain operating speeds, or mission segments, etc., imposed by the original BADA formulation outlined in section 3. The original formulation was specified as follows, with overall fuel flow a direct function of the TSFC (η) and total thrust based on MCP climb conditions.

$$f_{nom} = \eta T$$

$$\eta = C_{f1}\left(1 + \frac{V_{TAS}}{C_{f2}}\right).$$

In addition, the original level flight cruise fuel consumption was modeled with a simple scale factor as follows:

$$f_{CR} = \eta T C_{fCR}.$$

When in descent or idle thrust conditions the BADA formulation originally defined the minimum fuel flow as a function of altitude above sea level (ft) where:

$$f_{\min} = C_{f3}\left(1 - \frac{h}{C_{f4}}\right).$$

Refer to section 3 to revisit the details regarding the original fuel consumption formulation under the baseline BADA framework. The limitations of this model were made evident within that report including plots of the family of curves representing η that were computed given the Bell-provided trim data along with the BADA-formatted fits.

The new fuel consumption model takes all trim data made available from Bell Helicopter and provides least-squares fits for each curve. This consolidates data for the MCP climb, long-range cruise, and MCP cruise conditions. The TSFC for idle or low-power setting is also captured given the available Bell trim data. The goal was to use an identical model structure and representation across all flight modes while capturing the effect of demanded airspeed, power setting, and altitude. The family of TSFC curves spans the speed range available within each CTR performance data set provided by Bell Helicopter, as well as covers the altitude range from SL up to 30k feet. The common model structure updated for use with all flight segments is as follows:

$$f_{nom} = \eta T.$$

This provides a higher fidelity family of curves for the TSFC for each CTR and removes the oversimplified model structure of the original BADA formulation. Overall, this technique provides more flexibility with the understanding that we have the data available and are best served by putting it to use rather than limiting analysis with model structure oversimplifications.

I-3 Supplemental Performance Deck Verification

In an effort to verify implementation of these updates into the CTR PD utility a series of trim points from the original performance data provided by Bell Helicopter Textron was used. Components of the energy equation within the PD were configured based on the conditions specified for each trim point, and the final thrust required, drag, and fuel consumption were noted and are presented for comparison to the Bell results. Comparisons for long-range cruise, maximum power cruise, and maximum power climb are presented for the CTR10, CTR30, and CTR120 airframes. Bell Helicopter did not provide trim data for the independently developed 90-passenger CTR vehicle.

Check case results for the CTR airframes follow. Each case presents the overall percent difference between the PD output and the Bell trim data for thrust, drag, and fuel burn rate. A positive percent difference signifies the PD overestimates a parameter. Overall, these check cases are trimmed at maximum gross weight (Mmax) unless specified in the graph with a note. Similarly, all cases are at standard-day conditions unless specified otherwise in the graph. The current PD supports only standard-day conditions. The labeling of any cases as being trimmed at Mmin or Mref correspond to the appropriate BADA-defined gross weight for that CTR airframe. Here Mmin is a specified minimum operational weight and Mref is a specified middle range gross weight.

I-3.1 CTR10 Verification

The verification results for the CTR10 are shown in figures I-2 through I-4.

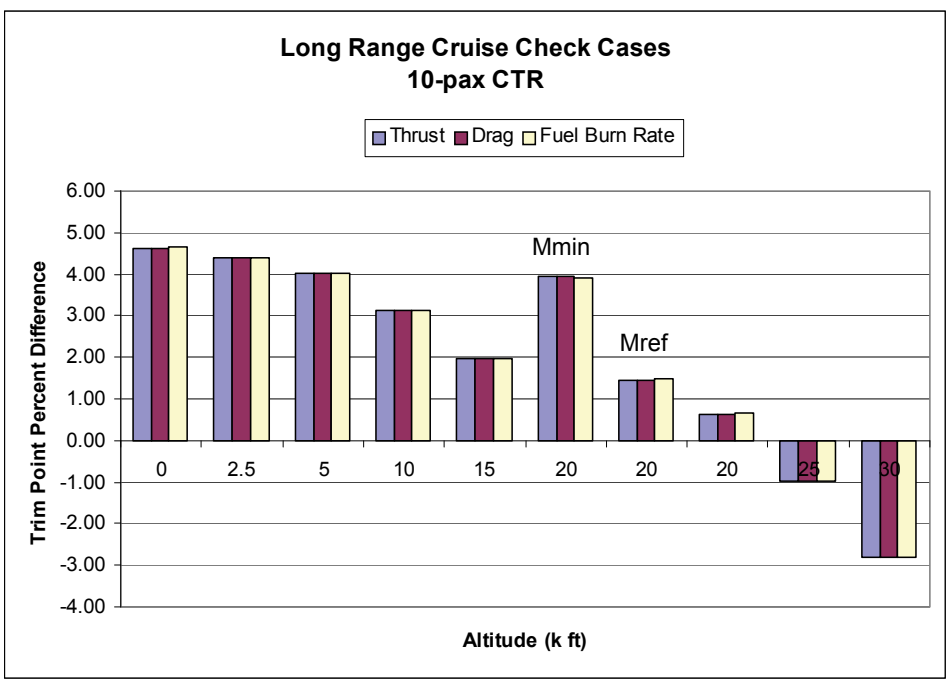

All cases configured at Gross Weight Mmax unless otherwise labeled above.

Figure I-2. CTR10 long-range cruise verification results.

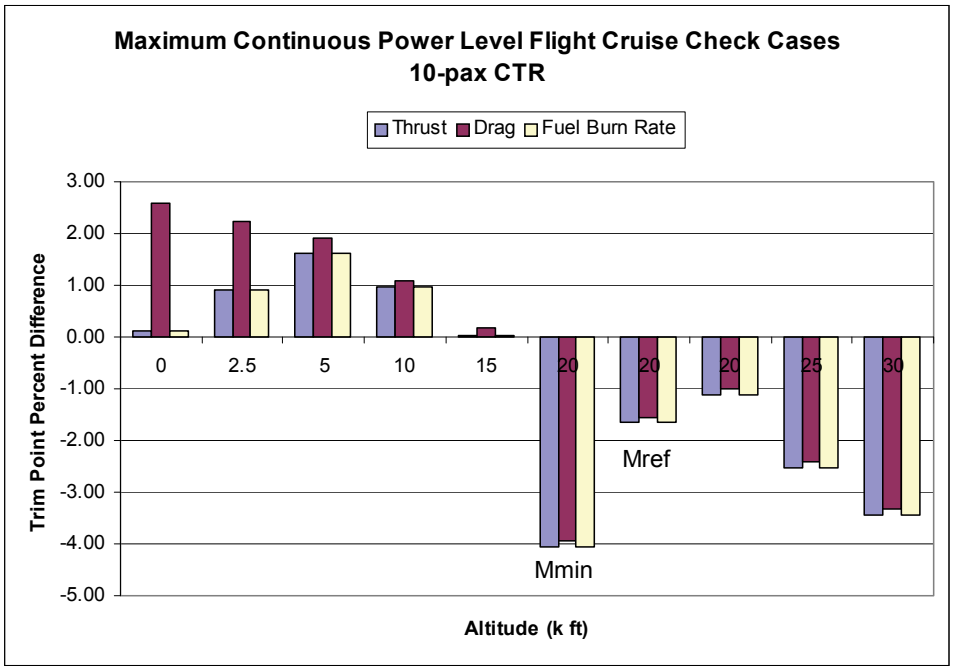

All cases configured at Gross Weight Mmax unless otherwise labeled above.

Figure I-3. CTR10 MCP cruise verification results.

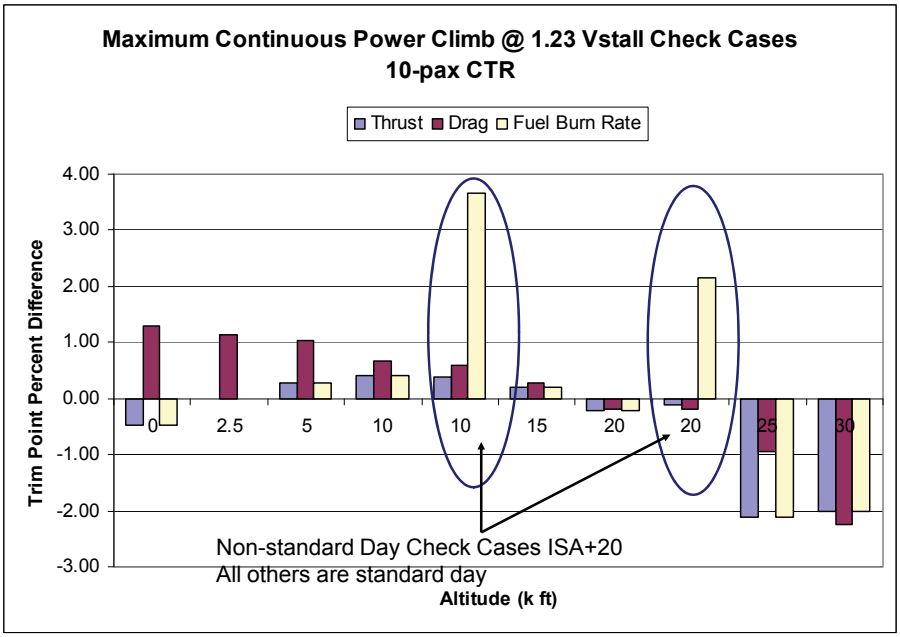

Figure I-4. CTR10 MCP climb verification results.

I-3.2 CTR30 Verification

The verification results for the CTR30 are shown in figures I-5 through I-7. The CTR30 experiences aerodynamic compressibility effects at MCP level cruise speeds that are not captured by the BADA model structure. These effects were not captured in the PD and, as such, it remains clear in the lower thrust required for trim as outlined in figure I-6.

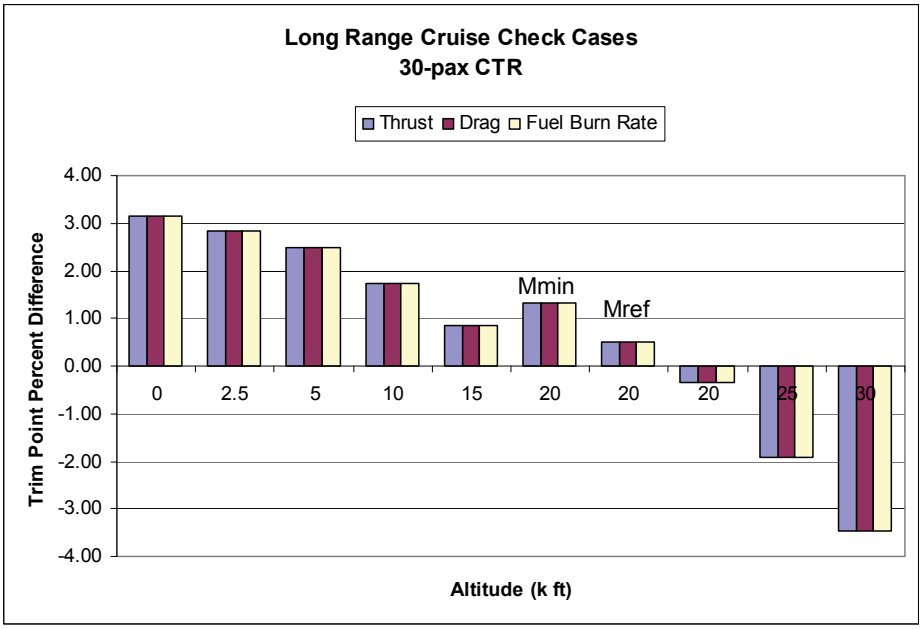

All cases configured at Gross Weight Mmax unless otherwise labeled above.

Figure I-5. CTR30 long-range cruise verification results.

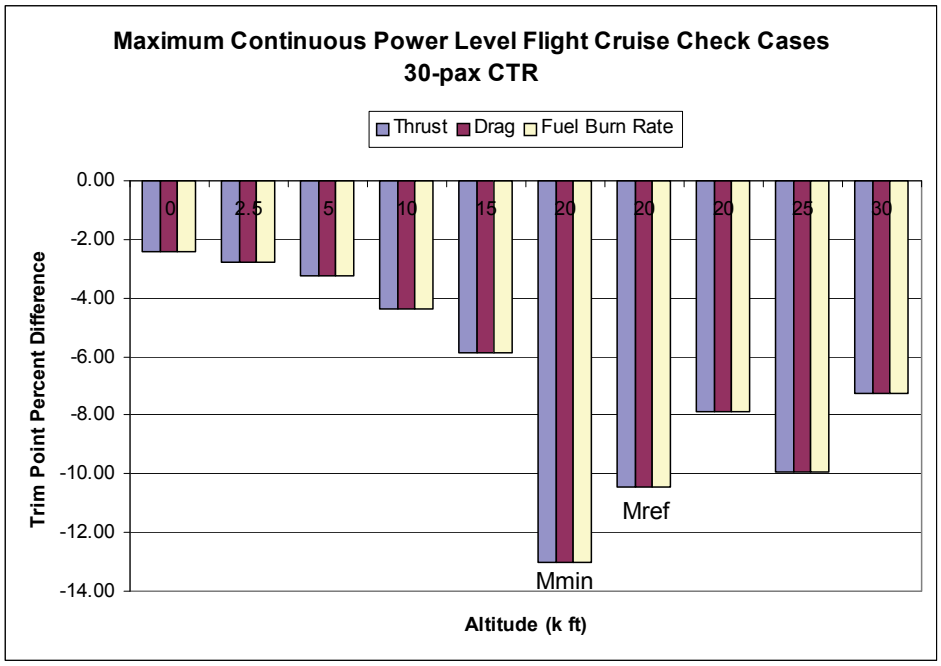

All cases configured at Gross Weight Mmax unless otherwise labeled above.

Figure I-6. CTR30 MCP cruise verification results.

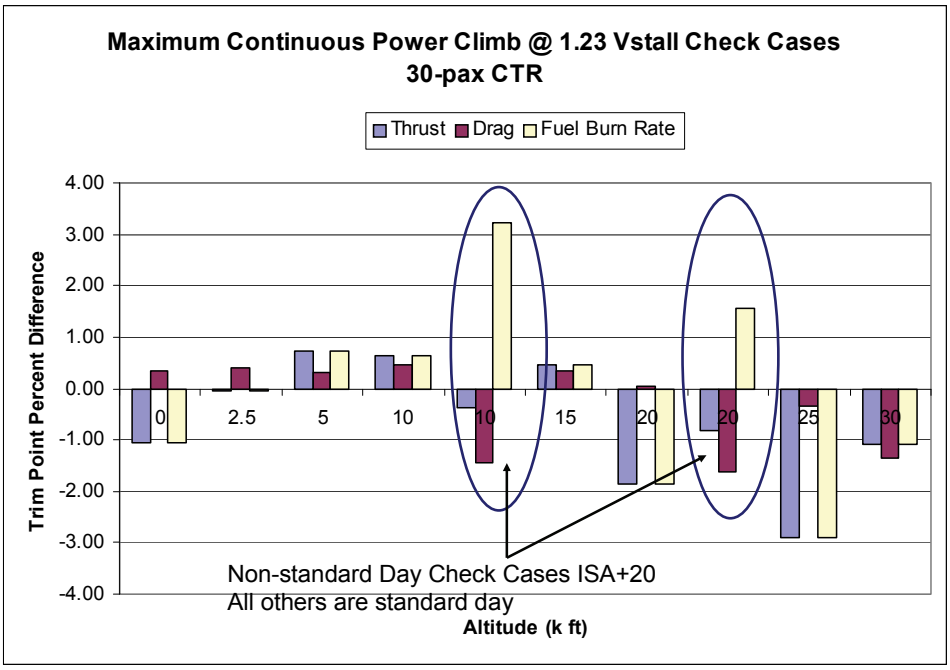

Figure I-7. CTR30 MCP climb verification results.

I-3.3 CTR120 Verification

The verification results for the CTR120 are shown in figures I-8 through I-10.

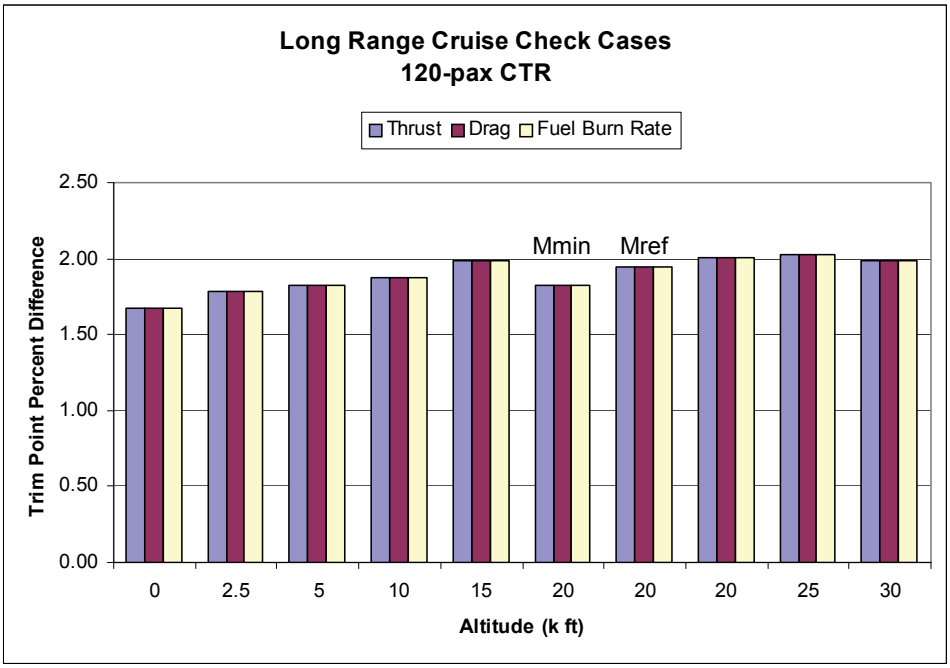

All cases configured at Gross Weight Mmax unless otherwise labeled above.

Figure I-8. CTR120 long-range cruise verification results.

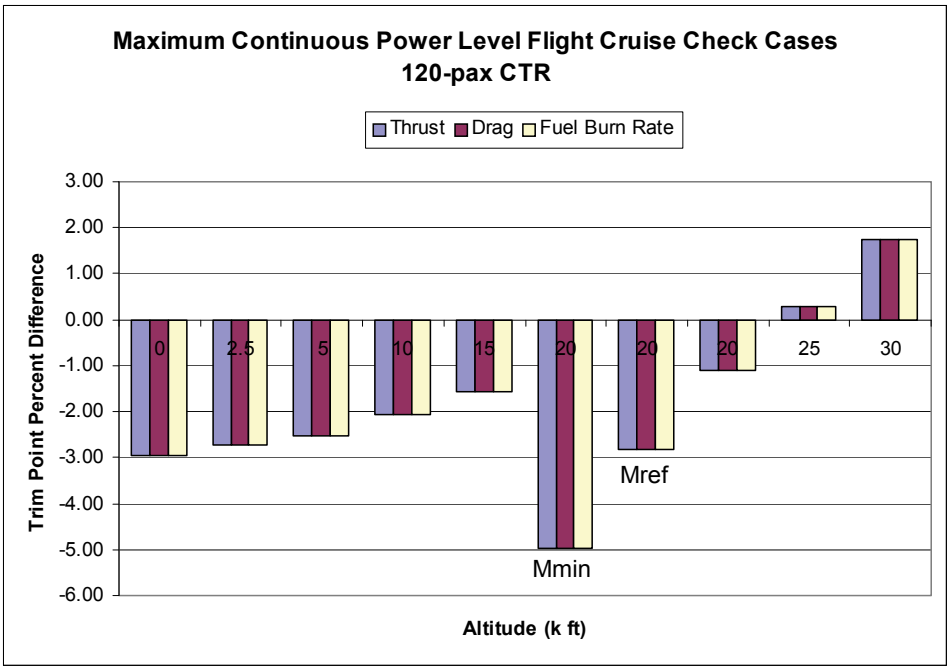

All cases configured at Gross Weight Mmax unless otherwise labeled above.

Figure I-9. CTR120 MCP cruise verification results.

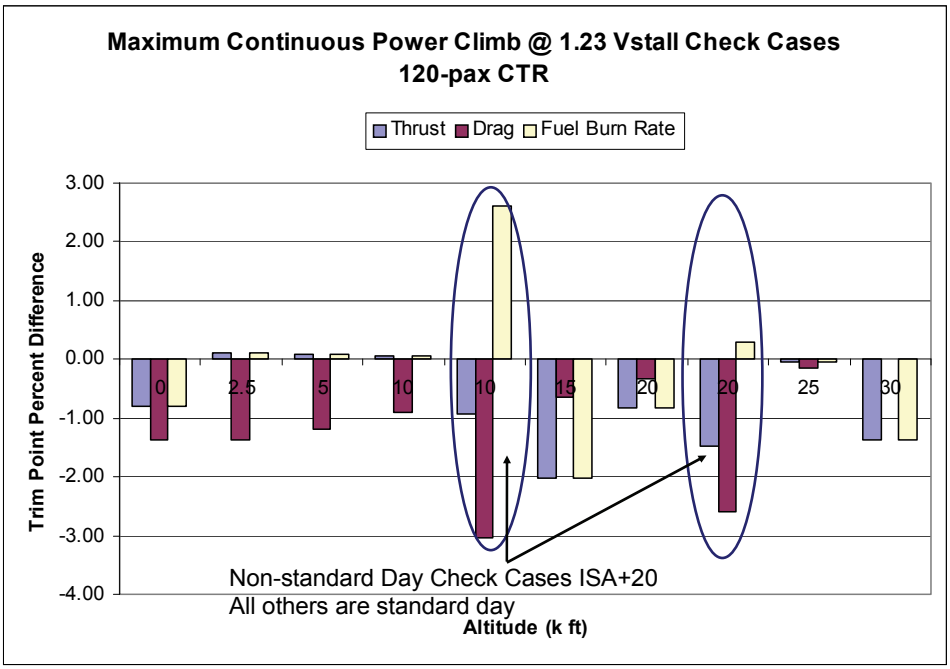

Figure I-10. CTR120 MCP climb verification results.

I-4 References

I-1. Paris, A. and Chung, W.: CTR Performance Deck User's Guide. Technical Note 022, Science Applications International Corporation (SAIC), McLean, VA, U.S. Government Prime Contract NNA09DA06T, Sept. 15, 2010.

I-2. Paris, A. and Chung, W.: CTR Performance Deck Verification. Technical Note 021, Science Applications International Corporation (SAIC), McLean, VA, U.S. Government Prime Contract NNA09DA06T, July 7, 2010.

APPENDIX J. TRADEOFF ANALYSIS OF CTR FLIGHT PROFILES

J-1 Introduction

To conduct a comprehensive tradeoff study of deploying a CTR fleet under NextGen, it is desirable to establish a set of baseline flight profiles for the CTR fleet (i.e., the CTR10, CTR30, CTR90, and CTR120 vehicles) in the Northeast Corridor (NEC) to be used in ACES and AvTerminal for the NAS throughput performance analysis. Since there are not any CTR commercial flight operations to refer to, a preliminary tradeoff analysis is developed based on designed CTR performance from the Year-1 effort to estimate the baseline flight profiles, which include climb and decent profiles, and cruise speed and altitude, as well as flight time and fuel burn performance. A performance deck (PD) software tool was developed based on static CTR performance in the airplane mode and energy method to evaluate the possible flight profiles for the four specific CTR passenger configurations according to weight, aerodynamics, thrust, and fuel burn characteristics. Acceleration and deceleration during climb and descent are considered to address passenger comfort.

J-2 Assumptions

1) Great-Circle routes are assumed.
2) Only the airplane mode of the flight profiles is evaluated.
3) Speed below 10,000 feet is limited to less than or equal to 250 knots.
4) Starting altitude is 600 feet—the estimated altitude at which the CTR will complete the conversion to airplane mode during the takeoff.
5) Each flight will end at the Initial Approach Fix altitude, which is 1,500 feet, while the CTR is still in airplane mode and leveling off from a descent at 200 knots.
6) Acceleration and deceleration are limited to ±0.03 g for passenger comfort.

J-3 Development of the Flight Profiles

Flight profiles, partially developed from the pilot-in-the-loop (PITL) simulations and shown in figures J-1 and J-2, were followed as the baseline procedures for the climb, cruise, and descent phases. Cruise speed and altitude were varied for each CTR passenger configuration to evaluate the flight time and fuel burn performance. Climb and descent flight profiles were then adjusted according to the cruise speed and altitude at the top of climb (TOC) and top of descent (TOD). For each designated city-pair, 10 nmi was assumed for takeoff, and approach and landing (i.e., points 1–4 in figure J-1 and points 8–12 in figure J-2, respectively) and was not included in the evaluations since the PD does not support non-airplane-mode operations. Therefore, all the flight time and fuel burn presented will only be from point 4 through point 8 during a full flight profile. This approach is applied throughout the discussion in this appendix.

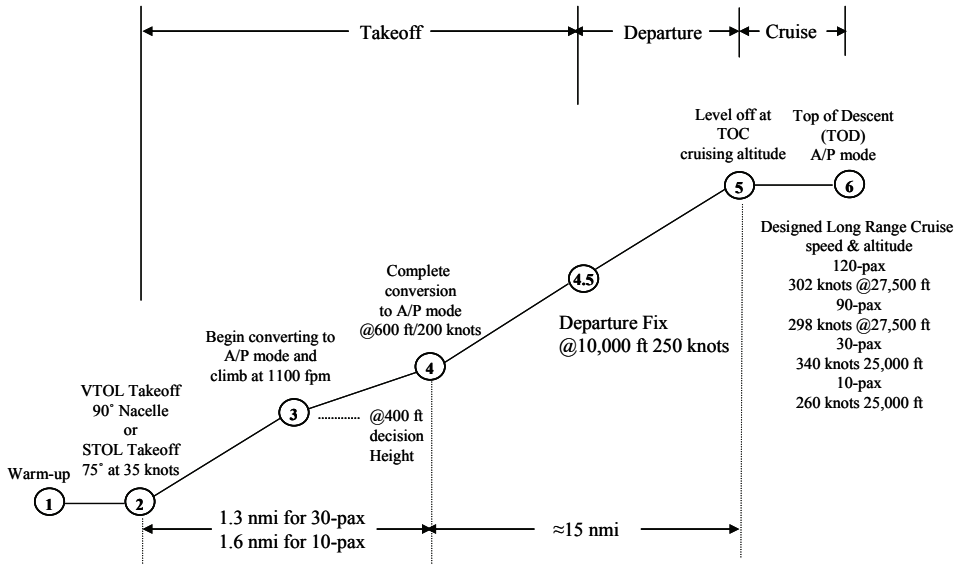

Figure J-1. Takeoff and climb profile for the CTR fleet.

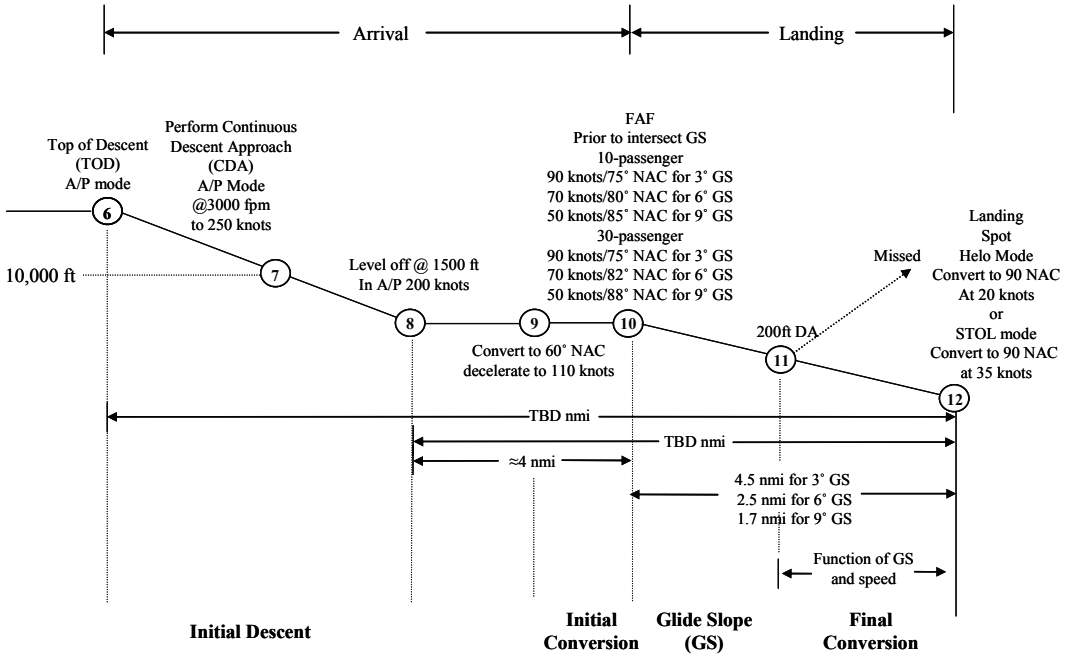

Figure J-2. Descent and landing profile for the CTR fleet.

J-3.1 Climb

The climb starts at 600 feet altitude at a speed of 200 knots in the airplane mode, i.e., point 4 in figure J-1. A speed of 250 KCAS is assumed at 10,000 feet altitude. Climb rate and speed are optimized according to maximum available thrust as shown in figures J-3(a) and J-3(b). Numbers of climb segments are chosen accordingly during the iterations. Accelerations are limited to ±0.03g.

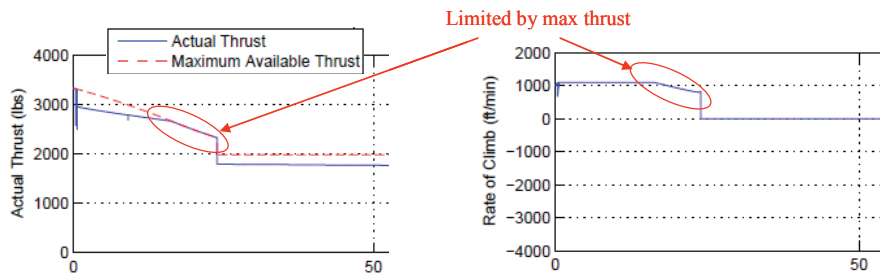

Figure J-3(a). Climb performance limited by maximum available thrust.

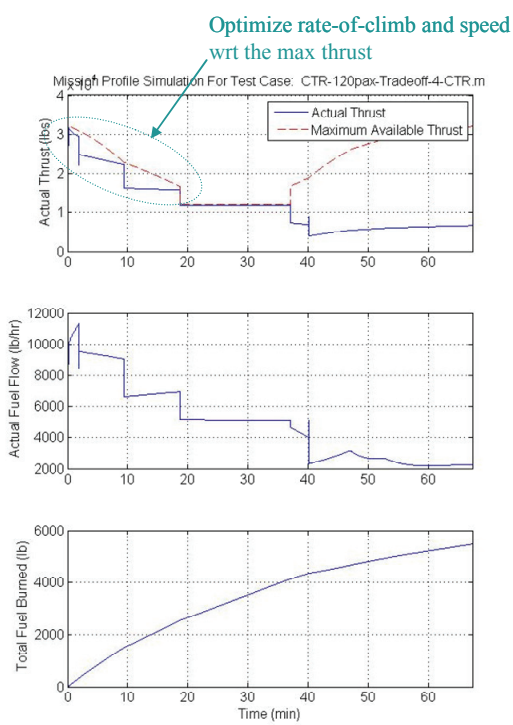

Figure J-3(b). Optimized climb performance relative to maximum available thrust.

J-3.2 Cruise

Cruise speed and altitude between points 5 and 6 in figure J-1 were varied to get a sensitivity evaluation with regard to the flight time and fuel burn for the entire flight, i.e., from point 4 in figure J-1 to point 8 in figure J-2.

J-3.3 Descent

Maximum descent rates were established as long as the decelerations were not exceeding ±0.03g. A target speed of 250 KCAS at 10,000 feet from the TOD was assumed in all profiles as shown at point 7 of figure J-2. The descent profile ends at point 8 in figure J-2 at a speed of 200 knots and an altitude of 1,500 feet.

J-4 CTR120 Flight Profiles

A 120-seat Airbus 319 flight track from Boston Logan International Airport (BOS) to Ronald Regan Washington National Airport (DCA), with a distance of 346 nmi, is shown in figure J-4. The complete flight time is 81 minutes with a scheduled trip time of 88 minutes.

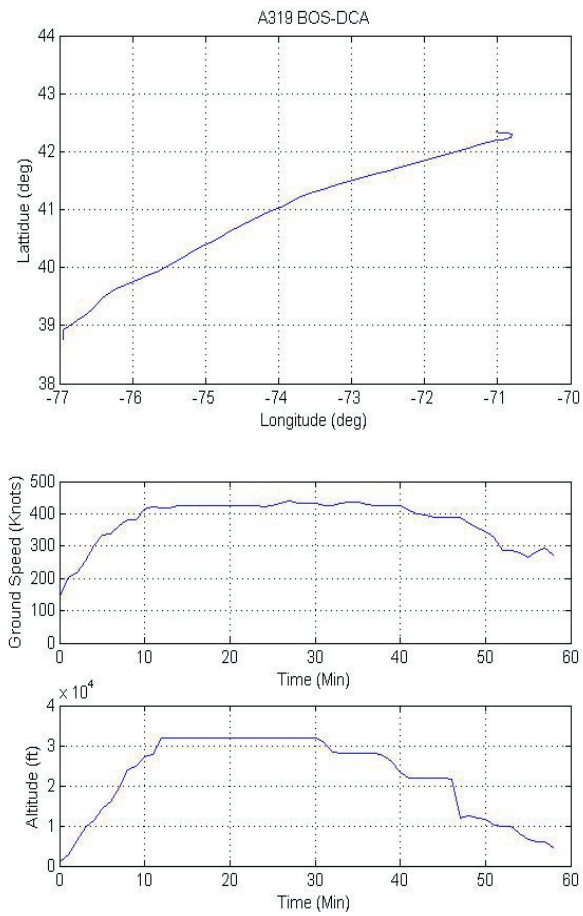

Figure J-4. An Airbus A319 track from BOS to DCA.

For the CTR120, the designed full fuel weight is 21,441 lbs. The fuel weight was reduced to 11,441 lbs for this evaluation since the fuel burn for the BOS–DCA flight is around 5,500 lbs. Even with the 10,000-lb fuel reduction, there is still plenty of fuel left for a return flight. The flight time and fuel burn data are shown in table J-1 (points 4–8 in figures J-1 and J-2) with varying cruise speed and altitude. The Long-Range Cruise (LRC) speed is 302 knots at a cruise altitude of 27,500 feet (Case #15 in table J-1), and the design target for the Maximum Continuous Power (MCP) speed is 345 knots (Case #6).

As shown in table J-1, the primary tradeoff is between flight time and fuel burn. Higher cruise altitude buns less fuel but requires longer flight time than operating at lower altitude. Higher speed achieves shorter flight time at the expense of more fuel burn. A Productivity Index (PI) developed by Bell Helicopter Textron is shown in equation J-1. The PI based on a payload of 26,000 lbs, an empty weight of 98,737 lbs, and a range of 336 nmi is shown in figure J-5, which suggests the optimal operating condition is Case #6 by flying a cruise altitude of 27,500 feet at an MCP speed of 345 knots as shown in green in table J-1.

$$\textit{Productivity Index (PI)} = (\textit{Payload} \times \textit{Range}) / ((\textit{Weight Empty} + \textit{Block Fuel}) \times \textit{Block Time}) \qquad \text{(J-1)}$$

To compare with the commercial flight, e.g., an A319 from BOS to DCA, which has a full flight time of 81 minutes, the following estimates were made. Assuming that the CTR fleet all have similar takeoff and landing performance (from PITL 30-passenger Run 13, a STO takeoff), it took less than two minutes to complete the conversion to airplane mode at an altitude of 600 feet and 200 knots (points 1–4 in figure J-1). On the descent side, from PITL 30-passenger Run 1, it took about 1 minute to transition from 250 knots airplane mode level flight to 110 knots 60 degrees nacelle (points 8–9 in figure J-2), and about 5 minutes from 110 knots 60 degrees nacelle to land with a 3-degree approach (points 9–12 in figure J-2) in Run 5. For the 6- and 9-degree approach, an extra 1 minute, i.e., 6 minutes from 110 knots 60 degrees nacelle to land, were observed in Runs 6 and 7 respectively to account for additional nacelle transition and a slower approach speed. Time spent in STOL approaches was found to be consistent with VTOL approaches.

TABLE J-1. CTR120 FLIGHT TIME AND FUEL BURN RESPONSE

Case	Distance (nmi)	Cruise Spd (knots)	Cruise Altitude (feet)	Initial Gross Weight* (lbs)	Time (min)	Fuel Burned (lbs)	Optimize wrt Max Thrust in climb	Max Thurst in cruise	Productivity Index (NM/Hr)
22	336	360	30000	137,648	66.93	5441.8	√	√	76.33
18	336	345	30000	137,648	68.63	5321.22	√		74.53
17	336	330	30000	137,648	69.56	5287.33	√		73.55
16	336	300	30000	137,648	73.11	5145.87	√		70.08
21	336	360	27500	137,648	65.13	5525.58	√	√	78.38
6	336	345	27500	137,648	66.98	5515	√		76.22
14	336	330	27500	137,648	69.17	5409.71	√		73.88
15	336	300	27500	137,648	72.85	5209.63	√		70.28
23	336	360	25000	137,648	65.68	5780	√	√	77.53
7	336	345	25000	137,648	67.26	5612.68	√		75.83
19	336	330	25000	137,648	68.68	5520.94	√		74.33
20	336	300	25000	137,648	72.65	5296.5	√		70.42

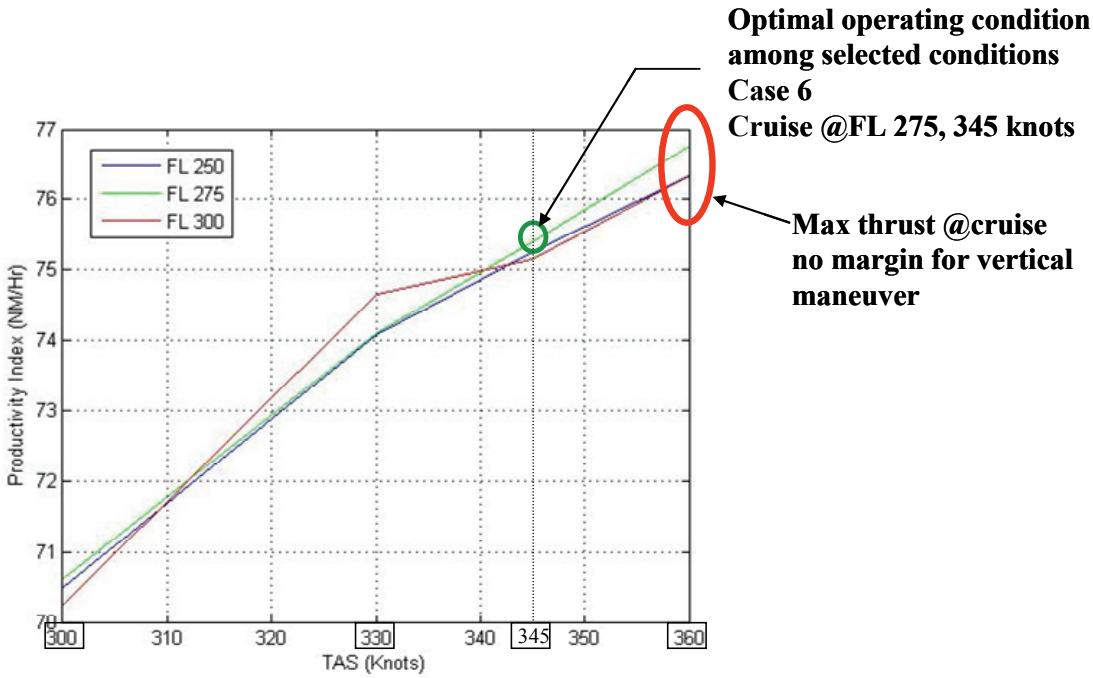

Figure J-5. Productivity Index (PI) of the CTR120 for BOS-DCA.

These PITL data resulted in a total flight time of 74.98 minutes (= 2 + 66.98 + 1 + 5) using the flight time from Case 6, table J-1, in airplane mode (points 4–8 in figures J-1 and J-2). Therefore the total flight time of the CTR120, from takeoff roll to landing, is competitive with the current fixed-wing fleet. Time histories from Case 6 are shown in figures J-6(a) through J-6(d). The eight extra minutes used in this estimate (i.e., two, one, and five minutes), as described are representative of the takeoff and initial climb (points 1–4), initial conversion (points 8–9), and approach and landing (points 9–12) respectively, and will be applied to the remaining flight profile development.

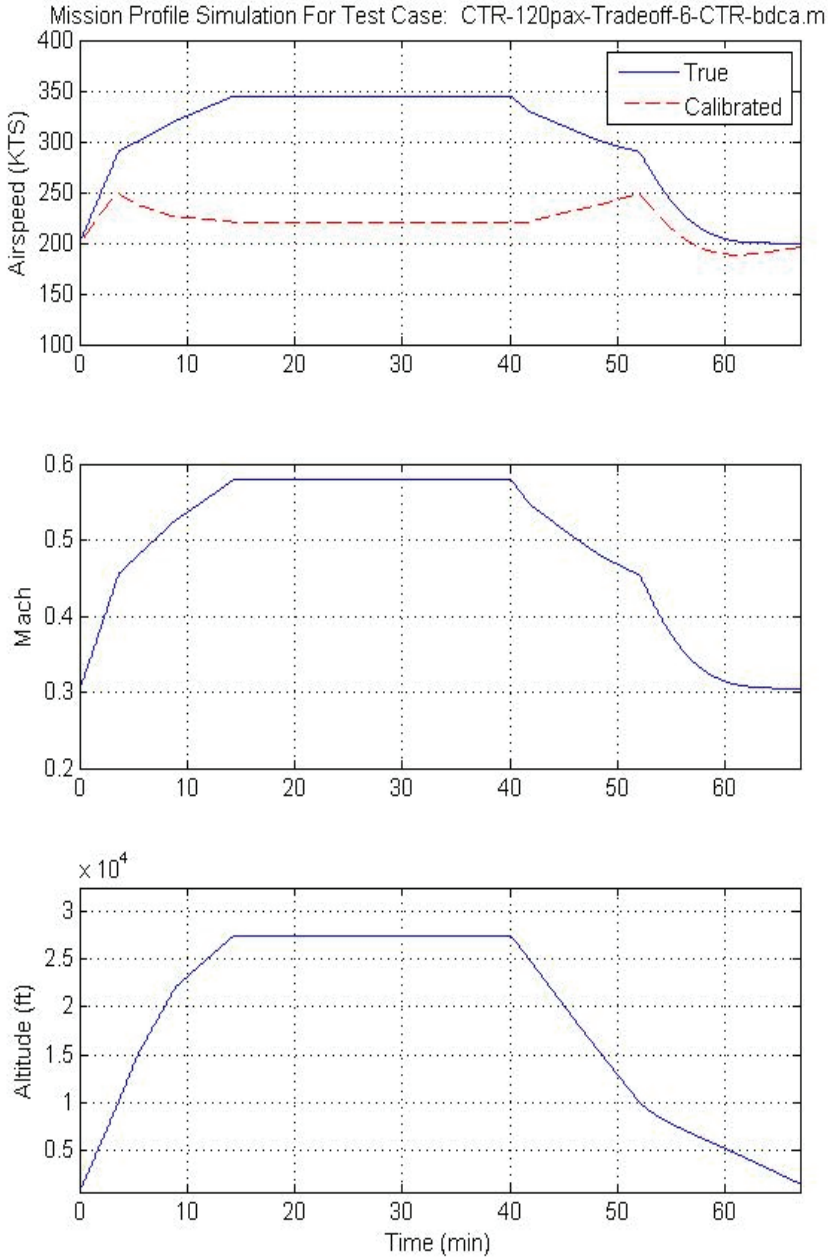

Figure J-6a. CTR120 flight profile time history.

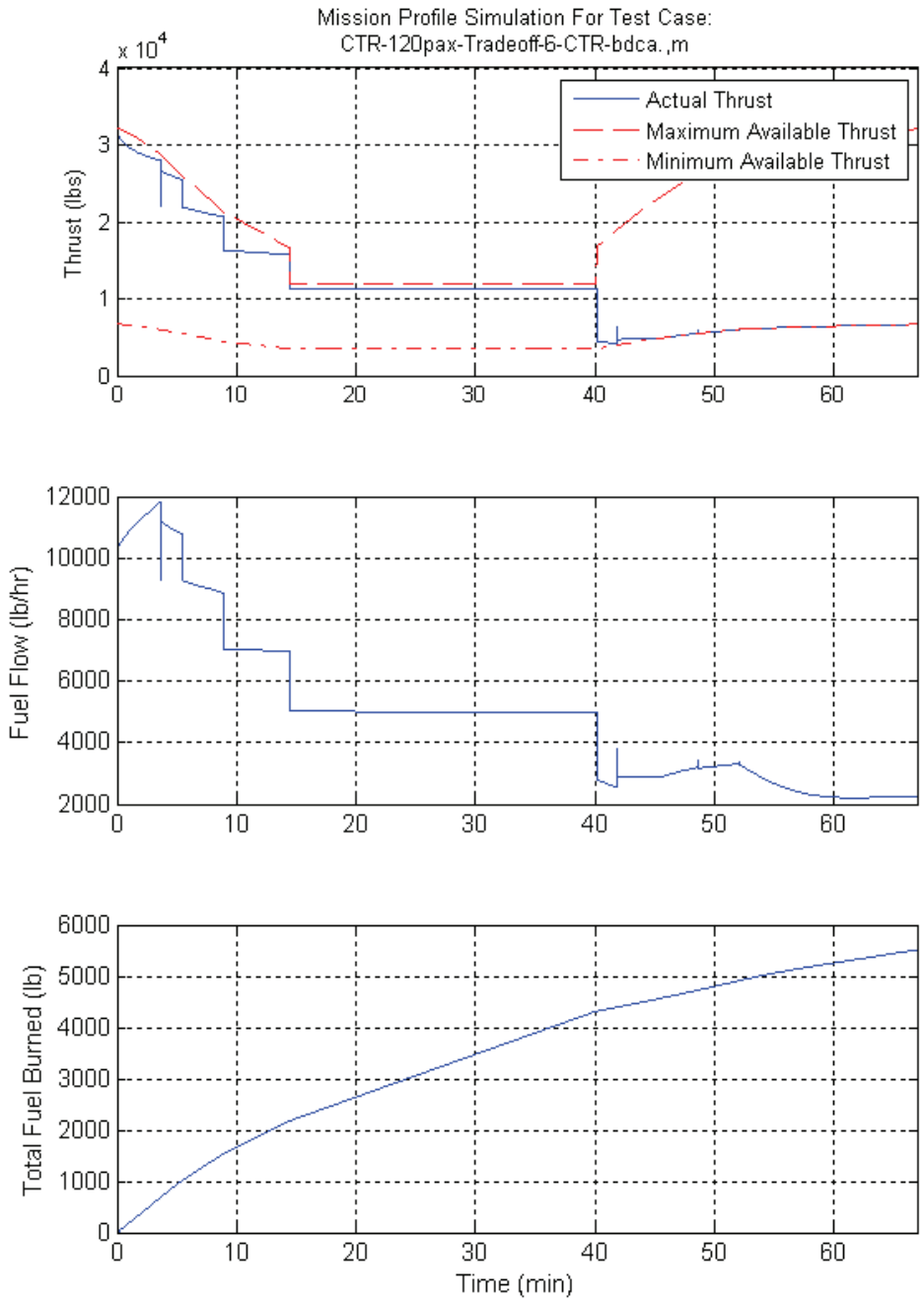

Figure J-6b. CTR120 flight profile time (cont.).

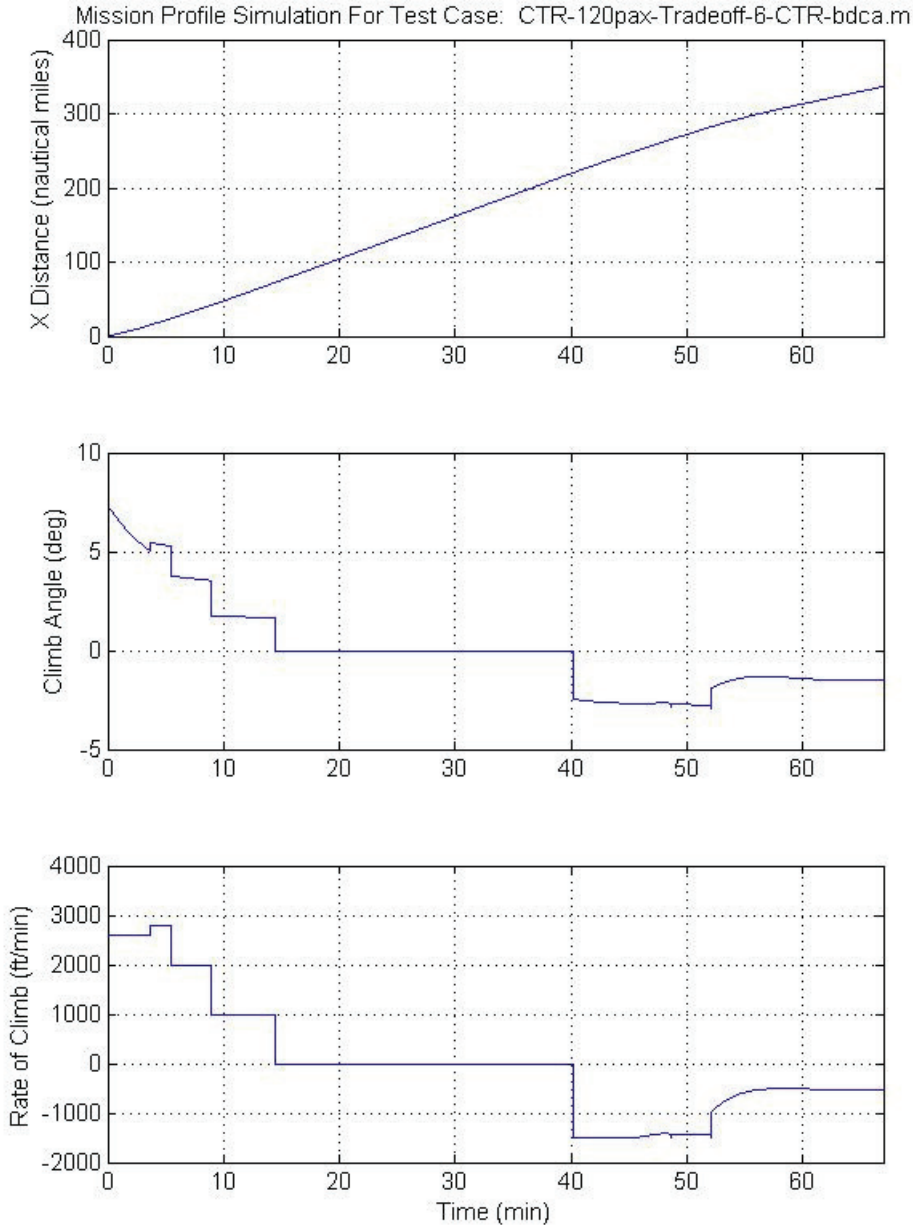

Figure J-6c. CTR120 flight profile time history (cont.).

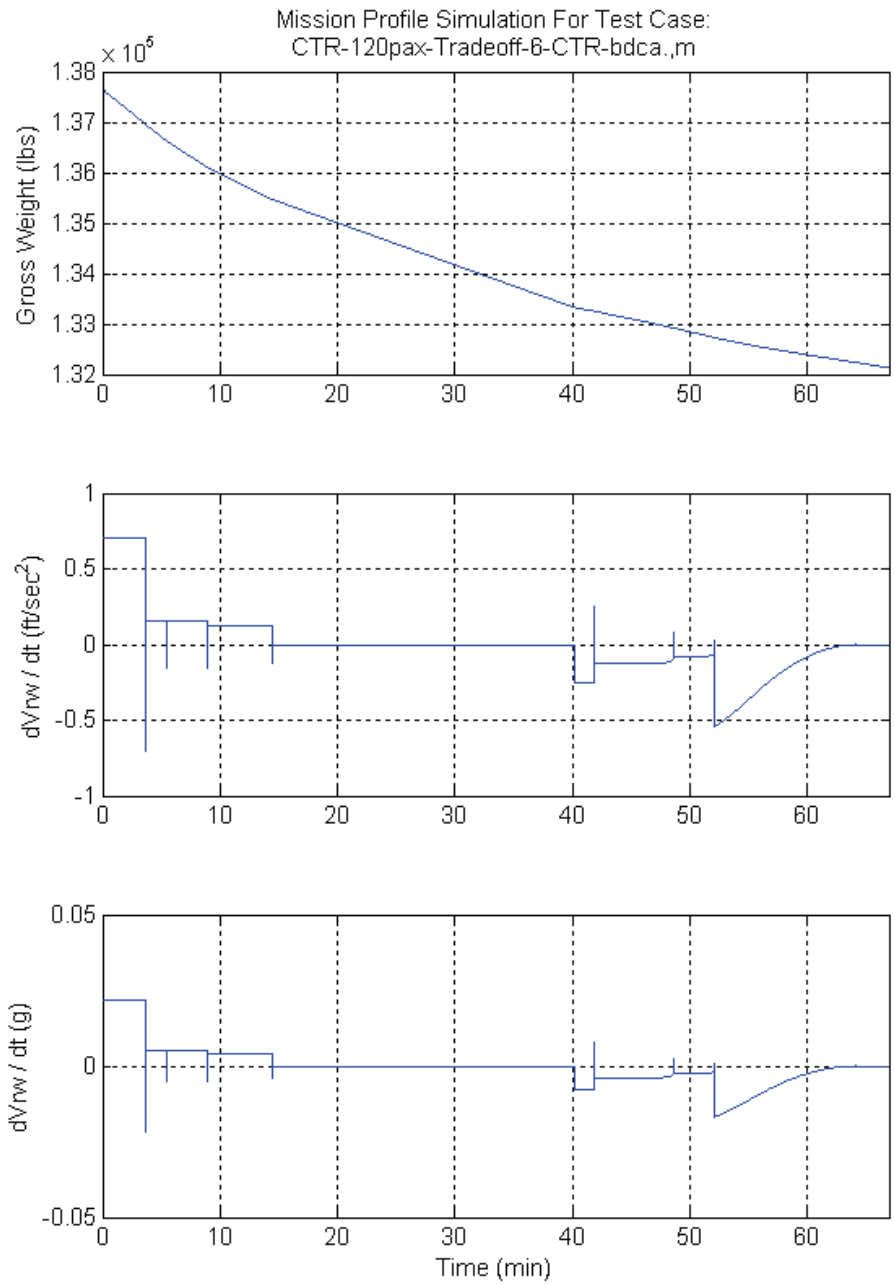

Figure J-6d. CTR120 flight profile time history (concluded).

J-5 CTR90 Flight Profiles

A 90-seat ERJ-175 flight track from Pittsburg International Airport (PIT) to Philadelphia International Airport (PHL), with a distance of 232 nmi, is shown in figure J-7. A total flight time of 50 minutes with a scheduled trip time of 65 minutes was registered as the flight cruised at 23,000 feet and 450 knots. Using the same assumptions made with the CTR120, a flight distance of 222 nmi for the CTR90 was used to develop flight profiles according to various cruise speeds and altitudes. The fuel weight of the CTR90 was reduced from 14,885 lbs to 9,885 lbs to adjust for the shorter flight. Table J-2 shows the flight time and fuel burn performance under the various cruise speeds and altitudes. The projected LRC speed is 300 knots at a cruise altitude of 27,500 feet, and is shown in Case #11, and the projected MCP speed is 345 knots as shown in Case #12 in table J-2.

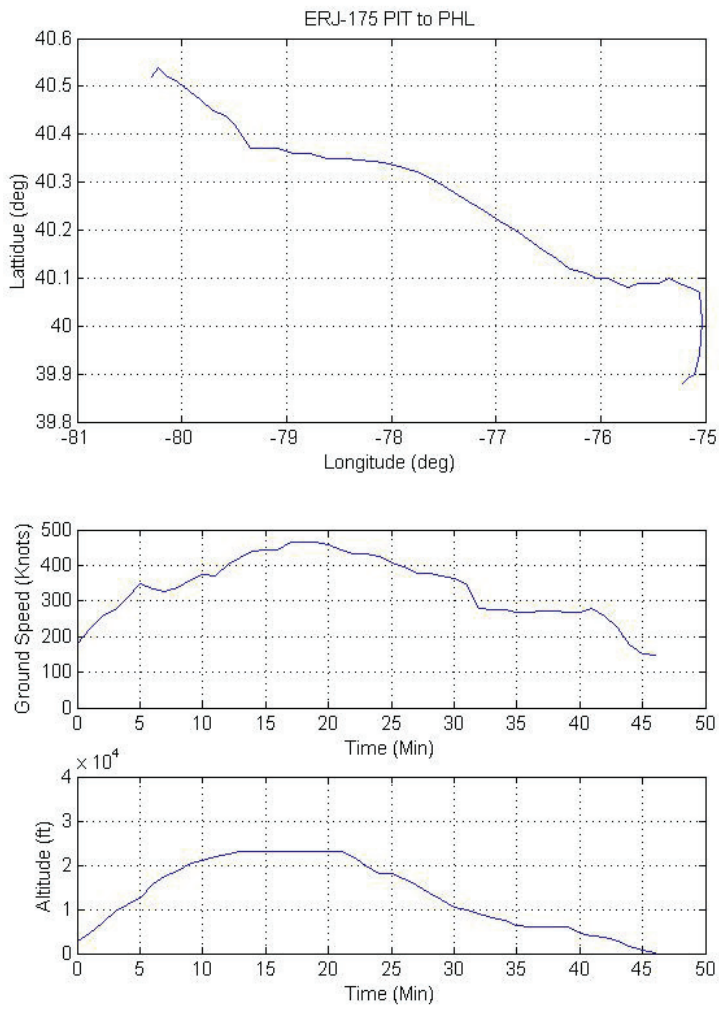

Figure J-7. An ERJ-175 track from PIT to PHL.

TABLE J-2. CTR90 FLIGHT TIME AND FUEL BURN RESPONSE

Case	Distance (nmi)	Cruise Spd (knots)	Cruise Altitude (feet)	Initial Gross Weight (lbs)	Time (min)	Fuel Burned (lbs)	Optimize wrt Max Thrust in climb	Max Thurst in cruise	Productivity Index (NM/Hr)
12	222	340	27500	114,911	46.23	3549.57	√	√	68.89
7	222	340	25000	114,911	45.88	3587.47	√		69.38
6	222	340	23000	114,911	45.76	3633.61	√		69.53
2	222	340	21000	114,911	45.66	3695.37	√		69.63
13	222	320	19000	114,911	45.36	3762.59	√	√	70.03

From table J-2, the trend is similar to the 120-passenger data in table J-1, i.e., at higher cruise altitude less fuel is consumed, but longer flight time is required than when operating at lower altitude. Case 2 has the best PI without hitting the maximum thrust in cruise as shown in green in table J-2, which suggests that for this specific origination-destination pair, a cruise speed of 340 knots and an altitude of 21,000 feet are optimal. Time histories from Case 2 are shown in figures J-8(a) through J-8(d).

The estimated total flight time for the CTR90 in Case 2 is 53.66 minutes (= 2 + 45.66 + 1 + 5) from runway roll to landing, 3.66 minutes longer than the commercial ERJ-175 showed previously. The primary reason is that the ERJ-175 was flying at a cruise speed above 400 knots at an altitude of 23,000 feet compared to the CTR flight at 340 knots at 21,500 feet (from Case 22 shown in figure 8(a)). To be competitive, more optimization of the CTR flight profile, such as trading off climb rate with speed and fuel burn, is needed.

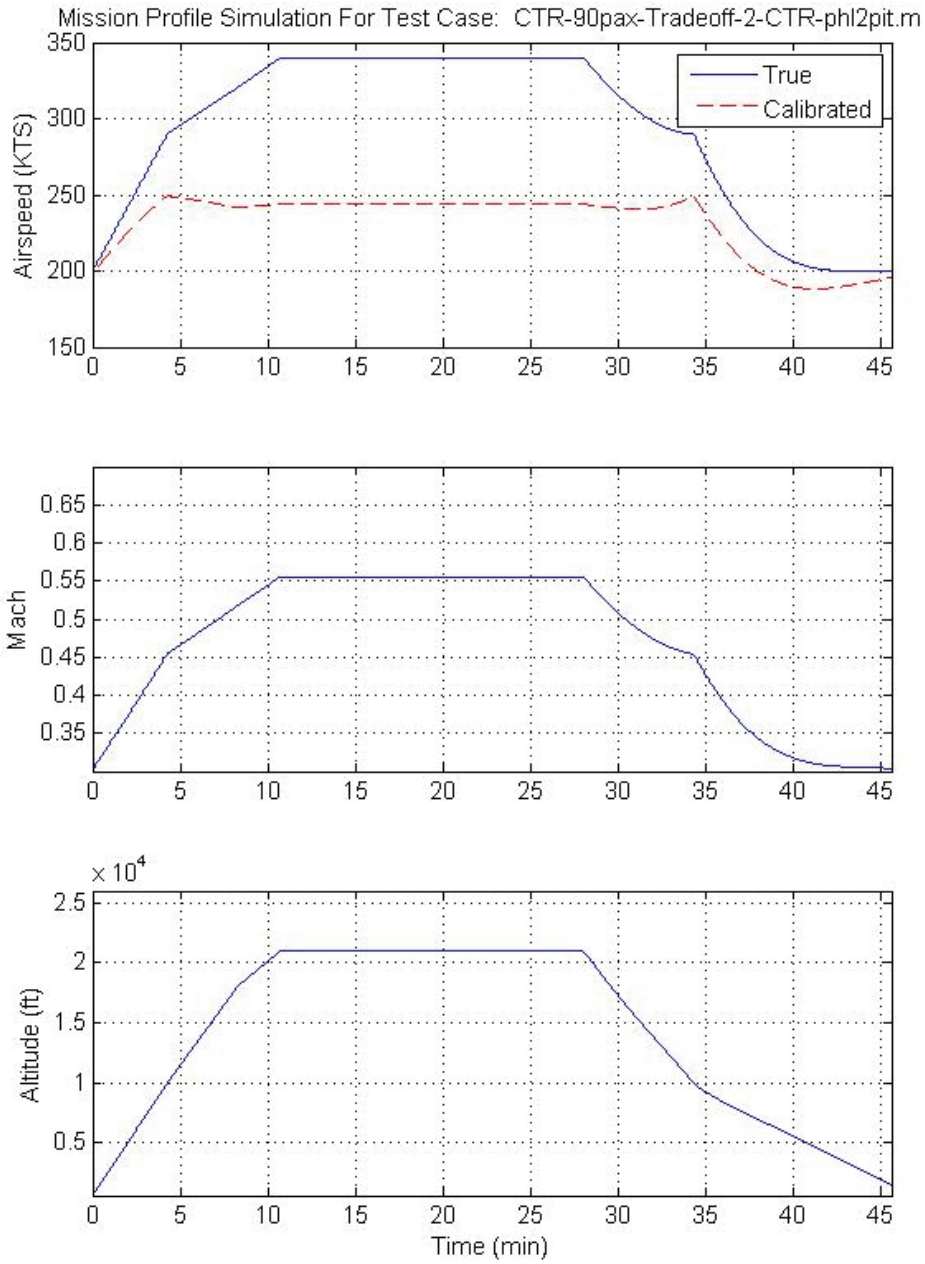

Figure J-8a. CTR90 flight profiles, Case 2.

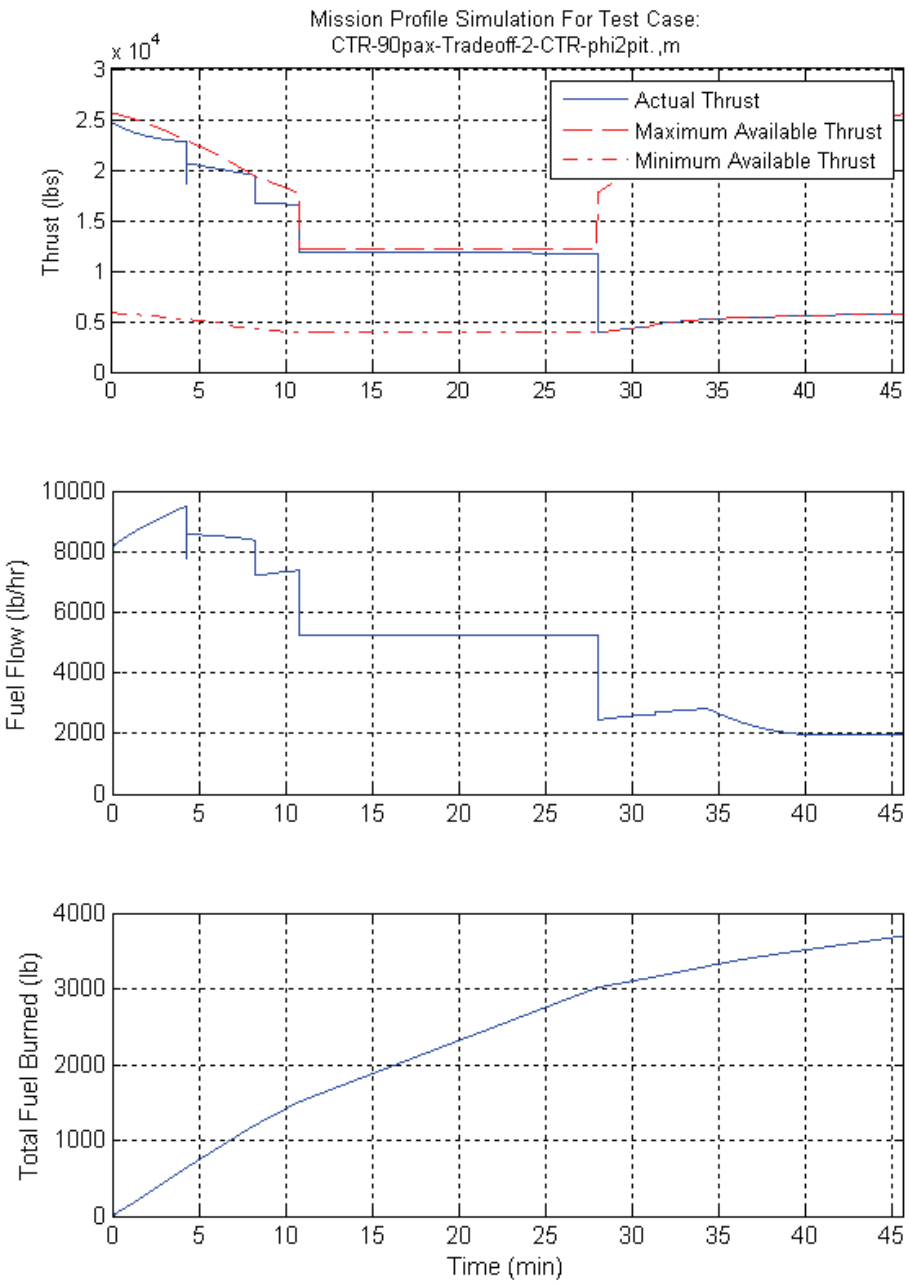

Figure J-8b. CTR90 flight profiles, Case 2 (cont.).

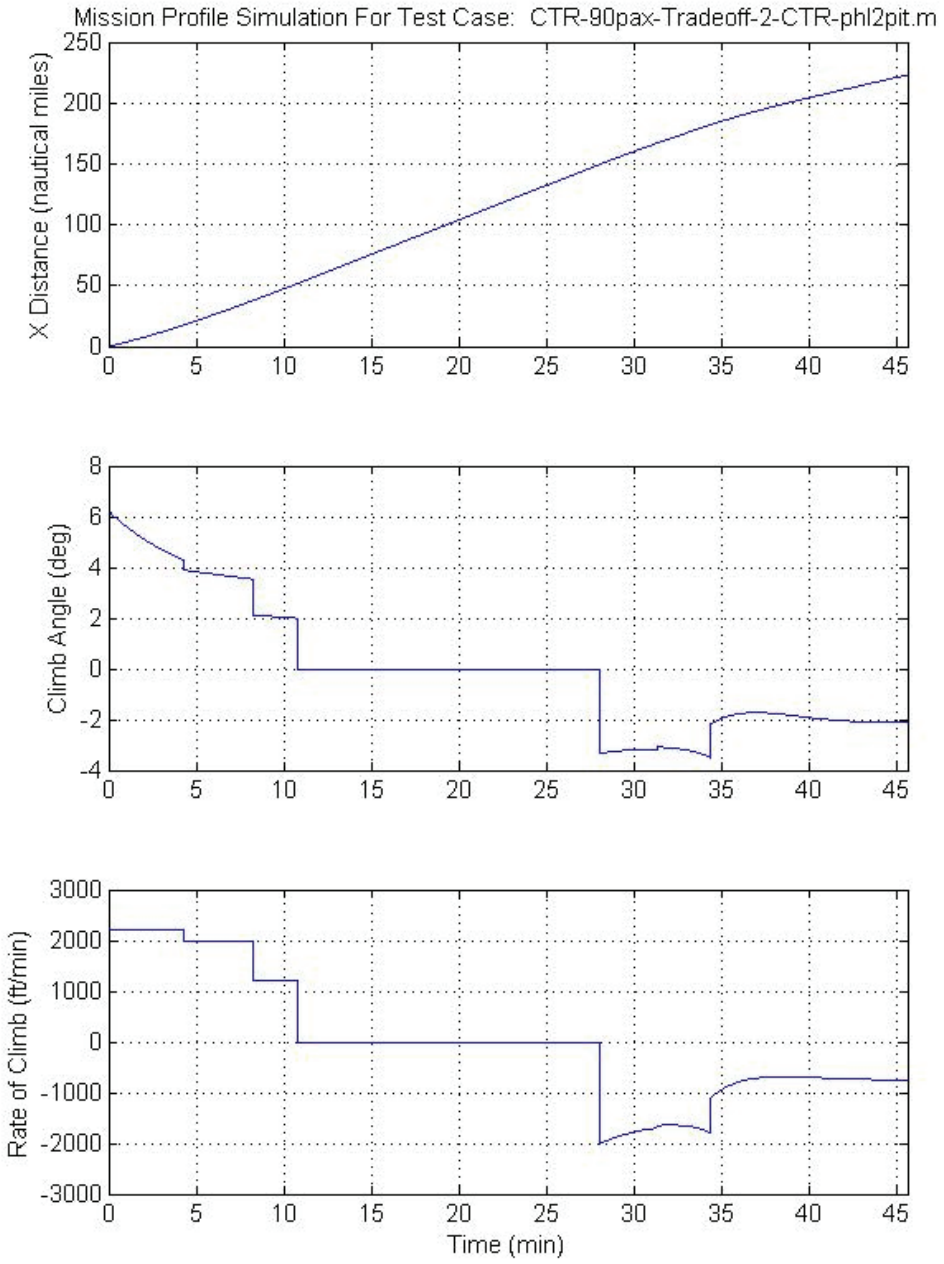

Figure J-8c. CTR90 flight profiles, Case 2 (cont.).

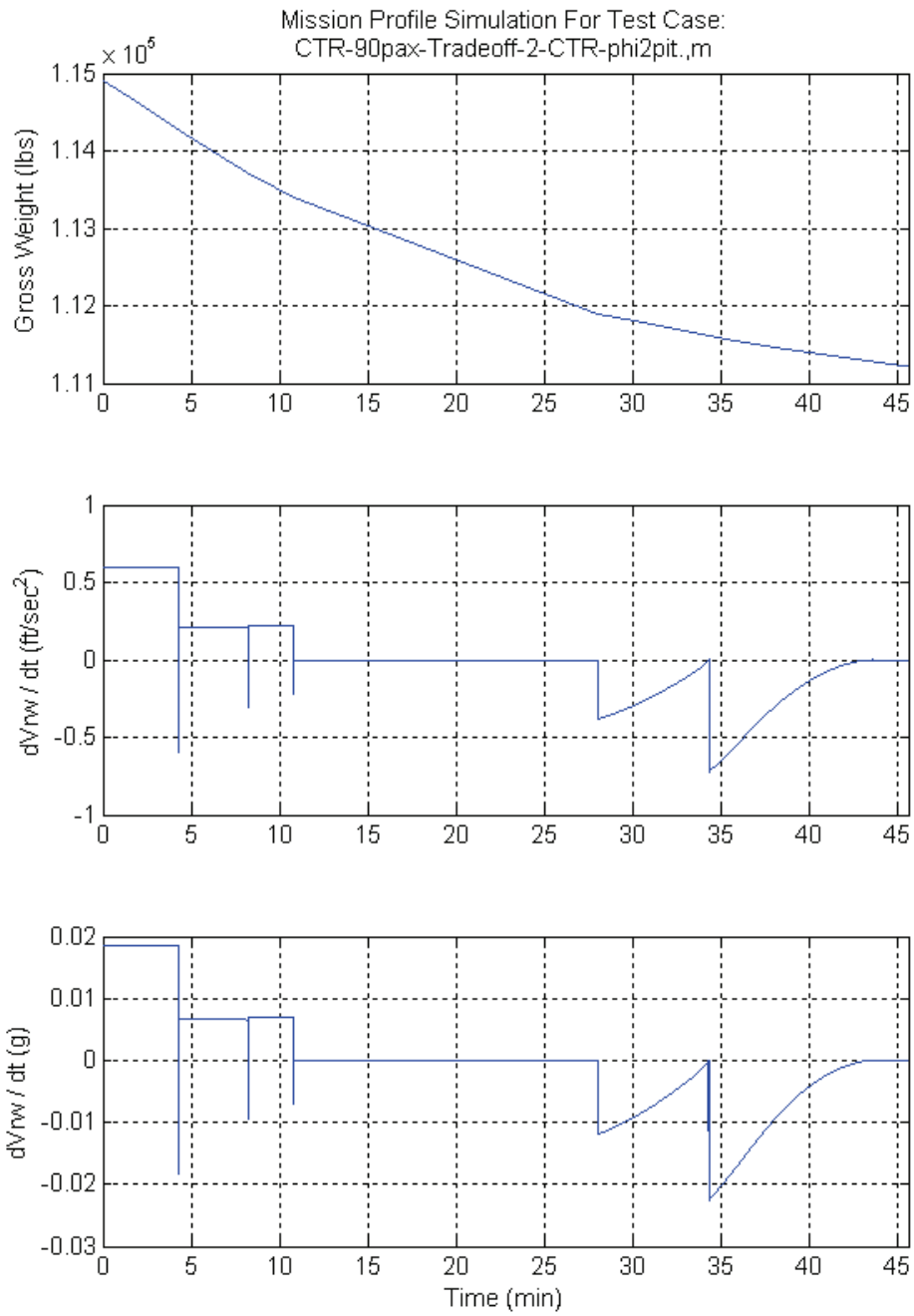

Figure J-8d. CTR90 flight profiles, Case 2 (concluded).

J-6 30-Passenger Flight Profiles

A 37-seat Dash 8-100 flight track from PHL to Baltimore Washington International Airport (BWI), with a distance of 78 nmi, a flight time of 33 minutes, and a scheduled trip time of 50 minutes, was shown in figure J-9. The Dash 8-100 climbed to a cruise altitude of 6,000 feet at a cruise speed of 220 knots. A variation of CTR30 flight profiles were evaluated and summarized in table J-3. Fuel weight was reduced from 7,000 lbs to 4,000 lbs to account for the shorter route. To be comparative to the Dash 8-100, only a cruise speed of 245 KCAS at three different cruise altitudes were evaluated.

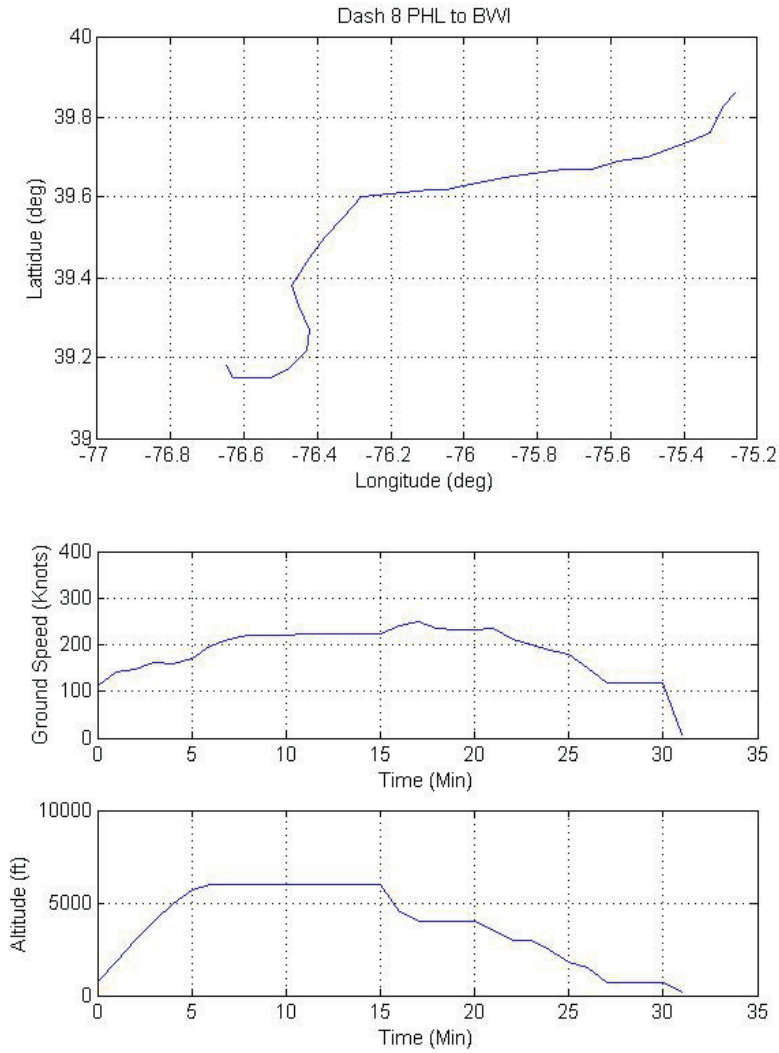

Figure J-9. A Dash 8-100 track from PHL to BWI.

TABLE J-3. CTR30 FLIGHT TIME AND FUEL BURN RESPONSE

Case	Distance (nmi)	Cruise Spd (knots)	Cruise Altitude (feet)	Initial Gross Weight (lbs)	Time (min)	Fuel Burned (lbs)	Optimize wrt Max Thrust in climb	Max Thurst in cruise	Productivity Index (NM/Hr)
10	68	285	9000	46,430	17.35	593.17	√		47.39
11	68	280	8000	46,430	17.14	593.26	√		47.97
12	68	275	7000	46,430	16.98	594.82	√		48.42

TABLE J-4. 30-PASSENGER FLIGHT TIME AND BURN DATA BETWEEN EWR AND PIT

Case	Distance (nmi)	Cruise Spd (knots)	Cruise Altitude (feet)	Initial Gross Weight (lbs)	Time (min)	Fuel Burned (lbs)	Optimize wrt Max Thrust in climb
13	267	340	16000	43,430	55.45	2162.18	√

The total flight time from Case 12 would be 24.98 minutes (= 2 + 16.98 + 1 + 5), which is competitive relative to the Dash 8-100 flight time of 33 minutes. Since the cruise altitude for this city-pair is below 10,000 feet, the CTR was operated well below the designed cruise speed of 340 knots. The time history of Case 12 is shown in figures J-10(a) through J-10(d).

Another case of evaluation, as shown in table J-4, was done using the CTR30 for longer routes, e.g., 277 nmi between Newark Liberty International Airport (EWR) and PIT, where the 30-passenger could be operated at designed cruise speed. The selected commercial flight was a 74-seat Dash 8 Q-400 between EWR and PIT flying at a cruise speed around 400 knots at 16,000 feet, with a flight time of 59 minutes and a scheduled trip time of 100 minutes. After including initial takeoff and conversion, and landing at the end (i.e., points 1–4 in figure J-1 and points 8-12 in figure J-2), the total flight time for the CTR30 would be 63.45 minutes (= 2 + 55.45 + 1 + 5), which is longer than the Dash 8 Q-400.

J-7 10-Passenger Flight Profiles

There is no commercial flight track available for 10-passenger. Table J-5 shows a single case if the CTR10 was operated between PHL and BWI. Fuel capacity was run at full 2,500 lbs. The flight time is similar to the CTR30, and the fuel burn is understandably lower due to the much small size of the aircraft. The total flight time is estimated at 29.66 minutes (= 2 + 21.66 + 1 + 5).

TABLE J-5. CTR10 FLIGHT TIME AND FUEL BURN RESPONSE

Case	Distance (nmi)	Cruise Spd (knots)	Cruise Altitude (feet)	Initial Gross Weight (lbs)	Time (min)	Fuel Burned (lbs)	Optimize wrt Max Thrust in climb
10	80	230	6000	16,800	21.66	286.1	√

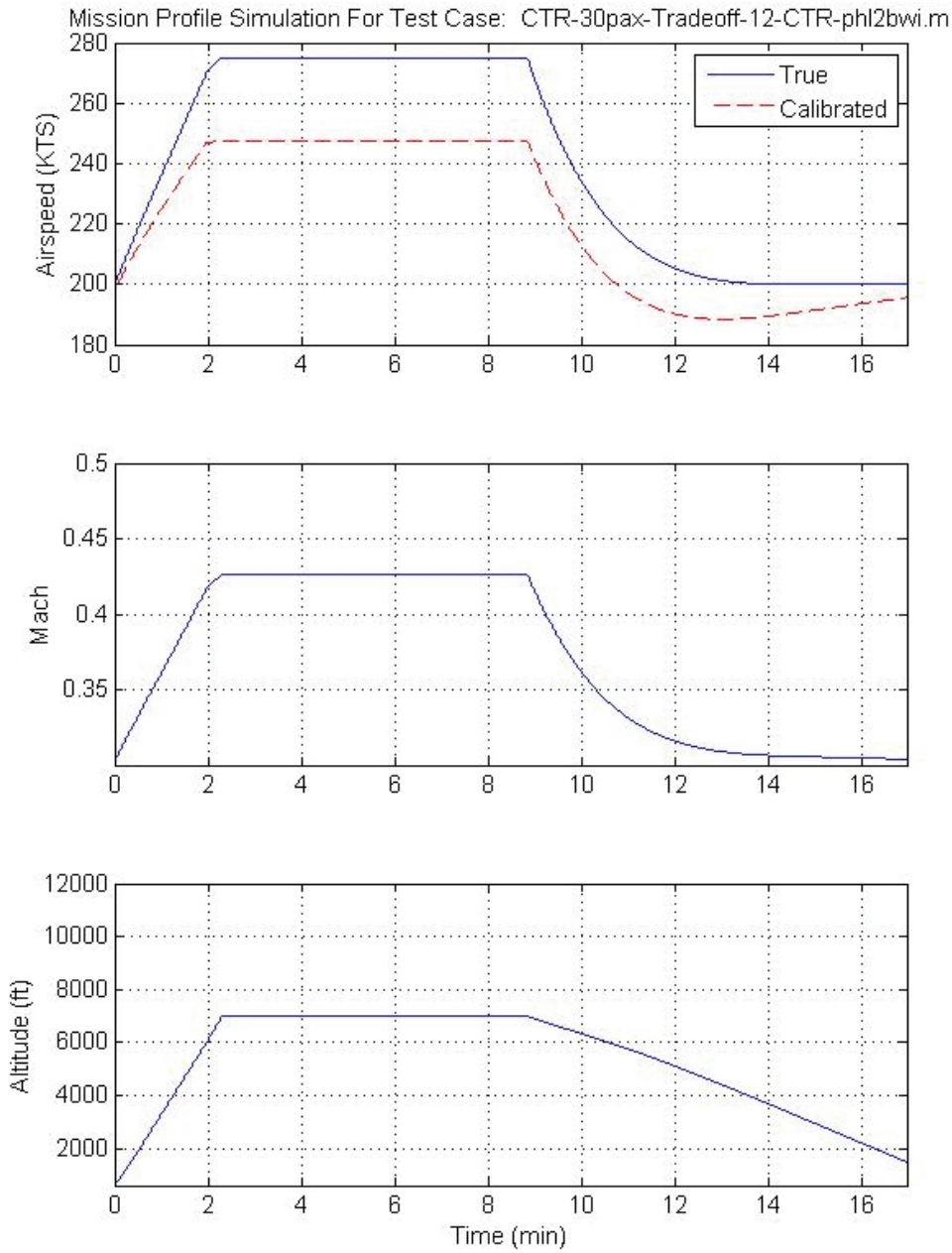

Figure J-10a. CTR30 flight profiles, PHL to BWI, Case 12.

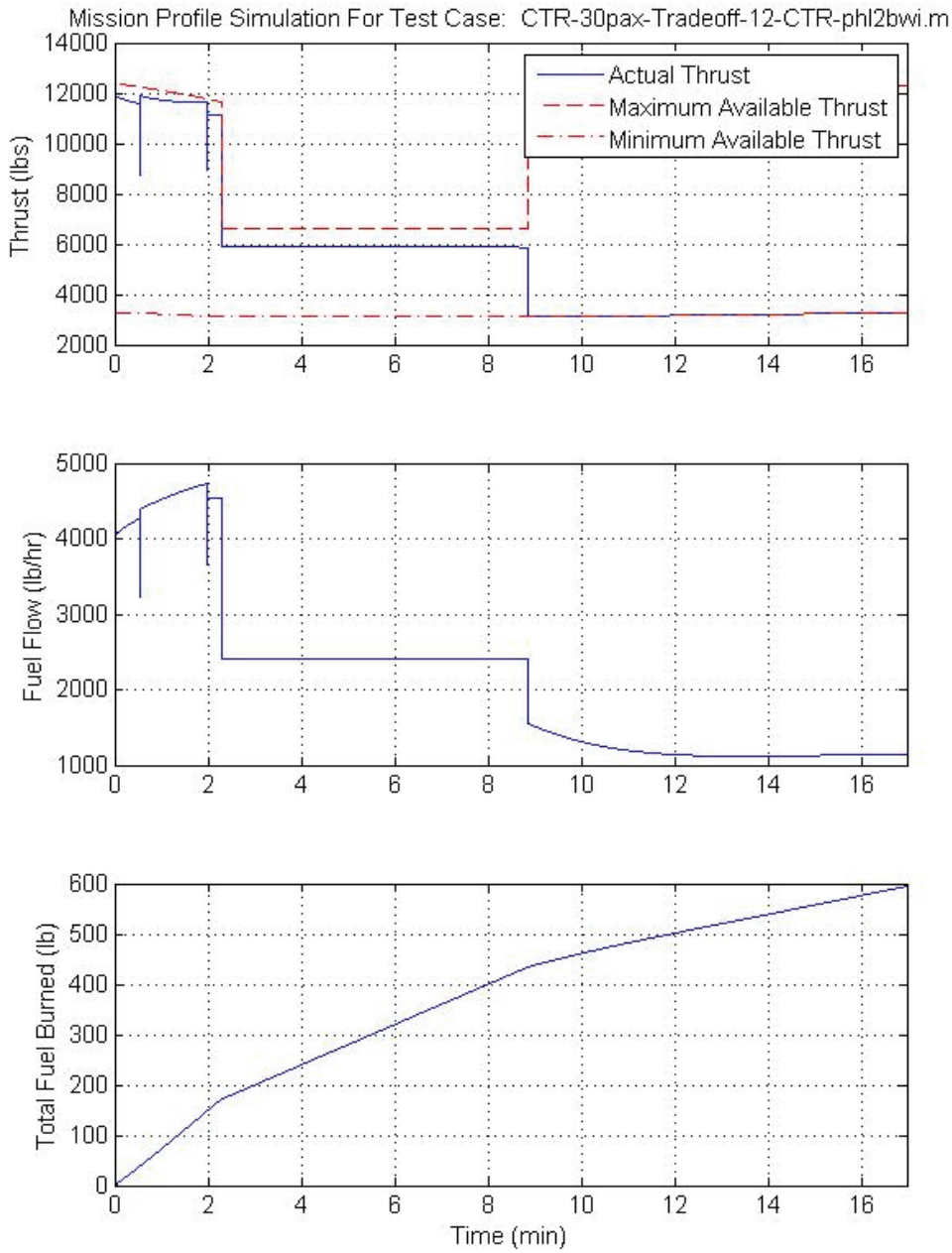

Figure J-10b. CTR30 flight profiles, PHL to BWI, Case 12 (cont.).

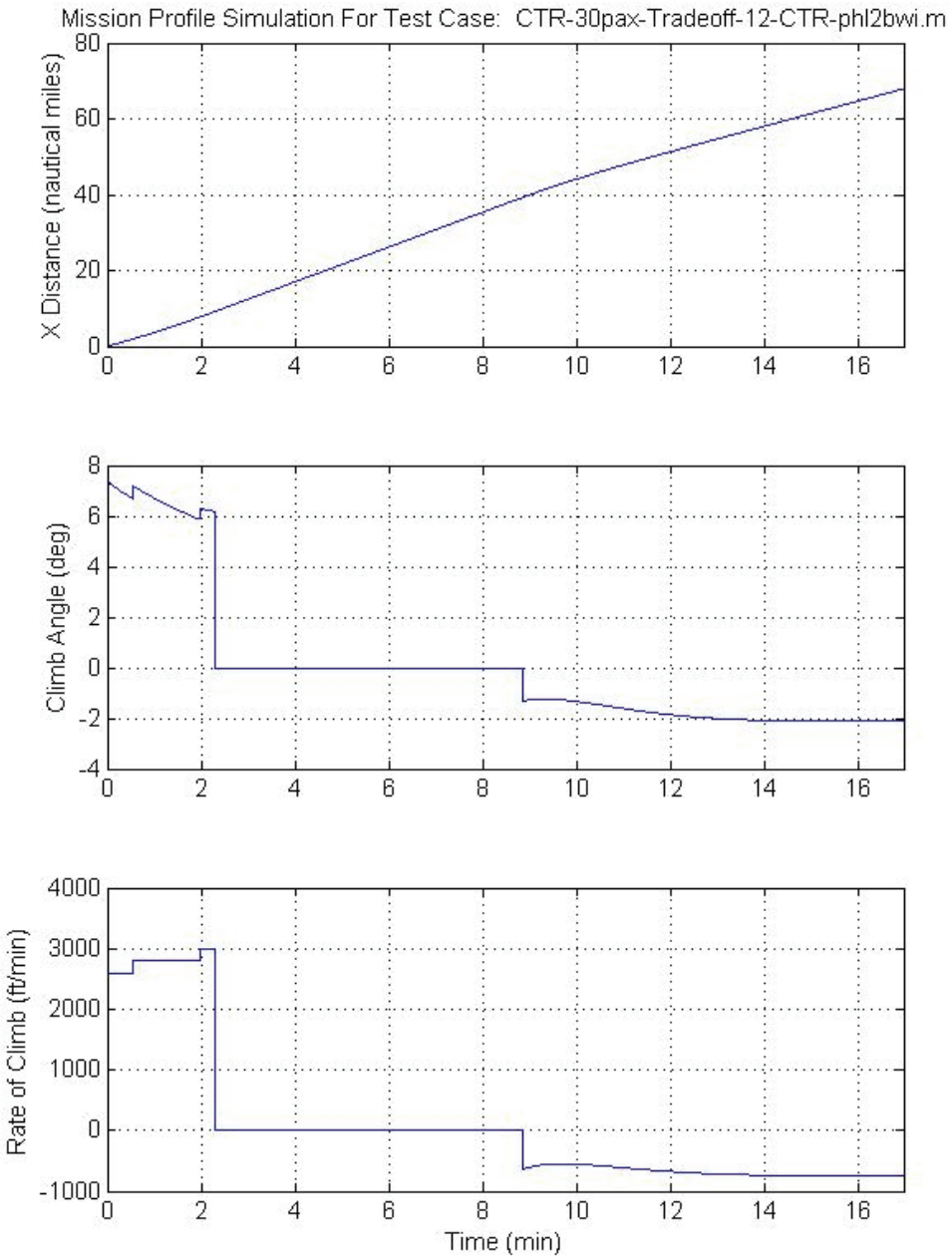

Figure J-10c. CTR30 flight profiles, PHL to BWI, Case 12 (cont.).

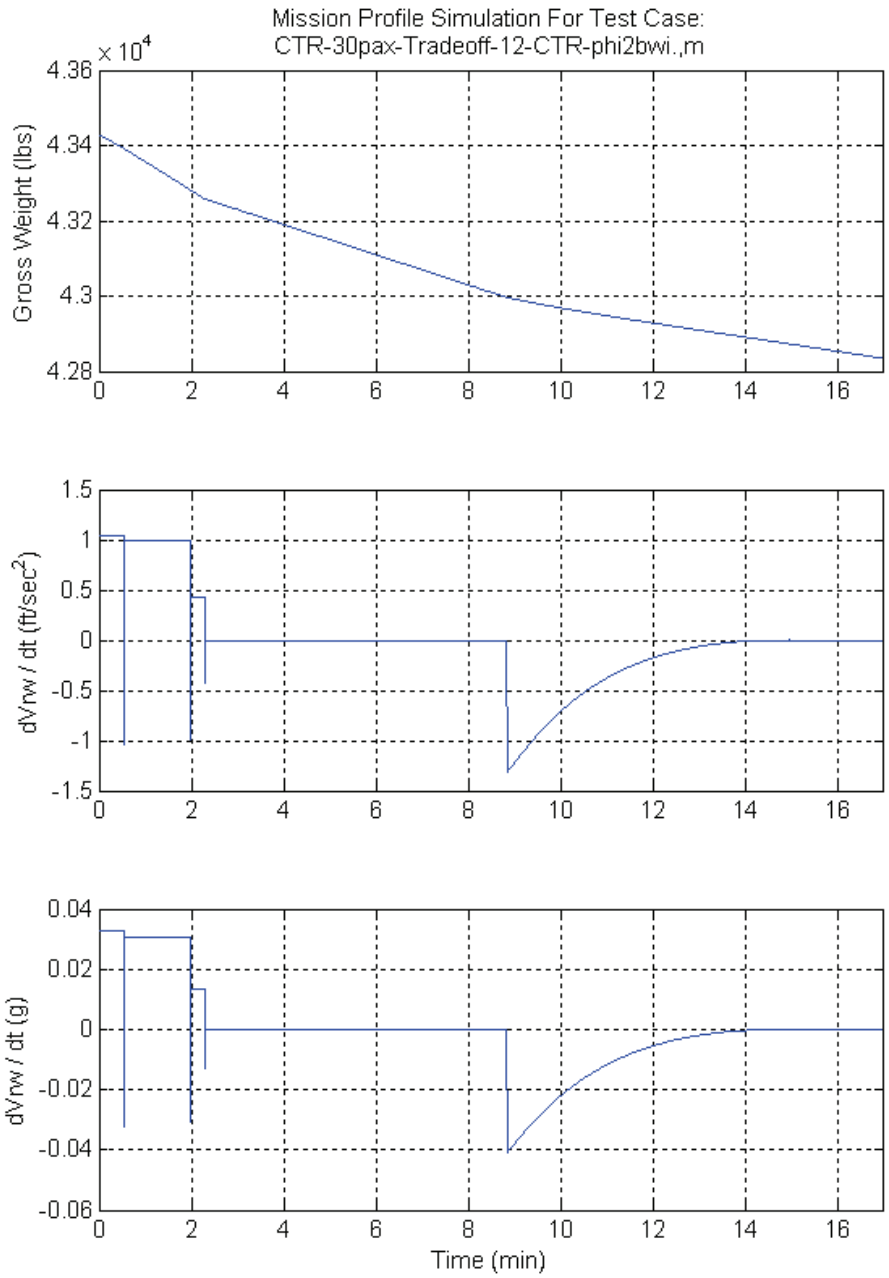

Figure J-10d. CTR30 flight profiles, PHL to BWI, Case 12 (concluded).

J-8 Summary

A summary of all commercial and CTR in-flight data is shown in table J-6. Data show that the CTR fleet can be competitive depending on the routes that commercial flights are taking and airplanes used. Estimates of taxi-out and taxi-in as described in ref. J-1 for the CTR STO and VTO operations need to be further refined.

TABLE J-6. SUMMARY OF FLIGHT TIME COMPARISON WITH COMMERCIAL FLIGHTS

	Passenger	Origin	Destination	Distance (NM)	Scheduled Trip Time (min)	Flt Time (min)	Cruise Gnd Spd (Knots)	Cruise Alt (feet)
A319	120	BOS	DCA	346	88	81	410	32000
120-pax CTR	120					74.98	345	27500
ERJ-175	90	PIT	PHL	232	65	50	450	23000
90-pax CTR	90					53.66	340	21000
Dash 8-100	37	PHL	BWI	78	50	33	220	6000
30-pax CTR	30					24.98	245	7000
Dash 8 Q400	74	EWR	PIT	277	100	59	400	16000
30-pax CTR	30					63.45	340	16000
10-pax CTR	10	PHL	BWI	90		29.66	230	6000

J-9 Concluding Remarks

1) The PD is flexible and reflects the designed CTR flight characteristics and physical properties. This tool can be used to develop CTR flight profiles and approach vectors, which include speed and altitude data, for the AvTerminal.
2) New strategy, e.g., optimizing the scheduled trip time (including taxi-out and taxi-in as shown in figure 6-4) is needed to operate the CTR fleet in order to be competitive with commercial flights, which have shorter flight time, especially for shorter routes where faster jets are being used.
3) At 120 passengers, the CTR is competitive in flight time when the commercial flights are operated at higher cruise altitudes.
4) At 90 passengers, the CTR is not as competitive in flight time since the commercial flights are operating at a similar altitude but at higher cruise speeds. Need to find a cruise altitude that is both practical and reduces the flight time.
5) At 30 passengers, cruise altitude is below 10,000 for shorter routes, and thus limits the cruise speed to below 250 KCAS, which takes away the higher cruise speed advantage of the CTR at this class; however it is competitive in flight time when compared to aircraft such as the Dash 8-100. At longer routes, the 30-plassenger is not quite competitive in flight time with the existing commercial flights for the same reason as the 90-passenger case.
6) At 10-passengers, the flight time performance is similar to the CTR30 for shorter routes.

J-10 References

J-1. Paris, A. and Chung, W.: CTR Performance Deck User's Guide. Technical Note 013, Science Applications International Corporation (SAIC), McLean, VA, U.S. Government Prime Contract NNA09DA06T, Sept. 15, 2010.

APPENDIX K. ACES TEST SCENARIOS SETUP

This section documents the Airspace Concept Evaluation System (ACES) simulation configuration for the runs. The input settings for the simulations are shown in table K-1. The main difference between simulations is the flight data set.

TABLE K-1. AUTO-CONFIGURE PROPERTIES (ACP) SETTINGS FOR SIMULATIONS

System Settings	
Start/Stop Dates	March 19, 2009 07:00 GMT March 20, 2009 23:00 GMT
Scenario	Weather date: March 19, 2009
Terminal Area Modeling	
Airport Taxi Times	Airport unimpeded taxi times were derived from Aviation System Performance Metrics (ASPM) and Airline Service Quality Performance (ASQP) historical data.
Airport State	No state files were used except for the bad weather simulations (weather date: March 19, 2009).
Airport Capacity	Input file featured the fully implemented NextGen airport capacities developed by the Joint Planning and Development Office (JPDO).
Airport Traffic Flow Management (TFM) Parameters	Default inputs were used.
Surface Traffic TFM Parameters	Not used. The focus of the simulations was system-wide and not confined to a specific airport.
Surface Traffic Air Traffic Control (ATC) Parameters	Not used. The focus of the simulations was system-wide and not confined to a specific airport.
Arrival Fix Spacing	Not used.
Surface Traffic Limitations	Not used. The focus of the simulations was system-wide and not confined to a specific airport.
Arrival/Departure Fix Spacing	Enabled. This feature enforces arrival and departure time separation within the terminal area.

TABLE K-1. AUTO-CONFIGURE PROPERTIES (ACP) SETTINGS FOR SIMULATIONS (concluded)

En Route Modeling	
Sector Grid	Default input file was used.
Center Boundary	Default input file was used.
Low Sector	Input file featured the fully-implemented NextGen airspace capacities developed by JPDO.
High Sector	Input file featured the fully-implemented NextGen airspace capacities developed by JPDO.
Super High Sector	Input file featured the fully-implemented NextGen airspace capacities developed by JPDO.
Delay Maneuvers	This feature was not used. Evaluation of the feature indicated little or no benefit in its use while increasing the duration of simulations.
Collision Detection and Resolution	Use of this feature was not within the scope of this research.
Advanced Airspace Concepts	Use of this feature was not within the scope of this research.
Flight Modeling	
AOC Operation	Use of this feature was not within the scope of this research.
Environment	
Wind	Disabled.

Vertiports are associated with an existing airport although they are simulated as independent entities. That is, operations from a vertiport are independent from those in nearby vertiports and its "parent" airport. Vertiport capacities were set to 12 arrivals per hour, 12 departures per hour, and a combined capacity no greater than 20 per hour. Boston Logan International Airport (BOS) was the exception and was double this capacity. This was necessary to keep delay to realistic levels due to the high volume of flights into and out of BOS and nearby fields in the flight data sets.

The terminal-area boundary for each vertiport was configured such that the CTR flight profile generated by the flight deck and ACES resembled each other. After some experimentation, a departure and arrival fix configuration of 40 and 10 nmi, respectively, was determined to produce the desired result. In addition, a separation of approximately 10 degrees between fixes was used to reduce the circuity of departure and arrival routes.

APPENDIX L. POSSIBLE VTOL/STOL LANDING LOCATIONS AT NEWARK LIBERTY INTERNATIONAL AIRPORT FOR CIVIL TILTROTOR AIRCRAFT

L-1 Background

Newark Liberty International Airport (EWR) along with John F. Kennedy International Airport (JFK) and New York LaGuardia International Airport (LGA), operated by the Port Authority of New York and New Jersey (PANYNJ), are the major airports that make up what is commonly referred to as the New York Metroplex. EWR was selected for the Year-2 study of the metroplex because:

1. EWR is the overnight small package center for the New York, New Jersey region. In 2006, nearly one million tons of air cargo moved through EWR.
2. In 2006, EWR had nearly 450,000 aircraft operations and moved nearly 36 million passengers.
3. In 2008, EWR had the second worst number of departure delays in the NAS (33 percent). The worst was Chicago O'Hare International Airport with 35-percent departure delays.[1]

L-2 Discussion

L-2.1 Airport Layout

The airport has two parallel runways (4R/22L and 4L/22R) with a third (crosswind) runway (11/29) used primarily by commuter aircraft. Runway 4R/22L is 9,980 feet long by 150 feet wide and Runway 4L/22R is 11,000 feet long by 150 feet wide. The distance between the parallel runways is 900 feet. Runway 11/29 is 6,800 feet long by 150 feet wide. There is also a 40-foot by 40-foot concrete helipad just north of taxiway "Z." There are more than 12 miles of 75-foot-wide taxiways entirely equipped with centerline lighting. Figure L-1 shows the general layout of the airport.

L-2.2 Assumptions

1. Essentially, the operation of the primary arrival and primary departure runway establishes the secondary arrival and departure that are used to handle peak hour flow conditions. Generally all of EWR aircraft traffic flows are variations on either a Southwest flow configuration (used approximately 55 percent of the time) and a Northeast flow configuration (used approximately 45 percent of the time). Usually all arriving aircraft are assigned to runway 4R/22L (the runway furthest from the terminal), while departures are assigned runway 4L/22R (the runway closest to the terminal). Runway 4L/22R is also used as a second arrival runway. This is only used intermittently since it reduces capacity for departures but data indicate that up to four peak hour arrivals can be accommodated. Runway 11/29 has very occasional use as an arrival runway. Its use is limited by two intersections with the main parallel runways. Runway 11 is used more frequently for departures during Northeast flow. While this shortens taxi times it does not contribute to overall departure capacity, again due to the two runway intersections.[2] This may change for two reasons: (i) the FAA has recently approved "Intersecting Runway Operations" to runway 29 and 4R,[3] and (ii) a Local Area Augmentation System has been installed on runway 29. This will lower the weather minimums for arrivals.

---

[1] A departure delay is a flight that departs from the gate more than 15 minutes after it's scheduled.

[2] FAA Regional Air Service Demand Study—Task E, May 2007.

[3] FAA Notice 2010-06-03, effective 06/03/2010 to 07/01/2010.

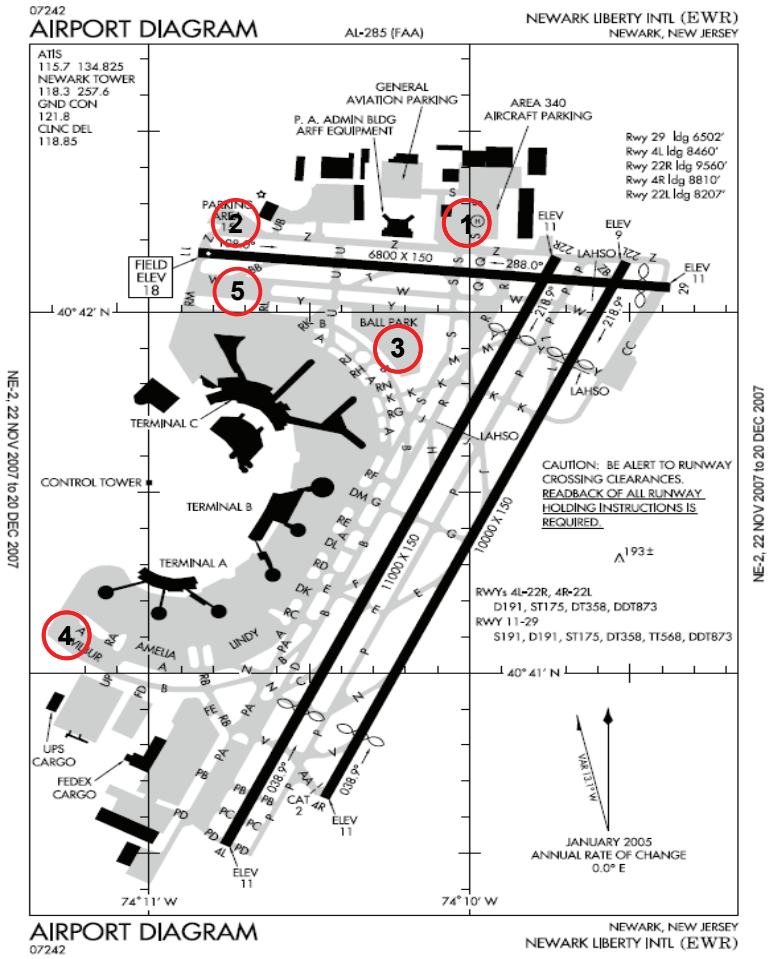

Figure L-1. EWR diagram with vertiport sites being evaluated.

2. For consistency with the evaluation done to determine CTR operations at Miami International Airport, as was performed early in the current study, the same criteria will be used to evaluate potential landing spots and useable taxiways at EWR. The criteria are:
   a. Upwind approach, landing, and departure are preferred.
   b. Approach and departure parallel to existing landing zone are preferred.
   c. Building/structures in close proximity to landing zone are to be avoided.
   d. Flights over neighborhoods, highways, taxiways, and runways are to be avoided.
   e. Consider distance from existing terminal infrastructure such as handling of passengers and luggage; landing zone close to existing terminals is preferred.
   f. Consider approach, landing, departure, and missed approach flight segments.
   g. Center of landing zone must be at least 700 feet from runway.
3. Production CTRs will have the full NextGen-required avionics from the manufacturer.
4. Vertiport design will follow FAA Advisory Circular (AC) "Vertiport Design," AC 150/5390-3, dated May 31, 1991. Vertiport infrastructure will exist to support flight operations.

5. The study will look at both VTOL and STOL CTR operations. In order to accurately assess gate-to gate operations in STOL between a CTR and fixed-wing aircraft, taxi times between these two classes of aircraft must be compared. To compute the taxi times for STOL operations at EWR, measure the taxi distance from the vertiport to takeoff position then divide by the typical CTR taxi speed. These times do not include the time needed to be towed to a startup (run-up) position and completing the startup checklist. These times are included in assumption number 7.
6. Navigation accuracy of RNP-0.30, or better, will exist to support appropriate approach/departure paths.
7. For VTOL operations, the following taxi-out and taxi-in scenarios will be used:

   Taxi-out;

   a. Aircraft at the gate loading passengers, baggage, etc. Crew performs the pre-flight check list (same as fixed-wing operation).
   b. Aircraft servicing is complete and all passengers seated and safety belts buckled. Tug can then push off gate. (FAR Part 121 requirement for all passengers to be seated and buckled before leaving gate.)
   c. The tug travels at 10 mph and therefore can move the aircraft approximately 880 feet in one minute.
   d. The center of site #5, Final Approach and Takeoff Area (FATO), is approximately 760–850 feet from the terminal where gate is located. Therefore, the tug can get the aircraft into takeoff position in one minute.
   e. While being towed to the takeoff position the auxiliary power system (APU) is running. (This is for passenger comfort and minimum power for communication, etc.)
   f. Once the aircraft is in the takeoff (or run-up position) the tug can disconnect and the crew can commence aircraft startup check list.[4]
   g. Commence aircraft startup check list. Startup check list can be completed in 7 minutes.[5]
   h. Final ATC clearance and commence takeoff.[6]

   Taxi-in:

   a. Touchdown in designated landing zone (LZ).
   b. Commence shutdown check list. Shutdown time is approximately 4–5 minutes.[7]
   c. Once rotors are stopped, the tug connects to aircraft and the CTR is towed to the gate. During towing the APU is on for the previously stated reasons. Towing to the gate is approximately one minute.[8]
   d. Aircraft arrives at gate and passengers disembark.[9]

---

[4] The aircraft cannot commence startup while being towed for two safety-related reasons; first, to minimize the impact of rotor downwash on personnel/ground vehicles/other aircraft in the area, and second, to minimize the potential for rotor whirl effect on the rotors from wind gust or wake vortex. This can be exacerbated by the action of towing. During startup pilots must concentrate on the roll control of the aircraft because of the effect of their relatively small landing gear footprint relative to the large force and moments generated by the rotors at the wing tips.

[5] Current V-22 experience shows the startup checklist to take anywhere from 5–10 minutes. We have allowed for additional automation and simplification of the checklist for the civil tiltrotor to allow for a 7-minute startup.

[6] Total taxi-out time is 8 minutes.

[7] Shutdown allows for engine cooldown time and for rotors to come to a complete stop (no rotor brake device assumed). Part of shutdown checklist is to start aircraft APU.

[8] The total taxi-in time is 5–6 minutes.

[9] The startup and shutdown times are based on twin-engine V-22 experience. It is unknown if a large CTR with four engines will be significantly different. Adverse weather, such as severe cold where additional warm-up time may be

L-3 Site Evaluation

L-3.1 Site #1

Site #1 in figure L-1 is north of runway 11/29 at the existing helipad; Site #1 could be fitted with a FATO at a dimension of 432.5 feet x 432.5 feet for the CTR120. Using the evaluation criteria previously mentioned, table L-1 summarizes the evaluation of Site #1.

TABLE L-1. SUMMARY OF SITE #1 EVALUATIONS

Critical Dimensions[10]	Positive Aspects of Site	Negative Aspects of Site	Taxi Path Distance/Time[11]	Site Rating
130 feet from FATO to vehicle storage building	Close proximity to runway 11/29 for STOL operations	Site surround by buildings on three sides	Western departure on 11/29 (0.21 miles/ 0.84 minute) Eastern departure on 11/29 (0.87 miles/ 3.84 minutes)	Medium
244 feet from FATO to cargo building	Close proximity of General Aviation Terminal at Signature Flight Services (just north of FATO)	Site not close to main terminal buildings		
80 feet south to a vehicle road	Clear approach from west to east and approaches parallel to main runways	Site close to end of runway 22R		
285 feet south to the center of taxiway	Current helipad location with lighting			

needed, was not considered. This could add 1–2 minutes to startup time. Finally, icing conditions, where the aircraft would need to be de-iced, were not considered. The CTR would need to be de-iced before startup, possibly at the gate, since de-icing with engines running and rotors turning is not acceptable.

[10] All dimensions are from the center of FATO (this applies for all site tables).

[11] Taxi distances determined from Google map "Path" analysis. Taxi time determined using a taxi speed of 15 mph and does not include any time delay for holding at taxiway crossings (this applies for all site tables).

L-3.2 Site #2

Site #2 as shown in figure L-1 is located at the east-end of runway 29 near parking area 15. Table L-2 provides a summary of the evaluation of Site #2.

TABLE L-2. SUMMARY OF SITE #2 EVALUATIONS

Critical Dimensions	Positive Aspects of Site	Negative Aspects of Site	Taxi Path Distance/Time	Site Rating
422 feet to drainage pond	Close proximity to runway 11/29	Too close to runway 11/29 (493 feet)	Western departure on 11/29 (0.46 miles/1.84 minutes) Eastern departure on 11/29 (0.09 miles/0.36 minutes)	Low
358 feet to airport vehicle road		Too close to Interstate 81		
511 feet from FATO to Brewster Road		The FATO covers part of a taxiway		
601 feet from FATO to Interstate 81		Not close to main terminals		

L-3.3 Site #3

Site #3 as shown in figure L-1 is in the central area of airport in an area informally called the "Ball Park." A summary of the evaluation of Site #3 is shown in table L-3.

TABLE L-3. SUMMARY OF SITE #3 EVALUATIONS

Critical Dimensions	Positive Aspects of Site	Negative Aspects of Site	Taxi Path Distance/Time	Site Rating
1,182 feet to terminal C	Close to main terminal	Approach and departure are over taxiways	Western departure on taxiway Eastern departure on taxiway (0.61 miles/ 2.44 minutes)	Medium
512 feet to taxiway	Approaches/departure can be made parallel to main runway traffic	For STOL operations, a longer distance to runway 11/29 than Site #1 or #2		
3,205 feet west of taxiway "Y" (potential eastern departure)	Approach and departure areas clear			
500 feet north to taxiway "Y" (potential western departure)				

L-3.4 Site #4

Site #4 as shown in figure L-1 shows the site just southwest of Terminal A. A summary of the evaluation of Site #4 is given in table L-4.

TABLE L-4. SUMMARY OF SITE #4 EVALUATIONS

Critical Dimensions	Positive Aspects of Site	Negative Aspects of Site	Taxi Path Distance/Time	Site Rating
535 feet from FATO to Terminal "A"	Only 360 feet to taxiway and runway 4R/22L	Rotor downwash could impact service road traffic	Departure parallel to main runway (0.66 miles/2.46 minutes)	High
435 feet to Southwest Service Road	Close to Terminal "A"	Could impact aircraft taxi traffic going to UPS and FedEx cargo areas		
565 feet to UPS Cargo building and 1114 feet to FedEx cargo building	Clear approaches for departure and arrival. Parallel to main runways			
Large building 717 feet to the west				

L-3.5 Site # 5

Figure L-1 shows Site # 5 between Terminal "C" and west end of runway 11/29; note the space availability for notional STOL taxi paths close to Site #5. A summary of evaluation for Site # 5 is shown in table L-5.

TABLE L-5. SUMMARY OF SITE #5 EVALUATIONS

Critical Dimensions	Positive Aspects of Site	Negative Aspects of Site	Taxi Path Distance/Time	Site Rating
780 feet from FATO to Terminal "C"	Only 0.20 miles from the eastern end of runway 11/29	Rotor downwash could impact taxiing traffic to northernmost terminal building	Departure to east on runway 11 (0.21 miles/ 0.84 minutes) Departure to the west from runway 11/29 (0.79 miles/3.16 minutes)	High
1355 feet from aircraft hanger	Close to Terminal "C"			
1145 feet to highway 9	Clear approaches for departure and arrival for both VTOL/STOL operations			

L-4 Recommendation

Site #5 is recommended for the CTR in NextGen performance analysis study. The site has clear approaches for departure and arrival for both VTOL/STOL operations. Close proximity to Hwy 9 helps mask the rotor noise on takeoff and landing. Also, close proximity to terminal "C" allows efficient transfer of luggage and passengers to connecting long-range/international flights and local transportation. Approach/departure procedures will need to review any potential rotor downwash impacts on taxiing aircraft and buildings.

APPENDIX M. AVTERMINAL ANALYSIS

The Sensis AvTerminal fast-time computerized modeling tool is designed to simulate operations and assess capacity and delay impacts for extended airport terminal areas. AvTerminal models terminal and en route airspace arrival and departure, and runway system takeoff and landing operations. AvTerminal implements a Focal-Point Scheduling Process, an integrated approach for modeling interactions among aircraft in various flight states. The Focal-point Scheduling Process sequences, maneuvers, and delays aircraft to resolve overtake and spacing conflicts among aircraft in the airspace and airport system. The process analyzes individual aircraft movements along 4-dimensonal flight trajectories (4DTs) through a network of focal points representing cruise and transition airspace fixes and runways, including multiple airports. AvTerminal uses 3-degree-of-freedom (3DOF) flight dynamics modeling to generate trajectories. The modeling logic manages and adjusts trajectories to create integrated streams of arrival and departure traffic representing realistic flight movement through the airspace and airports. AvTerminal processes a flight schedule and evaluates traffic throughput and delay at airspace and runway system focal points.

AvTerminal implements a method for accurately integrating a trajectory while taking large steps in appropriate integration variables. This dramatically reduces the size of the computation compared to simulation. The trajectory is integrated in an open-loop fashion over a prescribed trajectory rather than being maneuvered in a closed-loop fashion to approximately follow the same prescribed trajectory. Where the aircraft will go is not a mystery; the analysis answers the question of when it will be at specified positions.

AvTerminal adopts a point mass approach to trajectory determination (ref. M-1). AvTerminal uses a 3DOF trajectory generator model. The energy balance logic calculates 4DTs by integrating point mass equations for three translation degrees of freedom (X, Y, Z) based on route and true air speed (TAS). The logic calculates the trajectory by solving point mass equations iteratively. Aircraft dynamics modeling determines force balance parameters, aerodynamics (lift, drag) and propulsion (thrust, fuel burn rate), using aircraft-type performance characteristics data (stall speed, climb speed, descent speed, cruise speed, and empty weight). The trajectory is divided into segments that are specified in terms of the energy coordinates: altitude and TAS. The flight path angle is assumed constant over each trajectory segment. Interpolation is used to determine the state at a specific time or location.

The energy balance method allows modeling altitude changes and speed changes with the same compact equations. This method models a wide range of conditions including climb, descent, acceleration, and deceleration. The method is very fast computationally.

Although AvTerminal supports accurate modeling of the terminal and its surrounding airspace, it was beyond the scope of the current study to perform detailed airspace design for CTR and conventional aircraft operations. The application of AvTerminal in the current project was limited to evaluating whether CTR takeoff, climb, descent, and landing performance in the terminal area could be matched to the Performance Deck (PD) and Fuel Burn Post Processor (FBPP) developed earlier as an outcome of PITL simulations. Prior to this study, several full adaptations of AvTerminal had been developed for Newark Liberty International Airport (EWR), to include terminal, runway system, and arrival and departure procedures. Also, in support of prior NASA airspace systems analysis, EWR operations had been analyzed as part of a technology and operational concept analysis for Extreme Short Takeoff and landing (ESTOL) aircraft (refs. M-2, M-3).

Available EWR terminal input data defined existing airspace and runway system procedures for conventional fixed-wing traffic operations. Airspace procedures describe routes, fixes, and applicable altitude and spacing requirements. Runway system procedures describe runway assignments and associated arrival/departure fixes. En route procedures refer to the inbound cruise and descent and outbound climb and cruise routes and speed/altitude profiles.

The preliminary investigation of AvTerminal, as applied to the CTR terminal area problem, supported a finding that AvTerminal could potentially be a useful tool for evaluation of non-interfering CTR arrival and departure corridors. To actually perform such an analysis would require extensive work in the design and simulation of airspace, procedures, weather impacts, and ConOps for CTR operations at specifically identified airports. This was the approach taken in the earlier ESTOL study (ref. M-3). A limitation in the current study was the broad focus on CTR operations in the NAS rather than on detailed airspace design and procedures at individual locations.

The investigation of the usefulness of AvTerminal for modeling CTR operations at EWR also uncovered some shortcomings in AvTerminal's reliance on BADA fuel burn estimation and its adaptation for modeling CTR fuel burns. Post-processing of CTR profile and track data was required to match PD values. For future applications, an automated accurate fuel burn model will be needed in AvTerminal to accommodate CTRs and other new air vehicle types.

Figures M-1 through M-6 illustrate the agreement obtained after adapting AvTerminal to model PD vertical profiles and fuel burns. The exercise of adapting and validating the AvTerminal model to replicate PD results served to confirm the validity of relying primarily on the PD for CTR performance analysis. Where differences were found to exist, issues were identified principally in the modeling of BADA data and in AvTerminal internal modeling of CTR performance. The degree of confidence in the PD grew to an extent that primary reliance was placed on the PD as the authoritative source for CTR performance analysis.

Figure M-1 shows the vertical profile comparison for the CTR120 vehicle, and figure M-2 shows the fuel burn match for the CTR120 vehicle. Figure M-3 shows the vertical profile comparison for the CTR90 vehicle, and figure M-4 shows the fuel burn match for the CTR90 vehicle. Figure M-5 shows the vertical profile comparison for the CTR30 vehicle, and figure M-6 shows the vertical profile comparison for the CTR10 vehicle.

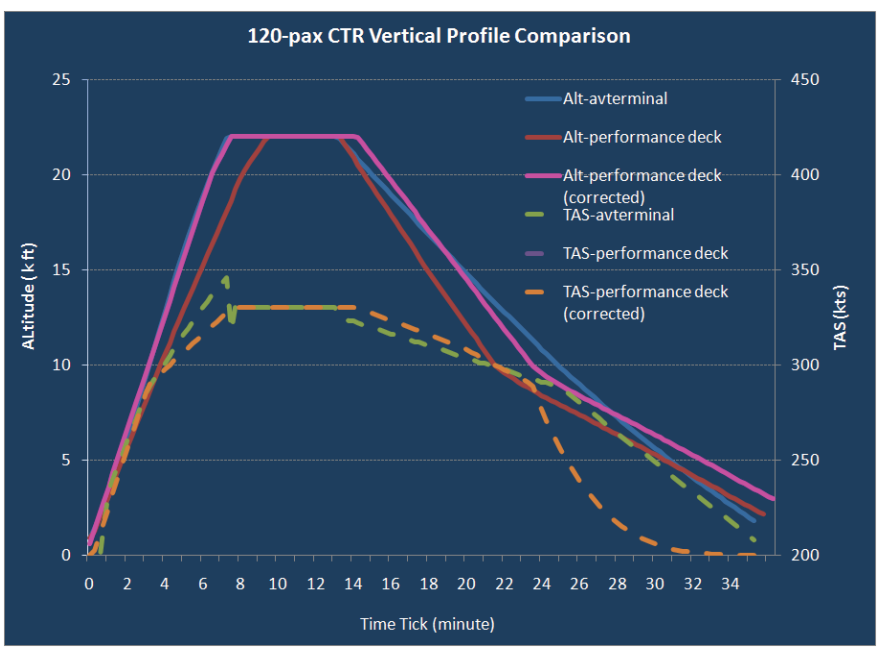

Figure M-1. Comparison of CTR120 AvTerminal and PD vertical profiles.

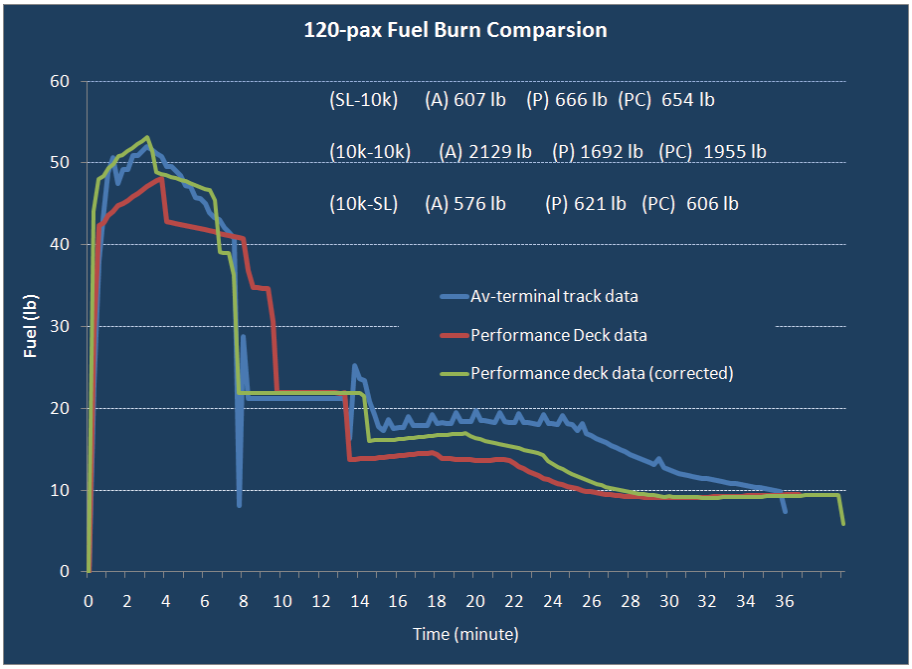

Figure M-2. Comparison of CTR120 AvTerminal and PD fuel burn.

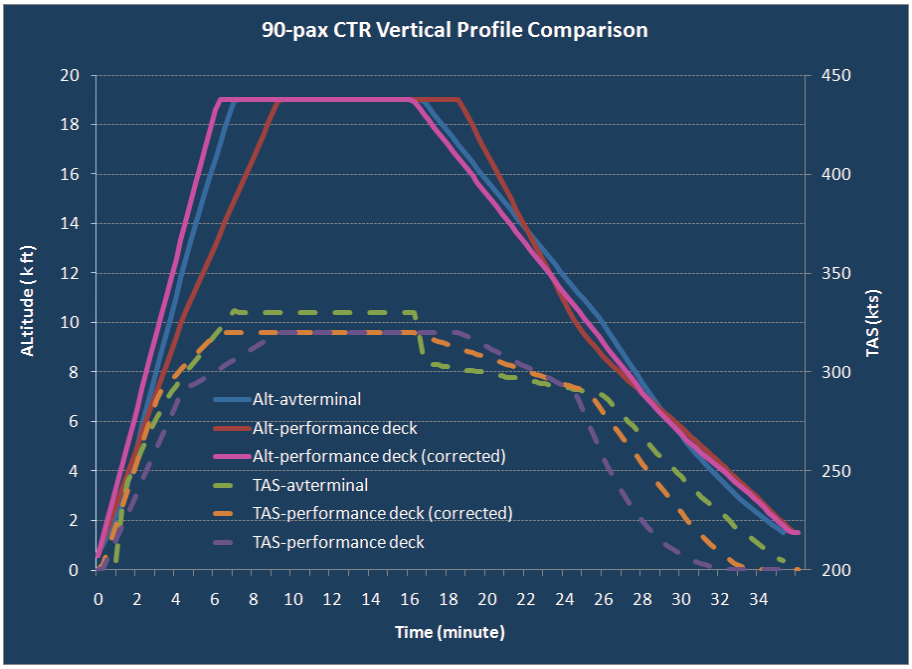

Figure M-3. Comparison of CTR90 AvTerminal and PD vertical profiles.

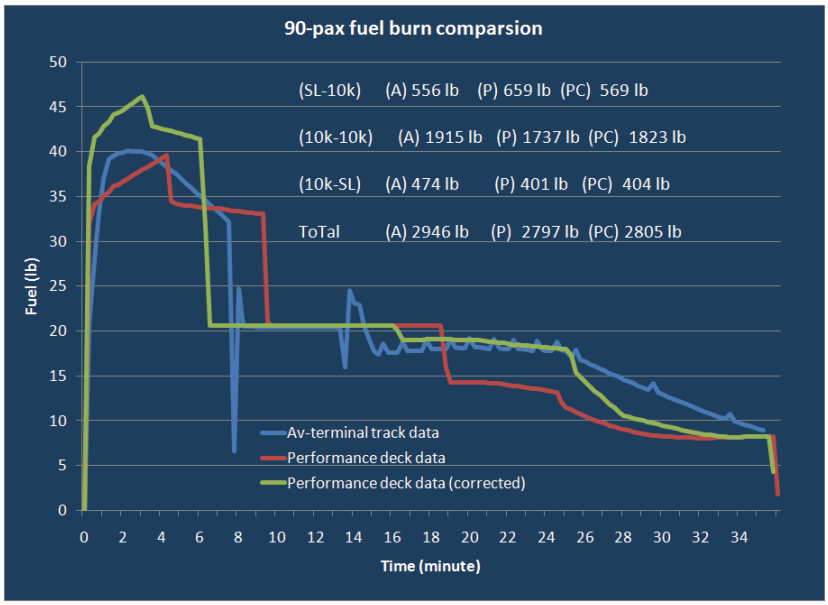

Figure M-4. Comparison of CTR90 AvTerminal and PD fuel burn.

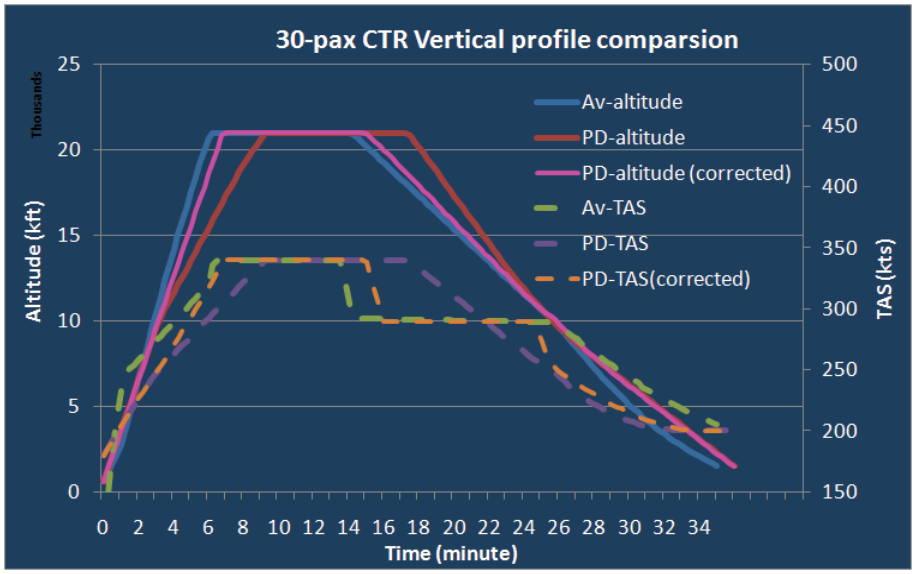

Figure M-5. Comparison of CTR30 AvTerminal and PD vertical profiles.

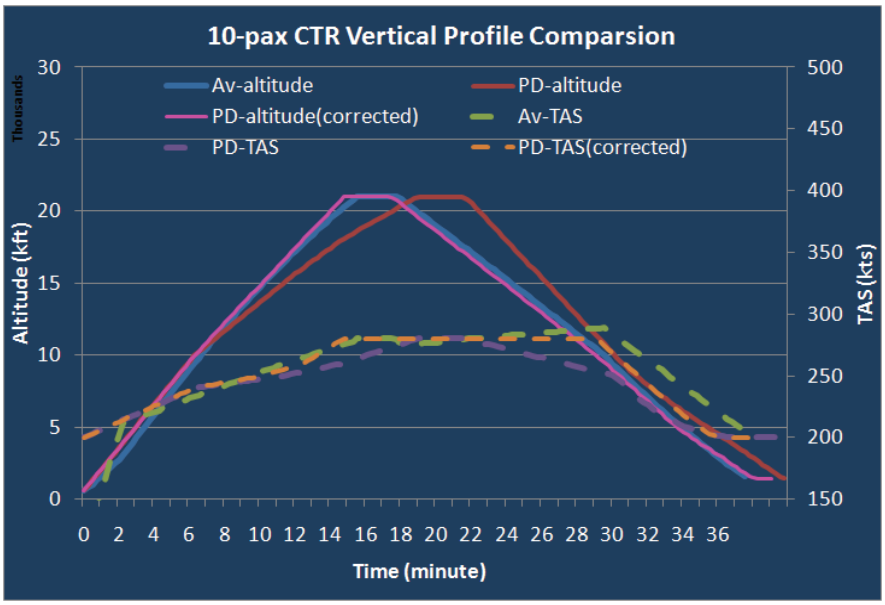

Figure M-6. Comparison of CTR10 AvTerminal and PD vertical profiles.

References:

M-1. Phillips, J. D.: An Accurate and Flexible Trajectory Analysis. Society of Automotive Engineers (SAE) Paper 975599, World Aviation Congress and Exposition, Anaheim, CA, Oct. 1997.

M-2. Couluris, G. J.; Phillips, J.; Hange, C. E.; and Wardwell, D. A.: CESTOL Impact on U.S. Airport Network Operations: Preliminary Analysis. International Power Lift Conference, London, UK, July 2008.

M-3. Couluris, G. J.; Hange, C. E.; Wardwell, D. A.; Signor, D.; and Phillips, J.: A Potential Impact Analysis of ESTOL Aircraft on Newark Airport Operations. AIAA Paper no. AIAA-2007-6700, AIAA Modeling and Simulation Technologies Conference and Exhibit, Hilton Head, SC, Aug. 2007.

APPENDIX N. CONVENTIONAL ITINERARIES ANALYSIS

N-1 Background

The analysis of conventional aircraft performance in this study pertains to the aircraft operating the 5,303 flights which are eligible for replacement by CTRs. The most important assumptions involve the handling of flight delays, fuel burn, trip time, and seat capacity. The primary source for these assumptions is the Sensis analysis of airline monthly and quarterly reports to the Department of Transportation (DOT).

The methodology and assumptions for computation of conventional aircraft performance (principally time and fuel burn) are presented in reference N-1, Conventional Aircraft Fleet Spreadsheet Analysis. Reference N-1 is configured with 10 worksheets (tabs) shown in table N-1. Descriptions of each tab are provided in section N-3 herein.

TABLE N-1. CONVENTIONAL AIRCRAFT WORKBOOK TABS

1. Conventional ACES Active Flight Listing
2. Conventional Flights Replaced by CTR Aircraft
3. Conventional Mixed-Equipage Operations Summary
4. Conventional Fix-based Operations Summary
5. Conventional Operations Metrics Detail
6. Conventional Operations Critical Metrics Assumptions
7. Conventional ACES Delay by Flight
8. Conventional Operations Unimpeded Time Calculation
9. Replaced Conventional Aircraft and Fuel Data
10. Conventional Operations Airport and Taxi Time Lookup

Note: In the workbook, tab titles are abbreviated.

N-2 Basic Approach

The basic approach was to derive airborne and ground taxi times based on routings assigned in ACES and estimated airport attributes and individual aircraft type characteristics. Table N-2 shows the basic assumptions used for analysis of conventional aircraft fuel burn, airborne time, and seating capacity. (Table N-2 is a copy of table 6-10, repeated here for convenience.)

TABLE N-2. CONVENTIONAL AIRCRAFT PERFORMANCE ASSUMPTIONS

Aircraft Type	Aircraft	Taxi lb per min	Fuel lb per LTO Cycle	Fuel lb per airborne minute	airborne min per track NM	ACES Enroute TAS KT	Nominal Seats
Airbus A319	A319	29	1676	78	0.148	406	123
Airbus A320	A320	34	2039	83	0.148	410	149
Airbus A321	A321	30	1789	103	0.148	442	170
Boeing 717-200	B712	25	1426	66	0.148	409	117
Boeing 727-100	B721	51	2765	133	0.148	474	110
Boeing 727-200	B722	51	2765	133	0.148	416	148
Boeing 737-300	B733	29	1663	75	0.148	416	132
Boeing 737-400	B734	30	1789	80	0.148	397	142
Boeing 737-500	B735	26	1531	73	0.148	417	111
Boeing 737-700	B737	29	1874	70	0.148	402	134
Boeing 737-800	B738	30	1940	83	0.148	417	152
Boeing 737-900	B739	28	1888	87	0.148	446	170
Beechcraft Airliner	BE99	7	340	6	0.287	209	15
Canadair Regional Jet CRJ-100	CRJ1	12	700	49	0.148	380	52
Canadair Regional Jet CRJ-200	CRJ2	12	700	49	0.148	367	49
Canadair Regional Jet CRJ-700	CRJ7	13	840	53	0.148	392	68
Canadair Regional Jet CRJ-900	CRJ9	16	920	58	0.148	405	86
McDonnell Douglas DC-9-30	DC93	34	1841	79	0.148	403	100
McDonnell Douglas DC-9-40	DC94	38	2125	79	0.148	398	110
McDonnell Douglas DC-9-50	DC95	38	2125	86	0.148	400	124
de Havilland Dash 8-100	DH8A	8	400	8	0.185	245	37
de Havilland Dash 8-200	DH8B	8	400	8	0.185	250	37
de Havilland Dash 8-300	DH8C	8	488	10	0.185	260	50
de Havilland Dash 8-400	DH8D	8	488	10	0.185	323	70
Embraer ERJ-135	E135	13	700	39	0.148	393	37
Embraer ERJ-145	E145	13	686	38	0.148	386	50
Embraer 175	E170	16	964	45	0.148	394	72
Embraer ERJ-190	E190	17	1069	66	0.148	405	100
Embraer EMB-145XR	E45X	12	700	49	0.148	411	50
McDonnell Douglas MD-82	MD82	33	2100	80	0.148	416	125
McDonnell Douglas MD-83	MD83	33	2100	80	0.148	417	125
McDonnell Douglas MD-88	MD88	33	2100	80	0.148	419	130
McDonnell Douglas MD-90	MD90	35	2145	82	0.148	430	149
Saab 340	SF34	8	488	10	0.233	257	33
Fairchild SA-227DC Metro	SW4	6	360	6	0.260	240	19

Note that conventional fuel and performance data is based on estimates reported in current aircraft operations, and does not make any allowance for improved fuel burn performance in 2025. Historically, between 1995 and 2009, average annual U.S. airline fuel efficiency improvement has been about 1.25 percent for small narrow-body aircraft (ref. N-1).

This methodology supports aggregation for individual test matrix points. The key indicators at the individual route and for specific test points are number of departures, taxi out and taxi in time, ACES track distance, Great Circle (GC) distance, circuity, unimpeded (delay-free) block time, total delay experienced at OPSNET 45 airports, and block fuel. From the aggregation of these variables, total block fuel, carbon dioxide (CO_2) emissions, passengers, seats, and load factor were calculated. Comparisons were made between conventional fixed-wing and CTR operations, and are presented in tables 6-14 through 6-28 of this report.

Note also that "mixed-equipage operations" and "fix-based operations" refer to assumptions used to generate aircraft routings for the ACES test points. The test points are discussed in section 6.4.5 of this report. ACES assigns waypoints to define aircraft navigation tracks representing those currently in actual use for flight planning, air-ground communications, and air navigation. These waypoints are termed "navigation fixes" and are defined by their latitude and longitude. In the ACES simulation, fix-based routings correspond to navigational aids and other identified points used to define NAS airway routings. Under fix-based routings, aircraft tracks consist of multiple flight legs connecting individual navigation fixes. Under NextGen, "direct to" (i.e., Great Circle) routings will be an option for aircraft with advanced avionics equipage. For "mixed-equipage" ACES simulation test points, 70 percent of fleet operations are assumed to operate on direct routes, and 30 percent of fleet operations are assumed to follow ACES-generated fix-based routes.

Delay was applied to all conventional flights in a uniform manner. In ACES, delay values are derived for each individual flight. In this study, delay values of up to 15 minutes are assumed to be taken at the departure gate with no fuel burn impact. The next 10 minutes of delay (up to a delay value of 25 minutes) are taken in taxi-out, and the next five minutes beyond that (up to a delay value of 30 minutes for an individual flight) are assumed to be taken in flight. The spreadsheet analysis was set up so that these default delay assumptions are easily changed.

Additional assumptions, including estimates of unimpeded airport taxi times, were obtained from analysis of airline monthly on-time reports to DOT.

During the study there was discussion of potentially achievable improvement in turbine engine fuel efficiency between 2010 and 2025. The discussion considered not only what could be achieved through improved materials, improved design, and improved turbofan and combustion efficiency, but also through improved flight procedures. A major constraint that limits improved fuel efficiency is the long service life of aircraft in fleet operation, and a limited rate of introduction of new aircraft into the operating fleet.

As background, during the 37th International Civil Aviation Organization (ICAO) General Assembly, held in Montreal in October 2010, ICAO member states adopted a resolution setting a goal of 2-percent average annual aviation fuel efficiency improvement up to the year 2050. In addition, the adopted resolution caps CO_2 emissions at the 2020 level.

The aviation industry had proposed a 1.5-percent average annual improvement through 2020. After ICAO adopted its 2010 resolution, the aviation industry supported the 2-percent annual target, with the reservation that the amount over 1.5 percent would need to be achieved through system operational improvements. Subsequent to the ICAO General Assembly, the FAA has proposed as a goal for discussion to "improve NAS energy efficiency (fuel burned per miles flown) by at least 2 percent annually" as a performance metric for 2018 (ref. N-2).

Overall required improvement between 2010 and 2025 is on the order of 25 percent (assuming an a 1.5-percent annual improvement rate), and 35 percent (assuming a 2-percent annual rate).

Given this context, tables 6-14 through 6-26 present notional "2025" levels of fuel burn and CO_2 emissions at an assumed level of 25 percent below 2010 levels.

N-3 Worksheet Descriptions

Conventional ACES Active Flight Listing

This worksheet shows the 58,100 conventional flights identified in the ACES NAS-wide simulation employed in this study. The flights are assigned to the regions used in the CTR analysis. For those flights eligible for CTR substitution, the CTR region and substituted CTR vehicle are shown. This worksheet represents the basis for selectively removing those conventional flights assumed to be replaced by CTRs, and generating ACES runs based on remaining conventional operations.

Conventional Flights Replaced by CTR Aircraft

This worksheet provides information on each of the 5,303 conventional flights eligible for CTR substitution. The main purpose of this worksheet is to support comparative analysis of changes in flights operated, itinerary mileages, and flight times for individual flights assumed to be replaced by CTRs under various assumptions. This worksheet is configured to take flight data in the format used in ACES to generate flight times and distances (ACES track distance and Great Circle distance).

Conventional Mixed-Equipage Operations Summary

The source data in this worksheet is contained in the **Conventional Operations Metrics Detail** worksheet. This summary is generated using a mixed-equipage assumption (70-percent flights capable of NextGen direct routing, 30-percent flights using traditional fix-based operation.) The summary data is a roll-up (under the mixed-equipage case) of individual conventional flight metrics; distances (GC and track), circuity, times (unimpeded and delay), seats operated, and fuel burn are calculated. For certain values (25-percent improved fuel burn, CO_2, and passengers) scale factors are applied to the summarized data.

Conventional Fix-Based Operations Summary

The source data in this worksheet is contained in the **Conventional Operations Metrics Detail** worksheet. This summary is generated using a 100-percent fix-based assumption (100-percent flights using traditional fix-based operation.) The summary data is a roll-up (under the fix-based case) of individual conventional flight metrics; distances (GC and track), circuity, times (unimpeded and delay), seats operated, and fuel burn are calculated. For certain values (25-percent improved fuel burn, CO_2, and passengers) scale factors are applied to the summarized data.

Conventional Operations Metrics Detail

This worksheet is the basis for the two preceding operations summary worksheets, and it contains the detailed calculations for each of the 5,303 flights eligible for CTR substitution under both mixed-equipage and fix-based routing assumptions. For each conventional individual flight the parameters of interest—distances (GC and track), circuity, segment times (unimpeded time and ACES delay values), seats operated, and fuel burn—are calculated. For each individual flight, the CTR region and substituted CTR type are also identified. This allows the data to be manipulated and the resulting table to be copied and pasted into the **Conventional Mixed-Equipage Operations Summary** and **Conventional Fix-based Operations Summary** worksheets. The resulting table represents a cross-tabulation and roll-up of the parameters of interest, and CTR regions and types.

The remaining worksheets contain assumptions used to derive values in the **Conventional Operations Metrics Detail** worksheet.

Conventional Operations Critical Metrics Assumptions

This worksheet contains specific assumptions applied to chargeable gate delay, taxi delay, and airborne delay, together with an assumption for 2025 fuel burn improvement. Since these are critical assumptions for cost buildup, they are identified in this worksheet.

Conventional ACES Delay by Flight

This worksheet contains the conventional aircraft delay values associated with each of 19 CTR-replacement test points, for each NAS-wide flight where ACES calculates delay (57,736 flights in all). Average delay values are derived for each test point for all airports and for OPSNET 45 airports.

Conventional Operations Unimpeded Time Calculation

This worksheet contains calculated unimpeded times for conventional aircraft by route (assuming average ACES track nmi) and by ACES aircraft type. The individual aircraft factors that drive the calculation in this worksheet are contained in the **Replaced Conventional Aircraft & Fuel Data** worksheet.

Replaced Conventional Aircraft and Fuel Data

This worksheet contains operational factors for each conventional aircraft type appearing in the ACES simulation. The factors in the worksheet are those that appear in table 6.10, as repeated in table N-2.

Conventional Operations Airport and Taxi Time Lookup

This worksheet contains several lookup tables. The principal table contains values for median taxi out and taxi in times for conventional operations at airports involving CTR substitution. A secondary table supports conversion between ICAO and IATA airport codes. A third table identifies airports as members of the Northeast Corridor nine (NEC9) core airports.

N-4 References

N-1. Anon. (Massachusetts Institute of Technology, Cambridge, MA): MIT Airline Data Project. http://airlinedataproject.mit.edu. Accessed Oct. 2011.

N-2. Anon. (Federal Aviation Administration, Washington, D.C.): Destination 2025. http://www.faa.gov/about/plans_reports/media/Destination2025.pdf. Accessed Dec. 2010.

APPENDIX O. CTR ITINERARIES ANALYSIS

O-1 Background

All CTR flights are assumed to operate on Great Circle (GC) direct routings and assume a default Vertical Takeoff and Landing (VTOL) mode of operation.

The methodology and assumptions for computation of CTR operational performance (time and fuel burn) are presented in reference O-1, Civil Tiltrotor Aircraft Fleet Spreadsheet Analysis. Reference O-1 is configured with 11 worksheets (tabs) shown in table O-1. Descriptions of each tab are provided in section O-3 herein.

TABLE O-1. CTR AIRCRAFT WORKBOOK TABS

1. CTR Operations Summary
2. CTR Metrics Detail
3. CTR Itinerary Cross Reference
4. CTR Operational Performance
5. CTR Takeoff and Landing Performance
6. CTR Parameter Settings
7. CTR Route Lookup
8. CTR Market Data
9. CTR Airport Latitude and Longitude
10. Job832 ACES Delay Run 2010-11-18
11. Job834 ACES Delay Run 2010-11-30

Note: In the workbook, tab titles are abbreviated.

O-2 Basic Approach

The basic approach was to derive airborne and ground taxi times based on routings assigned in ACES and on estimated airport attributes for vertiport-based CTR operations. The CTR workbook contains estimates of CTR time, distance, and fuel burn by phase of flight that were derived from, and validated in detail by, reference to the Fuel Burn Post Processor (FBPP) described in section 3.6. The CTR workbook can be configured to provide results for each route and CTR vehicle analyzed for either VTOL or STOL conversion, for any configuration specified in section 3.6.4, tables 3-20 through 3-27.

The CTR inertial distance transited, time to transit, and fuel burned for each phase of flight are illustrated in table O-2. The values are driven directly by copies of the lookup tables presented in section 3.6.4, tables 3-20 to 3-27.

TABLE O-2. CTR BASIC OPERATIONAL BUILDUP (DISTANCE, FUEL, TIME)

Taxi Out	Distance, nmi Fuel, lbs Time, minutes
Climb pt 2 > pt 4	Distance, nmi Fuel, lbs Time, minutes
Fuel Burn Post Processor	Distance, nmi Fuel, lbs Time, minutes
Descend and Land pt 8 > pt 12	Distance, nmi Fuel, lbs Time, minutes
Taxi In	Distance, nmi Fuel, lbs Time, minutes

In order to analyze CTR operations over the full range of routes and CTR sizes in the Test Matrix (discussed in section 6.4.5) and regional scenarios (sections 6.6 through 6.8), CTR fuel burn and flight time performance calculations were fitted to FBPP, as discussed in section 3.6, test points, using an iterative approach to minimizing least-squares residual differences. The goodness-of-fit results for the model used in section 6 for flight time and fuel burn for all individual CTR vehicles, as measured by the coefficients of determination (R^2), ranged from 0.998556 to 0.999943.

The CTR workbook can be configured to provide results for each route and CTR vehicle analyzed for either VTOL or STOL conversion, for any configuration specified (3-, 6-, or 9-degree glide slope) in tables 3-20 through 3-27. The CTR Aircraft Assumptions workbook is designed to be flexible in handling different CTR configurations, different assignment of CTR vehicles to routes, and different itineraries.

The fuel burn difference between STOL and VTOL was found to be less than one percent (section 6.10).

O-3 Worksheet Descriptions

CTR Operations Summary

The source data in this worksheet is contained in the **CTR Metrics Detail** worksheet. The summary data is a roll-up of individual CTR flight metrics; distances (GC and track), circuity, times (unimpeded and delay), seats operated, and fuel burn are calculated. For certain values (carbon dioxide and passengers) scale factors are applied to the summarized data.

CTR Metrics Detail

This worksheet is the basis for the preceding operations, **CTR Operations Summary** worksheet, and contains the detailed calculations for each of the 4,412 CTR flights eligible to substitute for conventional flights in the ACES simulation. For each CTR individual flight the parameters of interest—GC distances, segment times (unimpeded time and ACES delay values), seats operated, and fuel burn—are calculated. For each individual flight, the CTR region and substituted CTR type are also identified. This allows the data to be manipulated and the resulting table to be copied and pasted into the **CTR Operations Summary** worksheet. The pivot table represents a cross-tabulation and roll-up of the parameters of interest and CTR regions and types.

The remaining worksheets contain assumptions use to derive values in the **CTR Metrics Detail** worksheet.

CTR Itinerary Cross Reference

This worksheet is the basis for driving values in the CTR Metrics Detail worksheet. This worksheet contains a lookup table setting forth the assignment of CTR types to routes and regions, as well as times and fuel burn for each CTR vehicle and route operated. The tables in this worksheet show, for the purpose of traceability, the assumptions generated in the following worksheets.

CTR Operational Performance

This worksheet develops the fuel burn, time, and distance for each phase of flight shown in table O-2, by CTR vehicle and route operated. Estimates of CTR time, distance, and fuel burn by phase of flight were derived from and validated in detail by reference to the Fuel Burn Post Processor (FBPP) as described in section 3.6. The CTR inertial distance transited, time to transit, and fuel burned for each phase of flight are illustrated in table O-2.

CTR Takeoff and Landing Performance

This worksheet contains copies of the lookup tables presented in section 3.6.4 (tables 3-20 to 3-27). These lookup tables are used to drive calculations in the preceding **CTR Operational Performance** worksheet.

CTR Parameter Settings

This worksheet contains lookup tables with factors used to model the FBPP, also used to drive calculations in the preceding **CTR Operational Performance** worksheet.

CTR Route Lookup Table

This worksheet contains several lookup tables. The principal table contains assumptions about flight schedule frequencies and seats that apply to individual CTR routes. A secondary table provides assumptions about CTR cruise altitudes and cruise speeds for individual CTR types and routes.

CTR Market Data

This worksheet contains market size data used as one basis to assign CTR variants to specific airport-pair markets. This data was used for sizing and CTR variant selection purposes only, and was not used as an input feeding the **CTR Operations Summary** worksheet.

CTR Airport Latitude and Longitude

This worksheet contains airport latitude and longitude data used to calculate airport-pair GC distance, as well as to validate airport-pair distances obtained from other sources.

Job832 ACES Delay Run 2010-11-18

This worksheet contains delay data generated by an ACES simulation test run (Job832) on November 18, 2010. This run followed several iterations with (a) different numbers of vertiports at CTR airports, and (b) different CTR departure and arrival times designed to reduce "bunching" of arrivals and departures at vertiports. The worksheet is included as an example of results in a late-stage iteration, preceding the final ACES study iteration.

Job834 ACES Delay Run 2010-11-30

This worksheet contains delay data generated by the final ACES simulation test run (Job834) in the study. This run was based on iterated values selected for (a) number of vertiports at each airport served by CTRs, and (b) schedule timing used in the final ACES simulation in the study.

O-4 References

O-1. Anon. (Science Applications International Corporation (SAIC)), McLean, VA: Civil Tiltrotor Aircraft Fleet Spreadsheet Analysis, Appendix_O_CTR_Aircraft_Workbook_2011-07-25.xlsx, U.S. Government Prime Contract NNA09DA06T, July 25, 2011.